SPATIAL AND TEMPORAL LAG EFFECTS IN BEDLOAD SEDIMENT TRANSPORT

VOLUME I

SPATIAL AND TEMPORAL LAG EFFECTS IN BEDLOAD SEDIMENT TRANSPORT

A thesis

submitted in partial fulfilment

of the requirements for the Degree

of

Doctor of Philosophy in Civil Engineering

in the

University of Canterbury

by

BRETT CLAYTON PHILLIPS

University of Canterbury

July 1984

Table of Contents

Abstract

Spatial lag effects and temporal lag effects are investigated under bedload sediment transport conditions. This investigation, which involves both experimental and theoretical studies, culminates in the formulation of a numerical model which includes schemes which successfully describe spatial and temporal lag effects.

An equation which characterises spatial lag effects and two possible relations for the spatial lag coefficient are investigated. Values of the spatial lag coefficient are calculated from measured data and compared with values predicted by the theoretical relations. This investigation verifies the proposed spatial lag equation and indicates the form of the spatial lag coefficient relation.

A temporal lag scheme which is able to predict the temporal variation of bed roughness and sediment transport capacity under non-steady flow conditions is developed and calibrated against measured data. An impulse model is used to predict the temporal variation of the variable which chracterises the temporal response of the alluvial system, the equivalent steady flow rate. The performance of the temporal lag scheme is tested against additional measured data which verifies the proposed temporal lag scheme.

A numerical model which incorporates the spatial lag equation and the temporal lag scheme is formulated. This model also incorporates an upstream sediment boundary scheme which takes account of the zone of separation in a scour hole. The performance of the numerical model is tested against data measured by a previous investigator. The ability of the numerical model to predict the spatial and temporal variation of the bed elevation and the bedload sediment transport rate under both steady and non-steady flow, non-equilibrium sediment transport conditions is verified.

Acknowledgements

The research for this thesis was carried out in the Department of Civil Engineering, University of Canterbury, and thanks are extended to its head, Professor R. Park for the opportunity to use the facilities and equipment of the Department.

Special thanks are extended to my supervisor, Dr. A.J. Sutherland, for his guidance, encouragement and probing criticism during this study.

Appreciation is also expressed to my technician, Mr. H. Pearce, for his technical advice and unstinting assistance during the experimental study.

I gratefully acknowledge the assistance of the academic and technical staff of the Civil Engineering Department, in particular:

Professor I.R. Wood for his guidance during Dr. Sutherland's absence;

Mr. E.P. Giddens for his helpful advice;

Messrs A. Stokes and I. Sheppard for their technical advice and assistance in the construction and performance of experiments;

Messrs K. Mulvey and P. Robinson for their technical advice and assistance in the construction of the electronic bed profiling system;

Mrs. J.E. Stewart for her excellent effort typing the manuscript;

Mrs. V. Grey and Mr. B. McClelland for the draughting of figures; and

Mr. L. Gardiner for the photography.

I wish to thank my fellow students for many rewarding discussions.

Special thanks are extended to my wife, Anne, for her whole-hearted support and encouragement during this time.

This research was funded by the National Soil and Water Conservation Organisation and the writer supported by the University Grants Committee of New Zealand. Their support is gratefully acknowledged.

List of Figures

List of Plates

List of Tables

List of Symbols

a	Constant of sediment transport capacity
$a_1 - a_3$	Constants
a_k	Elemental area of flow
a_Q	Slope of discharge limb in temporal lag superposition solution
a_T	Time scale constant
A	Cross sectional area of flow
A_b	Area of deposition/scour at a section
A_1	Grain area constant
A_2	Grain volume constant
A_3	Constant of exchange time
A_ξ	Amplitude of property ξ
b	Constant of sediment transport capacity
$b_1 - b_5$	Constants
b_k	Elemental width of flow
b_Q	Slope of flow hydrograph
b_T	Time scale constant
B	Channel width at water surface
B_w	Channel bottom width
B1, B2	Flow routing coefficients
B3, B4	Sediment routing coefficients
c	Dimensional coefficient
c_s	Time series coefficient
C	Chezy coefficient
C_d	Celerity of dune bed form
C_{SL}	Spatial lag coefficient
C_t	Temporal lag constant
C1, C2	Flow routing coefficients
C3, C4	Sediment Routing Coefficients
d	Representative grain diameter
d_{35}	Diameter for which 35% of sediment is finer
d_{50}	Diameter for which 50% of sediment is finer

d_{65}	Diameter for which 65% of sediment is finer
Dgr	Nondimensional grain size
D1, D2	Flow routing coefficients
D3, D4	Sediment routing coefficients
e_s	Local erosion rate
f_b	Bed friction factor
f_b'	Grain friction factor
f_b''	Bed form friction factor
Fr	Froude number
g	Gravitational constant
g_s	Sediment mass transport rate per unit width
g_T	Impulse response function
g_{sc}	Sediment mass transport capacity per unit width
g_{sc_u}	Unsteady sediment mass transport capacity per unit width
g_{se}	Equilibrium sediment mass transport rate per unit width
g_{s_*}	Nondimensional sediment transport rate
g_{s_*}'	Nondimensional sediment transport rate
g_v	Volumetric sediment transport rate per unit width
g_{v_o}	Initial volumetric sediment transport rate per unit width
g_{v_∞}	Final volumetric sediment transport rate per unit width
G_V	Total volumetric sediment transport rate
G_{VC}	Total volumetric sediment transport capacity
G1, G2	Flow routing coefficients
G3, G4	Sediment routing coefficients
h	Scour depth
$h_{\text{℄}}$	Centre-line scour depth
h_m	Uniform scour depth predicted by numerical model
H	Local maximum scour depth.
H'	Local maximum scour depth on forward time line
$H_{\text{℄}}$	Local maximum centre-line scour depth
H_m	Local maximum uniform scour depth produced by numerical model
i_b	Fraction of total bedload of a particular size fraction
i_B	Fraction of bed area covered by a particular grain size
k_k	Sub-conveyance
k_s	Representative roughness height
K	Total conveyance

ℓ Distance to diffusion model degradation front from upstream boundary

L Distance to point of local maximum scour from fixed bed

L' Distance to point of local maximum scour from fixed bed on forward time line

L_s Grain step length

M_s Cumulative mass of sediment

n_b Manning (total) bed roughness value

$n_{b'}$ Grain Manning roughness value

$n_{b''}$ Bed form Manning roughness value

n_{b_e} Equivalent steady flow Manning bed roughness value

n_{b_u} Unsteady Manning bed roughness value

N Dimensionless erosion rate

N_d Number of particles deposited/unit area/unit time

N_e Number of particles eroded/unit area/unit time

p Einstein probability of erosion

p_k Elemental wetted perimeter

P Total wetted perimeter

q Flow rate per unit width

q_b Base flow rate per unit width

q_c Critical or threshold flow rate per unit width

q_e Equivalent steady flow rate per unit width

q_{e_o} Equivalent steady flow rate per unit width under an instantaneous step change in discharge

q_ℓ Lateral inflow per unit length

q_L Instantaneous (absolute) discharge per unit width on a superposition solution discharge limb

q_{max} Maximum or peak flow rate per unit width

q_R Excess discharge ratio

q_{R_o} Excess discharge ratio under an instantaneous step change in discharge

Q Total flow rate

r_{b_k} Elemental hydraulic radius of the bed

r_{xy} Correlation coefficient

R_b Total hydraulic radius of the bed

$R_{b'}$ Grain related hydraulic radius of the bed

$R_{b''}$ Bed form related hydraulic radius of the bed

R_{b_e} Equivalent steady flow (total) hydraulic radius of the bed

Re_*	Bed related grain Reynolds number
Re'_*	Grain related grain Reynolds number
S_d	Bed form steepness
S_f,	Friction or energy slope
$S_{f'}$	Grain related friction slope
$S_{f''}$	Bed form related friction slope
S_s	Specific gravity of sediment
S_t	Strouhal number
S_o	Bed slope
t	Time
t_o	Time at which superposition solution discharge limb commences
t_1	Exchange time
t_{90}	Time scale of temporal lag
t^*	Total temporal lag
T	Equilibrium time scale of dune bed form development from a plane bed
T_d	Propagation time of a dune bed form
T_e	Time scale of superposition solution
T_Q	Characteristic time of the flow hydrograph
u_s	Sediment velocity
u_{*_b}	Bed shear velocity
u_{*_b}'	Grain related bed shear velocity
$u_{*_{b_e}}$	Equivalent steady flow bed shear velocity
u_{*_c}	Critical or threshold bed shear velocity
U	Average flow velocity
U_c	Critical or threshold average flow velocity
U_{c_e}	Equivalent steady flow critical average velocity
U_e	Equivalent steady flow average velocity
V_b	Total volume of bed eroded over a given reach length per unit width
V_d	Total volume of bed material deposited/unit area/unit time
V_e	Total volume of bed material eroded/unit area/unit time
x	Longitudinal distance
x_R	Reach length
x_o	Location of mobile upstream boundary for diffusion models
y_b	Lateral coordinate of bed geometry
Y	Average flow depth
Y_e	Equivalent steady flow depth

Y_E	Average flow depth after temporal lag effects have dissipated
Y_o	Reference upstream flow depth
Z	Water surface elevation or stage
Z_b	Bed elevation
$Z_{b_{AV}}$	Average bed elevation predicted by numerical model
$Z_{b_{\mathbb{C}}}$	Centre-line bed elevation
α	Velocity distribution correction factor
α'	Resistance relation constant
α_K	Diffusion model factor
α_L	Step length constant (Yalin)
α_n	Manning resistance relation constant
α_s	Nondimensional sediment transport relation constant
α_o	Scour depth relation constant
α_o'	Scour depth relation constant
α_1	Constant
β'	Resistance relation constant
β_n	Manning resistance relation constant
β_s	Nondimensional sediment transport relation constant
β_o	Scour depth relation constant
β_1	Constant
δ	Upstream flow parameter
$\Delta H_{\mathbb{C}}$	Local maximum centre-line scour depth correction
η	Diffusion model variable (fixed upstream boundary)
η'	Diffusion model variable (mobile upstream boundary)
θ	Shields Parameter
θ'	Grain Shields Parameter
θ_c	Critical or threshold Shields Parameter
θ_c'	Critical or threshold grain Shields Parameter
Θ	Finite difference scheme weighting coefficient
κ	Diffusion coefficient
λ	Step length constant (Einstein)
λ'	Bed Porosity
λ_χ	Model/Prototype variable ratio of variable x
ν	Kinematic viscosity
ξ	General variable

$\pi_{t_{90}}$ Nondimensional time scale of temporal lag

π_T Nondimensional equilibrium time scale of dune bed development from a plane bed

ρ_s Sediment density

ρ_w Fluid density

σ_g Geometric standard deviation of grain size

τ_o Total bed shear stress

τ'_o Grain related bed shear stress

τ''_o Bed form related bed shear stress

ϕ_ξ Phase delay of property ξ

χ Nondimensional variable

ψ Flow Intensity

ψ' Grain related flow intensity

ω Sediment fall velocity

ω_q Cyclic discharge frequency

Chapter 1 | Introduction

1.1 PROBLEM STATEMENT

Large, steep, gravel-bed rivers are characteristic of New Zealand's South Island river systems. The stability of these rivers with regard to the mitigation of floods, maintenance of ground water levels, maintenance of the integrity of stop banks, bridges, pipelines and transmission lines and to the effects of hydro-electric structures is of economic importance. In gravel-bed rivers, it is the bedload component of sediment discharge which brings about significant morphological changes and is causing the more severe problems.

The bulk of the annual bedload discharge in gravel rivers occurs over relatively short periods of time during a few storm runoffs e.g. the Waimakariri River, N.Z. (Griffiths (1979)) and the Wairoa - Waimea Rivers, N.Z. (Pemberton (1979)). These flows are non-steady and little is known of their quantitative effects on channels and sediment yields. Commenting on the future needs in the sediment field, Wolman (1977) suggested: (p.51)

> "Both erosion and transport in natural streams vary with time. Perhaps a major need is to understand the way in which discontinuous (transient) transport processes take place in channels"

and concluded (p.24)

> "From both a theoretical and practical point of view, more attention is needed to unsteady or transient phenomena of erosion and transportation".

Likewise, when discussing dynamic models, Hey, Bathurst and Thorne (1982) stated: (p.12)

> "Mathematical modelling techniques are being developed for the prediction of scour and fill for gravel-bed rivers but their application is limited by the lack of, or deficiencies in, the process equations. Equally the non-availability of information on systematic long term changes in the flow and hydraulic geometry of gravel-bed rivers precludes the evaluation of the various modelling techniques".

A study recently completed by Bell (1980) has provided much useful background information of the type envisaged by Wolman (1977). However, this data base is limited and there exists the need for further experimental and theoretical research directed firstly: at further understanding the physics of unsteady or transient bedload transport under steady and non-steady flows and secondly; at formulating a mathematical model which is based on equations which quantify transient sediment responses and is thus better able to make quantitative predictions of the alluvial system behaviour, in particular, the estimation of bedload transport rates and yields and the effect of bed roughness on bedload transport rates.

1.2 SCOPE OF THESIS

The work herein forms part of a continuing research programme aimed at understanding the response of an alluvial system to constrained sediment boundary conditions under steady and non-steady water flows. In particular, spatial lag effects, which are viewed as the inability of an alluvial system to immediately overcome constrained sediment boundary conditions, and temporal lag effects, which are viewed as the inability of an alluvial system to immediately respond to imposed changes in discharge.

These lag effects were investigated experimentally by recording the spatial and temporal response of an alluvial system to non-steady flows under constrained sediment boundary conditions. In this study, constrained sediment boundary conditions were created by the presence of a rigid bed and zero sediment input stream of the test reach. Non-steady flow conditions were created by linearly increasing the flow rate from a base discharge up to a constant discharge over a selected period of time.

Under these conditions, a scour hole developed at the upstream

end of the test reach. Measurements of various bed and flow properties at sections within this scour hole were used to determine the validity of a proposed spatial lag equation while measurements taken downstream of the scour hole were used to develop a temporal lag model. The resulting spatial lag equation and temporal lag scheme were then incorporated in a numerical model. Spatial lag effects are directly incorporated in the model by the adoption of the spatial lag equation while temporal lag effects are indirectly incorporated in the model through relations for the bedload transport capacity and bed roughness values under unsteady flow conditions. The performance of the model was tested against the data of Bell (1980).

The experimental and theoretical studies were conducted in three stages. Firstly, an exploratory numerical model, which only incorporated the spatial lag equation, was formulated and tested. These simulations posed questions which could only be answered by an experimental investigation. These questions formed part of the wider experimental investigation into spatial and temporal lags which was conducted in the second stage. In the light of the results obtained, the third stage involved the modification and inclusion of a temporal lag scheme in the numerical model. The full model was then used to simulate various runs conducted by Bell (1980) and the model results compared with the data.

Chapter 2 is a review of the literature relevant to this study, it includes a brief discussion of current mathematical models and formulates objectives for the research programme.

Chapters 3 and 4 are devoted to descriptions of the design and procedures of the experimental programme, the apparatus used and of typical measurements.

Analyses of the steady flow equilibrium transport data are presented in Chapter 5. Side-wall correction methods and initial motion criteria are investigated and bed roughness and equilibrium sediment transport relations are obtained.

In Chapter 6, the non-steady flow experiments are discussed. Observations and typical results are also presented.

The analysis of spatial lag effects is presented in Chapter 7. The proposed spatial lag equation is derived, as are two theoretical relations for the bedload spatial lag coefficient. Values of the bedload spatial lag coefficient, obtained from the experimental

measurements of individual terms in the spatial lag equation, are compared with the theoretical relations and a bedload spatial lag coefficient relation is adopted.

Temporal lag effects are analysed in Chapter 8. A temporal lag scheme which is able to predict values of non-steady bed roughness and sediment transport capacity is developed and calibrated against measured data. The performance of the temporal lag scheme is also tested against further experimental data.

In Chapter 9, a numerical model based on the unsteady flow equations and the spatial lag equation is developed. The temporal lag scheme developed in Chapter 8 is also incorporated in the numerical model.

A comparison of the results of the numerical model simulations, of various runs conducted by Bell (1980), and the data of Bell (1980) are presented in Chapter 10. The ability of the model to simulate spatial lag effects, alone, and combined spatial and temporal lag effects is investigated. Comparisons with alternative mathematical models are also presented.

A set of conclusions and recommendations for future work is given in the final chapter.

Experimental detail, formulae and their derivations, selected data and results and a full listing of the numerical model are presented in the Appendices.

A full compilation of all experimental data, including bed and water surface profiles, lateral bed profiles, bedload transport readings and rates and velocity profiles is presented in the companion Volume II. Also included in Volume II are the various computer programs which were used to analyse the experimental data.

Chapter 2 | Literature Review

2.1 INTRODUCTION

A review of previous research into the spatial lag effects and temporal lag effects associated with steady and non-steady flow non-equilibrium bedload transport is presented. The implications of this previous research are discussed and objectives for the current research programme formulated.

2.2 SPATIAL LAG

When "constrained" sediment boundary conditions are imposed on an alluvial system it has been found that the alluvial system is unable to immediately overcome these constraints. Constrained sediment boundary conditions include the presence of a rigid bed upstream of a mobile reach, e.g. a dam spillway, and sediment inflow rates which are lesser or greater than the capacity of the flow to transport sediment at the upstream boundary. A certain distance is required before the alluvial system reaches an equilibrium state. This phenomenon is viewed as spatial lag.

2.2.1 Experimental Research

Spatial lag effects are most commonly investigated under steady flow non-equilibrium transport conditions. Non-equilibrium sediment transport conditions are created when the sediment inflow rate is either less than the capacity rate of sediment transport, which leads to erosion of bed material (degradation), or greater than the capacity rate of sediment transport, which leads to the deposition of sediment (aggradation).

Experimental research into the bed degradation process has centred on the response of the alluvial bed to the presence of a rigid

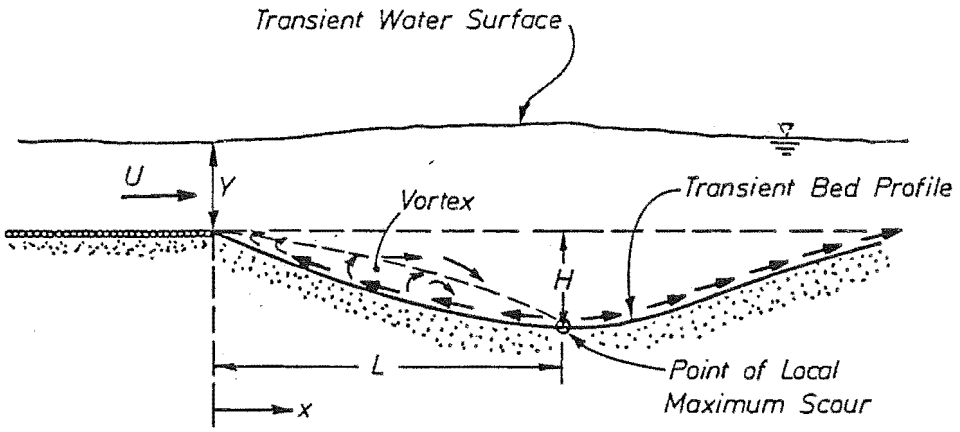

Figure 2.1 Typical Bed Degradation Due to Zero Upstream Sediment Inflow (After Dietz (1969))

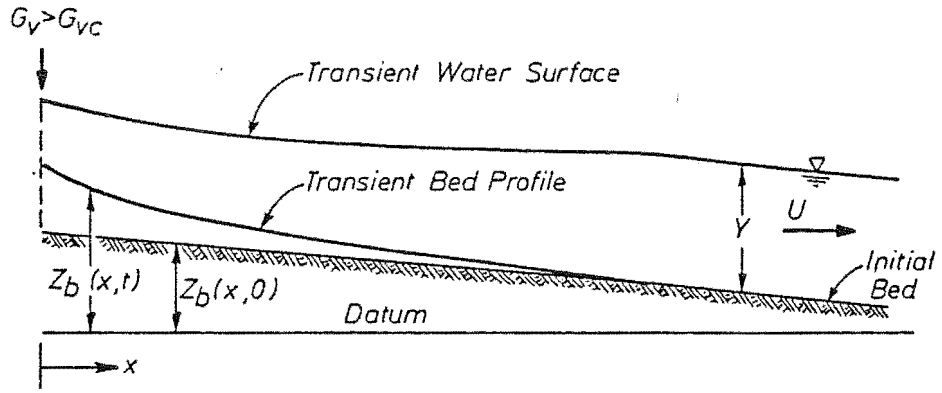

Figure 2.2 Typical Bed Aggradation Due to Upstream Sediment Overloading (After Mehta, Garde and Ranga Raju (1983))

upstream bed and zero sediment inflow at the upstream boundary of the mobile reach. These sediment boundary conditions cause a scour hole, of the form shown in Fig. 2.1, to develop at the upstream end of the mobile reach. This degradation continues and propagates downstream until a new equilibrium state is reached; in this case, when threshold conditions are encountered. The flow field in the scour hole, Fig. 2.1, is dominated by the presence of a fluid vortex. The presence of the fluid vortex also causes the point of local maximum scour, which is located at the toe of the vortex, to occur at a point downstream of the fixed to mobile bed interface.

The interest of previous researchers, including Dietz (1969), Mosonyi and Schoppman (1968) and Breusers (1965), has centred on the local scour process and the effects of various upstream fixed bed roughnesses and upstream bed slopes on the spatial and temporal distribution of the local maximum scour depth. The aim of this research has been to fit relations to the principal phases of the four distinct scour phases identified by Cuhna (1975) and listed in Section 6.23.

Dietz (1969) developed non-dimensional relations for both principal phases and calibrated them with data collected from experiments involving a variety of bed materials, including polystyrol (d_{50} = 1.55 mm, 2.81 mm), brown coal (1.1 mm, 3.4 mm, 7.8 mm) and sand (d_{50} = 0.12 mm). Similarily, Breusers (1965) investigated the first principal phase of scour for bed materials, including sand, bakelite and polystyrene, while Mosonyi and Schoppmann (1968) investigated the effect upstream bed slope had on this phase of scour for a sand bed. These calibrated relations allow the temporal variation of the local maximum scour depth and the expected maximum scour depth to be predicted.

Until recently little research had been conducted with the aim of determining the sediment transport rates within a developing scour hole. Consequently, the research of Bell (1980), who conducted an investigation into bed degradation processes due to the sudden cessation of sediment inflow at the upstream boundary has provided valuable experimental data. The results of Bell (1980), which include the temporal and spatial variations of bed elevation and bedload transport rates, can be used to more fully test mathematical models which seek to simulate spatial lag effects. Nakagawa and Tsujimoto (1980) also presented a limited set of bedload transport data which demonstrates spatial lag effects.

Experimental research into bed aggradation processes has centred on the response of the bed to sediment overloading at the upstream boundary of a mobile reach. This sediment boundary condition causes the bed to aggrade, in the manner demonstrated in Fig. 2.2, at the upstream end of the mobile reach. This aggradation continues and propagates downstream until a new equilibrium state is reached when the sediment transport capacity at the steeper slope is equal to the rate of sediment supply at the upstream boundary. Under these conditions, the maximum aggradation depth occurs at the upstream boundary and not at some point downstream as is the case for the maximum scour depth when bed aggradation occurs.

The interest of previous researchers, including Mehta, Garde and Ranga Raju (1983), Jain (1981), Soni (1981(a)) and Soni, Garde and Ranga Raju (1980), (1977), has centred on the temporal variation of the transient bed profile under various rates of sediment overloading. The aim of their research has been to measure transient bed profiles and use this data to calibrate the diffusion models developed by these researchers (Section 2.2.3). Mehta, Garde and Ranga Raju (1983) investigated the response of a sand bed (d_{50} = 0.5 mm, 0.7 mm) to sediment overloading; Soni, Garde and Ranga Raju (1980) (1977) conducted similar experiments, also with a sand bed (d_{50} = 0.32 mm).

Little research has been conducted into the transient sediment transport rates under sediment overloading conditions; Soni (1981(b)) is one of the few researchers to have investigated this aspect of bed aggradation.

2.2.2 Spatial Lag Equations

A general equation which describes spatial lag effects, of the form suggested by Bennett (1974) where the local erosion or deposition rate is assumed proportional to the difference between the sediment transport rate and sediment transport capacity, an idea first introduced by Einstein (1968), is

$$(1 - \lambda') \frac{\partial A_b}{\partial t} = C_{SL}(G_V - G_{VC}) \qquad (2.1)$$

where A_b = Area of scour or deposition at a section,
C_{SL} = Spatial lag coefficient,
G_V = Total sediment transport rate, by volume, and
G_{VC} = Total sediment transport capacity, by volume.

Bennett (1974) also suggested that the spatial lag coefficient is: "probably a strong function of bed sediment fall velocity, mean shear velocity and depth of flow".

An equation of the form proposed by Foster and Meyer (1972) for the erosion of soil in rills is obtained by re-arranging Eq. 2.1 thus

$$\frac{e_s}{C_{SL}G_{VC}} + \frac{G_V}{G_{VC}} = 1 \qquad (2.2)$$

where the local erosion rate, e_s, is given by

$$e_s = -(1 - \lambda') \frac{\partial A_b}{\partial t} \qquad (2.3)$$

and $C_{SL}G_{VC}$ is associated with the erosion capacity. Furthermore, Foster and Meyer were able to cite experimental evidence of Meyer and Monke (1965) and Willis (1971) that illustrates a tendency for flows over non-cohesive beds to entrain sediment according to Eq. 2.2.

Le Feuvre, Altinbilek and Carstens (1970) also investigated local bed erosion rates in a pipe for different flow conditions and sediments but formulated their relation for local erosion rates in terms of the flow velocity near the bed, angle of repose of the material, slope of the bed and sediment characteristics.

A spatial lag equation of the form given by Eq. 2.1, was also obtained by Wellington (1978) from an analysis of Einstein's (1950) formulation of a bedload transport equation. Furthermore, Wellington (1978) derived spatial lag coefficient relations for both bedload and suspended load transport conditions. The bedload spatial lag coefficient relation is (Wellington (1978))

$$C_{SL} = \frac{1 - p}{\lambda d_{50}} \qquad (2.4)$$

where d_{50} = Median grain size,
p = Einstein's probability of erosion, and
λ = Einstein's step length constant.

The derivation of this relation is presented in Section 7.2.

Wellington (1978) also derived a relation for the suspended load spatial lag coefficient using the work of Sumer (1977). An amended derivation of this relation was provided more recently by Phillips (1981). Since it is proposed to only investigate the bedload phase

of sediment transport, this relation is not presented herein.

To date, the calibration of the general spatial lag equation, Eq. 2.1, and the comparison of the spatial lag coefficient relations, Eqs. 2.4 and 2.5 with observed data does not appear to have been attempted by any researcher. Instead, previous researchers have only concentrated on specific aspects of the spatial lag phenomenon under steady flow conditions, Section 2.2.1, and thus no complete set of experimental data is available with which to test the general spatial lag equation. Even the very comprehensive results of Bell (1980) lack necessary data.

2.2.3 Mathematical Models

While modelling sediment transport in alluvial streams it is normally assumed, in the light of uncertainty regarding transient sediment phenomena, that the sediment transport capacity of the flow is filled instantaneously at every point in space and time (Bennett (1974)). Hence, many mathematical models, having first solved the equations of flow continuity and flow momentum, solve the sediment continuity equation while assuming that the sediment transport rate is given by

$$G_V = G_{VC} = f(\text{local flow conditions}) \qquad (2.5)$$

Mathematical models which have adopted this approach when simulating spatial lag effects include the bed degradation models proposed by Hwang (1975), Cunge and Perdreau (1973), Gessler (1971), Aksoy (1971) and Komura (1971).

However, when constrained sediment boundary conditions are present, Bell (1980) demonstrated that a certain distance is required before the transport capacity is reached and Eq. 2.11 holds. Wellington (1978) recognised this phenomenon and formulated the only numerical model to incorporate the general spatial lag equation, Eq. 2.1, in a sediment routing scheme. Wellington (1978) incorporated the spatial lag equation in both his bedload and suspended load routing schemes. An option incorporated by Wellington (1978) in his model, however, was to neglect bedload spatial lag effects and instead use an alternative bedload routing scheme based on the assumption that the sediment was transported at a capacity rate at all times and locations. Wellington (1978) did not test his numerical model against field or laboratory data but instead demonstrated its use for the case of assumed channel and sediment properties. In these demonstration runs, Wellington (1978),

adopted the alternative bedload routing scheme, Eq. 2.11, and only used the spatial lag equation when routing suspended load sediment.

For steady flow, non-equilibrium sediment transport conditions many researchers have simplified and manipulated the flow continuity, flow momentum, the sediment continuity equation, and the condition given by Eq. 2.11 to obtain a parabolic partial differential equation of the diffusion type,

$$\frac{\partial z_b}{\partial t} = \kappa \frac{\partial^2 z_b}{\partial x^2}$$

where Z_b = Bed elevation, and
κ = Diffusion coefficient

which is then solved for various initial and boundary conditions (see Section 10.3.4).

Mathematical models which have adopted this approach to simulate spatial lag effects due to sediment overloading, include the diffusion models of: Gill (1983(a)), Mehta, Garde and Ranga Raju (1983), Soni (1981 (a), (b)), Jain (1981), Soni, Garde and Ranga Raju (1980), (1977) and de Vries (1973). A major feature of these models is their simplicity. Only a limited number of checks on the foregoing diffusion models using laboratory and field data have been made; the most recent being that of Mehta, Garde and Ranga Raju (1983). They obtained good agreement between measured and predicted transient bed profiles, however this agreement was only obtained after diffusion coefficients of best fit had been determined.

More recently, diffusion models which simulate spatial lag effects due to the sudden reduction of sediment inflow have been proposed by Gill (1983(b)) and Yalin (1983). To date, no checks on the foregoing diffusion models using laboratory or field data have been made.

Various researchers have also proposed relations for the diffusion coefficient; so far three different relations have been proposed (See Section 10.3.4). Only the first relation has been tested. This relation has been tested indirectly by researchers including Mehta et al (1983), Soni et al (1980), (1977) and Jain (1981) by comparing measured and predicted transient bed profiles. As Mehta et al (1983) most recently found, the values of the diffusion coefficient predicted by this relation have not performed particularly well and have needed modification.

A feature of all diffusion models is that they are developed for steady flow conditions and are unable to simulate spatial lag effects under non-steady flow conditions. In contrast, mathematical models which adopt the general spatial lag equation are able to simulate spatial lag effects under steady and non-steady flow conditions and overcome the inherent constraints imposed by diffusion models.

2.3 TEMPORAL LAG

When unsteady flow conditions are imposed on an alluvial system it has been found that the alluvial system is unable to respond immediately to the changing flow. A certain time is required before the bed form geometry, sediment transport rate and flow depth adjust to the new flow regime. This phenomenon is viewed as a temporal lag.

2.3.1 Experimental Research

Temporal lag effects have been most commonly investigated by observing and measuring the temporal variation of bed forms under unsteady flow conditions. Reviews by Yalin (1972) and Simons and Senturk (1977) demonstrate that researchers have achieved some success in describing empirically the relationship of bed form type and the geometric properties of bed forms with gross parameters describing steady flow conditions. Field and laboratory observations during non-steady flows have demonstrated, however, that the development of bed forms lags the development predicted by steady flow bed form relations, using instantaneous flow properties.

Field observations of bed form temporal lag have been documented, predominantly on sand bed rivers, by Neill (1969) in the Red River and in the tidal reaches of the Weser River by Nasner (1973).

Laboratory evidence of bed form temporal lag has been obtained by Nakagawa and Tsujimoto (1983(b)), Bell (1980), Griffiths (1976), Jensen (1973) and Simons, Richardson and Haushild (1962) for flood waves; Yalin and Bishop (1977), Yalin (1975), Gee (1975), Gee (1973) and Raichlen and Kennedy (1965) for step changes in discharge; and Grant and Madsen (1982) and Bayazit (1969) for oscillating flows.

Nakagawa and Tsujimoto (1983(b)) found, for a uniform sand (d_{50} = 0.7 mm), that the dune height and wavelength followed the rising discharge limb of the hydrograph with a certain lag. Similarily, the dune height followed the descending limb of the hydrograph, while the

dune wavelength remained constant. Bell (1980), Griffiths (1976) and Jensen (1973) measured the geometric properties of dunes under triangular translation waves using gravel (d_{50} = 2.11 mm), gravel (d_{50} = 4.02 mm) and polystyrene balls (d_{50} = 1.5 mm) respectively. The dune height was found to follow the flow hydrograph with a certain lag, while the dune wavelength continued to increase throughout the wave passage. Yalin (1975) and Raichlen and Kennedy (1965) studied the growth of sand dunes from a plane bed and found that the change in bed form size is initially rapid, followed by a period of slower growth as an equilibrium state was approached. Gee (1975), (1973) examined the bed form response to a change from one steady flow equilibrium state to another steady flow state using sand grains (d_{50} = 0.3 mm and d_{50} = 1.00 mm) and concluded that dune growth proceeded more rapidly than dune destruction and that bedload transport is a necessary condition for changes to occur in dune dimensions.

Comparatively little experimental research has been conducted into the temporal lags associated with transport of sediments by non-steady flows. Experimental evidence of bedload transport temporal lag has been obtained by Bell (1980) and Griffiths (1976) under flood waves, and Bell (1980) for step changes in discharge from threshold conditions. Bell (1980) found that the bedload transport rates lagged the comparable steady flow transport rates and that the sediment yields were significantly less than the predicted comparable steady flow yields. Griffiths (1976) also found that the sediment transport rate lagged the comparable steady flow rate and concluded that the differences were caused by changes in entrainment of the bed material occurring more slowly than changes in discharge.

2.3.2 Mathematical Models

Mathematical models which simulate the response of dune bed forms to non-steady flows have been proposed by Nakagawa and Tsujimoto (1983(a)), Fredsøe (1981), (1979), Puls, Sundermann and Vollmers (1977) and Allen (1976 (a), (b)).

Allen (1976(b)) separated the response of dune bed forms into two components:

(i) Change due to modification of individual bed forms, and

(ii) Change due to the creation/destruction process where the original dunes are replaced by others better adjusted to the new flow conditions.

The first process was assumed, by Allen, to take place much faster than the second. Allen also introduced several empirical constants and assumptions to formulate the rate of change of dune configurations with time. The model was then used to numerically simulate the temporal response of an alluvial system to non-steady flows where the discharge was strictly periodic with a long base period, e.g. one year.

Puls, Sundermann and Vollmers (1977) based their model on the general two dimensional Navier-Stokes equations and a transport rate scheme which modelled the sediment transfer processes of erosion, transport and sedimentation and the effects of turbulence. This scheme was assumed to be more suitable for bedform analysis than an equilibrium transport formula.

Fredsøe (1979), (1981) modelled the response of dunes to sudden step changes in discharge, by assuming the change in bed form configuration was by modification of individual bed forms. The temporal response of dune steepness to a discharge impulse was assumed and described by an exponential function. Fredsøe tested his model by simulating the stepped discharge, experimental results of Gee (1973) and comparing the measured and predicted variations of flow depth. The agreement between the measured data and model predictions was satisfactory. After linearising his general equation set, Fredsøe applied his model to weakly, periodically varying flows, where it was assumed the changes in the flow were small, and determined values of the phase lags and amplitudes of the bed form steepness, flow depth and grain resistance. A comparison of model results with data measured under these flow conditions was not undertaken.

Nakagawa and Tsujimoto (1983(a)) based their model on the assumptions that the temporally lagged response of dune height to a step change in discharge was described by an exponential relation and that the dune steepness was constant during sand wave development. They also determined numerically the phase lags and amplitudes of the bed form height and flow depth under periodically varying flows. No comparison with measured data was provided.

In all cases, the short term fluctuations due to individual storm runoffs were ignored. Such an assumption will be more severe for gravel rivers, where the bulk of the bedload yield and the greatest changes in bed form geometry occur in these individual flow events.

2.4 SPATIAL AND TEMPORAL LAGS

When both constrained sediment boundary conditions and non-steady flows are imposed on an alluvial system the response of an alluvial system displays both spatial and temporal lags.

2.4.1 Experimental Research

Laboratory evidence of combined spatial and temporal lag effects was recently obtained by Bell (1980) for flood waves. Bell (1980) measured the temporal variation of the bedload transport rate at five sections along a mobile reach, downstream of a fixed bed, under triangular translation waves. In all cases studied there was zero upstream sediment inflow. The results of his non-steady flow, non-equilibrium transport experiments demonstrated an asymmetry in the sediment hydrograph and reduced sediment yields. These results reflect the strong influences of a developing scour hole and bed form temporal lag on bedload yields and transport rates.

2.4.2 Mathematical Models

Attempts to model non-steady flow, non-equilibrium transport conditions have been made by many researchers in a variety of ways. These analytical models adopt the St. Venant Equations of motion and the sediment continuity equation and also assume that the sediment transport rate is equal to the sediment transport capacity, Eq. 2.11, at all times. An indication of the myriad number of models which has been formulated was given by Bell (1980) when he listed seventeen models. These models fall into two broad categories.

The first category of model regards the flow as steady during each time step, which reduces the governing flow equations to the steady flow equations of motion. This approach is further subdivided into two routing techniques, both of which use finite difference solution methods. In an uncoupled model the flow and bedlevel computations are completed sequentially and the required flow adjustments are made at the end of each time step. In a coupled model the governing flow and sediment equations are solved simultaneously when bed deformations are assumed to be large during each time step. Examples of this category of model are the uncoupled model of Thomas and Prasuhn (1977) and the coupled model of Ponce, Garcia and Simons (1979).

The second category of model solves the complete dynamic equations of motion, particularly if rapid flow changes cause the local acceleration

terms to be significant, over each time step. Mathematical models in this category employ one of two numerical schemes: the method of characteristics or finite difference methods. Once again the latter numerical scheme can be coupled or uncoupled. Examples in this category of model are the model of Chang (1969), which adopts the method of characteristics, the uncoupled model of Wellington (1978) and the coupled model of Chen and Simons (1975).

In spite of there being many attempts, it would appear that no model formulated so far, which seeks to simulate non-steady flow, non-equilibrium transport, has adopted a spatial lag equation of the form given in Eq. 2.1 and specifically recognised temporal lag effects in its sediment routing scheme.

2.5 IMPLICATIONS

This literature survey indicates areas in which research work would be most useful. Specific aspects are:

(1) As stated by Bennett (1974): "there is a need to investigate the effects of unsteadiness and of flow nonuniformities on sediment transport characteristics. This would clarify if whether or not it is proper to define the response of the sediment load to changes in transport and detachment capacity by a first-order reaction rate law (Eq. 2.1). If such an expression is proper, the investigation should define the coefficient (C_{SL})."

Mathematical models have been reasonably well explored theoretically but, with the exception of Wellington (1978), have relied on the assumption that the sediment transport rate is at capacity at all times. Bell (1980) clearly demonstrated such an assumption to be unsatisfactory under conditions of strong bed degradation.

A laboratory investigation of the type envisaged by Bennett (1974), would test the validity of the proposed spatial lag equation. The formulation of a mathematical model which incorporates a calibrated spatial lag equation would lead to better simulations of spatial lag effects under steady and non-steady flows.

(2) Laboratory investigations of temporal lag effects have so far concentrated on the response of bed forms to step changes in discharge with comparatively little research being undertaken into the associated sediment transport temporal lag. Various researchers have formulated

bed form temporal lag models from these investigations and determined the phase lags and amplitudes of bed form steepness, bed roughness and flow depth for periodically varying flows.

In gravel rivers, however, the bulk of the bedload yield and changes in bed form geometry occur during individual flood events. Hence, further experimental research is required to investigate the temporal response of bedload transport to non-steady flow conditions with the aim of formulating a temporal lag model which is able to predict the temporal variation of bed roughness, flow depth and bedload transport rate under non-steady flow conditions. Such a model should then be used to investigate temporal lag effects due to individual flood events.

(3) Attempts to mathematically model non-steady, non-equilibrium transport conditions have been made by many researchers. All these models, however, rely on the unsatisfactory assumption that the sediment transport rate is at capacity at all times and locations. Further, none of these models specifically recognise temporal lag effects in their sediment routing schemes.

A mathematical model which incorporates the spatial lag equation and specifically includes temporal lag effects in its sediment routing scheme is required. The performance of such a model should be tested against measured data; the experimental data of Bell (1980), for flood waves, provides an excellent data base for such test purposes.

Thus, it is believed that this study makes a contribution by

(i) Seeking to comprehend spatial and temporal lag effects in bedload transport under steady and non-steady flow conditions by

(ii) Formulating a numerical model which specifically recognises spatial and temporal lag effects, and by

(iii) Comparing numerical model simulations with experimental data recorded by Bell (1980) and with data obtained during this study.

Chapter 3 | Laboratory Experiments: Design and Apparatus

3.1 INTRODUCTION

A series of laboratory experiments was conducted in the Fluid Mechanics Laboratory, University of Canterbury, during the period 1982-83. The aims of the experimental programme, which stem from the literature review and the results from initial, exploratory runs of the numerical model were as follows:

- To determine an equilibrium sediment transport relation under a variety of flow conditions, including a range of friction slopes.
- To measure individual terms in the spatial lag equation in order to calculate values of the spatial lag coefficient. These values of the spatial lag coefficient to be then compared with those values predicted by the proposed theoretical relations.
- To measure the effect of non-steady flows on sediment transport and bed form development to facilitate development of a temporal lag model for bedload sediment transport.
- To measure the flow and sediment behaviour so that the actual, measured behaviour could be compared with the behaviour predicted by exploratory runs of the initial numerical model.

3.2 LABORATORY EXPERIMENTS: SCALING AND DESIGN

3.2.1 Model Scaling

For many of the rivers in New Zealand, the bed slope is steep and the bed, composed of coarse gravel, is wide. In these rivers, significant bedload transport generally only occurs in times of floods; Griffiths (1979), Pemberton (1979). The experimental model was chosen

to simulate typical flow and bedload transport characteristics of these rivers.

To simulate typical river conditions relevant scaling relationships must be satisfied. For the case of non-steady two phase flow, Yalin (1971) derived five dimensionless variables which completely determine the alluvial system. These dimensionless variables are

$$\chi_1 = Re_* = \frac{u_{*_b} d_{50}}{\nu} \qquad \text{Grain Reynolds Number}$$

$$\chi_2 = \theta = \frac{u_{*_b}^2}{(S_s - 1) g\, d_{50}} \qquad \text{Shields Parameter}$$

$$\chi_3 = \frac{Y}{d_{50}} \qquad \text{Relative Roughness} \qquad (3.1)$$

$$\chi_4 = S_s = \frac{\rho_s}{\rho_w} \qquad \text{Grain Specific Gravity}$$

$$\chi_5 = S_t = \frac{u_{*_b} T_Q}{Y} \qquad \text{Strouhal Number}$$

where d_{50} = Median grain size,
g = Gravitational acceleration,
T_Q = Characteristic time of the flow hydrograph,
u_{*_b} = Bed shear velocity,
Y = Flow depth,
ρ_s = Density of sediment grains,
ρ_w = Density of fluid, and
ν = Kinematic viscosity.

Since the same fluid and sediment were used in the model and prototype, S_s was the same for both. Since flow conditions in the model and prototype will be in the rough turbulent regime ($Re_* > 70$) grain Reynolds Number can be neglected. Therefore, for dynamic similarity

$$\lambda_{\chi_2} = \lambda_{\chi_3} = \lambda_{\chi_5} = 1 \qquad (3.2)$$

where $\lambda_\chi = \frac{\chi_M}{\chi_P}$

and χ_M = Model variable, and
χ_P = Prototype variable.

This reduces to the following scale relationships for the system variables

$$\lambda_Y = \lambda_d = \lambda_\ell = \text{undistorted scale length,}$$

$$\lambda u_{*_b} = \sqrt{\lambda_\ell} \tag{3.3}$$

$$\lambda_{T_Q} = \sqrt{\lambda_\ell}$$

For a model grain size, d_{50} = 1.8 mm, and assuming a typical prototype size, d_{50} = 20 mm, implies a length scale of 1/11.1. Hence

$$\lambda_d = \lambda_Y = \frac{1}{11.1} \tag{3.4}$$

This is greater than the minimum scale of Yalin (1971)

$$\lambda_\ell > \left(\frac{70}{Re_{*_P}}\right)^{2/3}$$

which, typically, for New Zealand rivers is $\lambda_\ell > \simeq 1/30$.

Thus, from Equation 3.3

$$\lambda_T = \lambda_{u_{*_b}} = \lambda_U = \frac{1}{3.33} \tag{3.5}$$

where λ_U is the velocity scale.

A most important modelling aspect is that the rate of rise for floods should be correctly modelled. A very fast rising river may rise at 0.5 m/hr (Bell (1980)) which scales to 0.15 m/hr using the above velocity scale. This rate was used as a guide for selecting hydrographs of varying steepness and duration. Since temporal lag effects in bedload transport are more pronounced under severe non-steady flow conditions, rise rates ranging from 0.1 m/hr to 1.45 m/hr were chosen for the laboratory model experiments.

3.2.2 Design of Experiments

Most experiments were planned with non-equilibrium transport conditions (i.e. zero upstream sediment input). Consequently, the flume was operated in an open-circuit fashion. To facilitate comparison of results with those of Bell (1980) the same independent variables were chosen; they were: flume slope (S_o), inlet discharge per unit width (q) and flume width (B). Thus, flow depth (Y), velocity (U), sediment

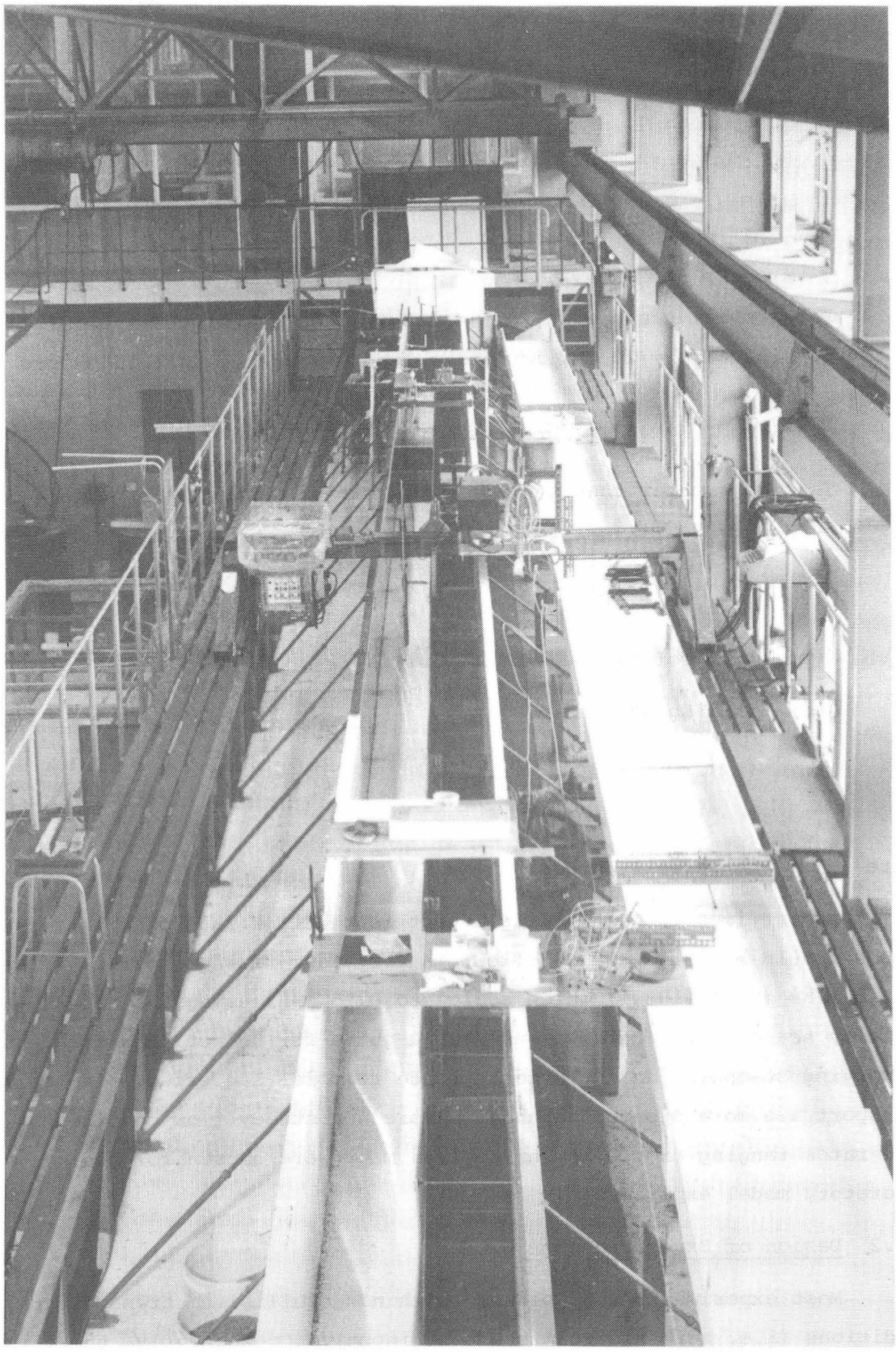

Plate 3.1 General View of Tilting Flume

transport rate (g_s) and roughness value (n) were the dependent variables. Since the Froude Number range was small, Fr ≃ 0.4 - 0.6, the roughness value and bedload transport rate relationships, with steady discharges, will be single-valued. Constraints imposed by the capacity of the bedload discharge measuring device were overcome by the careful selection of the magnitude and range of the independent variables B, S_o and q with

$$q_c \leq q \leq q_{max} \tag{3.6}$$

where q_c = critical or threshold discharge per unit width, and
q_{max} = maximum discharge per unit width.

3.3 EXPERIMENTAL PROGRAMME

The experimental programme consisted of 60 different runs in the flume. The conditions of each series of experiments are summarised below:

- Constant Parameters
  - Flume length = 30 m
  - Flume width = 0.305 m
  - Grain Size = 1.8 mm.
- Steady Flow Experiments
  - Series SE - Constant discharge, equilibrium sediment transport.
- Non-Steady Flow Experiments
  - Series SC - Inclined step change from threshold conditions to constant discharge.
  - Series GS - Inclined step change from threshold conditions to constant discharge (reduced reach length).

Details of individual series and procedures involved are given in Chapter 4.

3.4 LABORATORY APPARATUS

3.4.1 Tilting Flume

The major laboratory component is a 30 m tilting flume, (Plate 3.1), which has been described in detail by Hill (1967) and Bell (1980). The flume consists of adjustable side wall elements which sit on a flat steel deck, 28.5 m in length and has a working section of 23 m. The sidewalls were set 600 mm apart. Changes in flume slope were achieved using screw jacks at the midpoint and upper end supports of the flume.

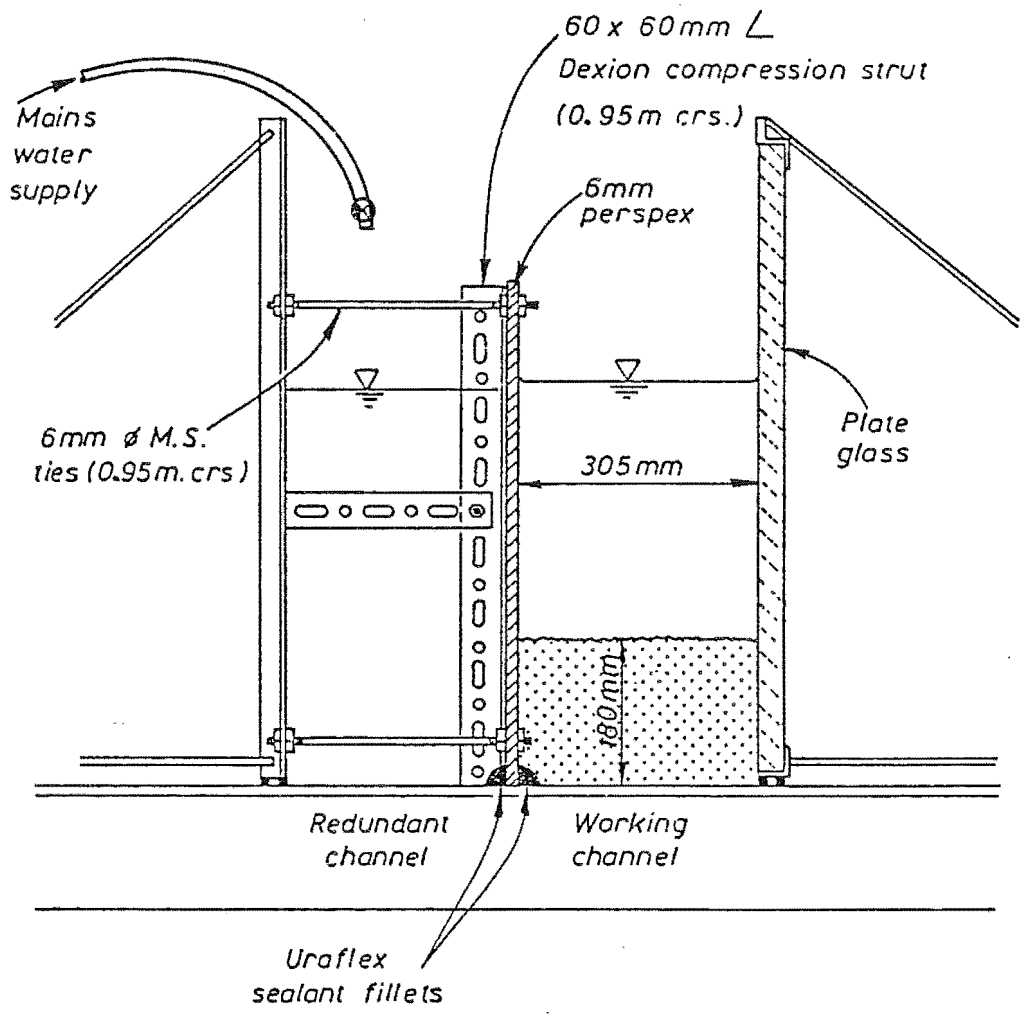

Figure 3.1 Flume Cross Section.

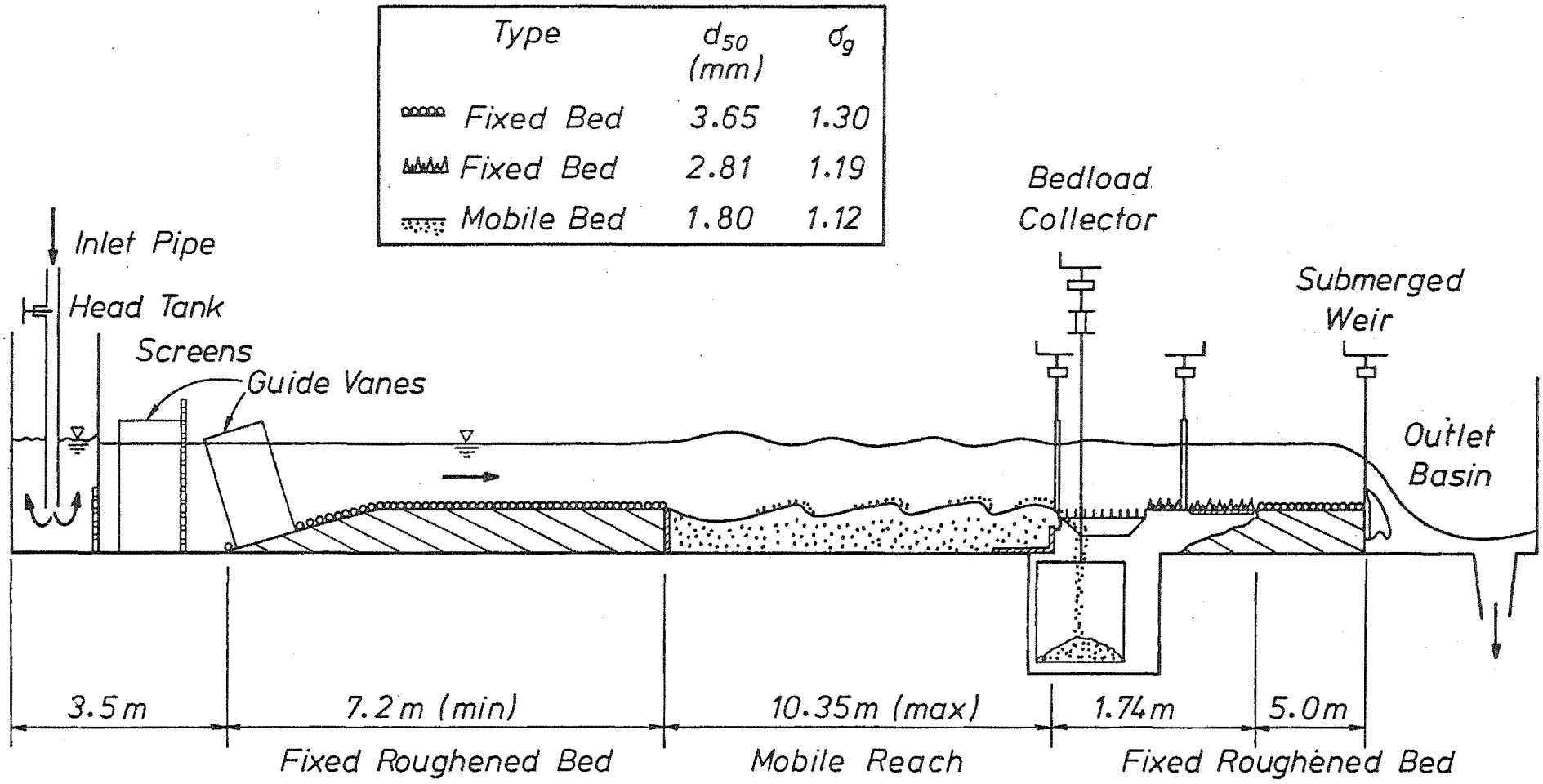

Figure 3.2 Schematic Longitudinal Flume Section

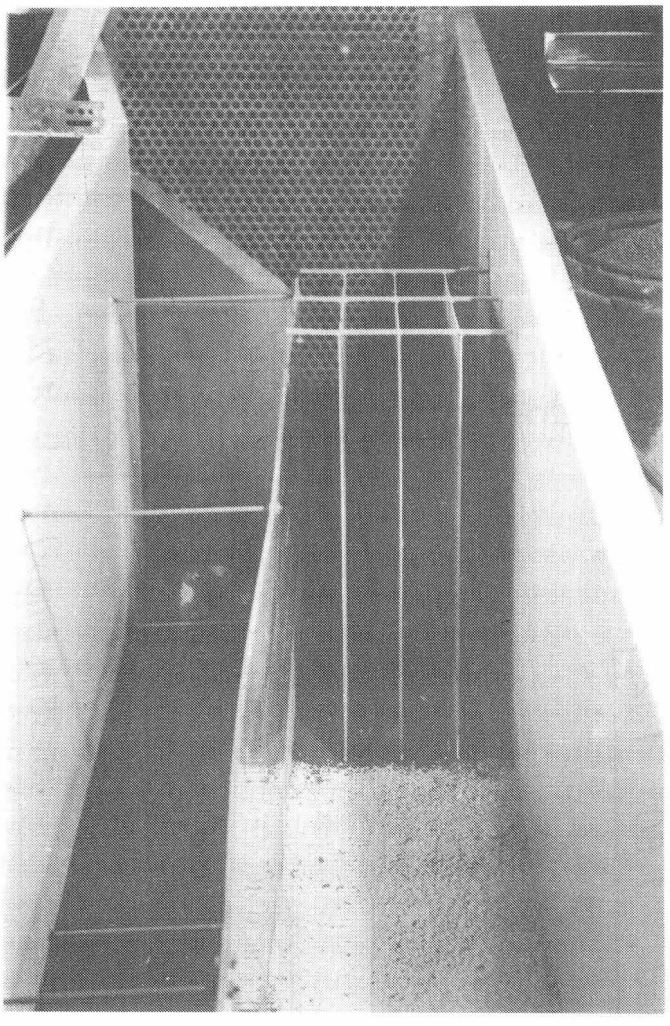

Plate 3.2 Upstream Flow Straighteners

The downstream support is freely hinged.

In order to allow direct comparison of results with those of Bell (1980) a 305 mm wide channel was constructed within the 600 mm flume using one existing flume wall and a new perspex wall, shown in Fig. 3.1. To prevent buckling of the walls due to hydrostatic pressures, the redundant channel was sealed and filled with mains water up to the main channel stage level.

A schematic longitudinal section of the flume is shown in Fig. 3.2. The essential components of the flume are

. Upstream Section
  - Reception tank for piped laboratory supply.
  - Contracting stilling basin containing flow straighteners.
  - Concrete ramp with flow straighteners leading onto a length of fixed bed. The roughness size and minimum length were selected to ensure a fully developed flow at the start of the test reach (see Appendix A.).

. Test Reach
  - A length of movable bed composed of uniform fine gravel particles to a depth of approximately 180 mm.

. Downstream Section
  - Bedload collector used to measure sediment transport rates at the end of the erodible reach.
  - Another length of rough fixed bed to accommodate backwater effects induced by the downstream control.
  - Stilling basin from which water drains back into the laboratory system.

3.4.2 Water Supply and Control

Water was supplied from a constant head tower and introduced at the upstream head tank of the flume through a valve controlled pipe (152 mm diameter).

A steady flow calibration curve, plotted from more than 60 flow measurements, gave the required valve setting for any given discharge. Valve settings were read from a fixed circular scale, mounted on the valve housing, using a pointer attached to the valve wheel. Non-steady flow hydrographs, in the form of an inclined step change in discharge, were generated manually by opening the valve in small steps at

predetermined times.

Flow straighteners and a perforated screen were inserted in the contracting section to dampen disturbances and provide an even flow distribution across the flume. In order to further align the flow a second set of flow straighteners was placed on the inclined ramp at the start of the fixed roughened bed (Plate 3.2).

At the downstream end of the channel a submerged weir gate was used to control the outlet backwater curve. The gate was made from steel plate and was raised and lowered using a screw threaded control rod. Weir settings were read from a fixed scale using a pointer attached to a weir gate support rod. During non-steady runs with inclined waves, the weir gate was raised in small steps in delayed synchronization with the opening valve. The delay accounted for the time the inclined wave took to reach the end of the test section. The weir gate setting for each step was obtained by interpolating between steady flow settings.

The water then returned to an underground sump through a calibrated pit which was used to measure steady flow rates.

3.4.3 Sediment Injection

For the series of equilibrium sediment transport experiments (SE runs) it was necessary to inject sediment just upstream of the movable bed. Sediment injection was done manually. This was achieved by weighing out the amount of sediment to be injected, every two minutes, within one minute and then sprinkling this measured amount of gravel into the flow during the second one minute period. Care was taken to ensure that the injected gravel was evenly spread across the flume and that all gravel fell onto the fixed bed upstream of the movable bed. This method was found to work very satisfactorily.

3.4.4 Bedload Discharge Measurement Devices

The devices used to measure bedload discharge were modified versions of the devices used by Bell (1980).

- Adjustable Bedload Collector

  In order to follow the degrading bed level during non-equilibrium sediment experiments a movable bedload collector was constructed. (Fig. 3.3 and Plates 3.3 - 3.6). The frame was suspended, by threaded rods at each end, from supports perpendicular to the flume. By rotating a support rod, the frame could be raised

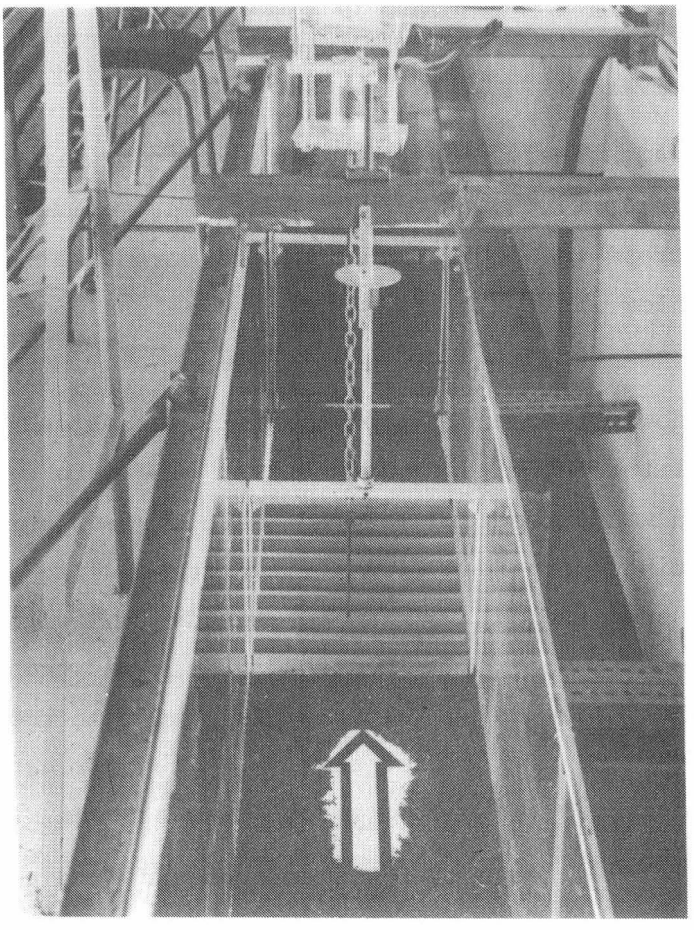

Plate 3.3 Bedload Collector - Lowered Position

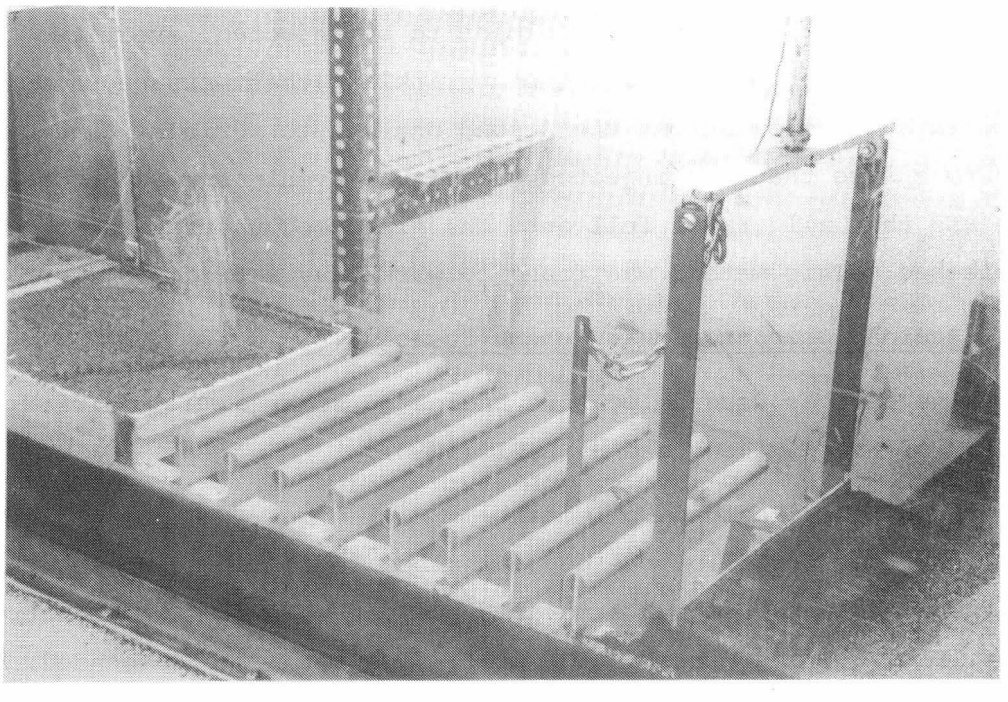

Plate 3.4 Bedload Collector - Lowered Position

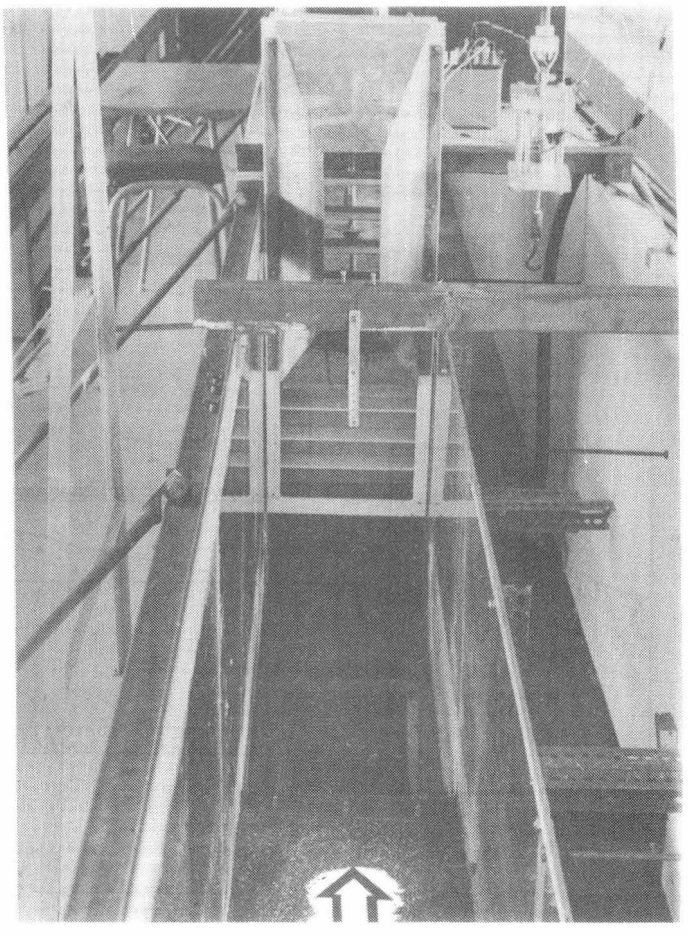

Plate 3.5 Bedload Collector - Raised Position

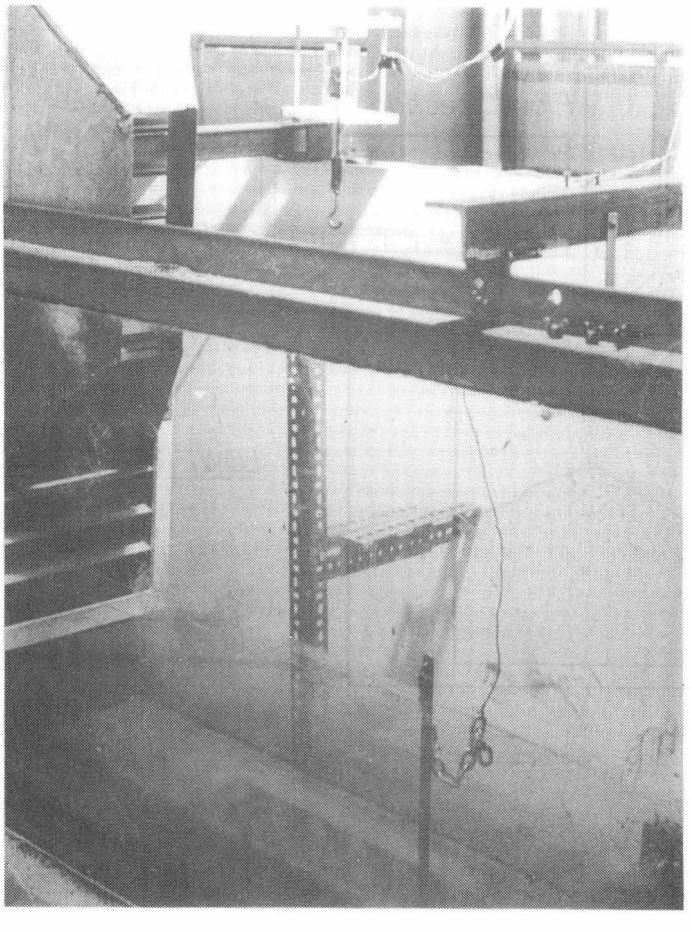

Plate 3.6 Bedload Collector - Raised Position

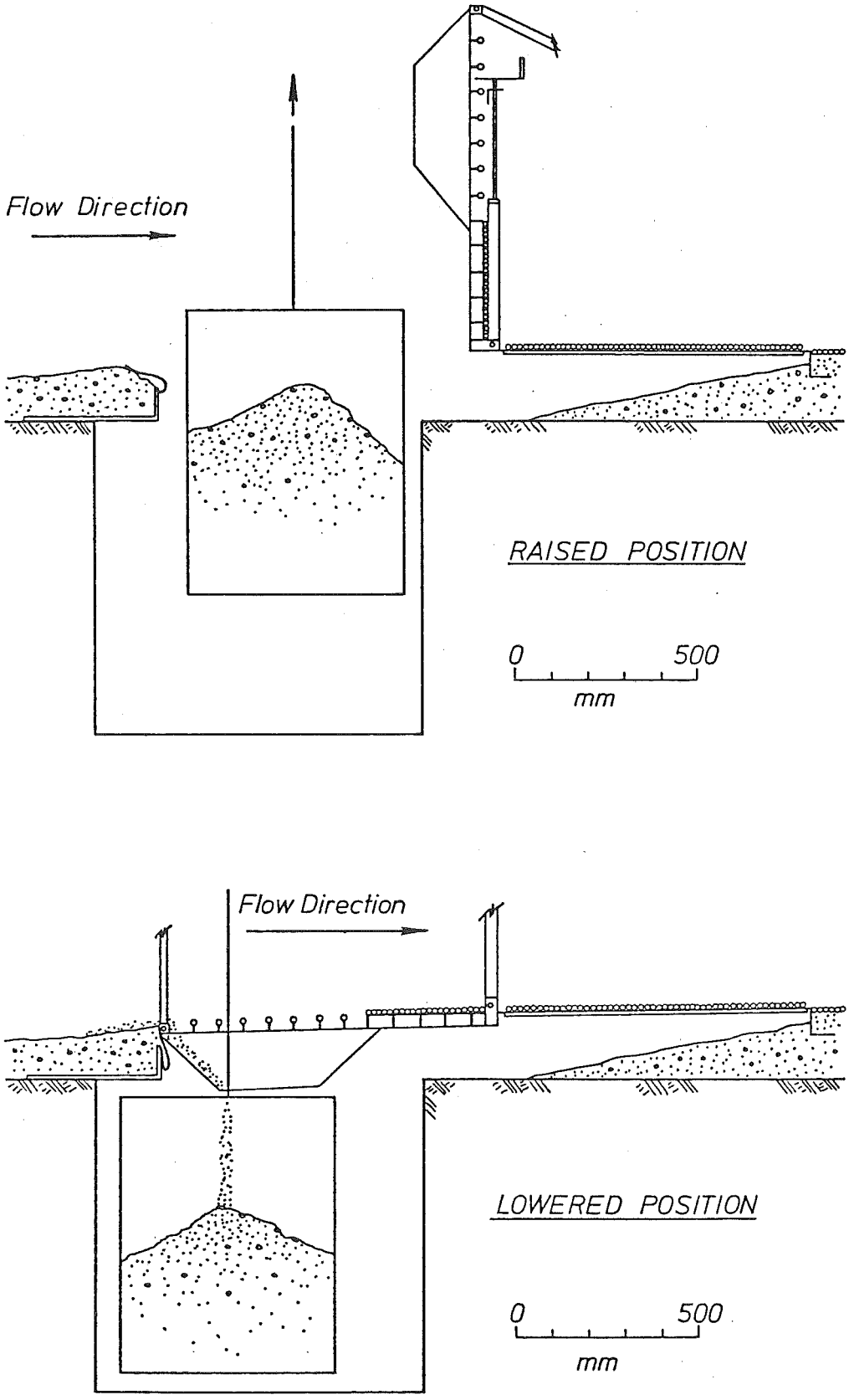

Figure 3.3 Schematic Bedload Collector Cross Section

or lowered at that end, with reference to an attached scale. At the upstream boundary a flexible rubber joint prevented loss of gravel from the test reach under the grill. This flexible joint connected the frame to a 100 mm high partition board located at the downstream end of the test reach. Two major features of the collector were: (1) that moving grains hopped directly from the test reach into the suspended basket; as distinct from Bell (1980) where grains moved across a smooth cover before falling into the basket, and (2) that the collector could be raised easily and the basket removed swiftly. Removal of the basket was facilitated by a quick release mechanism on the upstream support rod. Once the rubber joint was released and the upstream support rod disengaged the grill and frame could be rotated into a vertical position and locked, and the basket removed. The downstream end of the bedload collector was also adjustable to better simulate the bed profile in the vicinity of the collector. This was achieved by the use of a 0.81 m board which was hinged at both ends and attached to the collector and the fixed downstream rough bed. Further, in order to simulate bed roughness, a layer of gravel particles was glued to the hinged board and grill cover (Fig. 3.2).

Load Cell and Circuitry

The sediment collection basket was suspended by a rod and chain from a thin-walled aluminium load cell on which four strain gauges were arranged. The load cell was connected to a Budd bridge and the output voltage from the bridge was displayed on a digital voltmeter/recorder. The voltage output could be recorded by a Datel Thermal printer at intervals of 0.5 s to 60 s (Plate 3.7).

It was possible to adjust the Budd bridge settings so that the recorded output voltage response was linear for expected total sediment yields (dry mass) ranging from 10 kg up to the capacity of the basket, 90 kg. This allowed even small sediment yields to be accurately measured. The method used to obtain this linear voltage response was as follows. It was known that the voltage output of the Budd bridge was linear over the range - 250 mV to + 250 mV. Before each run commenced the submerged, empty basket was hung from the load cell. For a predetermined Budd bridge

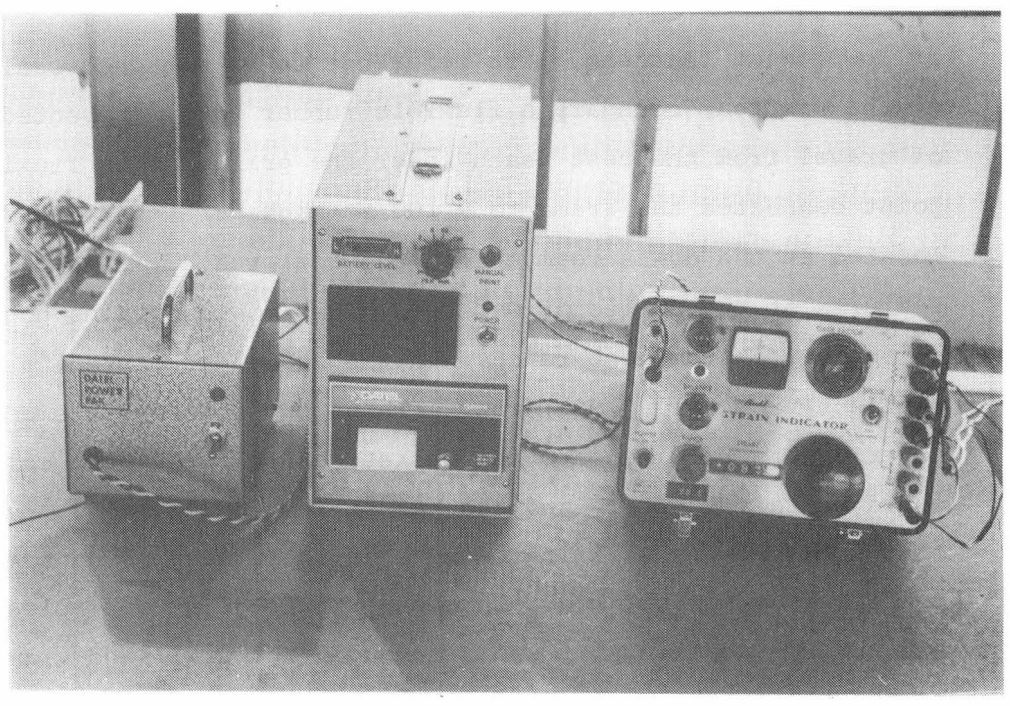

Plate 3.7 Bedload Recording Devices

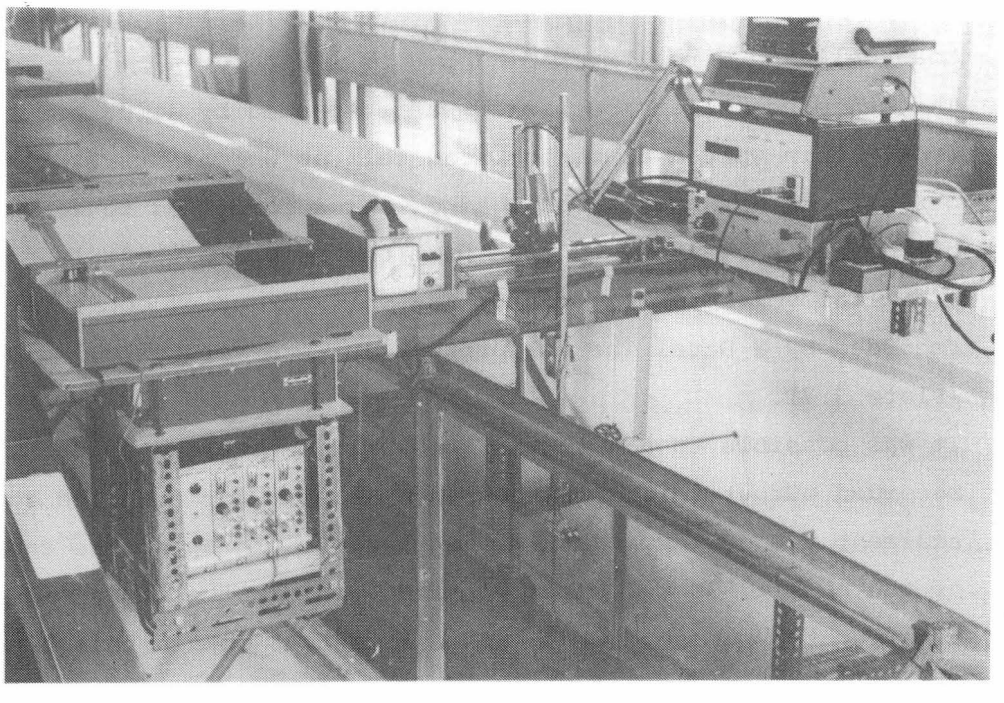

Plate 3.8 General Layout of Carriage Instruments

"sensitivity" setting, the "strain" setting on the Budd bridge was adjusted until the voltage output reached - 250 mV, i.e. the "zero" setting. A calibrated mass, 6.226 kg, (= 10 kg submerged gravel) was then hung from the load cell and the new voltage reading was recorded. The load cell conversion coefficient was then obtained by dividing 10 kg by the change in voltage output. The upper limit of the linear voltage output range is reached when the dry mass of sediment, calculated by multiplying the conversion coefficient by 500 mV, is collected. Various maximum expected yield ranges were set by adjusting the "sensitivity" setting. The weighing system was calibrated over several yield ranges and the change in accumulated dry weight against change in output voltage was found to be linear within any given range. The calibration of the load cell, undertaken before each run commenced, was checked at the end of each run by drying and weighing the gravel collected in the basket. The maximum error between predicted and measured total weight was 5%.

3.4.5 Stage and Bed Level Measuring Devices

The devices used to determine stage and bed levels were mounted on a movable carriage at a position corresponding to the centreline of the channel. The general layout is shown in Plate 3.8.

- Water Level Recorders

  During the SE series of experiments, water surface elevations were measured, relative to the carriage rails, by a point gauge to the nearest 0.2 mm. After the SE series was completed, modifications were made allowing continuous, longitudinal water surface profiles to be recorded at any given time. The modified measurement system used a Churchill Wave Recorder (Plate 3.9 and Fig. 3.4). A resistance water level probe was mounted on the point gauge previously used to measure stage and linked to the Wave Recorder. The analog output from the Wave Recorder drove the Y-axis of an HP Chart Recorder while the X-axis, longitudinal location, was driven by a potentiometer. A Y-axis scale of 1/1 was set, using the Y-axis gain control. In order to calibrate the water surface record it was necessary to measure the water surface at one known point, normally Chainage = - 0.5 m, and to align the record with this measured point. The system worked

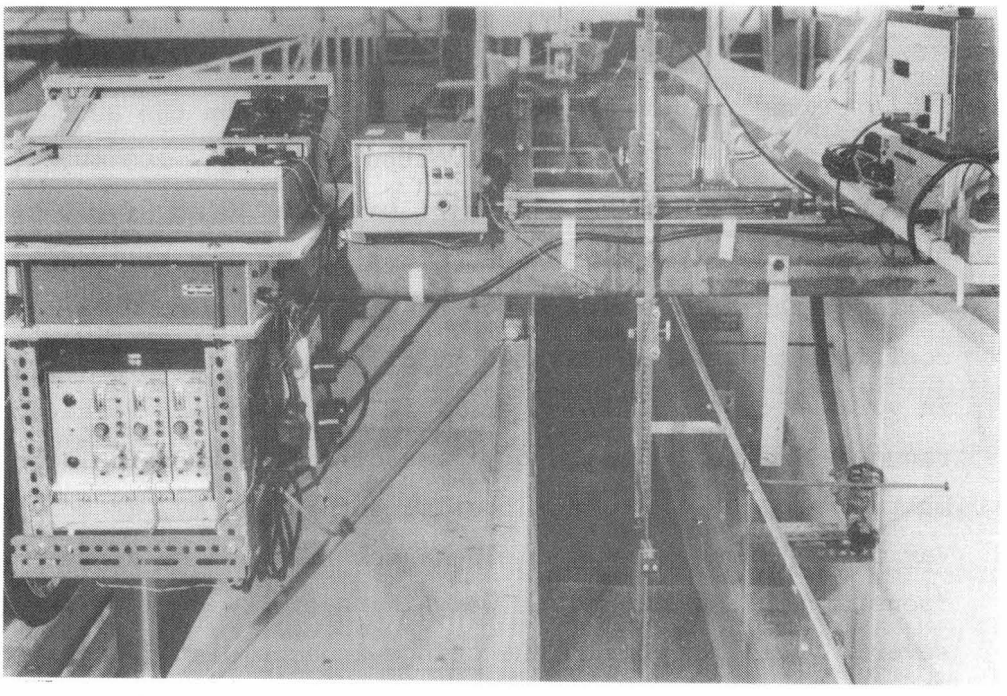

Plate 3.9 Wave Recorder and Chart Recorders

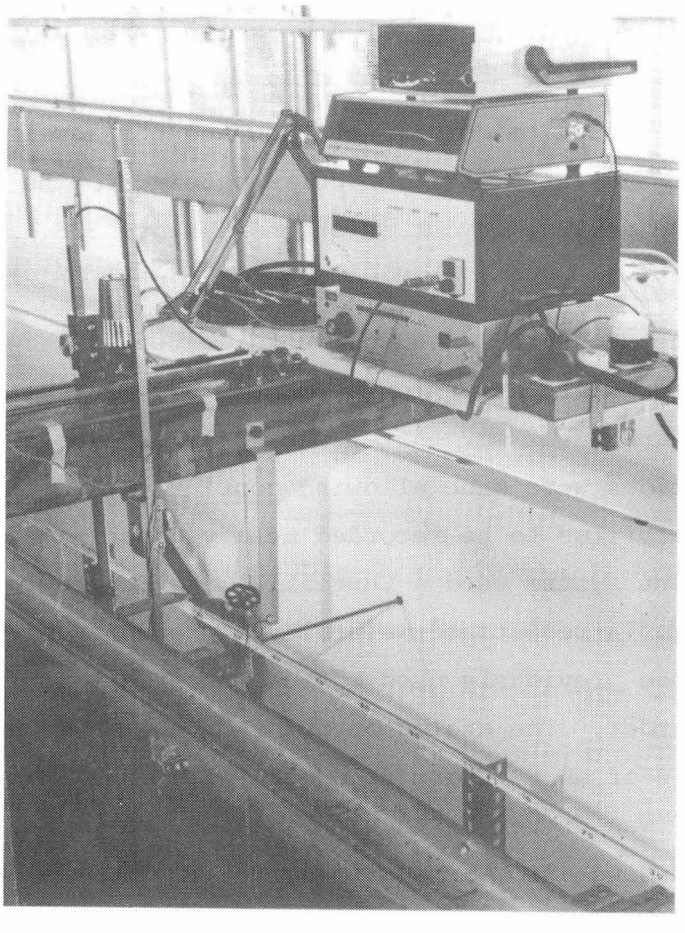

Plate 3.10 Ultrasonic Depth Meter

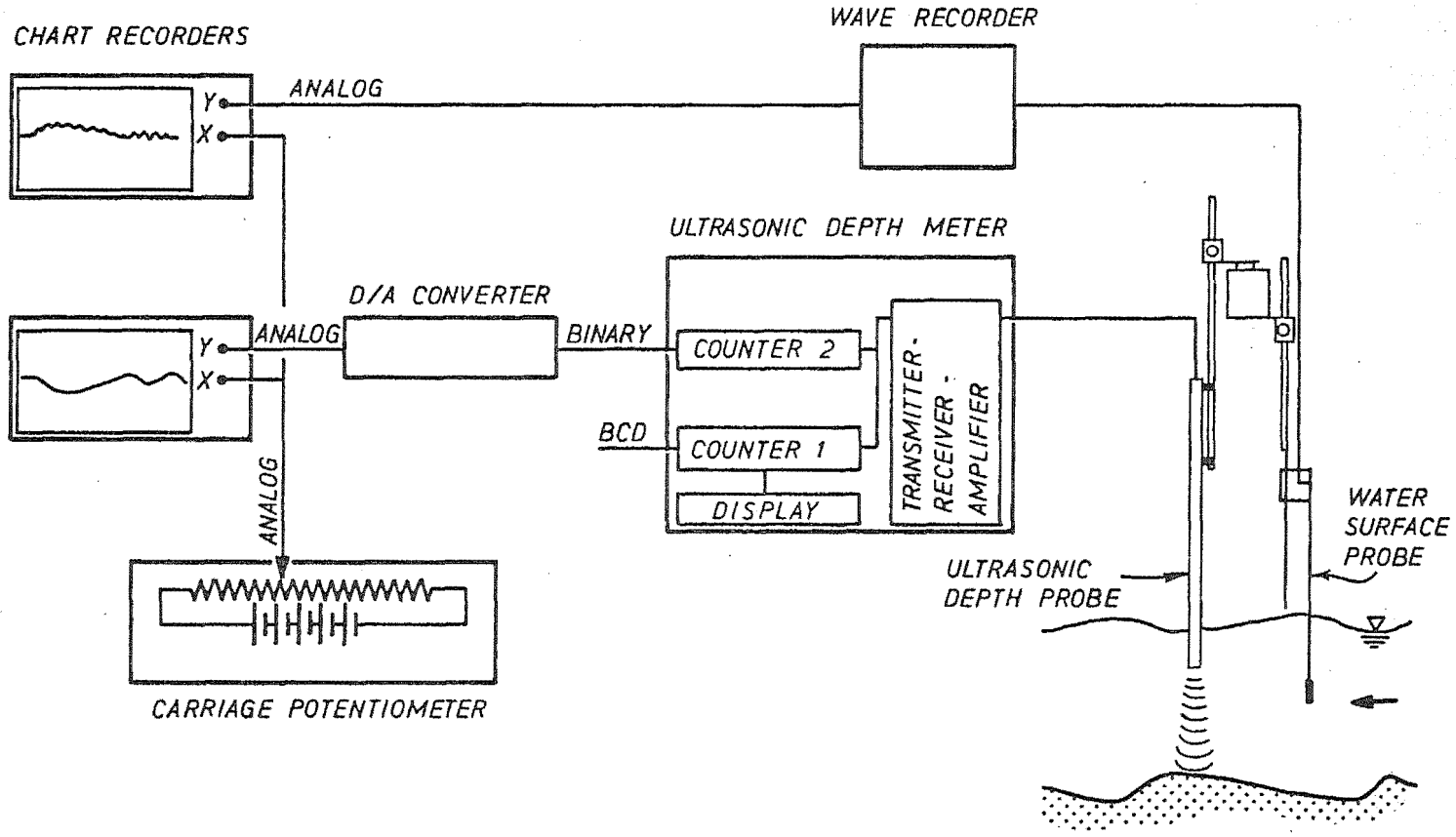

Figure 3.4 Schematic Electronic Circuitry of Bed Profile and Water Surface Measuring Devices

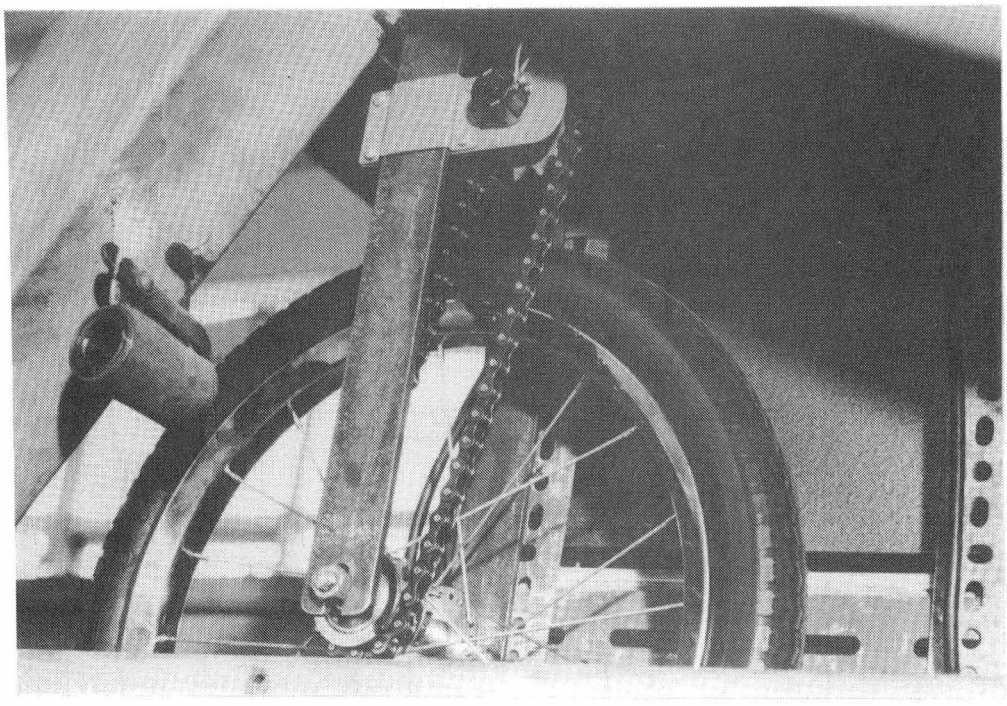

Plate 3.11 Carriage Wheel/Potentiometer Arrangement

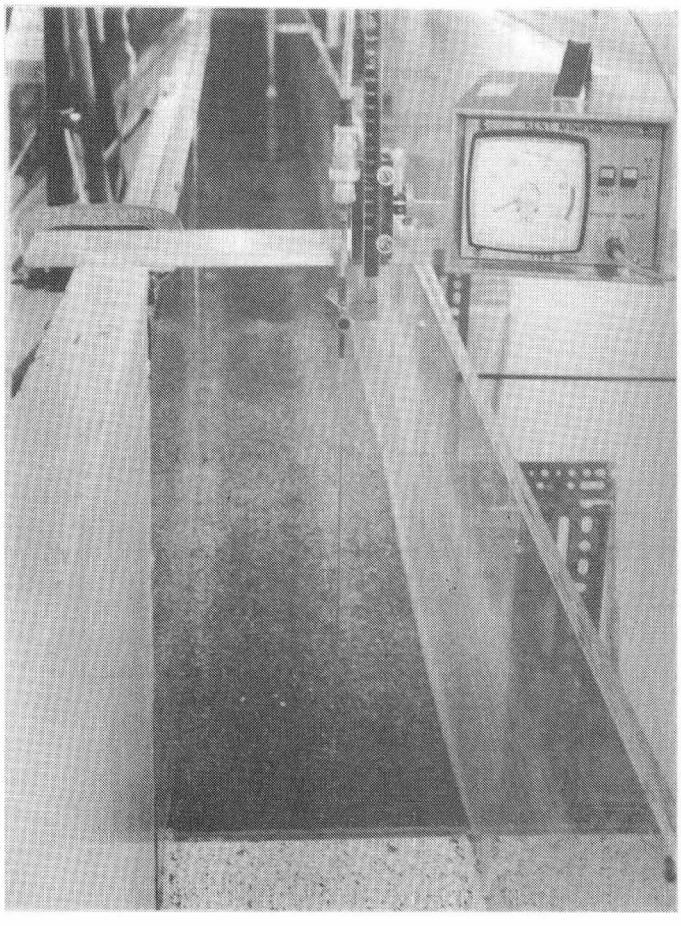

Plate 3.12 Kent Lea Miniflo Probe and Meter

well and was a significant improvement on discrete point gauge measurements. The X-axis is discussed in detail in a later section.

. Ultrasonic Depth Meter

An ultrasonic depth meter was constructed, using as a model an ultrasonic depth meter developed by the Central Laboratories, Ministry of Works and Development. Full details of the design and performance of this meter have been described by Spinks and Keller (1976). The circuit of the main unit is comprised of an ultrasonic transmitter, an ultrasonic receiver and a gate circuit to separate transmitted and received pulses and to transmit these pulses in correct sequence to electronic timer/counters (Fig. 3.4). The visual display electronic timer was driven by a 10 MHz crystal giving a counting resolution of 0.1 μs. The source of the ultrasonic beam was a 2 MHz piezo-electric crystal probe (20 mm diameter). The probe was mounted at the end of a 20 mm diameter tube, 440 mm long, and sealed with silicone rubber. The tube was clamped on to a point gauge which in turn was mounted on a transverse carriage which was mounted on the main carriage. Thus, the probe could be raised and lowered with changing water level and could be moved transversely across the flume.
The electronic timer measures the time it takes a transmitted ultrasonic pulse to bounce off the bed and register on the ultrasonic receiver. The pulse time can be easily converted into the distance from the bottom of the probe to the bed, if the velocity of sound in water is known. For a temperature range of $\pm$ 12°C, Spinks and Keller (1976) found that the velocity of sound in water only varied by $\pm$ 2%. Hence, it was assumed that the velocity of sound in water was constant for the range of temperatures encountered in the experimental programme.
In order to record continuous, longitudinal bed profiles a second, Binary electronic counter was added to the circuitry. This counter was driven by a 1 MHz crystal giving a resolution of 1 μs, which was equivalent to a depth resolution of 0.73 mm. The Binary output from this counter was converted to an analog signal using a Binary Digital-to-Analog Converter which in turn drove the Y-axis of a second HP Chart Recorder, while the X-axis, longitudinal location, was driven by a potentiometer. This is

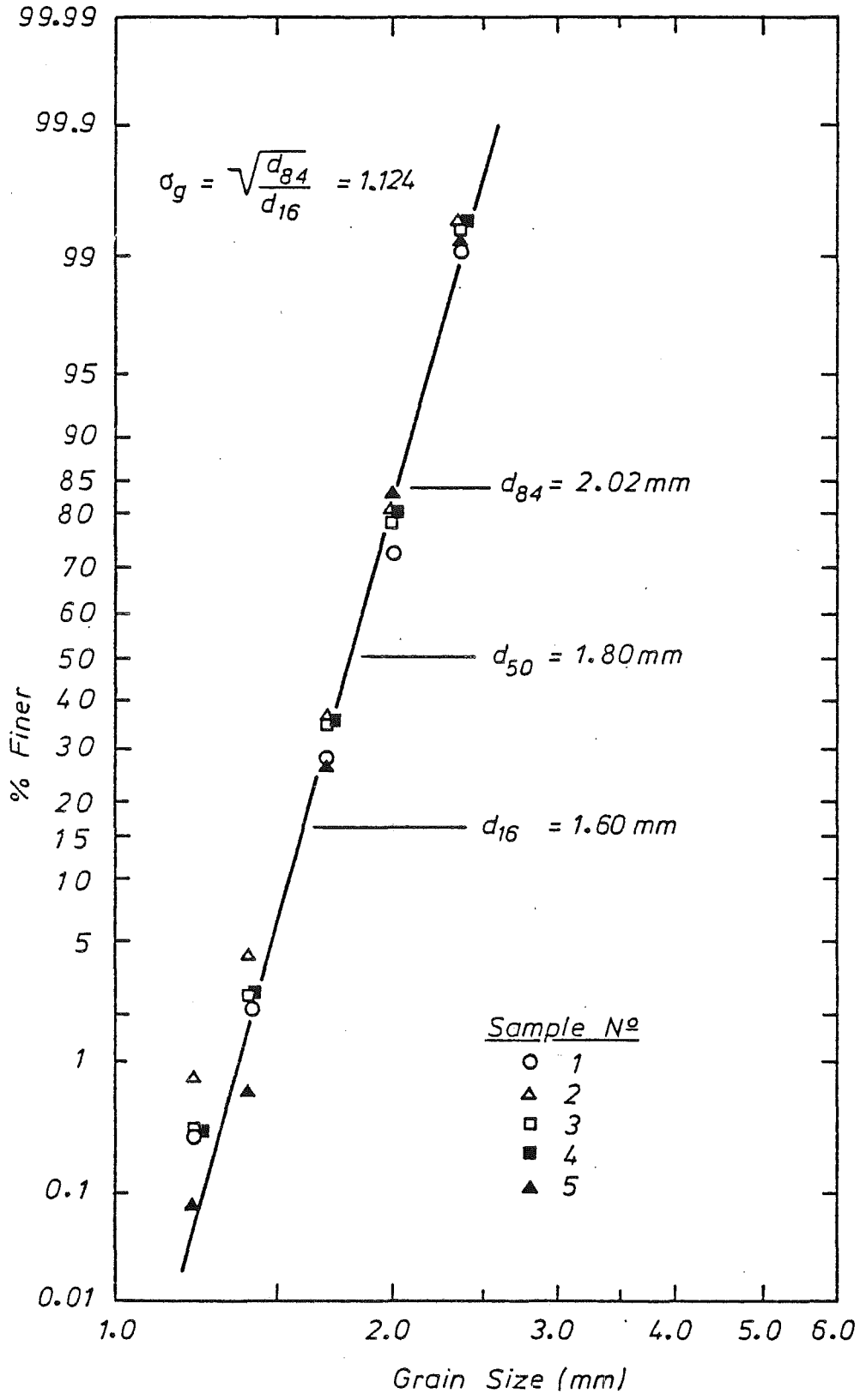

Figure 3.5 Grain Size Distribution

shown in Plate 3.10 and schematically in Fig. 3.4. A Y-axis scale of 1/1 was also set on this recorder, using the Y-axis gain control. Each bed profile record was referenced to the fixed upstream bed.

. X-Axis

Definition of longitudinal location, down the test reach, of the various probes was obtained using a 10-turn linear potentiometer and a constant voltage source. A 400 mm bicycle wheel was mounted on the side of the carriage where it ran along the base of a carriage rail (Plate 3.11). This wheel was used to drive the 10-turn potentiometer using a bicycle chain and fixed sprockets. The analog output from the potentiometer drove the X-axis of both the bed profile and water surface chart recorders. Two X-axis gain control settings were used to set two X-scales. These scales were: 1/50 and 1/20.

As previously mentioned, the gain controls of both chart recorders were used to calibrate the probe outputs in order to obtain desired scale responses. This calibration gave a linear response to any given signal, over the expected ranges, for both chart recorders. These calibrations were checked periodically throughout the experimental runs.

3.4.6 Velocity Meter

Velocity profiles were measured using a Kent Lea Miniflo Probe and Meter (Plate 3.12). A low velocity probe was mounted on a movable point gauge and point velocity measurements were recorded using the Miniflow Meter. Hair and lint in the water supply proved to be a problem. To avoid errors due to the fouling of the propellor, the velocity probe was carefully inspected before and periodically during each run for any hair or lint which was removed before measurements were undertaken. The velocity probe was also independently re-calibrated by the Ministry of Works and Development in a towing tank to ensure the accuracy of velocity measurements.

3.5 BED MATERIAL

The bed material was supplied by North End Sand Supplies, Kaiapoi, with an initial d_{50} = 2.1 mm and a geometric standard deviation, σ_g = 1.46. This source material was then sieved once between mesh screens of 2.38 mm and 1.58 mm spacing. The resultant bed material was a fine, uniform

Size	Specific Gravity	Porosity	Fall Velocity (m/s)	Angle of Repose
d_{50} = 1.8 mm	2.647, 2.651	.407	Fast = .247	35, 35
	2.667, 2.655	.405	Median = .20	35, 35.5
d_{84} = 2.02 mm	2.659, 2.624	.415	Slow = .15	35, 35
	2.661, 2.635	.408		35, 35.5
d_{16} = 1.60 mm				
σ_g = 1.124				
Average	2.65	.409	0.191	35°

Table 3.1 Summary of Bed Material Properties

gravel with a median size of 1.8 mm with subrounded and rounded grains. The grain size distribution curve was obtained from a sieve analysis of 5 random samples, each of 600 g. The grain size distribution curve is given in Fig. 3.5. Relevant properties of this bed material are summarised in Table 3.1 and described in Appendix A.

Chapter 4 | Laboratory Experiments: Measurements and Procedures

4.1 INTRODUCTION

This chapter describes typical measurements and the experimental procedures used for each series of experiments conducted.

4.2 EXPERIMENT IDENTIFICATION CODE

The identification code for each particular run is a combination of up to 9 letters and numbers. The first two letters identify the particular series to which the run belongs and the following two numbers identify the bed slope of the run. Two more numbers identify the run number within a series and further Roman numerals identify the inclined flow number or the reach length of the series depending on the type of measurements being made. A summary of the identification code components is given in Table 4.1. Three typical examples are:

- SE1506 - Run No. 6 for the case of steady discharge with equilibrium sediment injection upstream, at a bed slope of 0.0015.
- SC2003-IV - Run No. 3 for the case of a Type IV stepped increase in discharge from threshold conditions at a bed slope of 0.002.
- GS2001-II - Run No. 1 for the case of a Type I stepped increase in discharge from threshold conditions, at a bed slope of 0.002 and for a reach length of 2.0 m.

The results of experiments conducted by Bell (1980) are also referred to in later chapters. Since these two identification codes are different, a summary of the identification code components of

SERIES	CODE	SLOPE	CODE	RUN	CODE	HYDROGRAPH NUMBER	CODE	REACH LENGTH	CODE
Steady Equilibrium	SE	0.00095	10	1	01			10.35 m	
Inclined Step Change in Discharge	SC	0.0015	15	2	02				
				3	03	1	I		
				4	04	2	II		
		0.002	20	.	.	3	III	9.5 m	
				.	.	4	IV		
				7	07	5	V		
	GS	0.0025	25					1.0 m	I
								2.0 m	II

Table 4.1 Components of Identification Code

Bell (1980) is given in Table 4.2.

4.3 MEASUREMENTS

Measurements were made using the following methods.

4.3.1 Water Discharge

A calibrated pit (Section 3.4.2) was used to measure the steady flow rate at least once during each run. Periodically, a second reading was done to verify the first reading. Measurement error was $\pm$ 0.5%. The measured values of steady flow rate were used to check the discharge calibration chart used to operate the inlet valve.

4.3.2 Water Surface and Bed Profiles

Initially, water surface elevations, with respect to the flume slope, were measured using a point gauge at twelve stations along the test reach (Fig. 4.1). The water surface profile was measured at least four times during any given run using this method. On completion of the SE series a new system was developed which enabled a continuous, longitudinal water surface profile to be recorded (Section 3.4.5) at any given time. Each recorded profile was aligned with a stage reading measured at a control section using a point gauge. A reference reading was recorded every time a profile was measured.

The bed profile was measured indirectly with the ultrasonic probe and recorded on a chart recorder (Section 3.4.5), giving a continuous, longitudinal record of the bed configuration. The upstream fixed bed was used as a reference for each bed profile record.

The datum level 0.2 m below the level of the top of the partition board between the fixed and mobile beds was chosen for each reach length.

4.3.3 Bedload Transport Rate

The bedload transport rate was measured indirectly, throughout the duration of all runs, by the bedload collector system (Section 3.4.4). Instantaneous sediment transport rates were obtained by converting a change in voltage to a change in mass of gravel, using the calibrated conversion coefficient, and differentiating the resultant cumulative mass versus time record. Conversion coefficients were calibrated, in the manner described in Section 3.4.4, prior to each run. At the end of each run the collected gravel was removed from the basket, dried on trays and weighed. The measured mass of the dried gravel was then

SERIES	CODE	SLOPE	CODE	RUN OR HYDROGRAPH NUMBERS	CODE	REACH LENGTH	CODE
Initial Motion	IM	0.003		1	01	0.74 m	07
		0.002		2	02	1.74 m	17
				3	03	3.5 m	35
Steady Equilibrium	SE	0.002		4	04	5.3 m	53
				5	05	9.3 m	93
Steady Non-Equilibrium	ST	0.002		6	06		
				7	07		
Non-Steady Triangular Wave	NS	0.002		8	08		
				9	09		
				10	10		

Table 4.2 Components of Identification Code of Bell (1980)

compared with the expected total dry mass. If the two masses differed then the correct conversion coefficient was calculated. This coefficient was obtained by dividing the measured total dry mass of gravel by the total recorded change in output voltage. The difference between these values of the conversion coefficient was found to be less than $\pm$ 5%.

4.3.4 Water Temperature

The temperature of the water was measured at the beginning and end of each run. The temperature ranged from 15 - 20°C with the maximum variation of temperature during any given run being 2.5°C.

4.3.5 Bed Forms

Bed profiles were recorded, at varying time intervals, directly on a chart recorder (Section 3.4.5). Measurements of bed form height and length and celerity could be made directly from these records.

4.3.6 Time

A digital clock timer, mounted on the carriage, provided the time base for all runs. The clock was zeroed then started at the beginning of each experiment; signified by the first valve movement. Stop watches were synchronised with this time base and used to control valve, downstream weir gate and bedload collector frame movements.

4.4 EXPERIMENTAL PROCEDURES

The procedure is outlined for a typical run in each series of experiments conducted. When classifying flow as "steady" or "non-steady" the criterion used was the state of the flow over the fixed upstream bed.

4.4.1 Steady Flow Equilibrium Transport (SE Series)

Equilibrium conditions over the whole bed in an open circuit flume are achieved when the average sediment output rate from an erodible reach is equal to the average sediment input rate at the upstream interface between the fixed and mobile beds.

Before each run commenced the sediment bed was graded parallel to the flume slope. The downstream weir gate was then set. This predetermined gate setting ensured that the flow depth was uniform down the length of the reach when the full steady discharge was applied. The flume was then gradually filled until the base flow rate, set using

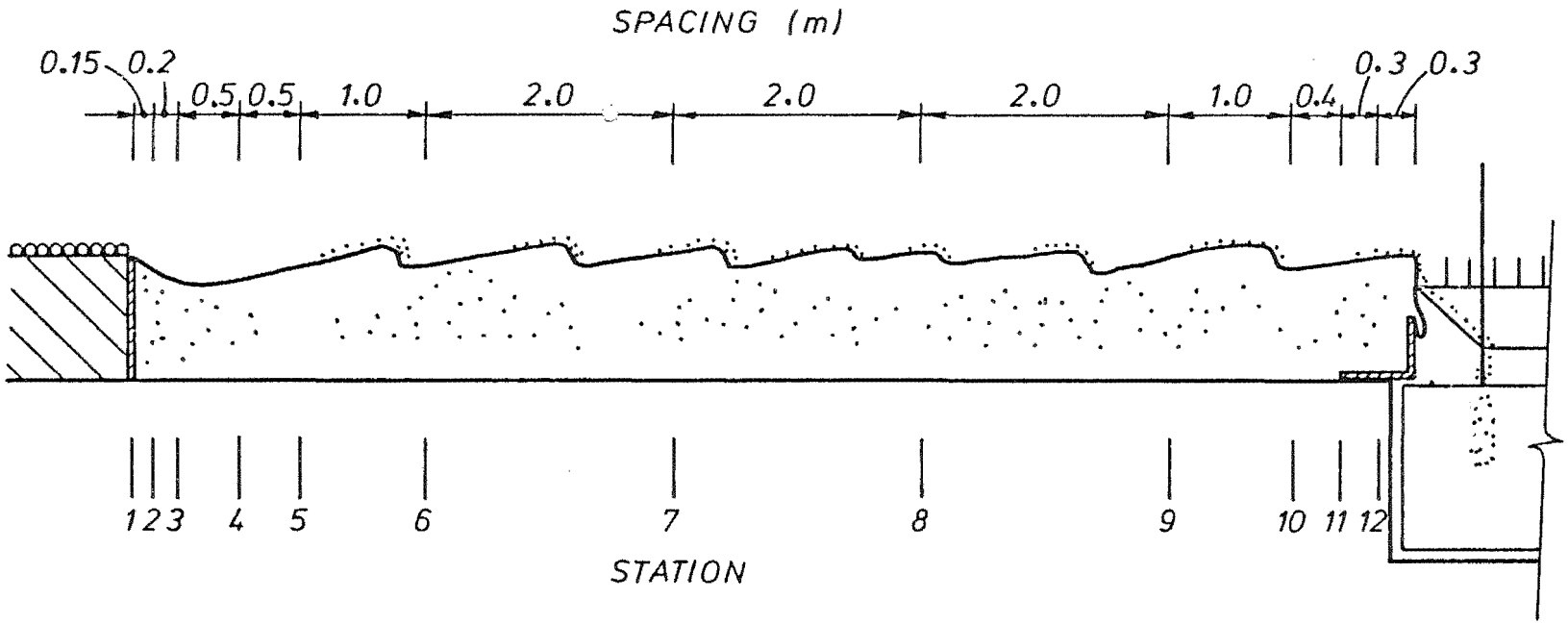

Figure 4.1 Water Surface Measuring Stations (SE Series)

the control valve, was reached. At this base discharge, the downstream gate setting caused a backwater profile to extend back up the full length of the mobile reach. Hence, at the start of each run the flow conditions over the plane bed were less than threshold flow conditions. To begin each run the desired flow rate was set quickly using the control valve and full sediment injection commenced (Section 3.4.3). The commencement of each run was synchronised with the automatic bedload recorder. The bedload recorder took readings of the cumulative gravel output from the test reach every 60 seconds.

Periodic measurements were made of the bed profile using the ultrasonic probe and measurements of water surface elevations at selected stations (Fig. 4.1) were made using a point gauge. Only point measurements of bed profile were recorded during the SE10 series as the continuous recording system was not developed until the end of this series. Flow rate and temperature were also measured.

Initial runs were undertaken at each discharge to determine gate settings and measure sediment transport rate output. These estimates of equilibrium transport rate were used as sediment injection rates in later runs. During final runs the bed profile was monitored and adjustments to the injection rate were made if scouring or deposition was evident in the upstream region of the mobile reach.

It was noted that changes in bed profile due to incorrect injection rates tended to be confined to the upstream region of the test reach and that as long as the injection rate was reasonably close to the equilibrium sediment transport rate that equilibrium bed conditions prevailed over most of the test reach and in particular at the downstream end where measurements were made. Hence the procedures adopted to ensure that equilibrium conditions were present during a run of 2 - 3 hours included

- Input transport rate being approximately equal to output transport rate, and
- That bed form non-uniformity due to incorrect injection rates be confined to the upstream region of the reach.

Since bed non-uniformity almost always occurred close to the fixed to mobile bed interface, water surface elevations are averaged from Stations 4 to 12 (Fig. 4.1) and not over the full 10.35 m long reach. Each experiment was run for three hours or until the sediment

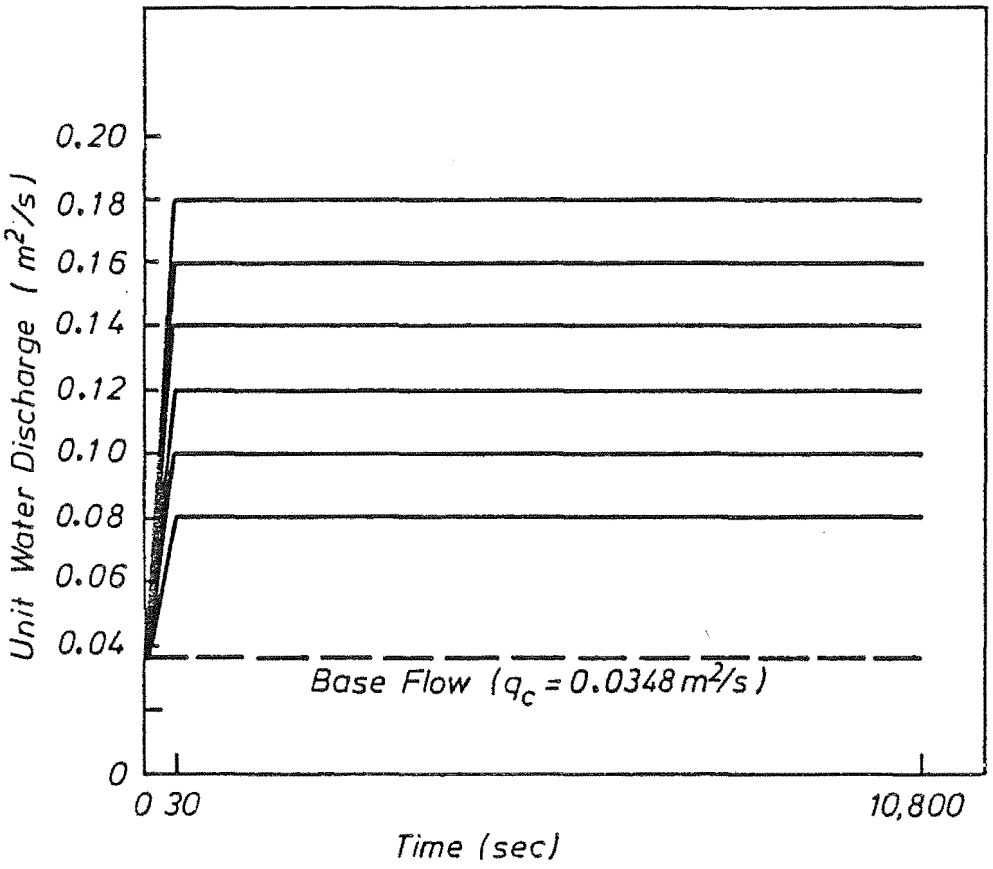

Figure 4.2 Flow Hydrographs (SC-I Series)

basket was completely filled. At the higher bed slopes and discharges this criterion reduced the duration of runs to two hours. Twenty-six runs were completed in this series. The flow properties of all runs are presented in Appendix C.

4.4.2 Step Change in Discharge - Non-Equilibrium Transport (SC Series)

. SC-I Series

Before this series commenced, a 1.0 m board coated with grains (d_{50} = 2.81 mm) was inserted immediately upstream of the test section. This was done to improve the flow transition from the fixed bed to the mobile bed. The new test reach length was 9.5 m. The bed was once again prepared by grading it parallel to the flume slope. However, in this series the downstream weir gate was set flush with the bed. The flume was then gradually filled until the base flow (q_b) was reached. It was found that at base flow and with this gate setting that the backwater curve just intruded into the downstream region of the mobile reach. Thus, at $t = 0^-$ s, the mean velocity was at threshold and the bed was plane. At t = 0 s the extra flow was superimposed on the base flow (over 30 s) and the downstream weir gate was raised to the required setting (over 30 s). Non-equilibrium conditions were created by having no sediment input at the upstream boundary for all time. The range of flows studied is given in Fig. 4.2 and their correlation with run numbers in Table 6.1.
Continuous, longitudinal water surface and bed profiles were recorded at various times; the cumulative bedload output was recorded every 60 seconds. The flow rate and temperature were also measured. Measurements of the lateral bed profiles at Stations 0.5, 1.0, 1.5 and 2.0 m and velocity profiles at Stations 0.0, 1.0 and 2.0 m were also made. Each experiment was run for three hours or until the sediment basket was completely filled. At the higher discharges the duration of runs decreased to two hours. Seven runs were completed in this series.

. SC-II, III, IV, V Series

Preparations for these series of runs followed the procedure outlined for the SC-I series. The required non-steady flow hydrograph was generated by opening the flow valve in small steps at predetermined times. This gave a stepped approximation

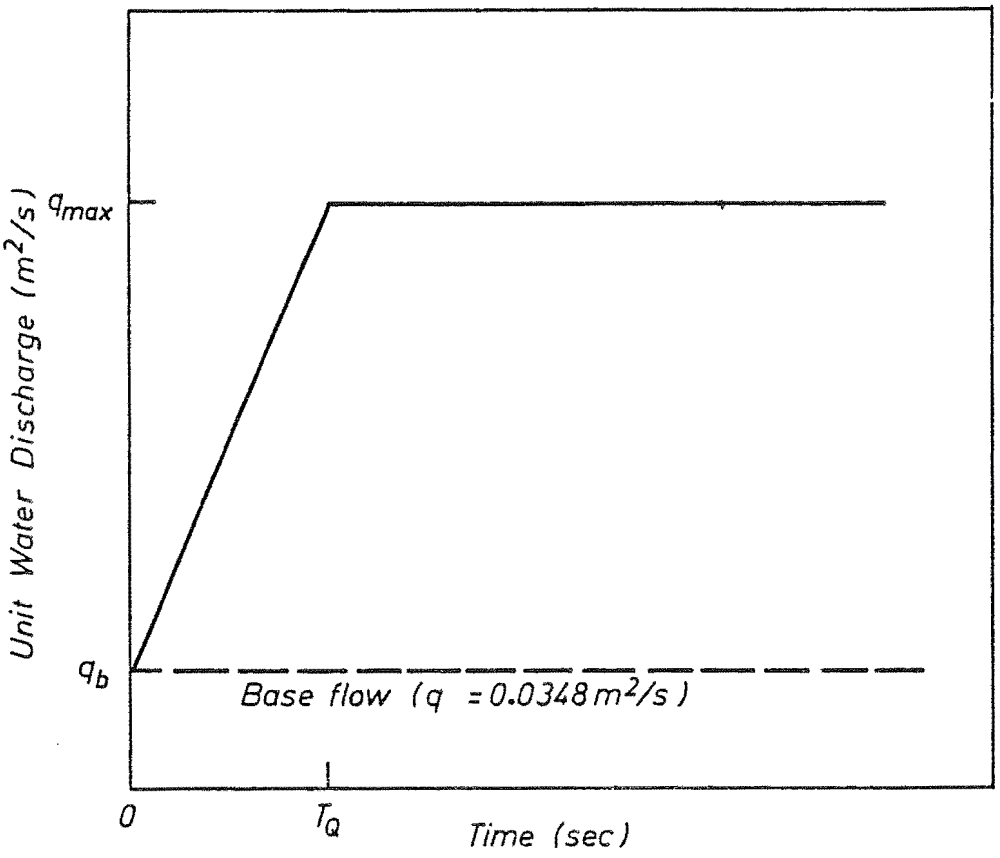

Figure 4.3 General Flow Hydrograph (SC Series)

HYDROGRAPH NUMBER	DISCHARGE RISE TIME (T_Q) (s)
I	30
II	300
III	600
IV	1200
V	1800

Table 4.3 Stepped Discharge Rise Times

to the required continuous inclined step change in discharge. The predetermined pattern of gate movements was commenced at t = 30 s instead of at t = 0 s thus ensuring that the discharge changes reached the downstream end of the test reach before gate movements began. A time step of 5 per cent of the rise time (Fig. 4.3) was adopted when determining valve and gate settings for these step changes. The range of flows studied was the same as that considered in the SC-I series (Fig. 4.2). The rise times studied are given in Table 4.3 (Fig. 4.3). As before, continuous, longitudinal water surface and bed profiles were recorded as was the cumulative bedload output. The flow rate and temperature were also recorded. In these series, interest was centred on the initial temporal response of the bed and runs were of between one and two hours duration. Sixteen runs were completed in these series.

4.4.3 Step Change in Discharge - Non-Equilibrium Transport (GS Series)

To determine values of the spatial lag coefficient, measurements of the sediment transport rate at degrading sections within scour holes were required. This was accomplished by lengthening the upstream fixed roughened bed progressively downstream; effectively moving the bedload sampling point into the general scour hole (Fig. 4.4). Initially, this gave a test reach length of 2.0 m (GS-II Series) then later a test reach length of 1.0 m (GS-I Series). When extending the fixed bed downstream care was taken to replicate the geometry of the original fixed bed which included installing a 1.0 m long board, coated with grains, upstream of the test reach (Fig. 4.4). To simulate conditions within the scour hole, at reduced reach lengths, it was necessary to lower the grill of the adjustable bedload collector as the bed degraded to prevent interference with bedload movement.

The procedure for each of these experiments was the same as for the parent SC-I runs. Thus, the range of discharge hydrographs considered was as given in Fig. 4.2. An additional task was the lowering of the adjustable bedload collector grill, as the bed degraded, according to predetermined settings. These settings were determined from the bed profile record of the parent SC-I run. To ensure that the grill movements did not promote scour of the bed, at the downstream end of the test reach, over and above that which occurred in the developing scour hole, 2 mm was subtracted from each grill setting. Hence, the grill

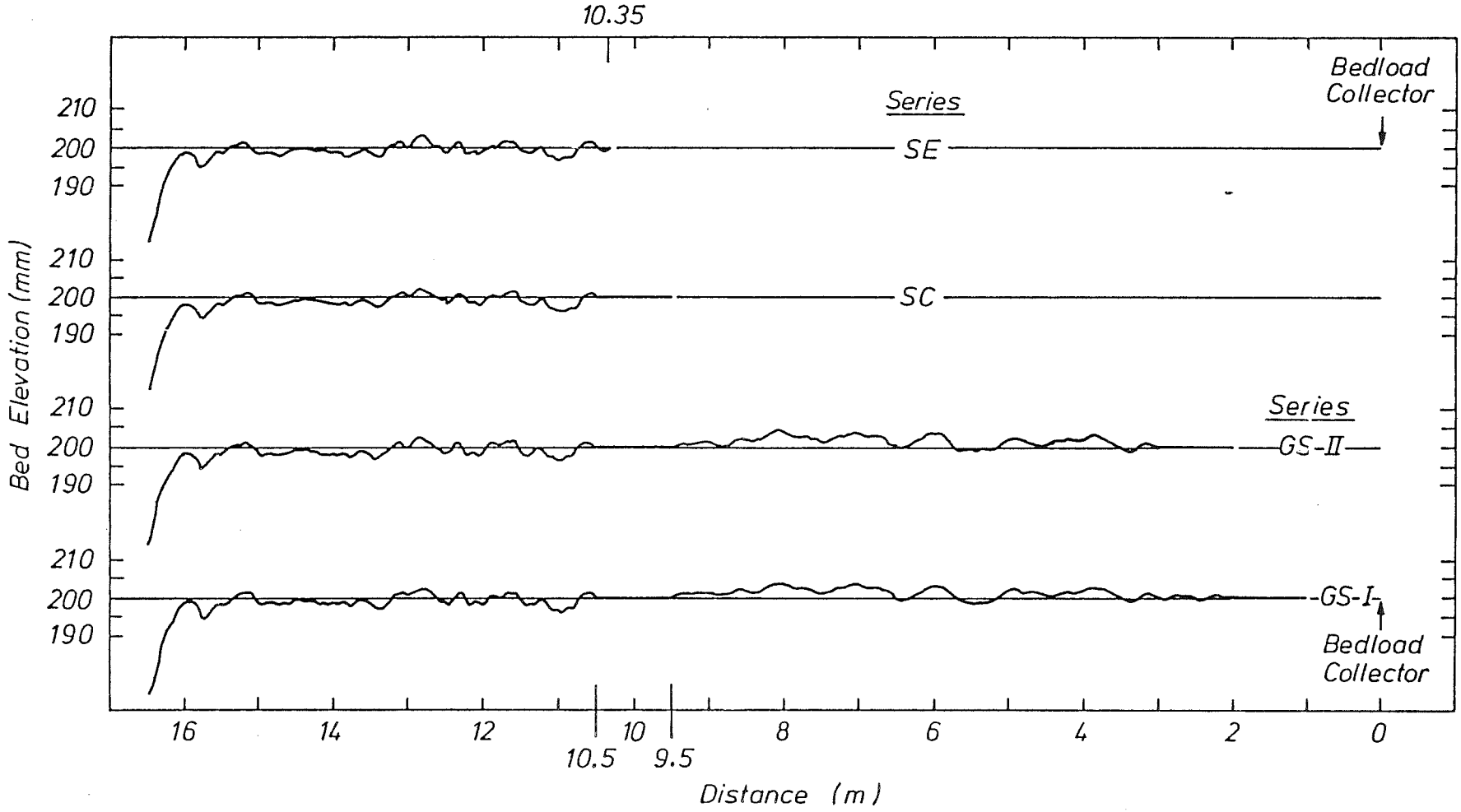

Figure 4.4 Fixed Upstream Bed Profiles

was always slightly higher than the measured bed profiles recorded during the parent SC-I runs.

The prime aim of these experiments was to measure sediment transport rates at given locations within the previously measured, general SC-I scour hole. Hence, a comparison procedure was needed, to ensure that the previously recorded SC-I scour hole profiles were being replicated within the short test reaches. The local maximum scour hole depth was selected as the criterion to be used when comparing the bed profiles. During initial runs at higher flow rates it soon become apparent that the scour hole in the reduced reach was degrading faster than had the parent SC-I scour hole. Consequently, it was found necessary to periodically adjust the downstream gate to obtain compatible scour hole profiles. At the highest discharge, the maximum adjustment in the downstream gate setting caused a 6% increase in the flow depth over the test reach. Interestingly, the magnitude of the gate adjustments was a function of discharge. This strongly suggested that these corrections were needed to counteract the absence of bed form development, downstream of the scour hole, exhibited in the parent SC-I runs. The fixed roughened bed downstream of the bedload trap was simply not able to simulate roughness due to bed form development.

Similar measurements to those taken for SC-I runs were recorded. Twelve runs were completed in these series.

Chapter 5 | Steady Flow Equilibrium Transport

5.1 INTRODUCTION

When analysing flume data it is necessary to account for the variable effect of the flume side-walls on flow properties. Two side-wall correction methods are considered. These are the methods of Vanoni and Brooks (1957) and Williams (1970). Both are used to analyse the flow data from the SE series of experiments and a preferred method selected. A further consideration is that the bed roughness itself is a combination of roughness due to sediment grains and due to bed form geometry. The procedure of Einstein (1950) is used to investigate this effect and a general equation which relates total and grain flow properties is developed.

In this study, an initial motion criterion is of twofold importance. Firstly, in the determination of when scouring ceases under steady flow non-equilibrium sediment conditions and, secondly in the formulation of an equilibrium sediment transport relation. The most commonly used initial motion criterion is that of Shields (1936). Several researchers have demonstrated that the rate of sediment transport near threshold conditions is strongly dependent on the applied bed shear stress. A rational approach to the definition of initial motion requires a measure of dimensionless erosion rate, as proposed by Neill (1968) and Neill and Yalin (1969). This approach is used to determine an initial motion criterion for the current series of experiments. The effect of grain Reynolds number on the general initial motion criterion is also investigated.

Under mobile bed conditions, the total bed roughness is a combination of roughness due to sediment grains and bed form geometry. Using Manning's equation and a relation between total and bed related

flow properties, bed and grain Manning roughness values are determined. A method, based on the relation presented by Engelund and Fredsφe (1982), whereby a multi-valued Manning resistance relation can be specified, is also demonstrated.

Observations and results are presented for the equilibrium transport series of experiments. These are discussed and compared with other sets of experimental data and established sediment transport formulae. An equilibrium sediment transport formula is also developed.

5.2 SIDE-WALL CORRECTION

5.2.1 Introduction

In flume experiments a gravel bed will normally be rougher than the wall surfaces; giving rise to a nonuniform distribution of boundary shear stress. As the bed becomes rougher or the flow depth decreases the wall shear stress decreases relative to the bed shear stress. Hence, during experiments the effect of the walls on the flow varies due to changing bed roughness; a side-wall correction is needed to standardise results. Separation of shear force into components of bed shear force and wall shear force was first proposed by Einstein (1942) and used by Johnson (1943) when he analysed and presented a compilation of published and unpublished sediment data. Johnson (1942) presented a method based on the Darcy-Weisbach formula which was subsequently modified by Vanoni and Brooks (1957). A simple, empirical relation to correct flume data for side-wall effects has also been proposed by Williams (1970). A further consideration is that bed roughness itself is a combination of roughnesses due to sediment grains and bed form geometry. This was recognised by Einstein (1950) and analysed more fully by Einstein and Barbarossa (1952). A simple graphical solution for this method was presented by Vanoni and Brooks (1957) and expanded by Toffaletti (1969). A computer subroutine based on this graphical solution, presented by Chen (1975), was used herein to calculate grain shear velocities.

5.2.2 Side-Wall Correction Procedure

Two side-wall correction methods were considered; Vanoni and Brooks (1957) method and the Williams (1970) relation. Vanoni and Brooks (1957) method is well established. Since full details of this method are readily available (Vanoni and Brooks (1957), A.S.C.E. (1975)) this procedure will not be presented herein.

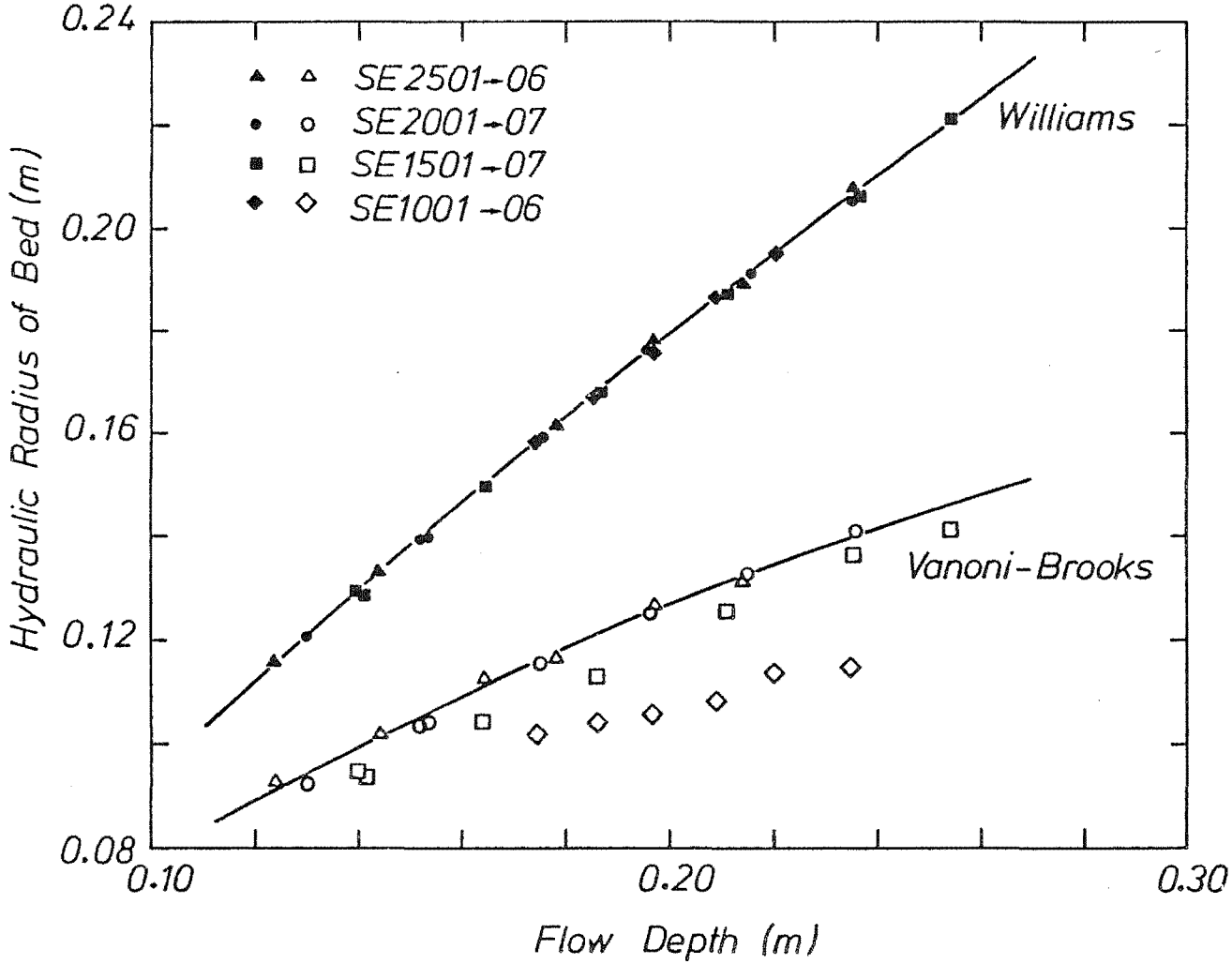

Figure 5.1 Hydraulic Radius of Bed Against Flow Depth.

Williams (1970) flume experiments are of interest because an adjustment factor which converts laboratory values of slope, unit stream power or shear stress into equivalent wide channel values for the same flow depth and unit sediment transport was presented. Using Williams (1970) correction factor, bed shear velocity, u_{*_b}, is given by (S.I. units).

$$u_{*_b} = \frac{u_*}{\sqrt{1 + 0.055\ Y/B^2}} \tag{5.1}$$

where $u_* = \sqrt{gYS_f}$

$u_{*_b} = \sqrt{gR_bS_f}$

and B = Flume width,

R_b = Hydraulic radius of the bed,

S_f = Friction slope

Y = Average flow depth.

Giving $$R_b = \frac{Y}{1 + 0.055\ Y/B^2} \tag{5.2}$$

5.2.3 Results

The measured flow data for the SE series were analysed using both side-wall correction schemes and values of the hydraulic radius of the bed, R_b, were obtained. These results are compared in Fig. 5.1 and presented in Appendix C.

Since the flume width was constant for all runs, B = 0.305 m, Eq. 5.2 became (S.I. Units).

$$R_b = \frac{Y}{1 + 0.591\ Y} \tag{5.3}$$

The Williams data presented in Fig. 5.1 was obtained by substituting values of flow depth into this relation.

Regression analysis of the data for the SE15, 20 and 25 series, obtained using Vanoni and Brooks (1957) method , gave

$$R_b = \frac{Y}{1 + 0.891\ Y/B} \qquad (r_{xy} = 0.983) \tag{5.4}$$

Giving, for B = 0.305 m

$$R_b = \frac{Y}{1 + 2.92\ Y} \tag{5.5}$$

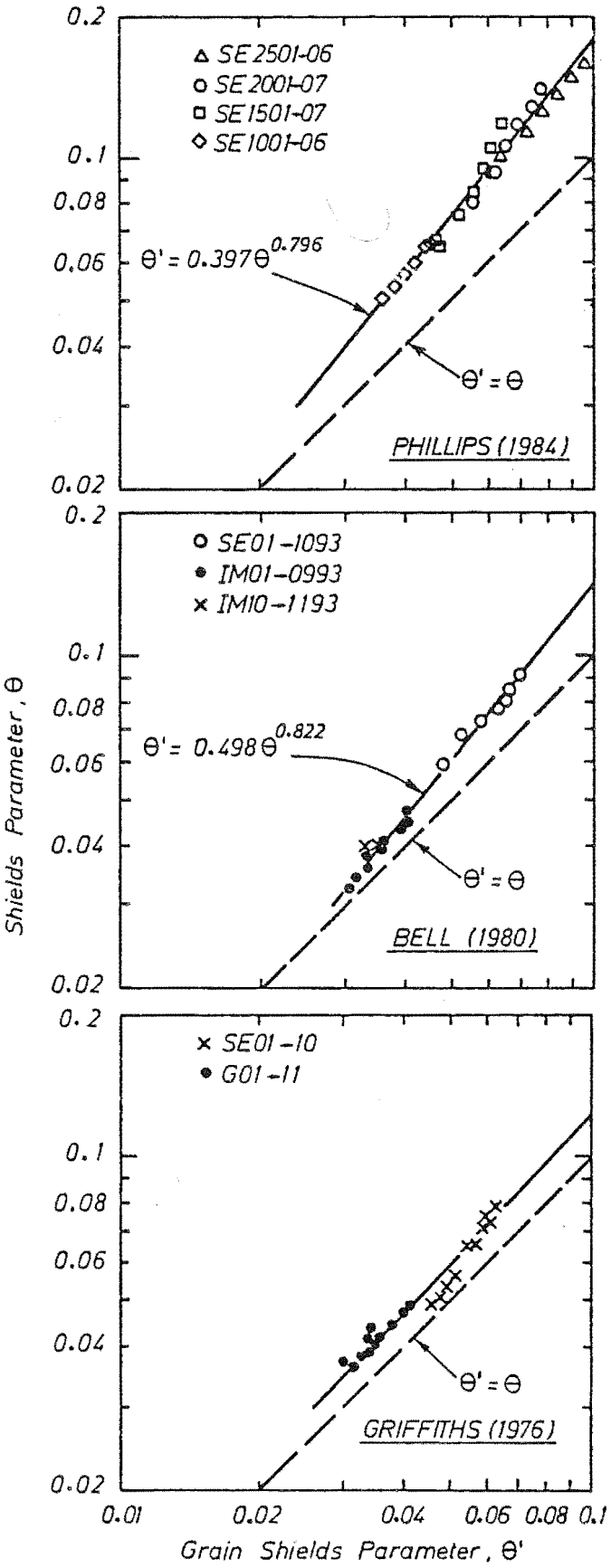

Figure 5.2 Shields Parameter Against Grain Shields Parameter

This relation is plotted in Fig. 5.1 as the Vanoni-Brooks curve.

The formulation of relations used in the temporal lag model presented in Chapter 8 was facilitated by using a power law relation to describe the side-wall correction. Over the expected flow range, Y = 0.08 -0.28 m, a least squares regression analysis was used to fit such a power relation to Eq. 5.3. Giving

$$R_b = 0.785\ Y^{0.921} \qquad (r_{xy} = 0.9999) \qquad (5.6)$$

or

$$Y = 1.30\ R_b^{1.086} \qquad (5.7)$$

The SE data, the data of Bell (1980) and of Griffiths (1976) were analysed using Einstein's (1950) procedure, (Section 5.2.1). The data plotted in Fig. 5.2 are in the form of Shields Parameter, θ, against Grain Shields Parameter, θ', (after Engelund and Fredsφe (1982)). A least squares regression analysis of the data gave, for the SE data

$$\theta' = 0.397\ \theta^{0.796} \qquad (r_{xy} = 0.9906) \qquad (5.8)$$

and for Bell's SE and IM data

$$\theta' = 0.498\ \theta^{0.822} \qquad (r_{xy} = 0.9972) \qquad (5.9)$$

where it was assumed that

$$\theta = u_{*_b}^{2}/(S_s - 1)g\ d_{50}$$

and

$$\theta' = u_{*_b}'^{2}/(S_s - 1)g\ d_{35}$$

the latter relation being of the form proposed by Einstein (1950).

5.2.4 Discussion

The results plotted in Fig. 5.1 show a marked difference between the two side-wall correction schemes considered. Williams (1970) side-wall correction method gives values of bed hydraulic radii which are markedly higher than those obtained using Vanoni and Brooks (1957) method. The Vanoni-Brooks data also displays slope dependence. A further, disquieting feature of this data is that at the lowest slope calculated R_b values are less than calculated values of the grain related hydraulic radius of the bed, R_b', (Appendix C).

Since the spatial lag analysis of Chapter 7 relied on the determination of flow properties within the scour hole, a region of

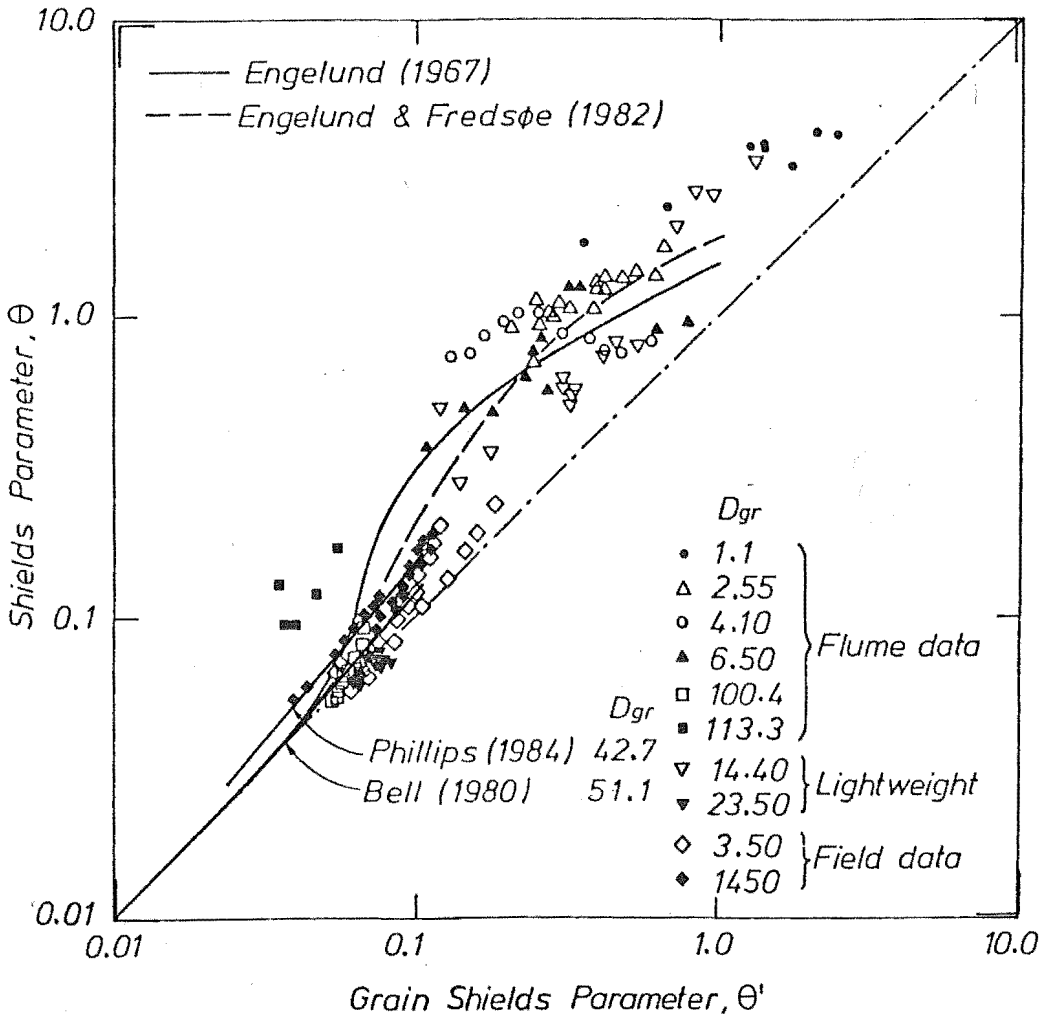

Figure 5.3 Engelund Relationships Between Shields Parameter and Grain Reynolds Number (After White, Paris and Bettess (1979).

reduced friction slope, it was essential that a side-wall correction be confidently applied under these conditions. It was decided to adopt Williams (1970) side-wall correction method since Vanoni-Brooks (1957) method could not be applied confidently at lower slopes. Bell (1980) also adopted Williams (1970) method.

When plotting Fig. 5.2, Shields Parameter values were obtained from values of bed shear velocity determined using Williams (1970) side-wall correction method. Grain Shields Parameter values were obtained from values of grain shear velocity determined using Einstein's (1950) procedure. It is evident from Fig. 5.2 and the regression coefficients, that the current data and the data of Bell (1980) are well fitted by the power relations given in Eqs. 5.8 and 5.9. Griffiths' data, however, appears inconsistent. The data indicates that either the four lowest discharge results in his SE series or the IM series results are probably incorrect. The internal consistency of the IM results indicates that it may be the SE results which are in error.

In Fig. 5.3, the calibrated relations given by Eqs. 5.8 and 5.9 are plotted and compared with the general relations proposed by Engelund (1967) and Engelund and Fredsφe (1982), as given by White, Paris and Bettess (1979). For the range of Shields Parameter values encountered in these experiments, $\theta < 0.2$, the calibrated relations agree well with the trend of the field data plotted in Fig. 5.3. The agreement between the calibrated relations and the general relations in this region is not as good.

The calibrated relations presented in Eqs. 5.8 and 5.9 were further used to obtain the resistance relations derived in Section 5.4.2.

5.3 INITIAL MOTION

5.3.1 Introduction

A turbulent flow exerts fluctuating hydrodynamic forces on a non-cohesive bed surface. In the case of flow conditions giving rise to the "beginning of movement" only the peaks of the turbulent fluctuations are able to displace grains. Since these fluctuations are statistically distributed, rare grain movements can take place even at low values of mean (time-average) bed shear (Neill and Yalin (1969)). As the flow intensity increases, this weak sediment transport is increased as greater numbers of grains are displaced. This has meant

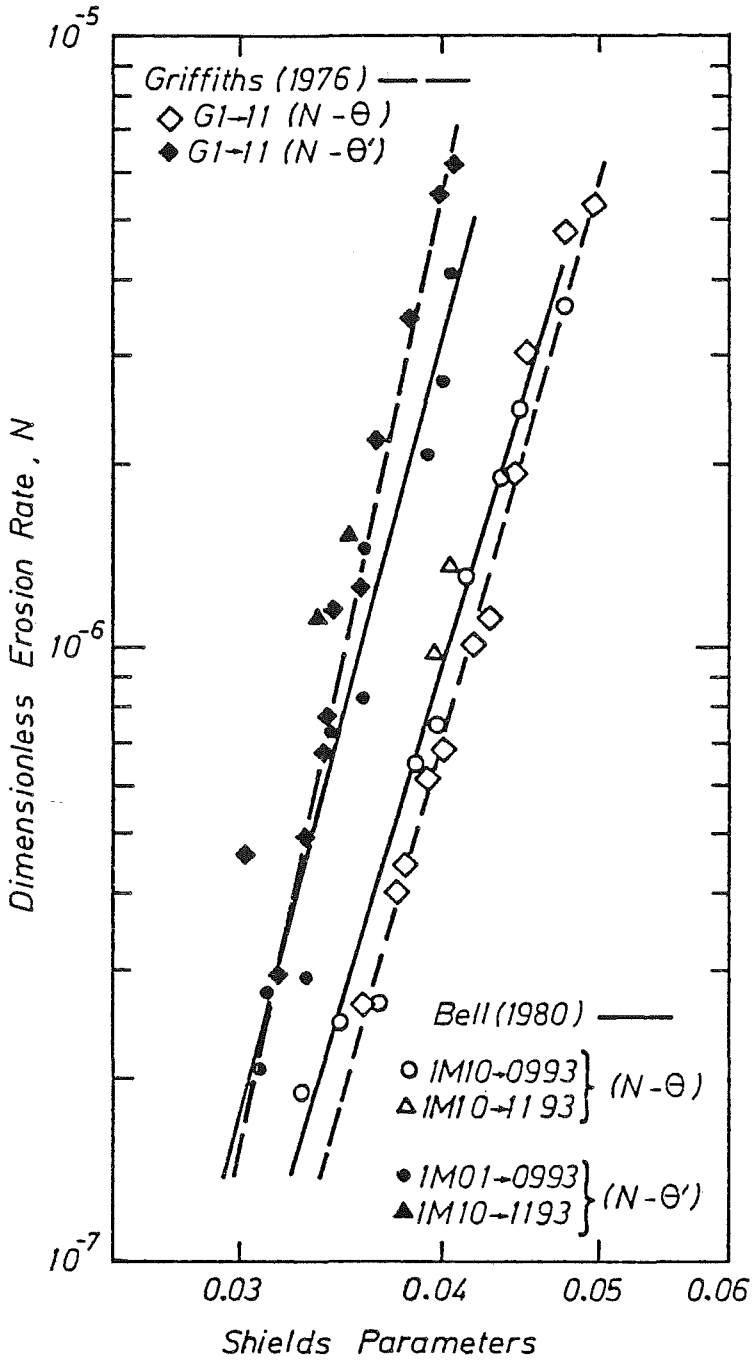

Figure 5.4 Nondimensinal Erosion Rate Against Shields Parameter.

that the definition of critical or initial motion has tended to be subjective thus giving rise to a wide array of initial motion criteria.

Shields (1936), in his classic work on initial motion, obtained values of critical mean bed shear stress by extrapolating back from measured sediment transport rates to "zero" transport conditions. He presented his results in the form

$$\frac{\tau_0}{\frac{(\rho_s - \rho_w)}{\rho_w} g\, d_{50}} = f\left(\frac{u_{*_b} d_{50}}{\nu}\right) \qquad (5.10)$$

or $$\theta = f(Re_*)$$

However, several researchers (Paintal (1971(a)), Taylor (1971), Pazis and Graf (1977)) have measured transport rates at values of Shields Parameter below the Shields curve. This has raised doubts about the validity of the extrapolation process used by Shields (1936) to define critical conditions.

A more rational approach has been presented by Neill (1968) and Neill and Yalin (1969). Their proposed definition of initial motion includes a measure of the "degree of movement", given by

$$N = \frac{N_e d_{50}^3}{u_{*_b}} = f(Re_*, \theta) \qquad (5.11)$$

where N_e = Number of grains detached/ unit area/unit time; and

N = Dimensionless erosion rate.

The initial motion criterion is obtained by choosing a value of N. Neill and Yalin (1969) proposed $N = 1 \times 10^{-6}$ as a suitable and measurable criterion.

One factor which will affect this approach, however, is the manner in which grains are packed on the bed surface. Fenton and Abbott (1977) demonstrated that threshold values of Shields Parameter possessed a marked dependence on the relative protrusion of the grain into the flow. It is likely, therefore, that this approach is unsuitable for graded sediments.

AUTHOR	θ	R_{e_*}	θ'	R_{e_*}'
Bell (1980)	.040	72	.0348	67
Griffiths (1976)	.0415	188	.0358	175

Table 5.1 Initial Motion Data for Criterion $N = 1 \times 10^{-6}$

5.3.2 Results

The data from the initial motion studies conducted by Bell (1980) and Griffiths (1976) are presented in Fig. 5.4 and results for the criterion $N = 1 \times 10^{-6}$ are given in Table 5.1. Side-wall effects were eliminated using Williams (1970) method.

Bell (1980) also presented a relation for weak sediment transport. For the flow conditions encountered in his IM series, given in Appendix C, he found the relation between weak sediment transport and Shields parameter to be

$$q_s = 3.36 \times 10^{10} \theta^{11.2} \text{ (kg/s/m)} \tag{5.12}$$

for the conditions

$$0.033 < \theta < 0.047$$

The similarity of the size of the bed material to that of Bell (1980) led, initially, to the assumption that the value of critical Shields Parameter for the bed material used in this study was equal to the value of critical Shields Parameter obtained by Bell (1980) from his IM data (Table 5.1). This assumption was checked in the following manner.

To date, a general relation between critical Shields Parameter and grain Reynolds Number, for the initial motion criterion $N = 1 \times 10^{-6}$, has not been presented due to the scarcity of data. However, it was possible to check the assumed value of the critical Shields Parameter by inferring a general curve from previously reported measurements of weak sediment transport.

Paintal (1971(a)) and Pazis and Graf (1977) both found a relationship between nondimensional weak sediment transport rate and Shields parameter to be of the form

$$q_{s_*} = \frac{q_s}{\rho_s d_{50} \sqrt{(s_s - 1) g d_{50}}} = \alpha_s \theta^{\beta_s} \tag{5.13}$$

where q_s = bedload mass transport rate/unit width/unit time.

The bedload transport rate can also be expressed as (after Einstein (1950))

$$q_s = \frac{N_e \lambda d_{50} A_2 d_{50}^3 \rho_s u_{*_b}}{u_{*_b}}$$

$$= N \lambda A_2 \rho_s d_{50} u_{*_b} \tag{5.14}$$

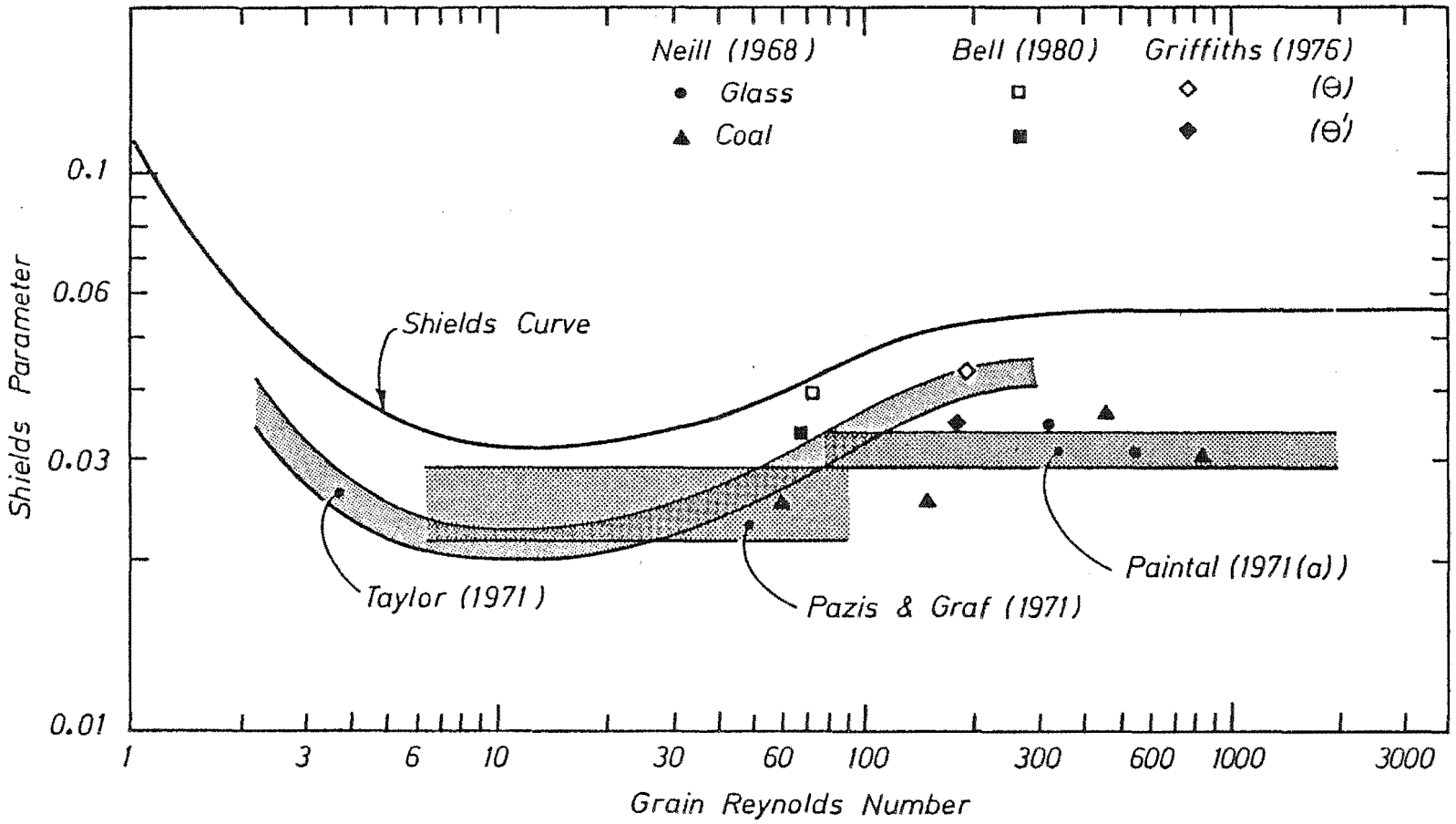

Figure 5.5 Initial Motion Criterion ($N = 1 \times 10^{-6}$) Against Shields Parameter and Grain Reynolds Number (After Taylor (1971))

where N = Nondimensional erosion rate, given by Eq. 5.11

and λd_{50} = Average step length; and

$A_2 d_{50}^3$ = Average grain volume.

Substituting Eq. 5.14 into Eq. 5.13 gives

$$g_{s_*} = N\lambda A_2 \sqrt{\theta} = \alpha_s \theta^{\beta_s} \tag{5.15}$$

Thus for assumed values of N and λA_2 it is possible to solve Eq. 5.15 for a critical value of Shields Parameter, given that the coefficients, α_s and β_s, are known. Near threshold conditions, values of the step length constant, λ, can vary from 20 - 200 (Fernandez Luque and Van Beek (1976), Yano, Tsuchiya and Michiue (1969)). For spherical grains $A_2 = \pi/6$; giving

$$10 \leq \lambda A_2 \leq 100 \tag{5.16}$$

Typical threshold values of Shields parameter, obtained by inserting the upper and lower limits given by Eq. 5.16 into Eq. 5.15, are given in Table 5.2 for the criterion $N = 1 \times 10^{-6}$. The coefficients obtained from Bell's (1980) weak sediment transport relation are also included in Table 5.2, allowing a comparison to be made with the coefficients obtained by previous researchers.

Taylor (1971) plotted contours of nondimensional sediment transport, g_{s_*}', on a plot of Shields parameter against grain Reynolds Number where

$$g_{s_*}' = \frac{g_s}{\rho_s u_{*_b} d_{50}} \tag{5.17}$$

Substitution of Eq. 5.14 into Eq. 5.17 gives

$$g_{s_*}' = N\lambda A_2 \tag{5.18}$$

The data obtained by solving Eqs. 5.15 and 5.18 for $N = 1 \times 10^{-6}$ and the upper and lower limits given by Eq. 5.16, are given in Fig. 5.5; also included are the results of Neill (1968) for conditions of "lower critical stage".

5.3.3 Discussion

The data plotted in Fig. 5.4 show that a critical value of Shields Parameter can be defined by a dimensionless sediment transport rate, as

AUTHORS	R_{e_*}	α_s	β_s	θ_c	
				Lower Limit	Upper Limit
Pazis and Graf (1971)	6 - 90	5.4×10^{7}	8.15	.0216	.0292
Paintal (1971(a))	80 - 2000	6.56×10^{18}	16.0	.029	.034
Bell (1980)		3.04×10^{10}	11.2		

Table 5.2 Properties of Weak Sediment Transport Relations

proposed in Eq. 5.11. The closeness of these two sets of data suggests that the amount of particle motion is independent of grain Reynolds Number in the rough turbulent zone which is commonly accepted to extend down to $Re_* = 70$. Below this limit the grain Reynolds Number is expected to become a more significant variable.

The data presented in Fig. 5.5 attempts to determine the significance of grain Reynolds Number on the assumed initial motion criterion, given by $N = 1 \times 10^{-6}$. The results inferred from Taylor (1971) are similar in shape to, but well below, Shields curve which Taylor (1971) postulated was equivalent to the contour defined by $g_{s_*}' = 1 \times 10^{-2}$, ($1 \times 10^{-4} < N < 1 \times 10^{-3}$). Similarily, Paintal (1971) noted a transition from weak to strong sediment transport at a nondimensional transport equivalent to $g_{s_*}' = 4.4 \times 10^{-2}$ ($4.4 \times 10^{-4} < N < 4.4 \times 10^{-3}$). This confirms the suggestion that Shields curve corresponds to a small but definite transport rate and not "zero" transport as Shields postulated.

In the transition range, $4 < Re_* < 70$, the results of Pazis and Graf (1977) and Taylor (1971) plotted in Fig. 5.5 only overlap if the step length constant, λ, varies from approximately 20, at $Re_* = 4$ up to 100 - 200 at $Re_* = 70$. At even higher values of grain Reynolds Number the data of Neill (1968) and the results of Paintal (1971(a)) are in reasonable agreement; both fall beneath the Taylor (1971) results. Assuming that Shields Parameter is constant in the fully rough zone; the Taylor (1971) results suggest that the fully rough zone is not encountered until $Re_* = 300$; a value much greater than the commonly accepted value of $Re_* = 70$.

The data of Bell (1980) and Griffiths (1976), obtained from Fig. 5.4 for $N = 1 \times 10^{-6}$ (Table 5.1), are also plotted in Fig. 5.5. The two data points plotted using grain related flow properties agree well with the other data presented. The two data points plotted using bed flow properties agree less well. The difference between these two sets of data reflects the difference, even at threshold conditions, between values of flow properties calculated using the calibrated side-wall correction relation of Williams (1970) and those calculated using Einstein's (1950) procedure.

Since the Bell (1980) value of critical grain Shields Parameter plotted close to the upper boundary of the Taylor (1971) results it was assumed that the curve defined by the upper boundary could be used to

estimate the critical grain Shields Parameter, θ_c', for a bed material of similar size. It was estimated that for the bed material used in the experimental programme that $\theta_c' \simeq 0.03$ and $Re_*' \simeq 48$. From Eq. 5.8

$$\theta_c = 0.039 \tag{5.19}$$

for the assumed criterion of initial motion, $N = 1 \times 10^{-6}$. Hence, the initial assumption that $\theta_c = 0.04$ was reasonable; however the value given in Eq. 5.19 was used herein. Using the bed resistance relation developed in Section 5.4.2, Eq. 5.40, and Mannings equation, this value of Shields Parameter gave a critical discharge, $q_c = 0.0244$ m^3/s/m. To contain the base flow backwater profile effects to the downstream rigid bed section, the base discharge which was set in the non-steady flow series was $q_b = 0.0348$ m^3/s/m which corresponds to $q_{s_*}' = 1.8 \times 10^{-3}$ ($1.8 \times 10^{-5} < N < 1.8 \times 10^{-4}$), a value which is closer to Taylor's (1971) proposed Shields initial motion criterion of $q_{s_*}' = 1 \times 10^{-2}$ ($1 \times 10^{-4} < N < 1 \times 10^{-3}$) than the criterion $N = 1 \times 10^{-6}$ upon which the q_c value was based.

At the base discharge, occasional grain movements were detected in keeping with weak sediment transport.

5.4 RESISTANCE

5.4.1 Introduction

In a wide, alluvial stream the stage-discharge response is governed by the total resistance offered by the bed. Unfortunately, a mobile plane bed is normally unstable and substantial hydraulic resistance due to the development of bed forms can be encountered. Many attempts to determine total hydraulic resistance have involved the separation of total resistance into two components. The first of these, the skin friction component which is signified by ', is associated with the granular properties of the bed material. The second component, the form drag which is signified by ", is associated with the resistance contributed by bed forms. Brownlie (1983) has reviewed six of many methods devised to determine total resistance in this manner.

Originally, Einstein and Barbarossa (1952) proposed that the hydraulic radius of the bed, R_b, could be split into two components, thus

$$R_b = R_b' + R_b'' \tag{5.20}$$

giving, since $\tau = \rho_s g R_b S_f$,

$$\tau_o = \tau_o' + \tau_o'' \tag{5.21}$$

An alternative approach proposed by Alam and Kennedy (1969) and Engelund (1967) was that energy slope be divided into two components, giving

$$S_f = S_f' + S_f'' \tag{5.22}$$

Assuming the Darcy-Weisbach resistance relation

$$\frac{U}{u_{*_b}} = \sqrt{\frac{8}{f_b}} \tag{5.23}$$

applies also for grain related and bed form related variables, one obtains from Eq. 5.21

$$f_b = f_b' + f_b'' \tag{5.24}$$

In recent times widespread use has been made of this friction-factor approach.

Resistance relations based on Manning's equation are still widely used in numerical models, KUWASER (Brown and Li (1979)), the Wellington (1978) model, HEC-2 and HEC-6 (Hydrologic Engineering Centre (1973-77)); an analysis of resistance using a Manning equation approach is presented below.

5.4.2 Manning Roughness Analysis

The Manning equation for total resistance is

$$U = \frac{c R_b^{2/3} S_f^{1/2}}{n_b} \tag{5.25}$$

or

$$\frac{U}{u_{*_b}} = \frac{c R_b^{1/6}}{\sqrt{g}\, n_b} \tag{5.26}$$

where n_b = Nondimensional Manning roughness value; and

c = Dimensional coefficient

= 1.0 $m^{1/3}/s$ (S.I. Units)

= 1.49 $ft^{1/3}/s$ (Imperial Units)

In terms of grain related flow properties, the Manning equation becomes

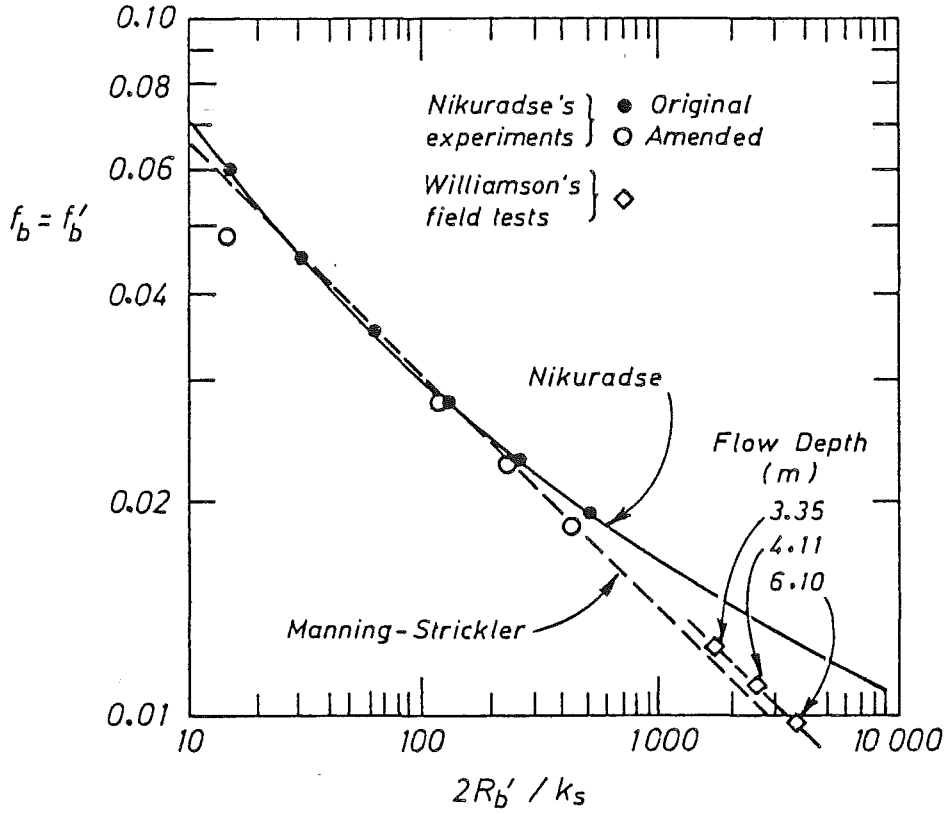

Figure 5.6 The Behaviour of Resistance Coefficients in Fully Rough Flow (After Henderson (1966))

$$U = \frac{cR_b'^{2/3} S_f^{1/2}}{n_b'} \tag{5.27}$$

where n_b' = Nondimensional Manning grain roughness value.

Recalling the Darcy-Weisbach equation for grain roughness

$$\frac{U}{u_{*_b}'} = \sqrt{\frac{8}{f_b'}} \tag{5.28}$$

and equating Equations (5.28) and (5.27) gives

$$n_b' = cR_b'^{1/6} \sqrt{\frac{f_b'}{8g}} \tag{5.29}$$

Similarily for total resistance

$$n_b = cR_b^{1/6} \sqrt{\frac{f_b}{8g}} \tag{5.30}$$

After applying several plausible corrections to Nikuradse's data, (Henderson (1966)), Williamson (1951) found that for fully rough flow conditions that grain friction factor, f_b', was given by (Fig. 5.6) the relation

$$f_b' = 0.113 \left(\frac{k_s}{R_b'}\right)^{1/3} \tag{5.31}$$

where k_s = Representative roughness height.

Substitution of Eq. 5.31 into Eq. 5.29 gives

$$n_b' = c\sqrt{\frac{0.113}{8g}}\, k_s^{1/6} \tag{5.32}$$

or

$$n_b' = \begin{cases} 0.038\, k_s^{1/6} & (k_s \text{ in m}) \\ 0.031\, k_s^{1/6} & (k_s \text{ in ft}) \end{cases} \tag{5.33}$$

This agrees closely with the empirical Strickler equation, given by Henderson (1966) as

$$n_b' = 0.034\, k_s^{1/6} \quad (k_s \text{ in ft})$$

$n = \frac{1}{21.1} d^{1/6}$

$= 0.0474\, d_m^{1/6}$

$0.04168\, d^{1/6}$ ft

Thus, in the zone of fully rough flow conditions, where Eq. 5.31 applies, the Manning grain roughness is independent of flow conditions and related solely to grain properties. However, for transition flow,

$Re_* \tilde{<} 70$, it is recognised that the Manning grain roughness will be a function of Reynolds Number, Re_*.

A general expression for Manning (total) roughness value can be obtained by dividing Eq. 5.25 by Eq. 5.27, giving

$$n_b = n_b' \left(\frac{R_b}{R_b'} \right)^{2/3} \tag{5.34}$$

From the definitions of Shields Parameter and grain Shields Parameter (Eq. 5.9) it is possible to re-arrange Eq. 5.34 and obtain

$$n_b = n_b' \left(\frac{d_{50}}{d_{35}} \right)^{2/3} \left(\frac{\theta}{\theta'} \right)^{2/3} \tag{5.35}$$

In order to solve Eq. 5.35 for n_b a relation between Shields Parameter and grain Shields Parameter must be adopted. Several such relations are available, including Engelund (1967) (Fig. 5.3)

$$\theta' = 0.06 + 0.4\ \theta^2 \qquad 0.1 < \theta < 1.5 \tag{5.36}$$

or, a modified form of Eq. 5.36 presented by Engelund and Fredsφe (1982) (Fig. 5.3)

$$\theta' = 0.06 + 0.3\ \theta^{1.5} \qquad 0.1 < \theta < 1.5 \tag{5.37}$$

or, as found in the side-wall analysis (Section 5.2.3), a general relation of the form

$$\theta' = \alpha' \theta^{\beta'} \tag{5.38}$$

Substituting Eq. 5.38 into Eq. 5.35 gives

$$n_b = n_b' \left(\frac{d_{50}}{d_{35}} \right)^{2/3} \left(\frac{\theta^{1-\beta'}}{\alpha'} \right)^{2/3} \tag{5.39}$$

which is a general relation for Manning (total) roughness value in terms of Shields Parameter.

5.4.3 Results

A general relation for Manning (total) roughness value was obtained by substituting the bed material properties (Appendix C) and calibrated α' and β' coefficients (Section 5.2.3, Fig. 5.2) into Eq. 5.33, with $k_s = d_{65}$ as suggested by Einstein and Barbarossa (1952), and

Eq. 5.39. Thus, for the current study

$$n_b' = 0.0133$$
$$n_b'' = 0.0256\ \theta^{0.136} \qquad (5.40)$$

Similarily, for Bell's (1980) data

$$n_b' = 0.0139$$
$$n_b'' = 0.0236\ \theta^{0.1185} \qquad (5.41)$$

Using the divided hydraulic radius approach of the bed approach of Einstein and Barbarossa (1952), the relation between total, grain and bed form related Manning roughness value is

$$n_b^{1.5} = n_b'^{1.5} + n_b''^{1.5} \qquad (5.42)$$

Since S.I. units were used at all times, the S.I. dimensional coefficient is automatically included in future references to Manning's equation, (Eq. 5.25 and 5.27).

5.4.4 Discussion

Several interesting points arose in the preceeding analysis. Firstly, in the fully rough zone it was demonstrated that Manning's grain roughness is independent of flow conditions and can be determined from Strickler's relation (Eq. 5.34). Hence, knowing Manning's grain roughness, the hydraulic radius of the bed associated with skin friction can be easily calculated from Eq. 5.27, the grain friction factor can then be obtained from Eq. 5.29. Alternatively, grain friction factor can be determined from a Moody diagram.

Secondly, it is possible to obtain a multi-valued Manning bed roughness by substituting into Eq. 5.35 a relation which describes both subcritical and supercritical flow regimes; such a relation, involving Shields Parameter and grain Shields Parameter, was presented graphically by Engelund and Fredsφe (1982). The relation presented in Fig. 5.3 and defined in Eq. 5.37 is the subcritical limb of this general relation. A general relation of this type would allow Manning bed roughness values to be determined over the complete range of flow conditions.

Thirdly, assuming the bed friction factor to be constant, then, from Eq. 5.30

$$n_b \propto R_b^{1/6} \qquad (5.43)$$

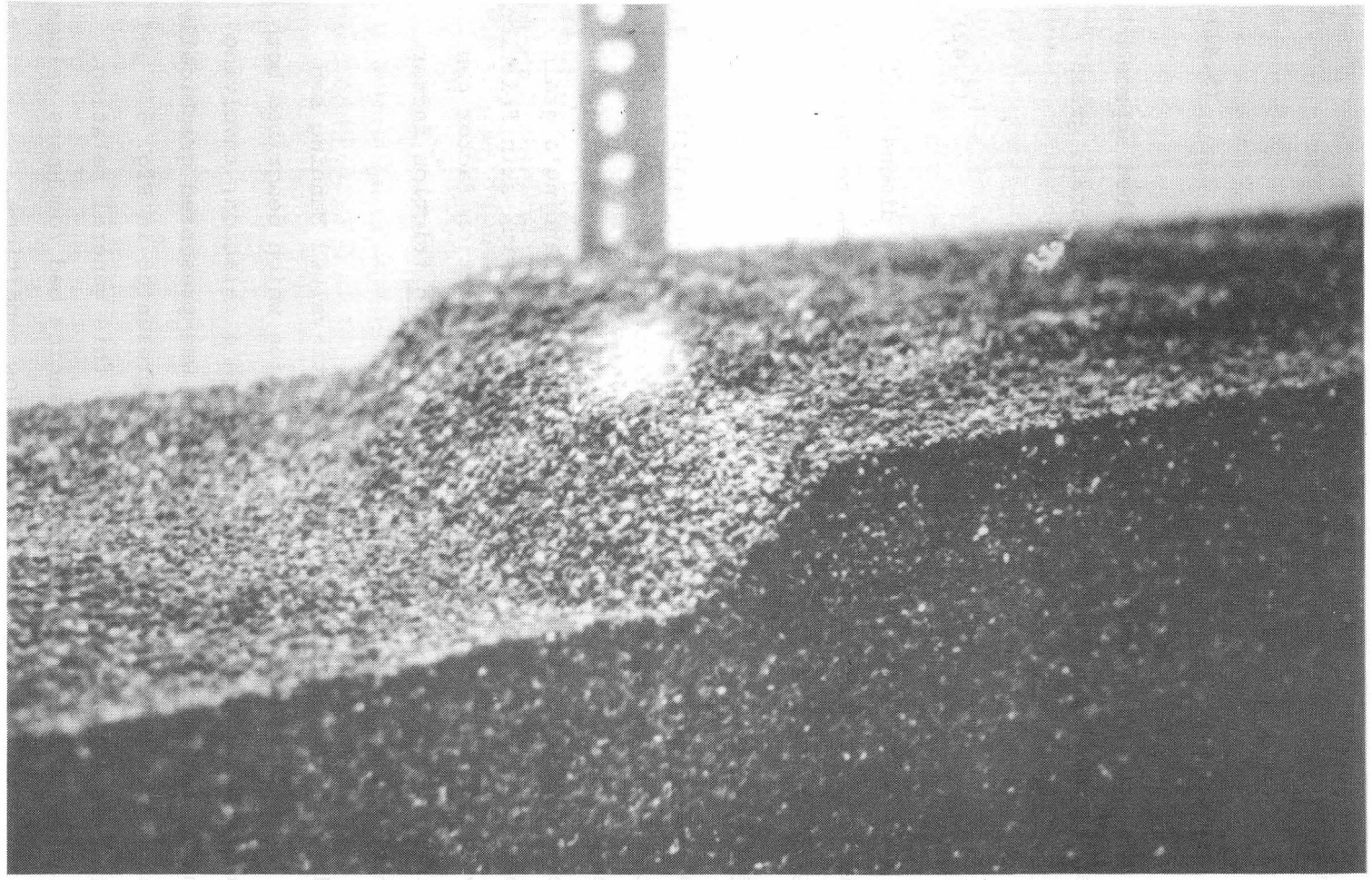

Plate 5.1 Typical Dune Bed Form Profile

The value of the exponent, 0.167, from Eq. 5.43 is close to those obtained from the data, 0.136, and 0.119 for Bell's (1980) data (Eqs. 5.40 and 5.41). These slight differences are due to the bed friction factor not being constant, due to the effects of varying bed forms.

Finally, this analysis emphasises that a Moody diagram can not be used to determine bed friction factors unless plane bed conditions prevail.

5.5 STEADY FLOW EQUILIBRIUM TRANSPORT (SE Series)

Observations and results are presented for the equilibrium transport series of experiments.

5.5.1 Observations

The experimental procedures used in this series of experiments were as outlined in Section 4.4.1. Before each run commenced, $t = 0^{-}$ s, the bed was plane and the base flow conditions were less than threshold (Section 4.4.1). At t = 0 s the desired flow rate was set quickly and sediment injection commenced at a predetermined rate. Exploratory runs gave estimates of the equilibrium sediment transport rates to be expected, these transport rates were used as the sediment injection rates in the final runs.

Soon after each run commenced the mobile bed began to deform and bed forms developed. For the range of bed slopes and water discharges considered, the majority of bed forms encountered were long two dimensional gravel bars (Plate 5.1, Fig. 6.4). Typically, these bed forms ranged in length from 0.8 - 1.5 m and in height from 12 - 36 mm. A typical bed form, which is shown in Plate 5.1, is distinguished by its steep face, flattened top and gently sloping tail. At higher discharges small dunes occasionally developed on the back of parent dunes. These bed forms propagated at celerities greater than those of the parent dunes until they approached the crest region of the parent dune where they slowed and were finally assimilated.

As bed forms developed two separate zones of motion were noted. Immediately downstream of a dune face grains were observed to be buffeted and rocked by turbulence and to move in a random manner. However, further downstream from the dune face random turbulent buffeting was less noticeable and grains were observed to roll uni-directionally downstream.

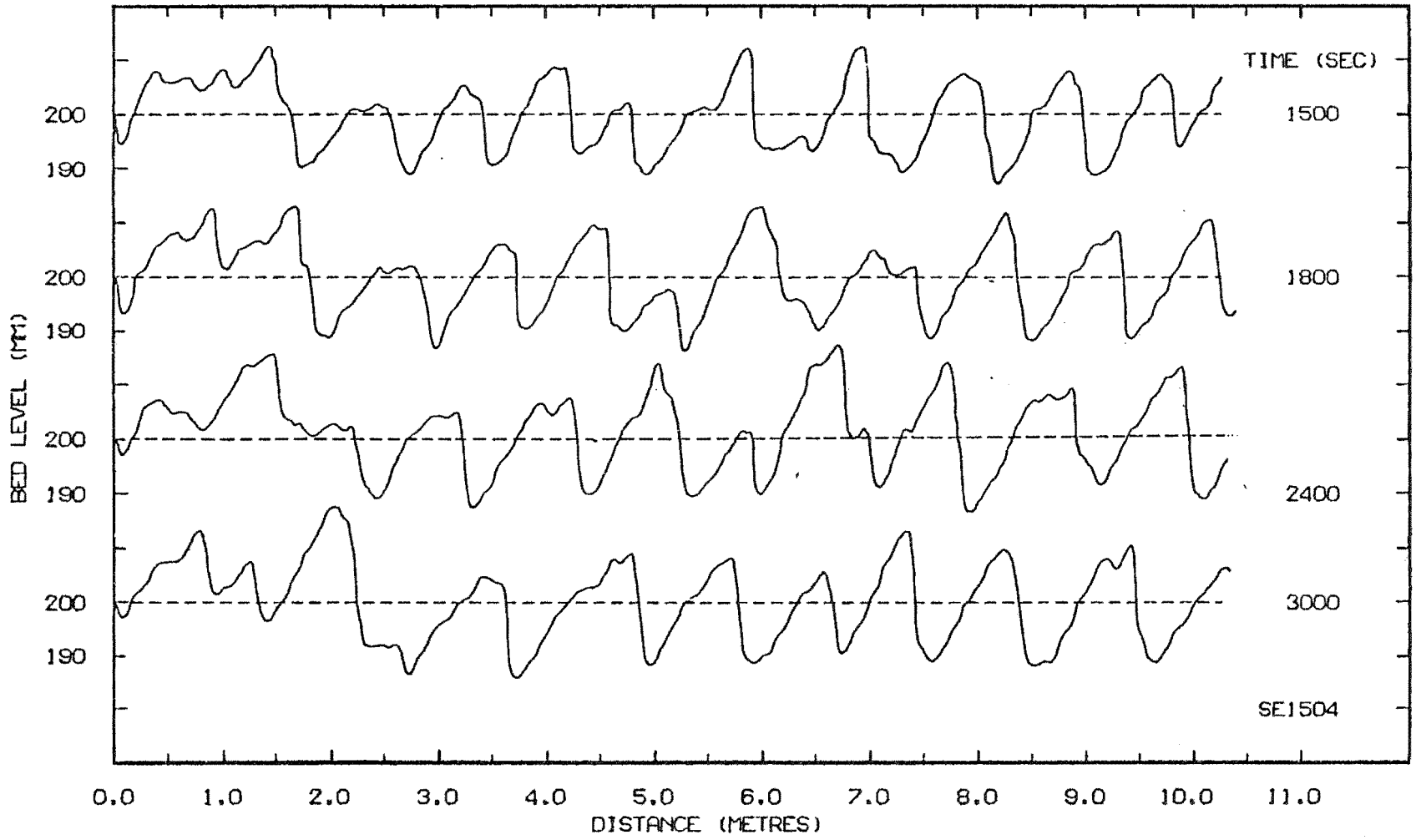

Figure 5.7 Typical Bed Profile Record (Run SE1504)

This motion did not occur as a sheet right across the flume but as narrow streams of motion which wavered back and forth across the width of the flume. Little detachment was noticed as grains reached a dune crest, rather they promptly slid down the dune face and were soon buried by the advancing bed form.

As the dunes developed, the water surface profile became out of phase with the bed profile i.e. a drop in the water surface profile occurred near the dune crest. Water surface profiles measured in the SC series (Fig. 6.4) clearly recorded this behaviour. A typical bed profile record for the SE series is given in Fig. 5.7. The full set of measurements is included in Volume II.

5.5.2 Results

Twenty-four runs were completed for a range of nine flow rates at four different flume slopes. Two extra runs were undertaken to assess the reproducibility of the results (see Appendix C).

Typical results, obtained for the sediment transport rate as a function of time, in the SE series of experiments are plotted in Fig. 5.8. Instantaneous smoothed transport rates were calculated from measured transport rates using the algorithm described by Bell (1980) in his Appendix B and summarised in Appendix B.

It takes time for an initially plane bed to deform and for bed forms to develop; hence an equilibrium state is not reached until some time after an experiment is commenced (Fig. 5.8). To determine the equilibrium bedload transport rate, g_{se}, an assumed relation was fitted to the cumulative mass curve recorded by the bedload collector system. Assuming that the transition from zero sediment transport at the commencement of an experiment to the equilibrium transport rate at a later time can be described by an exponential function, then

$$\frac{g_s}{g_{se}} = \left(1 - e^{-C_t t}\right) \tag{5.44}$$

Integrating 5.44 gives

$$M_s = B\int_0^t g_s dt = g_{se}\left(t + \frac{(e^{-C_t t} - 1)}{C_t}\right)B \tag{5.45}$$

where M_s = Cumulative mass of sediment, and

C_t = A temporal lag coefficient.

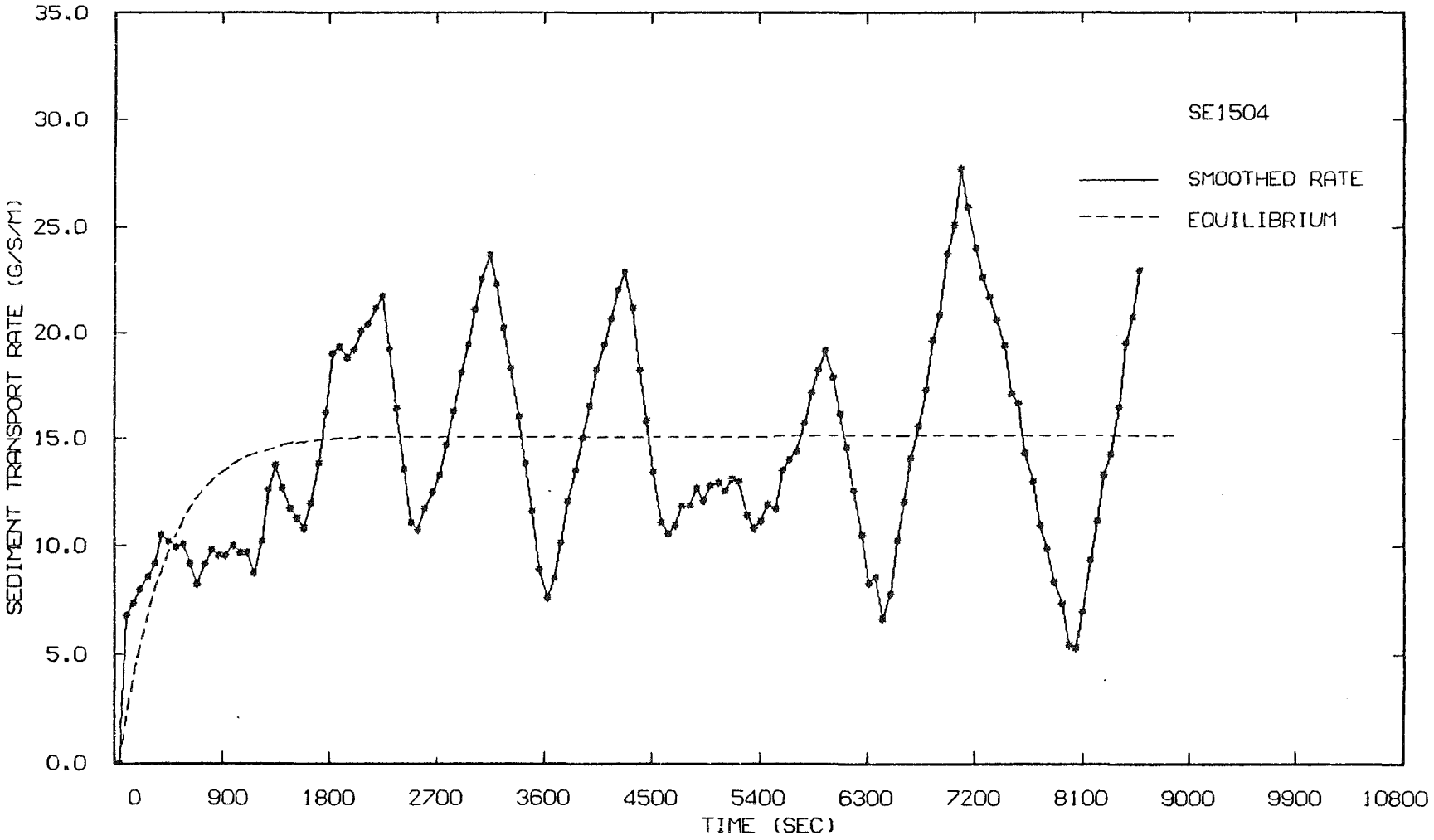

Figure 5.8 Sediment Transport Rate Against Time (SE1504)

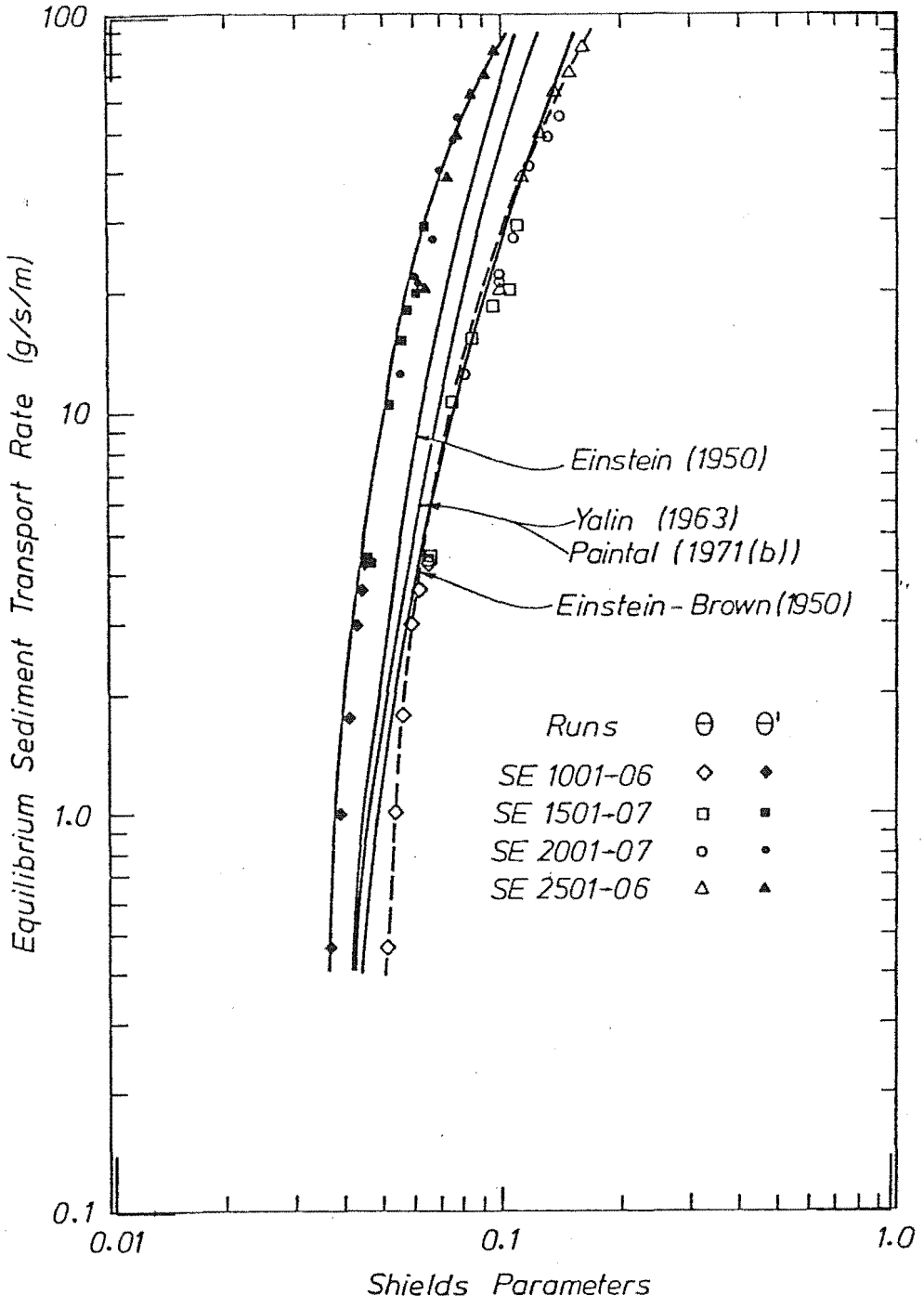

Figure 5.9 Equilibrium Sediment Transport Rate Against Shields Parameters.

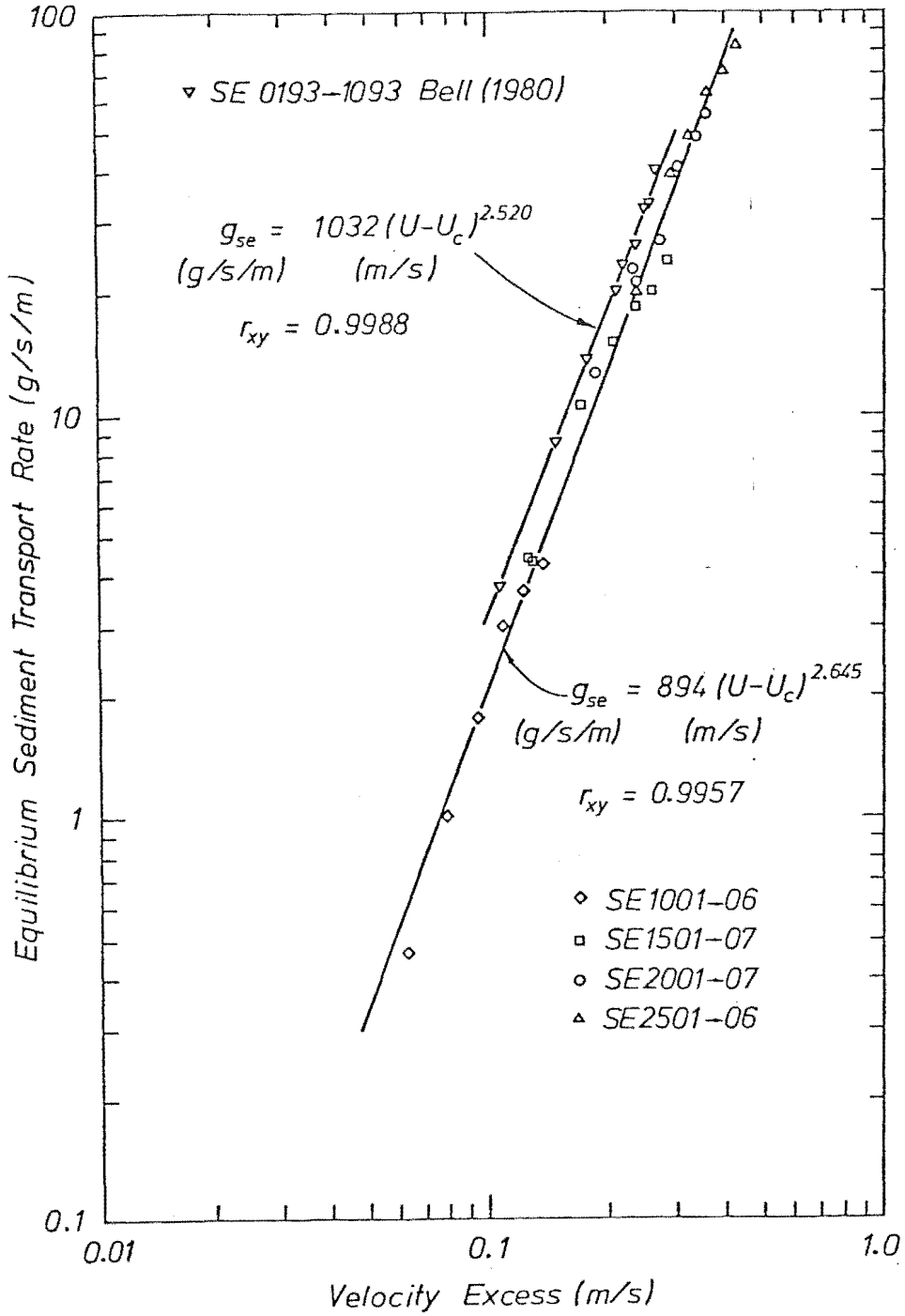

Figure 5.10 Equilibrium Sediment Transport Rate Against Velocity Excess

For each run, values of g_{se} and C_t were found by fitting Eq. 5.45 to the cumulative mass curve. An optimisation routine, based on a modified pattern search algorithm presented by Monro (1971), which minimised the sum of the errors squared was used. The "equilibrium" curve shown in Fig. 5.8 was obtained by inserting the optimum values of g_{se} and C_t in Eq. 5.44.

Values of the equilibrium bedload transport rate are tabulated, together with the corresponding flow data, in Appendix C and are plotted in Figs. 5.9 and 5.10. Curves predicted by various published formulae are included for comparison in Fig. 5.9.

Before the experimental programme began, a numerical model which recognised spatial lag effects was developed and exploratory runs were undertaken (Chapter 1). The sediment capacity relation adopted in this model was a function of a velocity excess term. Hence, the equilibrium sediment transport data was plotted against the velocity excess term, $U - U_c$, in Fig. 5.10; the data of Bell (1980) is also included. Least squares regression analysis of the data gave

$$\underset{(g/s/m)}{g_{se}} = 894 \underset{(m/s)}{(U - U_c)}^{2.645} \qquad (r_{xy} = 0.9957) \qquad (5.46)$$

where the critical velocity is assumed to be

$$U_c = U \frac{u_{*_c}}{u_{*_b}} \qquad (5.47)$$

and the critical bed shear velocity, u_{*_c}, is obtained from the value of critical Shields Parameter determined in Section 5.3.2, thus

$$u_{*_c} = \sqrt{(S_s - 1) g \, d_{50} \theta_c} \qquad (5.48)$$

Similarily, a regression analysis of Bell's (1980) data gave

$$\underset{(g/s/m)}{g_{se}} = 1032 \underset{(m/s)}{(U - U_c)}^{2.520} \qquad (r_{xy} = 0.9988) \qquad (5.49)$$

5.5.3 Discussion

The reproducibility of the results was checked with two extra runs and confirmed by the agreement between these runs and the parent runs, displayed in Figs. 5.9 and Fig. 5.10 and Appendix C, which was very good.

The performance of the equilibrium formula, shown in Fig. 5.9, is generally poor, particularly when the grain related data is compared with the Einstein (1950) curve. The bedload formula of Einstein-Brown (1950) was found to best fit the bed related data. At low flow intensities, the two sets of data plotted in Fig. 5.9 do not converge. This is to be expected since, even at the threshold of movement, the grain related values and bed related values of Shields Parameter, θ_c' and θ_c, were different (Section 5.3.3).

Before commencing the analysis of spatial lag effects, it was necessary to select a relation which was able to predict sediment transport capacities under varying friction slopes. The data plotted in Fig. 5.10 demonstrate that a relation based on velocity excess is able to do this. Hence, Eq. 5.46 was adopted and used to calculate sediment transport capacities in the spatial lag analysis presented in Chapter 7.

Since the exponents of the relations given by Eqs. 5.46 and 5.49 agree to within 5%, it was assumed, for the bed material of Bell (1980), that the sediment transport relation given by Eq. 5.49 could also be used to calculate bedload transport capacities under conditions of varying friction slope. Hence, Eq. 5.49 was used in the numerical simulations of Bell's (1980) results which are presented in Chapter 10.

5.6 SUMMARY

When analysing results from flume experiments, it is necessary to account for the variable effect of the flume side-wall. The method adopted in this study to correct the flume data for side-wall effects was that of Williams (1970). For a 0.305 m wide flume, the Williams (1970) side-wall correction is of the form

$$R_b = \frac{Y}{1 + 0.591\ Y} \tag{5.3}$$

The procedure of Einstein (1950) was used to determine flow properties due to grain resistance. A general relation between bed related and grain flow properties was also determined, it was of the form

$$\theta' = 0.397\ \theta^{0.796} \tag{5.8}$$

Near threshold conditions, several authors demonstrated that the rate of weak sediment transport was strongly dependent on the applied

bed shear stress. Hence, a rational approach to the definition of initial motion requires a measure of dimensionless sediment transport. Such an approach was proposed by Neill and Yalin (1969) and led them to an initial motion criterion of the form $N = 1 \times 10^{-6}$. The threshold value of Shields Parameter for this study was obtained from an investigation of the effect of grain Reynolds Number on this initial motion criterion. This threshold value is

$$\theta_c = 0.039 \tag{5.19}$$

Under mobile bed conditions the total resistance offered by the bed is due to two components; one component due to the granular properties of the bed material (skin friction) and the second component due to the form drag of bed forms. An analysis of grain resistance, using Manning's equation, found that in the fully rough zone that grain Manning roughness was independent of flow properties. A method whereby a multi-valued Manning resistance relation could be specified was also demonstrated. Using this approach an equation relating Manning bed roughness to Shields Parameter, of the form

$$n_b = 0.0256\ \theta^{0.136} \tag{5.40}$$

was obtained.

The equilibrium transport formula which best fitted the equilibrium transport data was that of Einstein and Brown (1950). A relation was also obtained between equilibrium sediment transport rate and velocity excess for a range of friction slopes. This relation, given by

$$\underset{(g/s/m)}{g_{se}} = 894\,\underset{(m/s)}{(U - U_c)}^{2.645} \tag{5.46}$$

was used in both the spatial and temporal lag analyses presented in Chapters 7 and 8 respectively. For the range of flow conditions studied in the series of equilibrium experiments the majority of bed forms encountered were two-dimensional dunes or gravel bars.

Chapter 6 | Non-Steady Flow Non-Equilibrium Transport

6.1 INTRODUCTION

Two of the prime aims of the experimental programme were to investigate spatial lag and temporal lag effects. These lag effects were investigated by recording the spatial and temporal response of the alluvial system to non-steady flows under constrained sediment boundary conditions. In this study, the constrained sediment boundary conditions were created by the presence of a rigid bed and zero sediment input upstream of the mobile reach. Non-steady flow conditions were created by linearly increasing the flow rate from a base discharge up to a chosen, constant discharge over a selected period of time.

Spatial lag effects, which are viewed as the inability of an alluvial system to immediately overcome constrained sediment boundary conditions, were investigated in the SC-I and GS series of experiments. In the SC-I series of experiments, the temporal variation of flow properties and bed elevations within scour holes, caused by the constrained sediment boundary conditions, were recorded. Bedload transport rates within these scour holes were recorded in the GS series of experiments.

Temporal lag effects, which are viewed as the inability of an alluvial system to immediately respond to an imposed change in discharge, were investigated in the SC-II, III, IV and V series and also in the SC-I series of experiments. In these experiments the temporal variations of bedload transport and bed form geometry were recorded at a section unaffected by the developing scour hole.

Observations and results from these series of experiments are presented. The specific manners in which these results were used in the analysis of spatial and temporal lag effects are presented in

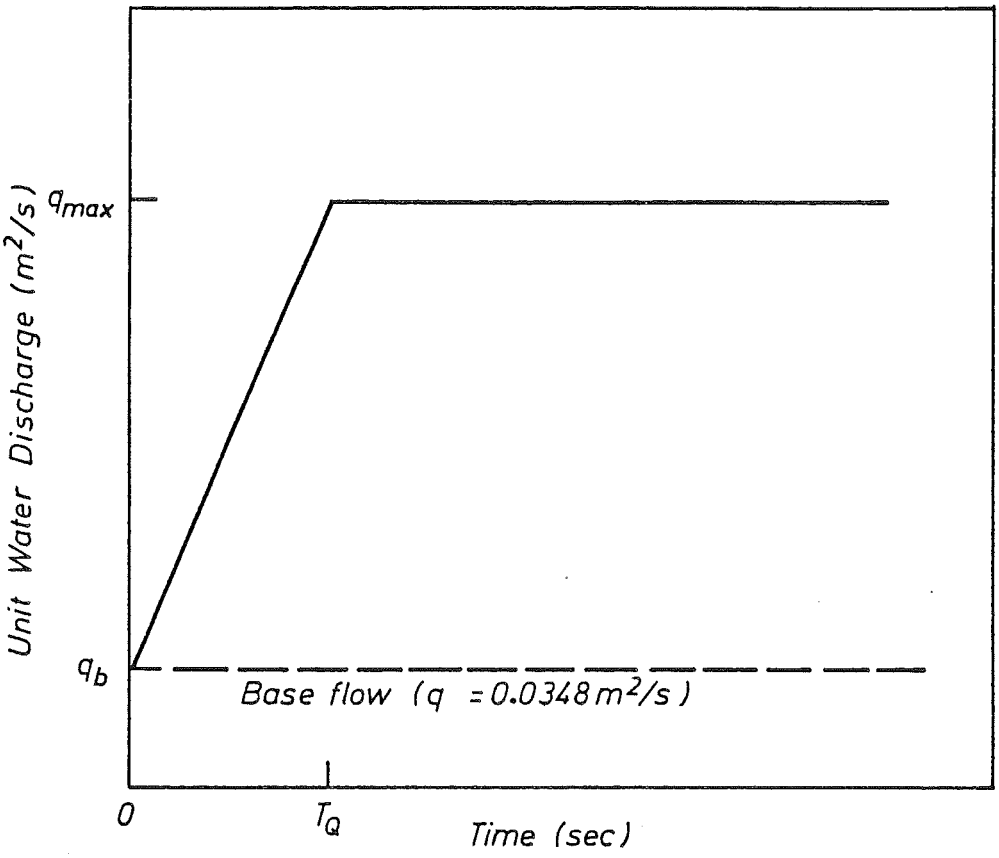

Figure 6.1 General Flow Hydrograph (SC Series)

Chapters 7 and 8 respectively.

6.2 STEPPED DISCHARGE - NON-EQUILIBRIUM TRANSPORT (SC Series)

The aims of the SC-I series of experiments were twofold. The first aim was to measure the temporal variation of flow properties and bed elevation under the non-equilibrium sediment conditions found within a scour hole. Hence, many measurements were taken at sections immediately downstream of the upstream boundary of the mobile reach. The second aim, which was also the aim of the SC-II, III, IV and V series of experiments, was to measure the temporal response of an initially flat mobile bed due solely to non-steady flow conditions. This aim was achieved by measuring the temporal variations of the bed form geometry, over the mobile reach, and the bedload transport rate at the downstream end of the mobile reach. Bedload transport rates were measured at this location because it gave the greatest time in which to take readings which were uninfluenced by the developing scour hole.

The flow hydrograph in all the experiments conducted was of the form given in Fig. 6.1. A full list of the experiments conducted and their associated flow hydrograph properties is given in Table 6.1. Each run was conducted in the manner detailed in Section 4.4.2. A total of twenty-three runs was completed in these series of experiments.

Observations and results for these experiments are presented and discussed below. Full results for all experiments are presented in Volume II.

6.2.1 Observations

During all runs the upstream sediment boundary conditions caused a scour hole, of the form shown in Fig. 6.2, to develop at the upstream end of the mobile reach. When the flow hydrograph was steeply inclined, the upstream scour hole quickly, and then more gradually developed and propagated downstream. The flume side-walls caused these scour holes to be strongly three-dimensional; an effect which is conveyed in Fig. 6.3. The effect of the side-walls was greatest on the lateral profile of the bed at the point of maximum scour at any given time (Fig. 6.2). Downstream of this point the influence of the side-walls decreased until the effect on bed form geometry was small. However, the side-walls did affect to some degree the lateral

RUN	q_{max} (m^2/s)	SC SERIES				
		I	II	III	IV	V
		DISCHARGE RISE TIME (s) (T_Q)				
		30	300	600	1200	1800
01	0.18	•		•	•	
02	0.10	•	•	•	•	•
03	0.12	•		•	•	
04	0.14	•		•	•	
05	0.16	•	•	•	•	•
06/07	0.18	• •		•	•	

(• Experiments Conducted)

Table 6.1 Experiments Conducted in SC Series

bed profile immediately downstream of a dune crest (Fig. 6.4). When the flow hydrograph was gently inclined, the development of this scour hole was more sedate.

At higher discharges the flow field in the scour hole was dominated by a fluid vortex, shown in Fig. 6.2, with a reverse flow, observed with the aid of dye, close to the bed. Sutherland (1983) measured just such a fluid vortex in his investigation of the flow field in a simulated scour hole. The maximum depth of scour at any given time occurred at the downstream extremity of this vortex, which typically was located 0.2 - 0.5 m downstream of the rigid bed (Fig. 6.2).

In the region of the vortex the motion of the grains was similar to that noted near a dune face and described previously (Section 5.5.1). The grains were buffeted, rocked and moved upstream and downstream longitudinally and laterally. The overall tendency, though, was to move down the slope showing gravity to be the dominant influence. At the boundary between the fixed and mobile beds the mobile bed always remained in contact with the edge of the fixed bed (Fig. 6.2) as reported by Bell (1980).

The water surface above the scour hole was observed to be out of phase with the bed, as shown in Fig. 6.2 and Fig. 6.5. The average level of this boil increased slowly with time as the scour hole deepened and was higher than the boils associated with the trough regions downstream of dune crests. Surface ripples were also present (Fig. 6.5); these being superimposed on the general water surface profile.

Under the non-steady flow conditions which prevailed in all runs, a transitional growth of bed forms from the initial plane bed conditions was observed. When the flow hydrograph was steeply inclined, the initial growth of dune bed forms was swift (Fig. 6.5). Dune heights increased more rapidly than dune lengths. The growth rate slowed noticeably at later times as the bed forms approached their presumable equilibrium configuration. The development of the bed forms appeared to be initiated by the small irregularities present in the plane bed at the start of each experiment. These small irregularities caused groups of particles to congregate locally at various locations along the test reach. These local particle concentrations promoted the growth of local mounds which, in turn, swiftly developed into dunes with a characteristic triangular shape. Typically, in the SC-I series

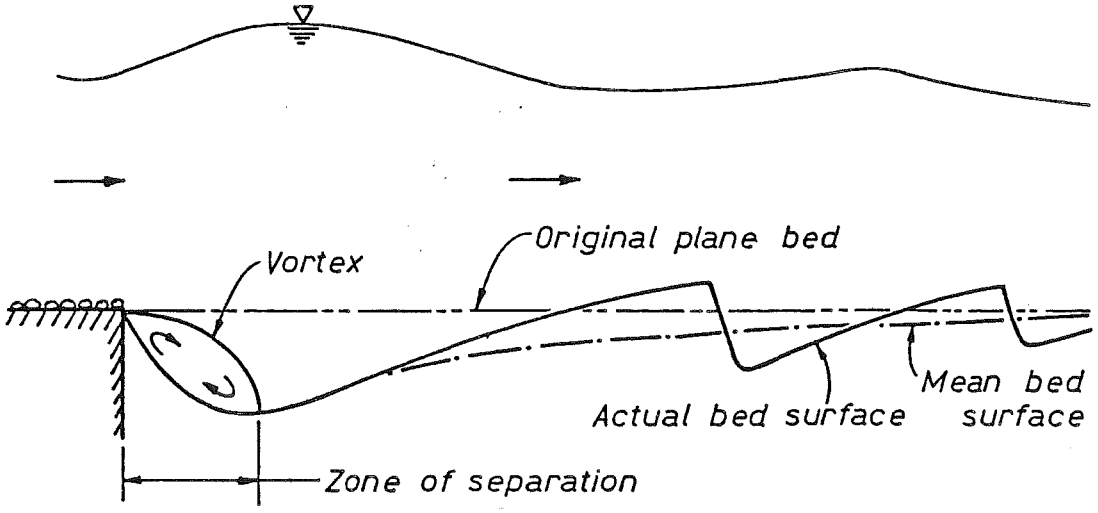

Figure 6.2 Flow Field in a Local Scour Hole Downstream of a Fixed Bed

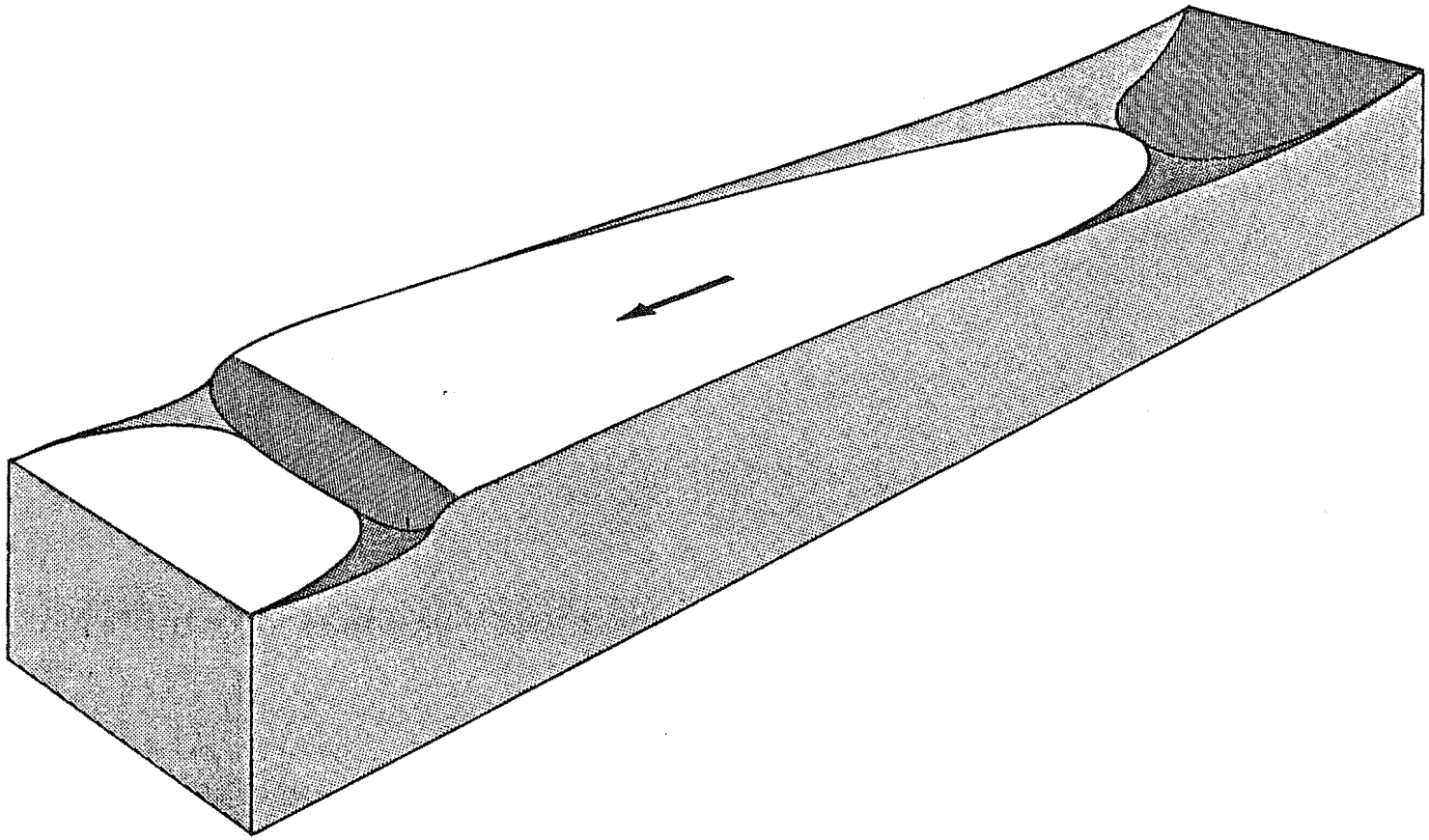

Figure 6.3 Idealized Scour Hole Geometry

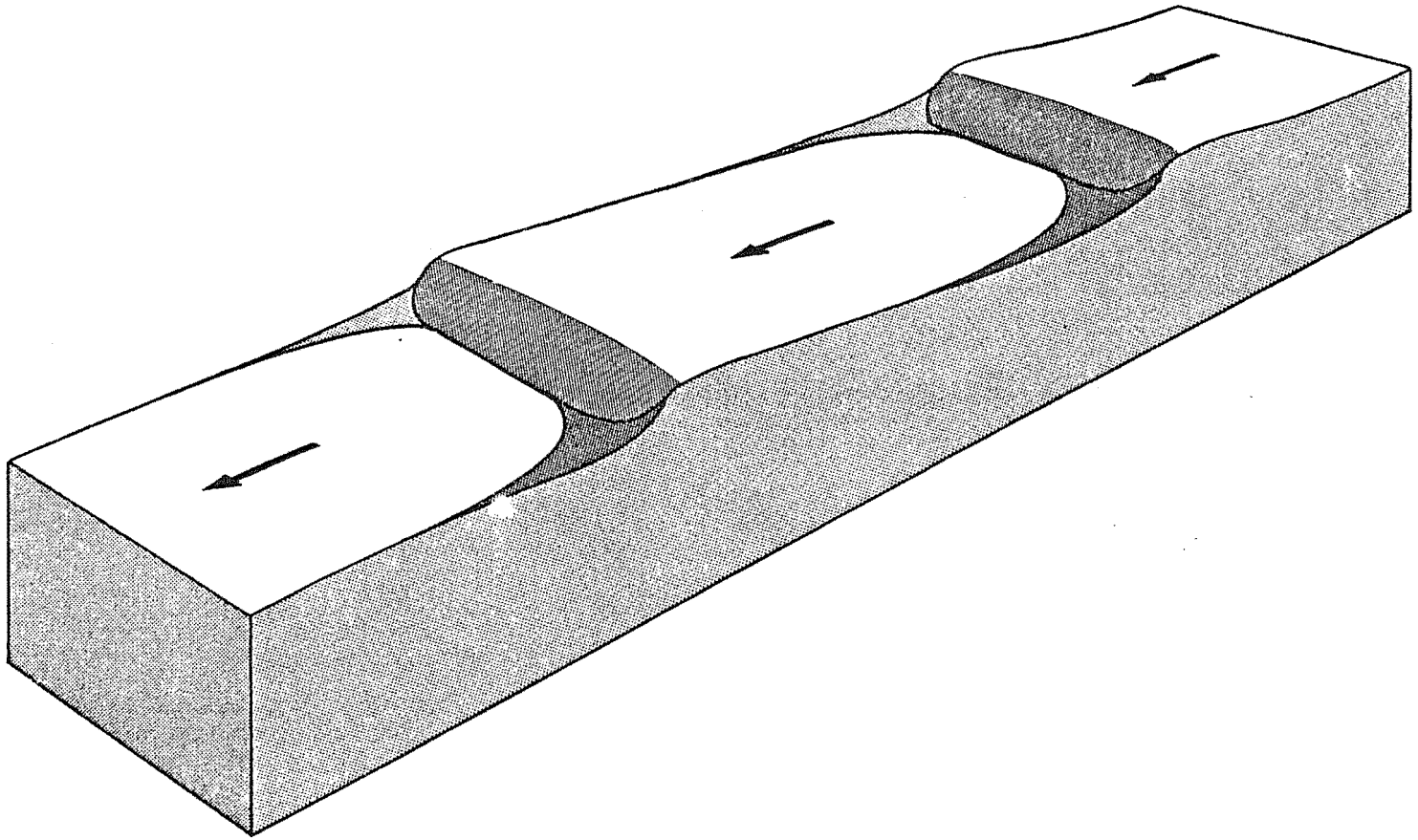

Figure 6.4 Idealized Bed Form Geometry

(Fig. 6.5(a)), significant bed forms developed within the first 300 seconds after a run commenced. The same bed form development occurred when the flow hydrograph was gently inclined, but at a more sedate rate.

At higher discharges, small dunes occasionally developed on the back of parent dunes. They propagated at celerities greater than those of the parent dunes until they approached the crest region of the parent dune. Here they slowed and were finally absorbed by the parent dune. The majority of bed forms encountered, however, were long two dimensional gravel bars (Fig. 6.4 and Plate 5.1).

The motion of grains downstream of the scour hole was the same as that previously described in the equilibrium series (Section 5.5.1).

6.2.2 Scour Hole Profiles

Two sets of continuous longitudinal water surface and bed profile measurements were recorded at various times during the SC-I series of experiments. The first set of recordings was taken over the full length of the test reach (Fig. 6.5) while the second set was taken at an increased horizontal plotter scale, over the 3.0 m length of mobile bed immediately downstream of the fixed bed (Fig. 6.6). During the SC-II, III, IV and V series of runs, recordings of the water surface and bed profiles were only taken over the full length of the flume. All these recordings were taken along the centre-line of the flume. The development of the scour hole and of the associated downstream bed forms could be traced from these records; see the sequence of chart records presented in Fig. 6.5. A more detailed view of the typical development of a scour hole with time, obtained from the second set of records, is demonstrated in Fig. 6.6.

Initially, the dimensions of the scour hole were comparable to those of the troughs formed downstream of the crests of the developing bed forms but the sediment boundary conditions soon caused the scour hole to grow and deepen rapidly. The development of the upstream bed form was integrally linked to the transport of bed material from this deepening scour hole.

As the transport capacity of the flow diminished in the scour hole bed material was eroded from the sloping back of the upstream bed form to satisfy the transport capacity of the flow further downstream. Consequently, at later times the location of the maximum scour depth remained relatively fixed while the scour hole as a whole became more

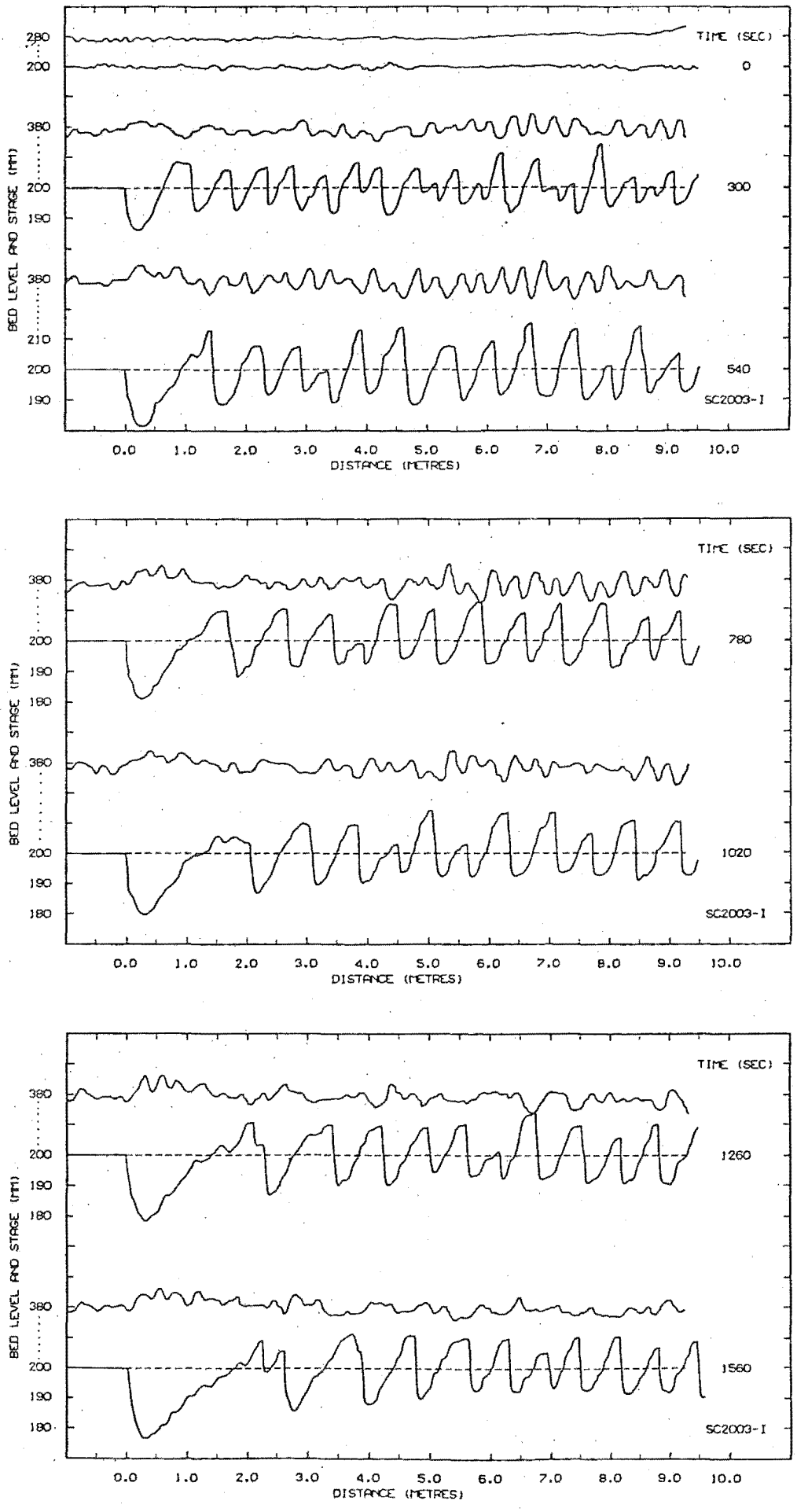

Figure 6.5(a) Typical Centre-Line Water Surface and Bed Profile Records (Run SC2003-I)

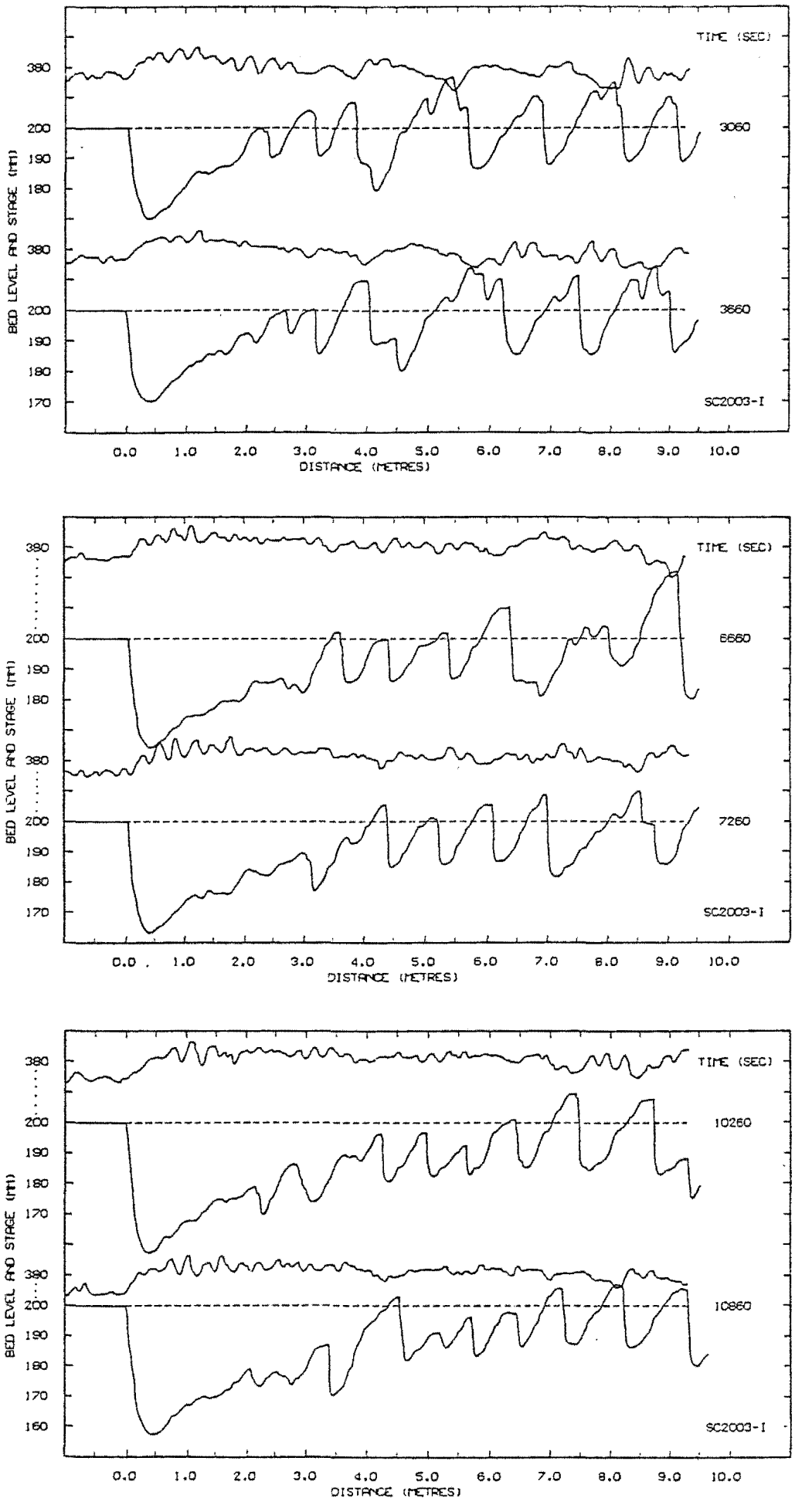

Figure 6.5(b) Typical Centre-Line Water Surface and Bed Profile Records (Run SC2003-I)

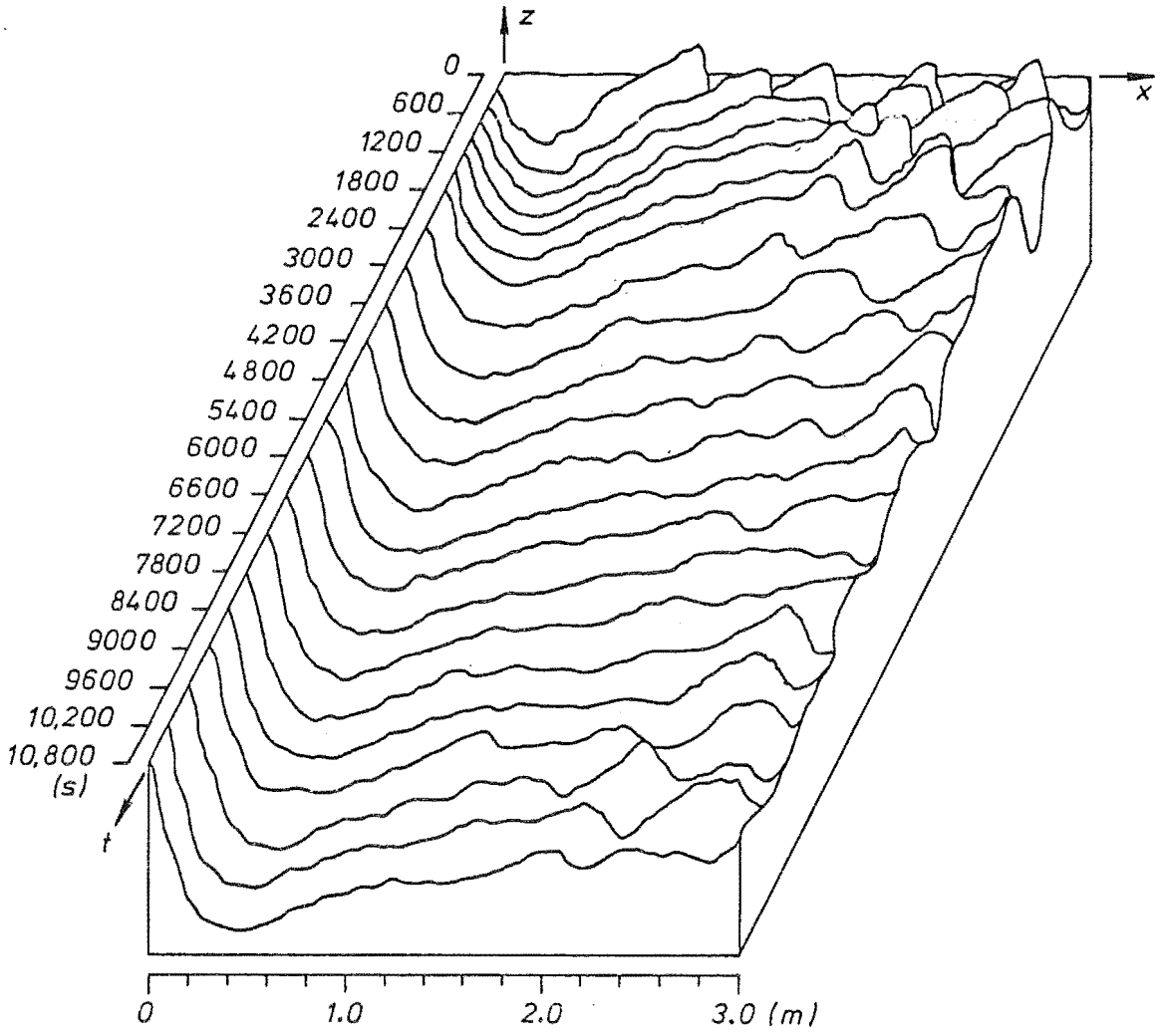

Figure 6.6 Scour Hole Profile Against Time
(Run SC2003-I)

elongated (Fig. 6.6).

At even later stages, particularly during the SC-I runs, the general scour hole defined by the mean bed trend line (Fig. 6.2) occupied the whole test reach. This can be seen to occur in Fig. 6.5(b) even though the actual bed profile locally crosses the original bed level at various points.

Scour hole profiles typical of those computed from mathematical models, for similar flow and sediment boundary conditions, are given in Figs. 6.7 and 6.8. A feature of such models is that they ignore the effect of the fluid vortex. Consequently, these models predict that the maximum depth of scour occurs at the fixed to mobile bed interface. Hence, they incorrectly predict the shape of the scour hole immediately downstream of the upstream boundary. A mathematical model can not fully model microscale features such as bed forms. Therefore, the bed profiles obtained from such models must be compared with the mean bed level trend line of measured results.

During all runs the flume side-walls caused the scour hole to be three-dimensional (Fig. 6.3); that is, the bed was curved both longitudinally and laterally. To determine average bed elevations within the scour hole, measurements were taken, at various times, of the lateral bed profile at Sections 0.5, 1.0, 1.5 and 2.0 m during all SC-I runs. Lateral bed profiles were not measured at the downstream end of the mobile reach during all SC runs because the influence side-walls had on the lateral bed geometry was slight. Examples of typical lateral bed profiles within a scour hole are given in Fig. 6.9. At any given time, the effect of the side-walls was greatest near the point of maximum scour; this effect decreased as the scour depth decreased downstream from this point. Also given in Fig. 6.9 are typical values of the correction, Δz_{b_Φ}, which must be added to the measurements of the centre-line bed elevation at a section to give the <u>average</u> bed elevation across the section.

6.2.3 <u>Maximum Scour Depth</u>

The variation of maximum scour depth, H, with time was determined from the bed profiles measured during each SC-I run, at various times; these results are plotted in Fig. 6.10.

According to Cuhna (1975), the time history of scour hole development consists of four distinct phases, which can be defined as

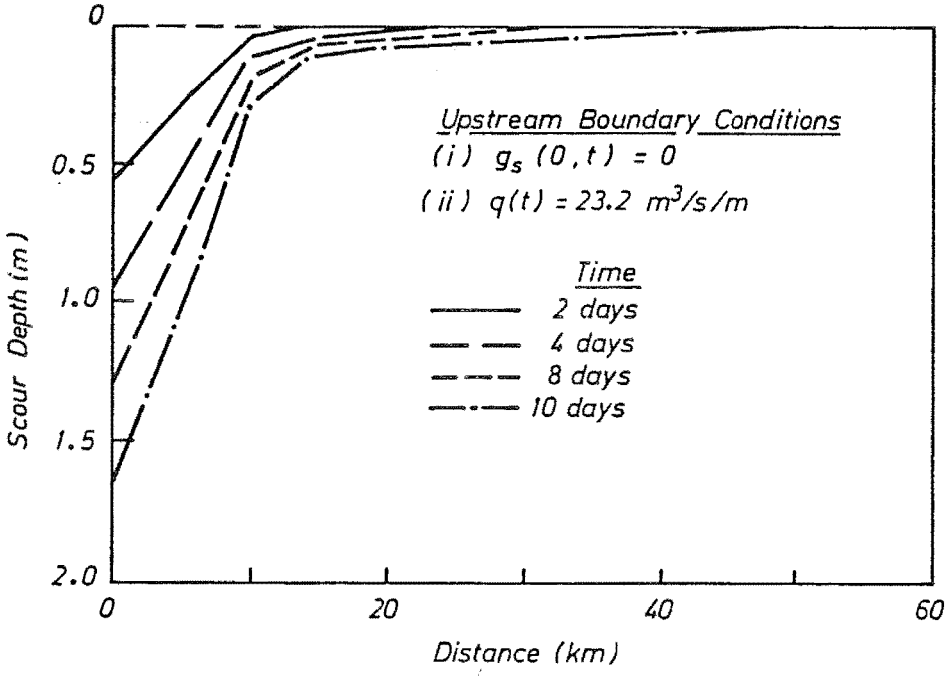

Figure 6.7 Typical Mathematical Model Prediction of Scour Hole Profiles (Adapted from Chen (1973) - After Bell (1980)

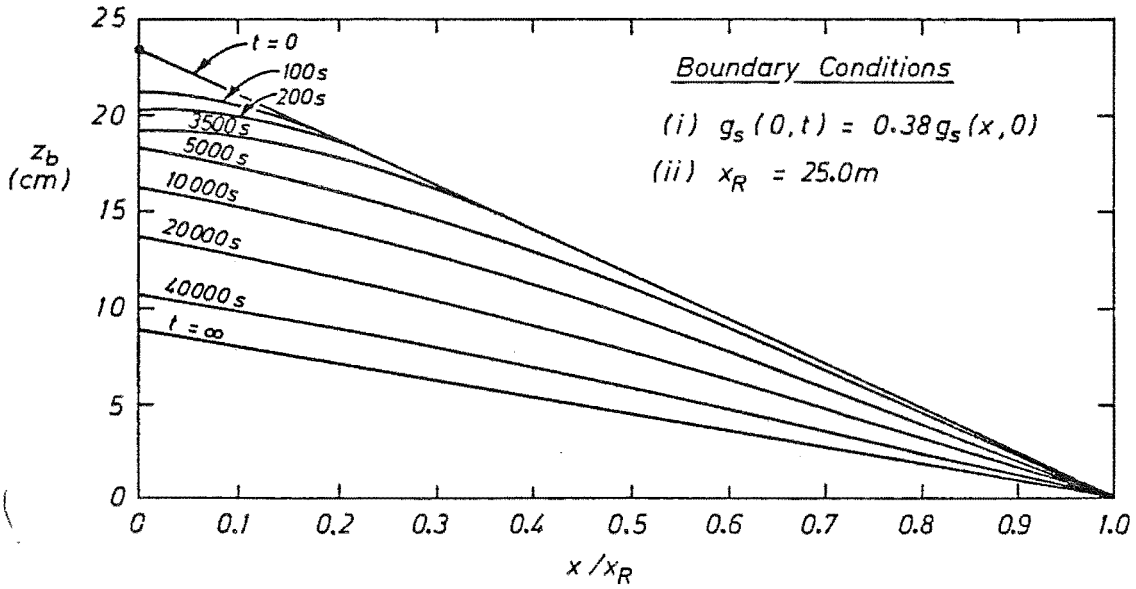

Figure 6.8 Typical Mathematical Model Prediction of Scour Hole Profiles (After Gill (1983(b))

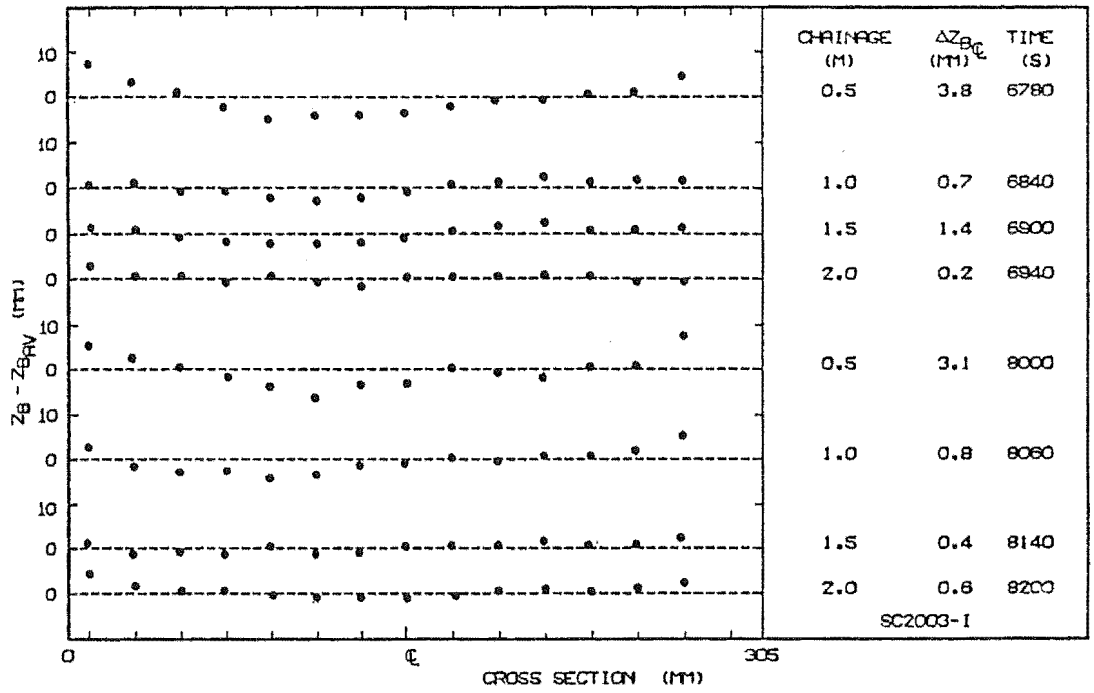

Figure 6.9 Typical Lateral Bed Profiles (Run SC2003-I)

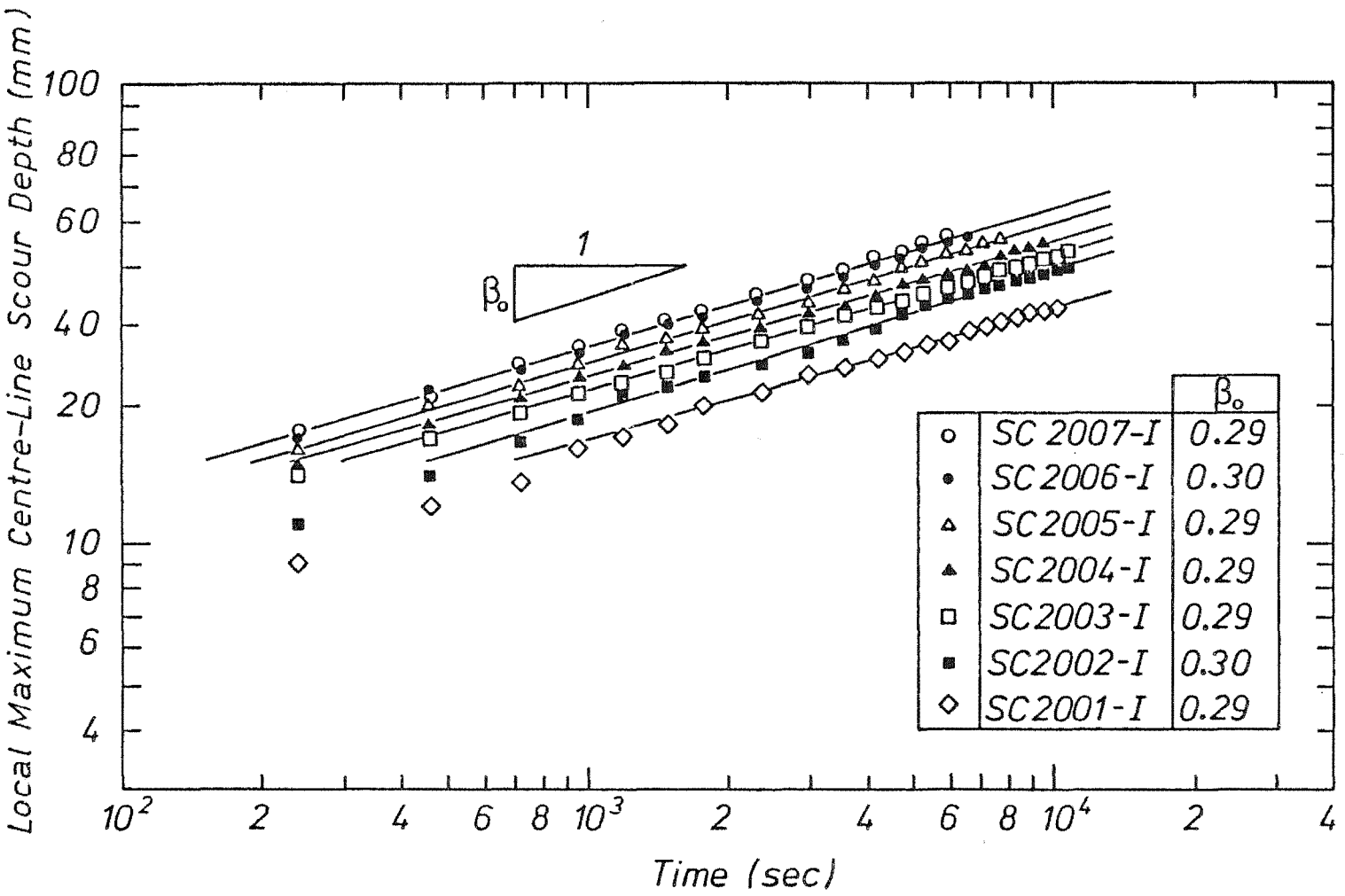

Figure 6.10 Local Maximum Centre-Line Scour Depth Against Time (SC-I Series)

(1) An initial transition phase where rapid scouring occurs;

(2) The first principal phase where the rate of scour slows, and where the maximum scour depth is given by

$$\frac{H}{Y_o} = \alpha_o t^{\beta_o} \qquad (6.1)$$

where α_o, β_o are constants which are functions of the properties of the flow and bed material and Y_0 is the depth of flow over the upstream fixed bed;

(3) A second transition phase where the second principal phase is approached asymptotically; and

(4) The second principal phase where the equilibrium scour depth is reached.

Such phases are also displayed in the results of Mosonyi and Schoppmann (1968) and Dietz (1969).

Only the first two phases were present in the results given in Fig. 6.10. At the lower discharges an initial transition period was noted before the first principal phase was reached. This period reduced in duration as the discharge increased; to the extent that at higher discharges only the principal phase was measured.

The principal phase data follows a power relation with time of the form

$$H(q, t) = \alpha_o' t^{\beta_o} \qquad (6.2)$$

where α_o', β_o are constants which are functions of the properties of the flow and bed material. The measured values of the exponent, β_o, shown in Fig. 6.10 were similar to those measured by Bell (1980) and lie in the range between 0.38 found by Breusers (1965) and Dietz (1969) and 0.2 found by Colaric, Pichon and Sananes (1967) for similar experiments. Likewise, Mosonyi and Schoppmann (1968), for similar flow conditions, found an exponent of 0.35 for the case where the upstream boundary was a vertical step and 0.27 for cases where the upstream fixed bed was an inclined ramp of varying slope.

6.2.4 Bedload Transport Rates

During all runs the sediment collection system was used to record the mass of the accumulated sediment, every sixty seconds, at the downstream end of the test reach, x = 9.5 m. The resultant

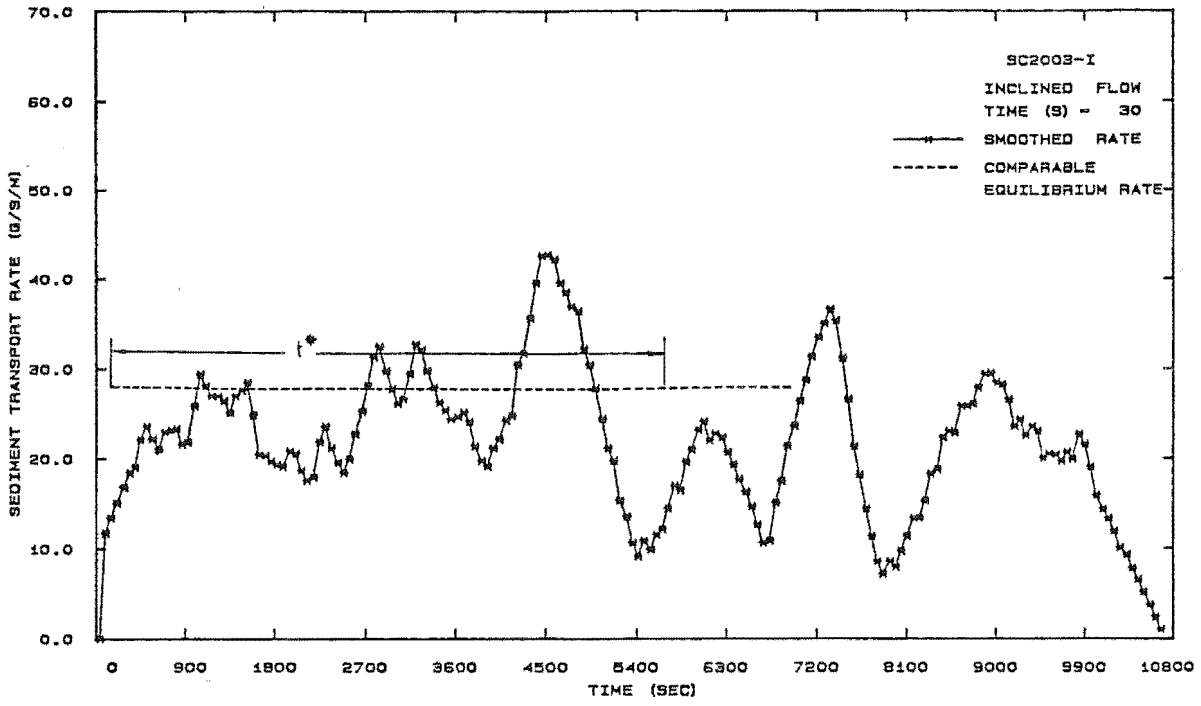

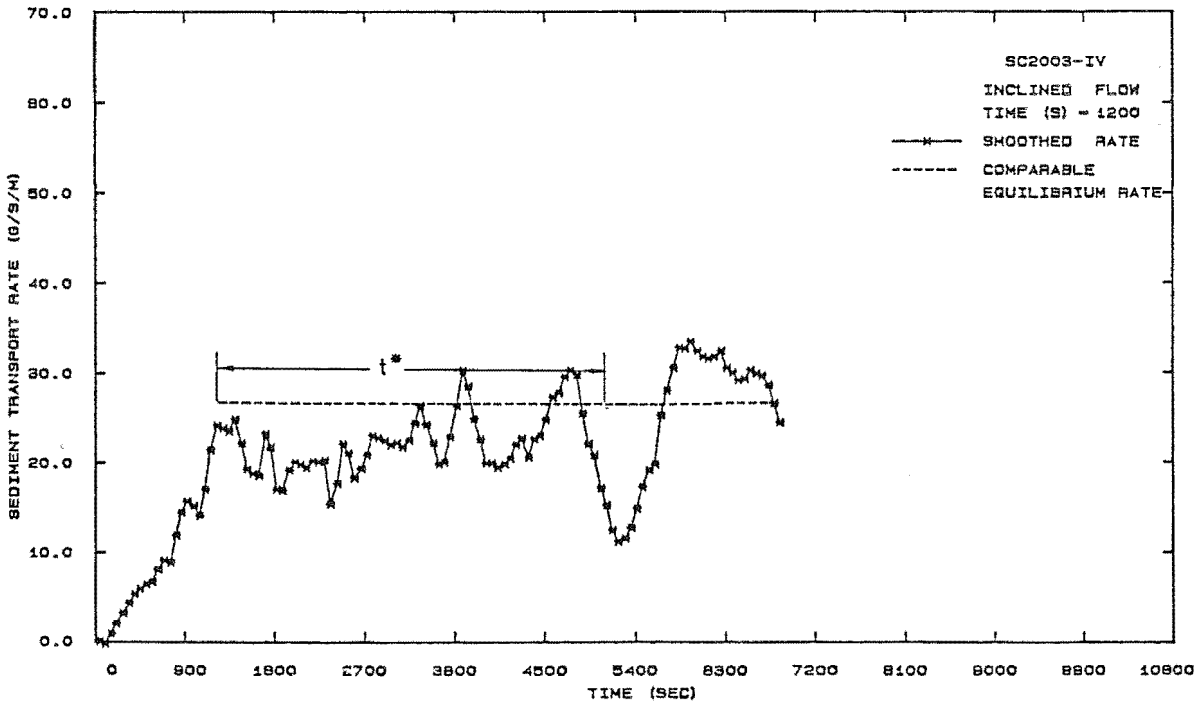

Figure 6.11 Sediment Transport Rate Against Time (Runs SC2003-I and SC2003-IV)

cumulative mass versus time curve was then used to calculate instantaneous smoothed bedload transport rates using the algorithm described in Appendix B. Two typical examples of the temporal variation of the bedload transport rate at the downstream end of the mobile reach are given in Fig. 6.11.

The response of the mobile bed to the unsteady flow conditions is dependent on the steepness of the flow hydrograph. When the maximum discharge is swiftly imposed on the base flow, the case of a steeply inclined hydrograph, the bed responds quickly and the sediment transport rate grows rapidly. At later times, the rate of increase of the bedload transport slows until a dynamic "equilibrium" sediment transport rate is reached (Run SC2003-I, Fig. 6.11).

The comparable equilibrium transport rate plotted in Fig. 6.11 is the value of the bedload transport rate measured in the equivalent SE run i.e. the steady equilibrium run with the same constant discharge and initial bed slope. This comparable equilibrium transport rate occurs at a time significantly later than that when the constant discharge is reached. This time difference is the temporal lag, t^*, and under these conditions it is large. Alternatively, when the maximum discharge is slowly imposed on the base flow the sediment transport rate increases more slowly but is more able to keep up with the changing flow conditions. Consequently, the equilibrium rate of sediment transport is reached sooner after the constant discharge is reached (Run SC2003-IV, Fig. 6.11). In this case, the temporal lag, t^*, is smaller. The precise manner in which temporal lag values were evaluated is presented and discussed in Chapter 8.

At later stages in the run, when the general scour hole, defined by the mean bed trend line, occupied the whole test reach the sediment hydrograph displayed a downward trend (Run SC2003-I, Fig. 6.11 for $t > 5400$ s). This occurs even though the actual bed profile locally crosses the original bed level (Fig. 6.5(b)) and bed forms cause local peaks in the sediment hydrograph. It was found that this behaviour was more pronounced at the higher discharges.

6.2.5 Velocity Profiles

The total bed resistance within a developing scour hole varies both spatially and temporally as the scour hole deepens and elongates. The calculation of spatial lag coefficients relied on the measurement

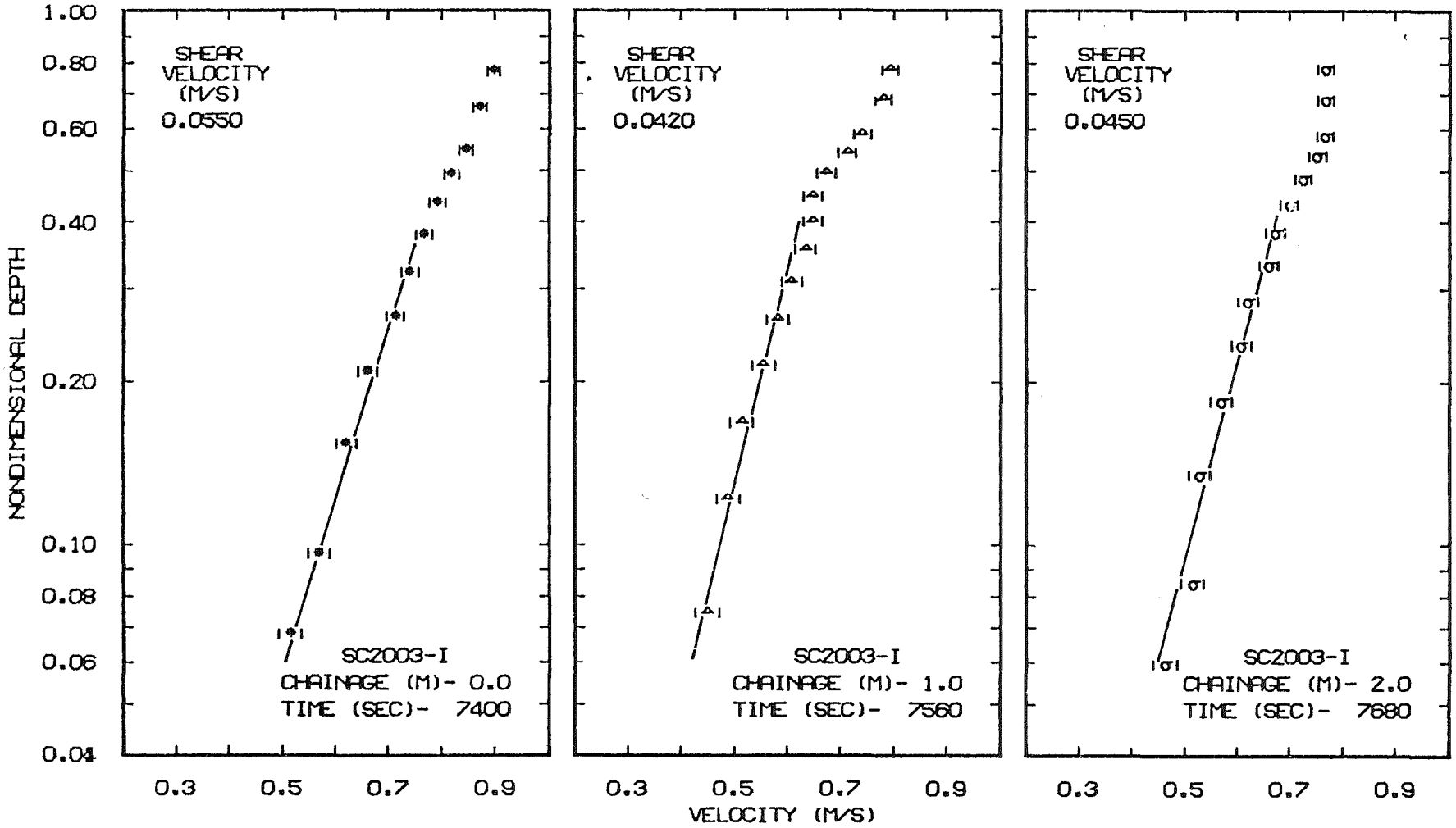

Figure 6.12 Typical Centre-Line Velocity Profiles (Run SC2003-I)

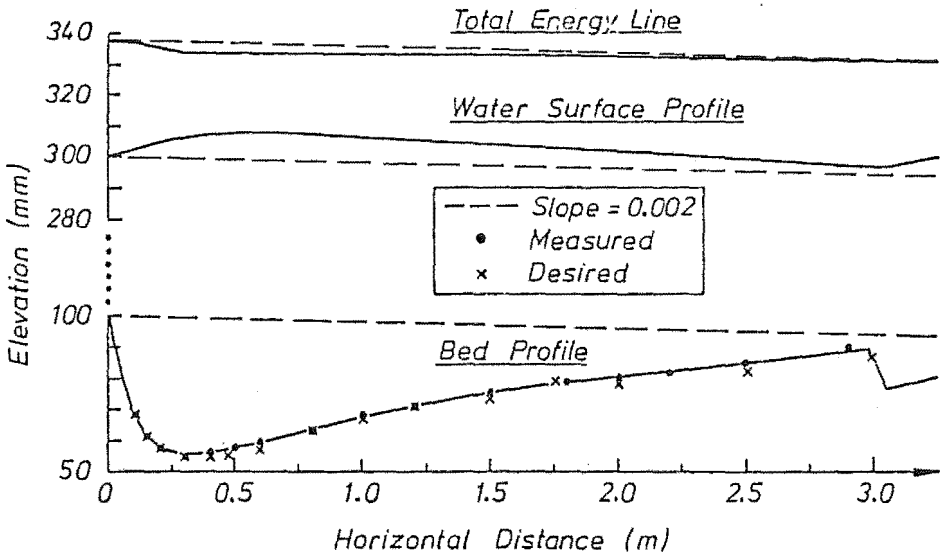

Figure 6.13 Total Energy Line, Water Surface and Bed Profile (After Sutherland (1983))

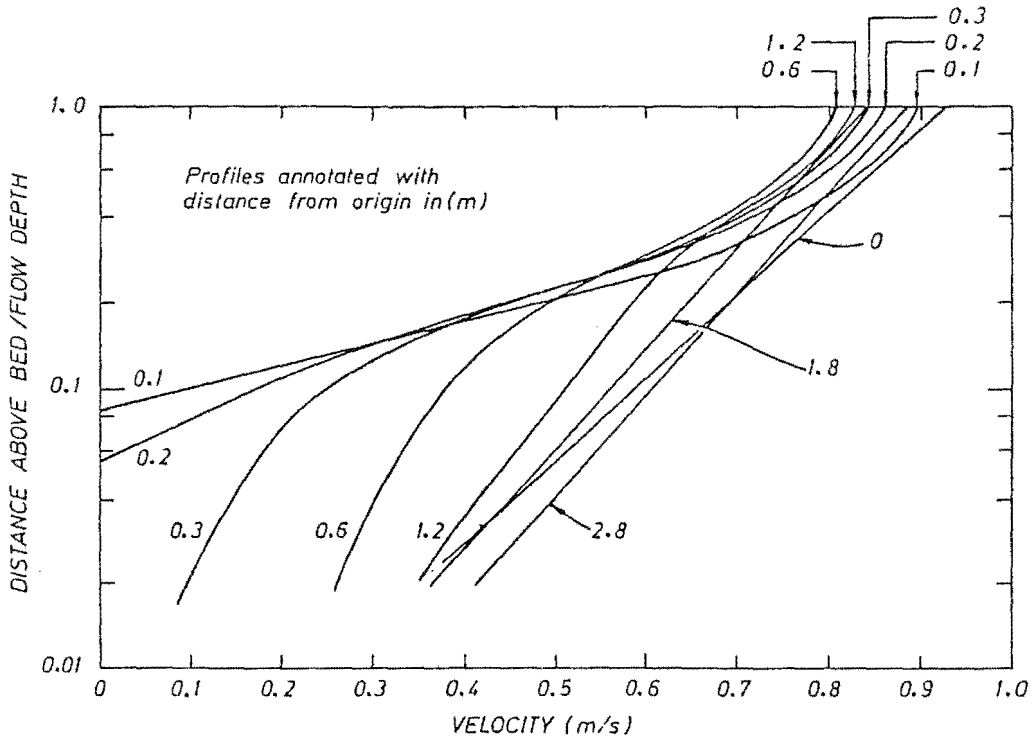

Figure 6.14 Velocity Profiles Within a Scour Hole (After Sutherland (1983))

of various flow and bed properties and on the determination of the temporal and spatial variation of bed resistance within scour holes (Section 7.3.3). The last requirement was indirectly achieved by measuring velocity profiles at two control sections, x = 1.0 m and 2.0 m, at various times during each SC-I run. Velocity profiles, which were measured on the flume centre-line, were also recorded at the end of the fixed upstream bed at x = 0.0 m. Measurements at this section confirmed that the flow was fully developed at the start of the test reach.

To collect all the required data during an SC-I run it was necessary to complete the measurement of each set of three velocity profiles within 10 minutes. With the bed continually degrading the readings had to be taken as swiftly as possible. However the velocity probe readings fluctuated as turbulent eddies passed the probe, thus an "average" reading could only be obtained after a reasonable length of time. As a compromise each reading of time-averaged velocity was estimated from the fluctuating readings given by the velocity probe over a 10-20 second period. Error bands associated with this measurement technique are included with all velocity profile plots. A representative set of centre-line velocity profile measurements is given in Fig. 6.12, where the elevation of a point above the bed was nondimensionalised using the centre-line flow depth at that section at that time.

It has been demonstrated, Raudkivi (1965) and Sutherland (1983), that velocity profiles deep within a scour hole are not fully logarithmic but that this state is approached as the flow travels downstream. This behaviour is demonstrated in Fig. 6.14 for the scour hole geometry given in Fig. 6.13 and is exhibited by the data presented in Fig. 6.12. Bed shear velocities were calculated by fitting a logarithmic profile to the lower section of each velocity profile and determining the corresponding bed shear velocity, u_{*_b}.

Although velocity profiles within a scour hole are not logarithmic it was considered that this method gave the best possible estimates of the temporal and spatial variation of bed shear velocity.

6.2.6 Bed Roughness

Assuming that Manning's equation holds (Eq. 5.26), bed roughness values were obtained, using average flow properties from

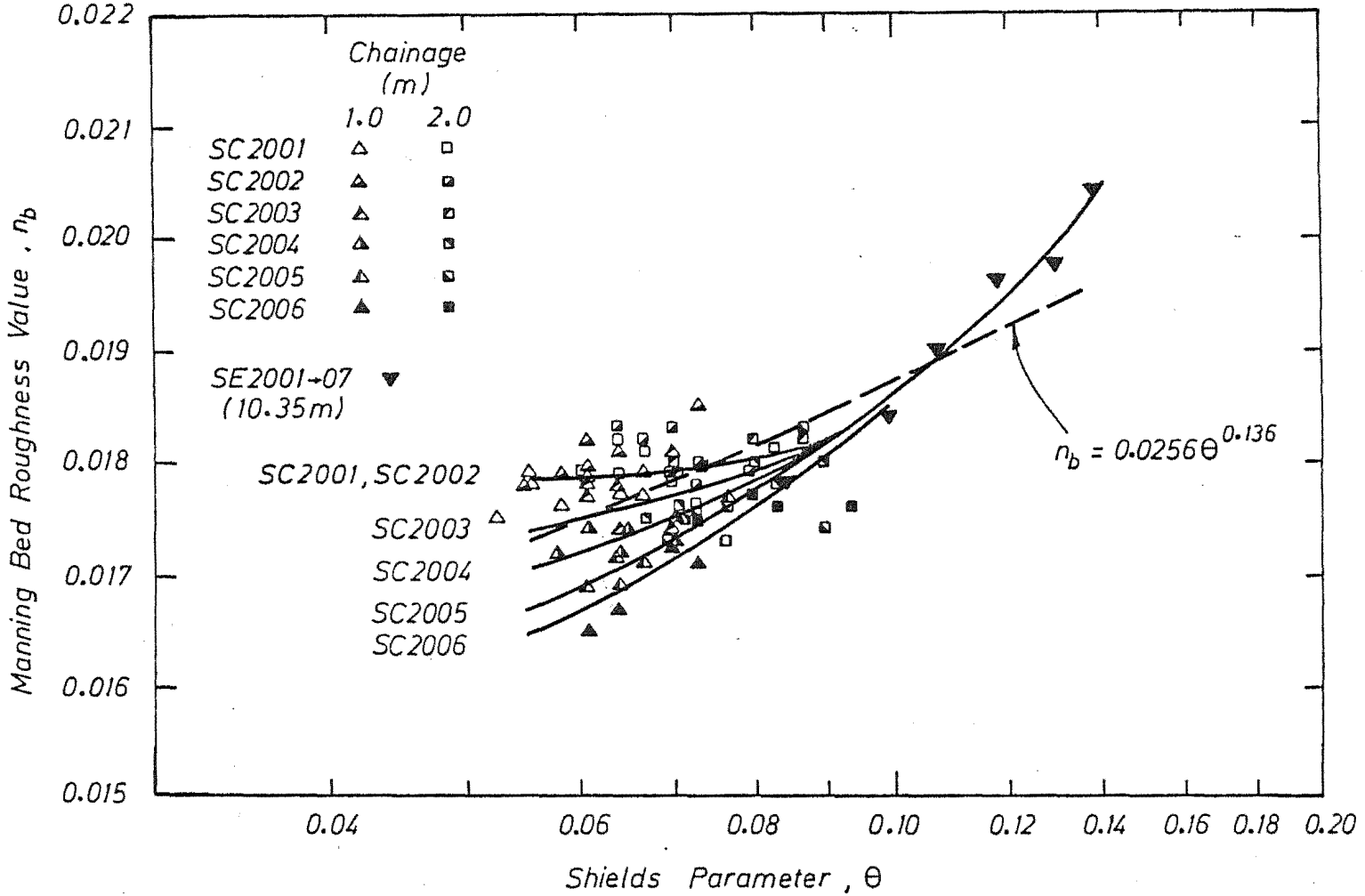

Figure 6.15 Bed Roughness Value Against Shields Parameter.

$$n_b = \frac{u_{*_b} R_b^{1/6}}{\sqrt{g}U} \qquad (6.3)$$

where all terms are as previously defined.

The bed roughness values obtained in this manner and the curves fitted to this data are plotted in Fig. 6.15 and presented in Appendix D. Values of Shields Parameter were calculated from

$$\theta = \frac{u_{*_b}^2}{(S_s - 1) g\, d_{50}} \qquad (6.4)$$

Within the general scour hole defined by the mean surface, Fig. 6.2, there is a variation in bed resistance. Near the point of local maximum scour, bed forms are absent and bed resistance is related only to grain properties. Further downstream, the scour hole becomes shallower, bed forms develop and the total bed resistance increases. This general trend is evident in Fig. 6.15.

In Fig. 6.15, a single curve could not be fitted to the data. This was unexpected in view of the general resistance relation determined in Section 5.4.3.

$$n_b = 0.0256\, \theta^{0.136} \qquad (6.5)$$

which is also shown in Fig. 6.15.

Separate curves were fitted to each set of data. The divergence of these curves at low values of Shields Parameter is considered to reflect the influence of side-walls on the geometry of scour holes.

At low discharges, the geometry of the shallow scour holes which develop is significantly influenced by the side-walls. Whereas, at higher discharges, the geometry of the deeper scour holes which form is less influenced by the side-walls. This effect is demonstrated by the discharge related values of centre-line bed elevation corrections which were applied to the data in Section 10.3.3. Hence, the data presented in Fig. 6.15 indicate that within the scour hole the overall roughness of a laterally curved bed is greater than that of a laterally plane bed at the same average bed elevation.

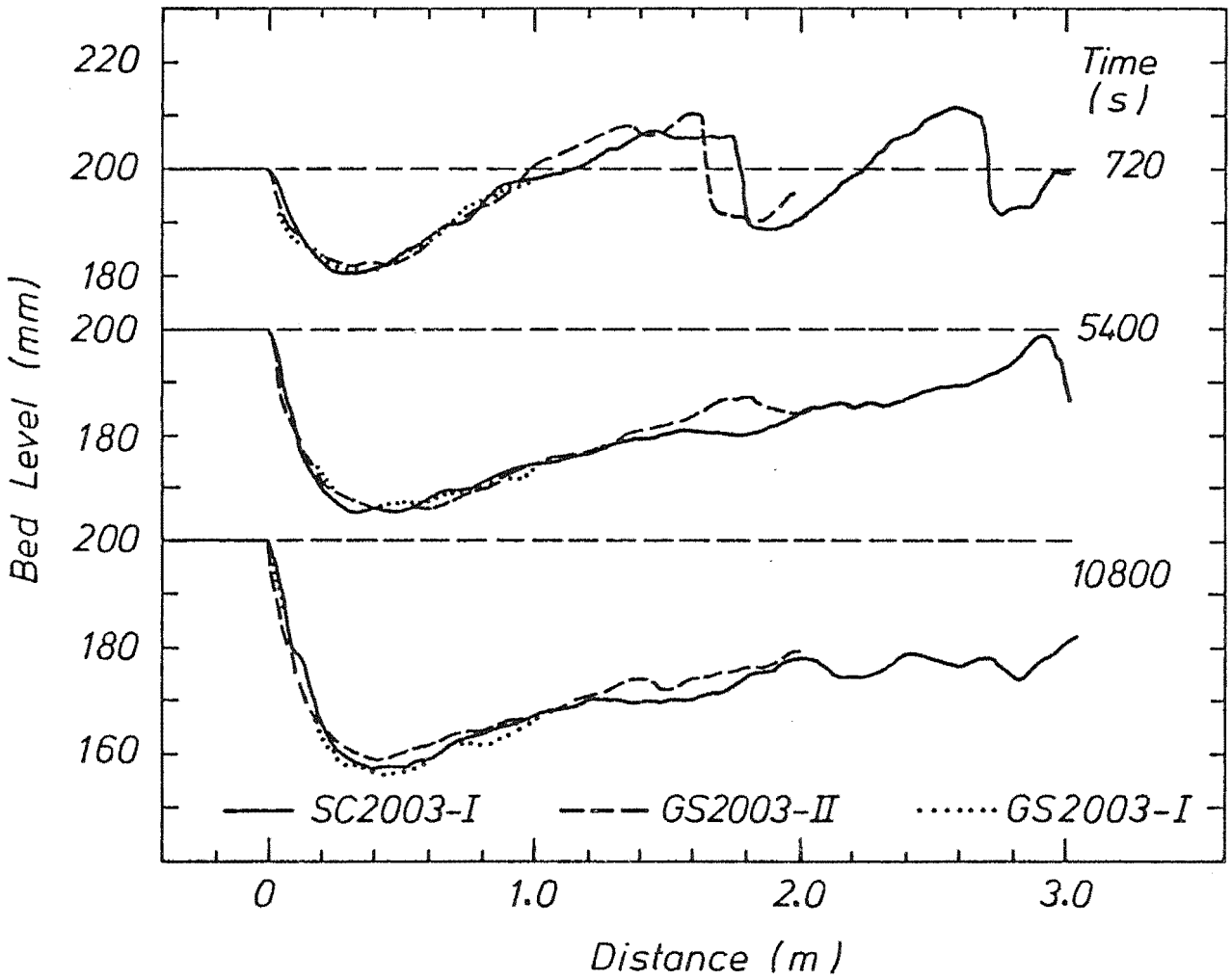

Figure 6.16 Centre-Line Scour Hole Profiles (Runs SC2003-I, GS2003-II, GS2003-I)

6.3 STEPPED DISCHARGE - NON-EQUILIBRIUM TRANSPORT (GS Series)

The aim of these experiments was to measure the temporal variation of bedload transport at two sections within previously measured scour holes. The GS-I series of experiments measured bedload transport rates at the section x = 1.0 m, while the GS-II series of experiments measured bedload transport rates at the section x = 2.0 m. The discharges studied in these experiments were the same as those studied in the SC series of runs (Table 6.1). The longitudinal and lateral geometry of the scour holes was also recorded. Observations and results from these series of experiments are presented and dicussed below. Full results are presented in Volume II.

6.3.1 Observations

During all runs the same flow and bed behaviour as that noted in the SC series of experiments was observed. Thus, the observations presented in detail in Section 6.2.1 apply also to these series of experiments.

The geometry of the bedload collector grill had some effect on the lateral profile of the bed near the end of the test reach. The upstream face of the collector was horizontal, so sediment banked against the side-walls near the end of the test reach was swept into the bedload collector. Thus, the lateral bed profile at the end of the test reach was horizontal. However, the effect the difference between this lateral profile and the curved lateral profile, which was measured in the parent SC-I runs, had on the measured values of bedload transport rate was considered to be negligible.

6.3.2 Scour Hole Profiles

The aim of measuring bedload transport rates within a previously measured scour hole was achieved by replicating the scour hole measured during a given SC-I run, within the shortened reach, at all times. Examples of the replication of scour holes for comparable runs at various times are given in Fig. 6.16.

The degree to which scour holes were being replicated was monitored continually throughout each run. The maximum scour depth was measured often and compared with the expected values i.e. those which had previously been determined from the parent SC-I run. If the measurements diverged from the expected values then the flow depth was

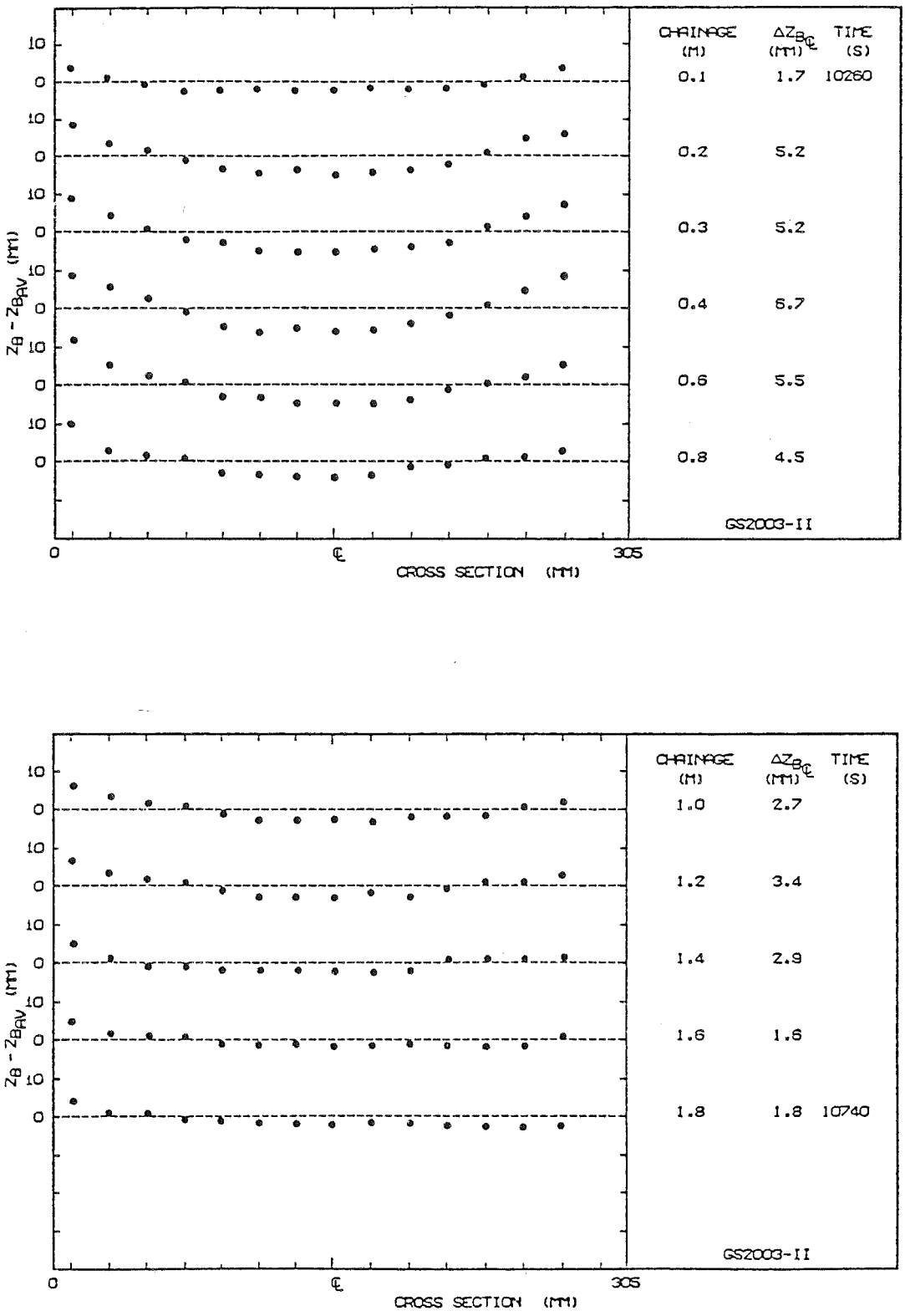

Figure 6.17 Typical Lateral Bed Profiles (Run GS2003-II)

adjusted until the readings converged again; the flow depth was controlled by adjusting the height of the downstream weir gate. The geometry of the scour hole was also controlled by the predetermined movements of the bedload collector grill (Section 4.4.3). Using these techniques the discrepancy between the actual and expected values of the maximum scour depth at any time was no greater than $\pm$ 2 mm, or one grain diameter.

The lateral profile of the bed at various sections within the scour hole was also measured at the end of each run, which added to the information on the three-dimensional geometry of the scour holes already obtained during the SC-I series of experiments. A typical set of lateral bed profile measurements is given in Fig. 6.17. These results demonstrate the significant effect of the side-walls on the geometry of the scour hole.

Using the measurements of longitudinal and lateral bed profiles, at the end of a run, it was possible to calculate a value of the total sediment yield and to compare this with the actual weighed sediment yield. Calculated values of total sediment yield were within $\pm$ 5% of actual yield values and were an extra check on results obtained from the bedload measuring devices.

6.3.3 Bedload Transport Rates

For each run, the cumulative sediment mass versus time curve, provided by the bedload collection system, was analysed in the manner previously described (Appendix B) and the variation of the instantaneous smoothed bedload transport rate with time obtained. This analysis gave the time history of the bedload transport rates at sections within developing scour holes. Examples of the variation of bedload transport rate with time are given in Figs. 6.18 and 6.19.

The effect of bed forms on the bedload transport rate is apparent in these plots. Bed forms were observed to develop in the test reach in response to the imposed flow conditions (Fig. 6.16) and to propagate downstream with time. The entrapment of bed forms in the collection system is reflected as early local peaks in the bedload transport records (Figs. 6.18 and 6.19). When the final bed form is swept out of the test reach and trapped in the bedload collector a concurrent maximum rate of bedload transport is observed. From this time onwards the scour hole completely occupies the test reach and

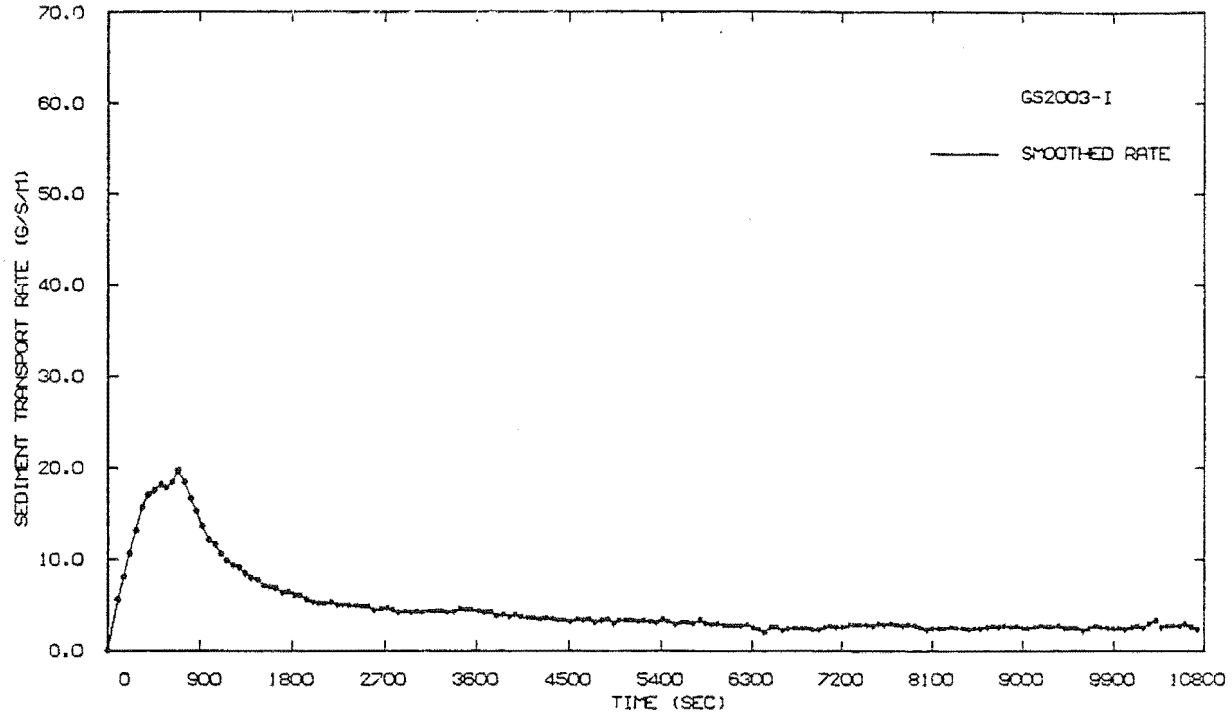

Figure 6.18 Sediment Transport Rate Against Time (Run GS2003-I)

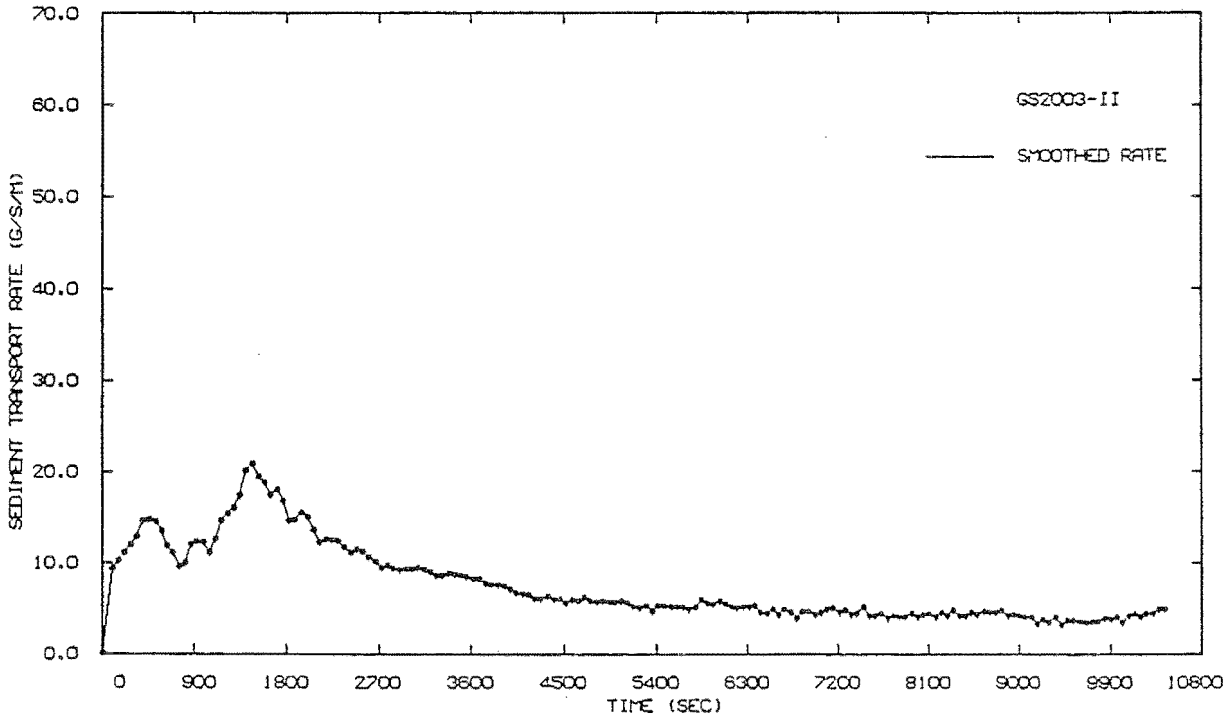

Figure 6.19 Sediment Transport Rate Against Time (Run GS2003-II)

consequently the rate of bedload transport declines and no further sharp peaks occur. Hence, it would appear from the bedload transport records that two, or possibly three, bed forms developed during a typical GS-II run (Fig. 6.19) but that only a single bed form developed in a typical GS-I run; an occurrence already noted from the bed profile records.

These plots of smoothed bedload transport rate against time were used to determine rates of bedload transport, at scouring sections, when values of the spatial lag coefficient were calculated (Section 7.3.2).

6.4 SUMMARY

Seven series of experiments were conducted to investigate spatial lag effects (Series SC-I, GS-I and GS-II) and temporal lag effects (Series SC-I, II, III, IV and V). In all these experiments the upstream sediment boundary conditions were constrained by the presence of a fixed bed and zero sediment injection at the upstream end of the test reach. Non-steady flow conditions were of the form given by an inclined step change in discharge from threshold conditions.

Observations and examples of measurements taken in these series of experiments were presented. The specific manner in which the data collected during these experiments were used in the analysis of spatial and temporal lag effects are presented in Chapters 7 and 8 respectively.

Chapter 7 | Spatial Lag Analysis

7.1 INTRODUCTION

Numerical models used to route sediment in alluvial channels normally assume that the sediment transport capacity is satisfied instantaneously at every point in time and space. However, when "constrained" sediment transport boundary conditions are encountered the transport capacity of the flow can not be satisfied everywhere. An equation which recognises this effect is the spatial lag equation, given by

$$(1 - \lambda') \frac{\partial A_b}{\partial t} = C_{SL}(G_V - G_{VC}) \qquad (7.1)$$

where A_b = Area of scour or deposition at a section,
C_{SL} = Spatial lag coefficient (dimension $(\text{Length})^{-1}$),
G_V = Total sediment transport rate, by volume,
G_{VC} = Total sediment transport capacity, by volume, and
λ' = Bed porosity.

A functional relation for the spatial lag coefficient, C_{SL}, was derived by Wellington (1978) using Einstein's (1950) formulation of a bedload transport equation. Wellington (1978) found that

$$C_{SL} = \frac{(1 - p)}{\lambda d_{50}} \qquad (7.2)$$

where d_{50} = Median grain size,
p = Einstein's probability of erosion, and
λ = Step length constant.

The derivations of this expression and of an alternative expression based on Yalin's (1972) analysis of Einstein's (1950) formulation are presented herein.

Two of the aims of the experimental programme were to test the validity of both the proposed spatial lag equation and the theoretical relation for the spatial lag coefficient. These aims were achieved by determining values of the spatial lag coefficient and comparing these with values calculated from theoretical relations. To determine values of the spatial lag coefficient it was necessary to

- Measure $\frac{\partial A_b}{\partial t}$ (SC-I series)
- Measure G_V (GS series)
- Determine G_{VC}

} At selected sections

In order to measure each individual term, it was necessary to consider sections at which strong aggradation or degradation occurred. At such sections the sediment transport rate and sediment transport capacity are <u>not</u> equal. The case studied in the SC-I series of experiments (Section 6.2) was that of bed degradation due to the development of a scour hole downstream of a fixed bed. Two control sections were selected within these scour holes. These sections were located 1.0 m and 2.0 m downstream of the fixed bed, respectively.

Measurements were taken of the temporal variation of the flow properties, bed elevation and bedload transport rate at these sections under a variety of flow rates. Typical measurements at these sections were presented and discussed in Chapter 6. Having obtained values of each of the three required terms from the measurements, values of the spatial lag coefficient were obtained by substituting these terms in a re-arranged form of spatial lag equation, Eq. 7.1, given by

$$C_{SL} = \frac{(1 - \lambda') \frac{\partial A_b}{\partial t}}{(G_V - G_{VC})} \qquad (7.3)$$

Values of the spatial lag coefficient obtained in this manner and their comparison with values obtained from theoretical relations are presented and discussed.

7.2 THEORETICAL RELATIONS

Wellington (1978) developed a theoretical relation for the spatial lag coefficient for bedload conditions from the Einstein (1950) formulation of a bedload transport relation. Wellington's (1978) development of this relation is presented below. Also presented is a

second relation which was developed from the critical analysis presented by Yalin (1972) of Einstein's (1950) formulation.

7.2.1 Sediment Erosion

The number of particles eroded from a reach of unit area per unit time is

$$N_e = \frac{i_b p}{A_1 d^2 t_1} \tag{7.4}$$

where the exchange time, t_1, is given by

$$t_1 = A_3 \sqrt{\frac{d}{g}\left(\frac{\rho_w}{\rho_s - \rho_w}\right)} \tag{7.5}$$

and A_1 = Constant of grain area,
A_3 = An exchange time constant,
d = Representative grain diameter,
i_b = Fraction of bed area covered by a particular grain size,
p = Probability of a particle being eroded, and

The total volume of bed material eroded per unit area per unit time, V_e, obtained by substituting Eq. 7.5 into Eq. 7.4 and multiplying by grain volume, is

$$V_e = \frac{i_b p A_2 d^3}{A_1 d^2 A_3} \sqrt{\frac{g(S_s - 1)}{d}}$$

$$= i_b p d \frac{A_2}{A_1 A_3} \sqrt{\frac{g(S_s - 1)}{d}} \tag{7.6}$$

where A_2 = Constant of grain volume.

To express V_e in terms of bed elevation changes, the porosity of the bed material, λ', must be incorporated, hence

$$\left.\frac{\partial Z_b}{\partial t}\right|_e = - \frac{i_b p d}{(1 - \lambda')} \frac{A_2}{A_1 A_3} \sqrt{\frac{g(S_s - 1)}{d}} \tag{7.7}$$

where $\left.\frac{\partial Z_b}{\partial t}\right|_e$ = Time rate of change of bed elevation due to erosion.

7.2.2 Sediment Deposition

The number of particles deposited in a reach of unit area per unit time is

$$N_d = \frac{i_B g_s}{\rho_s \mu_x A_2 d^3} \tag{7.8}$$

where g_s = Total mass transport per unit width in the bed layer,

i_B = Fraction of total bedload of a particular size fraction, and

μ_x = Average step length.

The volume of sediment deposited per unit area and time, V_d, is therefore

$$V_d = \frac{i_B g_s}{\rho_s \mu_x} \tag{7.9}$$

Expressing this in terms of local bed elevation changes

$$\left.\frac{\partial Z_b}{\partial t}\right|_d = \frac{i_B g_s}{\rho_s (1 - \lambda') \mu_x} \tag{7.10}$$

where $\left.\frac{\partial Z_b}{\partial t}\right|_d$ = Time rate of change of bed elevation due to deposition.

Alternatively

$$\left.\frac{\partial Z_b}{\partial t}\right|_d = \frac{G_V}{(1 - \lambda') B_w \mu_x} \tag{7.11}$$

where $G_V = B_w g_s / \rho_s$

= Volume transport rate of a particular sediment size in the bed layer, and

B_w = Channel bottom width.

Einstein (1950) assumed that the particles move with small steps of fixed length, L_s, given by

$$L_s = \lambda d \tag{7.12}$$

and where λ is a constant. Einstein proposed the value of λ to be 100.

Since the eroding probability is p everywhere, the step length is distributed with

$$P[x = i\lambda d] = (1 - p)p^{i-1}, \quad i = 1, 2, 3, \ldots. \tag{7.13}$$

and has a mean given by

$$\mu_x = \sum_{i=1}^{\infty} (i\lambda d)\ (1 - p)p^{i-1} = \frac{\lambda d}{(1 - p)} \tag{7.14}$$

Thus, Eq. 7.11 becomes

$$\left.\frac{\partial Z_b}{\partial t}\right|_d = \frac{G_V(1 - p)}{(1 - \lambda')B_w \lambda d} \tag{7.15}$$

7.2.3 Nett Sediment Erosion/Deposition

By combining Equations 7.7 and 7.15 a relation for the nett erosion or deposition at the bed may be derived.

Thus, for bedload

$$\frac{\partial Z_b}{\partial t} = \frac{(1 - p)}{(1 - \lambda')B_w \lambda d}\left[G_V - \frac{i_b p}{(1 - p)}\frac{\lambda A_2}{A_1 A_3} B_w \sqrt{(S_s - 1)gd^3}\right] \tag{7.16}$$

where the right hand term in Eq. 7.16 is Einstein's volumetric transport capacity for a particular sediment size, G_{VC}, under equilibrium conditions. Such an expression for equilibrium transport capacity was found by assuming that equilibrium conditions exist when the nett erosion/deposition is zero. Rearranging Eq. 7.16 and noting that

$$\frac{\partial A_b}{\partial t} = B_w \frac{\partial Z_b}{\partial t} \tag{7.17}$$

gives

$$(1 - \lambda')\frac{\partial A_b}{\partial t} = \frac{(1 - p)}{\lambda d}(G_V - G_{VC}) \tag{7.18}$$

Thus, the rate of change of bed area at a section is proportional to the difference between the actual transport rate and transport capacity and from Eq. 7.1 the spatial lag coefficient, C_{SL}, is given by

$$C_{SL} = \frac{(1 - p)}{\lambda d} = \frac{1}{\mu_x} \tag{7.19}$$

In terms of mass transport rate per unit width, Eq. 7.18 becomes

$$(1 - \lambda')\frac{\partial A_b}{\partial t} = C_{SL}\frac{B_w}{\rho_s}(g_s - g_{sc}) \tag{7.20}$$

An alternative expression for the spatial lag coefficient can also be derived from the critical analysis of Einstein's (1950) formulation presented by Yalin (1972). Three main points were raised by Yalin (1972). They were that

- Einstein (1950) incorrectly defined the lower limit of the integral expression used to obtain the probability of erosion, p, and that in fact the correct lower limit is $-\infty$;

- The exchange time, assumed by Einstein (1950) to be a function of the time of the grain, d/w, is in fact a function of the time of the flow, d/u_*. Yalin (1972) concluded this from an analysis of the detachment of individual grains due to turbulent fluctuations; and
- For the case of rough turbulent flow and for grain motion in the vicinity of the bed that the average step length is given by

$$\mu_x = \alpha_L \theta' d \tag{7.21}$$

It is not totally clear from Yalin's (1972) presentation whether he proposed that the average step length is a function of bed related flow properties i.e. θ or that it is a function of grain related flow properties i.e. θ'. However, after Yalin (1972) had formulated a new transport relation using the approach of Einstein (1950), he fitted this relation to the same data that Einstein (1950) used to calibrate his transport relation. Since Einstein (1950) used grain related flow properties when calculating flow intensity values, it was assumed, by implication, that Yalin (1972) adopted the same approach. Hence, the average step length is defined in Eq. 7.21 as a function of grain Shields Parameter.

More recently, Phillips (1981) found that near threshold conditions the average step length was more accurately described by the relation

$$\mu_x = \alpha_L(\theta' - \theta'_c)d \tag{7.22}$$

where θ' = Grain Shields Parameter, and
θ'_c = Critical grain Shields Parameter.

At large values of Shields Parameter, Eq. 7.22, reduces to the expression proposed by Yalin (1972). From Eqs. 7.19 and 7.22, an alternative equation for the spatial lag coefficient is

$$C_{SL} = \frac{1}{\alpha_L(\theta' - \theta'_c)d} \tag{7.23}$$

Two different theoretical relations for the spatial lag coefficient have now been derived using the approach of Einstein (1950) i.e. considering that the rate of sediment transport is a function of the nett erosion/deposition at a section.

7.3 SPATIAL LAG EQUATION - INDIVIDUAL TERMS

Values of the spatial lag coefficient were obtained by substituting measured and calculated values of the various terms into a re-arranged form of the spatial lag equation, Eq. 7.1, where

$$C_{SL} = \frac{(1 - \lambda') \frac{\partial A_b}{\partial t}}{(G_V - G_{VC})} \tag{7.24}$$

Substituting Eq. 7.17 into Eq. 7.24, and noting that

$$G_V = \frac{B_w g_s}{\rho_s} \tag{7.25}$$

and

$$G_{VC} = \frac{B_w g_{sc}}{\rho_s} \tag{7.26}$$

gives

$$C_{SL} = \frac{\rho_s (1 - \lambda') \frac{\partial z_b}{\partial t}}{(g_s - g_{sc})} \tag{7.27}$$

where g_s = Bedload <u>mass</u> transport rate per unit width, and
g_{sc} = Bedload <u>mass</u> transport capacity per unit width.

Spatial lag coefficients were calculated by substituting measured or calculated values of each term, at various times, into Eq. 7.27.

An initial analysis of the values of the spatial lag coefficients obtained, in this manner, from the data collected at the two control sections (x = 1.0 m and 2.0 m) was conducted. The comparison of this data with the theoretical relations was unable to clearly establish the validity of either relation due to the narrow range of flow conditions, as given by Shields Parameter, which were encountered at these sections. Consequently, values of each of the required terms were obtained at two further sections, x = 0.6 m and 3.0 m.

The manner in which each term was obtained, at all four sections, is presented below. All values of individual terms used in the spatial lag analysis are presented in Appendix D.

7.3.1 <u>Scour Rates</u>

The measured rate of scour at a section, at any given time, was obtained from the bed profiles recorded during each SC-I run, thus

$$\frac{\partial Z_b}{\partial t} = \frac{\Delta Z_{b_{AV}}}{\Delta t} \tag{7.28}$$

where $Z_{b_{AV}}$ = The average bed elevation at a section.

The average bed elevation at a section was obtained by correcting the measured value of the centre-line bed elevation for side-wall effects, thus

$$Z_{b_{AV}} = Z_{b_{\mathbb{Q}}} = \Delta Z_{b_{\mathbb{Q}}} \tag{7.29}$$

Typical measured values of the centre-line bed elevation correction, $\Delta Z_{b_{\mathbb{Q}}}$, for the sections x = 1.0 m and 2.0 m are given in Fig. 6.9. The centreline bed elevation corrections which were applied at the section x = 0.6 m, during each SC-I run, were estimated from the values of the bed corrections measured at the section x = 0.5 m during each SC-I run and the bed correction values measured at the section x = 0.6 m during each GS-I and GS-II run (Figs. 6.9 and 6.17). The centreline bed elevation corrections which were applied at the section x = 3.0 m, during each SC-I run, were estimated from the bed correction values measured at the section x = 2.0 m during each SC-I run.

Values of the rate of scour at a section, at a given time t, were obtained by averaging bed elevation changes over consecutive periods of 1200 seconds, thus

$$\frac{\partial Z_b}{\partial t} = \frac{Z_{b_{AV}}(t + 600) - Z_{b_{AV}}(t - 600)}{1200} \tag{7.30}$$

A period of 1200 seconds was selected for two reasons. Firstly, the low rates of scour which were encountered at the two control sections, typically 0.004 - 0.0015 mm/s, could only be calculated by averaging bed elevation changes over a reasonable length of time. Secondly, velocity profiles and lateral bed profiles were only measured every twenty minutes. Also, at times greater than thirty minutes during an SC-I run, bed and water surface profiles were only measured at ten minute and, at later stages, twenty minute intervals. Hence, at low discharges up to seven values of the scour rate were calculated while the reduced run lengths at higher discharges gave four values.

The calculation of rates of scour at a section did not commence until the scouring process was well established at each section. The times at which readings were obtained are included in the spatial lag

results presented in Appendix D.

The average depth of flow at a section, at each time, was also calculated. Assuming that the water surface elevation, Z, did not vary across the flume at a section, the average flow depth was calculated thus

$$Y = Z_{\text{℄}} - Z_{b_{AV}} \tag{7.31}$$

where Y = Average flow depth,

$Z_{\text{℄}}$ = Water surface elevation, measured at the flume centreline, and

$Z_{b_{AV}}$ = Average bed elevation.

Measured values of the water surface elevation were obtained from the water surface profiles recorded during each SC-I run. Values of the average flow depth were used in the calculation of bedload transport capacity, described in Section 7.3.3.

7.3.2 Bedload Transport Rates

At the two control sections, x = 1.0 m and 2.0 m, the rates of bedload sediment transport at the required times were simply read from the relevant tables (Volume II). At the two extra sections, x = 0.6 m and 3.0 m, the rate of bedload transport was obtained by calculating the change in total volume of bed, over the specified reach length, over time and converting this change in bed volume into an equivalent mass of sediment. The effect of the side-walls on the bed geometry was also accounted for in bed volume calculations. This was achieved by correcting the centre-line bed elevation readings, scaled from the SC-I bed profile records at intervals of 0.1 or 0.2 m, by using the corrections measured in the GS-I and GS-II series as estimates of the bed elevation corrections within the scour hole.

The method used to calculate bedload transport rates was

$$g_s(x_R) = (1 - \lambda')\rho_s \frac{\Delta V_b}{\Delta t} \tag{7.32}$$

where x_R = Reach length, and

V_b = The total volume of bed eroded over the reach, per unit width, from t = 0 to t = t.

The volume of the eroded bed per unit width is given by

$$V_b = B_w \int_0^{x_R} [Z_b(x, 0) - Z_{b_{AV}}(x, t)]dx \qquad (7.33)$$

where $Z_b(x, 0)$ = The elevation of the bed at t = 0, and

$Z_{b_{AV}}(x, t)$ = The average bed elevation at time, t, given by Eq. 7.29.

As before, the changes in bed volume were averaged over 1200 seconds. Thus, Eq. 7.32 becomes

$$g_s(x_R, t) = (1 - \lambda')\rho_s \frac{(V_b(t + 600) - V_b(t - 600))}{1200} \qquad (7.34)$$

Using this method, the bedload transport rate at each required time was calculated for all sections. This allowed calculated values of the rate of bedload transport to be compared with values measured in the GS-I and GS-II series. The agreement between most of these two sets of values was within 10%, which was considered good. However, at the two lowest discharges in the GS-I series the calculated values of bedload transport rate were significantly less than the measured values. From the results of the spatial lag analysis (Appendix D) it would appear that the measured values were higher than expected. This arises from the difficulty of measuring the rate of bedload transport over short reach lengths.

The good agreement between most of the calculated and measured transport rates meant that the calculated bedload transport rates at sections x = 0.6 m and 3.0 m were used with confidence. Although the calculated rates of bedload transport at Stations 1.0 and 2.0 m were similar to the measured transport rates, the measured transport rates were used in the determination of values of the spatial lag coefficient at these two sections simply because these transport rates had been physically measured.

7.3.3 Bedload Transport Capacity

The capacity of the flow to transport sediment as bedload was calculated by inserting instantaneous values of the flow properties into the bedload transport capacity relation obtained under equilibrium conditions, Eq. 5.46. Thus the bedload transport capacity was given by

$$\underset{(g/s/m)}{g_{sc}} = 894\underset{(m/s)}{(U - U_c)}^{2.645} \qquad (7.35)$$

where $$U_c = U \frac{u_{*c}}{u_{*b}}$$

and the various flow properties were determined in the following manner.

The average flow velocity at a section was obtained from

$$U = \frac{q}{Y} \tag{7.36}$$

where the measured average flow depth, Y, was obtained from Eq. 7.31 and the discharge per unit width, q, was measured during each run.

Using Williams (1970) side-wall correction method, the average hydraulic radius of the bed was given by

$$R_b = \frac{Y}{1 + 0.591Y} \tag{7.37}$$

The bed shear velocity was then calculated using Manning's equation, thus

$$u_{*b} = \frac{Un_b\sqrt{g}}{R_b^{1/6}} \tag{7.38}$$

where bed roughness values, n_b, within a scour hole for a given SC-I run were obtained from the relevant curve given in Fig. 6.15. Since the bed roughness value appears in both axes of the plot, bed roughness values were obtained after some trial and error. Further, the curves of bed roughness value against Shields Parameter given in Fig. 6.15, which were obtained from velocity profile readings at x = 1.0 and 2.0 m, were used to determine the bed roughness values at x = 0.6 m and 3.0 m.

Even though the flow conditions within a developing scour hole differed from equilibrium flow conditions e.g. non logarithmic velocity profiles, it was considered that this method could be used to determine values of the bedload transport capacity.

It was found that values of the spatial lag coefficient could not always be calculated in the proposed manner (Appendix D) because occasionally

$$g_s > g_{sc} \tag{7.39}$$

An inequality such as this reflects both the difficulties encountered when measuring transient sediment transport rates and calculating sediment

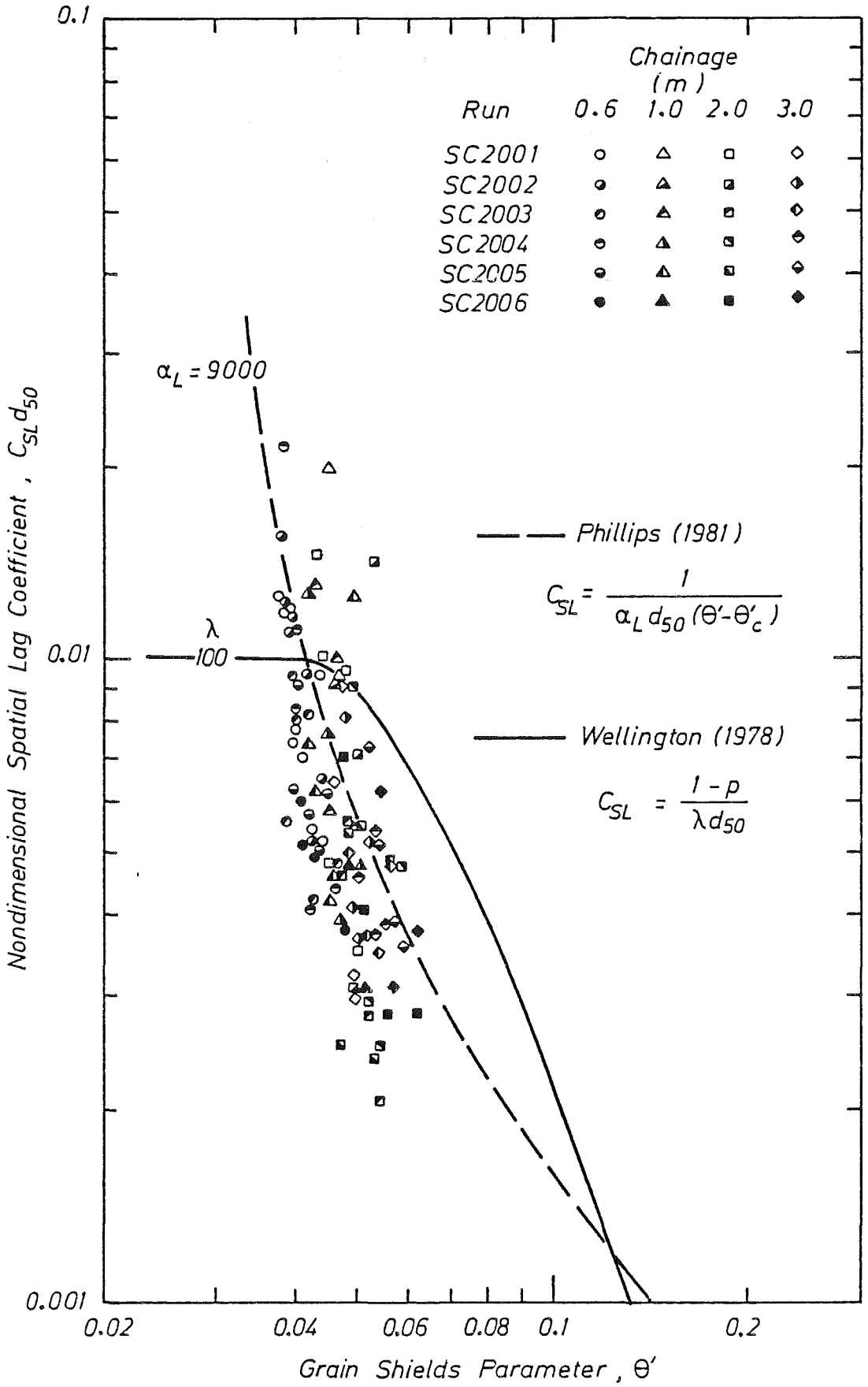

Figure 7.1 Nondimensional Spatial Lag Coefficient Against Grain Shields Parameter

transport capacities within a scour hole.

7.4 SPATIAL LAG COEFFICIENT - RESULTS

Spatial lag effects were analysed by calculating values of the spatial lag coefficient in the manner previously described (Section 7.3). The results of this analysis and their comparison with the theoretical relations are presented below.

7.4.1 Results

The results of the spatial lag analysis are presented in Figs. 7.1 and 7.2 and Appendix D. Nondimensional values of the spatial lag coefficient, $C_{SL}d_{50}$, are plotted against grain Shields Parameter in Fig. 7.1 while, in Fig. 7.2, the same nondimensional values are plotted against Shields Parameter. Also plotted in Figs. 7.1 and 7.2 are curves obtained from the theoretical relations based on the analyses of Wellington (1978) and Phillips (1981).

In terms of grain Shields Parameter, θ', the two relations are given by

$$C_{SL} = \frac{1 - p}{\lambda d_{50}} \tag{7.40}$$

where λ is the Einstein (1950) step length constant and the probability of erosion, p, is given by (Einstein (1950))

$$p = 1 - \frac{1}{\sqrt{2\pi}} \int_{-\infty}^{T'} e^{-t^2/2}\, dt \tag{7.41}$$

where $T' = \frac{B'\psi'}{\eta_o} - \frac{1}{\eta_o}$,

$\eta_o = 0.364$,

$\psi' = \frac{1}{\theta'}$,

$B' = f(Dgr) = 0.07$ for $Dgr \geq 25$, and

Dgr = Nondimensional grain size

$$= \left[\frac{(S_s - 1)g d_{50}^3}{\nu^2}\right]^{1/3};$$

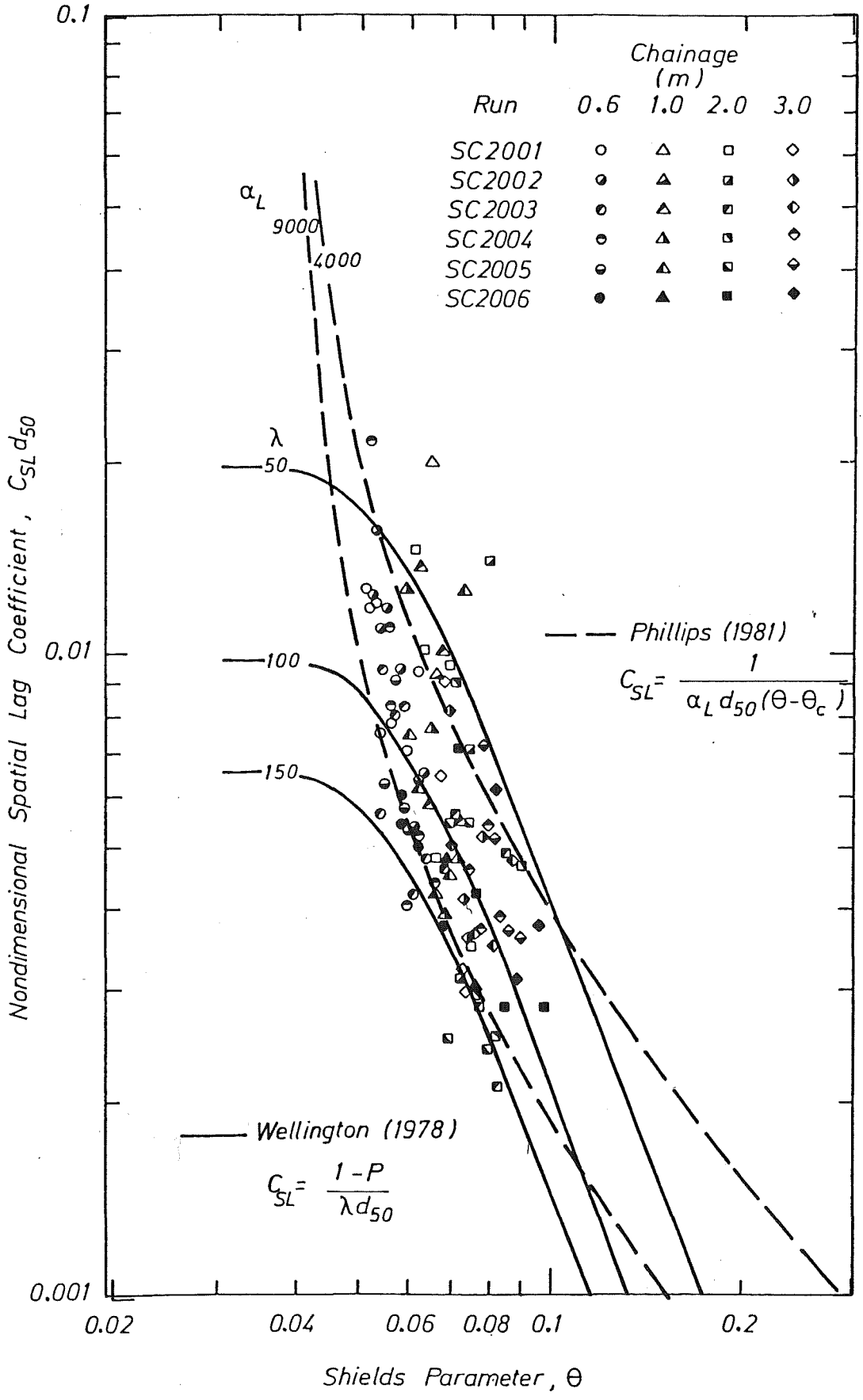

Figure 7.2 Nondimensional Spatial Lag Coefficient Against Shields Parameter.

and $$C_{SL} = \frac{1}{\alpha_L d_{50}(\theta' - \theta'_c)} \tag{7.42}$$

where α_L = A grain step length constant.

With regard to the step length constants, Einstein (1950) stated in his formulation of a sediment transport relation under equilibrium conditions that

$$\lambda = 100 \tag{7.43}$$

and the results of the analysis of mean step length of grains in motion presented by Phillips (1981) indicated that

$$\alpha_L \simeq 9000 \tag{7.44}$$

The use of bed related instead of grain related flow properties in the two theoretical relations was also investigated because of the doubt which surrounded the use of grain related flow properties. In terms of Shields Parameter, θ, the two theoretical relations became

$$C_{SL} = \frac{1 - P}{\lambda d_{50}} \tag{7.45}$$

where $$P = 1 - \frac{1}{\sqrt{2\pi}} \int_{-\infty}^{T} e^{-t^2/2}\, dt,$$

$$T = \frac{B'\psi}{\eta_o} - \frac{1}{\eta_o}, \text{ and}$$

$$\psi = \frac{1}{\theta};$$

and $$C_{SL} = \frac{1}{\alpha_L d_{50}(\theta - \theta_c)} \tag{7.46}$$

The curves plotted in Fig. 7.2 were obtained from Eqs. 7.45 and 7.46 for various values of the appropriate step length constant.

7.4.2 Discussion

The derivation of a relation for the spatial lag coefficient by Wellington (1978) was based on the work of Einstein (1950). A feature of the work of Einstein (1950) was that his sediment transport relation was formulated in terms of grain related flow properties. Similarly, the relation derived from Phillips' (1981) analysis of the mean step

length of grains in motion was also based on grain related flow properties. Consequently, the two relations for the spatial lag coefficient should theoretically be related to such properties.

The results presented in Fig. 7.1 for grain Shields Parameter should, therefore, be in good agreement with the proposed relations given by Eqs. 7.40 and 7.42. The agreement between the data and the Wellington (1978) relation, Eq. 7.40, is very poor. The agreement between the data and the relation based on Phillips' (1981) analysis, Eq. 7.42, is better but still unsatisfactory.

The agreement between the data and the alternative theoretical relations, based on Shields Parameter and given by Eqs. 7.45 and 7.46, shown in Fig. 7.2 is good. In the case of the Wellington (1978) relation, Eq. 7.45, most of the data is bounded by the curved defined by

$$50 < \lambda < 150 \tag{7.47}$$

Such values are not unreasonable since various researchers have reported results from step length studies which gave values of the step length constant ranging from 16 (Fernandez Luque and Van Beek (1976)) up to 200 (Yano, Tsuchiya and Michiue (1969)). A feature of the relation given by Eq. 7.45 is that the spatial lag coefficient approaches a constant value of $1/\lambda d_{50}$ as threshold conditions are approached. This behaviour is not evident in the data.

The data also compares very favourably with the curves given by the Phillips (1981) relation, Eq. 7.46, bounded by

$$4000 < \alpha_L < 9000 \tag{7.48}$$

Instead of predicting constant values of the spatial lag coefficient near threshold conditions this relation predicts values which increase swiftly as threshold conditions are approached. The trend of the data appears to agree with this behaviour.

Both the relations given by Eqs. 7.45 and 7.46 agree well with the data for a range of step length constants. However, it was concluded that the trend of the data was best described by the Phillips (1981) relation given by Eq. 7.46. A further advantage of this relation is its simplicity. Also, the fact that reasonable results were obtained (Fig. 7.2) supports the validity of the proposed spatial lag equation, given by

$$(1 - \lambda') \frac{\partial A_b}{\partial t} = C_{SL}(G_V - G_{VC}) \qquad (7.1)$$

for conditions where a constrained sediment boundary condition causes transient sediment transport rates.

Interestingly, Bennett (1974) stated that the total load spatial lag coefficient is: "probably a strong function of bed sediment fall velocity, mean stream velocity, and depth of flow". The proposed relation for the spatial lag coefficient is a strong function of flow properties and grain size but, in the case of bedload, is unrelated to the fall velocity of the bed material.

Unfortunately, the proposed relation has not been verified over as wide a range of flow conditions as would have been liked. Normally the data of other researchers could be called on but in this case there is no other suitable source of data. Even the data of Bell (1980) could not be used due to the unavailability of water surface elevation data and the lack of lateral bed profile measurements. Additional data could be obtained by conducting similar experiments, to those reported here, for a range of smaller grain sizes or, alternatively, conducting experiments under conditions of sediment overload at the upstream boundary. The majority of bed aggradation experiments reported in the literature only provide data on transient bed profiles with no information on flow depths or transport rates. The few researchers who do report data on the transient sediment discharge obtained these results by determining changes in bed volume from bed profiles. No complete set of data involving measurements of bed profiles, sediment transport rates and flow properties under conditions of sediment overloading appears to be available.

Bell (1980) conducted similar experiments and the results he obtained were simulated using a numerical model (Chapter 9). This model adopts the spatial lag equation which has been verified by this analysis. A comparison of the numerical model results with results obtained from a diffusion model and with Bell's (1980) results is given in Chapter 10.

7.5 SUMMARY

The proposed form of the spatial lag equation was tested by measuring individual terms in the equation and determining values of the spatial lag coefficient. These coefficient values were then compared

with predictions obtained from four theoretical relations. These relations were based on Einstein's (1950) formulation of a sediment transport relation and the results of an analysis of the step length of grains in motion.

In order to measure each individual term in the spatial lag equation, at various sections, it was necessary to consider conditions where strong scour was occurring. The case studied was one of a developing scour hole where the bed degraded swiftly.

Values of each individual term were obtained from the comprehensive set of measurements taken during the SC-I and GS series of experiments. This data base included measurements of the water surface and bed profiles, lateral bed profiles, velocity profiles and rates of bedload transport. Values of the spatial lag coefficient were obtained by substituting measured values of these terms into the spatial lag equation.

It was concluded from a comparison between the data and the various theoretical relations that the spatial lag data was best fitted by the relation given by

$$C_{SL} = \frac{1}{\alpha_L d_{50}(\theta - \theta_c)} \tag{7.42}$$

where the upper and lower bounds of this relation were given by $\alpha_L = 4000$ and $\alpha_L = 9000$ respectively.

It was also concluded that the spatial lag equation

$$(1 - \lambda') \frac{\partial A_b}{\partial t} = C_{SL}(G_V - G_{VC}) \tag{7.1}$$

which is based on accepted sediment transport theory, is valid.

Chapter 8 | Temporal Lag Analysis

8.1 INTRODUCTION

In alluvial streams the sediment transport rate, flow resistance and bed configuration are all integrally linked. The interrelations between them under steady equilibrium flow conditions have been investigated by many researchers.

When the flow is unsteady, however, bed forms do not usually respond instantaneously to the change in flow conditions. If the flow discharge changes rapidly enough, the geometric dimensions of the bed forms are not related to the instantaneous hydraulic conditions because it takes time for the bed forms to change their geometrical properties. Consequently, in the lower flow regime, where dunes are the dominant bed form, the time-lagged development of bed forms under unsteady flow conditions is reflected simultaneously in the time-lagged response of the flow resistance and rate of bedload sediment transport.

Many previous researchers, including Allen (1974), Allen (1976(a)(b)), Fredsφe (1979), Fredsφe (1981) and Nakagawa and Tsujimoto (1983(a)(b)) have concentrated on the time-lagged development of bed forms under unsteady flow conditions. In contrast, the temporal lag study presented herein analyses the time-lagged response of bedload sediment transport to unsteady flow conditions. The temporal development of the flow resistance and bed forms is also indirectly analysed.

Temporal lag effects were investigated experimentally in the SC-I, II, III, IV and V series of runs by recording the temporal variation of bedload sediment transport at the Section x = 9.5 m, located at the downstream end of the test reach (Section 6.2.4). Bed and water surface profiles were also recorded at various times.

A temporal lag scheme which can be applied in a numerical model

is developed and presented below. The performance of this scheme, which was developed by analysing the data collected during the SC-I series of experiments, is evaluated by comparing the sediment hydrographs predicted by the temporal lag scheme with the sediment hydrographs measured during the SC-II, III, IV and V series of experiments.

8.2 TEMPORAL LAG ANALYSIS

The temporal lag analysis presented below is based on an analysis of the bedload sediment hydrographs measured during the SC-I series of experiments.

8.2.1 Data Analysis Method

Two important assumptions were made when analysing the SC-I sediment hydrographs. The first was related to the rate of change of the mean bed elevation at the test section, x = 9.5 m, and the second to the temporal variation of the friction slope at this section.

During the SC-I runs, the constrained sediment boundary conditions caused a scour hole to develop. This scour hole deepened and propagated downstream with time (Fig. 6.5). In the downstream region of the test reach, though, it was noted that the mean bed elevation, if it was changing at all, was decreasing extremely slowly over the first twenty or thirty minutes of a run (see Fig. 6.5). At much later times, the rate of change of the mean bed elevation accelerated rapidly when the scour hole reached this region (Fig. 6.5). Hence, over the initial twenty to thirty minutes of each SC-I run, in which temporal lag effects were analysed, it was assumed that

$$\frac{\partial z_b}{\partial t} \simeq 0 \tag{8.1}$$

Inserting this condition into the spatial lag equation, Eq. 7.1, and substituting Eq. 7.17, gives

$$(1 - \lambda') B_w \frac{\partial z_b}{\partial t} = C_{SL}(G_V - G_{VC}) = 0 \tag{8.2}$$

Hence

$$G_V(t) = G_{VC}(t) \tag{8.3}$$

Alternatively, substituting Eqs. 7.25 and 7.26 into Eq. 8.3 gives

$$g_s(t) = g_{sc}(t) \tag{8.4}$$

which says that the sediment hydrograph is a record of the temporal variation of the bedload transport capacity under unsteady flow conditions.

The second assumption made was that at the test section, x = 9.5 m, that the friction slope was constant, over the same initial twenty to thirty minute period of an SC-I run, and equal to bed slope. Thus

$$S_f = S_o \tag{8.5}$$

It was considered that the manner in which the experiments were conducted, (see Section 4.4.2), simulated this condition at the downstream end of the test reach.

The aim of the analysis presented below is to determine values of a variable which can be used to calculate integrally linked time-lagged values of the flow resistance and sediment transport capacity under unsteady flow conditions. This aim was achieved by analysing the SC-I sediment hydrographs, using relations developed under steady flow conditions, and obtaining values of a new variable, q_e, the equivalent steady flow rate.

At any instant, the equivalent steady flow rate is that flow rate which when inserted into a sediment transport capacity relation, determined under steady flow conditions, gives the same sediment transport capacity as that which occurs under unsteady flow conditions. That is, instantaneous values of the unsteady discharge, q, should not be used with a sediment capacity relation determined under steady flow conditions but rather instantaneous values of the equivalent steady discharge, q_e, must be used.

The following method was used to obtain values of the equivalent steady discharge. The subscript, e, is used to denote an equivalent steady flow variable. Throughout this analysis, the friction slope, S_f, which occurs under unsteady flow conditions is assumed to also apply under equivalent steady flow conditions.

From Eq. 8.4, the bedload transport rate is given by

$$g_s = g_{sc} \tag{8.6}$$

and, from Eq. 5.46 and using equivalent steady flow variables

$$g_{sc} = 894(U_e - U_{c_e})^{2.645} \tag{8.7}$$

where, in terms of equivalent flow properties

$$U_e = \frac{R_{b_e}^{2/3} S_f^{1/2}}{n_{b_e}} \tag{8.8}$$

$$U_{c_e} = U_e \frac{u_{*_c}}{u_{*_{b_e}}} \tag{8.9}$$

and

$$u_{*_{b_e}} = \sqrt{g R_{b_e} S_f} \tag{8.10}$$

Substituting Eqs. 8.7 - 8.10 into Eq. 8.6 and re-arranging, gives

$$\left(\frac{g_s}{894}\right)^{1/2.645} = \frac{R_{b_e}^{2/3} S_f^{1/2}}{n_{b_e}} - \frac{R_{b_e}^{1/6} u_{*_c}}{\sqrt{g}\, n_{b_e}} \tag{8.11}$$

The Manning roughness value was assumed to be given by (Section 5.4.2, Eq. 5.40)

$$n_{b_e} = \alpha_n \theta_e^{\beta_n} \tag{8.12}$$

where

$$\theta_e = \frac{R_{b_e} S_f}{(S_s - 1) d_{50}} \tag{8.13}$$

Thus, from Eqs. 8.12 and 8.13

$$R_{b_e} = \alpha_1 \frac{n_{b_e}^{\beta_1}}{S_f} \tag{8.14}$$

where

$$\alpha_1 = \frac{(S_s - 1) d_{50}}{\alpha_n^{\beta_1}} \tag{8.15}$$

and

$$\beta_1 = 1/\beta_n \tag{8.16}$$

Substituting Eq. 8.14 into Eq. 8.11 gives

$$\frac{\alpha_1^{2/3}}{S_f^{1/6}} n_{b_e}^{2\beta_1/3 - 1} - \frac{\alpha_1^{1/6} u_{*_c}}{S_f^{1/6}\sqrt{g}} n_{b_e}^{\beta_1/6 - 1} - \left(\frac{g_s}{894}\right)^{1/2.645} = 0 \tag{8.17}$$

or, alternatively

$$a_1 n_{b_e}^{b_1} + a_2 n_{b_e}^{b_2} + a_3 = 0 \qquad (8.18)$$

where

$$\left.\begin{aligned} a_1 &= \alpha_1^{2/3} / S_f^{1/6} \\ a_2 &= \frac{-\alpha_1^{1/6} u_{*c}}{S_f^{1/6} \sqrt{g}} \\ a_3 &= -\left(\frac{g_s}{894}\right)^{1/2.645} \\ b_1 &= \frac{2\beta_1}{3} - 1 \end{aligned}\right\} \qquad (8.19)$$

and

$$b_2 = \frac{\beta_1}{6} - 1$$

In the experimental programme, the bed material properties and coefficients which were obtained from analyses of steady flow data were

	Section
$S_s = 2.65$, $d_{50} = 0.0018$ m	3.5
$u_{*c} = 0.337$ m/s	5.3
$\alpha_n = 0.0256$, $\beta_n = 0.136$	5.4

For $S_f = 0.002$ and the above values, Eq. 8.18 becomes

$$3.696 \times 10^6 \, n_{b_e}^{3.902} - 1.026 \, n_{b_e}^{0.2255} - 0.0766 \, g_s^{0.3781} = 0 \qquad (8.20)$$

Thus, for a given value of the bedload transport rate, g_s, Eq. 8.20 can be solved for n_{b_e}, the equivalent steady flow value of Manning roughness. An iterative Newton-Raphson procedure was used to solve Eq. 8.20.

The equivalent steady flow rate can now be found. Substituting the equivalent steady flow hydraulic radius of the bed, R_{b_e}, obtained from Eq. 8.14 into the side-wall correction formula allows the equivalent steady flow depth, Y_e, to be calculated. Hence, from Eq. 5.3

$$Y_e = \frac{R_{b_e}}{1 - 0.591\ R_{b_e}} \tag{8.21}$$

or, alternatively, from Eq. 5.7 for $0.076 < R_{b_e} < 0.24$

$$Y_e = 1.3\ R_{b_e}^{1.086} \tag{8.22}$$

From flow continuity and Manning's equation, Eq. 8.8, the equivalent steady discharge per unit width is

$$q_e = \frac{Y_e R_{b_e}^{2/3} S_f^{1/2}}{n_{b_e}} \tag{8.23}$$

Nondimensional values of the equivalent steady discharge per unit width were also calculated, using the following relation

$$q_R = \frac{q_e - q_b}{q_{max} - q_b} \tag{8.24}$$

where (Fig. 8.1)

q_b = Base discharge = 0.0348 $m^3/s/m$ (Section 5.3.3),

q_{max} = Maximum or peak discharge for a given run, and

q_R = Excess discharge ratio.

The method outlined above was used to analyse each SC-I sediment transport hydrograph over the first twenty to thirty minutes of each run and to obtain the temporal variations of the equivalent steady flow Manning roughness, n_{b_e}, and the equivalent steady flow rate, q_e. These equivalent steady flow hydrographs, which were nondimensionalised using Eq. 8.24, were then used to develop a temporal lag model which is able to predict temporally lagged values of bedload transport capacity and bed roughness. This scheme is outlined in the following sections.

8.2.2 Impulse Response Model

When, in an alluvial stream, the flow discharge changes rapidly enough the bed forms, flow resistance and sediment transport rate are unable to keep pace with the rate of change of energy supply and a new equilibrium state is only reached at some later time. This is particularly apparent when an instantaneous step discharge, an impulse, is applied. In the SC-I series of experiments, which simulated a

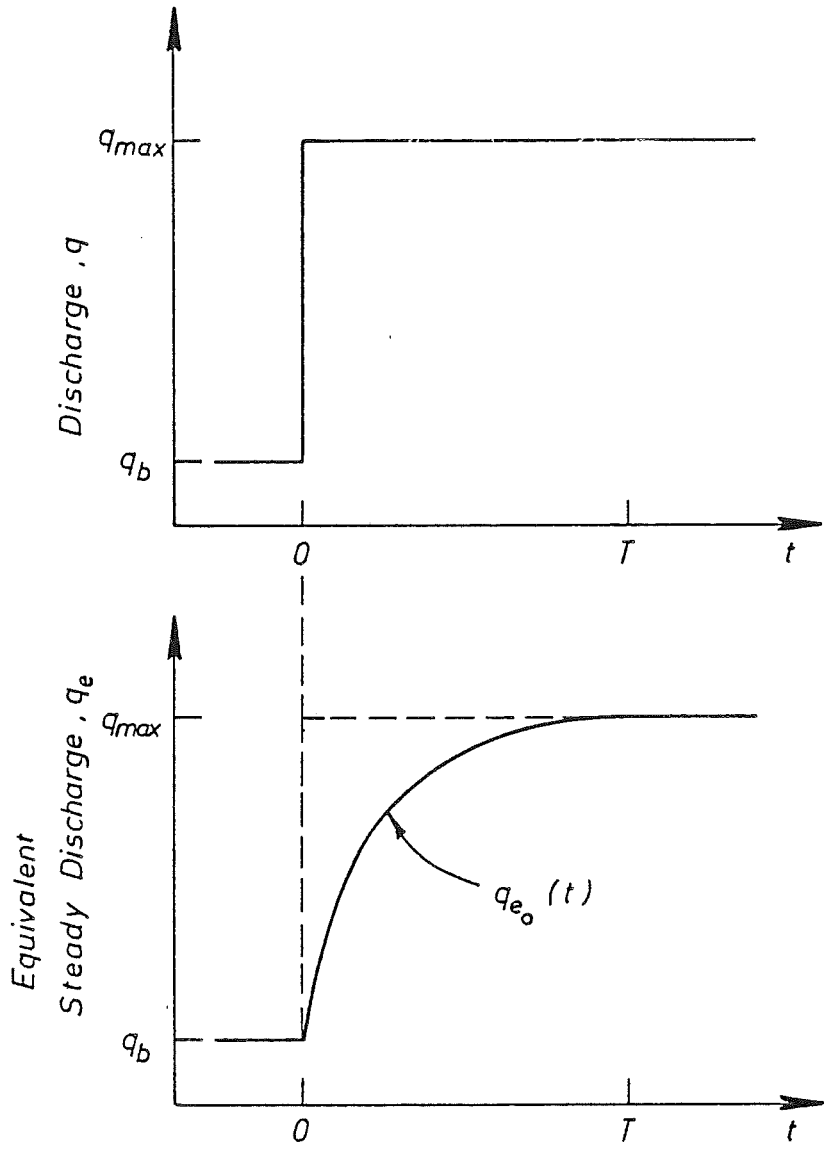

Figure 8.1 Idealized Temporal Response of the Equivalent Steady Flow Rate to a Discharge Impulse

discharge impulse, it was found that the equivalent steady flow hydrographs, which were obtained in the manner outlined in the preceding section, lagged the actual flow hydrographs. An idealized example of this behaviour is given in Fig. 8.1.

Mathematically, the lagged response of the equivalent steady flow rate, $q_e(t)$, to the temporal variation of the flow rate, $q(t)$, can be expressed by the equation

$$q_e(t) - q_b = \int_o^t (q(t') - q_b)\, g_T(t - t')dt' \qquad (8.25)$$

where $g_T(t)$ = Impulse response function which describes response of the equivalent steady discharge to an instantaneous step change in discharge, and

Eq. 8.25 is a form of Duhamel's superposition integral (Hildebrand (1976)). The impulse response function, $g_T(t)$ can be obtained from the measured temporal respone of q_{e_o}, the equivalent steady flow rate to an instantaneous step change in discharge from q_b to q_{max}, and Eq. 8.25, written as

$$g_T(t) = \frac{1}{(q_{max} - q_b)} \frac{d}{dt} (q_{e_o}(t) - q_b) \qquad (8.26)$$

Since the SC-I runs simulated an instantaneous step change in discharge, the values of the equivalent steady discharge, obtained in the manner outlined in Section 8.2.1, are in fact q_{e_o} values and when used in Eq. 8.26 determine the impulse response function, as defined in Eq. 8.25.

8.2.3 Time Scale

To determine the nondimensional form of the temporal response of the equivalent steady flow rate, q_{e_o}, it was necessary to determine values of a time scale which characterises this temporal response. This time scale was used to collapse the measured data onto a single curve (Fig. 8.4) and was defined as the time, t_{90}, at which (Fig. 8.1)

$$q_{e_o} - q_b = 0.9(q_{max} - q_b) \qquad (8.27)$$

or, alternatively, from Eq. 8.24

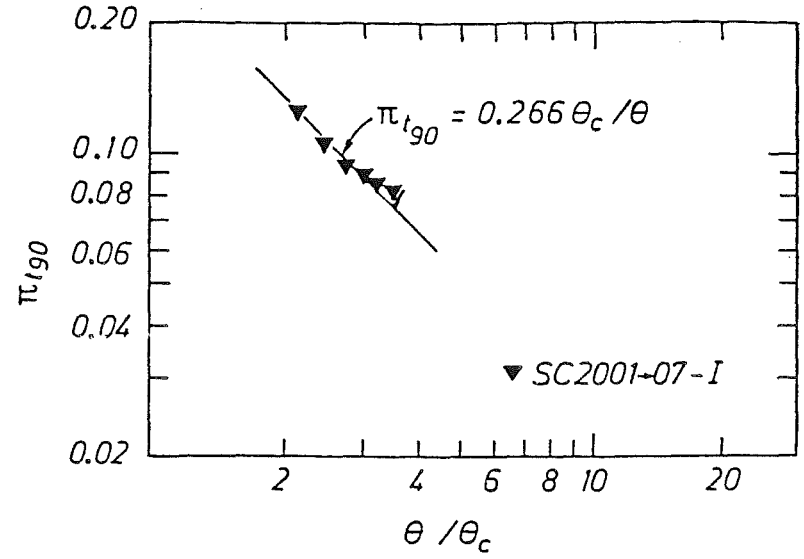

Figure 8.2 Nondimensional Time Scale Against Flow Intensity Ratio

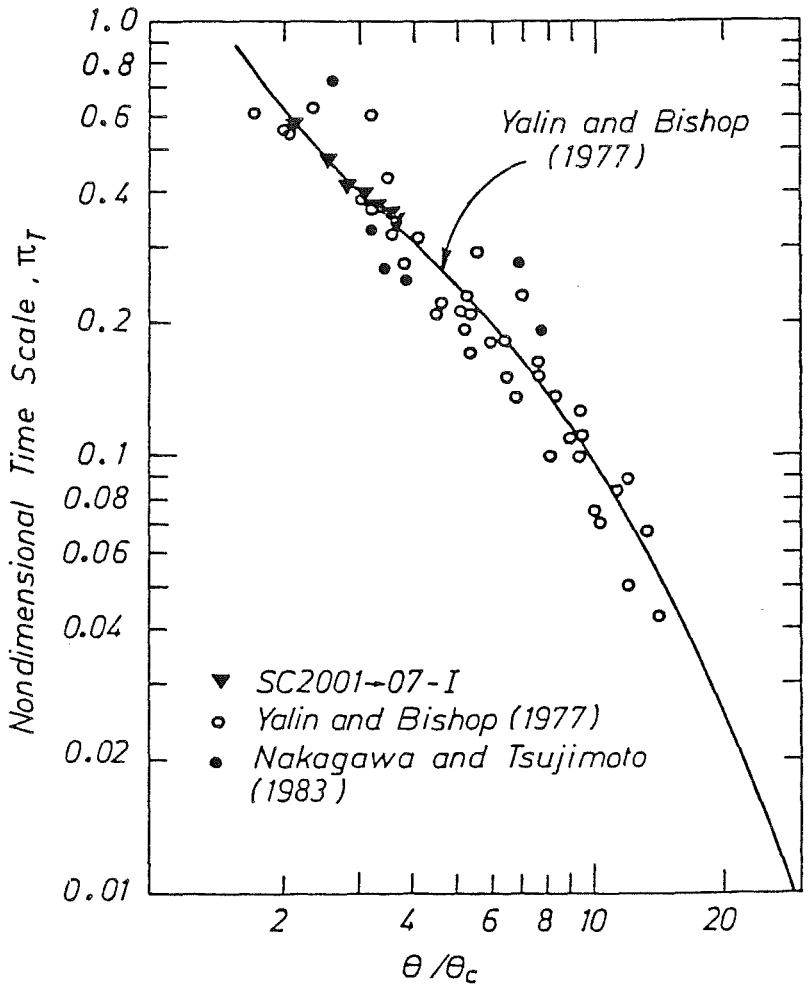

Figure 8.3 Nondimensional Equilibrium Time Against Flow Intensity Ratio (After Yalin and Bishop (1977))

$$q_{R_o} = \frac{q_{e_o} - q_b}{(q_{max} - q_b)} = 0.9 \qquad (8.28)$$

For each SC-I run, the value of this time scale, t_{90}, was found by plotting the variation of the excess discharge ratio, q_{R_o}, against time and determining the time at which $q_{R_o} = 0.9$ from the trend line fitted to the data. Seven values of this time scale were obtained in this manner, that is one from each of the seven SC-I runs.

Previous researchers, including Yalin and Bishop (1977) and Nakagawa and Tsujimoto (1983(a)), have similarily investigated the time it takes a dune bed to develop from a plane bed to an equilibrium state under unsteady flow conditions. The time scale adopted by these researchers was the time, T, at which equilibrium bed conditions were reached, (see Fig. 8.1).

The time scale adopted in this study, t_{90}, was nondimensionalised in the manner proposed by Yalin and Bishop (1977), namely

$$\pi_{t_{90}} = t_{90} \frac{\theta_c^{3/2} \sqrt{(S_s - 1) g d_{50}^3}}{Y_E^2} \qquad (8.29)$$

where the flow depth, Y_E, is the flow depth which occurs after temporal lag effects have dissipated i.e. when $t > T$ (Fig. 8.1) but before the time at which the advancing scour hole causes the bed to degrade. This flow depth corresponds to flow depth which occurs during the SE runs of the same bed slope and discharge given in Appendix C; these values of flow depth were inserted in Eq. 8.29. The nondimensional values of the time scale, obtained from Eq. 8.29, are presented in Appendix E and plotted, in the manner of Yalin and Bishop (1977), in Fig. 8.2.

The data was well fitted by the relation

$$\pi_{t_{90}} = 0.266 \left(\frac{\theta_c}{\theta}\right) \qquad (8.30)$$

Once $q_{e_o}(t)$ had been found (Eq. 8.35), as described in Section 8.2.4, it was possible to determine the time scale percentile which corresponds to the time scale, T, of Yalin and Bishop (1977). It was found, from Eq. 8.35 and the data of Yalin and Bishop (1977) given in Fig. 8.3, that

$$T = t_{97.6} = 4.51\ t_{90} \qquad (8.31)$$

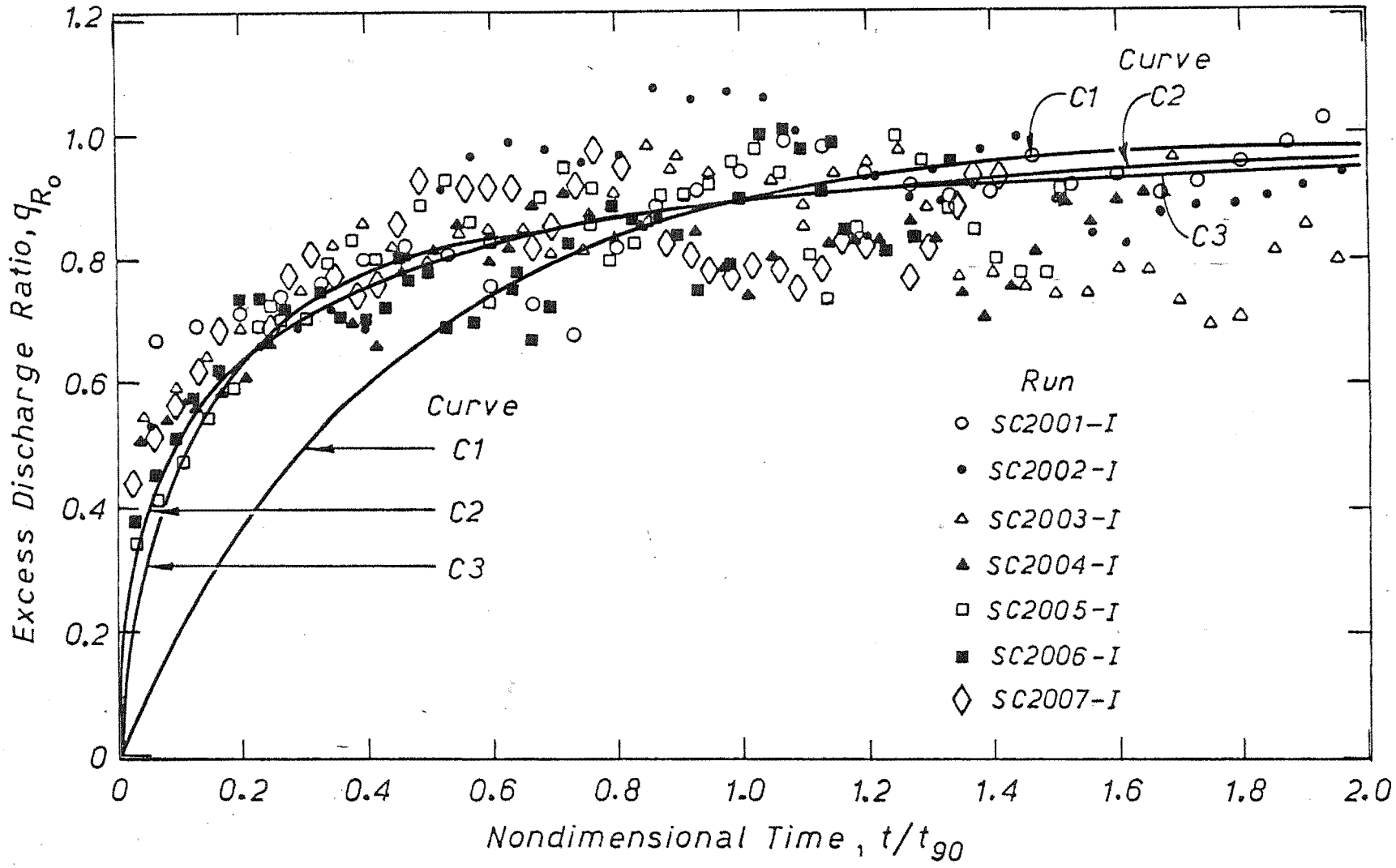

Figure 8.4 Excess Discharge Ratio Against Nondimensional Time (SC-I Series).

Nondimensional values of this time scale, π_T, were calculated using Eq. 8.31 and are compared with the data of Yalin and Bishop (1977) and Nakagawa and Tsujimoto (1983(a)) in Fig. 8.3, where

$$\pi_T = T \frac{\theta_c^{3/2} \sqrt{(S_s - 1) g d_{50}^3}}{Y_E^2} \tag{8.32}$$

The agreement between the new data and the previously published data is excellent.

8.2.4 Impulse Response Function

Knowing the time scale, t_{90}, it was possible to obtain the impulse response function, $g_T(t)$, by determining the relation which best described the temporal variation of the variable, q_{e_o}, and then substituting this relation into the general expression for the impulse response function, given by Eq. 8.26. The relation which best described the temporal variation of the variable, q_{e_o}, was obtained by finding the curve which best fitted data plotted in the form of excess discharge ratio, q_{R_o}, against nondimensional time, t/t_{90}. This data, to which three curves were fitted, is given in Fig. 8.4, where

$$q_{R_o} = \frac{q_{e_o} - q_b}{q_{max} - q_b} \tag{8.28}$$

These curves were

$$\text{Curve C1} : q_{R_o} = 1 - e^{-2.302\, t/t_{90}} \tag{8.33}$$

$$\text{Curve C2} : q_{R_o} = 1 - e^{-2.302\sqrt{t/t_{90}}} \tag{8.34}$$

$$\text{Curve C3} : q_{R_o} = \frac{t/t_{90}}{0.111 + t/t_{90}} \tag{8.35}$$

Previous researchers, including Fredsøe (1977) and Nakagawa and Tsujimoto (1983(a)) have assumed that an exponential function suitably described the lag variable they were considering. In this case, the exponential function given by curve C1 does not fit the data well. During the initial period the curve C1 is well below the band of data points. At later times, the agreement improves, but the overall fit

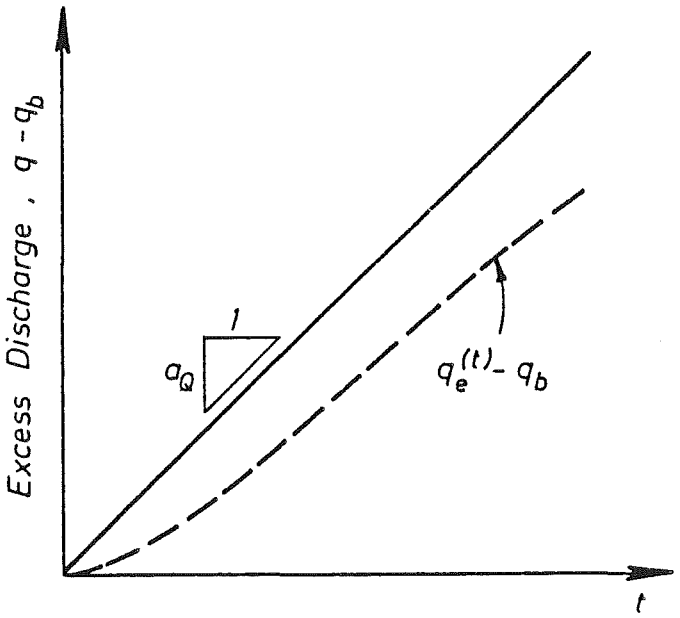

Figure 8.5 Linearly Increasing Discharge Case

of curve C1 to the data is unsatisfactory.

Two curves which do fit the data well at all times are the curves C2 and C3. There was no data available very close to the origin so the goodness of fit of these curves at the origin could not be tested. Since curves C2 and C3 fitted the data equally well, the choice of a relation was made on the basis of the ease with which the relation could be differentiated and integrated. On this basis, the relation which defined curve C3, Eq. 8.35, was adopted.

The impulse response function can now be derived from the equation of definition, Eq. 8.26, as follows.

Substituting Eq. 8.28 into Eq. 8.35 and re-arranging gives

$$q_{e_o}(t) - q_b = \frac{t}{0.111\ t_{90} + t}\ (q_{max} - q_b)$$

$$= \frac{t}{T_e + t}\ (q_{max} - q_b) \qquad (8.36)$$

where $$T_e = 0.111\ t_{90} \qquad (8.37)$$

= A modified equivalent steady discharge time scale.

Substituting Eq. 8.36 into Eq. 8.26 gives

$$g_T(t) = \frac{d}{dt}\left(\frac{t}{T_e + t}\right)$$

$$= \frac{T_e}{(T_e + t)^2} \qquad (8.38)$$

8.2.5 General Impulse Response Model

The use of the general response equation, Eq. 8.25, to determine the lagged response of the equivalent steady discharge is demonstrated for the case where the discharge hydrograph is assumed to be a linearly increasing discharge from a base discharge, q_b, for all time (Fig. 8.5). The solution obtained for this discharge case is then used to formulate the general solution for a complex flow hydrograph.

For the case where the change in discharge commences at t = 0, the flow hydrograph is given by (Fig. 8.5)

$$q(t) - q_b = a_Q t \qquad (8.39)$$

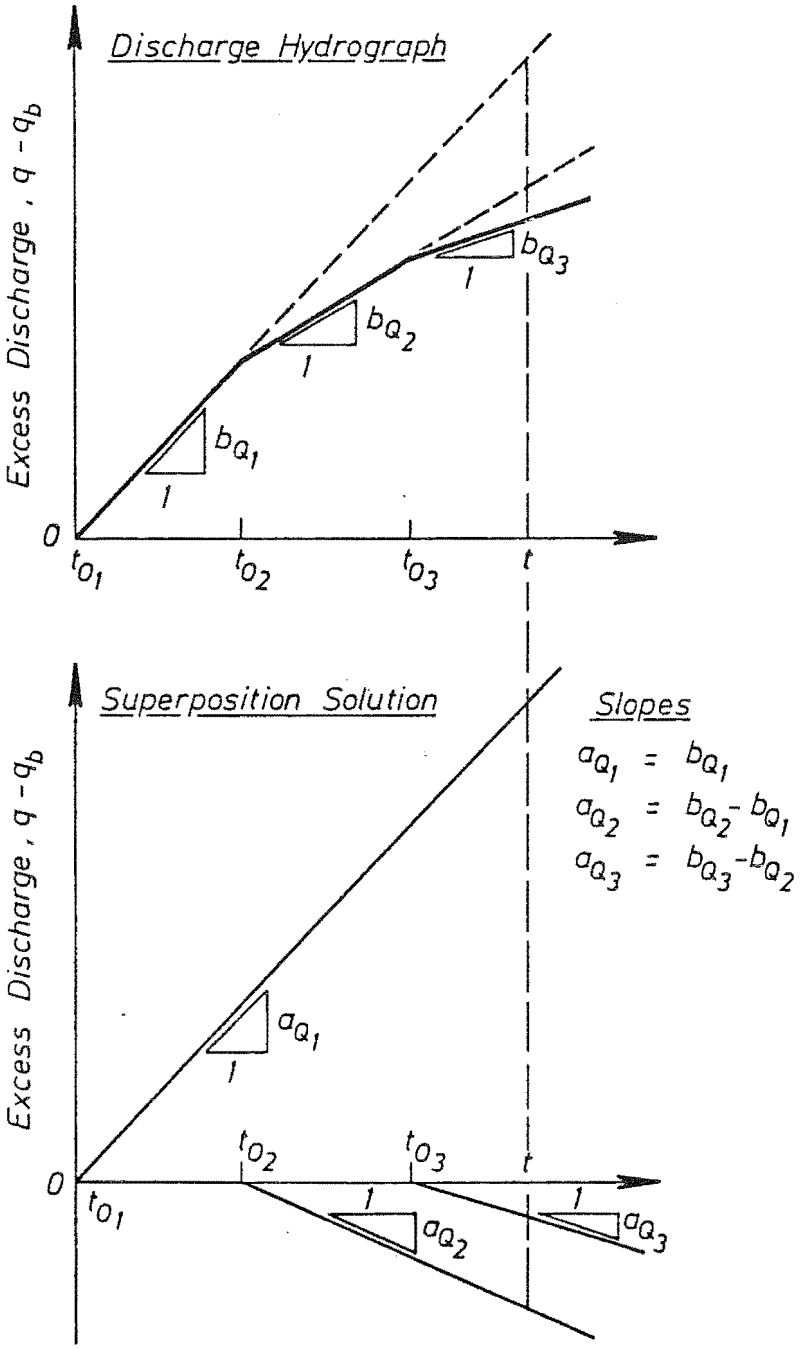

Figure 8.6 General Superposition Solution For a Complex Flow Hydrograph

The general solution for this case is obtained by substituting the impulse response function, Eq. 8.38, and the discharge relation, Eq. 8.39, into the general equation, Eq. 8.25, thus

$$q_e(t) - q_b = \int_o^t a_Q t' \frac{T_e}{(T_e + t - t')^2} dt' \tag{8.40}$$

Assuming that the time scale, T_e, is constant, the solution of the integral expression is

$$q_e(t) - q_b = a_Q \left[t + T_e \ln \left(\frac{T_e}{T_e + t} \right) \right] \tag{8.41}$$

The principle of superposition is then used to formulate the general solution for a complex flow hydrograph. This is demonstrated in Fig. 8.6, in which a complex hydrograph is assumed composed of m straight line segments. This complex hydrograph is decomposed into a series of time-lagged linearly increasing discharge limbs (Fig. 8.6); the general solution is obtained by superimposing the solutions obtained for each individual limb. Hence, the general solution is (Eq. 8.41)

$$q_e(t) = q_b + \sum_{i=1}^{m} a_{Q_i} \left[(t - t_{o_i}) + T_{e_i} \ln \left(\frac{T_{e_i}}{T_{e_i} + t - t_{o_i}} \right) \right] \tag{8.42}$$

where $m = r$ for $t_{o_r} < t < t_{o_{r+1}}$ and $r \geq 1$, and

a_{Q_i} = Slope of the i^{th} discharge limb in the superposition solution,

t_{o_i} = Time at which i^{th} discharge limb commences, and

T_{e_i} = Time scale of i^{th} discharge limb.

In the case considered in Fig. 8.6, the slope of the first discharge limb is positive while subsequent discharge limb slopes are negative. That is (Fig. 8.6)

$$\begin{aligned} a_{Q_1} &> 0 \\ a_{Q_{2,3,\ldots}} &< 0 \end{aligned} \tag{8.43}$$

8.2.6 Time Scale Relations

The general solution for a complex hydrograph, given by Eq. 8.42, was determined by superimposing time-lagged solutions, obtained using

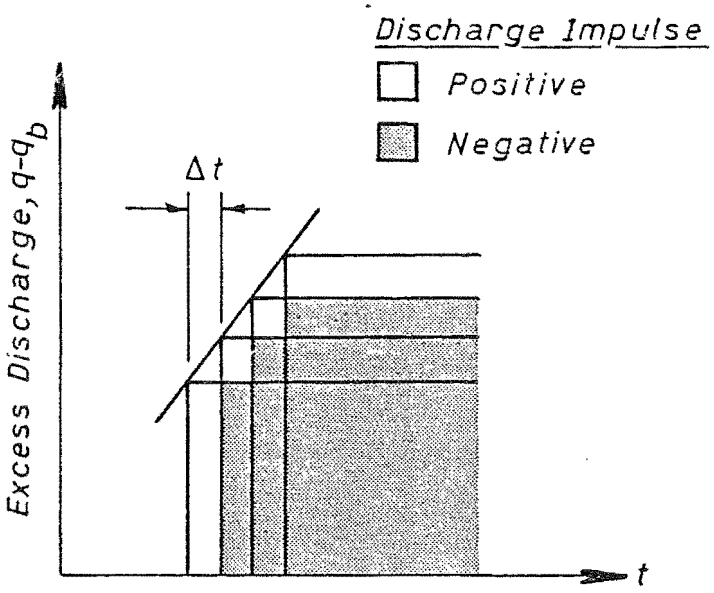

Figure 8.7 Superposition Method for General Impulse Solution for Varying Discharge.

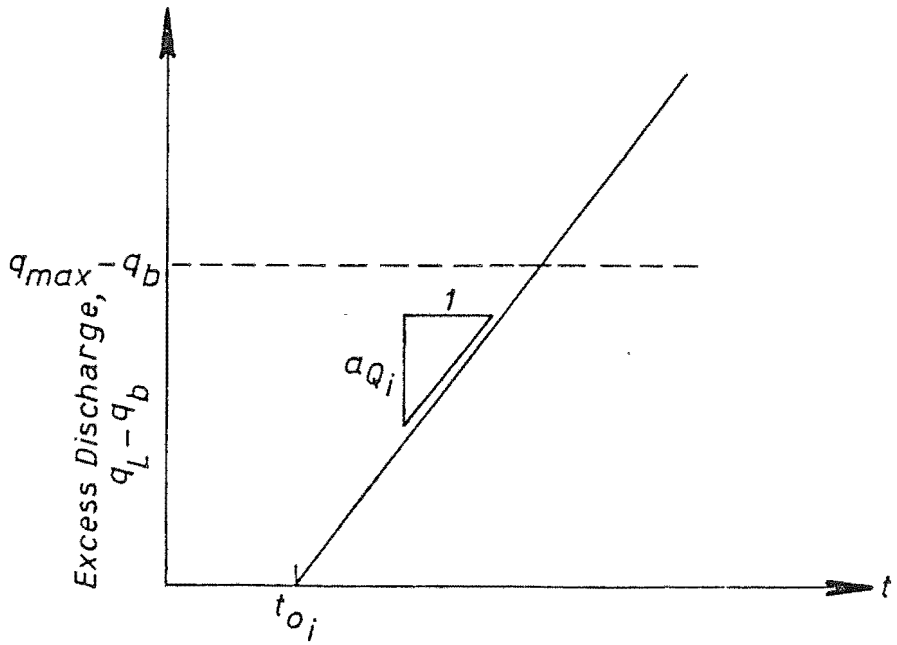

Figure 8.8 Geometry of the i^{th} Limb in Superposition Solution for a Complex Flow Hydrograph

Duhamel's superposition integral (Eq. 8.25), for a series of linearly increasing discharge limbs. The solution for the case of a linearly increasing discharge, given by Eq. 8.41, was in turn obtained by assuming that the time scale, T_e, was constant. However, a closer examination of the manner in which Duhamel's superposition integral, Eq. 8.25, was formulated indicates that T_e is not constant.

Duhamel's superposition integral is obtained by approximating a continuous function, in this case discharge, by a stepped function. The stepped function, in turn, is obtained by superimposing positive and negative discharge impulses. An example of this method is given in Fig. 8.7. It was also found, (Eqs. 8.37, 8.29 and 8.30 and Fig. 8.2), that the time scale, T_e, is a function of the height of a discharge impulse.

Since Duhamel's superposition integral was obtained by superimposing discharge impulses of various heights it follows that T_e is not constant but, in the limit, is a function of the instantaneous excess discharge at any given time (Fig. 8.7).

Three possible time scale relations were investigated. These relations were all based on a general solution derived from Eq. 8.29 (see Appendix E) and Eq. 8.27 for the case of an instantaneous step change in discharge to a constant maximum discharge, q_{max}, (Fig. 8.1). For the sediment properties and flume slope of 0.002 of this study, this relation is

$$T_e = 652.2\ q_{max}^{0.7285} \tag{8.44}$$

The first time scale relation considered is an equation which theoretically only holds for the case of a single instantaneous step change in discharge. For the i^{th} limb of the general superposition solution (Fig. 8.6) given in Fig. 8.8, this relation is

$$\text{Relation R1} \qquad T_{e_i} = 652.2\ q_{max}^{0.7285} \tag{8.45}$$

where q_{max} = Maximum or peak discharge of the flow hydrograph.

The second relation is (Fig. 8.8)

$$\text{Relation R2} \qquad T_{e_i} = \begin{cases} 652.2\ q_{L_i}^{0.7285} & q_{L_i} \leq q_{max} \\ 652.2\ q_{max}^{0.7285} & q_{L_i} > q_{max} \end{cases} \tag{8.46}$$

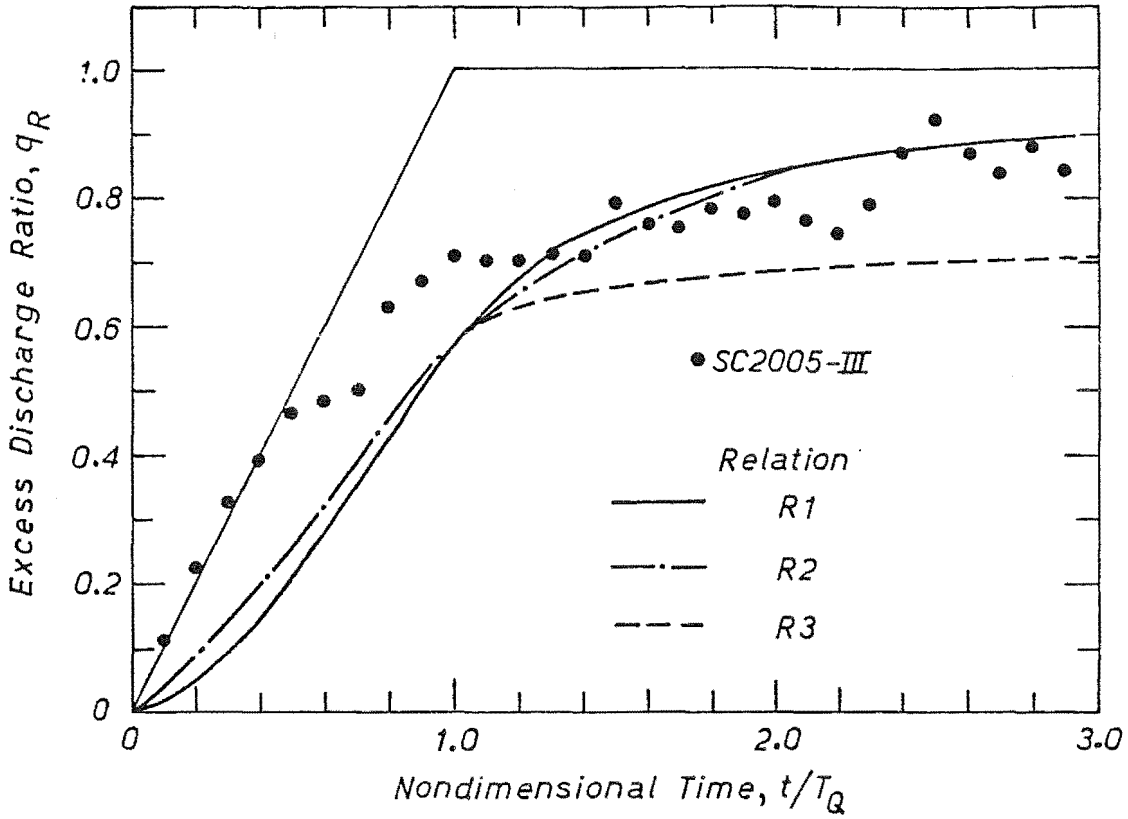

Figure 8.9 Excess Discharge Ratio Against Nondimensional Time (Run SC2005-III: q_{max} = 0.16 $m^3/s/m$, T_Q = 600 s)

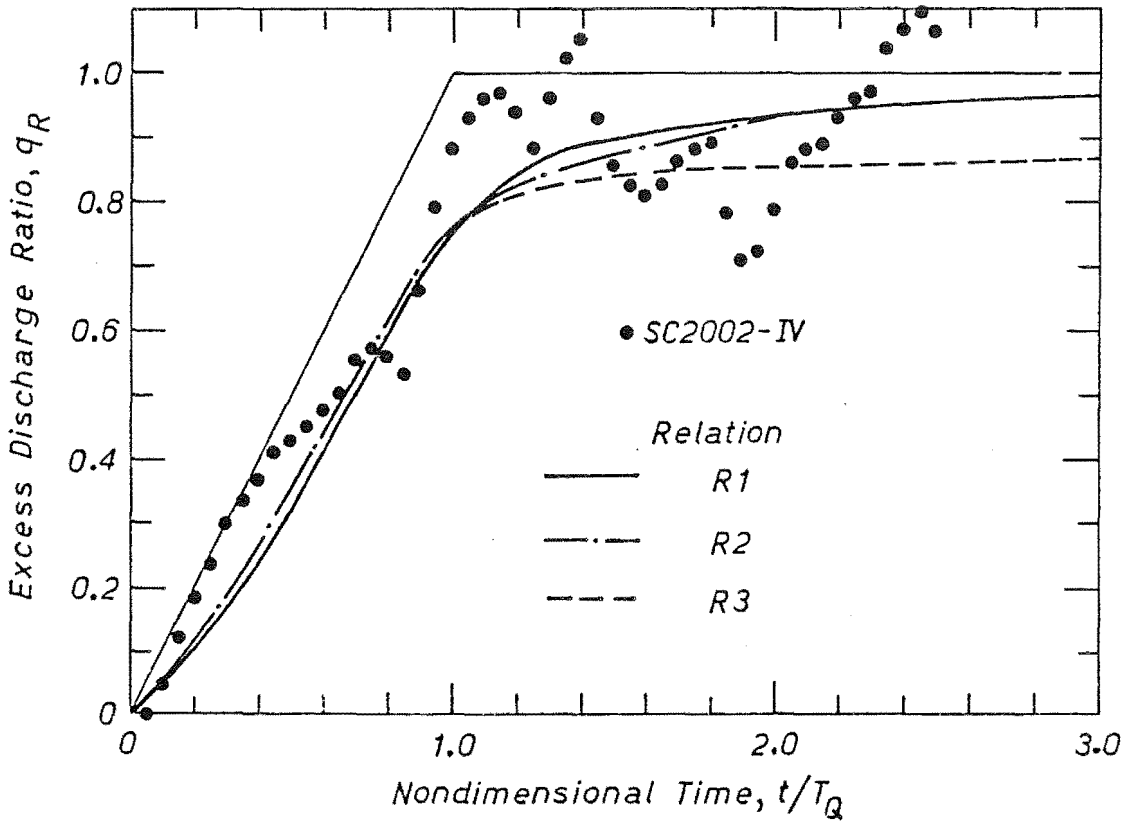

Figure 8.10 Excess Discharge Ratio Against Nondimensional Time (Run SC2002-IV: q_{max} = 0.10 $m^3/s/m$, T_Q = 1200 s)

where q_{L_i} = Instantaneous (absolute) discharge on the i^{th} limb at time t (Fig. 8.8),

$$= q_b + |a_{Q_i}|(t - t_{o_i}) \qquad (8.47)$$

The third relation is an equation which is theoretically consistent with the superposition approach used to derive the general impulse relation (Fig. 8.7). It is

Relation R3 $$T_{e_i} = 652.2\ q_{L_i}^{0.7285} \qquad (8.48)$$

The selection of a suitable time scale relation was based on a comparison of data obtained from two SC runs with the temporal variations of the lag variable, q_e, which were predicted when using each time scale relation. Data was obtained by analysing the sediment hydrographs measured during the SC2005-III and SC2002-IV runs in the manner outlined in Section 8.2.1. Each predicted temporal variation of the lag variable was obtained by assuming that the solution for a linearly increasing discharge limb, Eq. 8.41, held at each point in time and that values of the lag variable could be obtained by inserting values of the time scale, given by Eqs. 8.45, 8.46 or 8.48, into Eq. 8.42. For the SC-I flow hydrographs given in Fig. 6.1, the superposition solution is composed of only two limbs and is readily obtained from Eq. 8.42.

The results of this analysis are presented in Figs. 8.9 and 8.10 where the excess discharge ratio is given by

$$q_R = \frac{q_e - q_b}{q_{max} - q_b} \qquad (8.49)$$

The temporal variations of the lag variable predicted using Relations R1 and R2 are similar, Figs. 8.9 and 8.10, however, the temporal variation predicted using Relation R3 is significantly beneath the values predicted using the other two relations for $t > T_Q$. The agreement between the data and the curves predicted using Relations R1 and R2 is reasonable whereas the agreement between the data and the curve predicted using Relation R3 for $t > T_Q$ was considered unsatisfactory. At times close to the origin, the curve predicted using Relation R2 agrees better with the data than does the curve predicted using Relation R1. Hence, the time scale relation adopted was Relation R2

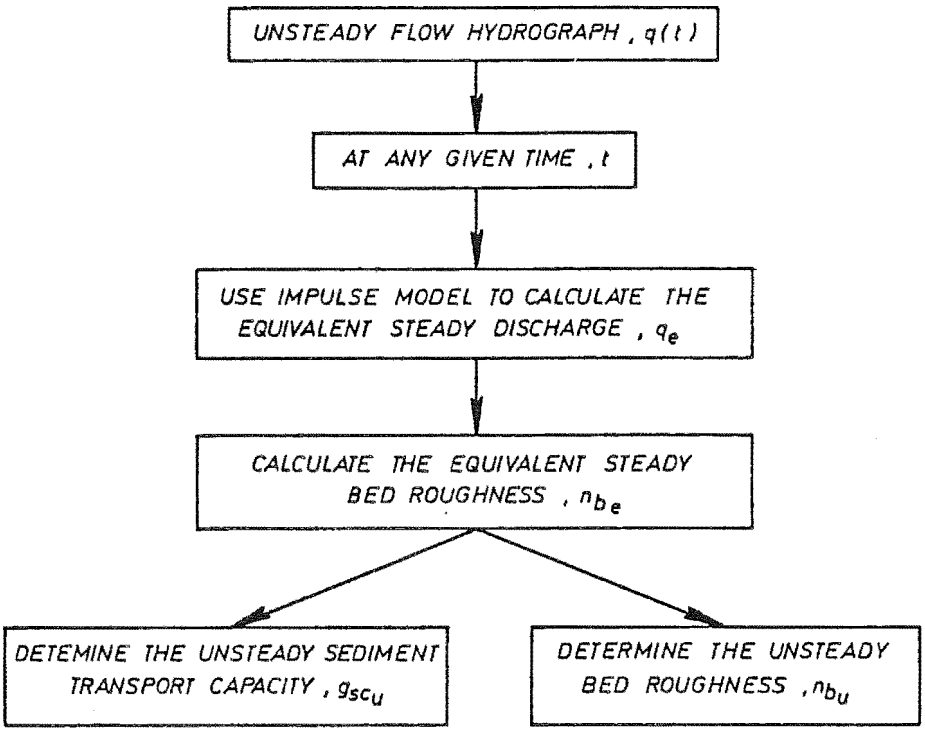

Figure 8.11 Flowcharge of Temporal Lag Model

because it partially alleviates the theoretical misgivings about a constant time scale and it performed satisfactorily when compared with measured data.

8.3 TEMPORAL LAG MODEL

The aim of the general temporal lag model is to predict values of the bed roughness and sediment transport capacity under unsteady flow conditions. In the proposed model, temporal lag effects are characterised by the equivalent steady flow rate, q_e. The manner in which the model calculates values of the bed roughness and sediment transport capacity under unsteady flow conditions is outlined in the flow chart given in Fig. 8.11. Each step of this flowchart is discussed below.

8.3.1 Impulse Model

The general impulse model presented in Section 8.2.5 is used to calculate values of the equivalent steady flow rate, q_e, at any given time. The general impulse model solution is

$$q_e(t) = q_b + \sum_{i=1}^{m} a_{Q_i}\left[(t - t_{o_i}) + T_{e_i}\,\ell n\left(\frac{T_{e_i}}{T_{e_i} + t - t_{o_i}}\right)\right] \qquad (8.46)$$

where all terms are as previously defined.

From the analysis of time scale relations presented in Section 8.2.6, a general time scale relation was adopted and is used in conjunction with the general solution given by Eq. 8.46. For the i^{th} limb of the general superposition solution, Eq. 8.46, the general time scale relation is

$$T_{e_i} = \begin{cases} a_T q_{L_i}^{b_T} & q_{L_i} \leq q_{max} \\ a_T q_{max}^{b_T} & q_{L_i} > q_{max} \end{cases} \qquad (8.46)$$

where

$$q_{L_i} = q_b + |a_{Q_i}|(t - t_{o_i}) \qquad (8.47)$$

q_{max} = Maximum or peak discharge of the flow hydrograph

and the coefficients a_T, b_T are functions of sediment and flow properties (see Eq. 8.37 and Appendix E).

8.3.2 Bed Roughness

The next step (Fig. 8.11) is to calculate the equivalent steady flow bed roughness. Under steady flow conditions, a relation for bed roughness value can be obtained from Manning's equation. This relation, the derivation of which is given in Appendix E, is

$$n_b = a_n S_f^{b_4} q^{b_5} \tag{8.50}$$

where

$$a_n = f(\alpha_n, \beta_n, S_s, d_{50}) \tag{8.51}$$

Similarly, from Eqs. 8.12, 8.22 and 8.23, a relation for the equivalent steady flow roughness value, n_{b_e}, can be derived. This relation is

$$n_{b_e} = a_n S_f^{b_4} q_e^{b_5} \tag{8.52}$$

Since, (Fig. 8.5)

$$q_e < q \tag{8.53}$$

It follows, from Eqs. 8.50 and 8.52 for $b_5 > 0$, that

$$n_{b_e} < n_b \tag{8.54}$$

When sediment is transported as bedload the sediment transport rate and the bed roughness, which reflects bed form geometry, are integrally linked because bed forms are the bedload transport mechanism. In this model, it is assumed that the linkage which exists between the sediment transport rate and bed roughness under steady flow conditions also exists under unsteady flow conditions. Hence, it is assumed that the bed roughness under unsteady flow conditions, n_{b_u}, is given by the equivalent steady flow bed roughness, n_{b_e}. Thus

$$n_{b_u} = n_{b_e} \tag{8.55}$$

In this way, the unsteady bed roughness values which are obtained from Eq. 8.52, or its equivalent Eq. 8.12, incorporate the inherent link between bed form geometry and bed roughness which was noted in Section 5.4.2. Hence Eq. 8.55 also describes the temporal lag associated with the development of bed forms.

8.3.3 Bedload Transport Capacity

The final step (Fig. 8.6) is to calculate the sediment transport

capacity under unsteady flow. Under steady flow conditions, a relation for the sediment transport capacity in terms of the bed roughness value, n_b, can be obtained, in a manner similar to that outlined in Section 8.2.1. This relation is

$$g_{sc} = a(a_1 n_b^{b_1} + a_2 n_b^{b_2})^b \tag{8.56}$$

where a, b are the coefficients of the transport capacity relation (Eq. 8.7) and the coefficients a_1, a_2, b_1, b_2 are as given in Eq. 8.19.

Similarly, Eqs. 8.4 and 8.18, give a relation for the unsteady sediment transport capacity in terms of the equivalent steady flow roughness value, n_{b_e}, where

$$g_{sc_u} = a(a_1 n_{b_e}^{b_1} + a_2 n_{b_e}^{b_2})^b \tag{8.57}$$

Since, (Eq. 8.54)

$$n_{b_e} < n_b \tag{8.58}$$

then, it follows from Eqs. 8.56 and 8.57 for b_1, b_2, $b > 0$, that

$$g_{sc_u} < g_{sc} \tag{8.59}$$

Hence, Eq. 8.57 describes the temporal lag associated with sediment transport under unsteady flow conditions.

The performance of this temporal lag model is discussed in the next section. It is also evaluated in Chapter 10.

8.4 TEMPORAL LAG MODEL PERFORMANCE

The performance of the temporal lag model was evaluated by comparing flow and sediment data measured during the SC-II, III, IV and V series of experiments with results predicted by the temporal lag model for unsteady flow conditions.

In all these series of experiments, the unsteady flow conditions were of the form of an inclined step change in discharge (Fig. 6.1). Under these conditions, values of the equivalent steady flow rate were obtained from (Eq. 8.46)

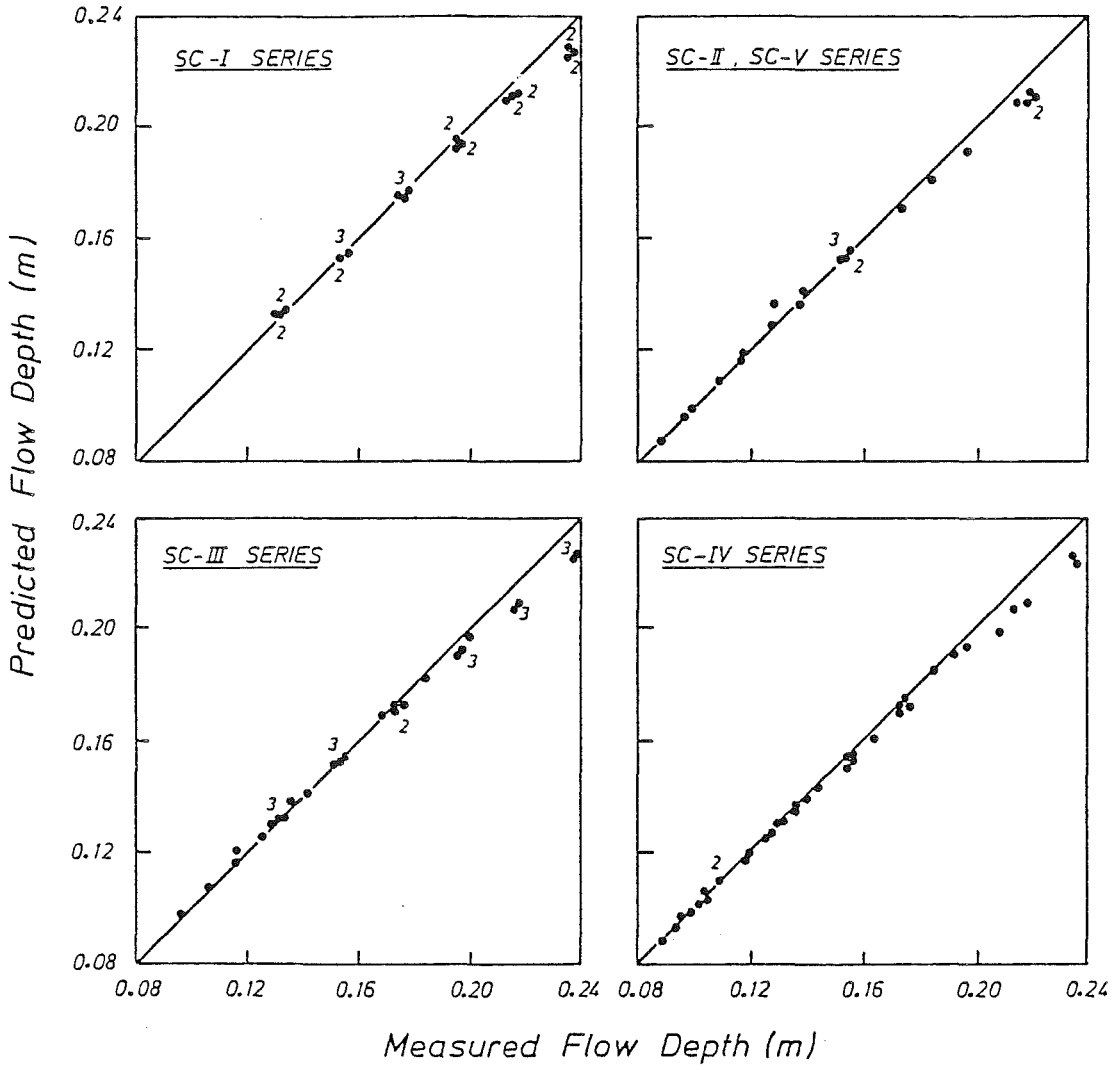

Figure 8.12 Measured Against Predicted Flow Depth (SC Series)

$$q_e(t) = q_b + \sum_{i=1}^{2} a_{Q_i}\left[(t - t_{o_i}) + T_{e_i}\,\ell n\left(\frac{T_{e_i}}{T_{e_i} + t - t_{o_i}}\right)\right] \qquad (8.60)$$

where (Fig. 6.1)

$$a_{Q_1} = \frac{q_{max} - q_b}{T_Q} \qquad (8.61)$$

and

$$a_{Q_2} = - a_{Q_1} \qquad (8.62)$$

Since it was assumed (Section 4.4) that it took 30 seconds for the flow to travel from the intake structure to the end of the mobile reach and t = 0 was referenced to the first value movement of the intake structure, then

$$t_{o_1} = 30 \qquad (8.63)$$

and

$$t_{o_2} = 30 + T_Q \qquad (8.64)$$

The time scale was given by the relation (Section 8.3.1)

$$T_{e_i} = \begin{cases} 652.2\, q_{L_i}^{0.7285} & q_{L_i} \leq q_{max} \\ 652.2\, q_{max}^{0.7285} & q_{L_i} > q_{max} \end{cases} \qquad (8.65)$$

where

$$q_{L_i} = q_b + |a_{Q_i}|(t - t_{o_i}) \qquad (8.47)$$

Values of the equivalent steady flow rate, obtained in the manner outlined above were then used to determine values of the unsteady bed roughness and unsteady sediment transport rate.

8.4.1 Bed Roughness

The temporal lag model predictions of the bed roughness under unsteady flow conditions were tested, indirectly, by comparing predicted flow depths with those flow depths measured at the downstream end of the test reach during the first twenty to thirty minutes of each run. At each time during this period when the water surface and bed profiles were recorded, the temporal lag model was used to calculate the equivalent steady flow rate. The unsteady bed roughness was determined from Eqs. 8.52 and 8.55, using the coefficients derived in Appendix E and predicted values of the flow depth were then calculated from the relation

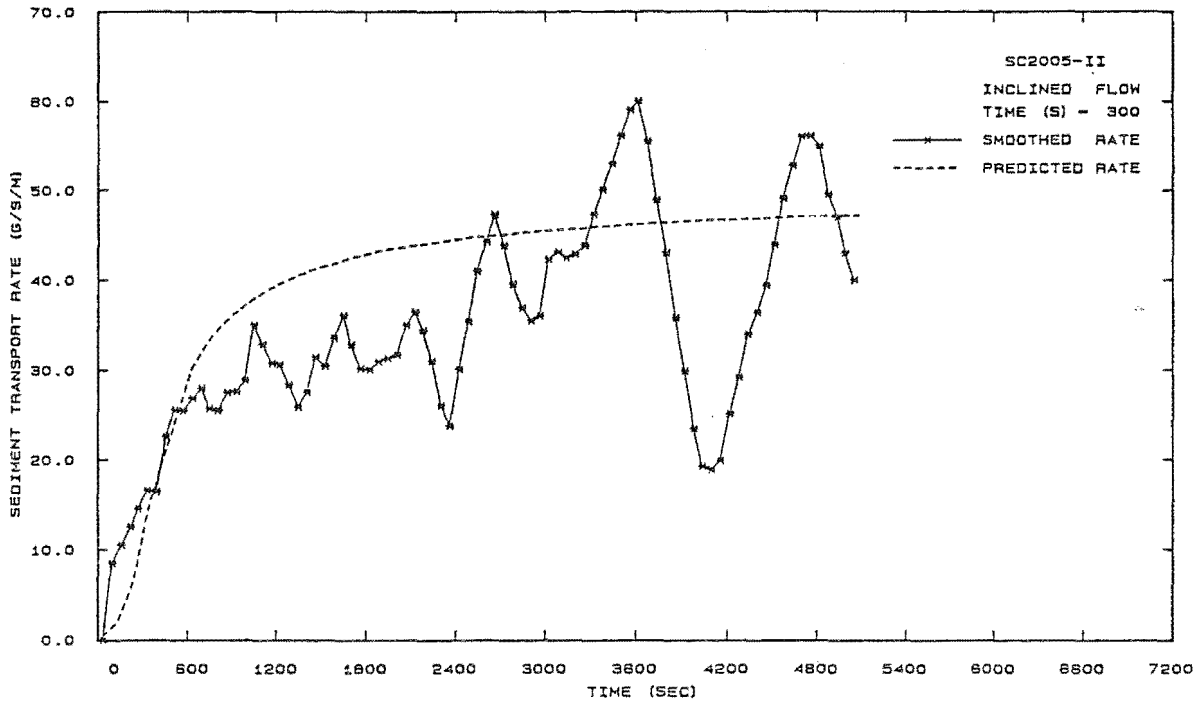

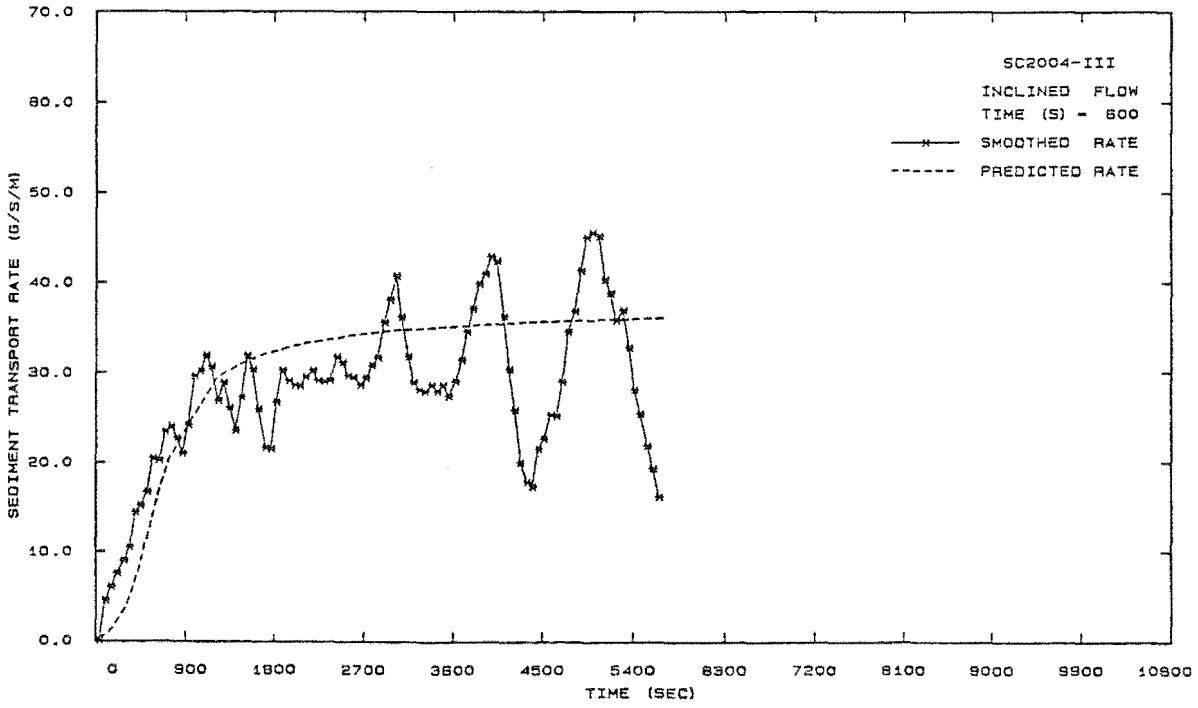

Figure 8.13 Measured Against Predicted Sediment Transport Rate (Runs SC2005-II and SC2004-III)

$$Y = 1.032 \times 10^{13}\ n_{b_u}^{7.985} \qquad (8.66)$$

The derivation of this equation is given in Appendix E.

Predicted and measured values of the flow depth are compared in Fig. 8.12. All data plotted in Fig. 8.12, including the times at which flow depths were measured and calculated, are tabulated in Appendix E. The agreement between the measured and predicted flow depths is good. Differences between measured and calculated values of flow depth range from 1% to -4%.

At large flow depths, which correspond to high discharges, the predicted values of the flow depth are slightly lower than the measured values. This difference is due to the steady flow bed roughness relation, Eq. 8.50, on which the unsteady flow bed roughness relation, Eq. 8.52, is based, predicting values of the bed roughness, at high discharges, which are slightly less than the bed roughness values obtained when flow data is inserted in a re-arranged Manning equation. This occurs because the coefficients α', β' of the relation between Shields Parameter and grain Shields Parameter, Eq. 5.8, were calibrated using data from four different bed slopes (Fig. 5.2) and not separately calibrated for each bed slope. This is reflected in the steady flow bed roughness relation because the coefficients a_n, b_4 and b_5, Eq. 8.50, are functions of the coefficients α_n and β_n, (see Appendix E), which themselves are functions of α' and β' through Eq. 5.39.

The good agreement between the measured and predicted flow depths confirms that the temporal lag model is able to predict bed roughness values under unsteady flow conditions.

8.4.2 Bedload Transport Rate

For each SC run, the temporal lag model was used to predict the temporal variation of the sediment transport rate under unsteady flow conditions. The temporal lag model was able to predict these sediment hydrographs because it was assumed, Eq. 8.4, that the rate of sediment transport, at the end of the mobile reach, was equal to the capacity rate of transport. The measured and predicted sediment hydrographs, for each SC run, were plotted and are presented in Appendix E. Four representative plots from the sixteen test runs are given in Figs. 8.13 and 8.14 (Table 6.1).

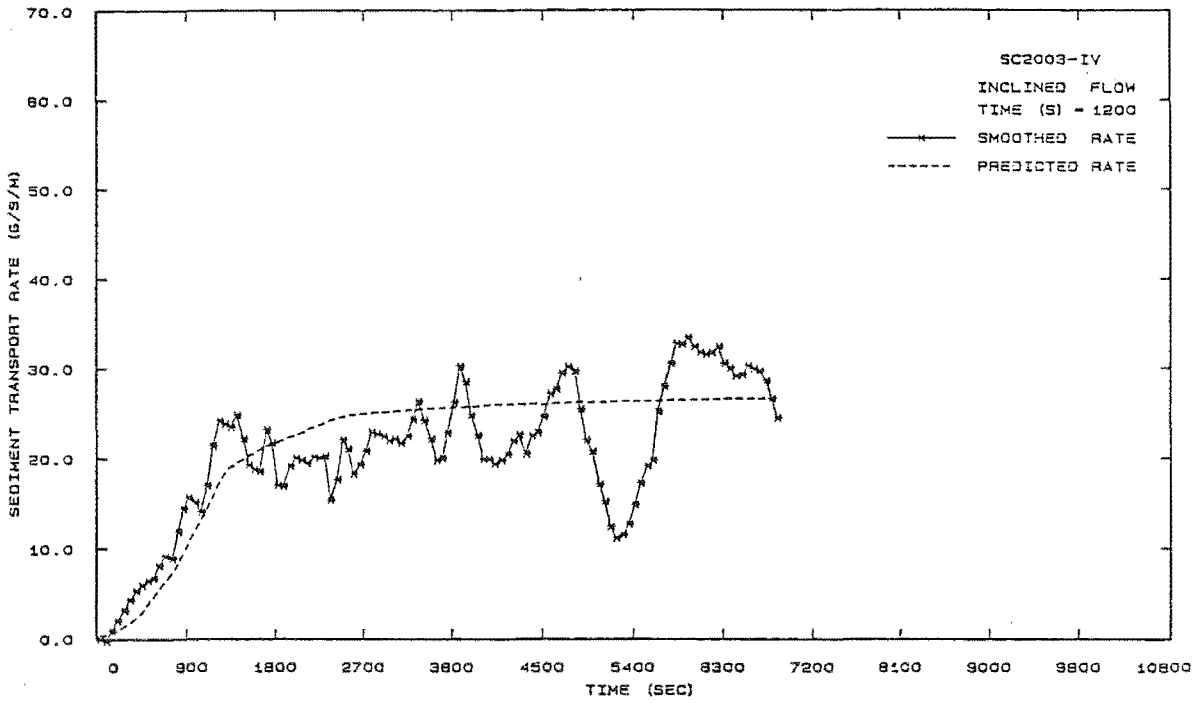

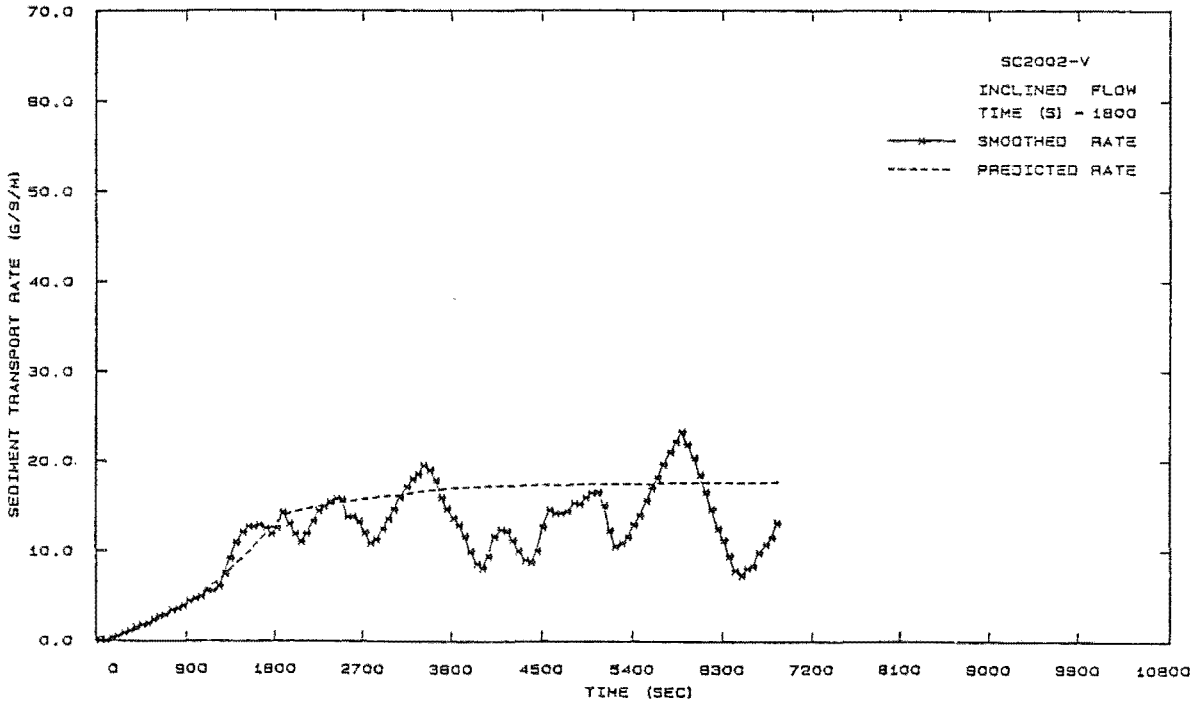

Figure 8.14 Measured Against Predicted Sediment Transport Rate (Runs SC2003-IV and SC2002-V)

The agreement between the measured and predicted sediment hydrographs is good, (Figs. 8.13 and 8.14), although the temporal lag model appears to overpredict the yield in all cases. The differences between the two hydrographs near the origin may arise from the method used to calculate instantaneous smoothed sediment transport rates. In this initial region, the algorithm used to calculate these values, (see Appendix B), cannot be applied immediately. A transition scheme is used until the full algorithm can be applied. In this case, the first five values of the sediment transport rate are calculated using such a transition scheme.

At large times in Figs. 8.13 and 8.14, the sediment transport rates predicted by the temporal lag model appear to be slightly higher than the trend of the measured transport rates. This behaviour may be due to spatial lag effects, which are assumed negligible in this analysis, slightly reducing the sediment transport rates and capacities at large times.

Overall, though, the measured sediment hydrographs agree well with the sediment hydrographs predicted by the temporal lag model over a wide range of unsteady flow conditions. A further comparison of predicted and measured sediment hydrographs, for the case of flood waves, is presented in Chapter 10.

It was concluded from these analyses that the proposed temporal lag model is able to predict the temporal variation of bed roughness and sediment transport capacity under unsteady flow conditions.

8.5 SUMMARY

A temporal lag model which predicts the variation of the bed roughness and sediment transport capacity under unsteady flow conditions has been developed and calibrated against measured data. The temporal response of these properties is characterised by a single variable, the equivalent steady flow rate. An impulse model was used to develop a general solution for the temporal variation of this variable under unsteady flow conditions. It was also found that the "equilibrium time scale" of Yalin and Bishop (1977) for the growth of dune bed forms from a plane bed, T, is in excellent agreement with the time scale, $t_{97.6}$, and that data for this time scale was in excellent agreeement with previously published data.

The temporal lag model was also used to calculate flow depths and sediment transport rates under a variety of unsteady flow conditions. These results were compared with measured data and the agreement was found to be good.

It was concluded that the proposed temporal lag model is able to predict the temporal variation of bed roughness and sediment transport capacity under unsteady flow conditions.

Chapter 9 | Non-Steady Sediment Transport - A Numerical Model

9.1 INTRODUCTION

Many researchers have found that the sediment phase of an alluvial system cannot respond immediately to imposed changes in discharge. A certain time is required before the sediment transport rate and bed form geometry can adjust to the new flow regime. This phenomenon has been viewed as temporal lag.

Similarly, the sediment phase cannot immediately overcome constrained sediment boundary conditions. A certain discharge is required before the sediment transport capacity of the flow is satisfied. This phenomenon has been viewed as spatial lag.

Spatial and temporal lag effects are evident in the results presented by Bell (1980). Bell (1980) studied the variation in sediment transport rate and bed form geometry induced by step changes in discharge and by the passage of flood waves. The data collected in the present study also demonstrates the effects of both spatial and temporal lag on bed form development and on the sediment transport rate.

Mathematical models which do not recognise the lag effects inherent in situations where constrained sediment boundary conditions exist e.g. a dam spillway, or where unsteady flow conditions occur cannot be reasonably applied to such conditions. Consequently, a numerical model which incorporates both spatial and temporal lag schemes and which is able to predict bedload sediment transport rates and changes in mean bed elevations under non-equilibrium sediment transport, steady and non-steady flow conditions has been assembled.

This model, an uncoupled one-dimensional, unsteady water and sediment routing model (UWASER), is based on the model presented by Wellington (1978). In the numerical simulations he undertook, Wellington

accounted for lags in the suspended bed material transport but assumed that the bedload transport reacted instantaneously to changes in local flow conditions. The sediment and flow equations adopted in this model, their associated boundary conditions and the methods used to solve them are detailed below.

9.2 FLOW ROUTING

An unsteady water and sediment routing model requires four basic equations. The first two equations describe the fluid flow, namely, the conservation of mass (continuity) and the conservation of momentum equations. The other two equations relate to the sediment transport phase and are discussed in Section 9.3.

9.2.1 Unsteady Flow Equations

Gradually varied, unsteady flow in open channels can be numerically simulated by a mathematical model based on the equations of continuity and momentum. The one-dimensional forms of these non-linear partial differential equations, where the stage and discharge are the dependent variables, are given in Eqs. 9.1 and 9.2 (Zoppou (1979)).

The flow continuity equation is

$$B \frac{\partial Z}{\partial t} + \frac{\partial Q}{\partial x} - q_\ell = 0 \tag{9.1}$$

and the momentum equation, for flow in a non-prismatic channel, is

$$\frac{\partial Q}{\partial t} - \frac{QB}{A}\frac{\partial Z}{\partial t} + \frac{\alpha Q}{A}\frac{\partial Q}{\partial x} - \frac{\alpha Q^2}{A^2}\left(B \frac{\partial Z}{\partial x} + \frac{\partial A}{\partial x}\bigg|_z\right) + gA \frac{\partial Z}{\partial x}$$

$$+ \frac{Q^2}{2A}\frac{\partial \alpha}{\partial x} + gA \frac{Q|Q|}{K^2} = - \frac{q_\ell Q}{A} \tag{9.2}$$

where A = Cross sectional area of flow,

B = Channel width at water surface,

g = Gravitational constant,

K = Channel conveyance,

Q = Discharge,

q_ℓ = Lateral inflow,

x = Longitudinal distance in the direction of the flow,

Z = Stage or elevation of the water surface above a horizontal datum, and

α = Velocity distribution correction factor

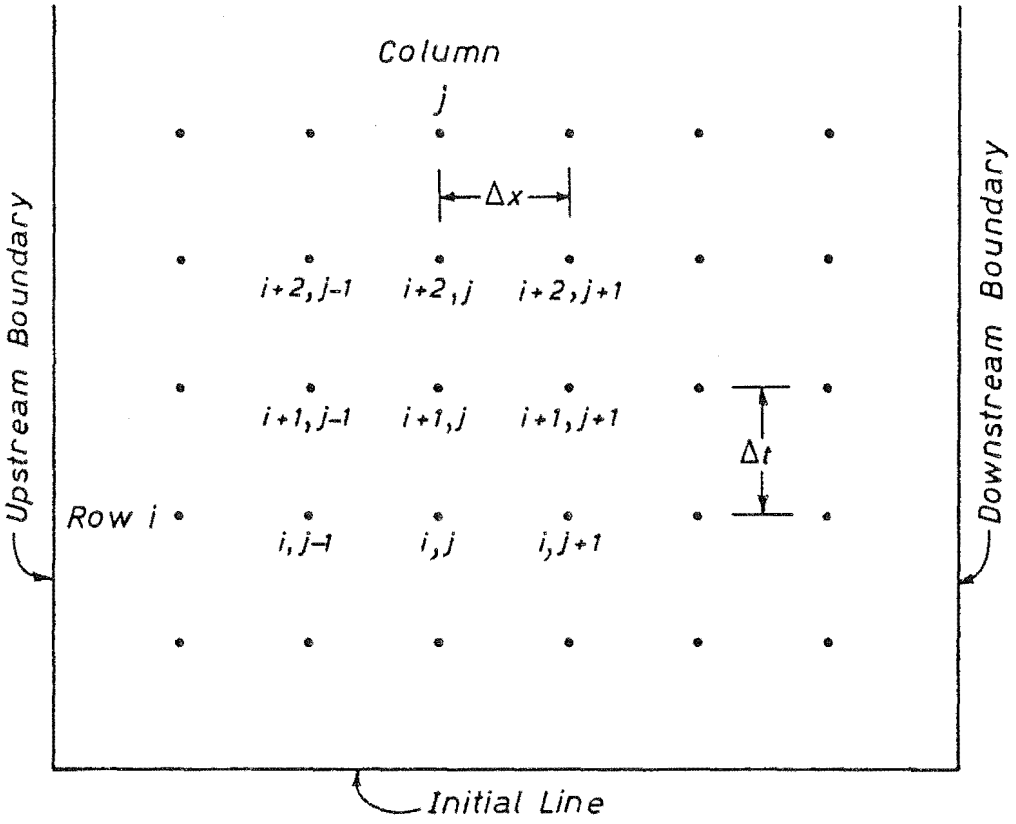

Figure 9.1 Fixed Grid in the (x, t) Plane (After Liggett and Cunge (1975))

and, the friction slope, S_f, is assumed given by

$$S_f = \frac{Q|Q|}{K^2} \tag{9.3}$$

The term $\partial A/\partial x\Big|_z$ represents the channel departure from non-prismatic conditions, and is the rate of change of area with respect to x, with the stage held constant. It is also assumed that the lateral inflow, q_ℓ, enters at right angles to the main flow and makes no dynamic contribution to the main stream.

The assumptions and limitations of the above equation have been discussed by both Zoppou (1979) and Liggett (1975). The manner in which the flow properties are evaluated for flow in a non-prismatic channel is detailed in Section 9.5.

9.2.2 Flow Routing Solution Scheme

Many techniques have been proposed for solving the above system of equations. Reviews of a wide range of these techniques have been presented by several researchers, including Zoppou (1979), Wellington (1978) and Liggett (1975).

Recognising that it is advantageous to be able to use a relatively long time increment when simulating stream behaviour over long periods of time and that a fixed grid method is more convenient, Wellington (1978) considered the stability, accuracy, efficiency and suitability of various solution techniques. He decided that an implicit finite difference scheme was most suitable.

Zoppou (1979) also advocated the use of implicit finite difference schemes because of the versatility offered by an unrestricted time increment and by the weighting coefficient.

Hence, the scheme adopted in this numerical model for solving the unsteady flow equations was an implicit finite difference scheme, specifically, the scheme presented by Wellington (1978).

An implicit finite difference scheme provides a solution for a group of advance points in the x-t plane, Fig. 9.1, using simultaneous equations which include all the unknown variables on the $(i + 1)^{th}$ time line and all the known variables on the i^{th} time line. The finite difference scheme developed by Wellington (1978), (and Zoppou (1979)), was based on the Priessmann (SOGREAH) finite difference scheme.

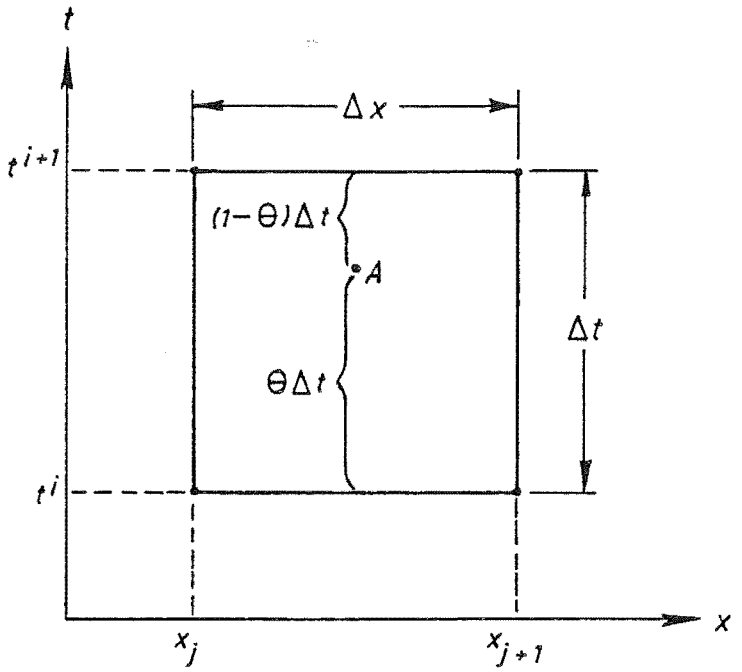

Figure 9.2 The Pressmann (SOGREAH) Scheme (After Liggett and Cunge (1975)).

The Priessmann scheme approximates the conditions at point A in Fig. 9.2 by applying the following equations to the continuity and momentum equations:

$$f(x, t) \simeq \frac{\theta}{2}\left(f_{j+1}^{i+1} + f_{j}^{i+1}\right) + \frac{(1-\theta)}{2}\left(f_{j+1}^{i} + f_{j}^{i}\right) \tag{9.4}$$

$$\frac{\partial f}{\partial x} \simeq \frac{\theta\left(f_{j+1}^{i+1} + f_{j}^{i+1}\right)}{\Delta x} + (1-\theta)\frac{\left(f_{j+1}^{i} + f_{j}^{i}\right)}{\Delta x} \tag{9.5}$$

$$\frac{\partial f}{\partial t} \simeq \frac{f_{j+1}^{i+1} - f_{j+1}^{i} + f_{j}^{i+1} - f_{j}^{i}}{2\Delta t} \tag{9.6}$$

where $f(x, t)$ = A flow or channel variable which is a function of x and t,

Δx = Distance increment,

Δt = Time increment,

θ = A weighting coefficient, where $0 \leq \theta \leq 1$,

and the subscripts i, j refer to co-ordinates on the t and x axes respectively.

Wellington (1978) chose to define the lateral inflow over the length of an element rather than defining q_ℓ at each computational point. To define the lateral inflow in this manner, Wellington (1978) found it necessary to adopt a slightly different form of Eq. 9.4. Thus

$$f(x, t) \simeq \theta\, f_{j+1/2}^{i+1} + (1-\theta)\, f_{j+1/2}^{i} \tag{9.7}$$

where $f_{j+1/2}^{i+1}$ and $f_{j+1/2}^{i}$ are the values of the parameter, f, at the location $(x_j + x_{j+1})/2$ on the i^{th} and $i+1^{th}$ time lines respectively.

Wellington (1978) then proceeded to discretize and linearise the continuity and momentum equations using Eqs. 9.5 - 9.7 and obtained equations of the form, for flow continuity

$$Hl_j \Delta Z_{j+1} + Bl_j \Delta Q_{j+1} = Cl_j \Delta Z_j + Dl_j \Delta Q_j + Gl_j \tag{9.8}$$

and for momentum

$$H2_j \Delta Z_{j+1} + B2_j \Delta Q_{j+1} = C2_j \Delta Z_j + D2_j \Delta Q_j + G2_j \tag{9.9}$$

The relations, derived by Wellington (1978), for each of the coefficients in Eqs. 9.8 and 9.9 are presented in full in Appendix F.

For a set of N computational points, Eqs. 9.8 and 9.9 give a

total of 2(N - 1) equations with 2N unknowns. For the solution to be determinate a further two relations must be defined, in the form of boundary conditions. Wellington (1978) adopted the Double Sweep technique developed by Priessmann (Liggett and Cunge (1975)) to solve the resulting determinate set of equations.

9.2.3 Flow Boundary Conditions

Three types of boundary condition can be used at both the upstream and downstream boundary, namely

$$\begin{aligned} &\text{(i)} \quad Z = Z(t) \text{ given} \\ &\text{(ii)} \quad Q = Q(t) \text{ given} \\ &\text{(iii)} \quad Q = f(Z) \text{ given} \end{aligned} \tag{9.10}$$

In this model the upstream boundary condition is assumed to be given by a discharge hydrograph, type (ii), and the downstream boundary condition by a uniform rating curve, type (iii).

It should be noted that errors may be introduced to the solution when a steady-state boundary condition is applied at the downstream boundary under unsteady flow conditions. However, unless data in the form of depth or discharge as a function of time is available at the downstream boundary, it is difficult to define a downstream boundary condition other than by a steady-state rating curve. For the purposes of investigating the response of the sediment phase to steady and unsteady flow conditions the assumed boundary conditions were considered sufficient.

9.3 SEDIMENT ROUTING

The third and fourth equations required for an unsteady water and sediment routing model describe the sediment phase. One of these equations must be an equation which represents sediment continuity. In this model, the fourth equation characterises the spatial and temporal lag effects in bed load transport and is the essential difference between this model and previous models.

9.3.1 Sediment Continuity Equation

The sediment continuity equation as given by Wellington (1978) is

$$\frac{1}{u_s}\frac{\partial G_V}{\partial t} - \frac{G_V}{u_s^2}\frac{\partial u_s}{\partial t} + (1 - \lambda')\frac{\partial A_b}{\partial t} + \frac{\partial G_V}{\partial x} = 0 \tag{9.11}$$

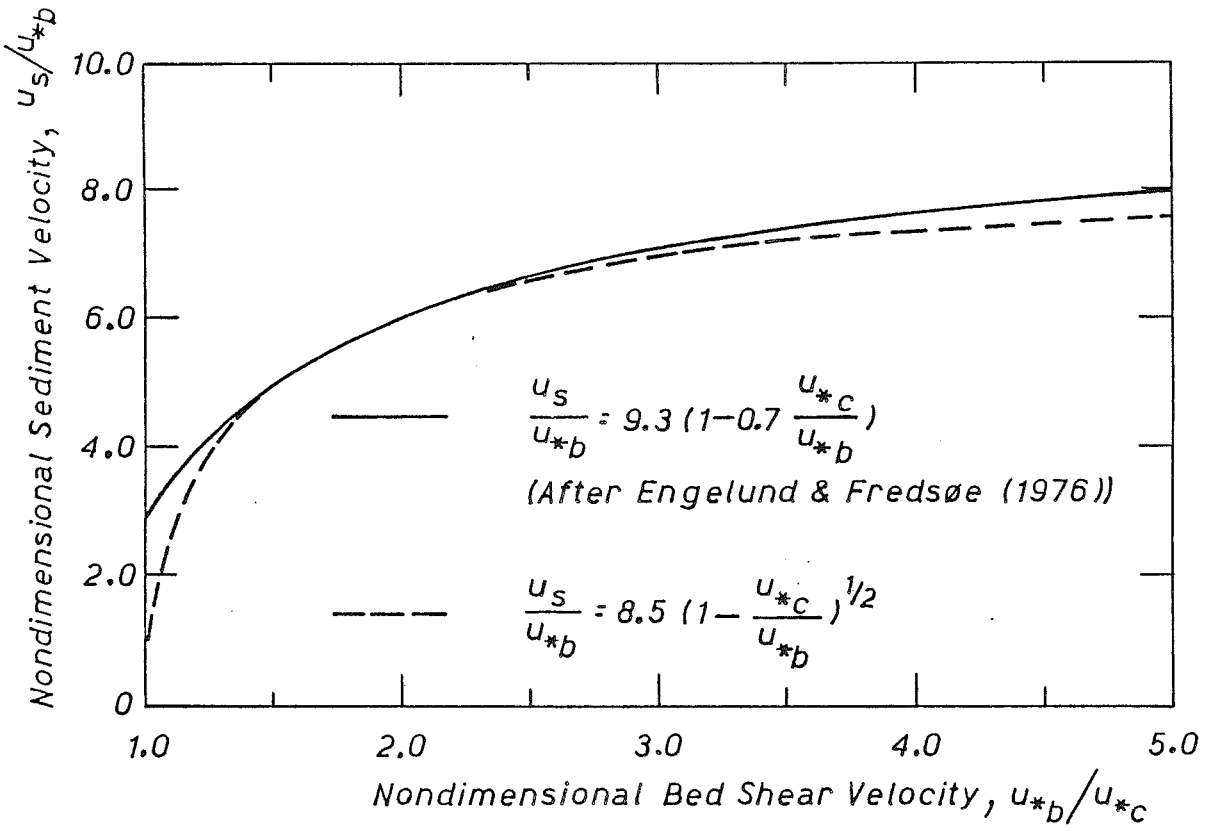

Figure 9.3 Nondimensional Sediment Velocity Against Nondimensional Bed Shear Velocity

where A_b = Area of deposition/scour of the bed at a section,
G_V = Sediment transport rate (by volume),
u_s = Mean sediment velocity, and
λ' = Bed porosity.

Alternatively, Eq. 9.11 can be expressed in terms of the bed elevation, Z_b, and the bed width, B_w, thus

$$\frac{1}{u_s}\frac{\partial G_V}{\partial t} - \frac{G_V}{u_s^2}\frac{\partial u_s}{\partial t} + (1 - \lambda')\, B_w \frac{\partial Z_b}{\partial t} + \frac{\partial G_V}{\partial x} = 0 \qquad (9.12)$$

9.3.2 Sediment Velocity Relation

Several relations for the mean sediment velocity have been proposed. Einstein (1950) considered that

$$\frac{u_s}{u_{*_b}'} = 11.6 \qquad (9.13)$$

whereas, Engelund and Fredsφe (1976) proposed that

$$\frac{u_s}{u_{*_b}} = 9.3\left(1 - 0.7\,\frac{u_{*_c}}{u_{*_b}}\right) \qquad (9.14)$$

Engelund and Fredsφe (1976) compared their relation with the data of Meland and Normann (1966) and Fernandez Luque (1974) and found good agreement over the range $0.84 < u_{*_b}/u_{*_c} < 3.2$.

More recently, Yalin (1983) suggested that

$$\frac{u_s}{u_{*_b}} = 8.5 \qquad (9.15)$$

Since the sediment transport capacity relation is a function of excess velocity, Eq. 7.35, it is predicted that the capacity of the flow to transport sediment ceases when threshold conditions are encountered at the bed. Equations 9.13, 9.14 and 9.15 are thus unsuitable since they predict a non-zero sediment velocity under threshold conditions. Hence, a new sediment velocity relation, which overcomes this difficulty, was developed. This relation is

$$\frac{u_s}{u_{*_b}} = 8.5\left(1 - \frac{u_{*_c}}{u_{*_b}}\right)^{1/2} \qquad (9.16)$$

and is compared with the relation of Engelund and Fredsφe (1976) in Fig. 9.3. The agreement between these two relations is within 5% over the range $1.3 < u_{*_b}/u_{*_c} < 5.0$.

The relation given in Eq. 9.16 behaves in the required manner as threshold conditions are approached. Interestingly, Eq. 9.16 also asymptotically approaches the relation of Yalin (1983), Eq. 9.15, for large bed shear velocity ratios i.e. $u_{*_b}/u_{*_c} > 10.0$.

9.3.3 Spatial Lag Equation

The analysis of the results presented in Chapter 7 demonstrated that when "constrained" sediment transport boundary conditions are encountered the sediment transport capacity of the flow cannot be satisfied everywhere. An equation found to describe this phenomenon is the spatial lag equation, given by

$$(1 - \lambda') \frac{\partial A_b}{\partial t} = C_{SL}(G_V - G_{VC}) \tag{9.17}$$

where

$$C_{SL} = \frac{1}{\alpha_L d_{50}(\theta - \theta_c)} \tag{9.18}$$

In the spatial lag analysis, the bedload transport capacity, G_{VC}, was calculated by inserting instantaneous values of flow properties which reflected the non-equilibrium flow conditions in the bedload transport capacity relation determined under equilibrium conditions. The same assumption is made in this model.

The equation of sediment continuity, Eq. 9.11, and the spatial lag equation, Eq. 9.17, comprise, with appropriate boundary conditions (Section 9.3.6), a determinate set of sediment equations.

9.3.4 Temporal Lag Equations

Before using the sediment equations, Eqs. 9.11 and 9.17, in the numerical simulation of the sediment phase one further aspect needs to be considered. This is the temporal response of an alluvial system to unsteady flow conditions i.e. temporal lag.

When the flow is unsteady it is found that the geometrical properties of the bed forms and the sediment transport rate are not related to local flow conditions because it takes time for the bed forms to change their geometrical properties. This phenomenon has been

viewed as a temporal lag, and was investigated in Chapter 8.

A feature of the temporal lag model proposed in Chapter 8 is that the temporal response of both bed forms and sediment transport is characterised by a single variable, q_e, the equivalent steady flow rate. An impulse model was used to develop a general solution for the temporal variation of this variable under unsteady flow conditions. This general solution is

$$q_e(t) = q_b + \sum_{i=1}^{m} a_{Q_i} \left[(t - t_{o_i}) + T_{e_i} \ln \left(\frac{T_{e_i}}{T_{e_i} + t - t_{o_i}} \right) \right] \qquad (9.19)$$

where all variables are as previously described in Section 8.2.5.

The bed roughness, under unsteady flow conditions, can be evaluated, Eqs. 8.52 and 8.55, from a relation of the form

$$n_{b_u} = f(S_f, q_e) \qquad (9.20)$$

At later times, when temporal lag effects have dissipated, the bed roughness is a function of local flow conditions, and

$$n_b = f(S_f, q) \qquad (9.21)$$

An important feature of the temporal lag model is the method used to calculate the bedload transport capacity under unsteady flow conditions. The unsteady bedload transport capacity is calculated by inserting instantaneous values of flow properties which reflect the temporal response of the alluvial system in the equilibrium bedload transport capacity relation. Thus, under unsteady flow conditions and from Eqs. 7.26, 8.7 and Appendix E, the bedload transport capacity, under unsteady flow conditions, is given by

$$G_{VC_u} = f(S_f, q_e) \qquad (9.22)$$

At later times, when temporal lag effects have dissipated, the response of the alluvial system is controlled by local flow conditions, and

$$G_{VC} = f(S_f, q) \qquad (9.23)$$

In this numerical model, sediment routing is accomplished by solving the sediment continuity equation, Eq. 9.11, and the spatial lag equation, Eq. 9.17, which incorporates Eq. 9.22. Hence, in the sediment routing phase, temporal lag effects are included in the spatial

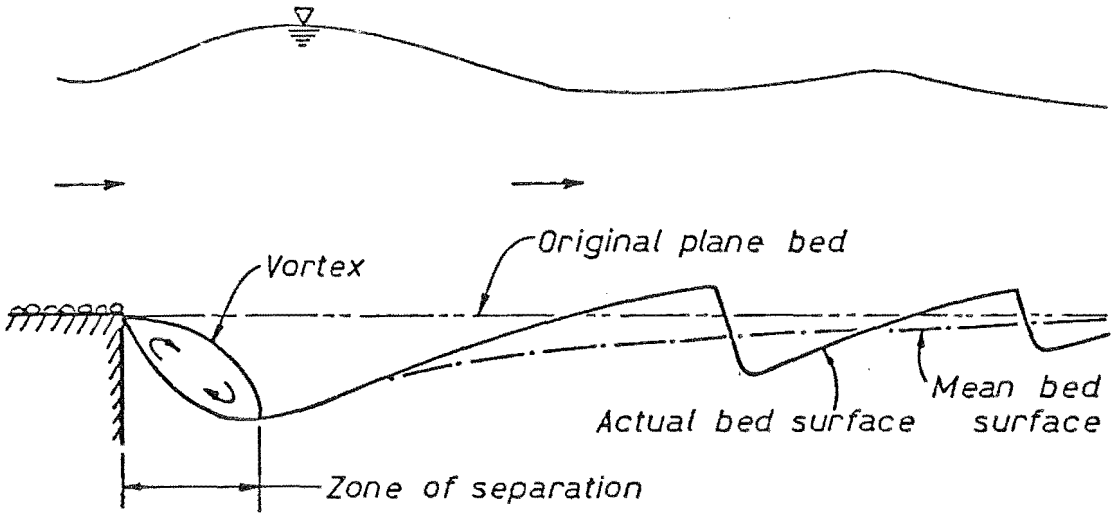

Figure 9.4 Flow Field in a Local Scour Hole Downstream of a Fixed Bed

lag equation via the bedload transport capacity term. The flow routing phase is also influenced by temporal lag effects via the bed roughness term in the expression for conveyance in Eq. 9.2.

9.3.5 Sediment Routing Solution Scheme

Wellington (1978), using the Priessman implicit scheme, developed a solution scheme for the two sediment equations given by Eqs. 9.11 and 9.17. He reported that early investigations into methods of discretizing the spatial lag equation showed that unless the term $C_{SL}G_V$ was formulated on the forward time line (t^{i+1}), Fig. 9.2, that local instabilities in scour and deposition were observed when large changes in sediment load occurred.

With this modification, the sediment continuity and spatial lag equations were discretized and linearized and equations of the following form obtained; for sediment continuity

$$H3_j \Delta G_{V_{j+1}} + B3_j \Delta A_{b_{j+1}} = C3_j \Delta G_{V_j} + D3_j \Delta A_{b_j} + G3_j \qquad (9.24)$$

and for the spatial lag equation

$$H4_j \Delta G_{V_{j+1}} + B4_j \Delta A_{b_{j+1}} = C4_j \Delta G_{V_j} + D4_j \Delta A_{b_j} + G4_j \qquad (9.25)$$

The relations for each of the coefficients in Eqs. 9.24 and 9.25 are presented in full in Appendix F.

For a set of N computational points, Eqs. 9.24 and 9.25 may be applied to give a total of 2(N - 1) equations with 2N unknowns. A further two relations, in the form of boundary conditions (Section 9.3.6), must be determined in order for the solution to be determinate. In this numerical model, this system of equations is solved by the Gaussian Elimination technique.

9.3.6 Sediment Boundary Conditions

Since it was intended that the numerical model be used to simulate the experiments conducted by Bell (1980) it was necessary to consider the influence an upstream fixed bed has on the geometry of the mobile bed immediately downstream of the fixed to mobile bed interface. In the field this condition exists, for example, at the end of a spillway apron.

Downstream of a fixed bed, where there is no sediment input, a mobile bed is scoured and a scour hole of the type shown in Fig. 9.4 is

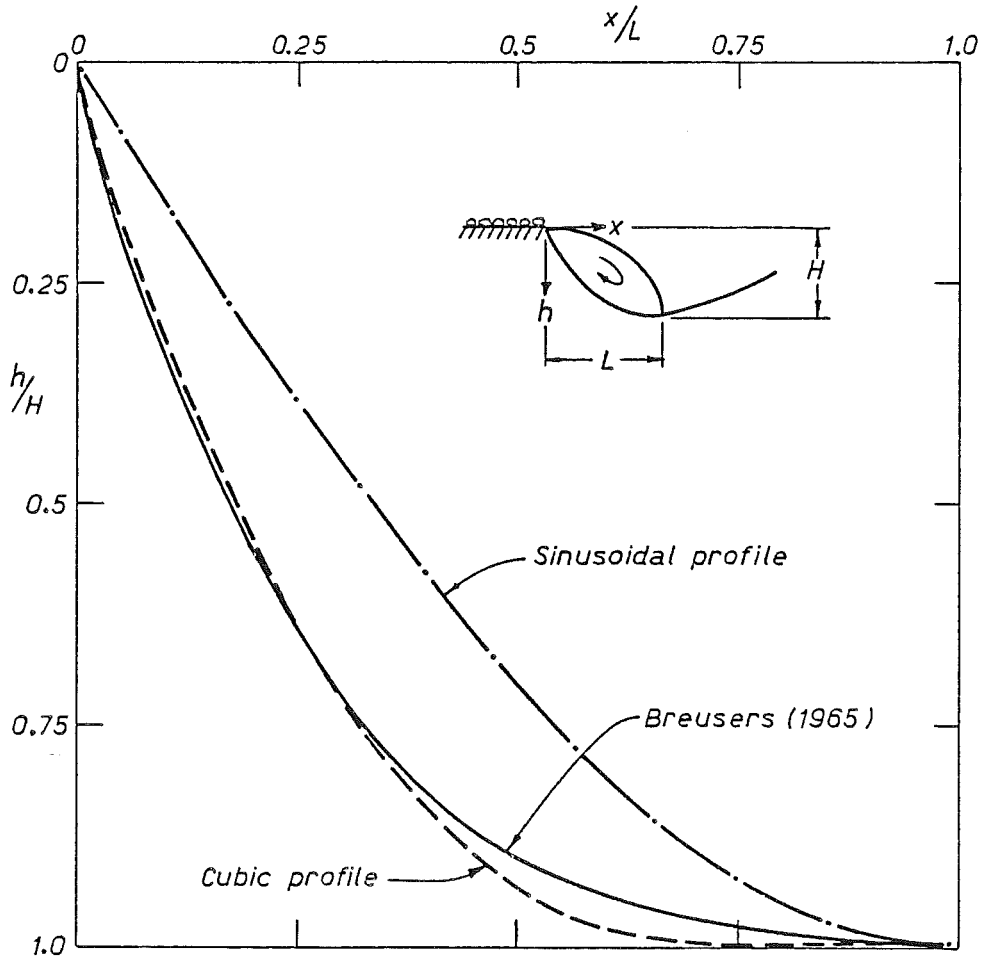

Figure 9.5 Scour Hole Profile in Zone of Separation

formed (Bell (1980), Dietz (1969), Mosonyi and Schoppmann (1968)). It has been noted that a zone of separation occurs and a fluid vortex forms (Fig. 9.4). The scour hole deepens under this fluid vortex until it reaches a local maximum depth at the downstream extremity of the vortex.

In this model the presence of the zone of separation is recognised by assuming the upstream sediment boundary condition to be located at the downstream end of the zone of separation, i.e. at the point of local maximum scour. The sediment boundary condition was developed for a rectangular channel, i.e. $B_w = B$, and took the form

$$G_V = G_V \text{ calculated} \tag{9.26}$$

The aim, when calculating values of the sediment transport rate at the upstream sediment boundary for use in Eq. 9.26, is to maintain compatability between sediment transport rates and the rate of scour. The spatial lag equation is used to achieve this compatability. Since the location of the point of maximum scour moves downstream with time the location of the upstream sediment boundary does likewise; hence this is a mobile boundary condition.

Before a scheme to calculate sediment transport rates at the upstream boundary could be formulated it was necessary to determine the general geometric properties of the bed under the fluid vortex.

Breusers (1965) measured and plotted typical scour hole profiles in the zone of separation. These profiles collapsed onto the nondimensional curve given in Fig. 9.5. A cubic equation of best fit was found to be

$$\frac{h}{H} = 1.5\left(\frac{x}{L}\right)^3 - 4.0\left(\frac{x}{L}\right)^2 + 3.5\left(\frac{x}{L}\right) \tag{9.27}$$

where h = Scour depth with respect to the plane bed at $t = 0$,

$= Z_b(x, 0) - Z_b(x, t)$

L = Distance to the point of local maximum scour from the fixed bed, and

H = Local maximum scour depth.

Integration of Eq. 9.27 gives a total volume of scour per unit width of 0.791 HL.

The second relation which was required was an equation which relates the location and depth of the point of local maximum scour to

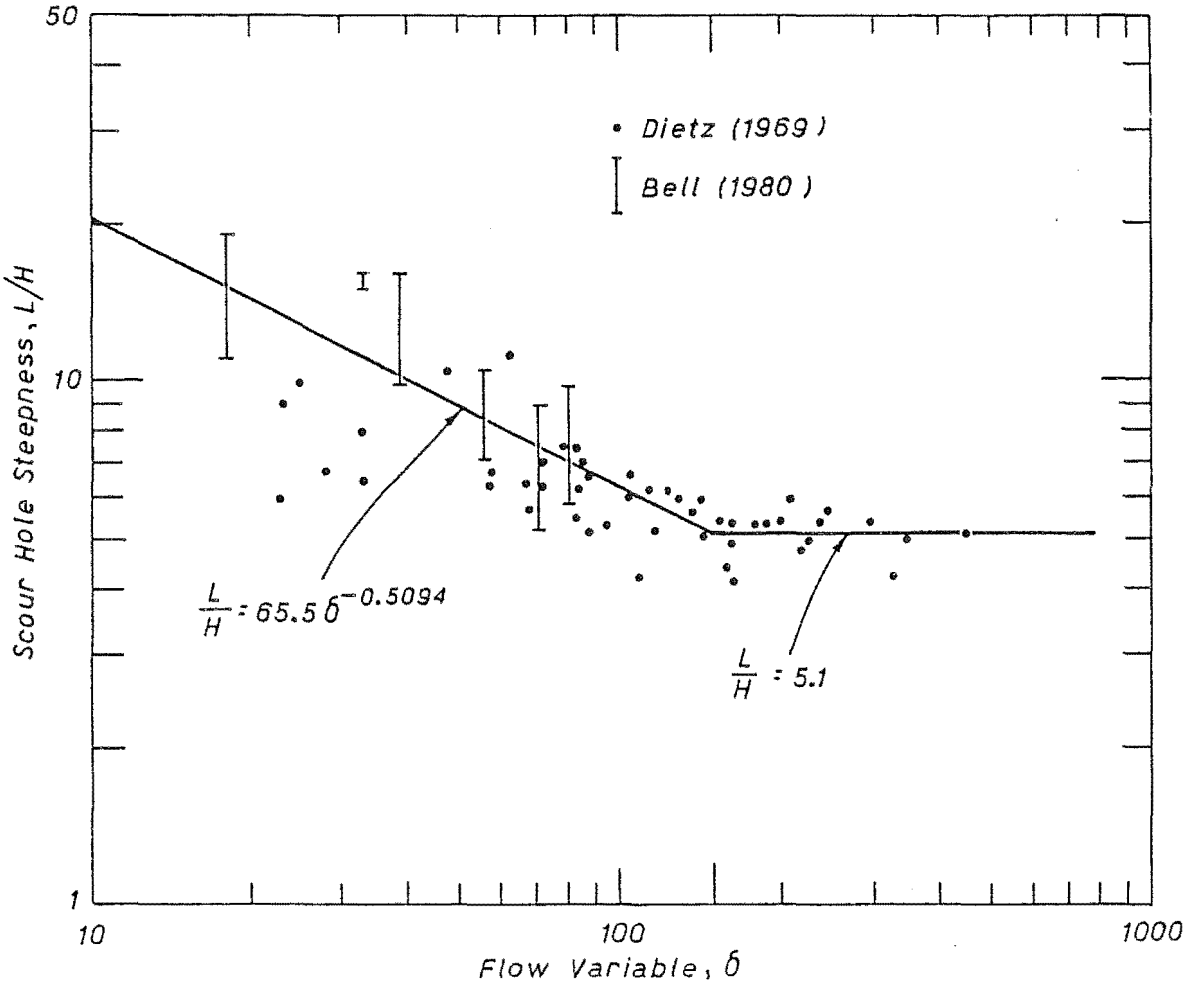

Figure 9.6 Scour Hole Steepness Against Upstream Flow Parameter

reference flow properties. Dietz (1969) presented experimental data of this kind in the form (Fig. 9.6)

$$\frac{L}{H} = f(\delta) \tag{9.28}$$

where, (Fig. 9.7)

$$\delta = \frac{U_1 - U_{c_1}}{\omega} \frac{1}{Dgr} \tag{9.29}$$

and Dgr = Dimensionless grain size, previously defined in Eq. 7.41,

U_1 = Average flow velocity at the fixed/mobile bed interface,

U_{c_1} = Threshold average velocity at the fixed/mobile bed interface, and

ω = Sediment fall velocity.

Data of this kind was also obtained by scaling local maximum scour hole depths and distance downstream from the interface of the point of local maximum scour from the scour hole profile records of Bell (1980). The data of Dietz (1969) and Bell (1980) are presented in Fig. 9.6. Two relations were fitted to the data, giving

$$\frac{L}{H} = \begin{cases} 65.5\ \delta^{-0.5094} & \delta \leq 150 \\ 5.1 & \delta > 150 \end{cases} \tag{9.30}$$

The movement of the point of local maximum scour depth is demonstrated in Fig. 9.7. During an increment in time, Δt, the location of the point of local maximum depth moves from point A to point B and from section 2 to section 2'. The upstream boundary scheme predicts the location of section 2', at any given time, and calculates the sediment transport rate on the forward time at this section. This scheme is outlined as follows.

At the end of a time increment, Δt, the volumetric sediment transport rate is given by

$$G_V(t + \Delta t) = \frac{B_w(1 - \lambda')\Delta V_b}{\Delta t} \tag{9.31}$$

where ΔV_b = Volume of bed scoured per unit width over the time increment, where

$$\Delta V_b = 0.791\ L'H' - 0.791\ LH - (L' - L)H \tag{9.32}$$

The spatial lag equation is

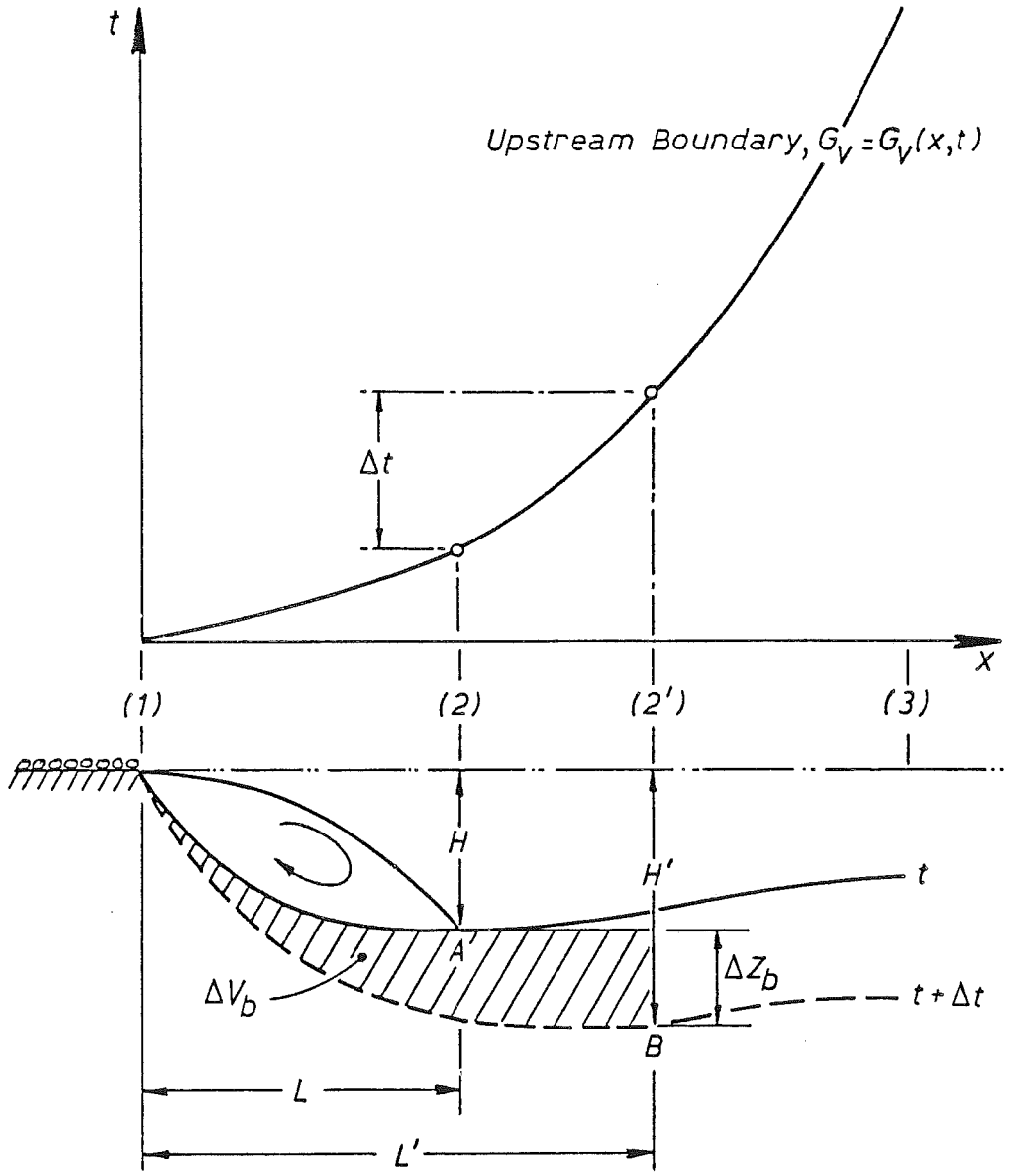

Figure 9.7 Definition Diagram for Upstream Sediment Boundary Condition

$$(1 - \lambda') \frac{\partial A_b}{\partial t} = C_{SL}(G_V - G_{VC}) \tag{9.33}$$

which becomes, on the forward time line

$$(1 - \lambda') \frac{\Delta A_b}{\Delta t} = C_{SL}(t + \Delta t)\ (G_V(t + \Delta t) - G_{VC}(t + \Delta t)) \tag{9.34}$$

Recalling that

$$\Delta A_b = B_w \Delta Z_b \tag{9.35}$$

and knowing values of the spatial lag coefficient and sediment transport capacity, Section 9.5.3, it is possible to solve Eqs. 9.31, 9.32, 9.34 and 9.35 for ΔZ_b and for $G_V(t + \Delta t)$. The method used to solve these equations is based on the discretized form of Eq. 9.33 given by

$$H4_2 \Delta G_{V_2} + B4_2 \Delta A_{b_2} = C4_2 \Delta G_{V_2} + D4_2 \Delta A_{b_2} + G4_2 \tag{9.36}$$

and is described in full in Appendix F. Once the value of ΔZ_b is known it is possible to locate section 2' and to then interpolate a value of the sediment discharge, on the current time line, at section 2', from known transport rates at Sections 2 and 3.

Thus, the upstream sediment boundary condition, which is assumed to be located at section 2', is

$$\Delta G_V = G_V(t + \Delta t) - G_V(t) \tag{9.37}$$

The upstream sediment boundary scheme formulated above was for the restrictive case of zero sediment inflow at the upstream end of the test reach, section 1 (Fig. 9.7). To obtain a more general scheme two small modifications were made.

Firstly, the equation used to calculate the sediment transport rate on the forward time line, Eq. 9.31, was modified. Assuming that the geometry of the scour hole is unaltered by the influx of sediment, the more general form of this equation is

$$G_V(t + \Delta t) = \frac{B_w(1 - \lambda')\Delta V_b}{\Delta t} + G_{V_1}(t + \Delta t) \tag{9.38}$$

where G_{V_1} = Volumetric rate of sediment inflow into the test reach.

Secondly, if at all times the sediment inflow into the test reach is known to be greater than the sediment transport capacity,

i.e. sediment overloading and aggradation, then a scour hole will not develop. Under these conditions the upstream sediment boundary is assumed to be located 1 mm downstream of the fixed/mobile bed interface. Thus, the upstream sediment boundary is effectively located at the upstream interface and does not move.

The downstream sediment boundary condition was assumed to be given by applying the spatial lag equation at the downstream boundary section. The discretized form of this boundary condition, which occurs at the N^{th} computational point, is

$$H4_N \Delta G_{V_N} + B4_N \Delta G_{V_N} = C4_N \Delta A_{b_N} + D4_N \Delta A_{b_N} + G4_N \qquad (9.39)$$

where the general form of the various coefficients is given in Appendix F.

9.3.7 Adjustment of Bed Levels and Flow Parameters

Since this is an uncoupled numerical model, that is flow routing is completed before sediment routing is commenced, it is necessary to adjust bed levels and flow parameters at the end of each time step.

The sediment routing scheme calculates the total area of bed erosion or deposition at each computational point during a given time increment. These values are then used to adjust the bed elevations at each computational point on the forward time lines. In this model, the method used is based on the scheme proposed by Brown and Li (1979) and evaluated by Phillips (1981). This method is outlined in Section 9.5.4.

Similarly, the flow parameters are adjusted to those values which were calculated on the forward time line during the flow routing phase.

Once all adjustments have been made flow routing and sediment routing for next time step increment is commenced.

9.4 PROGRAM DATA REQUIREMENTS

Only the general nature of the data required to operate both the flow and sediment routing phases of the numerical model are outlined here. The specific manner in which these data are supplied to the model is given in Appendix F and can also be ascertained by examining the program listing given in Appendix F.

Once the channel reach has been identified, it is necessary to divide this reach into sub-reaches, which need not necessarily be of

equal length. It is assumed that in each sub-reach the lateral channel geometry and bed material characteristics are reasonably uniform. The cross sectional geometry of each sub-reach is then ascertained and assumed to apply at the computational point which is normally defined, in terms of the longitudinal distance from the upstream boundary, at the centre of the sub-reach. In the cases of the first (or upstream) and last (or downstream) sub-reaches these computational points are defined as being located at the upstream and downstream boundary, respectively, of these sub-reaches and thus of the channel reach.

A feature of the model is the ability to generate cross sectional channel data. If the channel geometry down the reach can be described by a series of widely spaced representative sections then this feature can be used to calculate the channel geometry at evenly spaced intermediate computational points between these sections. Linear interpolation is used to calculate these intermediate channel geometries. The use of this feature markedly reduces the required amount of channel input data.

Flow data required include: the initial flow rate and stage at all computational points, the upstream flow hydrograph and the lateral inflow hydrographs for all sub-reaches. Another feature of the model is the ability to describe a sub-reach lateral inflow hydrograph by a hydrograph number. That is, the model only requires that a numbered set of representative lateral inflow hydrographs be defined. The lateral inflow hydrograph for each sub-reach is thus referenced to this family of lateral hydrographs by a hydrograph number. This feature also reduces the required amount of input data.

The assumed downstream flow boundary condition, a steady flow rating curve, is not required since the model automatically generates the steady flow rating curve at the downstream boundary.

The sediment data required include: the values of the various bed material properties, the initial bed roughness values and sediment transport rates at all computational points and the sediment hydrograph at the upstream flow boundary.

Only the initial bed roughness values are required because the general bed roughness equation, derived in the analysis of resistance, is incorporated in the model. Thus, at later times the bed roughness values are automatically calculated within the model.

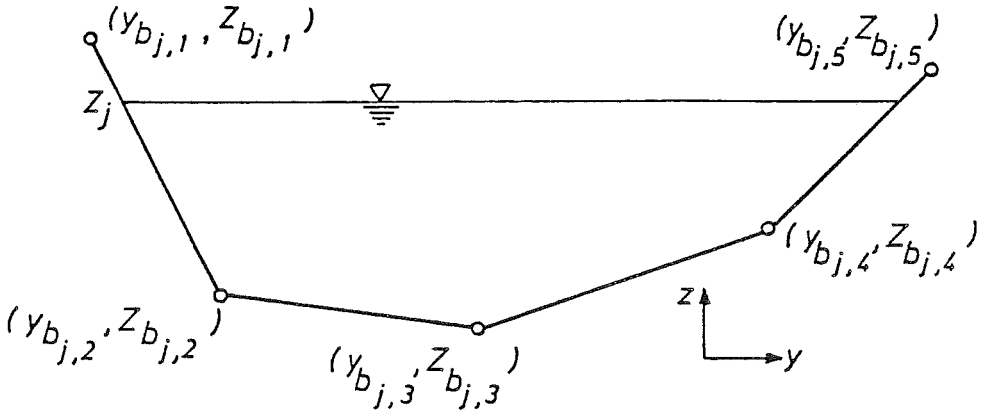

Figure 9.8 Coordinate System for Channel Cross Section at j^{th} Computational Point

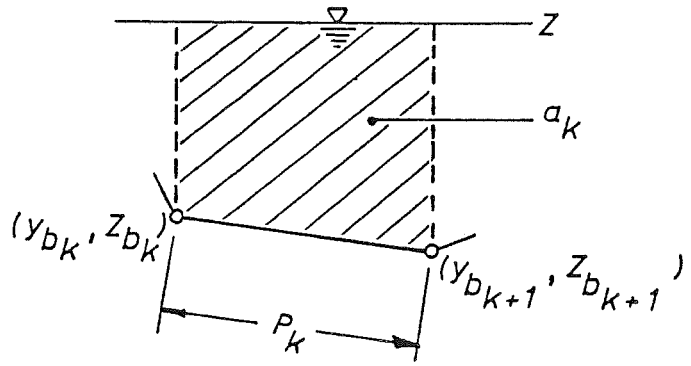

Figure 9.9 Typical Cross Section Element

Although the location of the upstream sediment boundary does not normally coincide with the location of the upstream flow boundary it is still necessary to describe the sediment inflow into the test reach because this sediment inflow forms part of the upstream sediment boundary scheme in Eq. 9.38. The downstream sediment boundary condition, which is obtained by applying the spatial lag equation at the downstream boundary computational point, is incorporated in the model and requires no additional data.

A full description of all the flow and sediment data required by the model is given in Appendix F.

9.5 PROGRAM COMPUTATIONS

The methods used to calculate the various flows and sediment properties are as follows.

9.5.1 Channel Geometry

At each computational point the channel cross section is defined by a set of (y_b, Z_b) coordinates. An example of the use of this coordinate system to define a non-prismatic channel cross section, for the j^{th} computational point, is given in Fig. 9.8. It is assumed in the model that the channel cross sections pertain to in-bank flow only. Since the upstream sediment boundary scheme was developed for a rectangular cross section it is also assumed that the cross section geometry in this initial region of the channel is rectangular.

9.5.2 Hydraulic Properties

A typical channel cross section element, used in the calculation of hydraulic properties, is shown in Fig. 9.9. The various hydraulic properties are calculated in the following manner.

- Area

  The total area of flow is computed by summing the elemental area between consecutive cross section coordinate points. The total area of flow is

$$A = \sum_{k=1}^{m} a_k \tag{9.40}$$

  where there are m elemental areas, a_k, given by

$$a_k = (Z - 0.5(Z_{b_k} - Z_{b_{k+1}}))\ (y_{b_{k+1}} - y_{b_k}) \tag{9.41}$$

If the water surface intersects the cross section element, then Eq. 9.41 for (k = 1, m) becomes

$$a_k = 0.5(Z - Z_{b_{k+1}})^2 \frac{(y_{b_{k+1}} - y_{b_k})}{|Z_{b_k} - Z_{b_{k+1}}|} \tag{9.42}$$

. Velocity

The average velocity of the flow is

$$U = Q/A \tag{9.43}$$

. Wetted Perimeter

The total wetted perimeter is computed by summing the elemental wetted perimeters. The total wetted perimeter is

$$P = \sum_{k=1}^{m} p_k \tag{9.44}$$

where the elemental wetted perimeter, p_k, is the length of cross section between coordinate points beneath the water surface, and is given by

$$p_k = \sqrt{(y_{b_k} - y_{b_{k+1}})^2 + (Z_{b_k} - Z_{b_{k+1}})^2} \tag{9.45}$$

If the water surface intersects the cross section element, then Eq. 9.45 for (k = 1, m) has to be slightly modified. Under these conditions (Fig. 9.8)

$$p_k = |(Z - Z_{b_{k+1}})| \sqrt{1 + \frac{(y_{b_k} - y_{b_{k+1}})^2}{(Z_{b_k} - Z_{b_{k+1}})^2}} \tag{9.46}$$

. Width

The total flow width at the surface is computed by summing the elemental widths. The total flow width is

$$B = \sum_{k=1}^{m} b_k \tag{9.47}$$

where the elemental width, b_k, is given by

$$b_k = (y_{b_{k+1}} - y_{b_k}) \tag{9.48}$$

If the water surface intersects the cross section element then

Eq. 9.48 for (k = 1, m) is given by

$$b_k = \left|(y_{b_{k+1}} - y_{b_k})\right| \frac{(Z - Z_{b_{k+1}})}{\left|Z_{b_k} - Z_{b_{k+1}}\right|} \tag{9.49}$$

. Hydraulic Radius

The elemental hydraulic radius of the bed, r_{b_k}, is

$$r_{b_k} = a_k/p_k \tag{9.50}$$

The total hydraulic radius of the bed, R_b, is from Eq. 9.53

$$R_b = \left(\frac{Kn_b}{A}\right)^{1.5} \tag{9.51}$$

. Conveyance

The total conveyance is computed by summing the sub-conveyances. The total conveyance is

$$K = \sum_{k=1}^{m} k_k \tag{9.52}$$

Assuming that the bed roughness is constant around the cross section, the sub-conveyance is computed from Manning's equations, thus

$$k_k = \frac{a_k r_{b_k}^{2/3}}{n_b} \tag{9.53}$$

. Friction Slope

The friction slope is

$$S_f = (Q/K)^2 \tag{9.54}$$

. Bed Shear Velocity

The bed shear velocity is

$$u_{*_b} = \sqrt{gR_b S_f} \tag{9.55}$$

. Shields Parameter

The Shields parameter is

$$\theta = \frac{u_{*_b}^2}{(S_s - 1)g\,d_{50}} \tag{9.56}$$

. Velocity Distribution Factor

The velocity distribution factor, α, defined in Eq. 9.57 accounts for the distribution of flow across the cross section but not the vertical shape of the velocity profile. Thus

$$\alpha = \frac{\sum_{k=1}^{m} k_k^3/a_k^2}{K^3/A^2} \tag{9.57}$$

9.5.3 Sediment Properties

. Sediment Velocity

The sediment velocity is computed from the relation

$$u_s = 8.5u_{*_b}\sqrt{1 - \frac{u_{*_c}}{u_{*_b}}} \tag{9.58}$$

. Spatial Lag Coefficient

The spatial lag coefficient is computed from the relation

$$C_{SL} = \frac{1}{\alpha_L d_{50}(\theta - \theta_c)} \tag{9.59}$$

. Bed Roughness

The bed roughness value was found from an analysis of flow resistance data to be given by the relation

$$n_b = \alpha_n \theta^{\beta_n} \tag{9.60}$$

. Sediment Transport Capacity

The total volumetric sediment transport capacity is computed from

$$G_{VC} = \frac{g_{sc} B_w}{\rho_s} \tag{9.61}$$

where the sediment transport capacity in mass rate per unit width is given by

$$g_{sc} = a(U - U_c)^b \tag{9.62}$$

and

$$U_c = U \frac{u_{*_c}}{u_{*_b}} \tag{9.63}$$

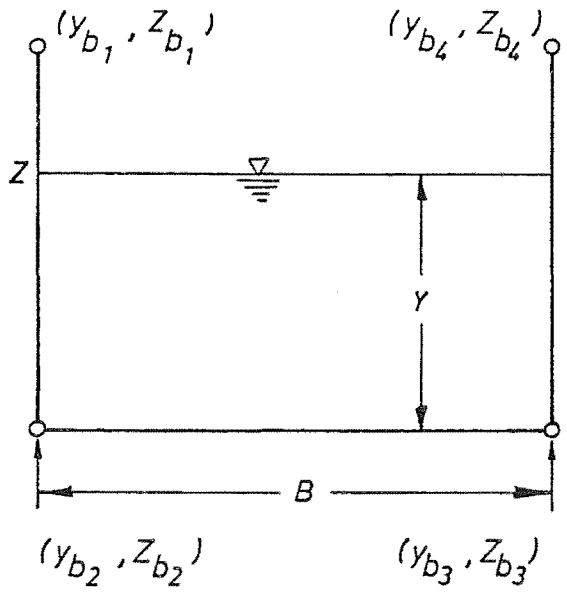

Figure 9.10 Typical Rectangular Channel Geometry

9.5.4 Distribution Scheme

The conveyance scheme proposed by Brown and Li (1979) is used to determine the bed elevation changes at each cross section coordinate point. At the end of each time increment, when flow and sediment routing have been completed, it is necessary to distribute the total area of scour/deposition, ΔA_b, around the cross section. Bed elevation changes at each coordinate point ($2 < k < m - 1$) are computed from the relation (Fig. 9.9)

$$\Delta Z_{b_k} = \frac{(k_{k-1} + k_k)\ \Delta A_b}{K\ (b_{k-1} + b_k)} \tag{9.64}$$

9.5.5 Rectangular Channel Relations

The program computations presented above are those undertaken in the general model. When the general model was used to simulate the experiments of Bell (1980) it was found that relation for total conveyance had to be modified. This was because the general method, Eq. 9.52, gives an equivalent value of total hydraulic radius equal to the flow depth for a rectangular cross section. This was unsatisfactory since it ignored side-wall effects. When applying the model to the case of the rectangular channel of Bell (1980), it was assumed that, (from Section 5.1.2)

$$R_b = \frac{Y}{1 + 0.591Y} \tag{9.65}$$

and that

$$K = \frac{AR_b^{2/3}}{n_b} \tag{9.66}$$

When the scour/deposition distribution scheme is applied to the 4-point rectangular channel (Fig. 9.10)

$$\Delta Z_{b_2} = \Delta Z_{b_3} = \frac{\Delta A_b}{B} \tag{9.67}$$

where

$$B = y_{b_3} - y_{b_2} \tag{9.68}$$

Thus the model predicts that the bed degrades/aggrades uniformly across the channel at any given section. This in fact does not occur

because of side-wall effects. Hence, a correction scheme which converts average bed elevations at a section into centre-line bed elevations must be used to compare model predictions with centre-line bed profile data. The scheme used for Bell's (1980) data is described in Section 10.3.3.

Since the model predicts that the bed is level across the channel at any section, then the flow depth (Fig. 9.10) is simply

$$Y = Z - Z_{b_2} = Z - Z_{b_3} \tag{9.69}$$

9.6 SUMMARY

An uncoupled, one-dimensional unsteady flow and sediment routing model (UWASER) has been developed. An innovative feature of this model is the ability to simulate both spatial and temporal lag effects under bedload transport conditions.

Flow routing is accomplished by solving the equations of flow continuity and momentum using an implicit finite difference scheme. These equations were discretized using a modified Priessmann (SOGREAH) scheme developed by Wellington (1978); a double sweep algorithm is used to solve these equations.

Sediment routing is accomplished by solving the equations of sediment continuity and the spatial lag equation. These equations were also discretized using a Priessmann scheme; a Gaussian Elimination scheme was used to solve these equations. An innovative feature of the sediment routing model is the definition of an upstream sediment boundary condition which takes account of the zone of separation immediately downstream of a rigid to mobile bed interface. Consequently, under scour conditions the sediment boundary, which is located at the toe of the fluid vortex, is some way downstream of the rigid to mobile bed interface and moves downstream with time.

Spatial lag effects are directly incorporated in the model by the adoption of the spatial lag equation. Temporal lag effects are indirectly incorporated in the model through relations for the bedload transport capacity and bed roughness values under unsteady flow conditions.

The model has been formulated for the general case of a non-prismatic channel but is restricted to conditions where only in-bank

flow occurs and the channel geometry in the region of the upstream sediment boundary is rectangular.

This model was used to simulate the steady and unsteady flow experiments of Bell (1980). The results of these simulations and their comparison with the data of Bell (1980) are presented in Chapter 10.

Chapter 10 | Non-Steady Sediment Transport - Numerical Model Results

10.1 INTRODUCTION

The performance of the numerical model was tested by simulating six of the series of experiments conducted by Bell (1980).

The first three simulated were the ST09, ST07 and ST05 series of experiments. These were steady flow, non-equilibrium sediment transport experiments and were conducted in such a manner that only spatial lag effects were present. Hence, the performance of the spatial lag scheme adopted in the numerical model was tested by comparing numerical model results with the results of Bell (1980) for these experiments.

An alternative model has been proposed by several researchers which also accounts for spatial lag effects; it is a diffusion model. The performance of a diffusion model under conditions of bed degradation were tested by comparing diffusion model results with the results of Bell (1980) for the ST09 experiments. The performances of both the numerical model and the diffusion model are also compared.

The final three series of Bell's (1980) experiments simulated were the NS02, NS03 and NS06 series of experiments. These were unsteady flow, non-equilibrium sediment transport experiments where both spatial lag and temporal lag effects were present. The performances of both the spatial lag and temporal lag schemes adopted in the numerical model were tested by comparing numerical model results with the results of Bell (1980) for the triangular flood waves studied in his experiments.

Many previous researchers have considered the time lagged development of bed forms under unsteady flow conditions. These researchers then applied their temporal lag models to flow conditions given by a weakly, periodically varying water discharge. The temporal response of the alluvial system predicted by the numerical model, under flood waves,

is compared with the temporal response predicted by a typical model of these previous researchers to ascertain if the temporal response of an alluvial system to solitary flood waves and to periodically varying flows is similar.

The sediment and flow conditions for Bell's (1980) experiments and the spatial lag and temporal lag equations adopted in the numerical model are detailed below.

10.2 SEDIMENT PROPERTIES AND LAG EQUATIONS

10.2.1 Sediment Properties

The properties of the bed material studied by Bell (1980) were

Grain Size Distribution,	d_{35} = 1.92 mm
	d_{50} = 2.11 mm
	d_{65} = 2.31 mm
	σ_g = 1.25
Bed Porosity,	λ' = 0.42
Specific Gravity,	S_s = 2.75
Fall Velocity,	ω = 0.18 m/s
Critical Shields Parameter	θ_c = 0.04
Critical Bed Shear Velocity,	u_{*c} = 0.0381 m/s

10.2.2 Bed Roughness and Sediment Transport Capacity

An analysis of the SE and IM data of Bell (1980), Sections 5.2.3 and 5.4.3, determined that the general bed roughness relation for the experiments of Bell (1980) is

$$n_b = 0.0236\ \theta^{0.1185} \tag{10.1}$$

or, alternatively (Appendix E)

$$n_b = 0.0359\ S_f^{0.091} q^{0.0726} \tag{10.2}$$

The sediment transport capacity relation (Section 5.5.2) is

$$\underset{(N/s/m)}{g_{sc}} = 10.12\ \underset{(m/s)}{(U - U_c)}^{2.520} \tag{10.3}$$

where the capacity rate of sediment transport is in dry weight transport rate per unit width, in the manner of Bell (1980).

The sediment transport data presented in Fig. 5.10, for the current study, demonstrated that a transport relation of the type given in Eq. 10.3 holds over a wide range of friction slopes. Hence, it was assumed (Section 5.5.3) that the relation given by Eq. 10.3 also holds over a range of friction slopes in all experiments.

10.2.3 Spatial Lag Equation

The spatial lag coefficient, in the spatial lag equation (Section 9.3.3), was given by

$$C_{SL} = \frac{1}{\alpha_L d_{50}(\theta - \theta_c)} \tag{10.4}$$

Trial runs of the numerical model indicated that the ST09 scour rates of Bell (1980) were best simulated when the lower bound value of the step length constant, α_L, (Section 7.4.1) was used. Hence, it was assumed that

$$\alpha_L = 4000 \tag{10.5}$$

10.2.4 Temporal Lag Equations

Under unsteady flow conditions, the temporal response of the sediment phase is characterised by the variable, q_e, the equivalent steady flow rate. Values of this variable are obtained in the manner in Section 9.3.4, where the time scale relation for the bed material of Bell (1980) is (Section 8.3.1 and Appendix E)

$$T_{e_i} = \begin{cases} 0.1718\ S_f^{-1.2748}\ q_{L_i}^{0.7208} & q_{L_i} \leq q_{max} \\ 0.1718\ S_f^{-1.2748}\ q_{max}^{0.7208} & q_{L_i} > q_{max} \end{cases} \tag{10.6}$$

and q_{max} is the peak or maximum discharge of the upstream flow hydrograph.

The unsteady bed roughness relation is (Appendix E)

$$n_{b_u} = n_{b_e} = 0.0359\ S_f^{0.091}\ q_e^{0.0726} \tag{10.7}$$

The unsteady sediment transport capacity relation is, from Eqs. 8.7 and 10.3,

$$\underset{(N/s/m)}{g_{sc_u}} = 10.12\ \underset{(m/s)}{(U_e - U_{c_e})}^{2.520} \tag{10.8}$$

where, (Appendix E and Eq. 10.7)

RUN	DISCHARGE ($m^3/s/m$)	FLOW DEPTH (m)	BED ROUGHNESS	BEDLOAD TRANSPORT RATE (N/s/m)
ST09	0.160	0.198	0.01784	0.439
ST07	0.127	0.170	0.01758	0.250
ST05	0.097	0.143	0.01724	0.118

Table 10.1 Initial Flow and Sediment Conditions (ST Series)

$$U_e = 3.317 \times 10^7 \, S_f^{-0.167} \, n_{b_e}^{4.616} \tag{10.9}$$

and

$$U_{c_e} = 24.23 \, u_{*_c} \, S_f^{-0.167} \, n_{b_e}^{0.4044} \tag{10.10}$$

10.3 STEADY FLOW NON-EQUILIBRIUM TRANSPORT

The manner in which Bell (1980) conducted the ST series of experiments in a 0.305 m wide flume is briefly outlined and the associated initial flow and sediment conditions are presented. The results obtained from numerical simulations of the ST09, ST07 and ST05 experiments are presented and compared with the data of Bell (1980).

Diffusion models are briefly discussed and the results of a diffusion model simulation of the ST09 experiments are presented. The results of the numerical model and diffusion model simulations are also compared.

10.3.1 Initial Conditions - ST Runs

Bell (1980) created non-equilibrium sediment transport conditions during the ST series of experiments by having zero sediment input at the upstream boundary of the test reach. To obtain a steady flow non-equilibrium system without introducing temporal lag effects in the sediment phase, Bell (1980) performed the experiments as steady flow equilibrium transport runs, in a manner similar to that described in Section 4.4.1, until he considered the equilibrium sediment transport rate was attained. The sediment mass input at the upstream boundary was then halted at the beginning of the ST run and measurements begun.

Consequently, the initial flow conditions were constant discharge and uniform flow depth over the complete length of the test reach. This constant discharge was maintained throughout the run. The initial friction slope was

$$S_f = S_o = 0.002 \tag{10.11}$$

The initial sediment conditions were uniform bed roughness and uniform capacity rate of sediment transport, as given by Eq. 10.3, over the complete length of the test reach. The sediment transport boundary condition at the upstream end of the test reach was

TIME = 1800.0 (S) = 30.000 (MINS)

FLOW ROUTING

SECTION NUMBER	CHAINAGE (M)	TOP WIDTH (M)	AREA (M**2)	CONVEYANCE	ALPHA	VELOCITY (M/S)	STAGE (M)	DISCHARGE (M**3/S)	THALWEG (M)
1	0.000	0.305	0.060	1.101	1.0000	0.8081	1.1980	0.0488	1.000
2	0.234	0.305	0.074	1.566	1.0000	0.6613	1.2086	0.0488	0.967
3	0.500	0.305	0.071	1.448	1.0000	0.6881	1.2065	0.0488	0.974
4	0.750	0.305	0.069	1.382	1.0000	0.7050	1.2050	0.0488	0.978
5	1.250	0.305	0.067	1.295	1.0000	0.7290	1.2025	0.0488	0.983
6	1.750	0.305	0.065	1.237	1.0000	0.7462	1.2005	0.0488	0.986
7	2.500	0.305	0.064	1.180	1.0000	0.7647	1.1978	0.0488	0.989
8	3.500	0.305	0.062	1.133	1.0000	0.7808	1.1948	0.0488	0.990
9	4.500	0.305	0.062	1.108	1.0000	0.7901	1.1922	0.0488	0.990
10	5.500	0.305	0.061	1.096	1.0000	0.7946	1.1899	0.0488	0.989
11	6.500	0.305	0.061	1.092	1.0000	0.7962	1.1878	0.0488	0.987
12	7.500	0.305	0.061	1.091	1.0000	0.7966	1.1858	0.0488	0.985
13	8.500	0.305	0.061	1.091	1.0000	0.7966	1.1838	0.0488	0.983
14	9.500	0.305	0.061	1.091	1.0000	0.7966	1.1818	0.0488	0.981
15	10.500	0.305	0.061	1.091	1.0000	0.7966	1.1798	0.0488	0.979
16	12.000	0.305	0.061	1.091	1.0000	0.7966	1.1768	0.0488	0.976
17	14.000	0.305	0.061	1.091	1.0000	0.7966	1.1728	0.0488	0.972
18	16.000	0.305	0.061	1.091	1.0000	0.7966	1.1688	0.0488	0.968
19	18.000	0.305	0.061	1.091	1.0000	0.7966	1.1648	0.0488	0.964
20	20.000	0.305	0.061	1.091	1.0000	0.7966	1.1608	0.0488	0.960
21	40.000	0.305	0.061	1.091	1.0000	0.7966	1.1208	0.0488	0.920
22	60.000	0.305	0.061	1.091	1.0000	0.7966	1.0808	0.0488	0.880
23	80.000	0.305	0.061	1.091	1.0000	0.7966	1.0408	0.0488	0.840
24	100.000	0.305	0.061	1.091	1.0000	0.7966	1.0008	0.0488	0.800

STORAGE VOLUME ERROR = 0.000 PERCENT

SEDIMENT ROUTING

SECTION NUMBER	SEDIMENT DISCHARGE (N/S/M) GS	GSC	CROSS SECTION BED ELEVATIONS (M) (POINT NO.) 1	2	3	4	SCOUR (MM)	MANNINGS N	FRICTION SLOPE	YIELD (KG)
1	0.0000	0.4153	2.0000	1.0000	1.0000	2.0000	0.0000	0.01730	0.00196	0.000
2	0.0175	0.0312	1.9995	0.9667	0.9667	1.9995	32.8713	0.01674	0.00097	1.486
3	0.0507	0.0704	1.9990	0.9740	0.9740	1.9990	25.0412	0.01699	0.00114	6.955
4	0.0822	0.1043	1.9985	0.9780	0.9780	1.9985	20.4862	0.01714	0.00125	9.728
5	0.1419	0.1660	1.9975	0.9830	0.9830	1.9975	14.4564	0.01734	0.00142	13.983
6	0.1965	0.2205	1.9965	0.9861	0.9861	1.9965	10.4400	0.01749	0.00156	17.013
7	0.2677	0.2892	1.9950	0.9886	0.9886	1.9950	6.3848	0.01763	0.00171	20.081
8	0.3412	0.3573	1.9930	0.9899	0.9899	1.9930	3.0959	0.01776	0.00185	22.376
9	0.3900	0.3999	1.9910	0.9897	0.9897	1.9910	1.2944	0.01783	0.00194	23.426
10	0.4167	0.4213	1.9890	0.9886	0.9886	1.9890	0.4366	0.01786	0.00198	23.826
11	0.4276	0.4290	1.9870	0.9869	0.9869	1.9870	0.1257	0.01786	0.00200	23.939
12	0.4305	0.4307	1.9850	0.9849	0.9849	1.9850	0.0544	0.01787	0.00200	23.958
13	0.4308	0.4308	1.9830	0.9830	0.9830	1.9830	0.0488	0.01787	0.00200	23.959
14	0.4308	0.4307	1.9810	0.9810	0.9810	1.9810	0.0499	0.01787	0.00200	23.958
15	0.4307	0.4307	1.9790	0.9789	0.9789	1.9790	0.0503	0.01787	0.00200	23.958
16	0.4307	0.4307	1.9760	0.9759	0.9759	1.9760	0.0501	0.01787	0.00200	23.958
17	0.4307	0.4307	1.9720	0.9719	0.9719	1.9720	0.0503	0.01787	0.00200	23.957
18	0.4307	0.4307	1.9680	0.9679	0.9679	1.9680	0.0501	0.01787	0.00200	23.957
19	0.4307	0.4307	1.9640	0.9639	0.9639	1.9640	0.0503	0.01787	0.00200	23.957
20	0.4307	0.4307	1.9600	0.9599	0.9599	1.9600	0.0502	0.01787	0.00200	23.957
21	0.4307	0.4307	1.9200	0.9199	0.9199	1.9200	0.0503	0.01787	0.00200	23.953
22	0.4307	0.4307	1.8800	0.8800	0.8800	1.8800	0.0498	0.01787	0.00200	23.947
23	0.4307	0.4307	1.8400	0.8400	0.8400	1.8400	0.0490	0.01787	0.00200	23.935
24	0.4307	0.4307	1.8000	0.8000	0.8000	1.8000	0.0460	0.01787	0.00200	23.903

SCOUR HOLE DATA

LENGTH (M) = 0.234 ,DEPTH (MM) = 33.05 ,L/H = 7.069

COMPATIBILITY ERROR = 0.548 PERCENT

SEDIMENT CONTINUITY

CUMULATIVE YIELD = 23.903 KG

SEDIMENT VOLUME ERROR = 0.373 PERCENT

GS07 = 0.0809 GS17 = 0.1954 GS35 = 0.3412 GS53 = 0.4114 GS93 = 0.4308

Table 10.2 Typical Numerical Model Results for t = 1800 s (Run ST09)

$$g_s = g_{sc} \quad \text{for } t = 0$$
$$g_s = 0 \quad \text{for } t > 0 \qquad (10.12)$$

10.3.2 Numerical Model Simulations

The numerical model was used to simulate the ST09, ST07 and ST05 experiments of Bell (1980) and to predict the temporal and spatial variation of the bed elevation and bedload transport rate.

The test reach simulated by the numerical model was assumed to be 0.305 m wide and 100 m long. The length of this reach ensured that the downstream boundary was located well downstream of the region of interest (x = 0 - 9.5 m) and was thus unaffected by spatial lag effects over the duration of a run. This 100 m long reach was divided into sub-reaches of variable length and computational points were defined. To facilitate the comparison of model results with the data of Bell (1980), computational points were located near each section at which Bell (1980) took measurements. At the beginning of each run, Section 2 was located at x = 0.25 m but at all later times the upstream sediment boundary scheme was used to locate this section (Section 9.3.6).

From an analysis of the data of Griffiths (1976), (Fig. 5.2), for a bed material of similar size to that used by Bell (1980) to form his plane, upstream fixed bed, it was estimated that the bed roughness value of the upstream fixed bed of Bell (1980) was 0.0173. Hence, the bed roughness value at Section 1, which is located at the fixed to mobile bed interface, was assumed to be constant with time and equal to 0.0173.

A typical example of the tables of results produced by the numerical model at each time step is given in Table 10.2. Scour hole data, in the form of the length of the zone of separation, L, the local maximum scour depth, H, and scour hole steepness, L/H, is listed as are the cumulative sediment yields at each section down the reach. The compatibility error is a measure of the degree to which the upstream sediment boundary scheme correctly predicts the local maximum scour depth while the sediment volume error checks that sediment continuity is being observed.

10.3.3 Numerical Model Results and Discussion

During the ST series of experiments, Bell (1980) investigated the spatial response of the bed to non-equilibrium sediment conditions

by measuring bedload transport rates at the downstream end of five different reaches. These reaches were created by lengthening the upstream fixed roughened bed in the downstream direction in a manner similar to that described in the GS series of experiments (Section 4.4.3). Bell (1980) effectively measured the bedload transport rate at five locations along the test reach. These sections were located at x = 0.74 m, 1.74 m, 3.53 m, 5.3 m and 9.3 m respectively. The manner in which Bell (1980) identified each of these runs is given in Table 4.2. The spatial and temporal variations of bedload transport measured by Bell (1980) are plotted in Figs. 10.3, 10.4 and 10.5. Bell (1980) also measured the temporal variation of the local maximum scour depth; these results are plotted in Fig. 10.1. Two typical examples of bed profiles measured by Bell (1980) are given in Fig. 10.2.

Since it is not clear how the bed roughness varies within a scour hole (Section 6.26 and Fig. 6.15), the numerical model was used twice to simulate each ST run. The first simulation undertaken was for the case where the bed roughness was assumed constant and equal to the initial bed roughness (Table 10.1). This initial, equilibrium bed roughness was considered to be the upper bound of possible bed roughness values for any given run. The second simulation undertaken was for the lower bound case, that is, where the bed roughness value was assumed to vary in the manner given by Eq. 10.1.

The numerical model results and their comparison with the results of Bell (1980) are as follows:

. Local Maximum Scour Depth

Before the model and experimental results were compared a correction, to account for the transverse bed profiles which occurred in the flume experiments, was applied to the model results to give the temporal variation of the local maximum scour depth at the flume centreline. The side-walls influence the lateral bed profile, giving a concave lateral profile, as demonstrated in Figs. 6.9 and 6.17, rather than the uniform profile predicted by the model (Eq. 9.67). This behaviour is particularly pronounced within the scour hole. The following correction method was adopted (Fig. 9.7)

$$H_{\text{¢}} = \begin{cases} H_m + \Delta H_{\text{¢}} & t \geq 360 \text{ s} \\ fH_m & t < 360 \text{ s} \end{cases} \qquad (10.13)$$

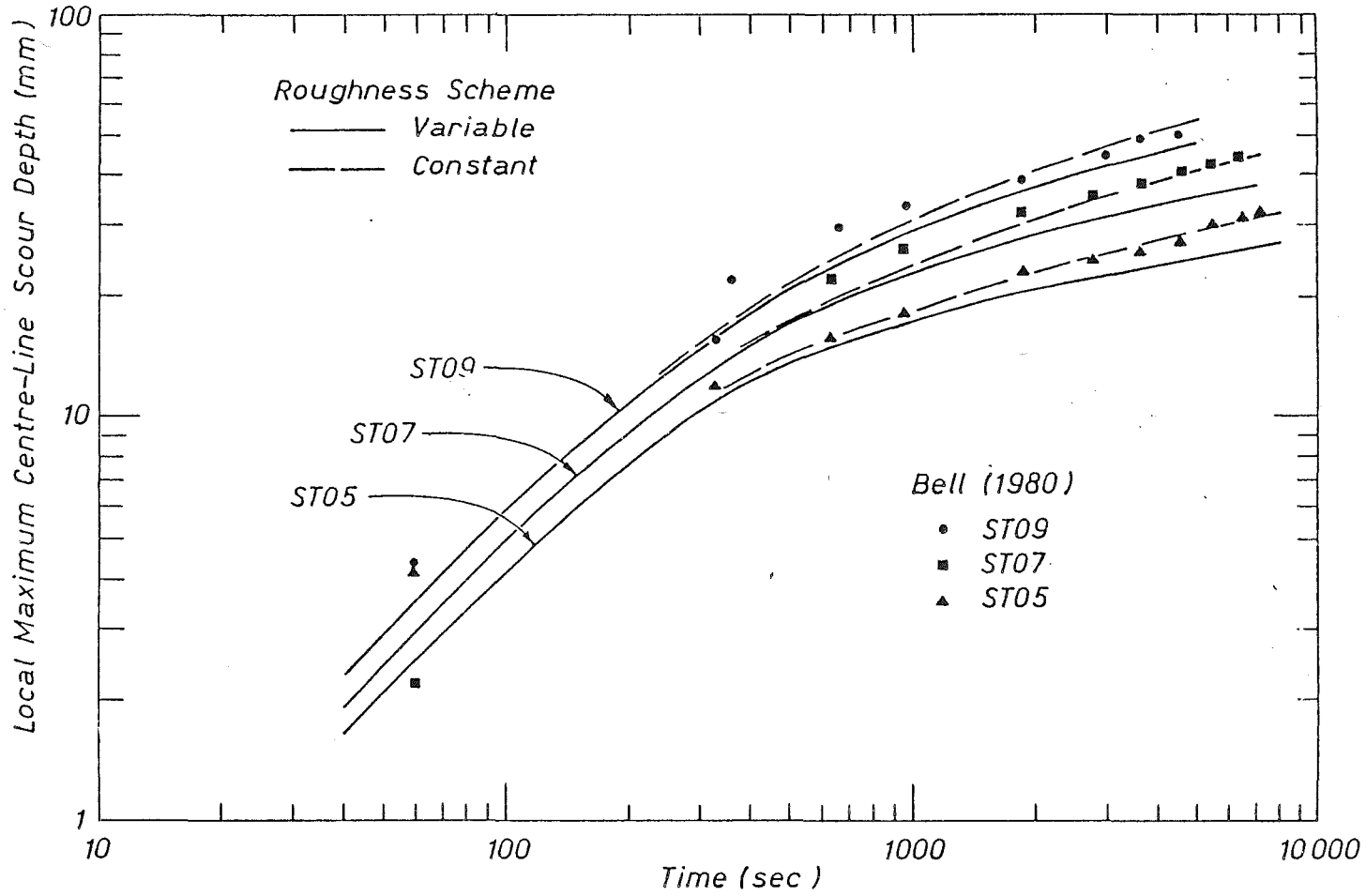

Figure 10.1 Local Maximum Centre-Line Scour Depth Against Time (Runs ST09, ST07, ST05)

where $f = H_{\text{¢}}/H_m$ at $t = 360$ s

and $H_{\text{¢}}$ = Centre-line maximum local scour depth,

H_m = Uniform local maximum scour depth predicted by the model,

$\Delta H_{\text{¢}}$ = Centre-line scour depth correction.

Measurements of lateral bed profiles near the point of local maximum scour indicated that the centre-line scour depth correction was constant during the first principal phase of scour (Section 6.2.3) but that the correction varies with discharge. Hence, it was assumed that after approximately six minutes, when the first principal phase of scour began, that the centre-line scour depth correction was constant. At times less than six minutes a multiplicative correction factor was considered more appropriate. The assumed centre-line scour depth corrections were estimated from the centre-line bed corrections obtained during the current study. These values were

$$\begin{aligned} &\text{Run ST09} \quad \Delta H_{\text{¢}} = 3.0 \text{ mm} \\ &\text{Run ST07} \quad \Delta H_{\text{¢}} = 3.8 \text{ mm} \\ &\text{Run ST05} \quad \Delta H_{\text{¢}} = 5.0 \text{ mm} \end{aligned} \tag{10.14}$$

These centre-line bed corrections values were assumed to be slightly larger than values measured during the current study because the scour rates encountered in Bell's study were greater than those measured in the current study and it was suspected that influence of side-walls was greater under Bell's conditions.

The corrected model results are compared with the data Bell (1980) obtained from the ST--05 series of experiments in Fig. 10.1. The agreement between the predicted and measured centre-line variations in the local maximum scour depth, displayed in Fig. 10.1, is good.

At times soon after a run commences, $0 < t < 300$ s, the roughness scheme adopted does not noticeably affect the predicted variation in the local maximum scour depth.

At times, $t > 300$ s, the scour depth variation predicted using variable bed roughness is always lower than that predicted using the constant bed roughness. This is because the bed shear velocities, which are proportional to the bed roughness value (see Eqs. 9.66, 9.54, 9.55), calculated using variable bed roughness are smaller than those predicted by a constant bed roughness. Consequently, the sediment transport capacities, (Eqs. 9.62 and 9.63), and the rates of scour predicted by the

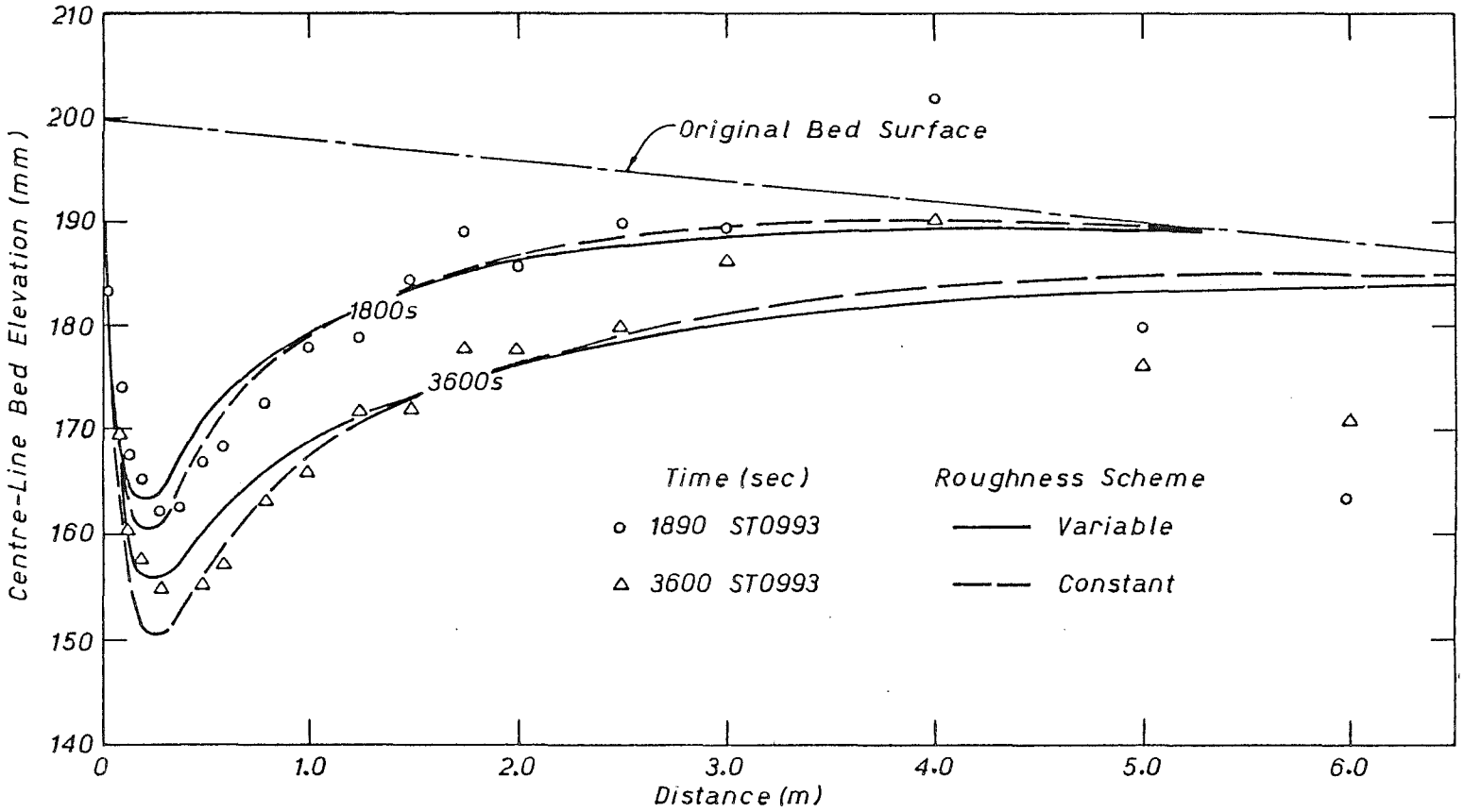

Figure 10.2 Longitudinal Centre-Line Bed Profiles (Run ST09).

spatial lag equation, (Eq. 9.17), are smaller.

At large times a constant maximum scour depth will be reached, in accord with the observations of Cuhna (1975), Mosonyi and Schoppmann (1968) and Dietz (1969). This occurs when, according to the model, threshold conditions are encountered at the point of local maximum scour.

The analysis of bed roughness within the scour hole indicated, (see Fig. 6.15), that at low discharges the bed roughness was constant while at higher discharges the bed roughness varied. The same trend appears to be displayed in Fig. 10.1. The data obtained during the ST05 run, a low discharge run, is well fitted by the constant bed roughness results while the ST09 data, obtained from a higher discharge run, falls between the results predicted by the constant and variable bed roughnesses.

. Bed Profiles

A correction was also applied to the bed profiles predicted by the model before these profiles were compared with the centre-line bed profiles measured by Bell (1980). The correction at any given section, x, and time, t, was

$$h_{\text{¢}}(x, t) = \frac{H_{\text{¢}}(t)}{H_m(t)} h_m(x, t) \qquad (10.15)$$

where $h_{\text{¢}}(x, t)$ = Centre-line scour depth at a section,

$h_m(x, t)$ = Uniform scour depth at a section predicted by the model

$= Z_b(x, 0) - Z_b(x, t)$

and $H_{\text{¢}}$ and H_m are as defined previously.

Two corrected model profiles are compared with two sets of bed elevations, measured by Bell (1980) during the ST0993 run, in Fig. 10.2. The agreement between the predicted and measured centre-line bed profiles is good, with the data falling between the sets of profiles predicted by the two roughness schemes. The difference between the data and model results at the downstream end of the scour holes is due to bed forms which cause the local bed elevation to rise and fall. The numerical model is unable to model individual bed forms, being only able to calculate the mean bed profile.

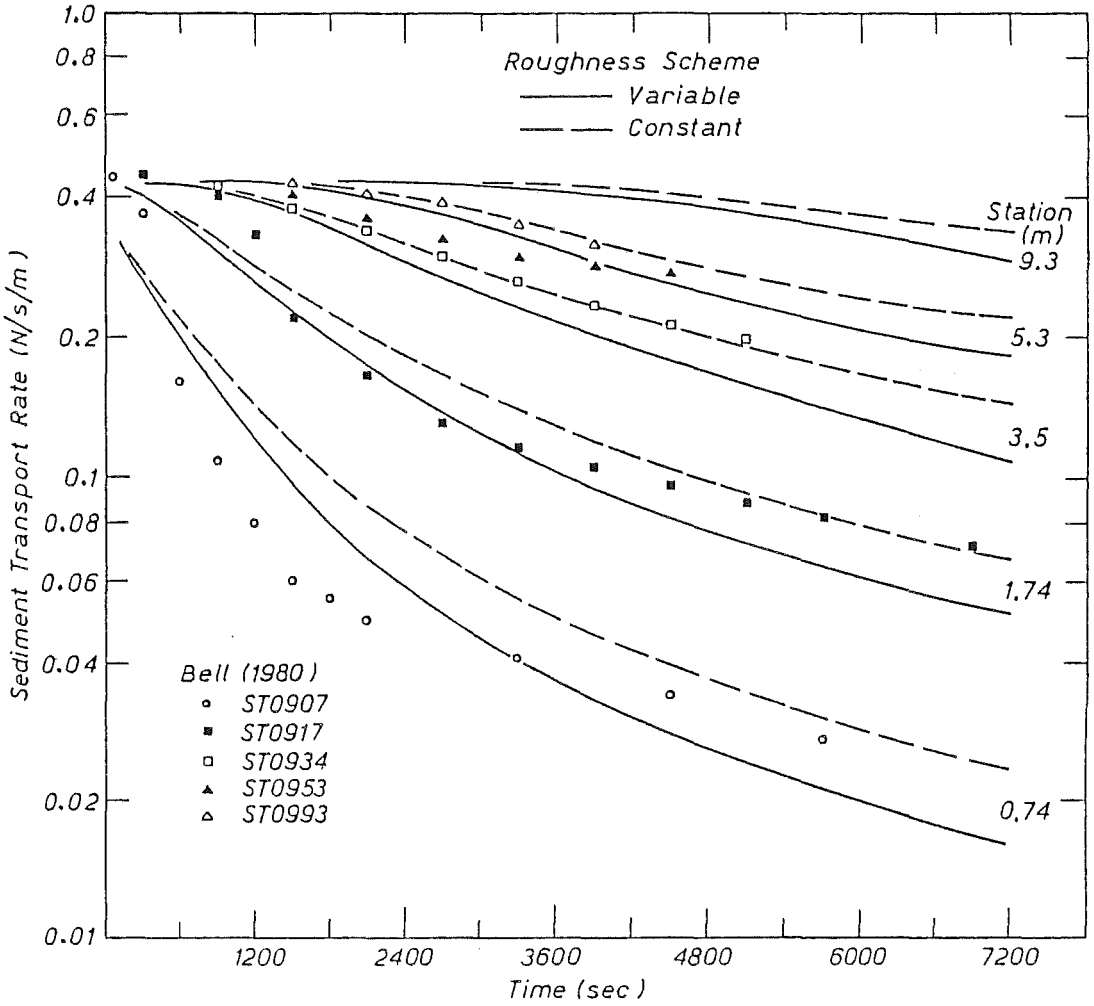

Figure 10.3 Sediment Transport Rate Against Time (Run ST09)

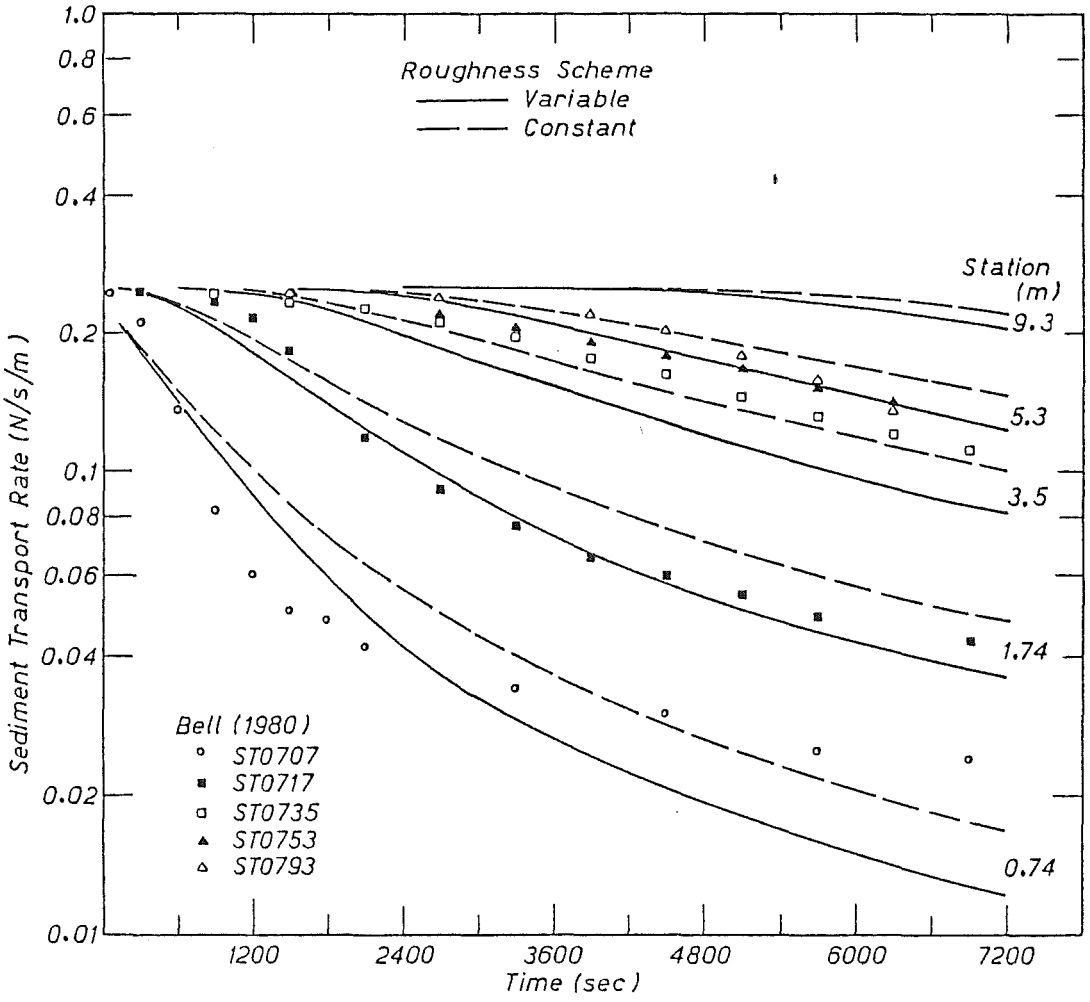

Figure 10.4 Sediment Transport Rate Against Time (Run ST07)

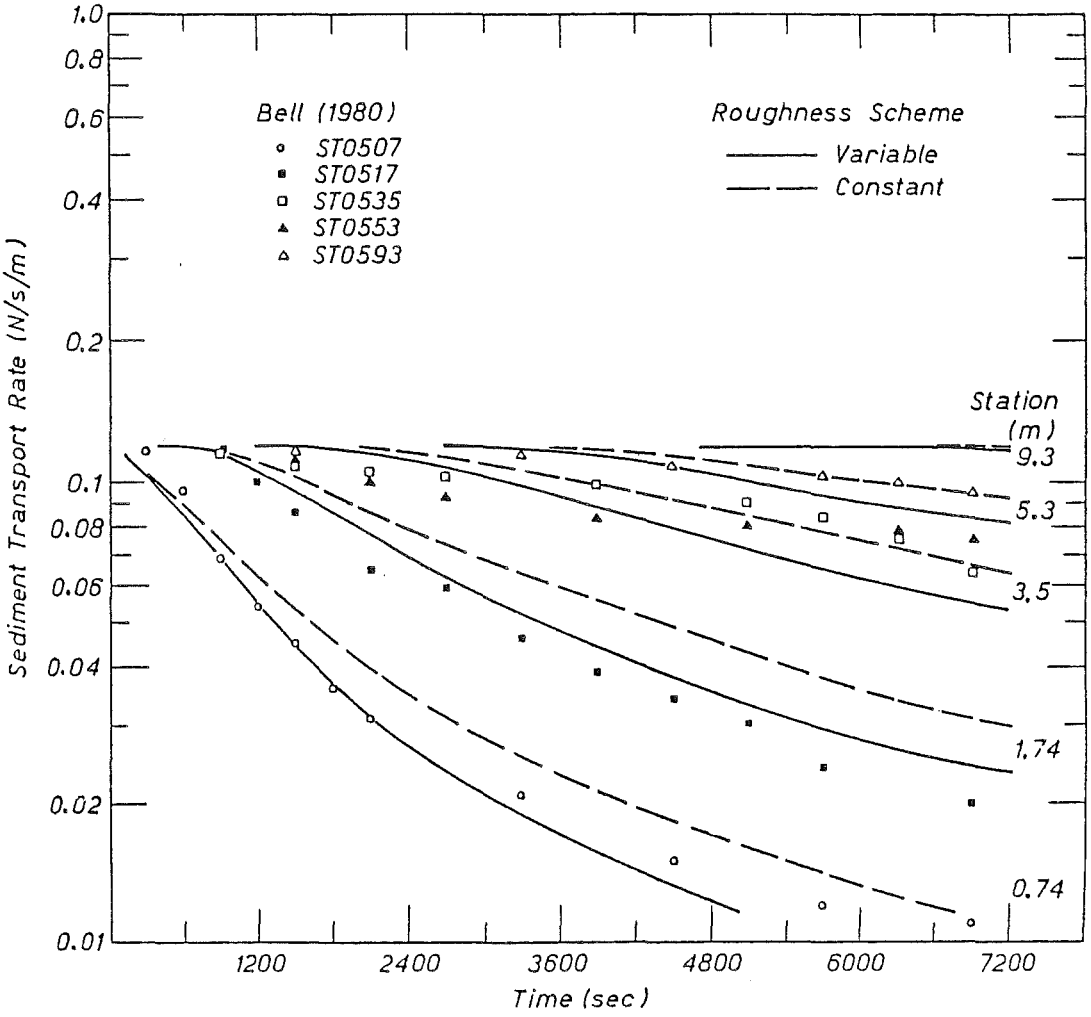

Figure 10.5 Sediment Transport Rate Against Time (Run ST05)

The model bed elevation results also demonstrate the effect of the two bed roughnesses on the scour hole geometry. The constant bed roughness causes the scour hole to be deep and relatively short while the variable bed roughness gives a scour hole which is slightly shallower near the zone of separation but is more elongated.

. Bedload Transport Rates

The predicted and measured temporal variations of the bedload transport rate at the five sections studied by Bell (1980) during the ST09, ST07 and ST05 experiments are given in Figs. 10.3, 10.4 and 10.5 respectively.

The lack of agreement between the predicted and measured sediment transport rates at Station 0.74 m may be due to the difficulties encountered when measuring sediment transport rates deep within a scour hole (Section 4.4.3). It may also be due to the model assuming that the initial bed roughness values hold at all points along the reach. Close to the upstream boundary of the mobile reach, the bed roughness, a component of which is due to bed forms, may not be the same as that assumed in the model because the assumed bed roughness may only occur downstream of the first equilibrium bed form which was typically 1 m long.

The agreement between the predicted band of bedload transport rates and the measured data at Stations 1.74 m, 3.5 m and 5.3 m is good, however, the agreement at Station 9.3 m is poor. In all runs, the model predicts the onset of change in the bedload transport rate at times which are much later than was measured at Station 9.3 m. An estimate of the earliest time at which changes in the bedload transport rate occur at the downstream end of the reach due to the cessation of sediment inflow can be determined by calculating the time an equilibrium bed form takes to propagate the length of the test reach.

Bell (1980) found in his experiments that the dune bed form celerity was given by

$$\underset{(m/s)}{C_d} = 5.9 \times 10^{-3} \underset{(m/s)}{U^{3.1}} \qquad (10.16)$$

Thus

$$T_d = \frac{9.3}{C_d} \qquad (10.17)$$

where T_d = Time a dune bed form takes to propagate the 9.3 m length of the test reach.

RUN	FLOW VELOCITY (m/s)	DUNE CELERITY (mm/s)	PROPAGATION TIME (s)	PREDICTED TIME OF ONSET OF CHANGE (s)
ST09	0.808	3.1	3000	≃ 3100
ST07	0.747	2.4	3875	≃ 4050
ST05	0.678	1.8	5167	≃ 6500

Table 10.3 Dune Bed Form Propagation Times (ST Series)

Values of the earliest times at which bedload transport rates might be expected to change were calculated from Eqs. 10.16 and 10.17 and are given in Table 10.3.

At Station 9.3 m, the ST09 and ST07 propagation times agree remarkably well with the predicted times of onset of change in bedload transport while the ST05 propagation time is less than the predicted time of onset of change in bedload transport (Table 10.3). Hence, the measured changes in bedload transport at Station 9.3 m are occurring at times much sooner than might have been expected from the propagation of the initial equilibrium bed forms down the test reach. It would appear that some, as yet unexplained, mechanism is causing changes in bedload transport rates at times equivalent to bed form celerities which are twice as great as those measured.

Overall, the agreement between the model predictions and measured data demonstrates that a model which incorporates the spatial lag equation and the upstream sediment boundary scheme is able to reasonably predict the temporal and spatial variation of the mean bed elevation and bedload transport rate under steady flow conditions with constrained sediment boundary conditions.

10.3.4 Diffusion Models

For steady flow, non-equilibrium sediment transport conditions many researchers have simplified and manipulated the governing equations of motion of water and sediment and obtained a parabolic partial differential equation of the diffusion type, where

$$\frac{\partial Z_b}{\partial t} = \kappa \frac{\partial^2 Z_b}{\partial x^2} \qquad (10.18)$$

Z_b = Bed elevation, and
κ = Diffusion coefficient

Previous researchers, including Soni, Garde and Ranga Raju (1980), (1977); Jain (1981); Soni (1981(a) and (b)); Mehta, Garde and Ranga Raju (1983) and Gill (1983(a)) have obtained solutions, using the diffusion equation, Eq. 10.18, and various initial and boundary conditions, for the case of sediment overloading at the upstream boundary of a mobile reach i.e. the bed aggradation case. Only a limited number of checks on the foregoing solutions using laboratory and field data have been made; the most recent being that of Mehta, Garde and Ranga Raju (1983).

More recently researchers, including Gill (1983(b) and Yalin (1983), have postulated that solutions can be obtained, using the diffusion equation, Eq. 10.18, and various initial and boundary conditions, for the case of bed degradation due to the sudden reduction or cutoff of sediment inflow at the upstream boundary. To date, no checks on the foregoing solutions using laboratory or field data appear to have been made. Hence, the performance of a diffusion model was compared with the data of Bell (1980) and with the performance of the numerical model.

The spatial and temporal variations of the sediment transport rate and scour depths are obtained by solving the diffusion and sediment continuity equations. In an infinitely long channel, the initial and boundary conditions are

$$\begin{aligned} g_v(x, o) &= g_{v_o} \\ g_v(o, t) &= g_{v_\infty} \\ Z_b(x, o) &= - S_o x \\ \frac{\partial Z_b}{\partial x}(o, t) &= - S_o - \frac{(g_{v_\infty} - g_{v_o})}{\kappa(1 - \lambda')} \end{aligned} \tag{10.19}$$

The fourth boundary condition conforms with a boundary condition proposed by Gill (1983(a)), namely

$$\frac{\partial Z_b}{\partial x}(o, t) = \frac{- g_{v_\infty}}{\kappa(1 - \lambda')} \tag{10.20}$$

if and only if the relation for the diffusion coefficient is as given in Eq. 10.26.

For the boundary conditions given in Eq. 10.19, the solution, in terms of error functions, for the temporal and spatial variation of the sediment transport rate is (Gill (1983(a)))

$$g_v(x, t) = g_{v_o} + (g_{v_\infty} - g_{v_o})\,(1 - \mathrm{erf}(\eta)) \tag{10.21}$$

where $\eta = \dfrac{x}{2\sqrt{\kappa t}}$

g_v = Volumetric sediment transport rate per unit width,

g_{v_o} = Initial volumetric sediment transport rate per unit width,

g_{v_∞} = Final volumetric sediment transport rate per unit width.

For the boundary conditions given in Eq. 10.19, the solution, in terms of error functions, for the temporal and spatial variation of the scour depth, h, is (Gill (1983(b), Jain (1981))

$$h(x, t) = Z_b(x, o) - Z_b(x, t)$$

$$= \frac{(g_{v_\infty} - g_{v_o})}{\kappa(1 - \lambda')} \left[x \, \text{erfc}(\eta) - 2\sqrt{\frac{\kappa t}{\pi}} \, e^{-\eta^2} \right] \qquad (10.22)$$

At the upstream boundary, x = 0, the variation in scour depth is

$$h(o, t) = - 2 \frac{(g_{v_\infty} - g_{v_o})}{(1 - \lambda')} \sqrt{\frac{t}{\kappa\pi}} \qquad (10.23)$$

Before these solutions can be used it is necessary to obtain a value of the diffusion coefficient, κ. To date, at least three equations have been proposed from which values of the diffusion coefficient may be obtained.

The first and most common relation, which was derived by assuming a sediment transport rate relation of the form

$$g_v = aU^b \qquad (10.24)$$

is (Mehta, Garde and Ranga Raju (1983))

$$\kappa_1 \simeq \kappa_{o_1} = \frac{b g_{v_o}}{3S_o(1 - \lambda')} \qquad (10.25)$$

Whereas, Gill (1983(a), (b)) derived a second relation, without resorting to an assumption about the form of a sediment transport relation, of the form

$$\kappa_2 \simeq \kappa_{o_2} = \frac{g_{v_o}}{S_o(1 - \lambda')} \qquad (10.26)$$

More recently, Yalin (1983) derived a third relation, from an evaluation of Bagnold's bed load formula, of the form (S.I. units)

$$\kappa_3 = \frac{13.31 \, q}{C(S_s - 1)} \qquad (10.27)$$

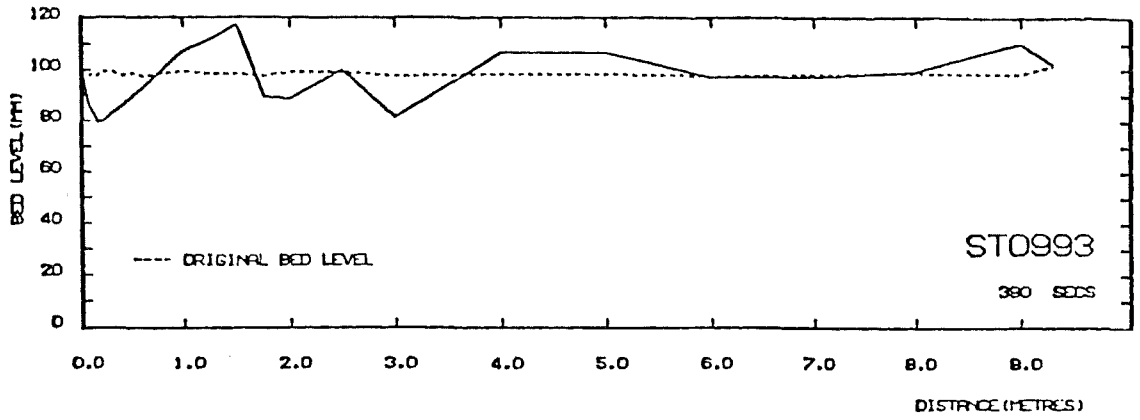

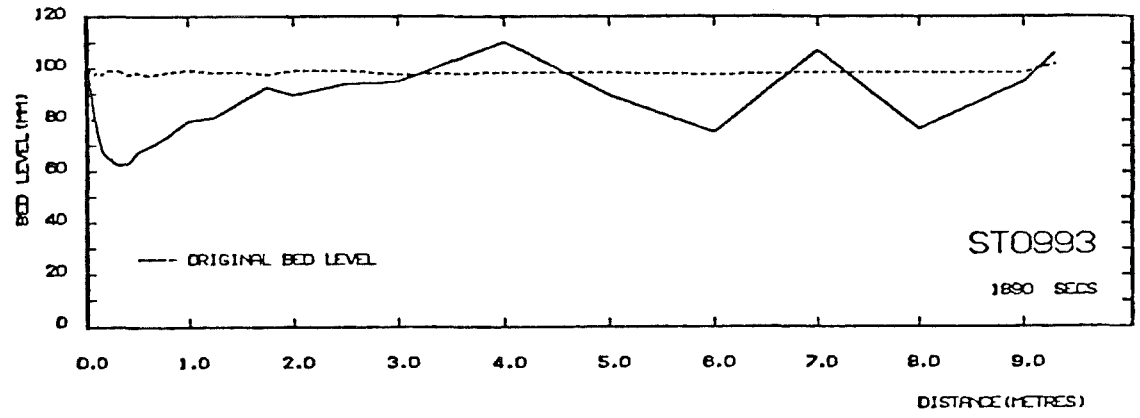

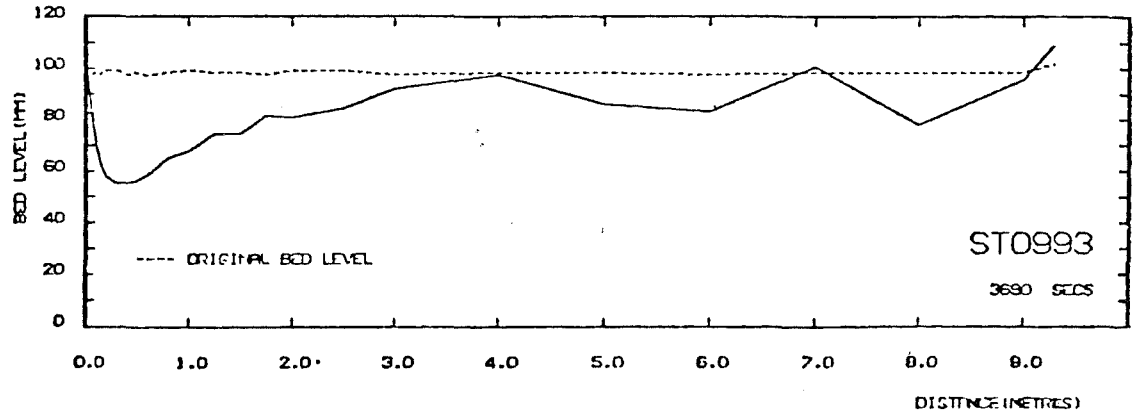

Figure 10.6 Typical Bed Profile Records (After Bell (1980)).

where q = Flow rate per unit width, and

C = Chezy roughness value

$$= \frac{R_b^{1/6}}{n_b}$$

10.3.5 Diffusion Model Results and Discussion

The solutions presented in Eqs. 10.21 and 10.22 and the various diffusion coefficient relations were tested by simulating the ST09 experiments of Bell (1980) and comparing predicted and measured scour depths and bedload transport rates.

Bell (1980) found from an analysis of his SE data that the exponent, b, of a transport relation of the form given by Eq. 10.24, was 8.0. Hence, for the ST09 experiments where (Table 10.1)

$$q = 0.160 \text{ m}^3/\text{s/m}$$

$$C \simeq 42.0 \text{ m}^{1/2}/\text{s}$$

$$g_{v_o} = 1.67 \times 10^{-5} \text{ m}^3/\text{s/m}$$

$$g_{v_\infty} = 0.0 \text{ m}^3/\text{s/m}$$

the various values of the diffusion coefficient, given by Eqs. 10.25, 10.26 and 10.27, are 0.0384, 0.0144 and 0.029 respectively.

Initial runs of the diffusion model indicated that the diffusion model results only fitted the data for values of the diffusion coefficient which were much smaller than even the value predicted by Gill (1983(a), (b)), (Eq. 10.26). Hence, a diffusion coefficient of best fit was obtained by fitting the model results to the data of Bell (1980). This diffusion coefficient was referenced to the relation of Gill (1983(a), (b)) because this relation is the only equation which was derived without resorting to an assumed sediment transport relation. Thus, the diffusion coefficient is assumed to be of the form

$$K = \alpha_K K_o = \frac{\alpha_K g_{v_o}}{S_o(1 - \lambda')} \qquad (10.28)$$

where, for the ST09 experiments, $K_o = 0.0144$.

The diffusion model results and their comparison with the results of Bell (1980) are as follows.

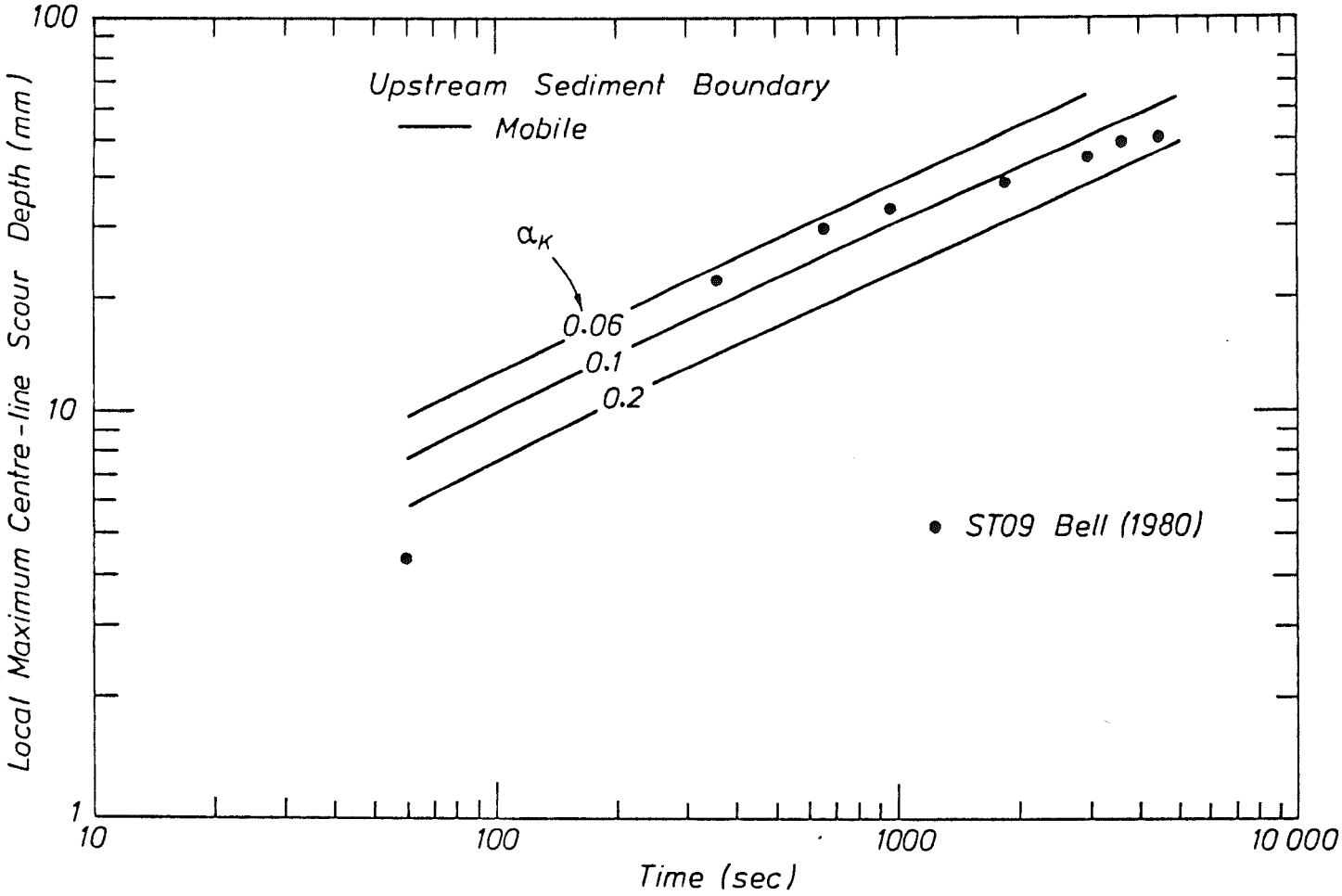

Figure 10.7 Local Maximum Centre-Line Scour Depth Against Time (Run ST09: $K = \alpha_K K_o$, $K_o = 0.0144$)

. Local Maximum Scour Depth

A feature of all previous diffusion models is that the upstream boundary is assumed to be stationary at x = 0. That is, diffusion models predict that the local maximum scour depth occurs at the fixed to mobile bed interface at all times. However, it has been shown, (see Fig. 10.6), that this is not the case but that the point of local maximum scour, which is located at the toe of the vortex formed in a scour hole (Fig. 9.7), moves downstream with time. Thus, the diffusion model is unsatisfactory in its present form.

The diffusion model can, however, be modified to enable it to predict the actual behaviour of the point of local maximum scour depth. This modification is the introduction of a moving origin located at $x_o(t)$, where

$$x_o(t) = \frac{L}{H} h(o, t) \qquad (10.29)$$

where h(o, t) is as given in Eq. 10.23, and the scour hole steepness, L/H, can be obtained by subsituting initial flow properties into the relation given by Eq. 9.30. For the ST09 experiments, Eq. 9.30 gives L/H = 7.0. This origin coincides with the location of the toe of the vortex and hence is the location of the point of local maximum scour.

Adopting a mobile upstream boundary, the spatial and temporal variation of the scour depth is (Eq. 10.22)

$$h(x, t) = \frac{(g_{v_\infty} - g_{v_o})}{\kappa(1 - \lambda')} \left[(x - x_o)\ \mathrm{erfc}(\eta') - 2\sqrt{\frac{Kt}{\pi}}\, e^{-\eta'^2} \right] \qquad (10.30)$$

where $\eta' = \dfrac{(x - x_o)}{2\sqrt{Kt}}$

The local maximum scour depth results obtained from the mobile boundary diffusion model, which were corrected for side-wall effects in the manner described in Section 10.3.3, are compared with the measured data in Fig. 10.7. The agreement between the data and the model predictions is best for $\alpha_K = 0.1$. This curve is also in good agreement with the numerical model results for 360 s < t < 1800 s. However, at times t > 1800 s the agreement between the diffusion model results, for $\alpha_K = 0.1$, and the data and numerical model results deteriorates. This highlights a second shortcoming of diffusion models.

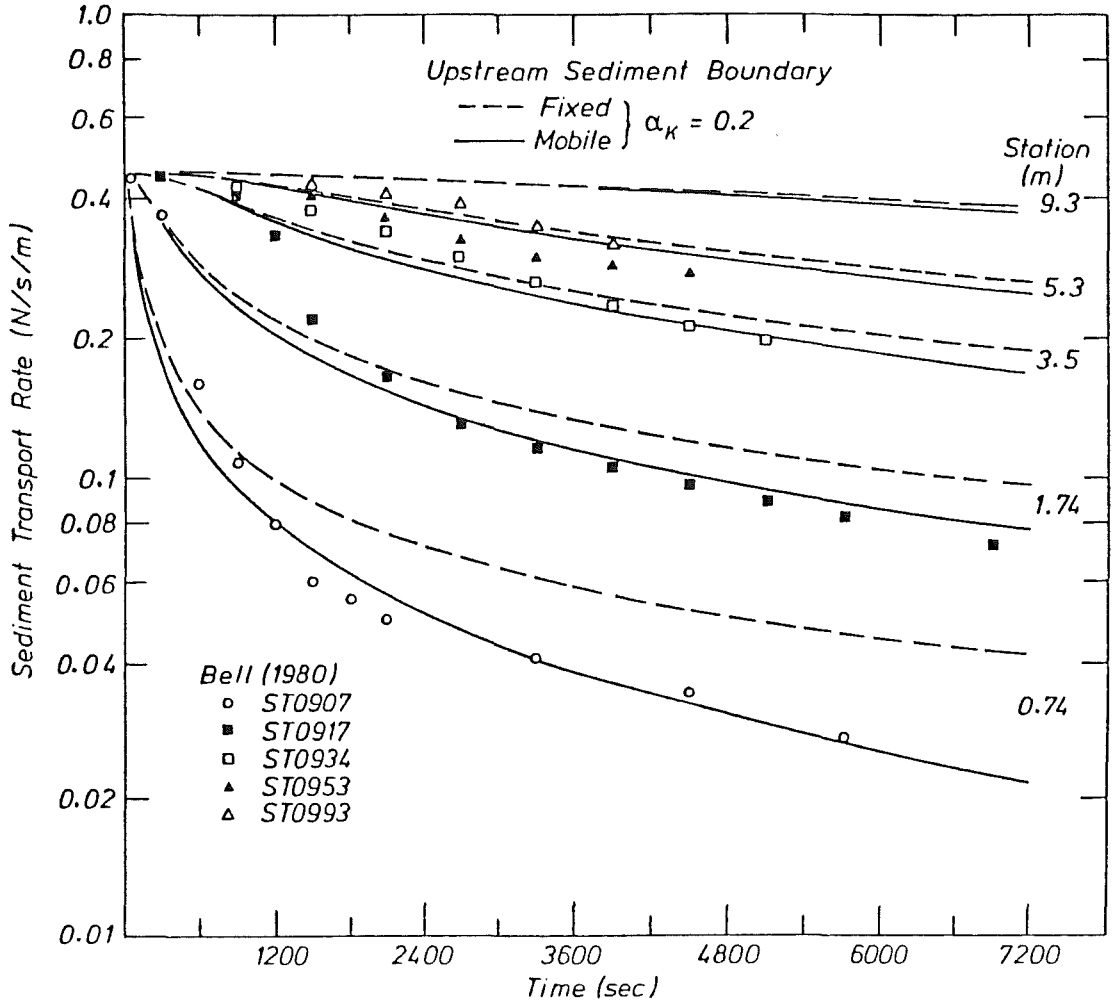

Figure 10.8 Sediment Transport Rate Against Time (Run ST09: $K = \alpha_K K_o$, $K_o = 0.0144$)

When sediment inflow ceases suddenly a scour hole develops and propagates in the manner outlined by Cuhna (1975) (Section 6.2.3) and at some later time, $t << \infty$, the local maximum scour depth reaches a maximum value when threshold conditions are encountered. A diffusion model predicts, however, that (Eq. 10.23)

$$h(o, t) = H(t) \alpha \sqrt{t} \tag{10.31}$$

That is, the maximum depth of scour is only reached at infinite time. Thus, the measured data, plotted in Fig. 10.7, which cross the contours of local maximum scour depth predicted by a diffusion model demonstrate that a diffusion model is unable to predict the onset of threshold conditions and must therefore be only used for moderate times. In this respect, the numerical model is better able to predict the variation of scour depths than is a diffusion model.

. Bedload Transport Rate

Incorporating the mobile boundary into the diffusion model, the spatial and temporal variation of the bedload transport rate is (Eq. 10.20)

$$g_v(x, t) = g_{v_o} + (g_{v_\infty} - g_{v_o}) (1 - \text{erf}(\eta')) \tag{10.32}$$

where all variables are as previously defined.

The temporal variations of the bedload transport rate, at the five sections of Bell (1980), predicted by both the stationary boundary and mobile boundary diffusion models, Eqs. 10.20 and 10.32, are plotted and compared with the ST09 data of Bell (1980) in Fig. 10.8.

The results plotted in Fig. 10.8 demonstrate the marked effect a mobile boundary scheme has on the diffusion model results which illustrates the significant effect the upstream vortex has on the temporal and spatial variation of bedload transport within a scour hole.

At Stations 0.74 m, 1.74 m, 3.5 m and 5.3 m the data was well fitted by the mobile boundary diffusion model results for $\alpha_K = 0.2$.

At Station 9.3 m the temporal variation of the bedload transport rate is much slower than that measured by Bell (1980) but is in agreement with the results predicted by the numerical model (Fig. 10.4).
Gill (1983(b)) demonstrated that the degradation front, ℓ, defined by the criterion $h(x, t)/h(0, t) = 0.01$, (Eqs. 10.22 and 10.23), was given by

$$\ell = 3.2 \sqrt{Kt} \tag{10.33}$$

RUN	DISCHARGE ($m^3/s/m$)	FLOW DEPTH (m)	BED ROUGHNESS	BEDLOAD TRANSPORT RATE (N/s/m)
NS02	0.0374	0.077	0.0161	0.0
NS03	0.0374	0.077	0.0161	0.0
NS06	0.0374	0.077	0.0161	0.0

Table 10.4 Initial Flow and Sediment Conditions (NS Series)

For the calibrated diffusion coefficient, $K = 0.00288$, Eq. 10.33 predicts that the degradation front reaches Station 9.3 m at t = 2930 s. This time is very similar to the time it takes a dune bed form to propagate the length of the flume, t = 3000 s (Table 10.3) but once again is much longer than the time at which Bell (1980) measured the onset of change in the sediment transport rate at Section 9.3 m.

10.3.6 Summary

It was concluded from a comparison of the performances of the numerical model and the mobile boundary diffusion model with the ST09 data of Bell (1980), that

- The mobile boundary diffusion model slightly better predicts the temporal variation of the bedload transport rate than does the numerical model,
- At Station 9.3 m, both models predict similar bedload transport rates with time but that the predicted temporal variations of the bedload transport are significantly different from that measured by Bell (1980),
- The temporal variation of the local maximum scour depth predicted by both the numerical and diffusion models agrees with the data at moderate times,
- Diffusion models will significantly overpredict long term scour depths because these models are inherently unable to predict the onset of threshold conditions, and
- The diffusion coefficient required to simulate the ST09 experiments of Bell (1980) was significantly smaller than that predicted by previous researchers.

10.4 NON-STEADY FLOW NON-EQUILIBRIUM TRANSPORT

The manner in which Bell (1980) conducted the NS series of experiments in a 0.305 m wide flume is briefly outlined and the associated initial flow and sediment conditions are presented. The results obtained from the numerical simulations of the NS02, NS03 and NS06 experiments are presented and compared with the data of Bell (1980). The results from a typical temporal lag model simulation of sediment behaviour under weakly, periodically varying water discharge by Fredsøe (1979) are compared with the numerical model results for solitary flood waves to determine if the

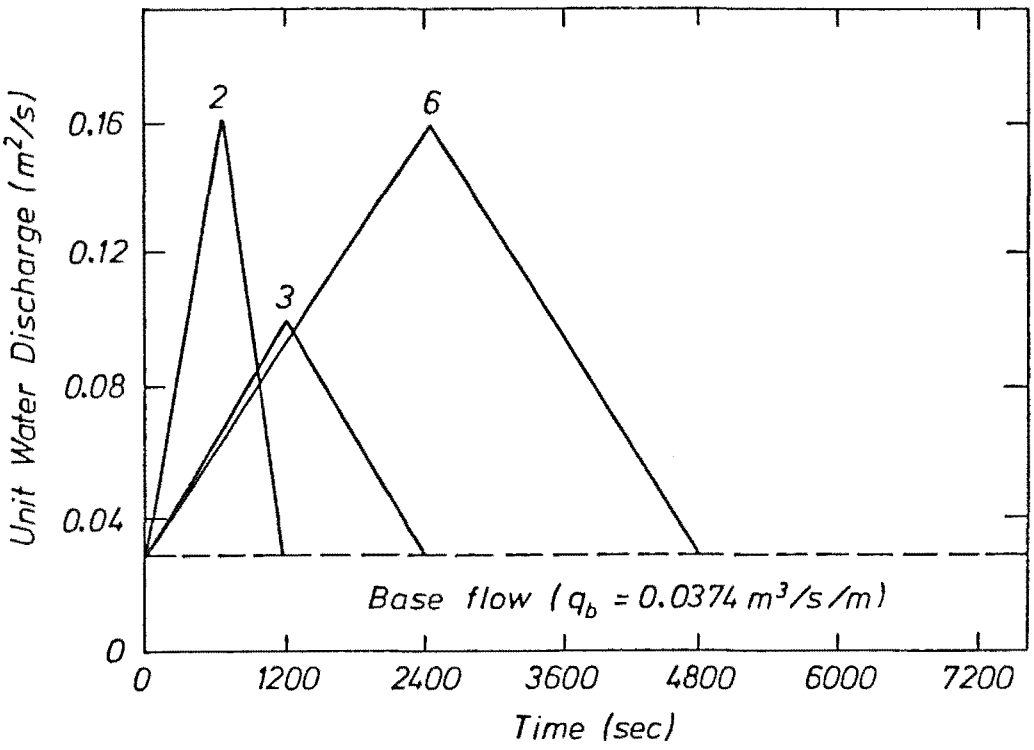

Figure 10.9 Flood Wave Hydrographs (NS Series)

sediment behaviour is similar.

10.4.1 Initial Conditions - NS Runs

Bell (1980) created non-equilibrium sediment transport conditions during the NS series of experiments by having zero sediment input at the upstream boundary of the test reach. Unsteady flow conditions were created by imposing a symmetrical flood wave on a base discharge. Consequently, both spatial and temporal lag effects were present.

The initial flow conditions were a constant base discharge and uniform flow depth over the complete length of the plane mobile bed. The initial friction slope was

$$S_f = S_o = 0.002 \tag{10.34}$$

The initial sediment boundary conditions were uniform plane bed roughness and zero rate of sediment transport over the complete length of the test reach. The sediment transport boundary condition at the upstream end of the test reach was

$$g_s = 0 \text{ for } t \geq 0 \tag{10.35}$$

The critical or base discharge adopted by Bell (1980) was 0.03 $m^3/s/m$, however the base discharge equivalent to the initial sediment transport conditions, $g_s = 0$ was found, from Eqs. 10.3, 10.1, Manning's equation and the side-wall correction relation, to be 0.0374 $m^3/s/m$. The difference between these two discharges is due to the adoption of slightly different initial motion criterion. Hence, when simulating the NS runs of Bell (1980) the initial flow conditions inserted in the model were the threshold conditions based on the initial motion criterion adopted when determining the sediment capacity relation i.e. $N = 1 \times 10^{-6}$ (Section 5.3.3).

The initial sediment and flow conditions for each simulation of the NS experiments are given in Table 10.4.

The flood wave hydrographs imposed on the base discharge for each simulation of the NS experiments are given in Fig. 10.9. The peak or maximum discharge for each flow hydrograph is

$$\begin{aligned} &\text{Run NS02} \quad q_{max} = 0.160 \ m^3/s/m \\ &\text{Run NS03} \quad q_{max} = 0.097 \ m^3/s/m \\ &\text{Run NS06} \quad q_{max} = 0.160 \ m^3/s/m \end{aligned} \tag{10.36}$$

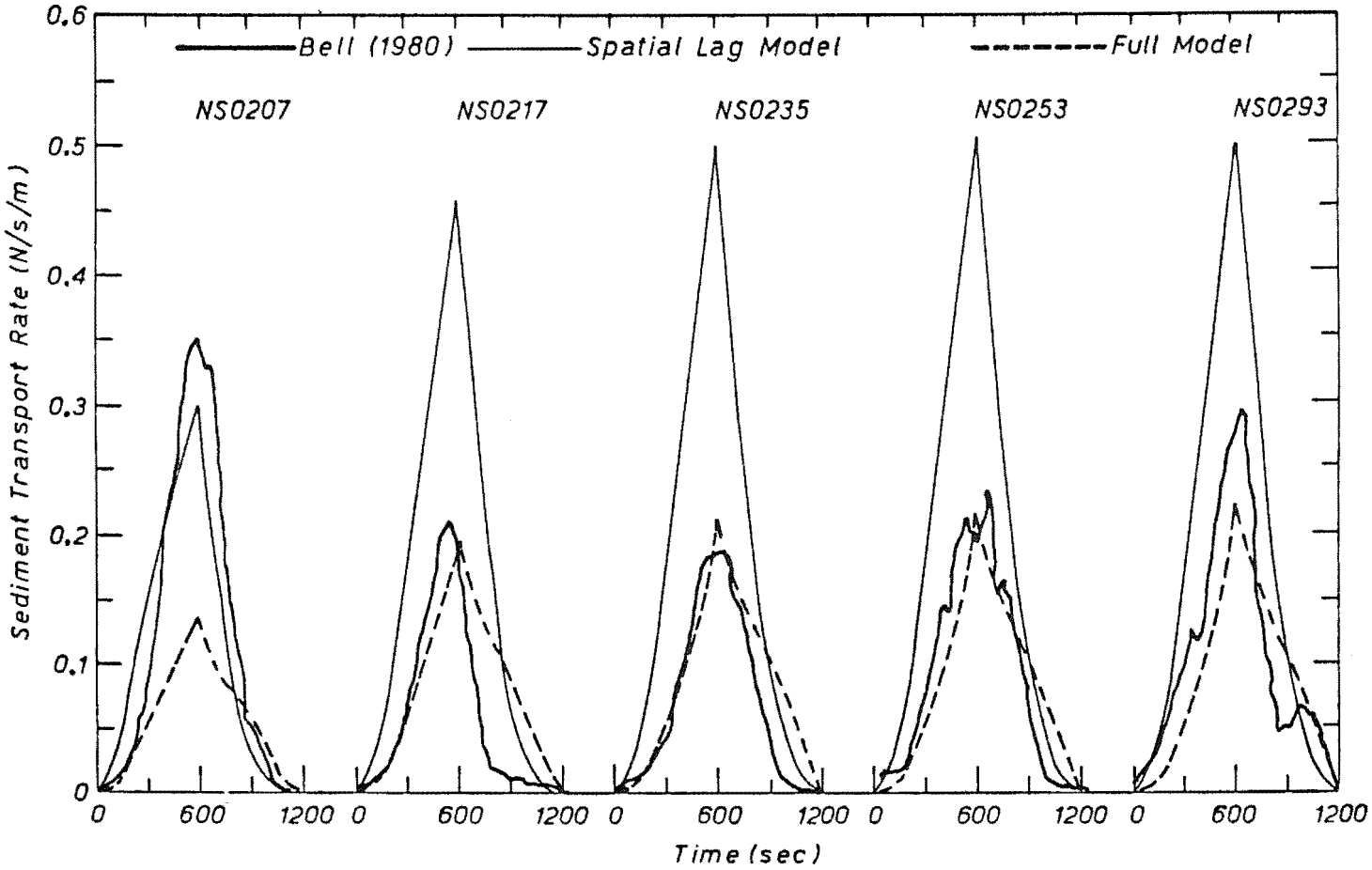

Figure 10.10 Sediment Transport Rate Against Time (Run NS02)

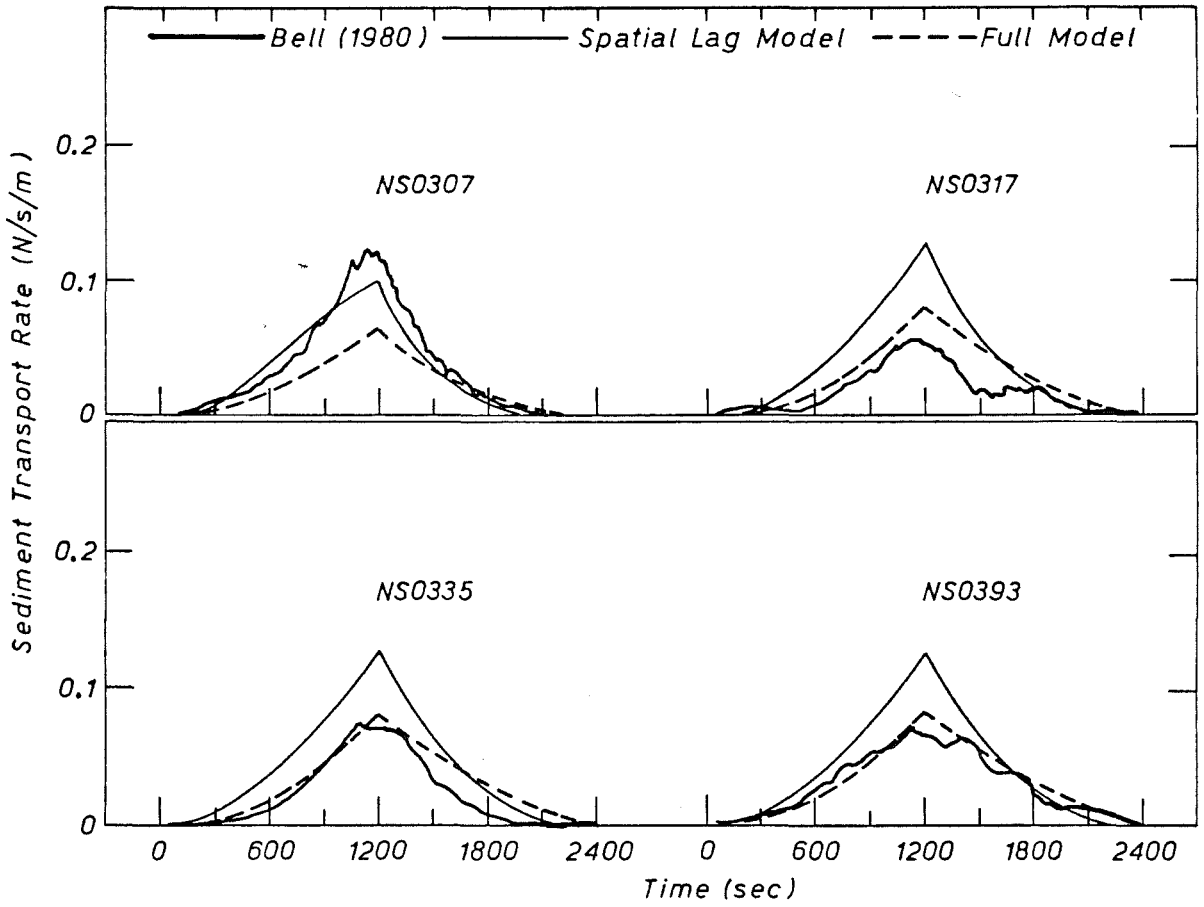

Figure 10.11 Sediment Transport Rate Against Time (Run NS03)

10.4.2 Numerical Model Results and Discussion

The numerical model was used to simulate the NS02, NS03 and NS06 experiments of Bell (1980) and to predict the temporal and spatial variations of bed elevation and bedload transport rate. Each simulation produced tables of results, at each time step, in the manner presented and described in Section 10.3.2 (Table 10.2).

As in the ST experiments, Bell (1980) measured the bedload transport rates at five sections along the test reach at Stations 0.74 m, 1.74 m, 3.53 m, 5.3 m and 9.3 m. The spatial and temporal variations of bedload transport rate measured by Bell (1980) are plotted in Figs. 10.10, 10.11 and 10.12 respectively. The individual run codes are as presented in Table 4.2.

To determine the effect of the temporal lag scheme on the predicted bedload transport rates, the numerical model was used twice to simulate each NS run. The first simulation undertaken was for the case where only spatial lag effects were modelled i.e. it was assumed that the sediment capacity relation was a function of local flow conditions. The second simulation undertaken was for the case where both spatial lag and temporal lag effects were modelled i.e. it was assumed that the transport capacity relation was not a function of local flow conditions but rather a function of the equivalent steady flow rate. In both simulations, the bed roughness was assumed to vary in the manner given by Eq. 10.1. The numerical model results and their comparison with the results of Bell (1980) are as follows.

. Bedload Transport Rate

The predicted and measured temporal variations of the bedload transport rate at various sections for the NS02, NS03 and NS06 experiments are plotted in Figs. 10.10, 10.11 and 10.12 respectively. The measured and predicted sediment yields for each run are given in Table 10.5.

The numerical model results plotted in Figs. 10.10, 10.11 and 10.12 demonstrate the significant effect the temporal lag scheme has on the predicted rates of bedload transport. Under the steep flow hydrograph of the NS02 runs, the temporal lag scheme predicts peak bedload transport rates which are less than half of the peak rates predicted by a model which only incorporates the spatial lag equation. Under the gentler flow hydrograph of the NS06 runs, the temporal lag scheme predicts peak bedload transport rates which are approximately three-quarters

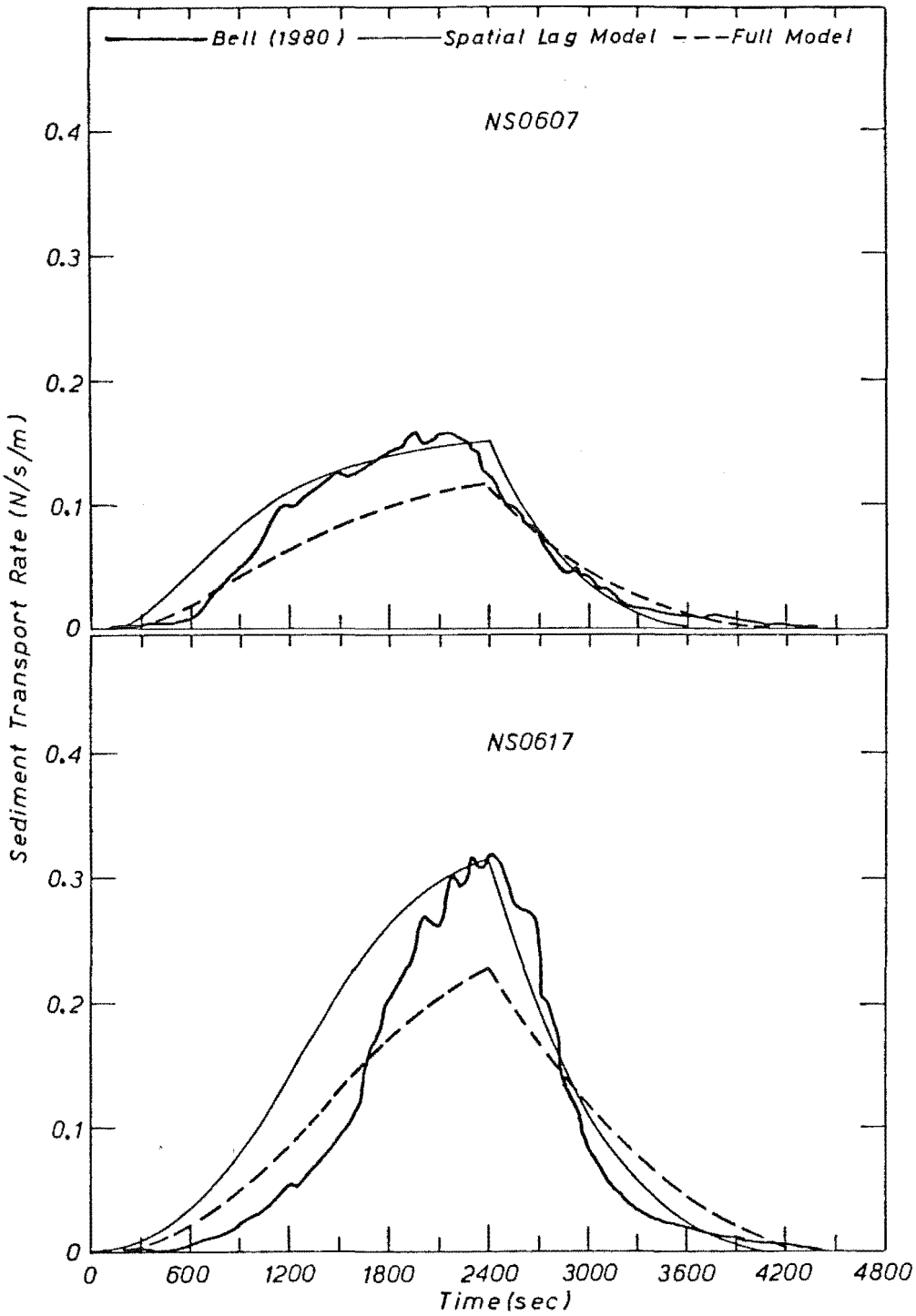

Figure 10.12(a) Sediment Transport Rate Against Time (Run NS06)

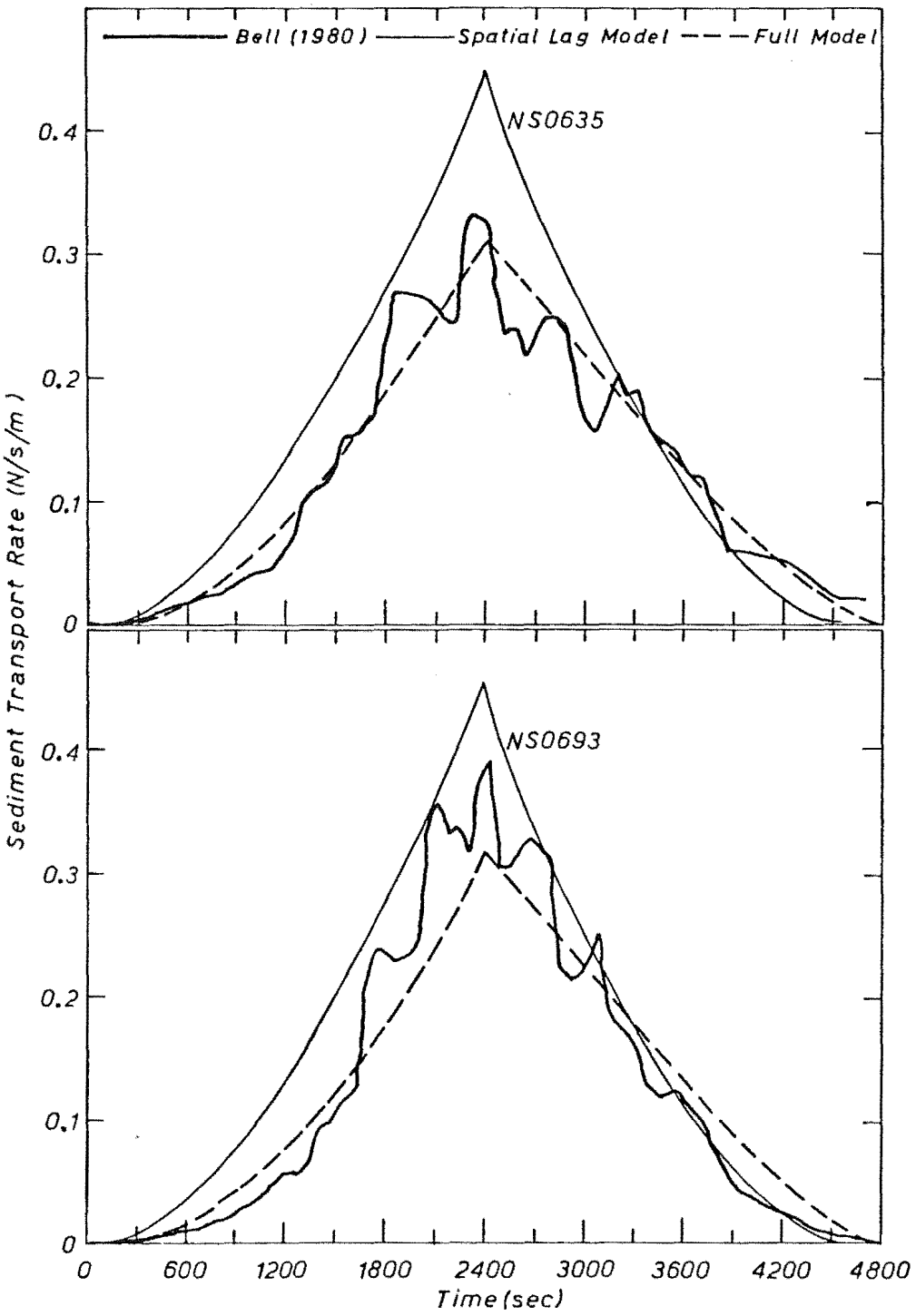

Figure 10.12(b) Sediment Transport Rate Against Time (Run NS06)

RUN	YIELD (KG)		
	MEASURED	MODEL	
		SPATIAL LAG ONLY	SPATIAL AND TEMPORAL LAG
NS0207	4.57	4.14	2.10
NS0217	2.28	5.92	2.93
NS0235	2.61	6.42	3.21
NS0253	3.28	6.43	3.26
NS0293	3.86	6.43	3.31
NS0307	2.62	2.45	1.63
NS0317	1.40	3.10	2.10
NS0335	1.70	3.10	2.11
NS0353	2.36	3.10	2.11
NS0393	2.24	3.10	2.11
NS0607	7.91	8.96	6.75
NS0617	12.20	19.60	12.36
NS0635	17.15	23.49	17.14
NS0653	16.70	23.71	18.58
NS0693	17.90	23.72	18.67

Table 10.5 Measured and Predicted Sediment Yields (Runs NS02, NS03 and NS06)

of the peak rates predicted by the spatial lag model. This trend was expected because the sediment phase is more able to keep up with slow changes in flow conditions than it is under swiftly changing flow conditions.

The asymmetry of both the simulated sediment hydrographs for the NS0607 and NS0617 runs, (Fig.10.13), clearly demonstrates the effect a developing scour hole may have on the sediment transport rates under the receding limb of the flood wave. This effect is less apparent in the NS02 and NS03 runs because the short duration of these flow events meant that the scour hole which formed was shallower than the scour hole which developed during the NS06 run.

For all runs except the NS--07 runs, the sediment hydrographs and sediment yields predicted by the numerical model which incorporates the temporal lag scheme i.e. the full model, are in excellent agreement with the measured hydrographs and yields. The tabulated values of sediment yield demonstrate that a model which only incorporates a spatial lag equation will overpredict sediment yields, especially under steep flow hydrographs.

The sediment yields at Station 0.74 m are consistently greater than even the sediment yields predicted by the spatial lag model. This, once again, appears to reflect the difficulty in measuring sediment transport rates over short reach lengths. It may also indicate that the bed roughness, due to bed form development, over a short reach is not the same as the bed roughness predicted by the model.

Overall, though, the performance of the model which incorporates both spatial and temporal lag schemes is excellent when compared with the measured data and demonstrates the significant effect temporal lag effects can have on sediment hydrographs and sediment yields.

10.4.3 Previous Temporal Lag Models

Many previous researchers have considered the time-lagged development of bed forms under unsteady flow conditions. Furthermore, they have applied their temporal lag models only to the case of a weakly, periodically varying water discharge. Typical of this approach, is the analysis and results presented by Fredsøe (1979). It was of particular interest to compare the behaviour of the proposed temporal lag model with that of the model of Fredsøe (1979).

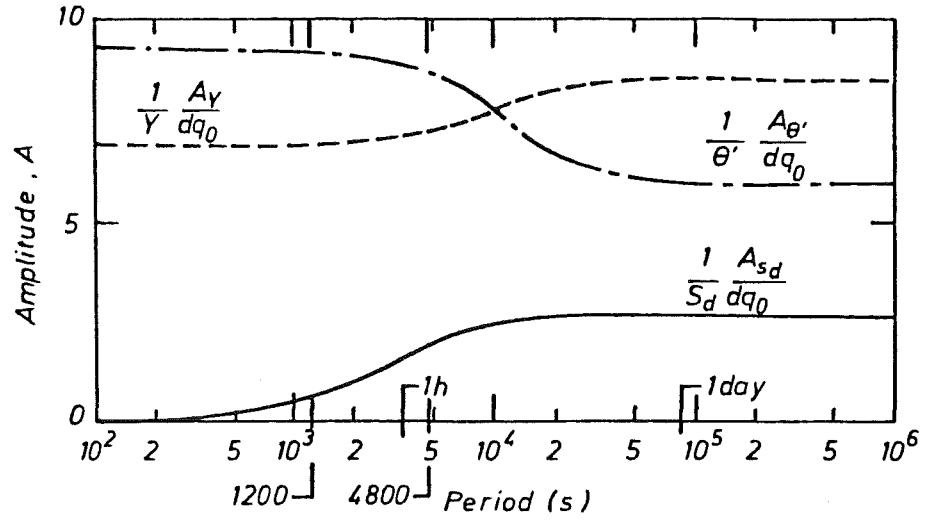

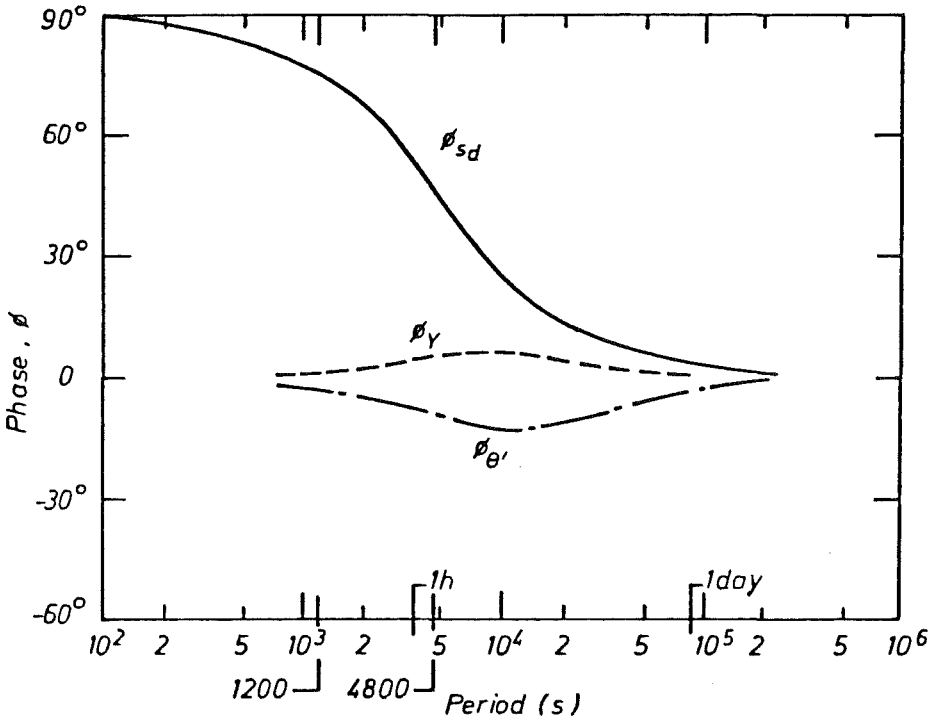

Figure 10.13 Variation of Amplitudes and Phases With Period For q = 0.10 $m^3/s/m$, S_o = 0.003, d_{50} = 1.0 mm which yields S_d = 0.0534 and Y = 0.15 m, (After Fredsøe (1979))

For a weakly, periodically varying water discharge, defined as

$$dq(t) = dq_o \sin(w_q t) \tag{10.37}$$

Fredsøe derived relations which described the temporally lagged behaviour of the bed form steepness, S_d, flow depth, Y, and grain Shields Parameter, θ', of the form

$$d\xi = A_\xi \sin(w_q t - \phi_\xi) \tag{10.38}$$

where $\xi = S_d$, Y or θ',

A_ξ = Amplitude of property ξ,

ϕ_ξ = Phase delay of property ξ,

w_q = Cyclic frequency of the varying discharge

and $d\xi$ describes the temporal variation of property ξ.

Fredsøe (1979), who considered that the grain Shields Parameter, θ', was a measure of the sediment transport rate, presented results which simulated a small stream e.g. a laboratory flume. These results are reproduced in Fig. 10.13. The flow and sediment properties are similar to those of Bell (1980).

It was of interest to compare the phase of the sediment transport, as measured by $\phi_{\theta'}$ by Fredsøe (1979), for periods similar to the wave period of runs NS02 and NS06 with the measured results of Bell (1980). In both the NS02 runs, (Fig. 10.10), and the NS06 runs, Fig. 10.12, the peak sediment transport is in phase with the flow hydrograph, (Fig. 10.9). For periods of similar duration, the trend of the phase, $\phi_{\theta'}$, in Fig. 10.13 is to decrease with increasing wave period. The temporal lag model and measured results in Figs. 10.10 and 10.12 also demonstrate that the peak sediment discharge increases with increasing wave duration (Section 10.4.2). However the results presented in Fig. 10.13 indicate that the amplitude of the sediment transport rate, $1/_{\theta'} A_{\theta'}/dq_o$, decreases with increasing wave duration.

The results of Fredsøe (1979) also indicate that the bed form development, as measured by ϕ_{S_d}, and the sediment transport rate, as measured by $\phi_{\theta'}$, are out of phase. In contrast, the bed roughness, which is a function of bed forms, and the sediment transport capacity are in phase in the proposed temporal lag model because they are both obtained from a single variable, the equivalent steady flow rate (see Fig. 8.6).

This comparison suggests that, since the results predicted by Fredsøe (1979) for a periodically varying discharge are dissimilar to those measured by Bell (1980) and simulated by the numerical model, that the temporal response of the bed roughness and the sediment transport rate are significantly affected by the pre-history of the alluvial system.

In the field, though, it is expected that the temporal response of an alluvial stream to constantly varying flows is composed of temporal responses to both periodically varying discharges and intermittent flood events.

10.5 SUMMARY

The performance of the proposed numerical model was tested by simulating six of the series of experiments conducted by Bell (1980).

The ST09, ST07 and ST05 runs of Bell (1980), were steady flow, non-equilibrium sediment transport experiments. These experiments were conducted in such a manner that only spatial lag effects were present. The predicted temporal variation of the centre-line local maximum scour depth was in good agreement with the measured data as was the agreement between predicted and measured temporal variations of the bedload transport rates at Stations 0.74 m, 1.74 m, 3.53 m and 5.3 m. In all numerical simulations the model predicted the onset of change in the bedload transport at Station 9.3 m at times much later than those measured by Bell (1980). The onset of change in the bedload transport rate at this station was equivalent to bed form celerities twice as great as those measured. The centre-line bed profiles were also in good agreement with the measured bed profiles of Bell (1980).

Diffusion models, which are an alternative to the numerical model, were investigated and several shortcomings under bed degradation conditions were revealed. The first shortcoming, that the upstream sediment boundary is stationary, was remedied by introducing a moving origin which is located at the toe of the vortex which develops in the scour hole. The temporal variations of the bedload transport rate predicted by the mobile boundary diffusion model, albeit for a greatly reduced diffusion coefficient than was predicted by various diffusion coefficient relations, were in excellent agreement with the measured bedload transport rates at Stations 0.74 m, 1.74 m, 3.53 m and 5.3 m. However, at Station 9.3 m, the mobile boundary

diffusion model results did not agree well with the measured data in a manner similar to that encountered in the numerical model simulations. A comparison of the measured and predicted temporal variations of the centre-line local maximum scour depth revealed the second shortcoming of diffusion models. This shortcoming is that diffusion models are unable to simulate the onset of threshold conditions on the bed and thus are unable to correctly predict the temporal variation of scour depths at large times. The third shortcoming of diffusion models is that they cannot be applied under unsteady flow conditions.

It was concluded that, overall, the numerical model was better able to predict the spatial and temporal variation of the bed elevation and bedload transport rate under steady flow non-equilibrium transport conditions than is a diffusion model.

The final three experiments simulated by the numerical model, the NS02, NS03 and NS06 experiments of Bell (1980), were unsteady flow non-equilibrium transport experiments. Both spatial and temporal lag effects were present in these experiments. The numerical model simulations of sediment hydrographs revealed the significant effect the temporal lag phenomenon can have on sediment hydrographs. The sediment hydrographs and sediment yields simulated by the full numerical model, which incorporates the spatial lag equation and temporal lag scheme, were in excellent agreement with the measured sediment hydrographs and sediment yields at all stations except Station 0.74 m. The measured sediment hydrographs at Station 0.74 m appear to reflect the difficulty in measuring sediment transport rates over short reach lengths and the possibility that the bed roughness over a short reach is not similar to that predicted by the numerical model.

The sediment hydrographs predicted by the full model were also compared with the temporal lag model results of Fredsφe (1979) for the case of a weakly, periodically varying discharge. This comparison suggested that the past discharge history significantly affects the temporal response of an alluvial system.

It was concluded from the comparison of measured and simulated results that the proposed numerical model, which incorporates a spatial lag equation and a temporal lag scheme, is well able to predict the spatial and temporal variations of the bed elevation and bedload transport rate under both steady and unsteady flow, non-equilibrium sediment transport conditions.

Chapter 11 | Conclusions and Recommendations

11.1 CONCLUSIONS

The aim of this study has been to investigate spatial and temporal lag effects in bedload transport under steady and non-steady flows. This investigation, which involved both experimental and theoretical studies, culminated in the formulation of a numerical model which includes schemes which successfully describe both spatial and temporal lag effects. Comparisons of model simulations and measured data confirmed the ability of the numerical model to simulate the response of an alluvial system to constrained sediment boundary conditions and steady and non-steady flows.

A brief recapitulation of aspects of the study and the essential conclusions, which are related to the aims formulated as a result of the literature review (Section 2.5) are presented below.

11.1.1 Spatial Lag

An equation,

$$(1 - \lambda') \frac{\partial A_b}{\partial t} = C_{SL}(G_V - G_{VC})$$

which characterises spatial lag effects and two possible relations for the spatial lag coefficient, C_{SL}, were investigated. Individual terms in the equation were measured at sections where the constrained sediment boundary conditions caused the bed to degrade swiftly i.e. at sections within a developing scour hole. Values of the spatial lag coefficient were calculated from these measured values using the spatial lag equation.

The spatial lag coefficient data was best fitted by the relation

$$C_{SL} = \frac{1}{\alpha_L d_{50}(\theta - \theta_c)}$$

where the upper and lower bounds for the empirically determined constant, α_L, are

$$4000 < \alpha_L < 9000$$

The numerical model developed herein (UWASER), which incorporated the above spatial lag equations and $\alpha_L = 4000$, was used to simulate three series of the steady flow, non-equilibrium transport experiments of Bell (1980); these experiments displayed only spatial lag effects.

It was found that

(i) The numerical model predicted well the temporal variation of the local maximum scour depth during all runs.

(ii) Predicted temporal variations of the bedload transport rate at all but the longest reach (9.3 m) were in good agreement with measured data. At Station 9.3 m, the numerical model predicted the onset of change in the bedload transport rates at times twice as great as those reported by Bell (1980). No explanation of this phenomenon has been found.

(iii) Predicted and measured centre-line bed profiles were in good agreement.

It was concluded from these studies that the proposed spatial lag equation together with a spatial lag coefficient relation of the form given above can define the response of an alluvial system to constrained sediment boundary conditions.

Diffusion models, which are an alternative model of spatial lag effects, were investigated and several shortcomings under bed degradation conditions were revealed. These shortcomings are

(i) The assumption, made in all diffusion models, that the upstream sediment boundary remains fixed. This assumption ignores the significant effect the fluid vortex has on the scour hole shape. This shortcoming was remedied herein by introducing a mobile upstream sediment boundary scheme.

(ii) Diffusion models are unable to simulate the onset of threshold conditions on the bed and are thus unable to correctly predict the temporal variation of scour depths at long times.

(iii) The diffusion coefficient relations predicted values which were 5 - 10 times greater than those which gave the best

agreement between model and experimentally measured values of the local maximum scour depth and bedload transport rates.

(iv) Diffusion models are unable to simulate spatial lag effects under non-steady flow conditions.

It was concluded that diffusion models should be used to simulate spatial lag effects, in the case of degrading beds, for short times only and that these simulations be only undertaken with diffusion coefficients that have been calibrated against experimental data.

11.1.2 Temporal Lag

A temporal lag scheme which is able to predict the temporal variation of bed roughness and sediment transport capacity under non-steady flow conditions was developed and calibrated against measured data.

The temporal response of the alluvial system is characterised by a single variable, the equivalent steady flow rate. An impulse model was used to develop a general solution for the temporal variation of this variable under non-steady flow conditions. Temporally lagged values of the bed roughness and sediment transport capacity are obtained by substituting values of the equivalent steady flow rate into bed roughness and sediment transport capacity relations obtained under steady flow conditions.

It was found that "equilibrium" time scale of this study was in excellent agreement with previously published "equilibrium" time scale data for the growth of dune bed forms from a plane bed.

The performance of the temporal lag scheme was tested by comparing predicted and measured flow depths and sediment transport rates under a variety of unsteady flow conditions. The agreement between predicted and measured values was found to be good; flow depths agreed to within $\pm$ 4%.

It was concluded that the proposed temporal lag scheme is able to predict the temporal variation of bed roughness and sediment transport rate under non-steady flow conditions.

11.1.3 Numerical Model (UWASER)

An uncoupled, unsteady flow and sediment routing model (UWASER) was developed. The innovative features of this model are

(i) The ability to simulate both spatial and temporal lag effects under bedload transport conditions.

(ii) The inclusion of an upstream sediment boundary scheme which takes account of the zone of separation which occurs at the upstream boundary of the alluvial reach under scour conditions.

Spatial lag effects are directly incorporated in the model through the use of the spatial lag equation. Temporal lag effects are indirectly incorporated in the model through relations for bedload transport capacity and bed roughness under unsteady flow conditions.

The numerical model was used to simulate three series of the non-steady flow, non-equilibrium transport experiments of Bell (1980). These experiments displayed both spatial lag and temporal lag effects. The numerical model simulations revealed

(i) The significant effect temporal lag can have on sediment hydrographs and yields. Reductions in bedload transport rates of up to 50% resulted from the inclusion of the temporal lag scheme in the numerical model.

(ii) The bedload hydrographs and yields predicted by the numerical model to be in excellent agreement with the measured sediment yields and hydrographs at all stations except station 0.74 m.

The measured bedload yields at station 0.74 m were significantly greater than those predicted by the model and appear to reflect the difficulty of measuring sediment transport rates over short reaches and the possibility that the bed roughness over short reaches is not similar to that predicted by the numerical model.

Sediment hydrographs, predicted by the numerical model, were compared with the temporal lag model results of Fredsøe (1979) for sediment transport under weakly, periodically varying discharge. This comparison suggested that the past discharge history significantly affects the temporal response of an alluvial system.

It was concluded from the comparison of all the measured and simulated results that the numerical model is well able to predict the spatial and temporal variations of the bed elevation and bedload transport rate under both steady and non-steady flow, non-equilibrium sediment

transport conditions.

11.2 RECOMMENDATIONS FOR FUTURE RESEARCH

This study has highlighted several areas of need in the field of sediment transport transients. The scope for further research is wide, not only in the laboratory but also in the field. The following recommendations are made.

11.2.1 Spatial Lag Studies

Further verification of the spatial lag equation and spatial lag coefficient relation is required. The proposed spatial lag coefficient relation has not been verified over as wide a range of flow and sediment conditions as would have been liked. Additional data is required at larger values of Shields Parameter and could be obtained by conducting similar experiments to those reported herein for a range of smaller grain sizes. Likewise, verification of the spatial lag equation under bed aggradation conditions is needed; this would involve sediment overloading experiments.

The numerical model simulations highlighted the need to further investigate the longitudinal variation of bed roughness within developing scour holes. Inclusion of a scheme which is better able to predict the variation of bed roughness would improve the ability of mathematical models to predict scour hole development and final equilibrium scour depths. The model simulations also highlighted differences between simulated and measured bedload transport at Station 9.3 m in the steady flow experiments of Bell (1980). These differences require investigation and the mechanism which causes this behaviour needs to be identified.

11.2.2 Temporal Lag Studies

There is a great need to collect further comprehensive sets of both field and laboratory data, including: bed profiles, bed form geometry, flow depth and sediment transport rates, under a variety of non-steady flows with and without spatial lag effects. To date, temporal lag schemes have only been used to simulate periodically varying flows; these flow conditions are of less relevance to gravel-bed rivers than are individual flood events. Temporal lag schemes need to be applied to individual flood events and compared with data measured, under these flow conditions, in the laboratory and in the field.

11.2.3 Numerical Models

Previous mathematical models, which have not incorporated spatial lag and/or temporal lag schemes, cannot be reasonably applied to situations where significant spatial and temporal lags exist. Mathematical models, of the form proposed herein, which include spatial and temporal lag effects need to be thoroughly tested against data measured under steady and non-steady flows with non-equilibrium transport conditions. Such comparisons can be expected to contribute to the refinement of future mathematical models.

Clearly much further work is needed before spatial and temporal lag effects due to steady and non-steady flows with non-equilibrium sediment transport can be fully comprehended.

References

AKSOY, S. (1971) "River Bed Degradation Downstream of Dams", *Proceedings of XIVth Congress*, IAHR, Paris, Vol. 3, Paper C33, p. 275-282.

ALAM, A.M.Z. and KENNEDY, J.F. (1969) "Friction Factors for Flow in Sand Bed Channels", *Journal of the Hydraulics Division*, ASCE, Vol. 95, No. HY6, p. 1973-1992.

ALLEN, J.R.L. (1974) "Reaction, Relaxation and Lag in Natural Sedimentary Systems: General Principles, Examples and Lessons", *Earth-Science Reviews*, Vol. 10, p. 263-342.

ALLEN, J.R.L. (1976(a)) "Computational Models for Dune Time-Lag: General Ideas, Difficulties and Early Results", *Sedimentary Geology*, Vol. 15, p. 1-53.

ALLEN, J.R.L. (1976(b)) "Bed Forms and Unsteady Processes: Some Concepts of Classification and Response Illustrated by Common One-Way Types", *Earth Science Processes*, Vol. 1, p. 361-374.

A.S.C.E. (1975) "Sedimentation Engineering", Prepared by the ASCE Task Committee for the Presentation of the Manual on Sedimentation of the Sedimentation Committee of the Hydraulics Division, V.A. Vanoni, Ed., *ASCE Manuals and Reports on Engineering Practice*, No. 54, 745 p.

BAYAZIT, M. (1969) "Resistance to Reversing Flow over Moveable Beds", *Journal of the Hydraulics Division*, ASCE, Vol. 95, No. HY4, p. 1109-1127.

BELL, R.G. (1980) "Non-Equilibrium Bedload Transport by Steady and Non-Steady Flows", *Report No. 80/23*, Dept. of Civil Eng'g, University of Canterbury, New Zealand, 237 p.

BENNETT, J.P. (1974) "Concepts of Mathematical Modelling of Sediment Yield", *Water Resources Research*, Vol. 10, No. 3, p. 485-492.

BREUSERS, H.N.C. (1965) "Conformity and Time Scale in Two-Dimensional Local Scour", *Publication No. 40*, Delft Hydraulics Laboratory, 8 p.

BROWN, G.O. and LI, R-M. (1979) "Sedimentation Study of the Yazoo River Basin", *User Manual for Program KUWASER*, Engineering Research Centre, Colorado State University, Colorado.

BROWNLIE, W.R. (1983) "Flow Depth in Sand Bed Rivers", *Journal of Hydraulic Engineering*, ASCE, Vol. 109, No. HY7, p. 959-990.

CHANG, F.M. (1969) "Computer Simulation of Riverbed Degradation and Aggradation by the Method of Chracteristics", *Proceedings of the XIIIth Congress*, IAHR, Koyoto, Vol. 1, Paper A37, p. 337-344.

CHEN, Y.H. (1975) "Mathematical Modelling of Water and Sediment Routing in Natural Channels", *Ph.D. Dissertation*, Colorado State University, Fort Collins, 253 p.

CHEN, Y.H. and SIMONS, D.B. (1975) "Mathematical Modelling of Alluvial Channels", *Symposium on Modelling Techniques*, Waterways, Harbours and Coastal Engineering Division, ASCE, San Francisco, Vol. 1, p. 466-483.

COLARIC, PICHON and SANANES (1967) "Etude des Affouillements a L'aval d'un Sevil Deversant", *Proceedings of the XIIth Congress*, IAHR, Fort Collins, Vol. 3, Paper C37, p. 322-329.

CUHNA, L.V. (1975) "Time Evolution of Local Scour", *"Proceedings of XVIth Congress*, IAHR, Sao Paulo, Vol. 2, Paper B36, p. 285-299.

CUNGE, J.A. and PERDREAU, N. (1973) "Mobile Bed Fluvial Models", *La Houille Blanche*, No. 7, p. 562-580.

de Vries, M. (1973) "River Bed Variations - Aggradation and Degradation", *Publication No. 107*, Delft Hydraulics Laboratory, Delft, 20 p.

DIETZ, J.W. (1969) "Kolkbidung in Feinen Oder Leichten Sohlmaterialien bei Stromendem Abfluß, *Mitteilungen Helft 155*, Versuchsanstalt fur Wasserbau and Kulturtechnik, Theodor-Rehbock-Flußbaulaboratorium, Universitat Fridericiana Karlsruhe, p. 1-20.

EINSTEIN, H.A. (1942) "Formulas for the Transportation of Bed Load", *Transactions*, ASCE, Vol. 207, p. 561-597.

EINSTEIN, H.A. (1950) "The Bed Load Function for Sediment Transportation in Open Channel Flows", *Technical Bulletin 1026*, U.S. Department of Agriculture, Soil Conservation Service, Washington D.C., 71 p.

EINSTEIN, H.A. (1968) "Deposition of Suspended Particles in a Gravel Bed", *Journal of the Hydraulics Division*, ASCE, Vol. 94, No. HY5, p. 1197-1205.

EINSTEIN, H.A. and BARBAROSSA, N.L. (1952) "River Channel Roughness", *Transactions*, ASCE, Vol. 117, p. 1121-1146.

ENGELUND, F. (1967) Closure to "Hydraulic Resistance of Alluvial Streams", *Journal of Hydraulics Division*, ASCE, Vol. 93, No. HY4, p. 287-296.

ENGELUND, F. and FREDSϕE, J. (1976) "A Sediment Transport Model for Straight Alluvial Channels", *Nordic Hydrology*, Vol. 7, p. 293-306.

ENGELUND, F. and FREDSϕE, J. (1982) "Sediment Ripples and Dunes", *Annual Review of Fluid Mechanics*, Vol. 14, p. 13-37.

FENTON, J.D. and ABBOTT, J.E. (1977) "Initial Motion of Grains on a Stream Bed: The Effect of Relative Protrusion", *Proceedings of the Royal Society of London*, Series A, Vol. 352, p. 523-537.

FERNANDEZ LUQUE (1974) "Erosion and Transport of Bed Sediment", *Dissertation* Kreps Repro B.V. - Mepel.

FERNANDEZ LUQUE, R. and Van BEEK, R. (1976) "Erosion and Transport of Bed Load Sediment", *Journal of Hydraulic Research*, IAHR, Vol. 14, No. 2, p. 127-144.

FOSTER, G.R. and MEYER, L.D. (1972) "A Closed-Form Soil Erosion Equation for Upland Areas", *Sedimentation*, Pub. and Ed. by H.W. Shen, Fort Collins, Chapter 12, 19 p.

FREDSØE, J. (1977) "Unsteady Flow in Straight Alluvial Channels", *Progress Report No. 44*, Inst. Hydrodynamic and Hydraulic Engineering, Technical University Denmark, p. 21-26.

FREDSØE, J. (1979) "Unsteady Flow in Straight Alluvial Streams: Modification of Individual Dunes", *Journal of Fluid Mechanics*, Vol. 91, Part 3, p. 497-512.

FREDSØE, J. (1981) "Unsteady Flow in Alluvial Streams. Part 2: Transition from Dunes to Plane Bed", *Journal of Fluid Mechanics*, Vol. 102, p. 431-453.

GEE, M.G. (1973) "Sediment Transport in Non-Steady Flow", *Technical Report HEL-22-3*, Hydraulic Engineering Laboratory, University of California, Berkeley, 93 p.

GEE, M.G. (1975) "Bed Form Response to Non-Steady Flows", *Journal of the Hydraulics Division*, ASCE, Vol. 101, No. HY3, p. 437-449.

GESSLER, J. (1971) "Aggradation and Degradation", *River Mechanics*, Ed. H.W. Shen, Vol. 1, Chapter 8, Colorado State University, Fort Collins, p. 8.1-8.24.

GILL, M.A. (1983(a)) "Diffusion Model for Aggrading Channels", *Journal of Hydraulic Research*, IAHR, Vol. 21, No. 5, p. 355-367.

GILL, M.A. (1983(b)) "Diffusion Model for Degrading Channels", *Journal of Hydraulic Research*, IAHR, Vol. 21, No. 5, p. 369-378.

GRANT, W.D. and MADSEN, O.S. (1982) "Moveable Bed Roughness in Unsteady Oscillating Flow", *Journal of Geophysical Research*, Vol. 87, No. C1, p. 469-481.

GRIFFITHS, G.A. (1976) "Transport of Bedload by Translation Waves in an Alluvial Channel", *Report No. 76-1*, Dept. of Civil Engineering, University of Canterbury, New Zealand, 152 p.

GRIFFITHS, G.A. (1979) "Recent Sedimentation History of Waimakariri River, N.Z.", *Journal of Hydrology*, New Zealand, Vol. 18, No. 1, p. 6-28.

HENDERSON, F.M. (1966) *Open Channel Flow*, The Macmillan Co., New York, N.Y., 522 p.

HEY, R.D., BATHURST, J.C. and THORNE, C.R. (1982) *Gravel-Bed Rivers: Fluvial Processes, Engineering and Management*, John Wiley and Sons, 875 p.

HILDEBRAND, F.B. (1976) *Advanced Calculus for Applications*, 2nd Ed., Prentice-Hall, 721 p.

HILL, I.K. (1967) "Fluvial Sediment Transport at Large Bed Shear Stress", *Ph.D. Dissertation*, University of Canterbury, New Zealand, 236 p.

HWANG, J.C. (1975) "Degradation of Sand-Bed Channels", *Proceedings of XVIth Congress*, IAHR, Sao Paulo, Vol. 2, Paper B23, p. 181-188.

Hydrologic Engineering Centre, "HEC-2, Water Surface Profiles" (1973) and "HEC-6, Scour and Deposition in Rivers and Reservoirs" (1977), *Computer Models*, U.S. Army, Corps of Engineers.

JAIN, S.C. (1981) "River Bed Aggradation due to Overloading", *Journal of Hydraulic Division*, ASCE, Vol. 107, HY1, p. 120-124.

JENSEN, P.D. (1973) "Dune Formation Under Non-Steady Conditions", *Proceedings of the XVth Congress*, IAHR, Istanbul, Vol. 1, Paper A23, p. 173-179.

JOHNSON, J.W. (1942) "The Importance of Side-Wall Friction in Bed-Load Investigations", *Civil Engineering*, Vol. 12, No. 6, p. 329-331.

JOHNSON, J.W. (1943) "Laboratory Investigations on Bed-Load Transportation and Bed Roughness", *Sedimentation Section Report SCS-TP-50*, Research Office of Soil Conservation Service, U.S.D.A., p. 116.

KENDALL, M.G. (1973) *Time-Series*, Charles Griffin & Co., London, 197 p.

KOMURA, S. (1971) "Prediction of River-Bed Degradation Below Dams", *Proceedings of the XIVth Congress*, IAHR, Paris, Vol. 3, Paper C31, p. 257-264.

LE FEUVRE, A.R., ALTINBILEK, H.D. and CARSTENS, M.R. (1970) "Sediment Pick-Up Function", *Journal of the Hydraulics Division*, ASCE, Vol. 96, No. HY10, p. 2051-2063.

LIGGETT, J.A. (1975) "Basic Equations of Unsteady Flow", *Unsteady Flow in Open Channels*, Ed. K. Mahmood and V. Yevjevich, Chapter 2, Water Resources Publications, Fort Collins, Colorado, p. 29-62.

LIGGETT, J.A. and CUNGE, J.A. (1975) "Numerical Methods of Solution of the Unsteady Flow Equations", *Unsteady Flow in Open Channels*, Ed. K. Mahmood and V. Yevjevich, Chapter 4, Water Resources Publications, Fort Collins, Colorado, p. 89-182.

MEHTA, P.J., GARDE, R.J. and RANGA RAJU, K.G. (1983) "Transient Bed Profiles in Aggrading Streams", *Proceedings of 2nd International Symposium on River Sedimentation"*, Nanjing, China.

MELAND, N. and NORMANN, J.O. (1966) "Transport Velocities of Single Particles in Bed-Load Motion", *Geografiska Annaler*, Vol. 48,A.

MEYER, L.D. and MONKE, E.J. (1965) "Mechanics of Soil Erosion by Rainfall and Overland Flow", *Transactions*, ASAE, Vol. 8, No. 4, p. 572-577.

MONRO, J.C. (1971) "Direct Search Optimisation in Mathematical Modelling and a Watershed Model Application", *NOAA Technical Memorandum NWS HYDRO-12*, U.S. Dept. of Commerce, Office of Hydrology, Silver Spring, Md., 52 p.

MOSONYI, E. AND SCHOPPMANN, B. (1968) "Ein Beitrag Erforschung von Ortlichen Auskolkungen hinter Geneigten Befestigungsstrecken in Abhangigkeit der Zeit", *Mitteilungen Helft 154*, Versuchsanstalt fur Wasserbau und Kulturtechnik, Theodor-Rehbrook-Flußbaulaboratorium, Universitat Fredericiana Karlsruhe, p. 1-33.

NAKAGAWA, H. and TSUJIMOTO, T. (1980) "Sand Bed Instability Due to Bed Load Motion", *Journal of the Hydraulic Division*, ASCE, Vol. 106, No. HY12, p. 2029-2051.

NAKAGAWA, H. and TSUJIMOTO, T. (1983(a)) "Time-Lag Appearing in Unsteady Flow with Sand Waves", *Journal of Hydroscience and Hydraulic Engineering*, Vol. 1, No. 1, p. 83-95.

NAKAGAWA, H. and TSUJIMOTO, T. (1983(b)) "Lag Behaviour of Unsteady Flow with Sand Dunes", *Proceedings of 2nd International Symposium on River Sedimentation*, Nanjing, China.

NASNER, H. (1973) "On the Behaviour of Tidal Dunes in Estuaries", *Proceedings of XVth Congress*, IAHR, Istanbul, Vol. 1, Paper A24, p. 181-188.

NEILL, C.R. (1968) "A Re-Examination of the Beginning of Movement for Coarse Granular Bed Materials", *Research Report INT 68*, Hydraulic Research Station, Wallingford.

NEILL, C.R. (1969) "Bed Forms of the Lower Red Deer River, Alberta", *Journal of Hydrology*, Vol. 7, No. 1, p. 58-85.

NEILL, C.R. and YALIN, M.S. (1969) "Quantitative Definition of the Beginning of Bed Movement", *Journal of the Hydraulic Division*, ASCE, Vol. 95, No. HY1, p. 585-587.

PAINTAL, A.S. (1971(a)) "Concept of Critical Shear Stress in Loose Boundary Open Channels", *Journal of Hydraulic Research*, IAHR, Vol. 9, No. 1, p. 91-113.

PAINTAL, A.S. (1971(b)) "A Stochastic Model of Bed Load Transport", *Journal of Hydraulic Research*, IAHR, Vol. 9, No. 4, p. 527-554.

PAZIS, G.C. and GRAF, W.H. (1977) "Weak Sediment Movement", *Journal of the Hydraulics Division*, ASCE, Vol. 103, No. HY7, p. 799-801.

PEMBERTON, D.G. (1979) "Shingle Management on the Wairoa-Waimea Rivers, Nelson", *New Zealand Engineering*, Vol. 34, No. 5, p. 98-101.

PHILLIPS, B.C. (1981) "Sediment Routing in Alluvial Streams", *M.Eng.Sc. Dissertation*, University of Melbourne, Australia, 470 p.

PONCE, V.M., GARCIA, J.L. and SIMONS, D.B. (1979) "Modelling Alluvial Channel Bed Transients", *Journal of the Hydraulic Division*, ASCE, Vol. 105, No. HY3, p. 245-256.

PULS, W., SUNDERMANN, J. and VOLLMERS, H. (1977) "A Numerical Approach to Solid Matter Transport Computation", *Proceedings of XVIIth Congress*, IAHR, Baden-Baden, Vol. 1, Paper A17, p. 130-135.

RAICHLEN, F. and KENNEDY, J.F. (1965) "The Growth of Sediment Bed Forms from an Initially Flattened Bed", *Proceedings of XIth Congress*, IAHR, Leningrad, Vol. 3, Paper 3.7, p. 1-8.

RAUDKIVI, A.J. (1965) "Turbulence and Vorticity in Loose Boundary Hydraulics", *Proceedings of 2nd Australasian Conference on Hydraulics and Fluid Mechanics*, University of Auckland, p. A135-A142.

SCHLICHTING, H. (1968) *Boundary Layer Theory*, 6th Ed., Prentice-Hall, N.Y., 748 p.

SHIELDS, A. (1936) "Application of Similarity Principles and Turbulence Research to Bed-Load Movement", Berlin, English Translation: W.P. Ott and J.C. van Uchelen, *California Institute Technical Publication No. 167*, Soil Conservation Service.

SIMONS, D.B., RICHARDSON, E.V. and HAUSHILD, W.L. (1962) "Depth Discharge Relations in Alluvial Channels", *Journal of the Hydraulic Division*, ASCE, Vol. 88, No. HY5, p. 57-72.

SIMONS, D.B. and SENTURK, F. (1977) *Sediment Transport Technology*, Water Resource Publications, Fort Collins, Colorado, 807 p.

SPINKS, A.H. and KELLER, R.J. (1976) "An Ultrasonic Depth Meter for Hydraulic Models", *Report No. 8-76/1*, Central Laboratories, Ministry of Works and Development, New Zealand, 22 p.

SONI, J.P. (1981(a)) "Laboratory Study of Aggradation in Alluvial Channels", *Journal of Hydrology*, Vol. 49, pp. 87-106.

SONI, J.P. (1981(b)) "An Error Function Solution of Sediment Transport in Aggrading Channels", *Journal of Hydrology*, Vol. 49, p. 107-119.

SONI, J.P., GARDE, R.J. and RANGA RAJU, K.G. (1977) "Nonuniform Flow in Aggrading Channels", *Journal of Waterways, Coastal and Ocean Division*, ASCE, Vol. 103, WW3, p. 321-333.

SONI, J.P., GARDE, R.J. and RANGA RAJU, K.G. (1980) "Aggradation in Streams Due to Overloading", *Journal of the Hydraulic Division*, ASCE, Vol. 106, HY1, p. 117-132.

SUMER, M. (1977) "Settlement of Solid Particles in Open-Channel Flow", Proceedings of the Hydraulic Division, ASCE, Vol. 103, HY11, p. 1323-1337.

SUTHERLAND, A.J. (1983) "Experimental Investigation of the Flow Field in a Simulated Scour Hole", *Research Report 83/6*, University of Canterbury, New Zealand, 33 p.

TAYLOR, B.D. (1971) "Temperature Effects in Alluvial Streams", *Report No. KH-R-27*, W.M. Keck Laboratory of Hydraulics and Water Resources, California Institute of Technology, 204 p.

THOMAS, W.A. and PRASUHN, A.L. (1977) "Mathematical Modelling of Scour and Deposition", *Journal of the Hydraulic Division*, ASCE, Vol. 103, No. HY8, p. 851-863.

TOFFALETTI, F.B. (1969) "Definitive Computations of Sand Discharge in Rivers", *Journal of the Hydraulic Division*, ASCE, Vol. 95, No. HY1, p. 225-248.

VANONI, V.A. and BROOKS, N.H. (1957) "Laboratory Studies of the Roughness and Suspended Load of Alluvial Streams", *Sedimentation Laboratory Report No. E68*, California Institute of Technology, Pasadena, 121 p.

WELLINGTON, N.B. (1978) "A Sediment-Routing Model for Alluvial Streams", *M.Eng.Sc. Dissertation*, University of Melbourne, Australia, 139 p.

WHITE, W.R., MILLI, H. and CRABBE, A.D. (1973) "Sediment Transport: An Appraisal of Available Methods", *Hydraulic Research Station Report No. INT 119*, 2 Vols., Wallingford.

WHITE, W.R., PARIS, E. and BETTESS, R. (1979) "A New General Method of Predicting the Frictional Characteristics of Alluvial Streams", *Hydraulic Research Station Report No. INT 181*, Wallingford, 13 p.

WILLIAMS, G.P. (1970) "Flume Width and Water Depth Effects in Sediment Transport Experiments", *U.S. Geological Survey*, Prof. Paper No. 562-H, 37 p.

WILLIAMSON, J. (1951) "The Laws of Flow in Rough Pipes", *La Houille Blanche*, Vol. 6, No. 5, p. 738.

WILLIS, J.C. (1971) "Erosion by Concentrated Flow", *Report ARS 41-179*, Agriculture Research Service, U.S. Dept. of Agriculture, Washington, D.C., 38 p.

WOLMAN, M.G. (1977) "Changing Needs and Opportunities in the Sediment Field", *Water Resources Research*, Vol. 13, No. 1, p. 50-54.

YALIN, M.S. (1963) "An Expression for Bed-Load Transportation", *Journal of the Hydraulics Division*, ASCE, Vol. 89, No. HY3, p. 221-250.

YALIN, M.S. (1971) *Theory of Hydraulic Models*, The Macmillan Co., London, 266 p.

YALIN, M.S. (1972) *Mechanics of Sediment Transport*, Permagon Press, 298 p.

YALIN, M.S. (1975) "Development of Sand Waves in Time", *Proceedings of XVth Congress*, IAHR, Sao Paulo, Vol. 2, Paper B27, p. 212-219.

YALIN, M.S. (1983) "River Bed Degradation Downstream of a Dam", *Proceedings of XXth Congress*, IAHR, Moscow, Vol. 2, Paper A.c.1, p. 237-243.

YALIN, M.S. and BISHOP, C.T. (1977) "On the Physical Modelling of Dunes", *Proceedings of XVIIth Congress*, IAHR, Baden-Baden, Vol. 1, Paper A4, p. 25-32.

YANO, K. TSUCHIYA, Y. and MICHIUE, M. (1969) "Studies on the Sand Transport in Streams with Tracers", *Bulletin of the Disaster Prevention Research Institute*, Vol. 18, Part 3, No. 141, Koyoto University, Japan, p. 1-16.

ZOPPOU, C. (1979) "Numerical Models and Solution of Unsteady Flow Equations for Open Channels", *M.Eng.Sc. Dissertation*, University of Melbourne, Australia, 233 p.

Appendix A | Experimental Considerations

A.1 FIXED BED LENGTHS

Fixed beds, whose surface was composed of rounded gravel particles (d_{50} = 3.65 mm) were placed upstream of the mobile reach, to allow the turbulent boundary layer to develop fully, and downstream of the mobile reach, to shift the backwater effects associated with the downstream weir gate away from the test reach (Fig. 3.2). These plane gravel beds were both sprayed with a fluid mixture of cement and water and allowed to harden. The upstream fixed bed was separated from the mobile reach by a partition board which was sealed to prevent seepage of water between the fixed and mobile beds. Similarily, a partition board was inserted just upstream of the downstream weir gate and also sealed to prevent seepage of water.

Using the analogy of the boundary layer growth on a rough plate and for a given maximum flow depth (Y) and equivalent grain roughness (k_s), the minimum length of the fixed upstream bed can be determined such that the boundary layer thickness is equal to the flow depth. Combining the coefficient of total skin-friction drag on a rough plate (Schlichting (1968)) and the universal velocity distribution for a completely rough region, gives

$$x = 0.153\, k_s \exp\{4.476\left[\log_{10}\left(\frac{30.1Y}{k_s}\right)\right]^{0.8}\} \qquad (A.1)$$

For the expected maximum flow depth, Y = 0.28 m, and an equivalent grain roughness, $k_s \simeq 2d_{50}$ = 7.3 mm, Eq. A.1 gives

$$x = 6.4 \text{ m}$$

The vertical velocity profiles at the fixed to mobile bed interface, measured during the SC-I series of experiments (Section 6.2.5),

confirmed that the boundary layer was indeed fully developed and thus the 7.2 m length of fixed upstream bed was deemed to be sufficient.

The length of the downstream fixed bed, 5.0 m, was dictated by the position of the bedload collector. This bed was able to contain the backwater curve from the submerged outlet weir at all discharges greater than the base discharge. At the base discharge and with the downstream weir gate set flush with the bed (Section 4.4.2) the bac water curve just intruded into the downstream end of the mobile reacn.

A.2 SEDIMENT PROPERTIES

The bed material was supplied by North End Sand Supplies, Kaiapoi with an initial $d_{50} = 2.1$ mm and a geometric standard deviation, $\sigma_g = 1.46$. This source material was then sieved once between mesh screens of 2.38 mm and 1.58 mm spacing. The resultant bed material was a fine uniform gravel, with $d_{50} = 1.8$ mm and $\sigma_g = 1.124$, consisting of sub-rounded and rounded grains. The grain size distribution of this material is shown in Fig. 3.5. Bed material properties are summarised in Table 3.1. Relevant sediment properties were determined in the following manner.

- Grain Size

  The grain size distribution curve was obtained by conducting a sieve analysis of five random 600 g samples of the bed material.

- Specific Gravity

  Eight samples of the bed material were oven dried, placed in a flask, weighed, then filled with distilled water and boiled in a vacuum dessicator. After removal from the dessicator, the flask was filled with distilled water up to a calibrated volume mark, weighed, and the water temperature measured. The specific gravity of the bed material was then determined from the various measurements.

- Porosity

  Four bed material samples were added to a weighed flask, filled with a known volume of distilled water and the flask and gravel weighed. The porosity of the bed material was obtained, using the formula

$$\rho_d = (1 - \lambda')\rho_s$$

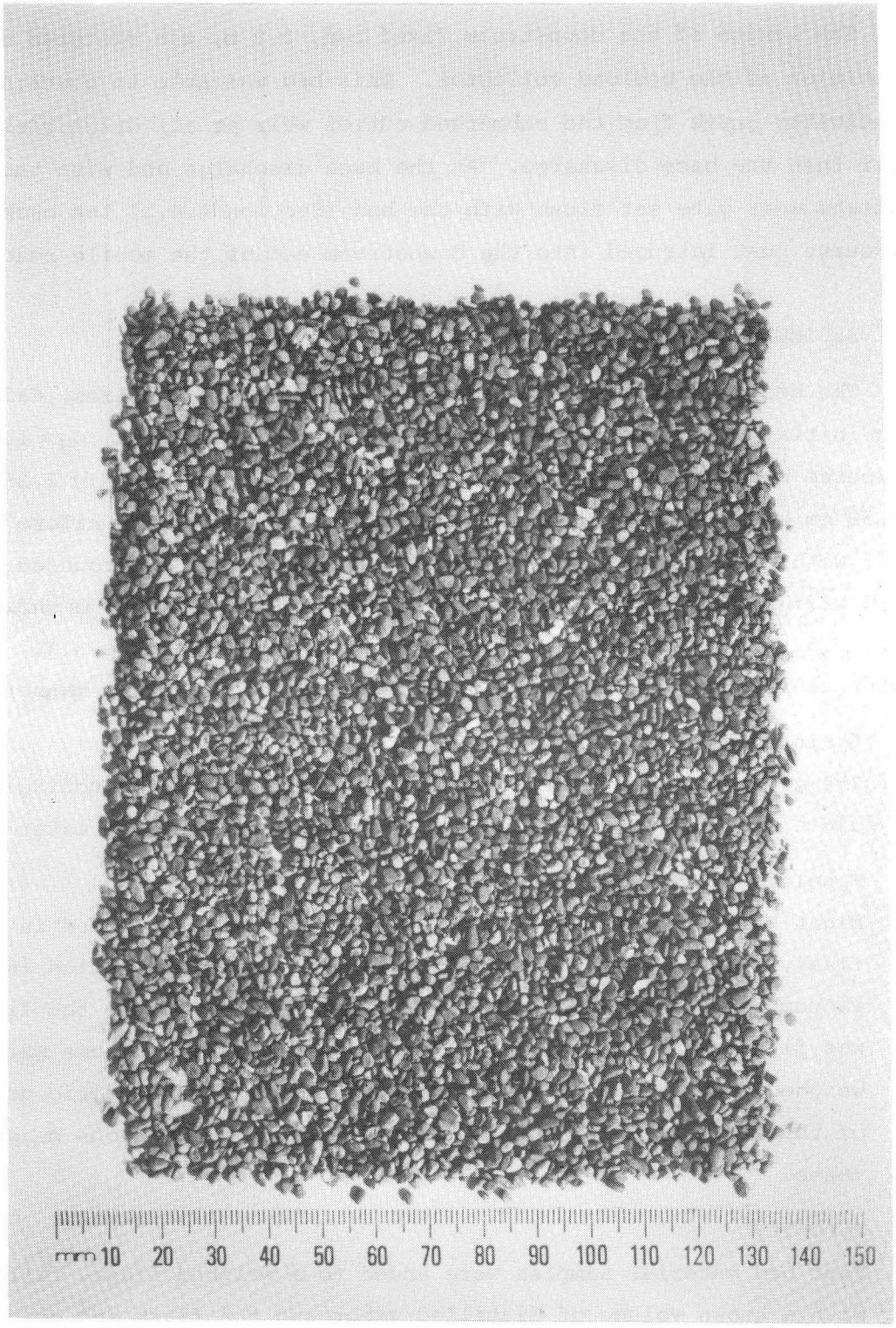

Plate A.1 Sediment Grain Shape (d_{50} = 1.8 mm)

- Fall Velocity

  Samples, each of 50 grains, were dropped into a 2 m column of water. Representative grains were selected and timed over a 500 mm test section located 250 mm above the floor of the column. At least four measurements of each of the fast, average and slow grain velocities were made and the average fall velocity determined.

- Submerged Angle of Repose

  Four cones of gravel were built against a side-wall of a water filled, perspex tank to maximum slopes just prior to a slump. Angles of repose were measured directly on the wall.

- Particle Shape

  The shape of the particles is shown in Plate A.1.

Appendix B | Time Series Analysis

B.1 BEDLOAD TRANSPORT RATE

The cumulative sediment yield during all runs was recorded in a constant temporal order. Hence the instantaneous bedload transport rates calculated from these records also display this temporal order and time-series analysis can be readily applied to smooth these sediment transport rates. The preferable procedure is to use a centred moving average filter.

The computational procedure is a lead-lag process where a polynomial is fitted to (2 m + 1) data points, which is termed the phase length, centred about the value of interest, which can be shown in the algebraic form

$$g_s(t) = \frac{\sum_{i=1}^{2m+1} c_{s_i} g_s'(t + (i - (m+1))\Delta t)}{\sum_{i=1}^{2m+1} c_{s_i}} \qquad (B.1)$$

where g_s = Smoothed sediment transport rate,
g_s' = Instantaneous sediment transport rate,
c_s = Time series coefficient, and
Δt = Sampling time increment.

Coefficients for polynomials up to the quintic order have been worked out and can be obtained from tables given by Kendall (1973). However, Bell (1980) found the linear polynomial, order one to be the most satisfactory smoothing polynomial. This polynomial was also adopted in this study.

As it stands the algorithm will not yield trend values for the first and last m data points. Coefficients for polynomials centred on

TIME-SERIES ANALYSIS - LINEAR ALGORITHM

TABLES OF COEFFICIENTS:

PHASE LENGTH = 9

1	2	3	4	5
17	56	22	32	1
14	47	19	29	1
11	38	16	26	1
8	29	13	23	1
5	20	10	20	1
2	11	7	17	1
-1	2	4	14	1
-4	-7	1	11	1
-7	-16	-2	8	1
45	180	90	180	9

PHASE LENGTH = 11

1	2	3	4	5	6
7	15	25	10	15	1
6	13	22	9	14	1
5	11	19	8	13	1
4	9	16	7	12	1
3	7	13	6	11	1
2	5	10	5	10	1
1	3	7	4	9	1
0	1	4	3	8	1
-1	-1	1	2	7	1
-2	-3	-2	1	6	1
-3	-5	-5	0	5	1
22	55	110	55	110	11

PHASE LENGTH = 13

1	2	3	4	5	6	7
25	44	19	32	13	20	1
22	39	17	29	12	19	1
19	34	15	26	11	18	1
16	29	13	23	10	17	1
13	24	11	20	9	16	1
10	19	9	17	8	15	1
7	14	7	14	7	14	1
4	9	5	11	6	13	1
1	4	3	8	5	12	1
-2	-1	1	5	4	11	1
-5	-6	-1	2	3	10	1
-8	-11	-3	-1	2	9	1
-11	-16	-5	-4	1	8	1
91	182	91	182	91	182	13

PHASE LENGTH = 15

1	2	3	4	5	6	7	8
29	91	161	35	119	49	77	1
26	82	146	32	110	46	74	1
23	73	131	29	101	43	71	1
20	64	116	26	92	40	68	1
17	55	101	23	83	37	65	1
14	46	86	20	74	34	62	1
11	37	71	17	65	31	59	1
8	28	56	14	56	28	56	1
5	19	41	11	47	25	53	1
2	10	26	8	38	22	50	1
-1	1	11	5	29	19	47	1
-4	-8	-4	2	20	16	44	1
-7	-17	-19	-1	11	13	41	1
-10	-26	-34	-4	2	10	38	1
-13	-35	-49	-7	-7	7	35	1
120	420	840	210	840	420	840	15

Table B.1 Time Series Coefficients
(After Kendall (1973))

these points were also obtained by Kendall (1973); these coefficients effectively fit a straight line through the first and last m data points. These coefficients, for a range of phase lengths, are given in Table B.1. The disadvantages of this smoothing scheme were briefly discussed by Bell (1980) and were fully discussed by Kendall (1973).

A phase length of 11 was adopted, in this study, for all analyses of sediment data. This phase length effectively smoothed instantaneous bedload transport rates over ten minute intervals.

Appendix C | Steady Flow Equilibrium Transport

C.1 SIDE-WALL CORRECTION

The data from the steady flow equilibrium (SE) experiments was analysed using the side-wall correction methods proposed by Williams (1970) and Vanoni and Brooks (1957). The divided bed shear stress approach of Einstein (1950) was also used to analyse the data for grain roughness effects. The results of this analysis of the SE data collected in this study, the SE data of Bell (1980) and of Griffiths (1976) are given in Tables C.1, C.2 and C.3 respectively.

C.2 INITIAL MOTION

The initial motion data of Bell (1980) and of Griffiths (1976) was analysed using both bed related flow properties, obtained by applying Williams (1970) side-wall correction, and grain related flow properties, obtained by the divided bed shear stress approach of Einstein (1950). The results of this analysis of the data of Bell (1980) and of Griffiths (1976) are given in Tables C.4 and C.5 respectively.

C.3 EQUILIBRIUM SEDIMENT TRANSPORT

C.3.1 Equilibrium Transport Formulae

The equilibrium sediment transport formulae were obtained from the following references:

. Einstein - Brown (1950)	- White, Milli and Crabbe (1973)	p.17
. Yalin (1963)	- White, Milli and Crabbe (1973)	p.29
. Einstein (1950)	- Einstein (1950)	p.37
. Paintal (1971(b))	- Paintal (1971(b)) (shown in the form of a plot of flow intensity against dimensionless sediment transport rate)	p.545

C.3.2 Equilibrium Transport Data

The SE data collected in this study, and by Bell (1980), is given in Tables C.6 and C.7 respectively. Also included in these tables are the results of a linear regression analysis of equilibrium sediment transport and velocity excess data.

SEDIMENT DATA : PHILLIPS (1984)

SEDIMENT : GRAVEL
SPECIFIC
GRAVITY : 2.65
D35 (MM) : 1.70
D50 (MM) : 1.80
D65 (MM) : 1.90

SIDE-WALL CORRECTION METHODS

RUN	DISCHARGE (M**2/S)	FLOW DEPTH (M)	SLOPE	VELOCITY (M/S)
SE1001	0.0908	0.1745	0.00095	0.5203
SE1002	0.1007	0.1855	0.00095	0.5429
SE1003	0.1098	0.1965	0.00095	0.5588
SE1004	0.1205	0.2092	0.00095	0.5760
SE1005	0.1303	0.2200	0.00095	0.5923
SE1006	0.1410	0.2353	0.00095	0.5992
SE1501	0.0798	0.1396	0.00150	0.5716
SE1502	0.0794	0.1397	0.00150	0.5684
SE1503	0.1006	0.1640	0.00150	0.6134
SE1504	0.1207	0.1864	0.00150	0.6475
SE1505	0.1392	0.2108	0.00150	0.6603
SE1506	0.1595	0.2350	0.00150	0.6787
SE1507	0.1786	0.2540	0.00150	0.7031
SE2001	0.0796	0.1295	0.00200	0.6147
SE2002	0.0998	0.1519	0.00200	0.6570
SE2003	0.0992	0.1520	0.00200	0.6526
SE2004	0.1215	0.1756	0.00200	0.6919
SE2005	0.1400	0.1958	0.00200	0.7150
SE2006	0.1621	0.2160	0.00200	0.7505
SE2007	0.1811	0.2357	0.00200	0.7683
SE2501	0.0803	0.1242	0.00250	0.6465
SE2502	0.1025	0.1445	0.00250	0.7093
SE2503	0.1219	0.1640	0.00250	0.7433
SE2504	0.1388	0.1780	0.00250	0.7798
SE2505	0.1606	0.1965	0.00250	0.8173
SE2506	0.1813	0.2138	0.00250	0.8480

		(WILLIAMS)		(VANONI-BROOKS)		(EINSTEIN)	
FLOW DEPTH (M)	MANNING N	HYD. RAD. (M)	MANNING N	HYD. RAD. (M)	MANNING N	HYD. RAD. (M)	MANNING N
0.1745	0.0185	0.1582	0.0173	0.1022	0.0129	0.1069	0.0133
0.1855	0.0185	0.1672	0.0172	0.1036	0.0125	0.1141	0.0134
0.1965	0.0186	0.1761	0.0173	0.1059	0.0123	0.1193	0.0134
0.2092	0.0189	0.1862	0.0174	0.1082	0.0122	0.1250	0.0134
0.2200	0.0190	0.1947	0.0175	0.1093	0.0119	0.1304	0.0134
0.2353	0.0196	0.2066	0.0180	0.1148	0.0122	0.1328	0.0134
0.1396	0.0182	0.1290	0.0173	0.0940	0.0140	0.0871	0.0133
0.1397	0.0183	0.1290	0.0174	0.0945	0.0141	0.0864	0.0133
0.1640	0.0189	0.1495	0.0178	0.1045	0.0140	0.0970	0.0133
0.1864	0.0195	0.1679	0.0182	0.1131	0.0140	0.1053	0.0133
0.2108	0.0208	0.1874	0.0192	0.1255	0.0147	0.1085	0.0133
0.2350	0.0217	0.2063	0.0199	0.1359	0.0151	0.1132	0.0134
0.2540	0.0221	0.2208	0.0201	0.1410	0.0149	0.1195	0.0134
0.1295	0.0186	0.1203	0.0177	0.0924	0.0149	0.0782	0.0133
0.1519	0.0194	0.1394	0.0183	0.1038	0.0150	0.0865	0.0133
0.1520	0.0195	0.1395	0.0184	0.1044	0.0152	0.0856	0.0133
0.1756	0.0203	0.1591	0.0190	0.1156	0.0153	0.0936	0.0133
0.1958	0.0211	0.1755	0.0196	0.1255	0.0157	0.0984	0.0133
0.2160	0.0215	0.1915	0.0198	0.1326	0.0155	0.1059	0.0133
0.2357	0.0222	0.2069	0.0204	0.1415	0.0158	0.1098	0.0133
0.1242	0.0193	0.1157	0.0184	0.0923	0.0158	0.0714	0.0133
0.1445	0.0194	0.1331	0.0184	0.1019	0.0154	0.0821	0.0133
0.1640	0.0202	0.1495	0.0189	0.1122	0.0156	0.0881	0.0133
0.1780	0.0203	0.1611	0.0190	0.1176	0.0154	0.0947	0.0133
0.1965	0.0207	0.1761	0.0192	0.1249	0.0153	0.1018	0.0133
0.2138	0.0211	0.1898	0.0195	0.1315	0.0152	0.1077	0.0133

		(WILLIAMS)		(VANONI-BROOKS)		(EINSTEIN)	
UST (M/S)	1/PSI	USTB (M/S)	1/PSIB	USTB (M/S)	1/PSIB	USTB (M/S)	1/PSIB
0.0403	0.0558	0.0384	0.0506	0.0309	0.0327	0.0316	0.0362
0.0416	0.0593	0.0395	0.0535	0.0311	0.0331	0.0326	0.0386
0.0428	0.0629	0.0405	0.0563	0.0314	0.0339	0.0333	0.0404
0.0442	0.0669	0.0417	0.0596	0.0318	0.0346	0.0341	0.0423
0.0453	0.0704	0.0426	0.0623	0.0319	0.0350	0.0349	0.0442
0.0468	0.0753	0.0439	0.0661	0.0327	0.0367	0.0352	0.0450
0.0453	0.0705	0.0436	0.0651	0.0372	0.0475	0.0358	0.0466
0.0453	0.0706	0.0436	0.0652	0.0373	0.0477	0.0357	0.0462
0.0491	0.0828	0.0469	0.0755	0.0392	0.0528	0.0378	0.0519
0.0524	0.0941	0.0497	0.0848	0.0408	0.0571	0.0394	0.0563
0.0557	0.1065	0.0525	0.0947	0.0430	0.0634	0.0400	0.0580
0.0588	0.1187	0.0551	0.1042	0.0447	0.0686	0.0408	0.0605
0.0611	0.1283	0.0570	0.1115	0.0456	0.0712	0.0419	0.0639
0.0504	0.0872	0.0486	0.0810	0.0426	0.0622	0.0392	0.0558
0.0546	0.1023	0.0523	0.0939	0.0451	0.0699	0.0412	0.0617
0.0546	0.1024	0.0523	0.0939	0.0453	0.0703	0.0410	0.0611
0.0587	0.1182	0.0559	0.1071	0.0476	0.0778	0.0429	0.0667
0.0620	0.1319	0.0587	0.1182	0.0496	0.0845	0.0439	0.0701
0.0651	0.1455	0.0613	0.1290	0.0510	0.0893	0.0456	0.0755
0.0680	0.1587	0.0637	0.1393	0.0527	0.0953	0.0464	0.0783
0.0552	0.1045	0.0533	0.0974	0.0476	0.0777	0.0418	0.0636
0.0595	0.1216	0.0571	0.1121	0.0500	0.0858	0.0449	0.0731
0.0634	0.1380	0.0606	0.1258	0.0525	0.0944	0.0465	0.0785
0.0661	0.1498	0.0628	0.1356	0.0537	0.0990	0.0482	0.0844
0.0694	0.1654	0.0657	0.1482	0.0554	0.1052	0.0500	0.0907
0.0724	0.1800	0.0682	0.1598	0.0568	0.1107	0.0514	0.0960

Table C.1 Side-Wall Analysis Results for SE Data

SEDIMENT DATA : BELL (1980)

SEDIMENT : GRAVEL
SPECIFIC
GRAVITY : 2.75
D35 (MM) : 1.92
D50 (MM) : 2.11
D65 (MM) : 2.31

SIDE-WALL CORRECTION METHODS

RUN	DISCHARGE (M**2/S)	FLOW DEPTH (M)	SLOPE	VELOCITY (M/S)
SE0193	0.0710	0.1170	0.00200	0.6068
SE0293	0.0870	0.1354	0.00200	0.6425
SE0393	0.1010	0.1463	0.00200	0.6904
SE0493	0.1160	0.1597	0.00200	0.7264
SE0593	0.1220	0.1650	0.00200	0.7394
SE0693	0.1310	0.1743	0.00200	0.7516
SE0793	0.1420	0.1847	0.00200	0.7688
SE0893	0.1420	0.1843	0.00200	0.7705
SE0993	0.1420	0.1843	0.00200	0.7705
SE1093	0.1480	0.1888	0.00200	0.7839

		(WILLIAMS)		(VANONI-BROOKS)		(EINSTEIN)	
FLOW DEPTH (M)	MANNING N	HYD. RAD. (M)	MANNING N	HYD. RAD. (M)	MANNING N	HYD. RAD. (M)	MANNING N
0.1170	0.0176	0.1094	0.0169	0.0841	0.0141	0.0806	0.0138
0.1354	0.0184	0.1254	0.0174	0.0940	0.0144	0.0878	0.0137
0.1463	0.0180	0.1347	0.0170	0.0965	0.0136	0.0978	0.0138
0.1597	0.0181	0.1459	0.0171	0.1010	0.0134	0.1056	0.0138
0.1650	0.0182	0.1503	0.0171	0.1027	0.0133	0.1085	0.0138
0.1743	0.0186	0.1580	0.0174	0.1069	0.0134	0.1112	0.0138
0.1847	0.0189	0.1665	0.0176	0.1108	0.0134	0.1151	0.0138
0.1843	0.0188	0.1662	0.0175	0.1103	0.0134	0.1155	0.0138
0.1843	0.0188	0.1662	0.0175	0.1103	0.0134	0.1155	0.0138
0.1888	0.0188	0.1698	0.0175	0.1110	0.0132	0.1186	0.0138

		(WILLIAMS)		(VANONI-BROOKS)		(EINSTEIN)	
UST (M/S)	1/PSI	USTB (M/S)	1/PSIB	USTB (M/S)	1/PSIB	USTB (M/S)	1/PSIB
0.0479	0.0634	0.0463	0.0593	0.0406	0.0455	0.0398	0.0480
0.0515	0.0733	0.0496	0.0679	0.0429	0.0509	0.0415	0.0523
0.0536	0.0792	0.0514	0.0729	0.0435	0.0523	0.0438	0.0582
0.0560	0.0865	0.0535	0.0790	0.0445	0.0547	0.0455	0.0629
0.0569	0.0894	0.0543	0.0814	0.0449	0.0556	0.0461	0.0646
0.0585	0.0944	0.0557	0.0856	0.0458	0.0579	0.0467	0.0662
0.0602	0.1000	0.0572	0.0902	0.0466	0.0600	0.0475	0.0685
0.0601	0.0998	0.0571	0.0900	0.0465	0.0597	0.0476	0.0687
0.0601	0.0998	0.0571	0.0900	0.0465	0.0597	0.0476	0.0687
0.0609	0.1023	0.0577	0.0920	0.0467	0.0601	0.0482	0.0706

Table C.2 Side-Wall Analysis Results for SE Data of Bell (1980)

SEDIMENT DATA : GRIFFITHS (1976)

SEDIMENT : GRAVEL
SPECIFIC
GRAVITY : 2.68
D35 (MM) : 3.76
D50 (MM) : 4.02
D65 (MM) : 4.23

SIDE-WALL CORRECTION METHODS

RUN	DISCHARGE (M**2/S)	FLOW DEPTH (M)	SLOPE	VELOCITY (M/S)
SE07	0.1480	0.1820	0.00200	0.8132
SE03	0.1620	0.1930	0.00200	0.8394
SE10	0.1730	0.2020	0.00200	0.8564
SE01	0.1890	0.2160	0.00200	0.8750
SE02	0.2280	0.2490	0.00200	0.9157
SE08	0.2360	0.2520	0.00200	0.9365
SE04	0.2700	0.2800	0.00200	0.9643
SE09	0.2850	0.2880	0.00200	0.9896
SE06	0.2940	0.2980	0.00200	0.9866
SE05	0.3210	0.3190	0.00200	1.0063

		(WILLIAMS)		(VANONI-BROOKS)		(EINSTEIN)	
FLOW DEPTH (M)	MANNING N	HYD. RAD. (M)	MANNING N	HYD. RAD. (M)	MANNING N	HYD. RAD. (M)	MANNING N
0.1820	0.0177	0.1643	0.0165	0.1028	0.0121	0.1455	0.0152
0.1930	0.0178	0.1732	0.0166	0.1049	0.0118	0.1525	0.0152
0.2020	0.0180	0.1805	0.0167	0.1069	0.0118	0.1572	0.0152
0.2160	0.0184	0.1915	0.0170	0.1109	0.0118	0.1623	0.0152
0.2490	0.0193	0.2171	0.0176	0.1193	0.0118	0.1738	0.0152
0.2520	0.0191	0.2193	0.0174	0.1161	0.0114	0.1798	0.0152
0.2800	0.0198	0.2402	0.0179	0.1222	0.0114	0.1879	0.0152
0.2880	0.0197	0.2461	0.0177	0.1191	0.0109	0.1954	0.0152
0.2980	0.0202	0.2534	0.0182	0.1241	0.0113	0.1945	0.0152
0.3190	0.0207	0.2684	0.0185	0.1271	0.0112	0.2004	0.0152

		(WILLIAMS)		(VANONI-BROOKS)		(EINSTEIN)	
UST (M/S)	1/PSI	USTB (M/S)	1/PSIB	USTB (M/S)	1/PSIB	USTB (M/S)	1/PSIB
0.0598	0.0539	0.0568	0.0487	0.0449	0.0304	0.0534	0.0461
0.0615	0.0572	0.0583	0.0513	0.0454	0.0311	0.0547	0.0483
0.0630	0.0598	0.0595	0.0534	0.0458	0.0317	0.0555	0.0498
0.0651	0.0640	0.0613	0.0567	0.0467	0.0329	0.0564	0.0514
0.0699	0.0737	0.0653	0.0643	0.0484	0.0353	0.0584	0.0550
0.0703	0.0746	0.0656	0.0650	0.0477	0.0344	0.0594	0.0569
0.0741	0.0829	0.0687	0.0711	0.0490	0.0362	0.0607	0.0595
0.0752	0.0853	0.0695	0.0729	0.0483	0.0353	0.0619	0.0619
0.0765	0.0882	0.0705	0.0750	0.0493	0.0367	0.0618	0.0616
0.0791	0.0945	0.0726	0.0795	0.0499	0.0376	0.0627	0.0634

Table C.3 Side-Wall Analysis Results for SE Data of Griffiths (1976)

SEDIMENT DATA : BELL (1980)

SEDIMENT : GRAVEL
SPECIFIC
GRAVITY : 2.75
D35 (MM) : 1.92
D50 (MM) : 2.11
D65 (MM) : 2.31

SIDE-WALL CORRECTION METHODS

RUN	DISCHARGE (M**2/S)	FLOW DEPTH (M)	SLOPE	VELOCITY (M/S)	NE (GR/M**2/S)
IM0193	0.0170	0.0411	0.00300	0.4136	0.694
IM0293	0.0180	0.0433	0.00300	0.4157	0.936
IM0393	0.0200	0.0459	0.00300	0.4357	1.030
IM0493	0.0210	0.0483	0.00300	0.4348	2.560
IM0593	0.0230	0.0502	0.00300	0.4582	2.990
IM0693	0.0240	0.0522	0.00300	0.4598	5.400
IM0793	0.0270	0.0550	0.00300	0.4909	7.890
IM0893	0.0280	0.0563	0.00300	0.4973	10.500
IM0993	0.0300	0.0601	0.00300	0.4992	15.800
IM1093	0.0360	0.0761	0.00200	0.4731	3.920
IM1193	0.0380	0.0777	0.00200	0.4891	5.540

		(WILLIAMS)		(EINSTEIN)	
FLOW DEPTH (M)	MANNING N	HYD. RAD. (M)	MANNING N	HYD. RAD. (M)	MANNING N
0.0411	0.0158	0.0401	0.0155	0.0345	0.0140
0.0433	0.0162	0.0422	0.0160	0.0347	0.0140
0.0459	0.0161	0.0447	0.0158	0.0371	0.0140
0.0483	0.0167	0.0470	0.0164	0.0370	0.0140
0.0502	0.0163	0.0488	0.0160	0.0398	0.0139
0.0522	0.0166	0.0506	0.0163	0.0400	0.0139
0.0550	0.0161	0.0533	0.0158	0.0439	0.0139
0.0563	0.0162	0.0545	0.0158	0.0448	0.0139
0.0601	0.0168	0.0580	0.0164	0.0450	0.0139
0.0761	0.0170	0.0728	0.0165	0.0558	0.0138
0.0777	0.0167	0.0743	0.0162	0.0586	0.0138

			(WILLIAMS)			(EINSTEIN)	
UST (M/S)	1/PSI	USTB (M/S)	1/PSIB	N	USTB (M/S)	1/PSIB	N
0.0348	0.0334	0.0344	0.0326	.190E-06	0.0318	0.0308	.205E-06
0.0357	0.0352	0.0352	0.0343	.249E-06	0.0320	0.0310	.275E-06
0.0368	0.0373	0.0363	0.0363	.267E-06	0.0330	0.0331	.293E-06
0.0377	0.0392	0.0372	0.0382	.647E-06	0.0330	0.0330	.729E-06
0.0384	0.0408	0.0379	0.0396	.742E-06	0.0342	0.0355	.821E-06
0.0392	0.0424	0.0386	0.0411	.131E-05	0.0343	0.0357	.148E-05
0.0402	0.0447	0.0396	0.0433	.187E-05	0.0360	0.0392	.206E-05
0.0407	0.0457	0.0400	0.0443	.246E-05	0.0363	0.0400	.272E-05
0.0421	0.0488	0.0413	0.0472	.359E-05	0.0364	0.0402	.408E-05
0.0386	0.0412	0.0378	0.0394	.974E-06	0.0331	0.0332	.111E-05
0.0390	0.0421	0.0382	0.0402	.136E-05	0.0339	0.0349	.153E-05

Table C.4 Initial Motion Data of Bell (1980)

SEDIMENT DATA : GRIFFITHS (1976)

SEDIMENT : GRAVEL
SPECIFIC
GRAVITY : 2.68
D35 (MM) : 3.76
D50 (MM) : 4.02
D65 (MM) : 4.23

SIDE-WALL CORRECTION METHODS

RUN	DISCHARGE (M**2/S)	FLOW DEPTH (M)	SLOPE	VELOCITY (M/S)	NE (GR/M**2/S)
G8	0.0680	0.1120	0.00230	0.6071	0.195
G1	0.0690	0.1170	0.00230	0.5897	0.310
G7	0.0750	0.1190	0.00230	0.6303	0.345
G9	0.0780	0.1220	0.00230	0.6393	0.480
G10	0.0810	0.1260	0.00230	0.6429	0.540
G2	0.0850	0.1320	0.00230	0.6439	0.820
G5	0.0890	0.1340	0.00230	0.6642	0.915
G3	0.0950	0.1410	0.00230	0.6738	1.600
G6	0.1000	0.1430	0.00230	0.6993	2.550
G4	0.1090	0.1520	0.00230	0.7171	4.190
G11	0.1160	0.1590	0.00230	0.7296	4.680

		(WILLIAMS)		(EINSTEIN)	
FLOW DEPTH (M)	MANNING N	HYD. RAD. (M)	MANNING N	HYD. RAD. (M)	MANNING N
0.1120	0.0184	0.1050	0.0176	0.0856	0.0153
0.1170	0.0195	0.1094	0.0186	0.0821	0.0154
0.1190	0.0184	0.1112	0.0176	0.0903	0.0153
0.1220	0.0185	0.1138	0.0176	0.0922	0.0153
0.1260	0.0187	0.1173	0.0179	0.0929	0.0153
0.1320	0.0193	0.1224	0.0184	0.0931	0.0153
0.1340	0.0189	0.1242	0.0180	0.0974	0.0153
0.1410	0.0193	0.1302	0.0183	0.0995	0.0153
0.1430	0.0188	0.1319	0.0178	0.1050	0.0153
0.1520	0.0190	0.1395	0.0180	0.1089	0.0153
0.1590	0.0193	0.1453	0.0182	0.1117	0.0152

			(WILLIAMS)			(EINSTEIN)	
UST (M/S)	1/PSI	USTB (M/S)	1/PSIB	N	USTB (M/S)	1/PSIB	N
0.0503	0.0381	0.0487	0.0358	.260E-06	0.0439	0.0312	.288E-06
0.0514	0.0398	0.0497	0.0373	.405E-06	0.0430	0.0299	.468E-06
0.0518	0.0405	0.0501	0.0379	.447E-06	0.0451	0.0329	.497E-06
0.0525	0.0415	0.0507	0.0388	.615E-06	0.0456	0.0336	.684E-06
0.0533	0.0429	0.0514	0.0399	.682E-06	0.0458	0.0338	.766E-06
0.0546	0.0450	0.0526	0.0417	.101E-05	0.0458	0.0339	.116E-05
0.0550	0.0456	0.0529	0.0423	.112E-05	0.0469	0.0355	.127E-05
0.0564	0.0480	0.0542	0.0443	.192E-05	0.0474	0.0362	.219E-05
0.0568	0.0487	0.0545	0.0449	.304E-05	0.0487	0.0382	.340E-05
0.0586	0.0518	0.0561	0.0475	.485E-05	0.0496	0.0397	.549E-05
0.0599	0.0541	0.0573	0.0495	.531E-05	0.0502	0.0407	.606E-05

Table C.5 Initial Motion Data of Griffiths (1976)

SEDIMENT DATA :PHILLIPS (1984)

SEDIMENT : GRAVEL
SPECIFIC
GRAVITY : 2.65
D35 (MM) : 1.70
D50 (MM) : 1.80
D65 (MM) : 1.90

EQUILIBRIUM SEDIMENT TRANSPORT DATA

RUN	FRICTION SLOPE	DISCHARGE (M**2/S)	FLOW DEPTH (M)	VELOCITY (M/S)	BED SHEAR VELOCITY (M/S)	INVERSE SHEAR INTENSITY	CRITICAL SHEAR INTENSITY	VELOCITY EXCESS (M/S)	SEDIMENT TRANSPORT (G/S/M)
SE1001	0.00095	0.0908	0.174	0.5203	0.0384	0.0506	0.0390	0.0635	0.462
SE1002	0.00095	0.1007	0.186	0.5429	0.0395	0.0535	0.0390	0.0792	1.003
SE1003	0.00095	0.1098	0.197	0.5588	0.0405	0.0563	0.0390	0.0938	1.770
SE1004	0.00095	0.1205	0.209	0.5760	0.0417	0.0596	0.0390	0.1099	2.951
SE1005	0.00095	0.1303	0.220	0.5923	0.0426	0.0623	0.0390	0.1236	3.607
SE1006	0.00095	0.1410	0.235	0.5992	0.0439	0.0661	0.0390	0.1389	4.210
SE1501	0.00150	0.0798	0.140	0.5716	0.0436	0.0651	0.0390	0.1293	4.302
SE1502	0.00150	0.0794	0.140	0.5684	0.0436	0.0652	0.0390	0.1287	4.374
SE1503	0.00150	0.1006	0.164	0.6134	0.0469	0.0755	0.0390	0.1726	10.452
SE1504	0.00150	0.1207	0.186	0.6475	0.0497	0.0848	0.0390	0.2084	15.187
SE1505	0.00150	0.1392	0.211	0.6603	0.0525	0.0947	0.0390	0.2365	18.321
SE1506	0.00150	0.1595	0.235	0.6787	0.0551	0.1042	0.0390	0.2635	20.033
SE1507	0.00150	0.1786	0.254	0.7031	0.0570	0.1115	0.0390	0.2874	29.138
SE2001	0.00200	0.0796	0.129	0.6147	0.0486	0.0810	0.0390	0.1882	12.548
SE2002	0.00200	0.0998	0.152	0.6570	0.0523	0.0939	0.0390	0.2335	22.698
SE2003	0.00200	0.0992	0.152	0.6526	0.0523	0.0939	0.0390	0.2321	21.200
SE2004	0.00200	0.1215	0.176	0.6919	0.0559	0.1071	0.0390	0.2744	27.570
SE2005	0.00200	0.1400	0.196	0.7150	0.0587	0.1182	0.0390	0.3043	41.338
SE2006	0.00200	0.1621	0.216	0.7505	0.0613	0.1290	0.0390	0.3378	48.931
SE2007	0.00200	0.1811	0.236	0.7683	0.0637	0.1393	0.0390	0.3618	55.738
SE2501	0.00250	0.0803	0.124	0.6465	0.0533	0.0974	0.0390	0.2374	20.384
SE2502	0.00250	0.1025	0.145	0.7093	0.0571	0.1121	0.0390	0.2909	39.193
SE2503	0.00250	0.1219	0.164	0.7433	0.0606	0.1258	0.0390	0.3295	49.495
SE2504	0.00250	0.1388	0.178	0.7798	0.0628	0.1356	0.0390	0.3615	63.213
SE2505	0.00250	0.1606	0.197	0.8173	0.0657	0.1482	0.0390	0.3980	70.885
SE2506	0.00250	0.1813	0.214	0.8480	0.0682	0.1598	0.0390	0.4290	82.295

SIDE-WALL CORRECTION METHOD USED: WILLIAMS (1970)

LINEAR REGRESSION ANALYSIS

GSE (G/S/M) = A*(U-UCRIT)**B (M/S)

A = 894.0
B = 2.6450
RXY = 0.9957

Table C.6 Equilibrium Sediment Transport Data

SEDIMENT DATA : BELL (1980)

SEDIMENT : GRAVEL
SPECIFIC
GRAVITY : 2.75
D35 (MM) : 1.92
D50 (MM) : 2.11
D65 (MM) : 2.31

EQUILIBRIUM SEDIMENT TRANSPORT DATA

RUN	FRICTION SLOPE	DISCHARGE (M**2/S)	FLOW DEPTH (M)	VELOCITY (M/S)	BED SHEAR VELOCITY (M/S)	INVERSE SHEAR INTENSITY	CRITICAL SHEAR INTENSITY	VELOCITY EXCESS (M/S)	SEDIMENT TRANSPORT (G/S/M)
SE0193	0.00200	0.0705	0.117	0.6026	0.0463	0.0593	0.0400	0.1076	3.772
SE0293	0.00200	0.0873	0.135	0.6448	0.0496	0.0679	0.0400	0.1499	8.563
SE0393	0.00200	0.1014	0.146	0.6931	0.0514	0.0729	0.0400	0.1798	13.761
SE0493	0.00200	0.1163	0.160	0.7282	0.0535	0.0790	0.0400	0.2102	20.082
SE0593	0.00200	0.1218	0.165	0.7382	0.0543	0.0814	0.0400	0.2208	23.649
SE0693	0.00200	0.1311	0.174	0.7522	0.0557	0.0856	0.0400	0.2380	26.504
SE0793	0.00200	0.1417	0.185	0.7672	0.0572	0.0902	0.0400	0.2563	33.129
SE0893	0.00200	0.1415	0.184	0.7678	0.0571	0.0900	0.0400	0.2560	32.314
SE0993	0.00200	0.1415	0.184	0.7678	0.0571	0.0900	0.0400	0.2560	32.314
SE1093	0.00200	0.1482	0.189	0.7850	0.0577	0.0920	0.0400	0.2674	40.367

SIDE-WALL CORRECTION METHOD USED: WILLIAMS (1970)

LINEAR REGRESSION ANALYSIS

GSE (G/S/M) = A*(U-UCRIT)**B (M/S)

A = 1031.8
B = 2.5200
RXY = 0.9988

Table C.7 Equilibrium Sediment Transport Data of Bell (1980)

Appendix D | Spatial Lag Results

D.1 BED ROUGHNESS VALUES

Bed roughness values were obtained from the velocity profiles, measured at Stations 1.0 m and 2.0 m during the SC2001-I to SC2006-I runs, in the manner described in Sections 6.2.5 and 6.2.6. These bed roughness values are given in Tables D.1.1 - D.1.3.

D.2 SPATIAL LAG COEFFICIENT VALUES

Values of the individual terms obtained from the data collected during the SC-I series of experiments and spatial lag coefficients, calculated in the manner described in Section 7.3, are given in Tables D.2.1 - D.2.6.

RUN: SC2001-I

DISCHARGE (M**2/S) : 0.0809
FLUME SLOPE : 0.0020
TEMPERATURE (C) : 18.3
REACH LENGTH (M) : 9.50

CHAINAGE (M) : 1.0

TIME (S)	FLOW DEPTH (M)	FLOW VELOCITY (M/S)	SHEAR VELOCITY (M/S)	INVERSE SHEAR INTENSITY	MANNING ROUGHNESS VALUE
2740	0.143	0.566	0.044	0.0664	0.0177
3950	0.146	0.554	0.043	0.0635	0.0177
5100	0.150	0.539	0.042	0.0605	0.0179
6320	0.151	0.536	0.041	0.0577	0.0176
7500	0.156	0.519	0.040	0.0549	0.0178
8720	0.157	0.515	0.040	0.0549	0.0179
9920	0.157	0.515	0.039	0.0522	0.0175

CHAINAGE (M) : 2.0

TIME (S)	FLOW DEPTH (M)	FLOW VELOCITY (M/S)	SHEAR VELOCITY (M/S)	INVERSE SHEAR INTENSITY	MANNING ROUGHNESS VALUE
2830	0.133	0.608	0.049	0.0824	0.0181
4080	0.137	0.591	0.046	0.0726	0.0176
5200	0.141	0.574	0.045	0.0695	0.0178
6450	0.146	0.554	0.044	0.0664	0.0181
7620	0.147	0.550	0.043	0.0635	0.0179
8880	0.149	0.543	0.043	0.0635	0.0182
10080	0.150	0.539	0.042	0.0605	0.0179

RUN: SC2002-I

DISCHARGE (M**2/S) : 0.1015
FLUME SLOPE : 0.0020
TEMPERATURE (C) : 17.4
REACH LENGTH (M) : 9.50

CHAINAGE (M) : 1.0

TIME (S)	FLOW DEPTH (M)	FLOW VELOCITY (M/S)	SHEAR VELOCITY (M/S)	INVERSE SHEAR INTENSITY	MANNING ROUGHNESS VALUE
2700	0.174	0.583	0.046	0.0726	0.0185
3900	0.176	0.577	0.044	0.0664	0.0179
5100	0.181	0.561	0.043	0.0635	0.0181
6300	0.183	0.555	0.042	0:0605	0.0179
7520	0.186	0.546	0.042	0.0605	0.0182
8720	0.187	0.543	0.041	0.0577	0.0179
9960	0.190	0.534	0.040	0.0549	0.0178

CHAINAGE (M) : 2.0

TIME (S)	FLOW DEPTH (M)	FLOW VELOCITY (M/S)	SHEAR VELOCITY (M/S)	INVERSE SHEAR INTENSITY	MANNING ROUGHNESS VALUE
2840	0.163	0.623	0.048	0.0791	0.0179
4080	0.168	0.604	0.046	0.0726	0.0178
5260	0.170	0.597	0.046	0.0726	0.0180
6460	0.172	0.590	0.045	0.0695	0.0179
7660	0.176	0.577	0.045	0.0695	0.0183
8880	0.178	0.570	0.044	0.0664	0.0182
10080	0.183	0.555	0.043	0.0635	0.0183

Table D.1.1 Bed Roughness Data (Runs SC2001-I and SC2002-I)

RUN: SC2003-I

DISCHARGE (M**2/S) : 0.1222
FLUME SLOPE : 0.0020
TEMPERATURE (C) : 17.5
REACH LENGTH (M) : 9.50

CHAINAGE (M) : 1.0

TIME (S)	FLOW DEPTH (M)	FLOW VELOCITY (M/S)	SHEAR VELOCITY (M/S)	INVERSE SHEAR INTENSITY	MANNING ROUGHNESS VALUE
2780	0.198	0.617	0.045	0.0695	0.0174
3900	0.204	0.599	0.045	0.0695	0.0181
5160	0.206	0.593	0.043	0.0635	0.0174
6340	0.210	0.582	0.043	0.0635	0.0178
7560	0.213	0.574	0.042	0.0605	0.0177
8760	0.214	0.571	0.042	0.0605	0.0178

CHAINAGE (M) : 2.0

TIME (S)	FLOW DEPTH (M)	FLOW VELOCITY (M/S)	SHEAR VELOCITY (M/S)	INVERSE SHEAR INTENSITY	MANNING ROUGHNESS VALUE
2900	0.187	0.653	0.050	0.0858	0.0182
4060	0.189	0.647	0.047	0.0758	0.0173
5300	0.194	0.630	0.048	0.0791	0.0182
6500	0.200	0.611	0.046	0.0726	0.0180
7680	0.202	0.605	0.045	0.0695	0.0179
8900	0.203	0.602	0.045	0.0695	0.0180

RUN: SC2004-I

DISCHARGE (M**2/S) : 0.1416
FLUME SLOPE : 0.0020
TEMPERATURE (C) : 19.6
REACH LENGTH (M) : 9.50

CHAINAGE (M) : 1.0

TIME (S)	FLOW DEPTH (M)	FLOW VELOCITY (M/S)	SHEAR VELOCITY (M/S)	INVERSE SHEAR INTENSITY	MANNING ROUGHNESS VALUE
2720	0.223	0.635	0.045	0.0695	0.0173
3920	0.226	0.627	0.045	0.0695	0.0175
5160	0.231	0.613	0.043	0.0635	0.0172
6360	0.234	0.605	0.043	0.0635	0.0174
7560	0.238	0.595	0.042	0.0605	0.0174
8740	0.241	0.588	0.041	0.0577	0.0172

CHAINAGE (M) : 2.0

TIME (S)	FLOW DEPTH (M)	FLOW VELOCITY (M/S)	SHEAR VELOCITY (M/S)	INVERSE SHEAR INTENSITY	MANNING ROUGHNESS VALUE
2860	0.207	0.684	0.051	0.0893	0.0180
4060	0.213	0.665	0.049	0.0824	0.0178
5320	0.219	0.647	0.048	0.0791	0.0180
6560	0.226	0.627	0.045	0.0695	0.0175
7700	0.227	0.624	0.045	0.0695	0.0176
8880	0.230	0.616	0.044	0.0664	0.0175

Table D.1.2 Bed Roughness Data (Runs SC2003-I and SC2004-I)

RUN: SC2005-I

DISCHARGE (M**2/S) : 0.1612
FLUME SLOPE : 0.0020
TEMPERATURE (C) : 19.2
REACH LENGTH (M) : 9.50

CHAINAGE (M) : 1.0

TIME (S)	FLOW DEPTH (M)	FLOW VELOCITY (M/S)	SHEAR VELOCITY (M/S)	INVERSE SHEAR INTENSITY	MANNING ROUGHNESS VALUE
2740	0.246	0.655	0.047	0.0758	0.0177
3920	0.252	0.640	0.044	0.0664	0.0171
5160	0.255	0.632	0.043	0.0635	0.0169
6380	0.259	0.622	0.043	0.0635	0.0172
7560	0.261	0.618	0.042	0.0605	0.0169

CHAINAGE (M) : 2.0

TIME (S)	FLOW DEPTH (M)	FLOW VELOCITY (M/S)	SHEAR VELOCITY (M/S)	INVERSE SHEAR INTENSITY	MANNING ROUGHNESS VALUE
2900	0.226	0.713	0.051	0.0893	0.0174
4060	0.240	0.672	0.050	0.0858	0.0183
5300	0.244	0.661	0.047	0.0758	0.0176
6500	0.249	0.647	0.046	0.0726	0.0176
7700	0.250	0.645	0.045	0.0695	0.0173

RUN: SC2006-I

DISCHARGE (M**2/S) : 0.1807
FLUME SLOPE : 0.0020
TEMPERATURE (C) : 20.3
REACH LENGTH (M) : 9.50

CHAINAGE (M) : 1.0

TIME (S)	FLOW DEPTH (M)	FLOW VELOCITY (M/S)	SHEAR VELOCITY (M/S)	INVERSE SHEAR INTENSITY	MANNING ROUGHNESS VALUE
2720	0.268	0.674	0.046	0.0726	0.0171
3930	0.276	0.655	0.045	0.0695	0.0173
5190	0.279	0.648	0.043	0.0635	0.0167
6340	0.282	0.641	0.042	0.0605	0.0165

CHAINAGE (M) : 2.0

TIME (S)	FLOW DEPTH (M)	FLOW VELOCITY (M/S)	SHEAR VELOCITY (M/S)	INVERSE SHEAR INTENSITY	MANNING ROUGHNESS VALUE
2860	0.250	0.723	0.052	0.0928	0.0178
4060	0.261	0.692	0.049	0.0824	0.0176
5330	0.267	0.677	0.048	0.0791	0.0177
6490	0.274	0.659	0.046	0.0726	0.0175

Table D.1.3 Bed Roughness Data (Runs SC2005-I and SC2006-I)

RUN: SC2001-I

DISCHARGE (M**2/S) : 0.0809
FLUME SLOPE : 0.0020
TEMPERATURE (C) : 18.3

SPATIAL LAG COEFFICIENT : VALUES DETERMINED EXPERIMENTALLY ARE PRESENTED BELOW

CHAINAGE (M) : 0.6

TIME (S)	MANNINGS ROUGHNESS VALUE	SHEAR VELOCITY (M/S)	FLOW VELOCITY (M/S)	CRITICAL VELOCITY (M/S)	SCOUR RATE (M/S)	SEDIMENT TRANSPORT RATE (M**2/S)	SEDIMENT TRANSPORT CAPACITY (M**2/S)	INVERSE SHEAR INTENSITY	SPATIAL LAG COEFFICIENT (1/M)
2400	0.0178	0.042	0.547	0.434	.255E-05	.768E-06	.106E-05	0.0620	0.00937
3600	0.0178	0.042	0.536	0.435	.254E-05	.400E-06	.782E-06	0.0592	0.00706
4800	0.0177	0.040	0.525	0.439	.156E-05	.311E-06	.524E-06	0.0559	0.00778
6000	0.0177	0.040	0.522	0.439	.150E-05	.250E-06	.465E-06	0.0551	0.00741
7200	0.0177	0.039	0.512	0.440	.104E-05	.225E-06	.317E-06	0.0527	0.01202
8400	0.0177	0.039	0.509	0.441	.818E-06	.203E-06	.276E-06	0.0519	0.01196
9600	0.0177	0.039	0.506	0.441	.690E-06	.181E-06	.239E-06	0.0512	0.01273

CHAINAGE (M) : 1.0

TIME (S)	MANNINGS ROUGHNESS VALUE	SHEAR VELOCITY (M/S)	FLOW VELOCITY (M/S)	CRITICAL VELOCITY (M/S)	SCOUR RATE (M/S)	SEDIMENT TRANSPORT RATE (M**2/S)	SEDIMENT TRANSPORT CAPACITY (M**2/S)	INVERSE SHEAR INTENSITY	SPATIAL LAG COEFFICIENT (1/M)
2400	0.0179	0.044	0.566	0.429	.307E-05	.167E-05	.175E-05	0.0678	0.04161
3600	0.0179	0.043	0.554	0.430	.172E-05	.126E-05	.135E-05	0.0647	0.01998
4800	0.0178	0.042	0.539	0.434	.232E-05	.120E-05	.867E-06	0.0601	
6000	0.0178	0.042	0.536	0.435	.183E-05	.110E-05	.782E-06	0.0592	
7200	0.0178	0.040	0.519	0.437	.131E-05	.862E-06	.446E-06	0.0549	
8400	0.0178	0.040	0.515	0.437	.135E-05	.789E-06	.394E-06	0.0541	
9600	0.0178	0.040	0.515	0.437	.813E-06	.512E-06	.394E-06	0.0541	

CHAINAGE (M) : 2.0

TIME (S)	MANNINGS ROUGHNESS VALUE	SHEAR VELOCITY (M/S)	FLOW VELOCITY (M/S)	CRITICAL VELOCITY (M/S)	SCOUR RATE (M/S)	SEDIMENT TRANSPORT RATE (M**2/S)	SEDIMENT TRANSPORT CAPACITY (M**2/S)	INVERSE SHEAR INTENSITY	SPATIAL LAG COEFFICIENT (1/M)
2400	0.0179	0.048	0.608	0.424	.206E-05	.377E-05	.384E-05	0.0802	0.03146
3600	0.0179	0.047	0.591	0.426	.166E-05	.235E-05	.285E-05	0.0749	0.00354
4800	0.0178	0.045	0.574	0.430	.247E-05	.171E-05	.198E-05	0.0693	0.00965
6000	0.0178	0.044	0.562	0.432	.160E-05	.118E-05	.153E-05	0.0660	0.00484
7200	0.0178	0.043	0.550	0.433	.169E-05	.988E-06	.116E-05	0.0629	0.01015
8400	0.0178	0.042	0.543	0.434	.134E-05	.861E-06	.959E-06	0.0610	0.01460
9600	0.0178	0.042	0.539	0.434	.104E-05	.115E-05	.867E-06	0.0601	

CHAINAGE (M) : 3.0

TIME (S)	MANNINGS ROUGHNESS VALUE	SHEAR VELOCITY (M/S)	FLOW VELOCITY (M/S)	CRITICAL VELOCITY (M/S)	SCOUR RATE (M/S)	SEDIMENT TRANSPORT RATE (M**2/S)	SEDIMENT TRANSPORT CAPACITY (M**2/S)	INVERSE SHEAR INTENSITY	SPATIAL LAG COEFFICIENT (1/M)
6000	0.0179	0.046	0.586	0.426	.192E-05	.194E-05	.264E-05	0.0736	0.00294
7200	0.0179	0.046	0.582	0.427	.153E-05	.194E-05	.244E-05	0.0724	0.00325
8400	0.0178	0.045	0.570	0.431	.153E-05	.165E-05	.182E-05	0.0682	0.00915
9600	0.0178	0.044	0.566	0.431	.115E-05	.148E-05	.167E-05	0.0671	0.00636

BED SHEAR VELOCITIES OBTAINED USING: WILLIAMS (1970) SIDE WALL CORRECTION METHOD

Table D.2.1 Spatial Lag Data and Results (Run SC2001-I)

RUN: SC2002-I

DISCHARGE (M**2/S) : 0.1015
FLUME SLOPE : 0.0020
TEMPERATURE (C) : 17.4

SPATIAL LAG COEFFICIENT : VALUES DETERMINED EXPERIMENTALLY ARE PRESENTED BELOW

CHAINAGE (M) : 0.6

TIME (S)	MANNINGS ROUGHNESS VALUE	SHEAR VELOCITY (M/S)	FLOW VELOCITY (M/S)	CRITICAL VELOCITY (M/S)	SCOUR RATE (M/S)	SEDIMENT TRANSPORT RATE (M**2/S)	SEDIMENT TRANSPORT CAPACITY (M**2/S)	INVERSE SHEAR INTENSITY	SPATIAL LAG COEFFICIENT (1/M)
2400	0.0178	0.043	0.567	0.446	.363E-05	.668E-06	.126E-05	0.0629	0.00653
3600	0.0178	0.042	0.558	0.447	.223E-05	.557E-06	.991E-06	0.0606	0.00546
4800	0.0178	0.041	0.549	0.448	.247E-05	.492E-06	.768E-06	0.0583	0.00954
6000	0.0177	0.040	0.540	0.452	.170E-05	.389E-06	.542E-06	0.0556	0.01182
7200	0.0177	0.040	0.534	0.453	.173E-05	.276E-06	.443E-06	0.0543	0.01099
8400	0.0177	0.039	0.529	0.454	.168E-05	.245E-06	.359E-06	0.0530	0.01567
9600	0.0177	0.039	0.526	0.454	.113E-05	.226E-06	.321E-06	0.0523	0.01272

CHAINAGE (M) : 1.0

TIME (S)	MANNINGS ROUGHNESS VALUE	SHEAR VELOCITY (M/S)	FLOW VELOCITY (M/S)	CRITICAL VELOCITY (M/S)	SCOUR RATE (M/S)	SEDIMENT TRANSPORT RATE (M**2/S)	SEDIMENT TRANSPORT CAPACITY (M**2/S)	INVERSE SHEAR INTENSITY	SPATIAL LAG COEFFICIENT (1/M)
2400	0.0179	0.045	0.587	0.441	.466E-05	.200E-05	.205E-05	0.0688	0.09492
3600	0.0179	0.044	0.577	0.443	.241E-05	.138E-05	.166E-05	0.0662	0.00928
4800	0.0178	0.042	0.561	0.447	.152E-05	.119E-05	.107E-05	0.0613	
6000	0.0178	0.042	0.555	0.448	.183E-05	.120E-05	.912E-06	0.0598	
7200	0.0178	0.041	0.546	0.449	.199E-05	.116E-05	.702E-06	0.0576	
8400	0.0178	0.041	0.543	0.449	.191E-05	.109E-05	.641E-06	0.0569	
9600	0.0178	0.040	0.534	0.450	.725E-06	.827E-06	.481E-06	0.0549	

CHAINAGE (M) : 2.0

TIME (S)	MANNINGS ROUGHNESS VALUE	SHEAR VELOCITY (M/S)	FLOW VELOCITY (M/S)	CRITICAL VELOCITY (M/S)	SCOUR RATE (M/S)	SEDIMENT TRANSPORT RATE (M**2/S)	SEDIMENT TRANSPORT CAPACITY (M**2/S)	INVERSE SHEAR INTENSITY	SPATIAL LAG COEFFICIENT (1/M)
2400	0.0180	0.048	0.623	0.435	.407E-05	.373E-05	.404E-05	0.0798	0.01421
3600	0.0179	0.046	0.604	0.440	.337E-05	.236E-05	.286E-05	0.0737	0.00716
4800	0.0179	0.046	0.597	0.440	.207E-05	.180E-05	.251E-05	0.0717	0.00310
6000	0.0179	0.045	0.590	0.441	.214E-05	.228E-05	.219E-05	0.0698	
7200	0.0178	0.044	0.577	0.445	.269E-05	.220E-05	.158E-05	0.0654	
8400	0.0178	0.043	0.570	0.446	.193E-05	.184E-05	.136E-05	0.0638	
9600	0.0178	0.042	0.555	0.448	.152E-05	.156E-05	.912E-06	0.0598	

CHAINAGE (M) : 3.0

TIME (S)	MANNINGS ROUGHNESS VALUE	SHEAR VELOCITY (M/S)	FLOW VELOCITY (M/S)	CRITICAL VELOCITY (M/S)	SCOUR RATE (M/S)	SEDIMENT TRANSPORT RATE (M**2/S)	SEDIMENT TRANSPORT CAPACITY (M**2/S)	INVERSE SHEAR INTENSITY	SPATIAL LAG COEFFICIENT (1/M)
4800	0.0181	0.048	0.615	0.433	.235E-05	.322E-05	.371E-05	0.0785	0.00517
6000	0.0180	0.047	0.604	0.437	.210E-05	.236E-05	.297E-05	0.0745	0.00364
7200	0.0180	0.046	0.597	0.438	.158E-05	.221E-05	.261E-05	0.0725	0.00414
8400	0.0179	0.045	0.590	0.441	.158E-05	.199E-05	.219E-05	0.0698	0.00815
9600	0.0179	0.044	0.580	0.442	.119E-05	.210E-05	.178E-05	0.0670	

BED SHEAR VELOCITIES OBTAINED USING: WILLIAMS (1970) SIDE WALL CORRECTION METHOD

Table D.2.2 Spatial Lag Data and Results (Run SC2002-I)

RUN: SC2003-I

DISCHARGE (M**2/S) : 0.1222
FLUME SLOPE : 0.0020
TEMPERATURE (C) : 17.5

SPATIAL LAG COEFFICIENT : VALUES DETERMINED EXPERIMENTALLY ARE PRESENTED BELOW

CHAINAGE (M) : 0.6

TIME (S)	MANNINGS ROUGHNESS VALUE	SHEAR VELOCITY (M/S)	FLOW VELOCITY (M/S)	CRITICAL VELOCITY (M/S)	SCOUR RATE (M/S)	SEDIMENT TRANSPORT RATE (M**2/S)	SEDIMENT TRANSPORT CAPACITY (M**2/S)	INVERSE SHEAR INTENSITY	SPATIAL LAG COEFFICIENT (1/M)
2400	0.0175	0.043	0.596	0.463	.395E-05	.747E-06	.162E-05	0.0646	0.00481
3600	0.0174	0.042	0.582	0.468	.204E-05	.581E-06	.109E-05	0.0604	0.00427
4800	0.0174	0.041	0.576	0.468	.235E-05	.640E-06	.942E-06	0.0591	0.00829
6000	0.0174	0.041	0.568	0.469	.252E-05	.415E-06	.748E-06	0.0572	0.00804
7200	0.0173	0.040	0.561	0.473	.173E-05	.345E-06	.540E-06	0.0548	0.00946
8400	0.0172	0.040	0.558	0.476	.780E-06	.305E-06	.453E-06	0.0536	0.00561

CHAINAGE (M) : 1.0

TIME (S)	MANNINGS ROUGHNESS VALUE	SHEAR VELOCITY (M/S)	FLOW VELOCITY (M/S)	CRITICAL VELOCITY (M/S)	SCOUR RATE (M/S)	SEDIMENT TRANSPORT RATE (M**2/S)	SEDIMENT TRANSPORT CAPACITY (M**2/S)	INVERSE SHEAR INTENSITY	SPATIAL LAG COEFFICIENT (1/M)
2400	0.0178	0.046	0.617	0.453	.509E-05	.186E-05	.283E-05	0.0723	0.00555
3600	0.0178	0.044	0.599	0.455	.336E-05	.165E-05	.200E-05	0.0675	0.01012
4800	0.0176	0.043	0.593	0.461	.222E-05	.120E-05	.160E-05	0.0646	0.00585
6000	0.0176	0.042	0.582	0.462	.237E-05	.105E-05	.123E-05	0.0618	0.01388
7200	0.0174	0.041	0.574	0.469	.112E-05	.958E-06	.873E-06	0.0584	
8400	0.0174	0.041	0.571	0.469	.127E-05	.902E-06	.809E-06	0.0578	

CHAINAGE (M) : 2.0

TIME (S)	MANNINGS ROUGHNESS VALUE	SHEAR VELOCITY (M/S)	FLOW VELOCITY (M/S)	CRITICAL VELOCITY (M/S)	SCOUR RATE (M/S)	SEDIMENT TRANSPORT RATE (M**2/S)	SEDIMENT TRANSPORT CAPACITY (M**2/S)	INVERSE SHEAR INTENSITY	SPATIAL LAG COEFFICIENT (1/M)
2400	0.0181	0.050	0.653	0.442	.560E-05	.434E-05	.556E-05	0.0853	0.00491
3600	0.0180	0.049	0.647	0.445	.335E-05	.318E-05	.488E-05	0.0823	0.00209
4800	0.0179	0.047	0.630	0.449	.390E-05	.218E-05	.366E-05	0.0767	0.00280
6000	0.0178	0.045	0.611	0.454	.237E-05	.208E-05	.253E-05	0.0707	0.00560
7200	0.0177	0.045	0.605	0.457	.138E-05	.184E-05	.215E-05	0.0683	0.00459
8400	0.0176	0.043	0.593	0.461	.206E-05	.170E-05	.160E-05	0.0646	

CHAINAGE (M) : 3.0

TIME (S)	MANNINGS ROUGHNESS VALUE	SHEAR VELOCITY (M/S)	FLOW VELOCITY (M/S)	CRITICAL VELOCITY (M/S)	SCOUR RATE (M/S)	SEDIMENT TRANSPORT RATE (M**2/S)	SEDIMENT TRANSPORT CAPACITY (M**2/S)	INVERSE SHEAR INTENSITY	SPATIAL LAG COEFFICIENT (1/M)
4800	0.0182	0.050	0.653	0.439	.406E-05	.483E-05	.573E-05	0.0862	0.00482
6000	0.0181	0.049	0.640	0.443	.258E-05	.379E-05	.457E-05	0.0812	0.00351
7200	0.0178	0.047	0.630	0.452	.202E-05	.295E-05	.352E-05	0.0758	0.00373
8400	0.0177	0.045	0.614	0.456	.202E-05	.214E-05	.257E-05	0.0707	0.00499

BED SHEAR VELOCITIES OBTAINED USING: WILLIAMS (1970) SIDE WALL CORRECTION METHOD

Table D.2.3 Spatial Lag Data and Results (Run SC2003-I)

RUN: SC2004-I

DISCHARGE (M**2/S) : 0.1416
FLUME SLOPE : 0.0020
TEMPERATURE (C) : 19.6

SPATIAL LAG COEFFICIENT : VALUES DETERMINED EXPERIMENTALLY ARE PRESENTED BELOW

CHAINAGE (M) : 0.6

TIME (S)	MANNINGS ROUGHNESS VALUE	SHEAR VELOCITY (M/S)	FLOW VELOCITY (M/S)	CRITICAL VELOCITY (M/S)	SCOUR RATE (M/S)	SEDIMENT TRANSPORT RATE (M**2/S)	SEDIMENT TRANSPORT CAPACITY (M**2/S)	INVERSE SHEAR INTENSITY	SPATIAL LAG COEFFICIENT (1/M)
2400	0.0173	0.044	0.621	0.476	.426E-05	.103E-05	.204E-05	0.0664	0.00445
3600	0.0172	0.043	0.608	0.480	.386E-05	.660E-06	.145E-05	0.0624	0.00520
4800	0.0171	0.042	0.597	0.484	.228E-05	.472E-06	.106E-05	0.0593	0.00411
6000	0.0170	0.041	0.588	0.488	.251E-05	.428E-06	.748E-06	0.0564	0.00835
7200	0.0170	0.040	0.580	0.489	.245E-05	.363E-06	.597E-06	0.0549	0.01110
8400	0.0169	0.039	0.571	0.493	.208E-05	.289E-06	.392E-06	0.0522	0.02150

CHAINAGE (M) : 1.0

TIME (S)	MANNINGS ROUGHNESS VALUE	SHEAR VELOCITY (M/S)	FLOW VELOCITY (M/S)	CRITICAL VELOCITY (M/S)	SCOUR RATE (M/S)	SEDIMENT TRANSPORT RATE (M**2/S)	SEDIMENT TRANSPORT CAPACITY (M**2/S)	INVERSE SHEAR INTENSITY	SPATIAL LAG COEFFICIENT (1/M)
2400	0.0174	0.045	0.635	0.472	.475E-05	.173E-05	.279E-05	0.0706	0.00474
3600	0.0174	0.045	0.627	0.473	.368E-05	.139E-05	.239E-05	0.0685	0.00391
4800	0.0173	0.043	0.613	0.477	.375E-05	.120E-05	.173E-05	0.0644	0.00765
6000	0.0172	0.042	0.603	0.481	.237E-05	.180E-05	.128E-05	0.0612	
7200	0.0172	0.042	0.595	0.482	.246E-05	.856E-06	.106E-05	0.0594	0.01282
8400	0.0171	0.041	0.588	0.485	.122E-05	.901E-06	.807E-06	0.0571	

CHAINAGE (M) : 2.0

TIME (S)	MANNINGS ROUGHNESS VALUE	SHEAR VELOCITY (M/S)	FLOW VELOCITY (M/S)	CRITICAL VELOCITY (M/S)	SCOUR RATE (M/S)	SEDIMENT TRANSPORT RATE (M**2/S)	SEDIMENT TRANSPORT CAPACITY (M**2/S)	INVERSE SHEAR INTENSITY	SPATIAL LAG COEFFICIENT (1/M)
2400	0.0180	0.051	0.684	0.451	.447E-05	.616E-05	.716E-05	0.0897	0.00472
3600	0.0177	0.049	0.665	0.461	.337E-05	.362E-05	.505E-05	0.0812	0.00251
4800	0.0177	0.047	0.647	0.462	.292E-05	.276E-05	.384E-05	0.0762	0.00288
6000	0.0176	0.045	0.627	0.467	.272E-05	.230E-05	.262E-05	0.0701	0.00903
7200	0.0174	0.044	0.624	0.473	.305E-05	.225E-05	.227E-05	0.0678	0.24499
8400	0.0174	0.044	0.616	0.474	.195E-05	.188E-05	.192E-05	0.0658	0.05263

CHAINAGE (M) : 3.0

TIME (S)	MANNINGS ROUGHNESS VALUE	SHEAR VELOCITY (M/S)	FLOW VELOCITY (M/S)	CRITICAL VELOCITY (M/S)	SCOUR RATE (M/S)	SEDIMENT TRANSPORT RATE (M**2/S)	SEDIMENT TRANSPORT CAPACITY (M**2/S)	INVERSE SHEAR INTENSITY	SPATIAL LAG COEFFICIENT (1/M)
4800	0.0180	0.049	0.662	0.453	.417E-05	.420E-05	.533E-05	0.0831	0.00391
6000	0.0179	0.048	0.650	0.457	.333E-05	.366E-05	.432E-05	0.0787	0.00539
7200	0.0179	0.047	0.644	0.458	.250E-05	.323E-05	.395E-05	0.0771	0.00372
8400	0.0178	0.046	0.635	0.461	.208E-05	.282E-05	.330E-05	0.0739	0.00464

BED SHEAR VELOCITIES OBTAINED USING: WILLIAMS (1970) SIDE WALL CORRECTION METHOD

Table D.2.4 Spatial Lag Data and Results (Run SC2004-I)

RUN: SC2005-I

DISCHARGE (M**2/S) : 0.1612
FLUME SLOPE : 0.0020
TEMPERATURE (C) : 19.1

SPATIAL LAG COEFFICIENT : VALUES DETERMINED EXPERIMENTALLY ARE PRESENTED BELOW

CHAINAGE (M) : 0.6

TIME (S)	MANNINGS ROUGHNESS VALUE	SHEAR VELOCITY (M/S)	FLOW VELOCITY (M/S)	CRITICAL VELOCITY (M/S)	SCOUR RATE (M/S)	SEDIMENT TRANSPORT RATE (M**2/S)	SEDIMENT TRANSPORT CAPACITY (M**2/S)	INVERSE SHEAR INTENSITY	SPATIAL LAG COEFFICIENT (1/M)
2400	0.0170	0.043	0.632	0.492	.470E-05	.105E-05	.185E-05	0.0643	0.00621
3600	0.0169	0.042	0.620	0.497	.330E-05	.674E-06	.133E-05	0.0607	0.00534
4800	0.0168	0.041	0.615	0.500	.240E-05	.660E-06	.111E-05	0.0590	0.00570
6000	0.0168	0.041	0.606	0.501	.200E-05	.629E-06	.864E-06	0.0570	0.00908
7200	0.0167	0.040	0.601	0.505	.200E-05	.360E-06	.699E-06	0.0553	0.00629

CHAINAGE (M) : 1.0

TIME (S)	MANNINGS ROUGHNESS VALUE	SHEAR VELOCITY (M/S)	FLOW VELOCITY (M/S)	CRITICAL VELOCITY (M/S)	SCOUR RATE (M/S)	SEDIMENT TRANSPORT RATE (M**2/S)	SEDIMENT TRANSPORT CAPACITY (M**2/S)	INVERSE SHEAR INTENSITY	SPATIAL LAG COEFFICIENT (1/M)
2400	0.0174	0.046	0.655	0.479	.546E-05	.299E-05	.345E-05	0.0731	0.01259
3600	0.0173	0.045	0.640	0.483	.370E-05	.165E-05	.251E-05	0.0684	0.00459
4800	0.0171	0.044	0.632	0.489	.282E-05	.125E-05	.196E-05	0.0650	0.00423
6000	0.0170	0.043	0.622	0.493	.256E-05	.106E-05	.150E-05	0.0620	0.00625
7200	0.0169	0.042	0.618	0.497	.189E-05	.983E-06	.126E-05	0.0602	0.00735

CHAINAGE (M) : 2.0

TIME (S)	MANNINGS ROUGHNESS VALUE	SHEAR VELOCITY (M/S)	FLOW VELOCITY (M/S)	CRITICAL VELOCITY (M/S)	SCOUR RATE (M/S)	SEDIMENT TRANSPORT RATE (M**2/S)	SEDIMENT TRANSPORT CAPACITY (M**2/S)	INVERSE SHEAR INTENSITY	SPATIAL LAG COEFFICIENT (1/M)
2400	0.0182	0.051	0.683	0.455	.439E-05	.705E-05	.678E-05	0.0879	
3600	0.0176	0.048	0.672	0.471	.418E-05	.297E-05	.480E-05	0.0791	0.00243
4800	0.0174	0.047	0.661	0.478	.429E-05	.294E-05	.376E-05	0.0745	0.00556
6000	0.0173	0.045	0.647	0.482	.339E-05	.223E-05	.288E-05	0.0703	0.00550
7200	0.0172	0.045	0.645	0.485	.170E-05	.191E-05	.263E-05	0.0688	0.00250

CHAINAGE (M) : 3.0

TIME (S)	MANNINGS ROUGHNESS VALUE	SHEAR VELOCITY (M/S)	FLOW VELOCITY (M/S)	CRITICAL VELOCITY (M/S)	SCOUR RATE (M/S)	SEDIMENT TRANSPORT RATE (M**2/S)	SEDIMENT TRANSPORT CAPACITY (M**2/S)	INVERSE SHEAR INTENSITY	SPATIAL LAG COEFFICIENT (1/M)
3600	0.0182	0.051	0.692	0.454	.458E-05	.622E-05	.757E-05	0.0906	0.00361
4800	0.0180	0.050	0.683	0.460	.334E-05	.545E-05	.639E-05	0.0860	0.00376
6000	0.0178	0.049	0.672	0.466	.334E-05	.447E-05	.514E-05	0.0809	0.00529
7200	0.0177	0.048	0.663	0.470	.291E-05	.397E-05	.440E-05	0.0778	0.00732

BED SHEAR VELOCITIES OBTAINED USING: WILLIAMS (1970) SIDE WALL CORRECTION METHOD

Table D.2.5 : Spatial Lag Data and Results (Run SC2005-I)

RUN: SC2006-I

DISCHARGE (M**2/S) : 0.1807
FLUME SLOPE : 0.0020
TEMPERATURE (C) : 20.3

SPATIAL LAG COEFFICIENT : VALUES DETERMINED EXPERIMENTALLY ARE PRESENTED BELOW

CHAINAGE (M) : 0.6

TIME (S)	MANNINGS ROUGHNESS VALUE	SHEAR VELOCITY (M/S)	FLOW VELOCITY (M/S)	CRITICAL VELOCITY (M/S)	SCOUR RATE (M/S)	SEDIMENT TRANSPORT RATE (M**2/S)	SEDIMENT TRANSPORT CAPACITY (M**2/S)	INVERSE SHEAR INTENSITY	SPATIAL LAG COEFFICIENT (1/M)
2400	0.0169	0.044	0.659	0.500	.507E-05	.121E-05	.261E-05	0.0677	0.00386
3600	0.0167	0.042	0.641	0.509	.362E-05	.826E-06	.160E-05	0.0619	0.00497
4800	0.0166	0.042	0.632	0.513	.312E-05	.596E-06	.122E-05	0.0592	0.00536
6000	0.0166	0.041	0.625	0.513	.240E-05	.606E-06	.103E-05	0.0578	0.00604

CHAINAGE (M) : 1.0

TIME (S)	MANNINGS ROUGHNESS VALUE	SHEAR VELOCITY (M/S)	FLOW VELOCITY (M/S)	CRITICAL VELOCITY (M/S)	SCOUR RATE (M/S)	SEDIMENT TRANSPORT RATE (M**2/S)	SEDIMENT TRANSPORT CAPACITY (M**2/S)	INVERSE SHEAR INTENSITY	SPATIAL LAG COEFFICIENT (1/M)
2400	0.0173	0.047	0.674	0.487	.638E-05	.172E-05	.400E-05	0.0746	0.00297
3600	0.0170	0.044	0.655	0.498	.399E-05	.160E-05	.251E-05	0.0674	0.00470
4800	0.0170	0.044	0.648	0.499	.317E-05	.224E-05	.219E-05	0.0657	
6000	0.0168	0.043	0.641	0.505	.260E-05	.174E-05	.170E-05	0.0626	

CHAINAGE (M) : 2.0

TIME (S)	MANNINGS ROUGHNESS VALUE	SHEAR VELOCITY (M/S)	FLOW VELOCITY (M/S)	CRITICAL VELOCITY (M/S)	SCOUR RATE (M/S)	SEDIMENT TRANSPORT RATE (M**2/S)	SEDIMENT TRANSPORT CAPACITY (M**2/S)	INVERSE SHEAR INTENSITY	SPATIAL LAG COEFFICIENT (1/M)
2400	0.0183	0.053	0.723	0.456	.555E-05	.812E-05	.102E-04	0.0979	0.00279
3600	0.0178	0.049	0.692	0.472	.565E-05	.403E-05	.619E-05	0.0839	0.00279
4800	0.0174	0.047	0.677	0.484	.422E-05	.324E-05	.432E-05	0.0761	0.00416
6000	0.0173	0.045	0.659	0.489	.332E-05	.264E-05	.314E-05	0.0709	0.00711

CHAINAGE (M) : 3.0

TIME (S)	MANNINGS ROUGHNESS VALUE	SHEAR VELOCITY (M/S)	FLOW VELOCITY (M/S)	CRITICAL VELOCITY (M/S)	SCOUR RATE (M/S)	SEDIMENT TRANSPORT RATE (M**2/S)	SEDIMENT TRANSPORT CAPACITY (M**2/S)	INVERSE SHEAR INTENSITY	SPATIAL LAG COEFFICIENT (1/M)
3600	0.0185	0.053	0.711	0.452	.542E-05	.797E-05	.949E-05	0.0965	0.00380
4800	0.0181	0.050	0.692	0.464	.500E-05	.510E-05	.679E-05	0.0868	0.00315
6000	0.0178	0.049	0.684	0.473	.458E-05	.479E-05	.557E-05	0.0818	0.00626

BED SHEAR VELOCITIES OBTAINED USING: WILLIAMS (1970) SIDE WALL CORRECTION METHOD

Table D.2.6 Spatial Lag Data and Results (Run SC2006-I).

Appendix E | Temporal Lag Results

E.1 DERIVATIONS

General equations for the temporal lag time scale, Manning bed roughness value, average flow velocity, bed shear velocity and flow depth are derived as follows.

E.1.1 Derivation of General Equation for Time Scale, t_{90}

For the range of discharges considered the non-dimensional time scale, $\pi_{t_{90}}$, was given by (Section 8.2.3)

$$\pi_{t_{90}} = 0.266 \frac{\theta_c}{\theta} \tag{E.1}$$

where

$$\pi_{t_{90}} = t_{90} \theta_c^{3/2} \frac{\sqrt{(S_s - 1) g d_{50}^3}}{Y_E^2} \tag{E.2}$$

Thus

$$t_{90} = \frac{0.266}{\sqrt{(S_s - 1) g d_{50}^3} \sqrt{\theta_c}} \frac{Y_E^2}{\theta} \tag{E.3}$$

From the side-wall analysis (Section 5.2.3)

$$Y_E = 1.30 R_b^{1.086} \tag{E.4}$$

Also

$$\theta = \frac{R_b S_f}{(S_s - 1) d_{50}} \tag{E.5}$$

Thus

$$Y_E = 1.30 \left[\frac{(S_s - 1) d_{50}}{S_f}\right]^{1.086} \theta^{1.086} \tag{E.6}$$

Substituting Eq. E.6 into E.3 gives

$$t_{90} = \frac{0.266}{\sqrt{(S_s - 1)g\, d_{50}^{\,3}\theta_c}} 1.30^2 \left[\frac{(S_s - 1)d_{50}}{S_f}\right]^{2.178} \theta^{1.178} \qquad \text{(E.7)}$$

From continuity and Manning's equation

$$q = \frac{Y_E R_b^{\,2/3} S_f^{\,1/2}}{n_b} \qquad \text{(E.8)}$$

The analysis of flow resistance (Section 5.4.2) showed Manning bed roughness to be given by

$$n_b = \alpha_n \theta^{\beta_n} \qquad \text{(E.9)}$$

Substituting Eq. E.5, E.6 and E.9 into Eq. E.8 gives

$$q = \frac{1.30}{\alpha_n} \left[\frac{(S_s - 1)d_{50}}{S_f}\right]^{1.753} S_f^{\,0.5}\, \theta^{1.753 - \beta_n} \qquad \text{(E.10)}$$

Rearranging Eq. 10 gives

$$\theta = \left\{\frac{\alpha_n}{1.30} \frac{1}{[(S_s - 1)d_{50}]^{1.753}} S_f^{\,1.253} q\right\}^{\frac{1}{1.753 - \beta_n}} \qquad \text{(E.11)}$$

Substituting Eq. E.11 into Eq. E.7 gives

$$t_{90} = \frac{0.266}{\sqrt{g\theta_c}} \frac{1.30^2}{d_{50}} \frac{[(S_s - 1)d_{50}]^{1.678}}{S_f^{\,2.178}} \left\{\frac{\alpha_n}{1.30} \frac{S_f^{\,1.253}}{[(S_s - 1)d_{50}]^{1.753}} q\right\}^{\frac{1.178}{1.753 - \beta_n}}$$

$$= \frac{0.266}{\sqrt{g\theta_c}} \frac{1.30^{2-a'}}{d_{50}} [(S_s - 1)d_{50}]^{1.678 - 1.753a'} \alpha_n^{a'} \frac{1}{S_f^{\,2.178 - 1.253a'}} q^{a'} \qquad \text{.... (E.12)}$$

where $a' = 1.178/(1.753 - \beta_n)$

Eq. E.12 is the general solution for the time scale, t_{90}, as a function of friction slope and discharge. Substituting the sediment properties for the current series of experiments and the series of Bell (1980) into Eq. E.12 gives

$$t_{90} = 2.264 \frac{q^{0.7285}}{S_f^{\,1.265}} \qquad \text{(E.13)}$$

where $S_s = 2.65$
$d_{50} = 0.0018$ m
$\theta_c = 0.039$
$\alpha_n = 0.0256$, and
$\beta_n = 0.136$

For the series of Bell (1980), Eq. E.12 gives

$$t_{90} = 1.873 \frac{q^{0.7208}}{S_f^{1.2748}} \qquad (E.14)$$

where $S_f = 2.75$
$d_{50} = 0.00211$ m
$\theta_c = 0.04$
$\alpha_n = 0.02356$, and
$\beta_n = 0.1187$

E.1.2 Derivation of General Equation for Manning Bed Roughness Value, n_b

Substituting Eq. E.9, for θ, into Eq. E.11 gives

$$n_b = \left\{ \frac{\alpha_n^{1.753/\beta_n} S_f^{1.253}}{1.30[(S_s - 1)d_{50}]^{1.753}} q \right\}^{\frac{\beta_n}{1.753 - \beta_n}} \qquad (E.15)$$

Substituting the various sediment properties into Eq. E.15 gives

$$n_b = 0.0434 \, S_f^{0.1054} \, q^{0.0841} \qquad (E.16)$$

and for the data of Bell (1980)

$$n_b = 0.0359 \, S_f^{0.091} \, q^{0.0726} \qquad (E.17)$$

E.1.3 Derivation of General Equation for Average Flow Velocity, U

The Manning equation is

$$U = \frac{R_b^{2/3} S_f^{1/2}}{n_b} \qquad (E.18)$$

Substituting for R_b in terms of θ, (Eq. E.5), and then for θ in terms of n_b, (Eq. E.9), yields

$$U = \left[\frac{(S_s - 1)d_{50}}{\alpha_n^{1/\beta_n}}\right]^{0.667} \frac{n_b^{0.667/\beta_n - 1}}{S_f^{0.167}} \quad \text{(E.19)}$$

Substituting the various sediment properties into Eq. E.19 gives

$$U = 1.312 \times 10^6 \, S_f^{-0.167} \, n_b^{3.094} \quad \text{(E.20)}$$

and for the data of Bell (1980)

$$U = 3.317 \times 10^7 \, S_f^{-0.167} \, n_b^{4.6164} \quad \text{(E.21)}$$

E.1.4 Derivation of General Equation for Bed Shear Velocity, u_{*_b}

The definition of bed shear velocity is

$$u_{*_b} = \sqrt{gR_b S_f} \quad \text{(E.22)}$$

Substituting the relations given in Eqs. E.5 and E.9 gives

$$u_{*_b} = \sqrt{\frac{(S_s - 1)g\, d_{50}}{\alpha_n^{1/\beta_n}}} \, n_b^{1/2\beta_n} \quad \text{(E.23)}$$

Substituting the various sediment properties in Eq. E.23 gives

$$u_{*_b} = 1.214 \times 10^5 \, n_b^{3.676} \quad \text{(E.24)}$$

and for the data of Bell (1980)

$$u_{*_b} = 1.368 \times 10^6 \, n_b^{4.212} \quad \text{(E.25)}$$

E.1.5 Derivation of General Equation for Flow Depth, Y

Using a side-wall correction relation and a roughness relation, the general equation is obtained by substituting for θ, (Eq. E.9), into Eq. E.6, which gives

$$Y = 1.30 \left[\frac{(S_s - 1)d_{50}}{\alpha_n^{1/\beta_n}}\right]^{1.086} \frac{n_b^{1.086/\beta_n}}{S_f^{1.086}} \quad \text{(E.26)}$$

Substituting the various sediment properties into Eq. E.26 gives

$$Y = 1.20 \times 10^{10} \, S_f^{-1.086} \, n_b^{7.985} \quad \text{(E.27)}$$

and for the data of Bell (1980)

$$Y = 2.32 \times 10^{12} S_f^{-1.086} n_b^{9.149} \qquad (E.28)$$

E.2 TIME SCALE DATA

Values of the temporal lag time scale, t_{90}, were obtained and nondimensionalized in the manner described in Section 8.2.3. These values are given in Table E.1.

E.3 EXCESS DISCHARGE RATIO DATA

Excess discharge ratio values were obtained from the measured bedload transport rates in the manner described in Section 8.2.1. These values of excess discharge ratio against nondimensional time, t/t_{90}, are plotted in Fig. 8.4 and given in Tables E.2.1 - E.2.7.

E.4 TEMPORAL LAG MODEL RESULTS - FLOW DEPTHS

Values of the flow depth measured from the water surface profile records and flow depth values predicted by the temporal lag model, at the downstream end of the mobile reach, are given in Tables E.3 - E.7.

E.5 TEMPORAL LAG MODEL RESULTS - BEDLOAD TRANSPORT RATES

The temporal variations of the measured and predicted bedload transport rate, at the downstream end of the mobile reach, are plotted in Figs. E.1.1 - E.1.4, E.2, E.3.1 - E.3.3, E.4.1 - E.4.3, and E.5.

RUN	SHIELDS PARAMETER	SHIELDS PARAMETER RATIO	STEADY FLOW DEPTH (m)	TIME SCALE (s)	NONDIMENSIONAL TIME SCALE
SC2001-I	0.0832	2.13	0.133	900	0.120
SC2002-I	0.0957	2.45	0.155	1040	0.103
SC2003-I	0.1073	2.75	0.176	1200	0.091
SC2004-I	0.1173	3.01	0.194	1420	0.089
SC2005-I	0.1269	3.25	0.212	1580	0.083
SC2006-I	0.1360	3.49	0.229	1800	0.082
SC2007-I	0.1365	3.59	0.230	1700	0.077

Table E.1 Time Scale Data (SC-I Series).

RUN: SC2001-I

DISCHARGE (M**2/S) : 0.0809
SLOPE : 0.0020
TEMPERATURE (C) : 18.3

TIME OF INCLINED DISCHARGE STEP-TQ (S) : 30.0
RESPONSE DISCHARGE TIME SCALE -T90 (S) : 900.0

TEMPORAL LAG ANALYSIS RESULTS

TIME (S)	SEDIMENT TRANSPORT RATE (G/S/M)	EQUIVALENT STEADY BED ROUGHNESS	EQUIVALENT STEADY DISCHARGE (M**2/S)	EXCESS DISCHARGE RATIO	NON DIMENSIONAL TIME
30	0.330	0.0170	0.0351	0.0057	0.0000
90	6.260	0.0179	0.0659	0.6738	0.0667
150	6.559	0.0180	0.0669	0.6956	0.1333
210	6.859	0.0180	0.0678	0.7169	0.2000
270	7.158	0.0180	0.0688	0.7379	0.2667
330	7.458	0.0180	0.0698	0.7585	0.3333
390	8.104	0.0181	0.0718	0.8020	0.4000
450	8.456	0.0181	0.0728	0.8251	0.4667
510	8.163	0.0181	0.0720	0.8059	0.5333
570	7.575	0.0180	0.0701	0.7665	0.6000
630	7.106	0.0180	0.0686	0.7342	0.6667
690	6.342	0.0179	0.0661	0.6798	0.7333
750	8.456	0.0181	0.0728	0.8251	0.8000
810	9.631	0.0182	0.0763	0.8997	0.8667
870	9.866	0.0182	0.0769	0.9142	0.9333
930	10.335	0.0182	0.0783	0.9429	1.0000
990	10.981	0.0182	0.0800	0.9815	1.0667
1050	11.040	0.0182	0.0802	0.9850	1.1333
1110	10.277	0.0182	0.0781	0.9393	1.2000
1170	9.983	0.0182	0.0773	0.9214	1.2667
1230	9.748	0.0182	0.0766	0.9070	1.3333
1290	9.866	0.0182	0.0769	0.9142	1.4000
1350	10.805	0.0182	0.0796	0.9710	1.4667
1410	10.042	0.0182	0.0774	0.9250	1.5333
1470	10.218	0.0182	0.0779	0.9358	1.6000
1530	9.807	0.0182	0.0768	0.9106	1.6667
1590	10.159	0.0182	0.0778	0.9322	1.7333
1650	10.688	0.0182	0.0792	0.9640	1.8000
1710	11.157	0.0182	0.0805	0.9919	1.8667
1770	11.862	0.0183	0.0824	1.0328	1.9333
1830	13.095	0.0183	0.0856	1.1024	2.0000
1890	13.859	0.0184	0.0876	1.1443	2.0667
1950	14.328	0.0184	0.0887	1.1697	2.1333
2010	14.152	0.0184	0.0883	1.1602	2.2000
2070	12.978	0.0183	0.0853	1.0958	2.2667
2130	11.627	0.0183	0.0818	1.0192	2.3333
2190	10.688	0.0182	0.0792	0.9640	2.4000
2250	9.102	0.0181	0.0748	0.8666	2.4667
2310	7.810	0.0181	0.0709	0.7824	2.5333
2370	7.340	0.0180	0.0694	0.7505	2.6000
2430	7.458	0.0180	0.0698	0.7585	2.6667

Table E.2.1 Excess Discharge Ratio Data (Run SC2001-I)

RUN: SC2002-I

DISCHARGE (M**2/S) : 0.1015
SLOPE : 0.0020
TEMPERATURE (C) : 17.4

TIME OF INCLINED DISCHARGE STEP-TQ (S) : 30.0
RESPONSE DISCHARGE TIME SCALE -T90 (S) : 1040.0

TEMPORAL LAG ANALYSIS RESULTS

TIME (S)	SEDIMENT TRANSPORT RATE (G/S/M)	EQUIVALENT STEADY BED ROUGHNESS	EQUIVALENT STEADY DISCHARGE (M**2/S)	EXCESS DISCHARGE RATIO	NON DIMENSIONAL TIME
30	0.330	0.0170	0.0351	0.0040	0.0000
90	7.498	0.0180	0.0699	0.5262	0.0577
150	8.488	0.0181	0.0729	0.5718	0.1154
210	9.479	0.0182	0.0758	0.6153	0.1731
270	10.469	0.0182	0.0786	0.6572	0.2308
330	11.459	0.0183	0.0813	0.6977	0.2885
390	12.025	0.0183	0.0828	0.7203	0.3462
450	11.247	0.0183	0.0808	0.6891	0.4038
510	14.501	0.0184	0.0891	0.8148	0.4615
570	17.330	0.0185	0.0959	0.9164	0.5192
630	19.028	0.0186	0.0998	0.9746	0.5769
690	19.523	0.0186	0.1009	0.9913	0.6346
750	19.099	0.0186	0.1000	0.9770	0.6923
810	18.533	0.0186	0.0987	0.9578	0.7500
870	18.957	0.0186	0.0996	0.9722	0.8077
930	22.352	0.0187	0.1071	1.0841	0.8654
990	21.716	0.0187	0.1057	1.0636	0.9231
1050	22.069	0.0187	0.1065	1.0750	0.9808
1110	21.645	0.0187	0.1056	1.0613	1.0385
1170	20.160	0.0186	0.1023	1.0125	1.0962
1230	19.523	0.0186	0.1009	0.9913	1.1538
1290	17.896	0.0185	0.0972	0.9360	1.2115
1350	17.189	0.0185	0.0956	0.9114	1.2692
1410	16.835	0.0185	0.0948	0.8990	1.3269
1470	19.311	0.0186	0.1004	0.9842	1.3846
1530	19.947	0.0186	0.1019	1.0055	1.4423
1590	16.835	0.0185	0.0948	0.8990	1.5000
1650	15.632	0.0185	0.0919	0.8562	1.5577
1710	14.784	0.0184	0.0898	0.8253	1.6154
1770	16.411	0.0185	0.0938	0.8840	1.6731
1830	16.764	0.0185	0.0946	0.8965	1.7308
1890	16.623	0.0185	0.0943	0.8915	1.7885
1950	17.259	0.0185	0.0958	0.9139	1.8462
2010	17.613	0.0185	0.0966	0.9262	1.9038
2070	18.179	0.0185	0.0979	0.9457	1.9615
2130	15.703	0.0185	0.0921	0.8587	2.0192
2190	13.723	0.0184	0.0872	0.7858	2.0769
2250	15.774	0.0185	0.0922	0.8613	2.1346
2310	18.957	0.0186	0.0996	0.9722	2.1923
2370	22.211	0.0187	0.1068	1.0796	2.2500
2430	23.696	0.0187	0.1100	1.1270	2.3077

Table E.2.2 Excess Discharge Ratio Data (Run SC2002-I)

RUN: SC2003-I

DISCHARGE (M**2/S) : 0.1222
SLOPE : 0.0020
TEMPERATURE (C) : 17.5

TIME OF INCLINED DISCHARGE STEP-TQ (S) : 30.0
RESPONSE DISCHARGE TIME SCALE -T90 (S) : 1200.0

TEMPORAL LAG ANALYSIS RESULTS

TIME (S)	SEDIMENT TRANSPORT RATE (G/S/M)	EQUIVALENT STEADY BED ROUGHNESS	EQUIVALENT STEADY DISCHARGE (M**2/S)	EXCESS DISCHARGE RATIO	NON DIMENSIONAL TIME
30	0.330	0.0170	0.0351	0.0030	0.0000
90	11.782	0.0183	0.0822	0.5423	0.0500
150	13.479	0.0184	0.0866	0.5927	0.1000
210	15.175	0.0184	0.0908	0.6408	0.1500
270	16.872	0.0185	0.0949	0.6871	0.2000
330	18.568	0.0186	0.0988	0.7319	0.2500
390	19.159	0.0186	0.1001	0.7472	0.3000
450	22.282	0.0187	0.1070	0.8256	0.3500
510	23.717	0.0187	0.1100	0.8605	0.4000
570	22.366	0.0187	0.1071	0.8277	0.4500
630	21.269	0.0187	0.1048	0.8006	0.5000
690	23.126	0.0187	0.1088	0.8463	0.5500
750	23.379	0.0187	0.1093	0.8524	0.6000
810	23.548	0.0187	0.1097	0.8565	0.6500
870	21.776	0.0187	0.1059	0.8132	0.7000
930	22.029	0.0187	0.1064	0.8194	0.7500
990	25.996	0.0188	0.1147	0.9147	0.8000
1050	29.625	0.0189	0.1220	0.9981	0.8500
1110	28.359	0.0189	0.1195	0.9693	0.9000
1170	27.177	0.0188	0.1171	0.9422	0.9500
1230	27.177	0.0188	0.1171	0.9422	1.0000
1290	26.671	0.0188	0.1161	0.9304	1.0500
1350	25.320	0.0188	0.1134	0.8988	1.1000
1410	27.177	0.0188	0.1171	0.9422	1.1500
1470	27.852	0.0188	0.1185	0.9577	1.2000
1530	28.696	0.0189	0.1202	0.9770	1.2500
1590	25.067	0.0188	0.1128	0.8928	1.3000
1650	20.594	0.0186	0.1033	0.7837	1.3500
1710	20.425	0.0186	0.1029	0.7794	1.4000
1770	19.750	0.0186	0.1014	0.7623	1.4500
1830	19.412	0.0186	0.1007	0.7537	1.5000
1890	19.159	0.0186	0.1001	0.7472	1.5500
1950	21.016	0.0186	0.1042	0.7943	1.6000
2010	20.763	0.0186	0.1037	0.7879	1.6500
2070	18.822	0.0186	0.0993	0.7385	1.7000
2130	17.640	0.0185	0.0966	0.7076	1.7500
2190	17.977	0.0185	0.0974	0.7165	1.8000
2250	21.944	0.0187	0.1062	0.8173	1.8500
2310	23.801	0.0187	0.1102	0.8626	1.9000
2370	21.354	0.0187	0.1050	0.8027	1.9500
2430	19.666	0.0186	0.1012	0.7602	2.0000

Table E.2.3 Excess Discharge Ratio Data (Run SC2003-I)

RUN: SC2004-I

DISCHARGE (M**2/S) : 0.1416
SLOPE : 0.0020
TEMPERATURE (C) : 19.6

TIME OF INCLINED DISCHARGE STEP-TQ (S) : 30.0
RESPONSE DISCHARGE TIME SCALE -T90 (S) : 1420.0

TEMPORAL LAG ANALYSIS RESULTS

TIME (S)	SEDIMENT TRANSPORT RATE (G/S/M)	EQUIVALENT STEADY BED ROUGHNESS	EQUIVALENT STEADY DISCHARGE (M**2/S)	EXCESS DISCHARGE RATIO	NON DIMENSIONAL TIME
30	0.330	0.0170	0.0351	0.0025	0.0000
90	14.514	0.0184	0.0892	0.5092	0.0423
150	15.682	0.0185	0.0920	0.5358	0.0845
210	16.849	0.0185	0.0948	0.5618	0.1268
270	18.017	0.0185	0.0975	0.5872	0.1690
330	19.185	0.0186	0.1002	0.6120	0.2113
390	21.938	0.0187	0.1062	0.6687	0.2535
450	23.689	0.0187	0.1100	0.7037	0.2958
510	24.940	0.0188	0.1126	0.7282	0.3380
570	23.522	0.0187	0.1096	0.7004	0.3803
630	21.687	0.0187	0.1057	0.6637	0.4225
690	27.943	0.0189	0.1187	0.7855	0.4648
750	29.778	0.0189	0.1223	0.8196	0.5070
810	31.280	0.0189	0.1253	0.8471	0.5493
870	28.611	0.0189	0.1200	0.7980	0.5915
930	30.112	0.0189	0.1230	0.8258	0.6338
990	33.699	0.0190	0.1299	0.8907	0.6761
1050	34.867	0.0190	0.1321	0.9114	0.7183
1110	32.948	0.0190	0.1285	0.8772	0.7606
1170	30.446	0.0189	0.1236	0.8319	0.8028
1230	31.864	0.0190	0.1264	0.8577	0.8451
1290	36.868	0.0191	0.1359	0.9465	0.8873
1350	31.613	0.0189	0.1259	0.8532	0.9296
1410	28.027	0.0189	0.1189	0.7870	0.9718
1470	26.275	0.0188	0.1153	0.7539	1.0141
1530	29.361	0.0189	0.1215	0.8119	1.0563
1590	31.947	0.0190	0.1266	0.8592	1.0986
1650	30.362	0.0189	0.1235	0.8304	1.1408
1710	30.779	0.0189	0.1243	0.8380	1.1831
1770	31.113	0.0189	0.1249	0.8441	1.2254
1830	32.448	0.0190	0.1275	0.8683	1.2676
1890	30.779	0.0189	0.1243	0.8380	1.3099
1950	26.192	0.0188	0.1151	0.7523	1.3521
2010	24.190	0.0187	0.1110	0.7135	1.3944
2070	26.442	0.0188	0.1157	0.7571	1.4366
2130	30.112	0.0189	0.1230	0.8258	1.4789
2190	34.283	0.0190	0.1310	0.9010	1.5211
2250	32.614	0.0190	0.1278	0.8713	1.5634
2310	34.616	0.0190	0.1317	0.9070	1.6056
2370	34.950	0.0190	0.1323	0.9128	1.6479
2430	38.203	0.0191	0.1383	0.9696	1.6901

Table E.2.4 Excess Discharge Ratio Data (Run SC2004-I)

RUN: SC2005-I

DISCHARGE (M**2/S) : 0.1612
SLOPE : 0.0020
TEMPERATURE (C) : 19.1

TIME OF INCLINED DISCHARGE STEP-TQ (S) : 30.0
RESPONSE DISCHARGE TIME SCALE -T90 (S) : 1580.0

TEMPORAL LAG ANALYSIS RESULTS

TIME (S)	SEDIMENT TRANSPORT RATE (G/S/M)	EQUIVALENT STEADY BED ROUGHNESS	EQUIVALENT STEADY DISCHARGE (M**2/S)	EXCESS DISCHARGE RATIO	NON DIMENSIONAL TIME
30	0.330	0.0170	0.0351	0.0021	0.0000
90	10.180	0.0182	0.0778	0.3404	0.0380
150	13.526	0.0184	0.0867	0.4107	0.0759
210	16.872	0.0185	0.0949	0.4751	0.1139
270	20.217	0.0186	0.1025	0.5353	0.1519
330	23.563	0.0187	0.1097	0.5925	0.1899
390	29.936	0.0189	0.1226	0.6950	0.2278
450	30.439	0.0189	0.1236	0.7028	0.2658
510	30.942	0.0189	0.1246	0.7106	0.3038
570	36.645	0.0191	0.1355	0.7964	0.3418
630	39.076	0.0191	0.1400	0.8319	0.3797
690	37.148	0.0191	0.1364	0.8038	0.4177
750	38.322	0.0191	0.1386	0.8209	0.4557
810	43.018	0.0192	0.1471	0.8883	0.4937
870	46.120	0.0192	0.1526	0.9317	0.5316
930	41.005	0.0191	0.1435	0.8597	0.5696
990	38.825	0.0191	0.1395	0.8283	0.6076
1050	35.806	0.0190	0.1339	0.7840	0.6456
1110	43.605	0.0192	0.1481	0.8965	0.6835
1170	47.797	0.0193	0.1555	0.9549	0.7215
1230	41.089	0.0192	0.1436	0.8609	0.7595
1290	37.567	0.0191	0.1372	0.8099	0.7975
1350	39.076	0.0191	0.1400	0.8319	0.8354
1410	43.772	0.0192	0.1484	0.8989	0.8734
1470	44.946	0.0192	0.1505	0.9154	0.9114
1530	45.785	0.0192	0.1520	0.9271	0.9494
1590	48.217	0.0193	0.1562	0.9607	0.9873
1650	49.558	0.0193	0.1586	0.9791	1.0253
1710	46.539	0.0193	0.1533	0.9375	1.0633
1770	37.483	0.0191	0.1370	0.8087	1.1013
1830	33.123	0.0190	0.1288	0.7439	1.1392
1890	40.083	0.0191	0.1418	0.8464	1.1772
1950	46.959	0.0193	0.1540	0.9434	1.2152
2010	51.319	0.0193	0.1616	1.0030	1.2532
2070	48.384	0.0193	0.1565	0.9630	1.2911
2130	43.605	0.0192	0.1481	0.8965	1.3291
2190	40.083	0.0191	0.1418	0.8464	1.3671
2250	37.148	0.0191	0.1364	0.8038	1.4051
2310	35.303	0.0190	0.1330	0.7766	1.4430
2370	35.051	0.0190	0.1325	0.7728	1.4810
2430	44.443	0.0192	0.1496	0.9083	1.5190

Table E.2.5 Excess Discharge Ratio Data (Run SC2005-I)

RUN: SC2006-I

DISCHARGE (M**2/S) : 0.1807
SLOPE : 0.0020
TEMPERATURE (C) : 20.3

TIME OF INCLINED DISCHARGE STEP-TQ (S) : 30.0
RESPONSE DISCHARGE TIME SCALE -T90 (S) : 1800.0

TEMPORAL LAG ANALYSIS RESULTS

TIME (S)	SEDIMENT TRANSPORT RATE (G/S/M)	EQUIVALENT STEADY BED ROUGHNESS	EQUIVALENT STEADY DISCHARGE (M**2/S)	EXCESS DISCHARGE RATIO	NON DIMENSIONAL TIME
30	0.330	0.0170	0.0351	0.0018	0.0000
90	15.178	0.0184	0.0908	0.3839	0.0333
150	19.349	0.0186	0.1005	0.4505	0.0667
210	23.521	0.0187	0.1096	0.5127	0.1000
270	27.693	0.0188	0.1182	0.5715	0.1333
330	31.865	0.0190	0.1264	0.6279	0.1667
390	39.811	0.0191	0.1413	0.7299	0.2000
450	40.050	0.0191	0.1417	0.7329	0.2333
510	38.778	0.0191	0.1394	0.7170	0.2667
570	41.321	0.0192	0.1440	0.7487	0.3000
630	41.639	0.0192	0.1446	0.7526	0.3333
690	38.063	0.0191	0.1381	0.7080	0.3667
750	36.871	0.0191	0.1359	0.6929	0.4000
810	39.255	0.0191	0.1403	0.7230	0.4333
870	42.990	0.0192	0.1470	0.7692	0.4667
930	44.500	0.0192	0.1497	0.7876	0.5000
990	37.109	0.0191	0.1363	0.6959	0.5333
1050	37.586	0.0191	0.1372	0.7019	0.5667
1110	39.891	0.0191	0.1414	0.7309	0.6000
1170	41.162	0.0192	0.1437	0.7467	0.6333
1230	35.520	0.0190	0.1334	0.6756	0.6667
1290	39.573	0.0191	0.1409	0.7269	0.7000
1350	48.393	0.0193	0.1565	0.8344	0.7333
1410	55.545	0.0194	0.1688	0.9181	0.7667
1470	53.161	0.0194	0.1647	0.8905	0.8000
1530	50.857	0.0193	0.1608	0.8635	0.8333
1590	50.777	0.0193	0.1607	0.8626	0.8667
1650	49.585	0.0193	0.1586	0.8485	0.9000
1710	41.400	0.0192	0.1442	0.7497	0.9333
1770	44.976	0.0192	0.1506	0.7934	0.9667
1830	54.432	0.0194	0.1669	0.9053	1.0000
1890	63.173	0.0195	0.1814	1.0048	1.0333
1950	63.889	0.0195	0.1826	1.0129	1.0667
2010	60.790	0.0195	0.1775	0.9780	1.1000
2070	55.148	0.0194	0.1681	0.9135	1.1333
2130	50.062	0.0193	0.1594	0.8542	1.1667
2190	48.950	0.0193	0.1575	0.8410	1.2000
2250	47.519	0.0193	0.1550	0.8240	1.2333
2310	49.267	0.0193	0.1581	0.8448	1.2667
2370	58.247	0.0194	0.1733	0.9491	1.3000
2430	59.121	0.0195	0.1747	0.9591	1.3333

Table E.2.6 Excess Discharge Ratio Data (Run SC2006-I)

RUN: SC2007-I

DISCHARGE (M**2/S) : 0.1795
SLOPE : 0.0020
TEMPERATURE (C) : 15.2

TIME OF INCLINED DISCHARGE STEP-TQ (S) : 30.0
RESPONSE DISCHARGE TIME SCALE -T90 (S) : 1700.0

TEMPORAL LAG ANALYSIS RESULTS

TIME (S)	SEDIMENT TRANSPORT RATE (G/S/M)	EQUIVALENT STEADY BED ROUGHNESS	EQUIVALENT STEADY DISCHARGE (M**2/S)	EXCESS DISCHARGE RATIO	NON DIMENSIONAL TIME
30	0.330	0.0170	0.0351	0.0018	0.0000
90	18.768	0.0186	0.0992	0.4452	0.0353
150	23.177	0.0187	0.1089	0.5119	0.0706
210	27.586	0.0188	0.1180	0.5748	0.1059
270	31.995	0.0190	0.1267	0.6348	0.1412
330	36.405	0.0191	0.1350	0.6926	0.1765
390	38.172	0.0191	0.1383	0.7152	0.2118
450	36.581	0.0191	0.1353	0.6949	0.2471
510	42.325	0.0192	0.1458	0.7674	0.2824
570	46.301	0.0193	0.1529	0.8161	0.3176
630	42.590	0.0192	0.1463	0.7706	0.3529
690	40.381	0.0191	0.1423	0.7431	0.3882
750	42.148	0.0192	0.1455	0.7652	0.4235
810	49.482	0.0193	0.1584	0.8543	0.4588
870	56.374	0.0194	0.1701	0.9354	0.4941
930	55.932	0.0194	0.1694	0.9302	0.5294
990	54.872	0.0194	0.1676	0.9179	0.5647
1050	54.872	0.0194	0.1676	0.9179	0.6000
1110	54.784	0.0194	0.1675	0.9169	0.6353
1170	46.920	0.0193	0.1540	0.8236	0.6706
1230	49.394	0.0193	0.1583	0.8533	0.7059
1290	55.667	0.0194	0.1690	0.9272	0.7412
1350	60.174	0.0195	0.1765	0.9791	0.7765
1410	58.671	0.0195	0.1740	0.9619	0.8118
1470	50.012	0.0193	0.1593	0.8607	0.8471
1530	47.273	0.0193	0.1546	0.8278	0.8824
1590	45.682	0.0192	0.1518	0.8086	0.9176
1650	43.562	0.0192	0.1480	0.7826	0.9529
1710	43.739	0.0192	0.1484	0.7848	0.9882
1770	44.887	0.0192	0.1504	0.7989	1.0235
1830	43.297	0.0192	0.1476	0.7794	1.0588
1890	42.236	0.0192	0.1457	0.7663	1.0941
1950	44.622	0.0192	0.1499	0.7956	1.1294
2010	48.510	0.0193	0.1567	0.8427	1.1647
2070	48.068	0.0193	0.1560	0.8374	1.2000
2130	48.068	0.0193	0.1560	0.8374	1.2353
2190	42.767	0.0192	0.1466	0.7728	1.2706
2250	47.273	0.0193	0.1546	0.8278	1.3059
2310	52.840	0.0194	0.1642	0.8941	1.3412
2370	57.081	0.0194	0.1713	0.9435	1.3765
2430	57.434	0.0194	0.1719	0.9476	1.4118

Table E.2.7 Excess Discharge Ratio Data (Run SC2007-I)

TEMPORAL LAG MODEL RESULTS - UNSTEADY FLOW DEPTH

RUN	TIME (S)	DISCHARGE (M**2/S)	EQUIVALENT EQUILIBRIUM DISCHARGE (M**2/S)	PREDICTED FLOW DEPTH (M)	MEASURED FLOW DEPTH (M)
SC2001-I	240	0.0809	0.0658	0.132	0.131
	480	0.0809	0.0723	0.133	0.132
	720	0.0809	0.0749	0.133	0.132
	960	0.0809	0.0763	0.133	0.133
	1200	0.0809	0.0771	0.134	0.132
SC2002-I	240	0.1015	0.0772	0.154	0.154
	480	0.1015	0.0873	0.155	0.154
	720	0.1015	0.0914	0.155	0.156
	960	0.1015	0.0937	0.155	0.156
	1200	0.1015	0.0952	0.155	0.155
SC2003-I	300	0.1222	0.0925	0.174	0.177
	540	0.1222	0.1034	0.175	0.177
	780	0.1222	0.1084	0.176	0.178
	1020	0.1222	0.1113	0.176	0.178
	1260	0.1222	0.1132	0.176	0.178
SC2004-I	300	0.1416	0.1027	0.192	0.196
	540	0.1416	0.1166	0.193	0.197
	780	0.1416	0.1232	0.194	0.198
	1020	0.1416	0.1270	0.194	0.198
	1260	0.1416	0.1295	0.194	0.197
SC2005-I	300	0.1612	0.1124	0.209	0.213
	540	0.1612	0.1294	0.210	0.213
	780	0.1612	0.1376	0.211	0.215
	1020	0.1612	0.1425	0.211	0.215
	1260	0.1612	0.1457	0.212	0.216
SC2006-I	300	0.1807	0.1215	0.225	0.236
	540	0.1807	0.1417	0.227	0.237
	780	0.1807	0.1516	0.228	0.237
	1020	0.1807	0.1575	0.228	0.238
	1260	0.1807	0.1614	0.228	0.237

Table E.3 Temporal Lag Model Results - Flow Depths (SC-I Series)

TEMPORAL LAG MODEL RESULTS - UNSTEADY FLOW DEPTH

RUN	TIME (S)	DISCHARGE (M**2/S)	EQUIVALENT EQUILIBRIUM DISCHARGE (M**2/S)	PREDICTED FLOW DEPTH (M)	MEASURED FLOW DEPTH (M)
SC2002-II	240	0.0847	0.0580	0.135	0.129
	480	0.0999	0.0793	0.152	0.154
	720	0.0999	0.0881	0.153	0.153
	960	0.0999	0.0912	0.154	0.153
	1200	0.0999	0.0930	0.154	0.153
SC2005-II	240	0.1312	0.0729	0.180	0.184
	480	0.1605	0.1108	0.208	0.219
	720	0.1605	0.1305	0.210	0.219
	960	0.1605	0.1380	0.210	0.220
	1200	0.1605	0.1425	0.211	0.220

Table E.4 Temporal Lag Model Results - Flow Depths (SC-II Series)

TEMPORAL LAG MODEL RESULTS - UNSTEADY FLOW DEPTH

RUN	TIME (S)	DISCHARGE (M**2/S)	EQUIVALENT EQUILIBRIUM DISCHARGE (M**2/S)	PREDICTED FLOW DEPTH (M)	MEASURED FLOW DEPTH (M)
SC2001-III	240	0.0517	0.0439	0.098	0.096
	480	0.0693	0.0570	0.119	0.116
	720	0.0789	0.0680	0.131	0.129
	1020	0.0789	0.0722	0.131	0.130
	1200	0.0789	0.0741	0.131	0.130
	1500	0.0789	0.0753	0.131	0.131
SC2002-III	240	0.0598	0.0478	0.108	0.105
	480	0.0859	0.0661	0.137	0.136
	720	0.1000	0.0817	0.153	0.151
	1020	0.1000	0.0884	0.153	0.153
	1200	0.1000	0.0918	0.154	0.153
	1500	0.1000	0.0938	0.154	0.153
SC2003-III	240	0.0671	0.0510	0.116	0.115
	480	0.1008	0.0737	0.153	0.154
	720	0.1191	0.0933	0.171	0.173
	960	0.1191	0.1008	0.172	0.173
	1200	0.1191	0.1073	0.173	0.175
	1500	0.1191	0.1101	0.173	0.175
SC2004-III	240	0.0748	0.0541	0.125	0.125
	480	0.1165	0.0811	0.168	0.169
	720	0.1391	0.1047	0.190	0.196
	960	0.1391	0.1144	0.191	0.197
	1200	0.1391	0.1230	0.191	0.196
	1500	0.1391	0.1269	0.192	0.196
SC2005-III	240	0.0823	0.0571	0.133	0.130
	480	0.1319	0.0880	0.182	0.184
	720	0.1588	0.1153	0.207	0.216
	960	0.1588	0.1272	0.208	0.217
	1200	0.1588	0.1380	0.209	0.217
	1500	0.1588	0.1430	0.209	0.217
SC2006-III	240	0.0903	0.0600	0.141	0.141
	480	0.1482	0.0949	0.196	0.200
	720	0.1796	0.1259	0.225	0.237
	960	0.1796	0.1403	0.226	0.237
	1200	0.1796	0.1535	0.227	0.238
	1500	0.1796	0.1596	0.227	0.238

Table E.5 Temporal Lag Model Results - Flow Depths (SC-III Series)

TEMPORAL LAG MODEL RESULTS - UNSTEADY FLOW DEPTH

RUN	TIME (S)	DISCHARGE (M**2/S)	EQUIVALENT EQUILIBRIUM DISCHARGE (M**2/S)	PREDICTED FLOW DEPTH (M)	MEASURED FLOW DEPTH (M)
SC2001-IV	240	0.0433	0.0396	0.088	0.089
	480	0.0521	0.0466	0.099	0.099
	720	0.0609	0.0539	0.110	0.109
	960	0.0697	0.0614	0.120	0.120
	1200	0.0785	0.0690	0.130	0.129
	1500	0.0789	0.0727	0.131	0.130
SC2002-IV	240	0.0474	0.0418	0.093	0.094
	480	0.0605	0.0518	0.109	0.108
	720	0.0737	0.0624	0.125	0.125
	960	0.0868	0.0732	0.139	0.140
	1200	0.1000	0.0841	0.153	0.156
	1500	0.1005	0.0897	0.154	0.154
SC2003-IV	240	0.0510	0.0436	0.097	0.095
	480	0.0679	0.0562	0.118	0.119
	720	0.0849	0.0694	0.137	0.136
	960	0.1018	0.0829	0.155	0.155
	1200	0.1187	0.0966	0.171	0.173
	1500	0.1194	0.1039	0.173	0.176
SC2004-IV	240	0.0551	0.0456	0.102	0.101
	480	0.0764	0.0609	0.127	0.127
	720	0.0976	0.0771	0.150	0.154
	960	0.1188	0.0936	0.171	0.173
	1200	0.1400	0.1103	0.191	0.192
	1500	0.1409	0.1194	0.193	0.196
SC2005-IV	240	0.0586	0.0472	0.107	0.103
	480	0.0834	0.0648	0.135	0.136
	720	0.1082	0.0832	0.161	0.163
	960	0.1330	0.1021	0.184	0.185
	1200	0.1579	0.1213	0.207	0.214
	1500	0.1589	0.1320	0.209	0.218
SC2006-IV	300	0.0697	0.0538	0.119	0.120
	480	0.0914	0.0689	0.143	0.144
	720	0.1202	0.0899	0.172	0.174
	960	0.1491	0.1114	0.199	0.208
	1200	0.1780	0.1332	0.224	0.236
	1500	0.1792	0.1458	0.226	0.237

Table E.6 Temporal Lag Model Results - Flow Depths (SC-IV Series)

TEMPORAL LAG MODEL RESULTS - UNSTEADY FLOW DEPTH

RUN	TIME (S)	DISCHARGE (M**2/S)	EQUIVALENT EQUILIBRIUM DISCHARGE (M**2/S)	PREDICTED FLOW DEPTH (M)	MEASURED FLOW DEPTH (M)
SC2002-V	240	0.0430	0.0395	0.087	0.088
	480	0.0516	0.0463	0.098	0.099
	720	0.0602	0.0535	0.109	0.109
	960	0.0688	0.0608	0.119	0.118
	1200	0.0774	0.0682	0.129	0.128
	1500	0.0882	0.0776	0.141	0.139
	1800	0.0989	0.0870	0.152	0.152
SC2005-V	240	0.0507	0.0435	0.097	0.098
	480	0.0673	0.0558	0.117	0.118
	720	0.0839	0.0688	0.136	0.138
	960	0.1005	0.0821	0.153	0.155
	1200	0.1171	0.0956	0.170	0.174
	1500	0.1379	0.1126	0.189	0.197
	1800	0.1586	0.1298	0.208	0.216

Table E.7 Temporal Lag Model Results - Flow Depths (SC-V Series)

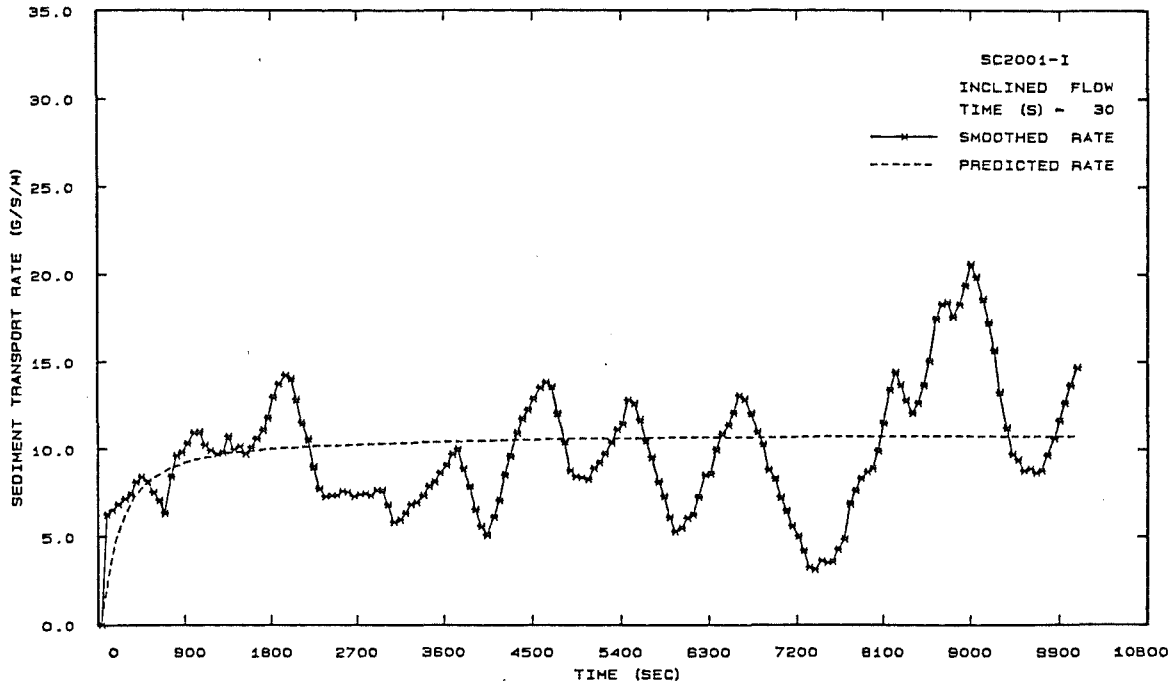

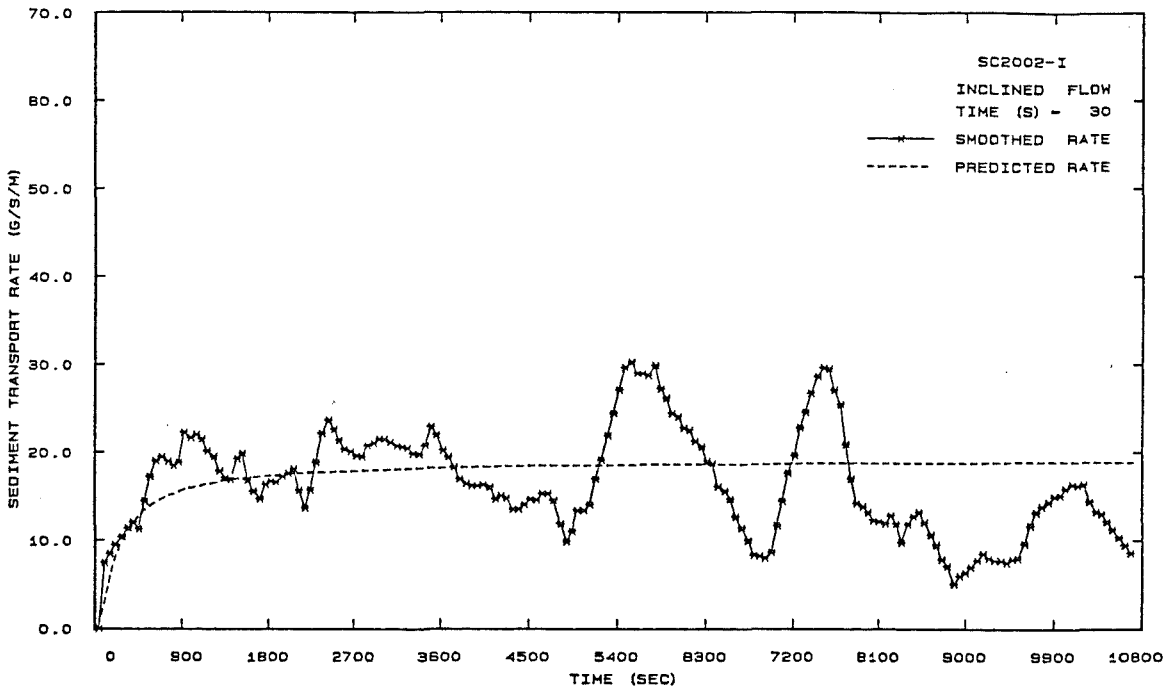

Fig. E.1.1 Temporal Lag Model Results - Bedload Transport Rates (Runs SC2001-I and SC2002-I)

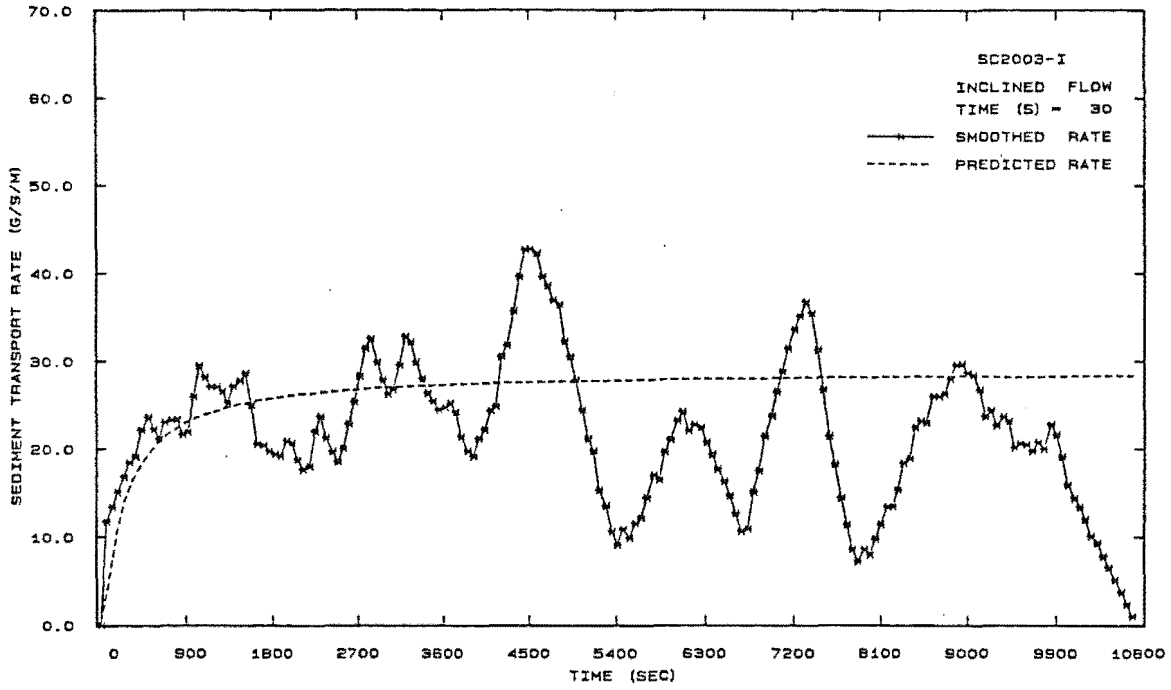

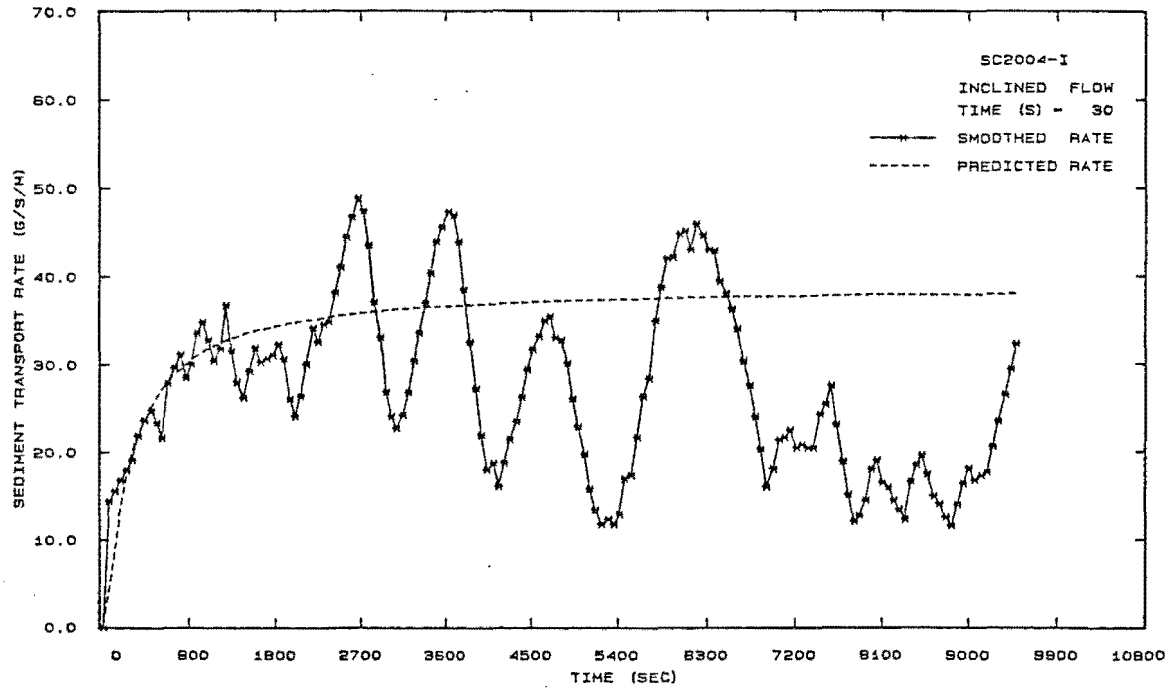

Fig. E.1.2 Temporal Lag Model Results - Bedload Transport Rates (Runs SC2003-I and SC2004-I)

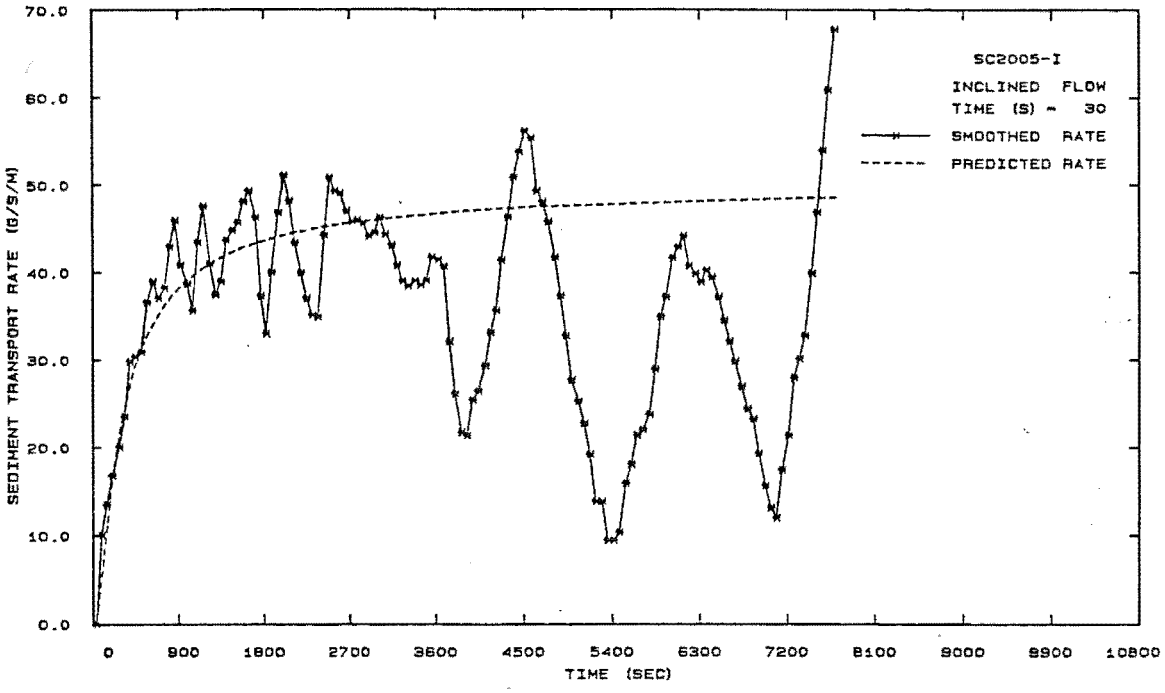

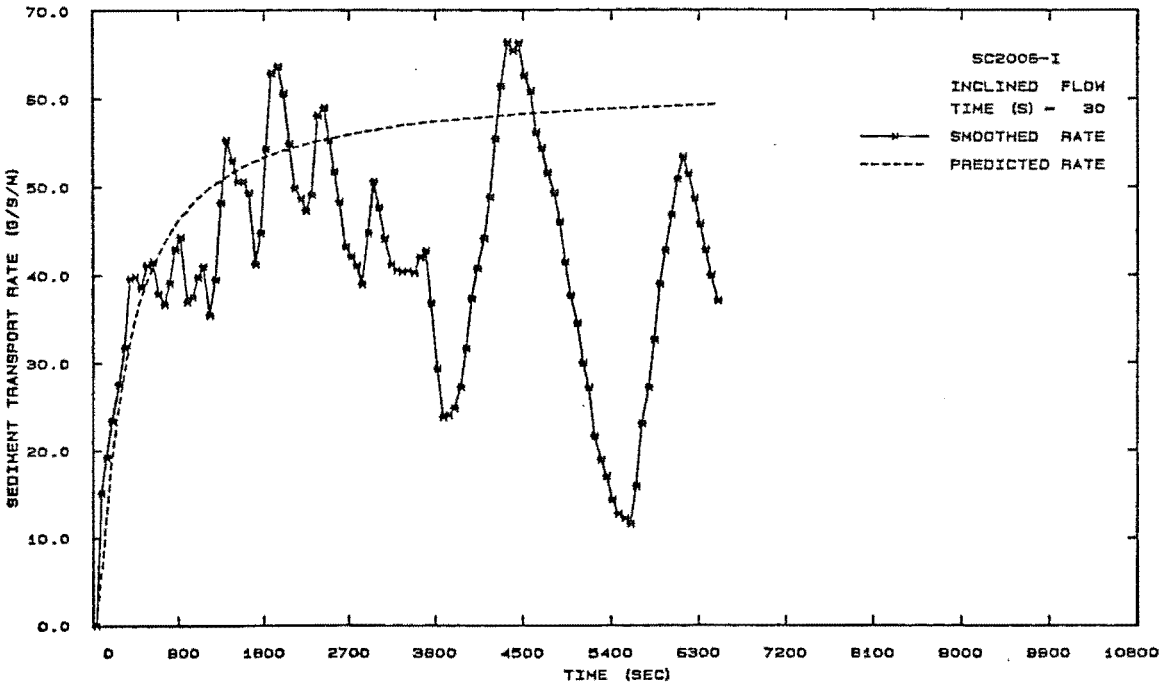

Fig. E.1.3 Temporal Lag Model Results - Bedload Transport Rates (Runs SC2005-I and SC2006-I)

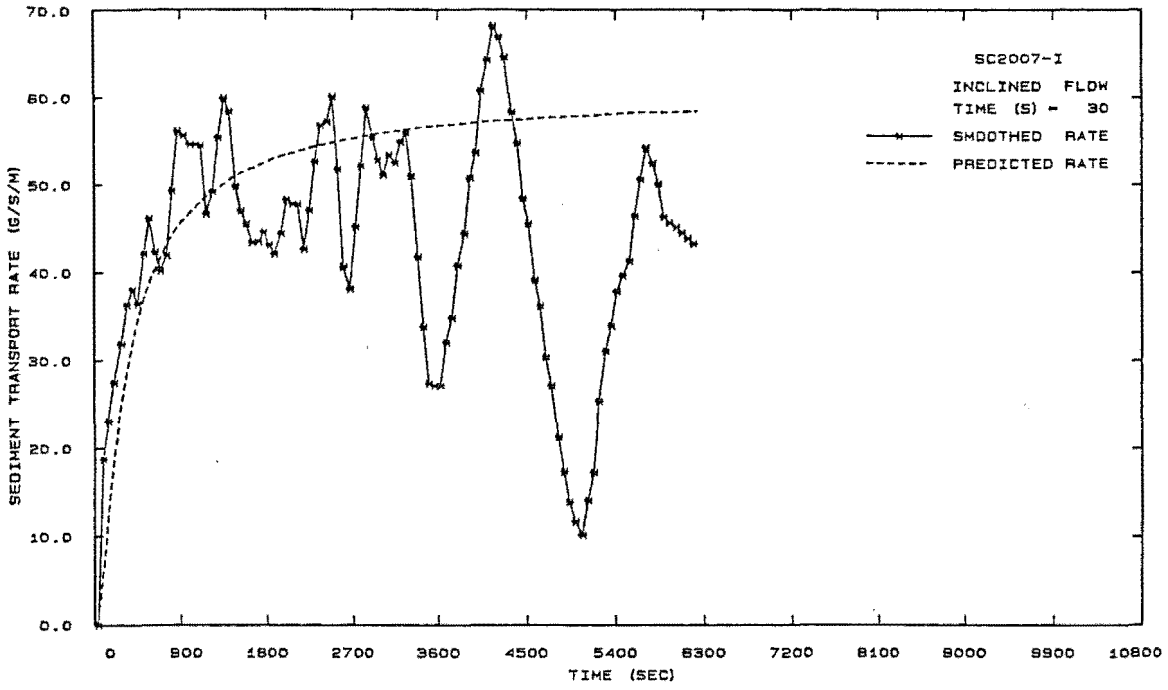

Fig. E.1.4 Temporal Lag Model Results - Bedload Transport Rates (Run SC2007-I)

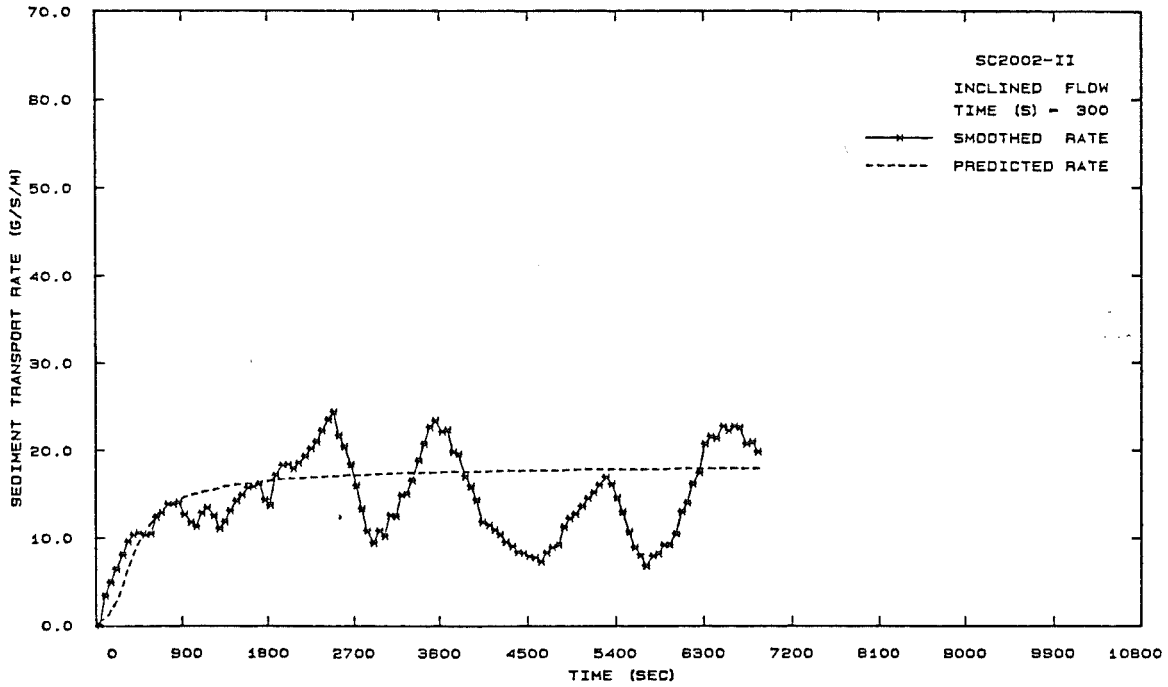

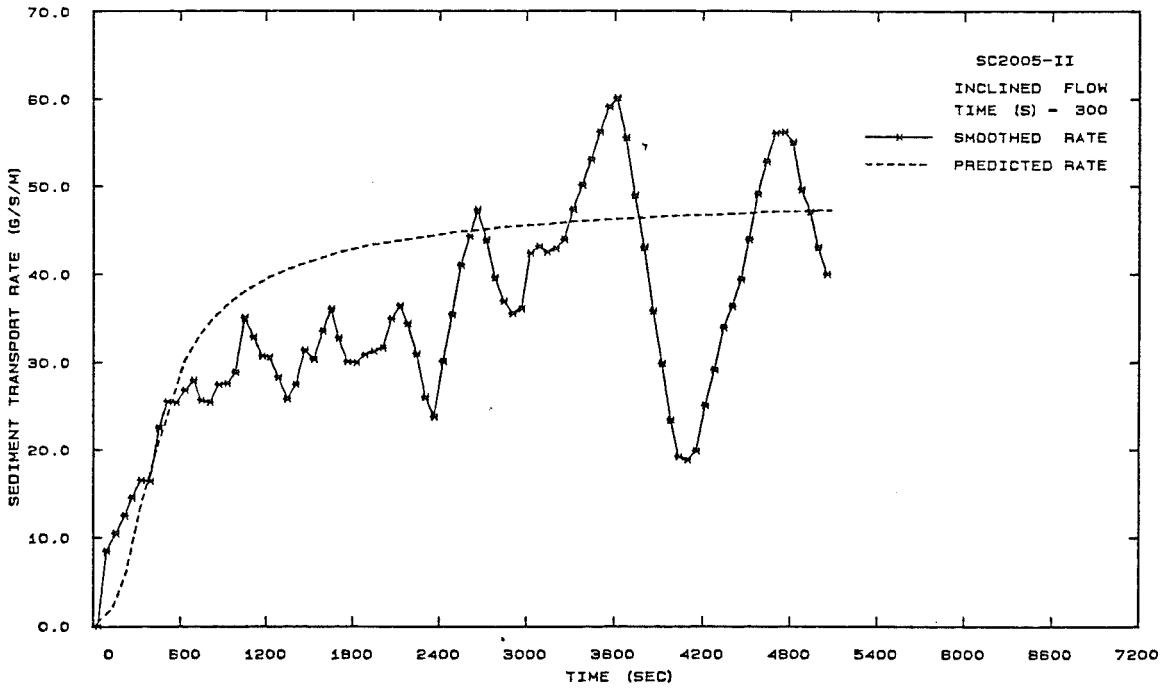

Fig. E.2 Temporal Lag Model Results - Bedload Transport Rates (Runs SC2002-II and SC2005-II)

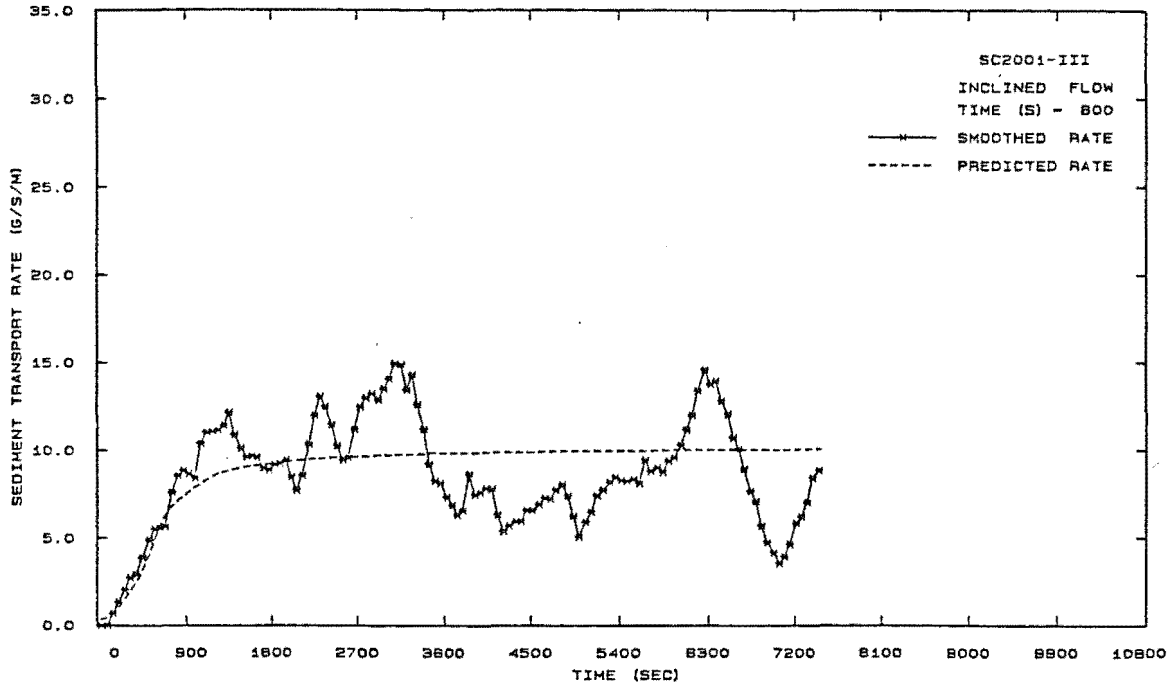

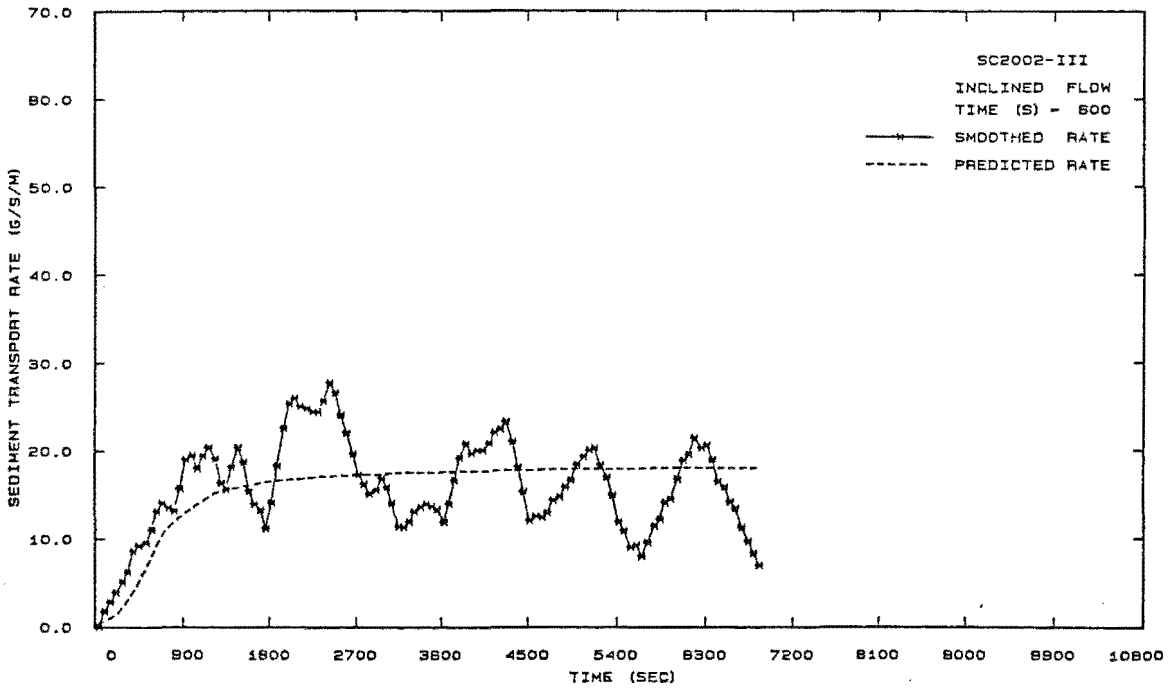

Fig. E.3.1 Temporal Lag Model Results - Bedload Transport Rates (Runs SC2001-III and SC2002-III)

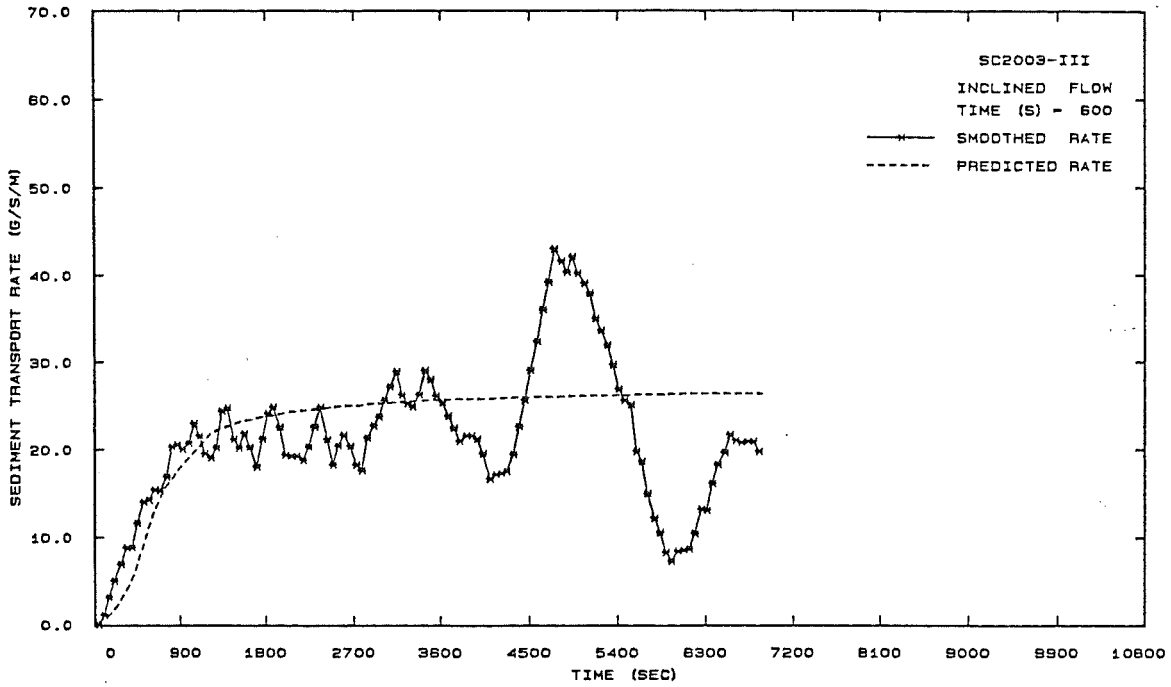

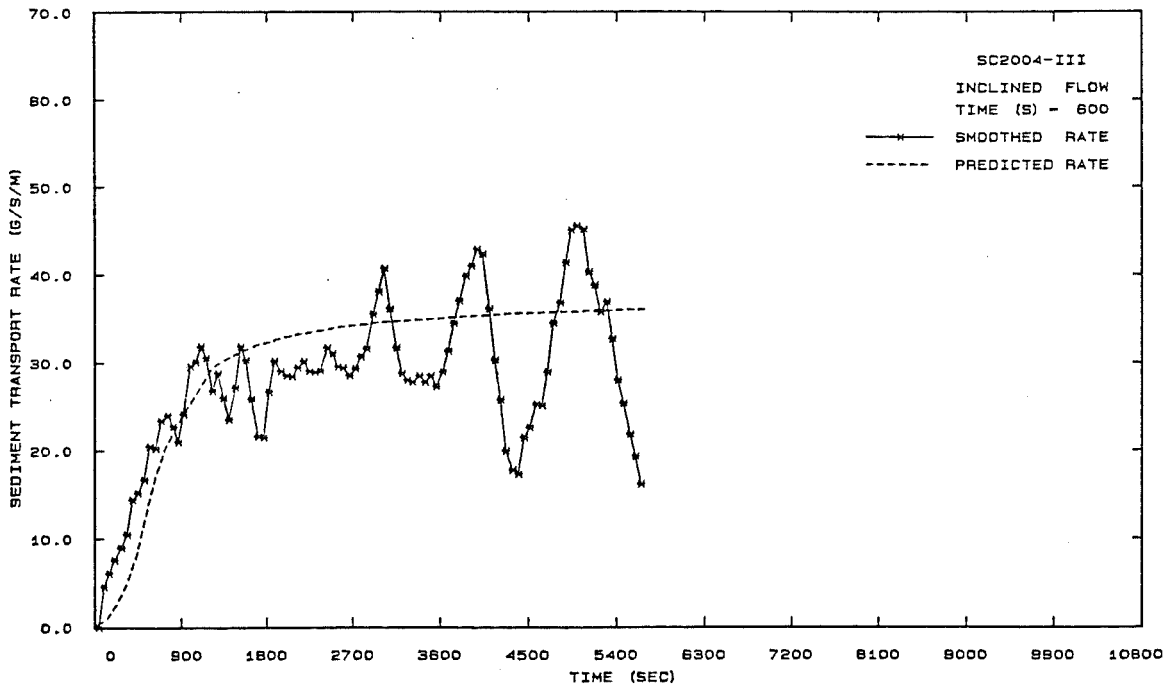

Fig. E.3.2 Temporal Lag Model Results - Bedload Transport Rates (Runs SC2003-III and SC2004-III)

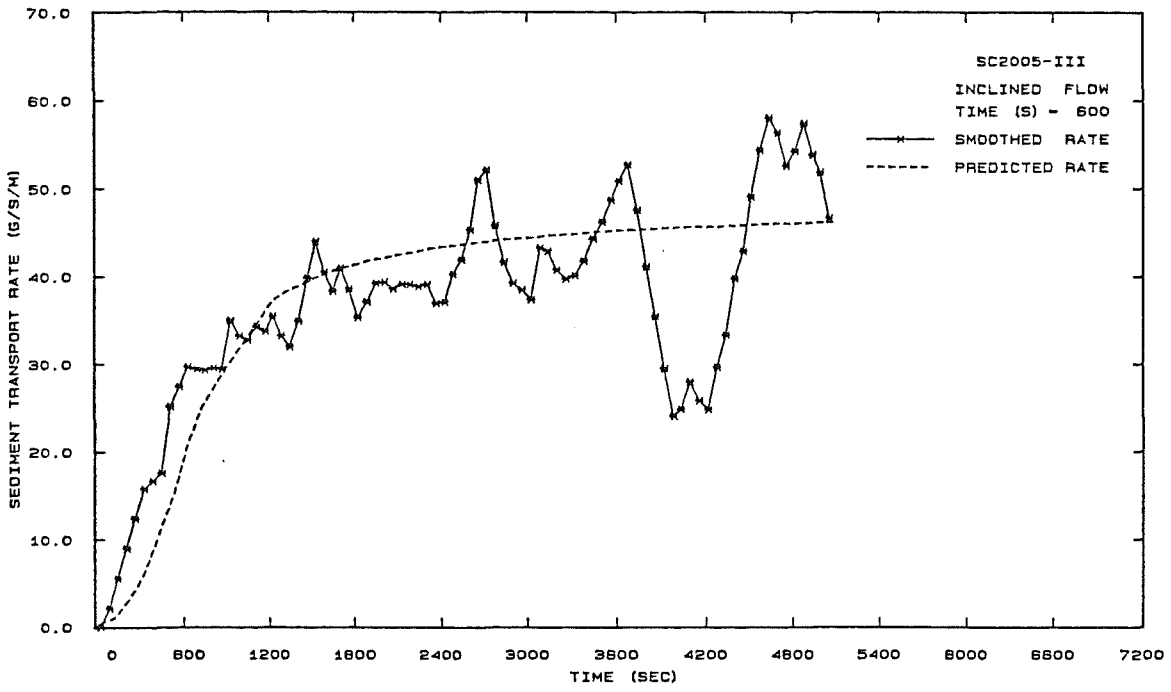

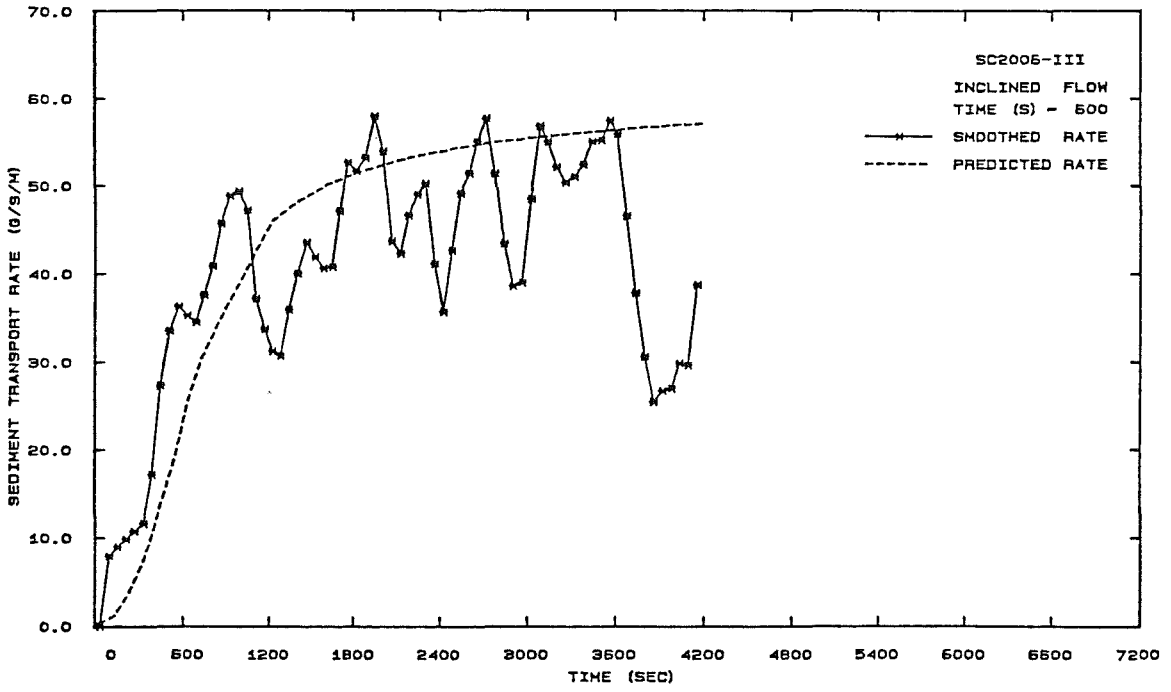

Fig. E.3.3 Temporal Lag Model Results - Bedload Transport Rates (Runs SC2005-III and SC2006-III)

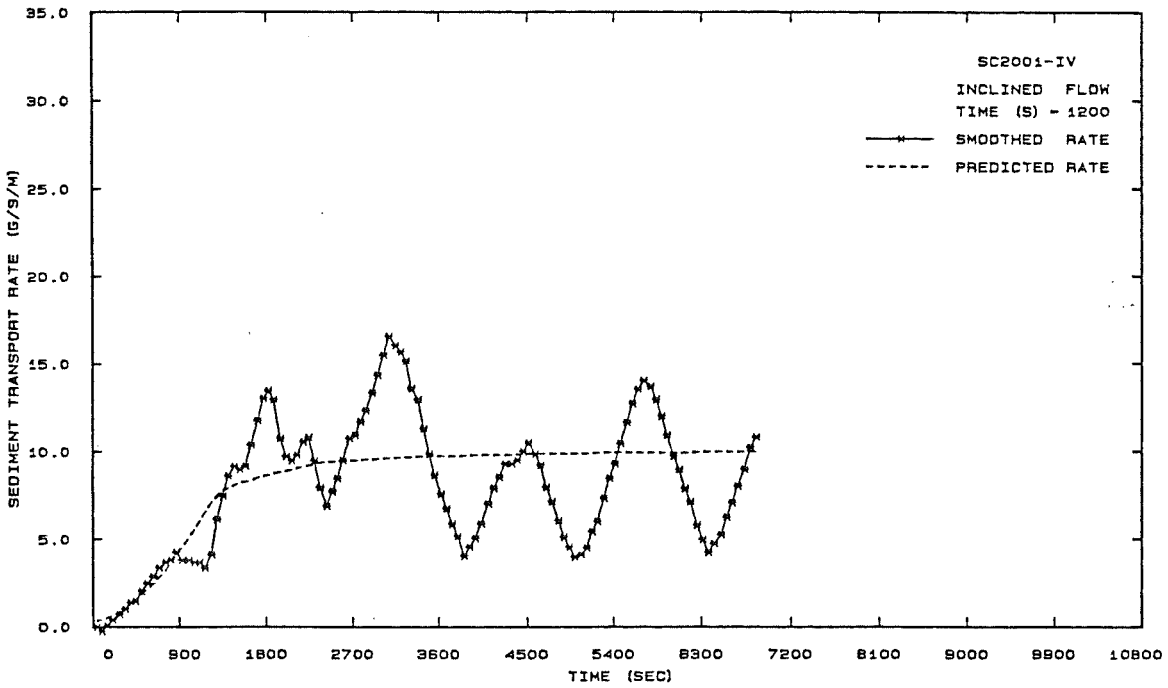

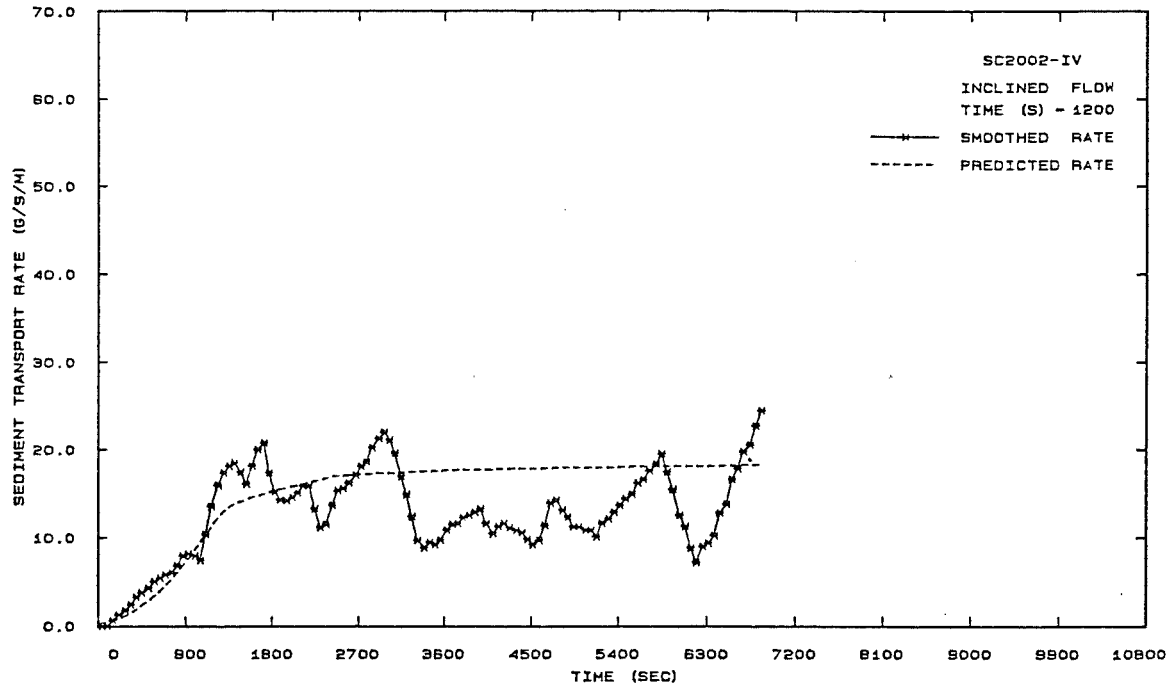

Fig. E.4.1 Temporal Lag Model Results - Bedload Transport Rates (Runs SC2001-IV and SC2002-IV)

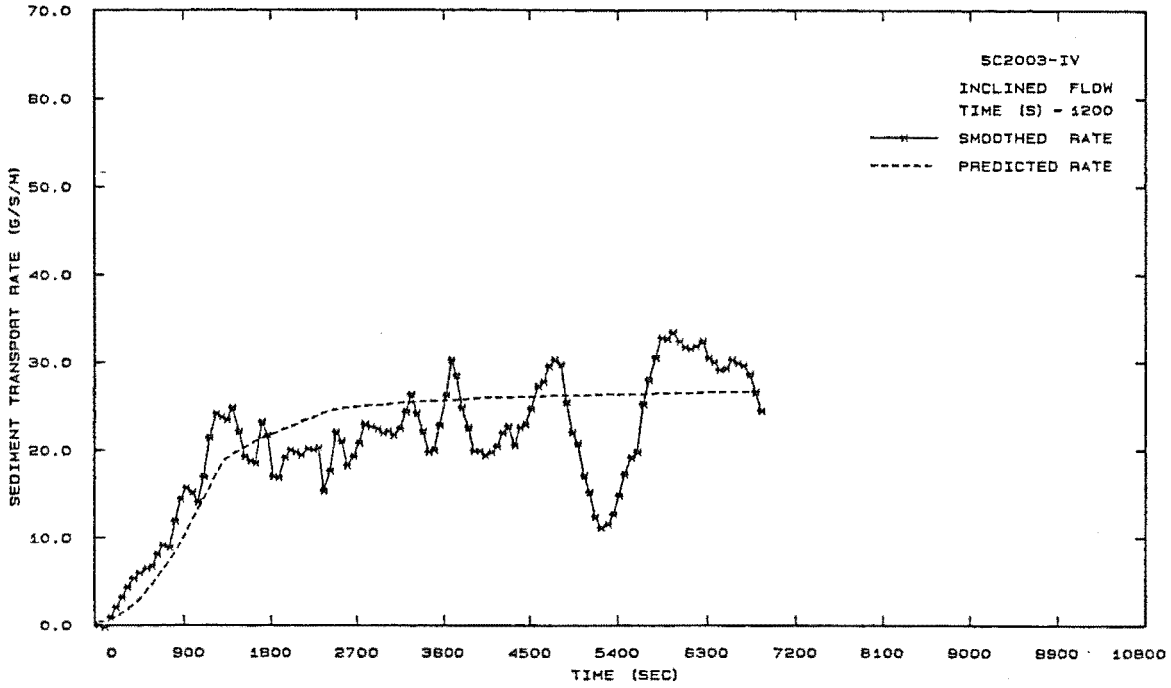

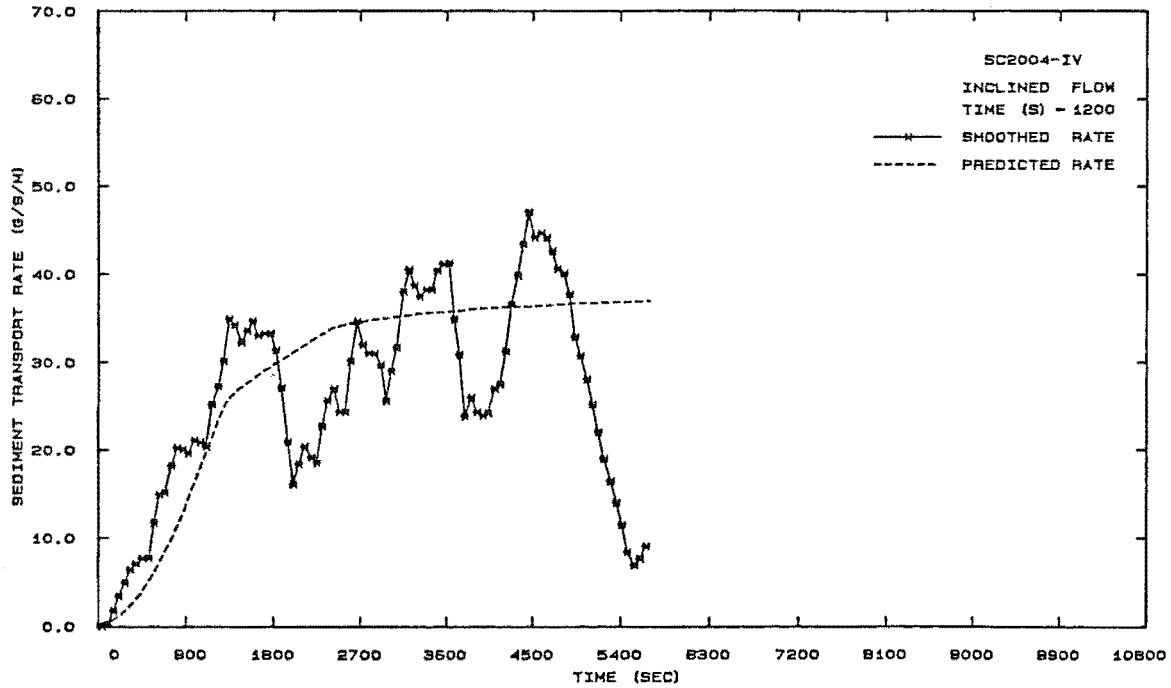

Fig. E.4.2 Temporal Lag Model Results - Bedload Transport Rates (Runs SC2003-IV and SC2004-IV)

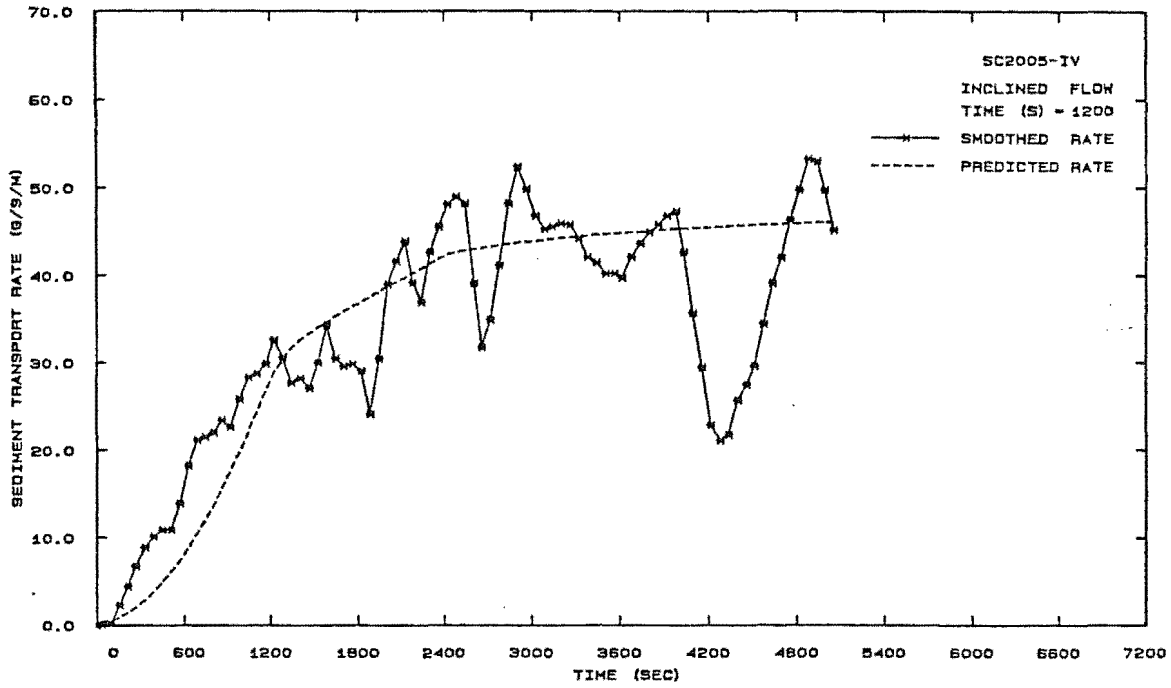

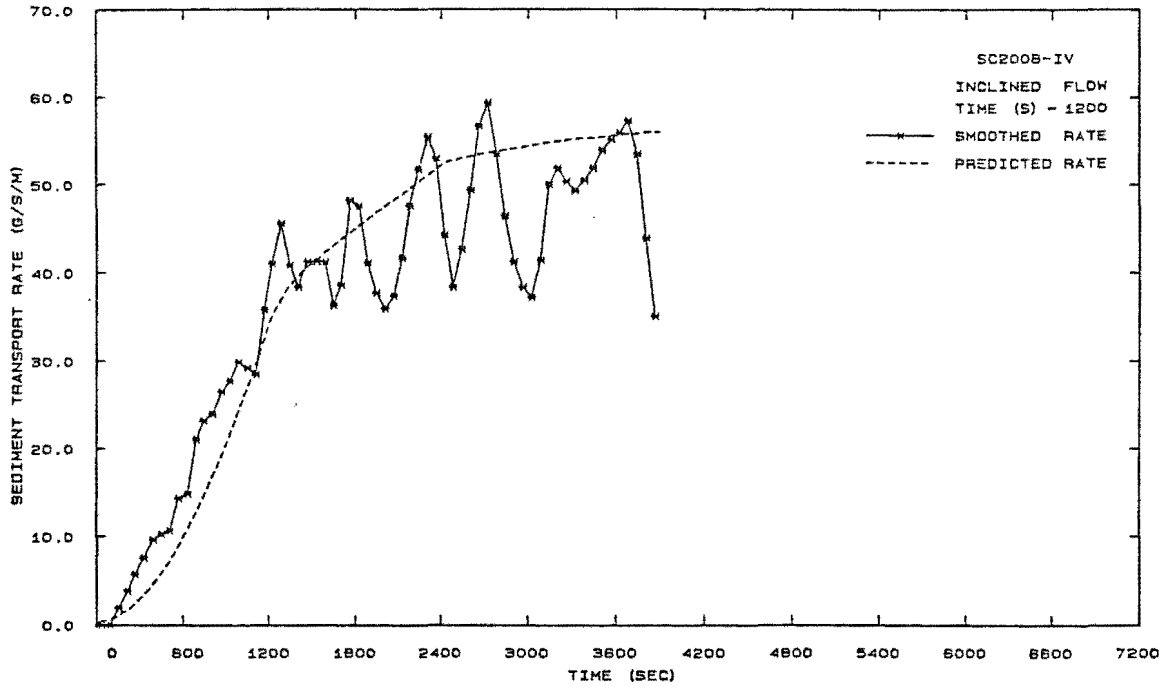

Fig. E.4.3 Temporal Lag Model Results - Bedload Transport Rates (Runs SC2005-IV and SC2006-IV)

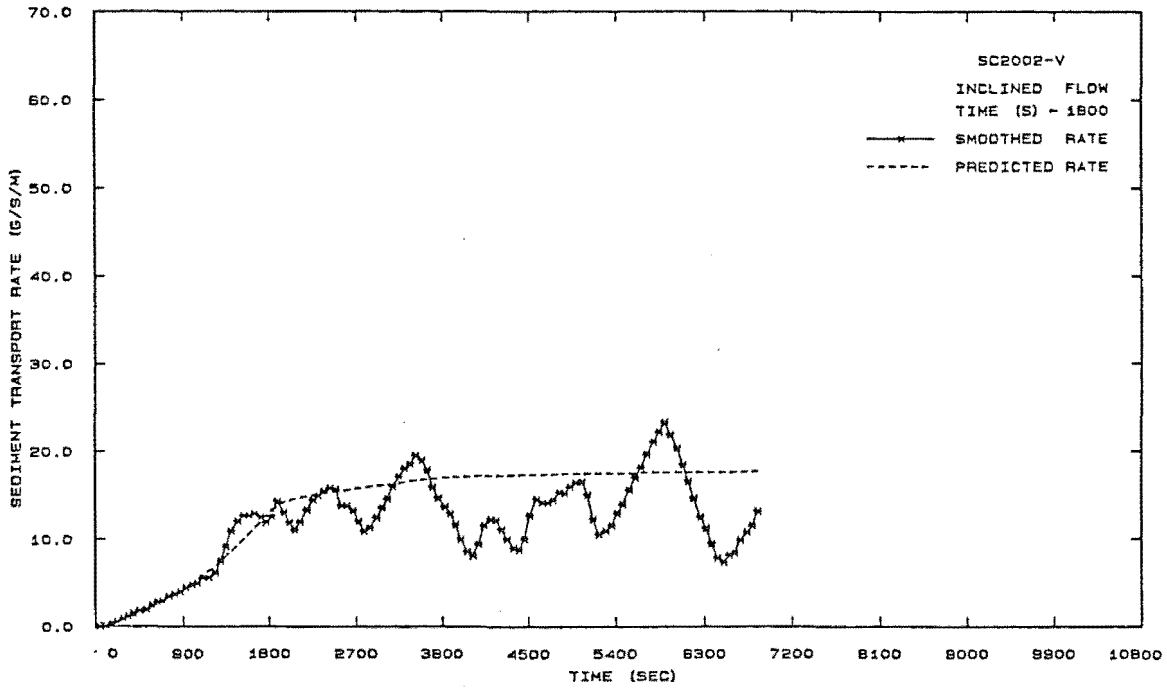

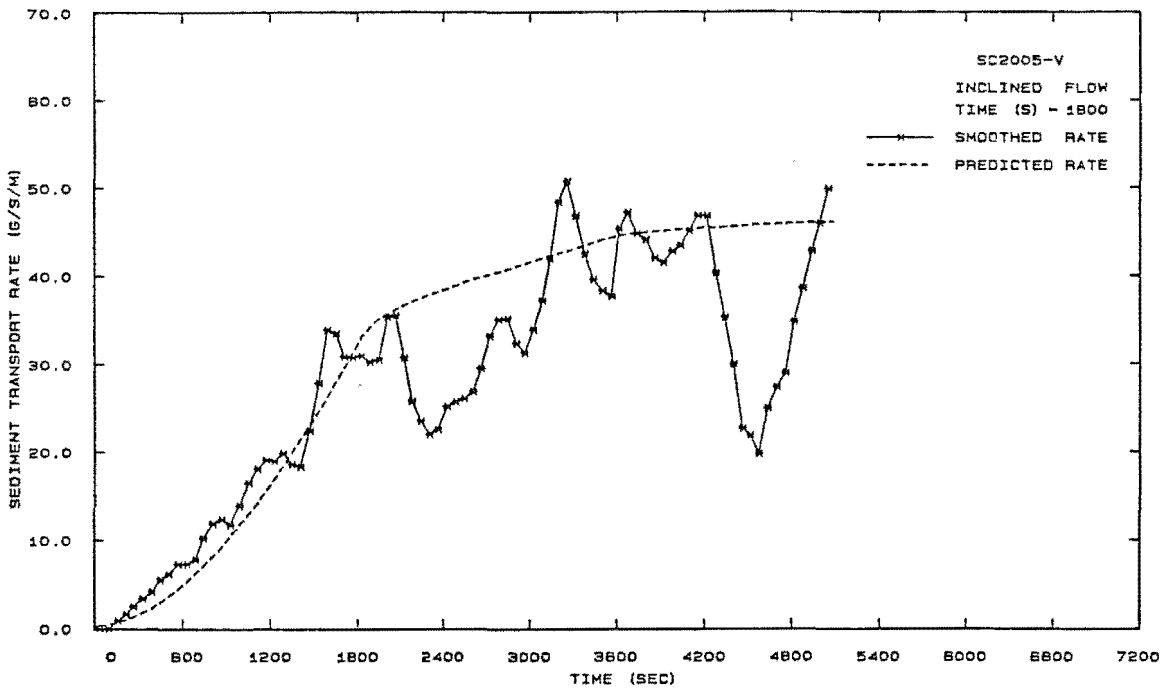

Fig. E.5 Temporal Lag Model Results - Bedload Transport Rates (Runs SC2002-V and SC2005-V)

Appendix F | Numerical Model Relations and Listing

F.1 IMPLICIT FINITE DIFFERENCE SCHEME COEFFICIENTS

The four basic equations used in the numerical model were discretized in the manner previously described in Sections 9.2.2 and 9.3.5. The discretized form of these equations and the full equation for each coefficient are as follows:

F.1.1 Flow Continuity

The discretized flow continuity equation is

$$Hl_j \Delta Z_{j+1} + Bl_j \Delta Q_{j+1} = Cl_j \Delta Z_j + Dl_j \Delta Q_j + Gl_j \qquad (F.1)$$

where

$$Hl_j = 1 - 4\theta \frac{\Delta t}{\Delta x} \left[\frac{Q_{j+1} - Q_j - \Delta x q_{\ell j}}{(B_{j+1} + B_j)^2} \right] \frac{dB_{j+1}}{dZ} \qquad (F.2)$$

$$Bl_j = 4\theta \frac{\Delta t}{\Delta x} \frac{1}{(B_{j+1} + B_j)} \qquad (F.3)$$

$$Cl_j = -1 + 4\theta \frac{\Delta t}{\Delta x} \left[\frac{Q_{j+1} - Q_j - \Delta x q_{\ell_j}}{(B_{j+1} + B_j)^2} \right] \frac{dB_j}{dZ} \qquad (F.4)$$

$$Dl_j = 4\theta \frac{\Delta t}{\Delta x} \frac{1}{(B_{j+1} + B_j)} \qquad (F.5)$$

$$Gl_j = 4 \frac{\Delta t}{\Delta x} \left[\frac{\Delta x(\theta \Delta q_{\ell_j} + q_{\ell_j}) - (Q_{j+1} - Q_j)}{(B_{j+1} + B_j)} \right] \qquad (F.6)$$

F.1.2 Flow Momentum

The discretized momentum equation is

$$H2_j \Delta Z_{j+1} + B2_j \Delta Q_{j+1} = C2_j \Delta Z_j + D2_j \Delta Q_j + G2_j \qquad (F.7)$$

where

$$H2_j = -\frac{1}{2}\left(\frac{Q_{j+1}B_{j+1}}{A_{j+1}} + \frac{Q_j B_j}{A_j}\right)$$

$$+ \theta \frac{\Delta t}{\Delta x}\left[(Q_{j+1} - Q_j)\left(\frac{Q_{j+1}}{A_{j+1}}\frac{d\alpha_{j+1}}{dZ} - \frac{Q_{j+1}B_{j+1}\alpha_{j+1}}{A_{j+1}^2}\right) + gB_{j+1}(Z_{j+1} - Z_j)\right.$$

$$\left. - (\alpha_{j+1} - \alpha_j)\frac{Q_{j+1}^2 B_{j+1}}{2A_{j+1}^2} + g(A_{j+1} + A_j) + \frac{1}{2}\left(\frac{Q_{j+1}^2}{A_{j+1}} + \frac{Q_j^2}{A_j}\right)\frac{d\alpha_{j+1}}{dZ}\right]$$

$$+ g\theta\Delta t\, B_{j+1}\frac{\left(Z_{b_{j+1}} - Z_{b_j}\right)}{\Delta x} - \frac{\theta\Delta t q_{\ell_j} Q_{j+1}B_{j+1}}{A_{j+1}^2}$$

$$- \theta\Delta t\left(\frac{\alpha_{j+1}Q_{j+1}^2}{A_{j+1}^2}\frac{dS_{a_{j+1}}}{dZ} + \frac{Q_{j+1}^2 S_{a_{j+1}}}{A_{j+1}^2}\frac{d\alpha_{j+1}}{dZ} - \frac{2B_{j+1}\alpha_{j+1}Q_{j+1}^2 S_{a_{j+1}}}{A_{j+1}^3}\right)$$

$$- \theta\frac{\Delta t}{\Delta x}\left[\frac{\alpha_{j+1}Q_{j+1}^2 B_{j+1}}{A_{j+1}^2} + \frac{\alpha_j Q_j^2 B_j}{A_j^2} + (Z_{j+1} - Z_j)\left(\frac{\alpha_{j+1}Q_{j+1}^2}{A_{j+1}^2}\frac{dB_{j+1}}{dZ}\right.\right.$$

$$\left.\left. + \frac{Q_{j+1}^2 B_{j+1}}{A_{j+1}^2}\frac{d\alpha_{j+1}}{dZ} - \frac{2\alpha_{j+1}Q_{j+1}^2 B_{j+1}^2}{A_j^3}\right)\right]$$

$$+ \frac{g\theta\Delta t Q_{j+1}|Q_{j+1}|}{K_{j+1}^2}\left(B_{j+1} - \frac{2A_{j+1}}{K_{j+1}}\frac{dK_{j+1}}{dZ}\right) \qquad (F.8)$$

$$B2_j = 1 + \theta\frac{\Delta t}{\Delta x}\left(\frac{\alpha_{j+1}Q_{j+1}}{A_{j+1}} + \frac{\alpha_j Q_j}{A_j} + (Q_{j+1} - Q_j)\frac{\alpha_{j+1}}{A_{j+1}} + (\alpha_{j+1} - \alpha_j)\frac{Q_{j+1}}{A_{j+1}}\right)$$

$$+ 2g\theta\Delta t\frac{A_{j+1}|Q_{j+1}|}{K_{j+1}^2} - 2\theta\Delta t\frac{\alpha_{j+1}Q_{j+1}S_{a_{j+1}}}{A_{j+1}^2} + 2\theta\frac{\Delta t}{\Delta x}(Z_{j+1} - Z_j)\frac{\alpha_j Q_j B_j}{A_j^2}$$

$$+ \theta\Delta t\frac{q_{\ell_j}}{A_{j+1}} \qquad (F.9)$$

$$C2_j = \frac{1}{2}\left(\frac{Q_{j+1}B_{j+1}}{A_{j+1}} + \frac{Q_jB_j}{A_j}\right) - \theta\frac{\Delta t}{\Delta x}\left[(Q_{j+1} - Q_j)\left(\frac{Q_j}{A_j}\frac{d\alpha_j}{dZ} - \frac{Q_jB_j\alpha_j}{A_j^2}\right)\right.$$

$$\left. + gB_j(Z_{j+1} - Z_j) - \frac{Q_j^2B_j}{2A_j^2}(\alpha_{j+1} - \alpha_j) - g(A_{j+1} + A_j) - \frac{1}{2}\left(\frac{Q_{j+1}^2}{A_{j+1}} + \frac{Q_j^2}{A_j}\right)\frac{d\alpha_i}{dZ}\right]$$

$$- g\theta\Delta t\, B_{j+1}\frac{\left(Z_{b_{j+1}} - Z_{b_j}\right)}{\Delta x} + \theta\Delta t\frac{q_{\ell_j}B_jQ_j}{A_j^2} + \theta\Delta t\left(\frac{\alpha_jQ_j^2}{A_j^2}\frac{dS_{a_j}}{dZ}\right.$$

$$\left. + \frac{Q_jS_{a_j}^2}{A_j^2}\frac{d\alpha_j}{dZ} - \frac{2B_j\alpha_jQ_j^2S_{a_j}}{A_j^3}\right) - \theta\frac{\Delta t}{\Delta x}\left[\frac{\alpha_{j+1}Q_{j+1}^2B_{j+1}}{A_{j+1}^2}\right.$$

$$\left. + \frac{\alpha_jQ_j^2B_j}{A_j^2} - (Z_{j+1} - Z_j)\left(\frac{\alpha_jQ_j^2}{A_j^2}\frac{dB_j}{dZ} + \frac{Q_j^2B_j}{A_j^2}\frac{d\alpha_j}{dZ} - \frac{2\alpha_jQ_j^2B_j^2}{A_j^3}\right)\right]$$

$$- \frac{g\theta\Delta tQ_j|Q_j|}{K_j^2}\left(B_j - \frac{2A_j}{B_j}\frac{dK_j}{dZ}\right) \qquad \text{(F.10)}$$

$$D2_j = -1 - \theta\frac{\Delta t}{\Delta x}\left(-\frac{\alpha_{j+1}Q_{j+1}}{A_{j+1}} - \frac{\alpha_jQ_j}{A_j} + (Q_{j+1} - Q_j)\frac{\alpha_j}{A_j} + (\alpha_{j+1} - \alpha_j)\frac{Q_j}{A_j}\right)$$

$$- 2g\theta\Delta t\frac{A_j|Q_j|}{K_j^2} + 2\theta\Delta t\frac{\alpha_jQ_jS_{a_j}}{A_j^2} + 2\theta\frac{\Delta t}{\Delta x}\frac{(Z_{j+1} - Z_j)\alpha_jQ_jB_j}{A_j^2} - \theta\frac{\Delta t}{A_j}q_{\ell_j}$$

.... (F.11)

$$G2_j = -\frac{\Delta t}{\Delta x}\left[(Q_{j+1} - Q_j)\left(\frac{\alpha_{j+1}Q_{j+1}}{A_{j+1}} + \frac{\alpha_jQ_j}{A_j}\right) + g(Z_{j+1} - Z_j)(A_{j+1} + A_j)\right.$$

$$\left. + (\alpha_{j+1} - \alpha_j)\left(\frac{Q_{j+1}^2}{2A_{j+1}} + \frac{Q_j^2}{2A_j}\right)\right] + \Delta t\left(\frac{\alpha_{j+1}Q_{j+1}^2S_{a_{j+1}}}{A_{j+1}^2} + \frac{\alpha_jQ_j^2S_{a_j}}{A_j^2}\right)$$

$$+ \frac{\Delta t}{\Delta x}(Z_{j+1} - Z_j)\left(\frac{\alpha_{j+1}Q_{j+1}^2B_{j+1}}{A_{j+1}} + \frac{\alpha_jQ_j^2B_j}{A_j^2}\right) - \Delta tq_{\ell_j}\left(\frac{Q_{j+1}}{A_{j+1}} + \frac{Q_j}{A_j}\right)$$

$$- \theta\Delta t\Delta q_{\ell_j}\left(\frac{Q_{j+1}}{A_{j+1}} + \frac{Q_j}{A_j}\right) - g\theta\Delta t(A_{j+1} + A_j)\left(\frac{Z_{b_{j+1}} - Z_{b_j}}{\Delta x}\right) \qquad \text{(F.12)}$$

and $$S_a = \left.\frac{\partial A}{\partial x}\right|_Z$$

F.1.3 Sediment Continuity

The discretised sediment continuity equation is

$$H3_j \Delta G_{V_{j+1}} + B3_j \Delta A_{b_{j+1}} = C3_j \Delta G_{V_j} + D3_j \Delta A_{b_j} + G3_j$$

where

$$H3_j = 2\theta \frac{\Delta t}{\Delta x} + \frac{2}{\theta(\Delta u_{s_{j+1}} + \Delta u_{s_j}) + (u_{s_{j+1}} + u_{s_j})} - \frac{\theta}{2} \frac{(\Delta u_{s_{j+1}} + \Delta u_{s_j})}{(u_{s_{j+1}} + \Delta u_{s_{j+1}})^2} \quad \ldots\ (F.13)$$

$$B3_j = (1 - \lambda') \quad (F.14)$$

$$C3_j = -\left[-2\theta \frac{\Delta t}{\Delta x} + \frac{2}{\theta(\Delta u_{s_{j+1}} + \Delta u_{s_j}) + (u_{s_{j+1}} + u_{s_j})} - \frac{\theta}{2} \frac{(\Delta u_{s_{j+1}} + \Delta u_{s_j})}{(u_{s_j} + \Delta u_{s_j})^2}\right] \quad \ldots\ (F.15)$$

$$D3_j = -(1 - \lambda') \quad (F.16)$$

$$G3_j = (\Delta u_{s_{j+1}} + \Delta u_{s_j}) \left[\frac{\theta}{2}\left(\frac{G_{V_{j+1}}}{(u_{s_{j+1}} + \Delta u_{s_{j+1}})^2} + \frac{G_{V_j}}{(u_{s_j} + \Delta u_{s_j})^2}\right) + \frac{(1 - \theta)}{2}\left(\frac{G_{V_{j+1}}}{u_{s_{j+1}}^2} + \frac{G_{V_j}}{u_{s_j}^2}\right)\right] - 2 \frac{\Delta t}{\Delta x}(G_{V_{j+1}} - G_{V_j}) \quad (F.17)$$

F.1.4 Spatial Lag

The discretised spatial lag equation is

$$H4_j \Delta G_{V_{j+1}} + B4_j \Delta A_{b_{j+1}} = C4_j \Delta G_{V_j} + D4_j \Delta A_{b_j} + G4_j \quad (F.18)$$

$$H4_j = -\Delta t(C_{SL_{j+1}} + \Delta C_{SL_{j+1}}) \quad (F.19)$$

$$B4_j = (1 - \lambda') \quad (F.20)$$

$$C4_j = \Delta t(C_{SL_j} + \Delta C_{SL_j}) \quad (F.21)$$

$$D4_j = -(1 - \lambda') \quad (F.22)$$

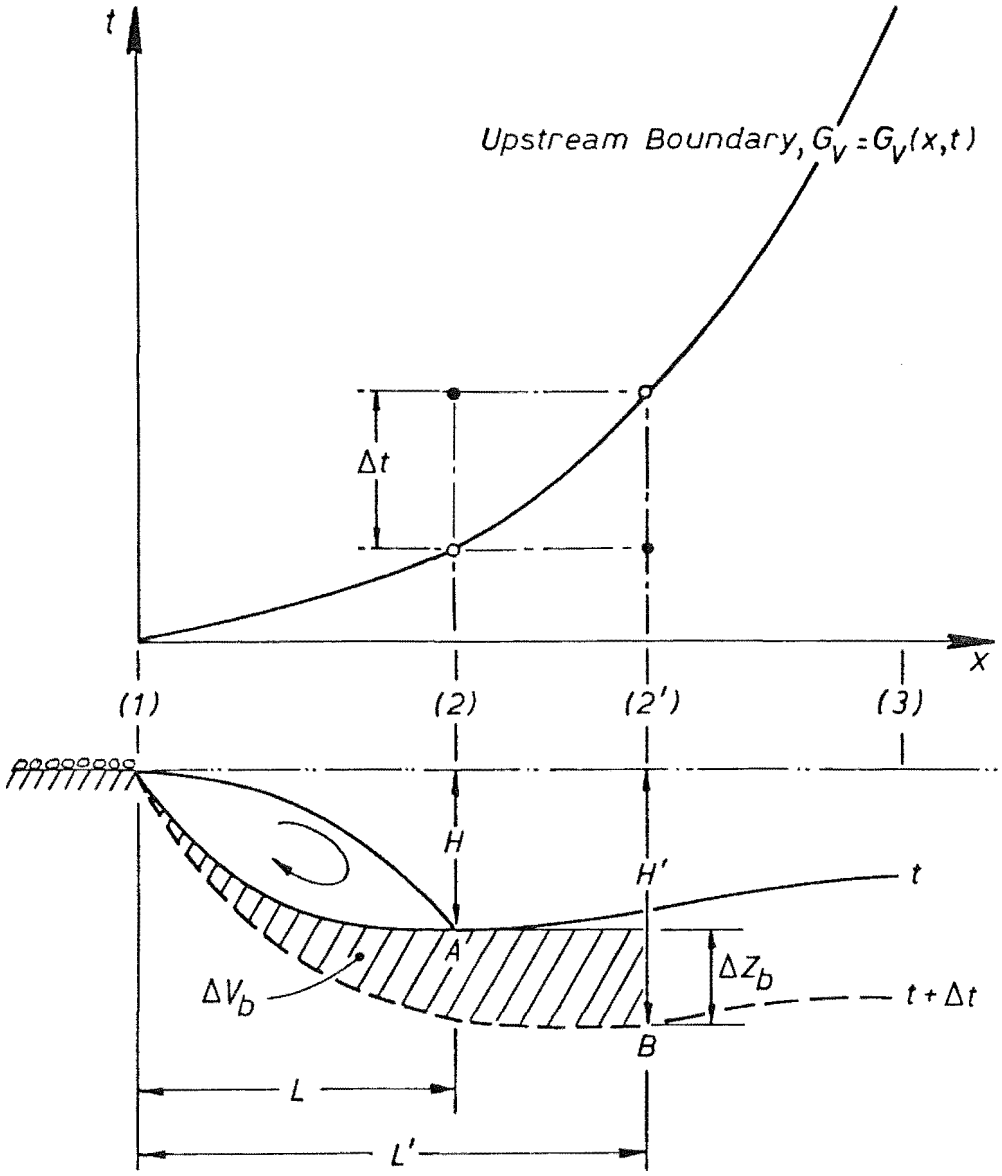

Figure F.1 Definition Diagram for Upstream Sediment Boundary Condition

$$G4_j = \Delta t[(C_{SL_{j+1}} + \Delta C_{SL_{j+1}})\ (G_{V_{j+1}} - \theta(G_{VC_{j+1}} + \Delta G_{VC_{j+1}}))$$

$$+ (C_{SL_j} + \Delta C_{SL_j})\ (G_{V_j} - \theta(G_{VC_j} + \Delta G_{VC_j}))$$

$$- (1 - \theta)\ (G_{VC_{j+1}} C_{SL_{j+1}} + G_{VC_j} C_{SL_j})] \qquad \text{(F.23)}$$

F.2 UPSTREAM SEDIMENT BOUNDARY SCHEME

The aim of the upstream boundary scheme is to calculate the sediment transport rate, at the toe of the vortex, on the forward time line. On the current time line, the toe of the vortex, is located at section 2 (Fig. F.1). However, on the forward time line, the toe of the vortex, is located a section 2'. In order to locate section 2' and to calculate the sediment transport rate on the forward time line it is necessary to solve the spatial lag equation. At section 2, the discretised form of this equation is

$$H4_2 \Delta G_{V_2} + B4_2 \Delta A_{b_2} = C4_2 \Delta G_{V_2} + D4_2 \Delta A_{b_2} + G4_2 \qquad \text{(F.24)}$$

Re-arranging, gives

$$(B4_2 - D4_2)\ \Delta A_{b_2} = (C4_2 - H4_2)\ \Delta G_{V_2} + G4_2 \qquad \text{(F.25)}$$

Substituting the expressions for each coefficient, from Eqs. F.19 - F.23, into Eq. F.25 gives

$$2(1 - \lambda')\Delta A_{b_2} = 2\Delta t(C_{SL_2} + \Delta C_{SL_2})\ \Delta G_{V_2}$$

$$+ 2\Delta t(C_{SL_2} + \Delta C_{SL_2})\ (G_{V_2} - \theta(G_{VC_2} + \Delta G_{VC_2}))$$

$$- 2\Delta t(1 - \theta)\ C_{SL_2} G_{VC_2} \qquad \text{(F.26)}$$

Re-arranging Eq. F.26 gives

$$(1 - \lambda')\frac{\Delta A_{b_2}}{\Delta t} = (C_{SL_2} + \Delta C_{SL_2})\ (G_{V_2} + \Delta G_{V_2})$$

$$- \theta(C_{SL_2} + \Delta C_{SL_2})\ (G_{VC_2} + \Delta G_{VC_2}) - (1 - \theta)\ C_{SL_2} G_{VC_2}$$

.... (F.27)

Since the boundary sediment scheme is only applicable under conditions of scour, it was assumed that for purposes of this scheme that scour is positive. Hence, Eq. F.27 becomes (Fig. F.1)

$$(1 - \lambda')\frac{\Delta A_{b_2}}{\Delta t} \simeq (1 - \lambda')B\frac{\Delta Z_b}{\Delta t} = -C(G_{V_2} + \Delta G_{V_2}) + G \qquad (F.28)$$

where ΔZ_b = Change local maximum scour depth over time Δt

and $$C = C_{SL_2} + \Delta C_{SL_2} \qquad (F.29)$$

$$G = \theta(C_{SL_2} + \Delta C_{SL_2})(G_{VC_2} + \Delta G_{VC_2}) + (1 - \theta)\, C_{SL_2} G_{VC_2} \qquad (F.30)$$

It should also be noted that the term $(G_{V_2} + \Delta G_{V_2})$ is the sediment transport rate on the forward time line, at section 2.

From the geometry of the scour hole it was found (Section 9.3.6) that the sediment transport rate on the forward time line, at section 2', is given by

$$(G_{V_{2'}} + \Delta G_{V_{2'}}) = \frac{(1 - \lambda')B\Delta V_b}{\Delta t} + G_{V_1} \qquad (F.31)$$

Since section 2 and 2' are close together it was assumed that, on the forward time line, that the sediment transport rates at section 2 and 2' are equal. Thus

$$(G_{V_2} + \Delta G_{V_2}) = (G_{V_{2'}} + \Delta G_{V_{2'}}) \qquad (F.32)$$

Substituting Eqs. F.32 and F.31 into Eq. F.28 and re-arranging gives

$$\frac{(1 - \lambda')B\Delta V_b}{\Delta t} + G_{V_1} = \frac{G}{C} - (1 - \lambda')\frac{B}{C}\frac{\Delta Z_b}{\Delta t} \qquad (F.33)$$

Re-arranging Eq. F.33 further, gives

$$\Delta V_b = \left(\frac{G}{C} - G_{V_1}\right)\frac{\Delta t}{(1 - \lambda')B} - \frac{\Delta Z_b}{C} \qquad (F.34)$$

Over the time increment, Δt, it was found (Section 9.3.6) that

$$\Delta V_b = 0.791H'L' - 0.791HL - H(L' - L) \qquad (F.35)$$

On the current time line the location, L, and depth of local maximum scour, H, and the scour hole steepness are known. Assuming that the scour hole steepness is constant over the time increment, then

$$\frac{L}{H} = \frac{L'}{H'} = S_H \tag{F.36}$$

thus

$$L' = S_H H' \tag{F.37}$$

Also, (Fig. F.1)

$$H' = H + \Delta Z_b \tag{F.38}$$

Thus, Eq. F.37 becomes

$$L' = S_H(H + \Delta Z_b) \tag{F.39}$$

Substituting Eqs. F.38 and F.39 into Eq. F.35 gives

$$V_b = 0.791\ S_H(H + \Delta Z_b)^2 - 0.791LH - H(S_H(H + \Delta Z_b) - L) \tag{F.40}$$

Substituting Eq. F.40 into Eq. F.34 and gathering terms gives

$$EE\Delta Z_b^2 + FF\Delta Z_b + GG = 0 \tag{F.41}$$

where

$$EE = 0.791\ \frac{L}{H}$$

$$FF = 0.582\ S_H H + \frac{1}{C}$$

$$GG = 0.209(LH - S_H H^2) - \frac{\Delta t}{(1 - \lambda')B}\left(\frac{G}{C} - G_{V_1}\right)$$

Once Eq. F.41 has been solved iteratively for ΔZ_b it is possible to calculate the location of section 2' from Eqs. F.38 and F.37.

Once section 2' has been located the sediment boundary is moved to this location; the sediment transport rate, on the current time line, is interpolated and the sediment boundary condition is calculated, where the boundary condition is

$$\Delta G_{V_{2'}} = G_{V_{2'}}(t + \Delta t) - G_{V_{2'}}(t) \tag{F.42}$$

In order to calculate the location of section 2' in the manner outlined above it is necessary to initially route the flow and obtain flow

properties on the forward time line. Once the upstream sediment boundary has been moved to section 2' the flow routing phase is again undertaken and the sediment boundary condition is defined. Once sediment routing is completed it is possible to compare the predicted change in bed elevation ΔZ_b with that obtained from the full sediment routing phase. This check is incorporated in the model (see Section 10.3.2).

F.3 INPUT DATA FOR NUMERICAL MODEL (UWASER)

Variable	Format	Description
GENERAL		
TITLE(16)	(16A5)	Title of simulation run.
INFO(16)	(16A5)	Information about simulation run.
OPTION	(I5)	= 0 Flow routing only, or = 1 Flow and sediment routing
THETA	(F10.4)	Weighting coefficient in finite difference scheme ($0 < \theta < 1$).
NDT		Number of time increments used in the simulation ($NDT \leq 20$).
DTS(I)	(I=1,NDT) (I5,/(3F10.3))	Time increments in the simulation (s).
TMAXS(I)		Maximum time until which a given time increment applies (TMAXS(NDT) is the maximum simulation time) (s).
TINCRS(I)		Time increments at which tables of results are printed.
CHANNEL GEOMETRY		
N	(2I5)	Number of computational points ($N \leq 50$).
NCROSS		Number of representative cross sections.

Variable	Format	Description
NSEC		Cross section number.
NP(NSEC)	(2I5,2F10.2,F10.5)	Number of points used to define a cross section (NP $\leq$ 12).
XNODE(NSEC)		Chainage of a cross section (m).
DDX		Uniform distance increment for internal cross sections between representative sections (m).
MANN(NSEC)		Manning bed roughness value for a cross section.
YB(NSEC,L) (L=1,NP(NSEC))	(8F10.4)	Lateral location of a cross section point (m).
ZB(NSEC,L)		Bed elevation of a cross section point (m).

The geometry, location and Manning bed roughness value of internal cross sections are linearly interpolated from the geometries and properties of adjacent representative cross sections.

INITIAL FLOW CONDITIONS

Q(J) (J=1,N)	(8F10.4)	Initial flow rate at a section (m^3/s).
Z(J) (J=1,N)	(8F10.4)	Initial water surface elevation at a section (m).

FLOW BOUNDARY CONDITIONS

NPQ	(I10,/(5F10.4))	Number of points used to define the upstream flow hydrograph (NPQ $\leq$ 20).
QQ(I) (I=1,NPQ)		Upstream flow hydrograph (m^3/s).
TQ(I) (I=1,NPQ)	(5F10.4)	Time associated with flow hydrograph (s).
NTYPE	(I5)	Number of representative lateral inflow hydrographs (NTYPE $\leq$ 50).

Variable	Format	Description
NQ	(I10,/(5F10.4))	Number of points used to define representative lateral inflow hydrographs (NQ ≤ 10).
QIL(I,J) (I=1,NQ) (J=1,NTYPE)		Lateral inflow hydrographs (m^3/s). Lateral inflow (+) and lateral outflow (-) are uniformly distributed along each sub-reach.
TIL(I,J) (I=1,NQ) (J=1,NTYPE)	(5F10.4)	Time associated with the representative lateral inflow hydrographs (s).
LCODE(I) (I=1,N-1)	(16I5)	Code number of the representative lateral inflow hydrograph which occurs at a given sub-reach.

SEDIMENT PROPERTIES

D35	(3F10.6,3F10.4,F10.9,F10.4)	Grain size which is 35% finer (m).
D50		Grain size which is 50% finer (m).
D65		Grain size which is 65% finer (m).
POROS		Porosity of bed material.
SG		Specific gravity of bed material.
THETC		Threshold value of Shields Parameter.
VISCOS		Fluid kinematic viscosity (m^2/s).
W		Grain fall velocity (m/s).
COEFA	(2F10.4)	Coefficient of assumed bedload capacity relation.
COEFB		Exponent of assumed bedload capacity relation (Relation assumes the units of bedload transport capacity are N/s/m).
NL	(I5)	Section number of mobile section in the upstream sediment boundary scheme.
GS(I) (I=1,N)	(5F10.5)	Initial sediment transport rate at a section (N/s/m).

Variable	Format	Description
SEDIMENT BOUNDARY CONDITIONS		
NPG	(I10,/5F10.5)	Number of points used to define the upstream sediment boundary hydrograph (NPG $\leq$ 20).
GB(I) (I=1,NPG)		Upstream sediment boundary hydrograph (N/s/m)
TG(I) (I=1,NPG)	(5F10.5)	Time associated with upstream sediment boundary hydrograph.

All boundary flow, lateral inflow and sediment hydrographs must be specified for times equal to or greater than the maximum simulation time.

F.4 NUMERICAL MODEL LISTING (UWASER)

F.4.1 UWASER Listing

A listing of the numerical model which simulates spatial lag effects is presented below. This model is in the form used to simulate flow and sediment conditions in a rectangular channel. Program modifications for the case of a complex channel geometry are also listed in the program (see subroutines ADJUST and PROPS). Temporal lag effects were simulated by modifying this program in the manner outlined in Section F.4.2.

```
C
C ***************************************************************************
C
C                              U W A S E R
C
C     UNSTEADY WATER AND SEDIMENT ROUTING MODEL DEVELOPED BY B.PHILLIPS
C     AT THE UNIVERSITY OF CANTERBURY, CHRISTCHURCH, NEW ZEALAND (1983)
C
C     THE PROGRAM ROUTES BOTH WATER AND SEDIMENT THROUGH A NON-UNIFORM
C     CHANNEL.FLOW ROUTING IS ACCOMPLISHED BY EMPLOYING IMPLICIT FINITE
C     DIFFERENCE TECHNIQUES TO SOLVE THE EQUATIONS OF FLOW CONTINUITY
C     AND MOMENTUM. SEDIMENT ROUTING IS ACCOMPLISHED BY EMPLOYING GAUSS
C     IAN ELIMINATION TECHNIQUES TO SOLVE THE EQUATIONS OF SEDIMENT CON
C     TINUITY AND LOCAL TRANSPORT
C
C
C ***************************************************************************
C
C
C                              VARIABLES
C                              *********
C
C     A         - CROSS SECTIONAL AREA OF FLOW
C     AA        - CHANGE IN CROSS SECTIONAL AREA W.R.T. DISTANCE FOR A
C                 GIVEN STAGE (DEVIATION FROM PRISMATIC CHANNEL)
C     ALPHA     - VELOCITY DISTRIBUTION COEFFICIENT
C     ALPDER    - RATE OF CHANGE OF ALPHA W.R.T. DEPTH
C     ASTAR     - DIMENSIONLESS GRAIN SIZE
C
C     B         - TOP WIDTH
C     BB        - RATE OF CHANGE OF AA W.R.T. DEPTH
C     BDERIV    - RATE OF CHANGE OF TOP WIDTH W.R.T. DEPTH
C     BDYVOL    - STORAGE VOLUME
C     BEDVL     - VOLUME OF BED ERODED OR DEPOSITED
C
C     COEF      - DEPOSITION RATE COEFFICIENT ON T TIME LINE
C     COEF1     - DEPOSITION RATE COEFFICIENT ON T+1 TIME LINE
C     COEFA     - COEFFICIENT IN EQUILIBRIUM SEDIMENT DISCHARGE FORMULA
C     COEFB     - EXPONENT IN EQUILIBRIUM SEDIMENT DISCHARGE FORMULA
C     CSOLVE    - MATRIX OF COEFFICIENTS FROM SEDIMENT FINITE DIFFERENCE
C                 SCHEME
C
C     DABED     - CHANGE IN AREA OF SCOUR/DEPOSITION DURING TIME
C                 INCREMENT DT
C     DCOEF     - CHANGE IN DEPOSITION RATE COEFFICIENT DURING TIME
C                 INCREMENT DT
C     DDX       - DISTANCE INCREMENT BETWEEN INTERNAL SECTIONS
C     DELTA     - FLOW PARAMETER (AFTER DIETZ (1969))
C     DEPTH     - FLOW DEPTH
C     DG        - CHANGE IN SEDIMENT DISCHARGE DURING TIME INCREMENT DT
C     DH        - CHANGE IN SCOUR DEPTH OVER TIME INCREMENT
C     DLAT      - CHANGE IN LATERAL INFLOW DURING TIME INCREMENT DT
C     DQ        - CHANGE IN DISCHARGE DURING TIME INCREMENT DT
C     DT        - TIME INCREMENT ADOPTED FOR THE RECTANGULAR MESH
C     DTS       - TIME INCREMENTS IN SIMULATION
C     DUSED     - CHANGE IN SEDIMENT VELOCITY DURING TIME INCREMENT DT
C     DZ        - CHANGE IN STAGE DURING TIME INCREMENT DT
C     D35       - GRAIN SIZE WHICH IS 35 % FINER
C     D50       - GRAIN SIZE WHICH IS 50 % FINER
C     D65       - GRAIN SIZE WHICH IS 65 % FINER
C
C     G         - GRAVITATIONAL CONSTANT = 9.81
C     GB        - INFLOW SEDIMENT HYDROGRAPH
C     GS        - SEDIMENT DISCHARGE
C     GSE       - SEDIMENT TRANSPORT CAPACITY - ON THE T TIME LINE
C     GSE1      -                             - ON THE T+1 TIME LINE
C     GSF       - SEDIMENT TRANSPORT RATE ON FOWARD TIME LINE
C
C     INFO      - GENERAL INFORMATION
C
C     K         - TOTAL CONVEYANCE
C     KDERIV    - RATE OF CHANGE OF TOTAL CONVEYANCE W.R.T. DEPTH
C
C     LCODE     - CODE NUMBER OF THE REPRESENTATIVE LATERAL INFLOW
C                 HYDROGRAPH FOR A GIVEN SUB-REACH
C
C     MANN      - MANNING'S N VALUE
C
C     N         - NUMBER OF COMPUTATIONAL POINTS (NODES) IN REACH N  <50
C     NCROSS    - NUMBER OF REPRESENTATIVE CROSS SECTIONS          N  <50
C     NDT       - NUMBER OF TIME INCREMENTS USED IN SIMULATION     NDT<20
C     NL        - SECTION NUMBER OF MOBILE SECTION IN UPSTREAM
C                 SEDIMENT BOUNDARY SCHEME
C     NP        - NUMBER OF POINTS USED TO DEFINE A CROSS SECTION NP <12
C     NPG       - NUMBER OF POINTS USED TO DEFINE SED. HYDROGRAPH NPG<20
C     NPQ       - NUMBER OF POINTS USED TO DEFINE FLOW HYDROGRAPH NPQ<20
```

```
C     NQ        - NUMBER OF POINTS USED TO DEFINE LATERAL INFLOW
C                 HYDROGRAPHS                                        NQ <10
C     NSEC      - CROSS SECTION NUMBER
C     NTYPE     - NUMBER OF REPRESENTATIVE LATERAL INFLOW
C                 HYDROGRAPHS                                      NTYPE<50
C
C     OPTION    - 0 - FLOW ROUTING ONLY
C                 1 - FLOW AND SEDIMENT ROUTING
C
C     P         - WETTED PERIMETER
C     POROS     - POROSITY OF BED MATERIAL
C
C     Q         - FLOW RATE
C     QLAT      - LATERAL INFLOW PER UNIT LENGTH
C     QIL       - REPRESENTATIVE LATERAL INFLOW HYDROGRAPH
C     QQ        - UPSTREAM FLOW HYDROGRAPH
C
C     R         - HYDRAULIC RADIUS
C
C     SDVOL     - SEDIMENT STORAGE VOLUME
C     SEDVL     - SEDIMENT STORAGE VOLUME
C     SG        - SPECIFIC GRAVITY OF BED MATERIAL
C     STORVL    - STORAGE VOLUME
C     SUBK      - SUB CONVEYANCES, COMPUTED ON THE FORWARD TIME LINE
C     SVGAIN    - SEDIMENT STORAGE VOLUME DIFFERENCE
C     SVLIN     - SEDIMENT INFLOW  VOLUME
C     SVLOUT    - SEDIMENT OUTFLOW VOLUME
C
C     T         - TIME AT WHICH PROPERTIES ARE KNOWN
C     T1        - TIME AT WHICH PROPERTIES ARE TO BE EVALUATED
C     TG        - TIME ASSOCIATED WITH INFLOW SEDIMENT HYDROGRAPH
C     THALWG    - MINIMUM BED ELEVATION OF A CROSS SECTION
C     THETA     - WEIGHTING COEFFICIENT IN FINITE DIFFERENCE SCHEME
C     THETC     - THRESHOLD VALUE OF SHIELDS PARAMETER
C     TIL       - TIME ASSOCIATED WITH LATERAL INFLOW HYDROGRAPH
C     TINCRS    - TIME INCREMENTS AT WHICH TABLES OF RESULTS ARE PRINTED
C     TITLE     - JOB IDENTIFIER
C     TMAX      - MAXIMUM TIME FOR THE FLOOD TO PROPAGATE THROUGH THE
C                 REACH
C     TMAXS     - MAXIMUM TIME UNTIL WHICH GIVEN TIME INCREMENT APPLIES
C     TQ        - TIME ASSOCIATED WITH FLOW HYDROGRAPH
C
C     USED      - SEDIMENT VELOCITY - ON T TIME LINE
C     USED1     -                   - ON T+1 TIME LINE
C     UCRIT     - FLOW VELOCITY AT THRESHOLD BED CONDITION
C     USCRIT    - SHEAR VELOCITY AT THRESHOLD BED CONDITION
C
C     V         - FLOW VELOCITY
C     VGAIN     - STORAGE VOLUME DIFFERENCE
C     VISCOS    - FLUID KINEMATIC VISCOSITY
C     VOLIN     - INFLOW  VOLUME
C     VOLOUT    - OUTFLOW VOLUME
C     VOLERR    - STORAGE VOLUME DIFFERENCE AS A PERCENTAGE OF THE
C                 INFLOW VOLUME
C     VOLERS    - SEDIMENT STORAGE VOLUME DIFFERENCE AS A PERCENTAGE
C                 OF THE SEDIMENT OUTFLOW VOLUME
C
C     W         - FALL VELOCITY OF BED MATERIAL
C
C     XNODE     - CHAINAGE OF COMPUTATIONAL POINTS FROM UPSTREAM BOUNDARY
C
C     YB        - HORIZONTAL ORDINATES OF POINTS DEFINING A CROSS SECTION
C
C     Z         - ELEVATION OF THE WATER SURFACE (STAGE) ABOVE AN
C                 ARBITRARY DATUM
C     ZB        - ELEVATIONS OF POINTS DEFINING A CROSS SECTION
C
C
C                       SUBROUTINE CALL
C                          SEQUENCE
C                          ********
C
C                        )
C                        (
C                     )--)
C                     (  (--- GEO
C                     )        )------ PROPS
C                     (  (-----(
C                     )  )
C                     (  (--- FCONT
C                     )        )------ PROPS
C                     (        (------ SIMPSN
C                     )  )-----)
C                     (  (
C                     )  )--- SCONT
C                     (        (------ SIMPSN
C                     )  )-----)
```

```
C               (  (
C               )  )--- SED
C               (        (------ PROPS
C               )  )-----)
C               (  (
C               )  )--- IMPLCT
C               (        (------ QLTF
C               )        )------ GEO
C               (                 (------ PROPS
C               )        )--------)
C               (  (-----(
C               )  )
C               (  (--- HOLE
C               )        )------ PROPS
C               (  (-----(
C               )  )
C               (  (
C               )  )--- IMPLCT
C               (        (------ QLTF
C               )        )------ GEO
C               (                 (------ PROPS
C               )        )--------)
C               (  (-----(
C               )  )
C               (  (--- SROUT
C               )        )------ SED
C               (                 (------ PROPS
C               )        )--------SOLVE
C               (  (-----(
C               )  )
C               (  (
C               )  )--- ADJUST
C               (        (------ PROPS
C               )  )-----)
C               (  (
C               )  )
C               (--(
C
C ***************************************************************************
C
C
```

```
      COMMON /A/ T,N,T1
      COMMON /B/ G,DT,QBASE,THETA,Q(50),OPTION
      COMMON /C/ QQ(20),TQ(20),NPQ
      COMMON /E/ MANN1(50),MANN(50),NP(50),XNODE(50),YB(50,12),ZB(50,12)
      COMMON /F/ DLAT(50),QI(10,50),TI(10,50),QLAT(50),NPQI(50)
      COMMON /G/ A(50),ALPHA(50),B(50),DX,K(50),DEPTH(50),P(50),R(50),
     1           THALWG(50),Z(50)
      COMMON /H/ DQ(50),DZ(50)
      COMMON /O/ BETA,D35,D50,D65,GS(50),POROS,SG,USCRIT,VISCOS,W
      COMMON /P/ GB(20),TG(20),NPG
      COMMON /Q/ COEF(50),COEF1(50),DCOEF(50),DUSED(50),GSE(50),GSE1(50)
     1           ,USED(50),USED1(50),DGSE(50)
      COMMON /R/ DABED(50),DG(50),GSF,NL
      COMMON /S/ COEFA,COEFB
C
      DIMENSION  DA(50),DIFY(24),DIFZ(24),DTS(20),INFO(16),LCODE(50),
     1           NPQL(50),QIL(10,50),TIL(10,50),TINCRS(20),TITLE(16),
     2           TMAXS(20 ),ZBED(50),YLD(50)
C
      REAL       K,KT,L,L1,LONH,MANN,MANN1
      INTEGER    OPTION,OPT1
C
C
C     INPUT
C     -----
C
C
      READ(5,24) (TITLE(J),J=1,16)

      READ(5,26) (INFO(J),J=1,16)
      READ(5,28) OPTION
      READ(5,40) THETA
      READ(5,30) NDT,(DTS(I),TMAXS(I),TINCRS(I),I=1,NDT)
      TMAX = TMAXS(NDT)
C
C     CHANNEL GEOMETRY
C     ----------------
C
```

```
      READ(5,32) N,NCROSS
      IF( N.GT.50 ) GO TO 14
      M = N-1
      G = 9.81
C
C     DETERMINE CROSS SECTION GEOMETRY OF REPRESENTATIVE SECTIONS
C
      DO 220 J = 1,NCROSS
      READ(5,34) NSEC,NP(NSEC),XNODE(NSEC),DDX,MANN(NSEC)
      MP = NP(NSEC)
      READ(5,36) (YB(NSEC,L),ZB(NSEC,L),L=1,MP)
      IF( NSEC.GT.1 ) GO TO 200
      NLOW = 1
      GO TO 220
C
C     DETERMINE CROSS SECTION GEOMETRY OF INTERNAL SECTIONS
C
  200 DO 204 I = 1,MP
      DIFY(I) = YB(NSEC,I) - YB(NLOW,I)
  204 DIFZ(I) = ZB(NSEC,I) - ZB(NLOW,I)
      DIFN = MANN(NSEC) - MANN(NLOW)
C
      NL = NLOW + 1
      DO 212 IJ = NL,NSEC
      XNODE(IJ) = XNODE(IJ-1) + DDX
      RATIO = (XNODE(IJ)-XNODE(NLOW)) / (XNODE(NSEC)-XNODE(NLOW))
      IF( RATIO.EQ.1. ) GO TO 216
C
      DO 208 IK = 1,MP
      YB(IJ,IK) = YB(NLOW,IK) + RATIO*DIFY(IK)
  208 ZB(IJ,IK) = ZB(NLOW,IK) + RATIO*DIFZ(IK)
      MANN(IJ) = MANN(NLOW) + RATIO*DIFN
      NP(IJ) = MP
  212 CONTINUE
  216 NLOW = NSEC
  220 CONTINUE
C
C     INITIAL FLOW CONDITIONS
C     -----------------------
C
      READ(5,38) (Q(J),J=1,N)
      READ(5,40) (Z(J),J=1,N)
C
C     FLOW BOUNDARY CONDITIONS
C     ------------------------
C
C     UPSTREAM BOUNDARY CONDITION SPECIFIED AS DISCRETE POINTS IN TIME
C
      READ(5,42) NPQ,(QQ(I),I=1,NPQ)
      READ(5,44) (TQ(I),I=1,NPQ)
      IF( TQ(NPQ).LE.TMAX ) GO TO 15
      IF( NPQ.GT.20 ) GO TO 16
C
C     REPRESENTATIVE LATERAL INFLOW HYDROGRAPHS ARE SPECIFIED AS
C     DISCRETE POINTS IN TIME
C
      READ(5,28) NTYPE
      DO 224 J = 1,NTYPE
      READ(5,42) NQ,(QIL(I,J),I=1,NQ)
      READ(5,44) (TIL(I,J),I=1,NQ)
      IF( NQ.GT.10 ) GO TO 16
      IF( TIL(NQ,J).LT.TMAX ) GO TO 18
      NPQL(J) = NQ
  224 CONTINUE
C
      READ(5,45) (LCODE(J),J=1,M)
      DO 232 IK = 1,M
      L = LCODE(IK)
      NPQI(IK) = NPQL(L)
      MUP = NPQI(IK)
      DO 228 IJ = 1,MUP
      QI(IJ,IK) = QIL(IJ,L)
  228 TI(IJ,IK) = TIL(IJ,L)
  232 CONTINUE
      IF( OPTION.EQ.0 ) GO TO 236
C
C     SEDIMENT PROPERTIES
C     -------------------
C
      READ(5,46) D35,D50,D65,POROS,SG,THETC,VISCOS,W
      READ(5,48) COEFA,COEFB
C
      USCRIT = SQRT(THETC*(SG-1.)*G*D50)
C
C     INITIAL CONDITIONS
C     ------------------
```

```
C
      READ(5,28) NL
      READ(5,50) (GS(I),I=1,N)
C
C     SEDIMENT BOUNDARY CONDITION
C     ---------------------------
C
C     UPSTREAM BOUNDARY CONDITION SPECIFIED AS DISCRETE POINTS IN TIME
C
      READ(5,52) NPG,(GB(I),I=1,NPG)
      READ(5,44) (TG(I),I=1,NPG)
      IF( TG(NPG).LT.TMAX ) GO TO 19
      IF( NPG.GT.20 ) GO TO 20
C
C     OUTPUT
C     ------
C
  236 WRITE(6,54)

      WRITE(6,56) (TITLE(J),J=1,16)
      WRITE(6,58) (INFO(J),J=1,16)
      WRITE(6,60)
      WRITE(6,62) THETA
      DO 240 J = 1,NDT
  240 WRITE(6,63) DTS(J),TMAXS(J),TINCRS(J)
      WRITE(6,64) M
      DO 244 I = 1,N
      MP = NP(I)
      WRITE(6,66) I,XNODE(I),MANN(I),MP
  244 WRITE(6,68) (L,YB(I,L),ZB(I,L),L=1,MP)
      WRITE(6,70)
      WRITE(6,72) (QQ(J),TQ(J),J=1,NPQ)
      WRITE(6,74)
      DO 248 J = 1,M
      WRITE(6,76) J
      NQI = NPQI(J)
  248 WRITE(6,78) (QI(L,M),TI(L,M),L=1,NQI)
      WRITE(6,80)
      DO 252 L = 1,N
  252 WRITE(6,82) L,Z(L),Q(L)
C
      IF( OPTION.EQ.0 ) GO TO 260
C
      WRITE(6,84)
      WRITE(6,86) D35,D50,D65,POROS,SG,USCRIT,VISCOS,W
      WRITE(6,88)
      WRITE(6,90) COEFA,COEFB
      WRITE(6,92)
      WRITE(6,94) (GB(I),TG(I),I=1,NPG)
      WRITE(6,96)
      WRITE(6,98) (J,GS(J),J=1,N)
C
      T     = 0.0
      TIME  = 0.0
      YIELD = 0.0
      QBASE = Q(1)
      DO 256 J = 1,N
  256 GS(J) = GS(J) / (G*SG*1000.)*B(J)
C
C
C     RESULTS
C     -------
C
C
  260 WRITE(6,100)
C
  264 IF( T.GE.TMAX ) STOP
C
C     DETERMINE TIME INCREMENT DT
C
      DTT = DT
      DO 272 IF = 1,NDT
  268 IF( T.GE.TMAXS(IF) ) GO TO 272
      DT = DTS(IF)
      TINCR = TINCRS(IF)
      GO TO 276
  272 CONTINUE
C
C     WRITE OUT RESULTS AT SPECIFIED TIME INCREMENTS
C
  276 DO 280 J = 2,N
      SVLOUT = DTT*(GS(J)-(1.-THETA)*DG(J))
      YLD(J) = YLD(J)+SVLOUT*SG*1000.
  280 CONTINUE
C
      IF( T.NE.TIME ) GO TO 304
```

```
      TIME = TIME + TINCR
      TMIN = T/60.
      WRITE(6,104) T,TMIN
      WRITE(6,106)
      DO 284 J = 1,N
C
C     TEST WHETHER FLOW IS SUPERCRITICAL
C
      CALL GEO (J,0,0)
C
      V = Q(J)/A(J)
      FN = V/SQRT(G*A(J)/B(J))
      IF( FN.LT.1.0 ) GO TO 284
      WRITE(6,108) J,FN
      IF( FN.GE.2.0 ) STOP
C
  284 WRITE(6,110) J,XNODE(J),B(J),A(J),K(J),ALPHA(J),V,Z(J),Q(J),
     1             THALWG(J)
C
C
C     CHECK FLOW CONTINUITY
C     ---------------------
C
      CALL FCONT (N,DTT,VOLERR)
C
      WRITE(6,115) VOLERR
C
      IF( OPTION.EQ. 0 ) GO TO 304
C
      WRITE(6,112)
      IF( T.EQ.0. ) GO TO 288
C
C     CHECK SEDIMENT CONTINUITY
C     -------------------------
C
      CALL SCONT (N,DTT,THETA,SVLOUT,VOLERR)
C
C     WRITE OUT RESULTS OF SEDIMENT ROUTING
C     -------------------------------------
C
  288 ZBED(NL) = ZBED(NL-1)+(XNODE(NL)-XNODE(NL-1))*(ZBED(NL+1)-
     1           ZBED(NL-1))/(XNODE(NL+1)-XNODE(NL-1))
C
      DO 300 J = 1,N
      IF( T.EQ.0. ) GS(J) = GS(J)*B(J)
      IF( T.EQ.0. ) MANN1(J) = MANN(J)
C
      CALL SED (1,J,Q(J))
C
      IF( T.EQ.0. ) ZBED(J) = ZB(J,2)
      MP     = NP(J)
      TRATE  = GS(J)*G*SG*1000./B(J)
      EQUILT = GSE(J)*G*SG*1000./B(J)
      IF( T.EQ.0. ) GO TO 296
      DO 292 IJ = 1,NPG
  292 GB(IJ) = GB(IJ)*B(1)
  296 CONTINUE
C
      SCOUR  = (ZBED(J)-ZB(J,2))*1000.
      SF     = (Q(J)/K(J))**2.
C
      IF( J.EQ.NL.AND.T.GT.0. )  COMERR = (1.-SCOUR/(H1*1000.))*100.
C
  300 WRITE(6,114) J,TRATE,EQUILT,(ZB(J,L),L=1,MP),SCOUR,MANN(J),SF,
     1             YLD(J)
C
      IF( T.EQ.0. ) GO TO 304
      HD     = H1*1000.
      LONH   = L1/H1
      WRITE(6,130) L1,HD,LONH
      WRITE(6,113) COMERR
      WRITE(6,117) YLD(N),VOLERR
C
  304 CALL IMPLCT
C
      IF( OPTION.EQ.0 ) GO TO 12
C
C     DETERMINE BED ROUGHNESS ON FOWARD TIME LINE
C
      DO 308 J = 2,N
      ST = Z(J)+DZ(J)
C
      CALL PROPS (1,J,ST,AT,BT,KT,PT,RT,RBT,ALPT,THAL)
C
      SF = ((Q(J)+DQ(J))/KT)**2.
      THETB = (RBT*SF)/((SG-1.)*D50)
      MANN1(J) = 0.02356*THETB**0.1187
```

```
      IF( MANN1(J).LE.0.01610 ) MANN1(J) = 0.01610
  308 CONTINUE
C
      NUP = NL-1
      IF( T.GT.0. ) NUP = NL
C
      L = XNODE(NUP)-XNODE(NL-1)
      H = ZBED(NUP)-ZB(NUP,2)
      IF( T.EQ.0. ) L = 0.0005
      IF( T.EQ.0. ) H = 0.00005
C
C     DETERMINE LOCATION OF MAXIMUM SCOUR ON FOWARD TIME LINE
C
      CALL HOLE (NUP,L,H,L1,H1)
C
      RATIO    = (L1+XNODE(NL-1)-XNODE(NUP))/(XNODE(NL+1)-XNODE(NUP))
      MP = NP(NL)
      DO 312 I = 1,MP
      YB(NL,I) = YB(NUP,I)+RATIO*(YB(NL+1,I)-YB(NUP,I))
  312 ZB(NL,I) = ZB(NUP,I)+RATIO*(ZB(NL+1,I)-ZB(NUP,I))
C
      XNODE(NL)= L1 + XNODE(NL-1)
      IF( T.EQ.0. ) GO TO 316
      MANN(NL) = MANN(NUP)+RATIO*(MANN(NL+1)-MANN(NUP))
  316 Z(NL)    =    Z(NUP)+RATIO*(   Z(NL+1)-   Z(NUP))
      Q(NL)    =    Q(NUP)+RATIO*(   Q(NL+1)-   Q(NUP))
      GS(NL)   =   GS(NUP)+RATIO*(  GS(NL+1)-  GS(NUP))
C
      CALL IMPLCT
C
C
      CALL SROUT
C
      CALL ADJUST
C
   12 IF( OPTION.EQ.0 ) T = T1
      GO TO 264
C
C     INPUT ERRORS LISTED
C
   14 WRITE(6,116)
      GO TO 22
   15 WRITE(6,118)
      GO TO 22
   16 WRITE(6,120)
      GO TO 22
   18 WRITE(6,124) II
      GO TO 22
   19 WRITE(6,126)
      GO TO 22
   20 WRITE(6,128)
C
   22 STOP
C
C     READ FORMATS
C
   24 FORMAT (16A5)
   26 FORMAT (16A5)
   28 FORMAT (I5)
   30 FORMAT (I5,/(3F10.3))
   32 FORMAT (2I5)
   34 FORMAT (2I5,2F10.2,F10.5)
   36 FORMAT (8F10.4)
   38 FORMAT (8F10.4)
   40 FORMAT (8F10.4)
   42 FORMAT (I10,/(5F10.4))
   44 FORMAT (5F10.4)
   45 FORMAT (16I5)
   46 FORMAT( 3F10.6,3F10.4,F10.9,F10.4)
   48 FORMAT (2F10.4)
   50 FORMAT (5F10.5)
   52 FORMAT (I10,/(5F10.5))
C
C     WRITE FORMATS
C
   54 FORMAT (1H1,//,58X,16HU  W  A  S  E  R,//,32X,67HUNSTEADY WATER AN
     1D SEDIMENT ROUTING MODEL DEVELOPED BY B.C.PHILLIPS,/,32X,66HAT THE
     2 UNIVERSITY OF CANTERBURY, CHRISTCHURCH, NEW ZEALAND (1983).,/)
   56 FORMAT (//,23X,86(1H*),/,23X,1H*,84X,1H*,/,23X,1H*,2X,16A5,2X,1H*,
     1/,23X,1H*,84X,1H*,/,23X,86(1H*),/)
   58 FORMAT (/,25X,16A5,/)
   60 FORMAT (//,57X,19(1H*),/,57X,19HSTREAM FLOW ROUTING,/,55X,23HUSING
     1 DYNAMIC EQUATIONS,/,55X,23(1H*),//,58X,16HINPUT PARAMETERS,/,58X,
     2 16(1H*),/)
   62 FORMAT (/,54X,23HWEIGHTING COEFFICIENT =,F6.2)
   63 FORMAT (/,45X,16HTIME INCREMENT =,F6.1,9H S, UP TO,F8.1,2H S,/,
     145X,21HRESULTS PRINTED EVERY,F8.1,2H S )
```

```
 64 FORMAT (/,58X,16HCHANNEL GEOMETRY,/,58X,16(1H*),//,54X,23HNUMBER O
   1F SUB REACHES =,I5,/)
 66 FORMAT (/,52X,14HSECTION NUMBER,I4,//,52X,20HRIVER CHAINAGE (M) =,
   1F8.2,/,52X,19HMANNING'S N VALUE =,F7.5,/,52X,29HNO. OF CROSS SECTI
   2ON POINTS =,I4,//,53X,26HPOINT HORIZONTAL ELEVATION,/)
 68 FORMAT (53X,I3,2F10.2)
 70 FORMAT (//,54X,24HFLOW BOUNDARY CONDITIONS,/,54X,24(1H*),//,57X,19
   1HUPSTREAM HYDROGRAPH,/,57X,19(1H-),//,58X,17HDISCHARGE    TIME,/,
   259X,16H(CUMECS)      (S),/)
 72 FORMAT (56X,F10.3,F10.1)
 74 FORMAT (//,53X,26HLATERAL INFLOW HYDROGRAPHS,/,53X,26(1H-),/)
 76 FORMAT (/,50X,9HSUB REACH,I4,19H  DISCHARGE    TIME,/,66X,
   116H(CUMECS)      (S),/)
 78 FORMAT (62X,F10.4,F9.1)
 80 FORMAT (//,55X,23HINITIAL FLOW CONDITIONS,/,55X,23(1H-),//,51X,30H
   1SECTION NO.  STAGE   DISCHARGE,/,65X,16H(M)      (CUMECS),/)
 82 FORMAT (51X,I6,F12.3,F11.4)
 84 FORMAT (//,58X,16(1H*),/,58X,16HSEDIMENT ROUTING,/,58X,16(1H*),/)
 86 FORMAT (/,57X,19HSEDIMENT PROPERTIES,/,57X,19(1H*),//,51X,18HGRAIN
   1 SIZE   D35 =,F8.5,4H (M),/,51X,18HDISTRIBUTION D50 =,F8.5,4H (M),
   2/,64X,5HD65 =,F8.5,4H (M),/,51X,18HBED POROSITY     =,F6.3,/,51X,
   318HSPECIFIC GRAVITY =,F6.3,/,51X,12HCRITICAL BED,/,51X,18HSHEAR ST
   4RESS     =,F7.4,7H  (M/S),/,51X,18HVISCOSITY         =,E9.2,8H(M**2
   5/S),/,51X,18HFALL VELOCITY    =,F7.4,7H  (M/S),/)
 88 FORMAT (/,53X,26HSEDIMENT DISCHARGE FORMULA,/,53X,26(1H*),//,52X,
   128HGS (N/S/M)  = A*(U-UCRIT)**B,/)
 90 FORMAT (60X,3HA =,E10.5,/,60X,3HB =,E10.5)
 92 FORMAT (//,52X,28HSEDIMENT BOUNDARY CONDITIONS,/,52X,28(1H*),///,
   152X,28HUPSTREAM SEDIMENT HYDROGRAPH,/,52X,28(1H-),//,58X,17HSEDIME
   2NT     TIME,/,58X,9HDISCHARGE,/,59X,15H(N/S/M)      (S),/)
 94 FORMAT (56X,F10.4,F9.1)
 96 FORMAT (//,58X,16HINITIAL SEDIMENT,/,56X,20HDISCHARGE CONDITIONS,/
   1,56X,20(1H-),//,51X,30HSECTION NO. SEDIMENT DISCHARGE,/,69X,7H(N/S
   2/M),/)
 98 FORMAT (51X,I6,F19.4)
100 FORMAT (1H1,//,63X,7(1H*),/,63X,7HRESULTS,/,63X,7(1H*),//)
104 FORMAT (//,48X,6HTIME =,F8.1,6H (S) =,F8.3,7H (MINS),/,48X,
   135(1H-),/)
106 FORMAT (/,60X,12HFLOW ROUTING,/,60X,12(1H-),//,16X, 98HSECTION   C
   1HAINAGE  TOP WIDTH   AREA   CONVEYANCE   ALPHA   VELOCITY   STAGE
   2  DISCHARGE   THALWEG,/,16X,37H NUMBER      (M)          (M)     (M**
   32),22X,35H(M/S)       (M)      (M**3/S)      (M),/)
108 FORMAT (10X,32HFLOW IS SUPERCRITICAL AT SECTION,I4,17H ,FROUDE NUM
   1BER =,F6.3,/)
110 FORMAT (16X,I5,F13.3,F11.3,F9.3,F10.3,F10.4,F9.4,F9.4,F11.4,F10.3)
112 FORMAT (//,58X,16HSEDIMENT ROUTING,/,58X,16(1H-),//, 5X,20HSECTION
   1     SEDIMENT,20X,32HCROSS SECTION BED ELEVATIONS (M),17X,35HSCOUR
   2  MANNINGS  FRICTION     YIELD,/,5X,20HNUMBER     DISCHARGE,29X,11
   3H(POINT NO.),30X,33H(MM)      N        SLOPE      (KG),/,
   417X,7H(N/S/M),22X,"1",9X,"2",9X,"3",9X,"4",/,14X,2HGS,8X,3HGSC,/)
113 FORMAT( /,5X,23HCOMPATIBILITY   ERROR =,F8.3,9H  PERCENT)
114 FORMAT (4X,I5,2F10.4,10X,4F10.4,10X,F10.4,2F10.5,F10.3)
115 FORMAT (/,16X,22HSTORAGE VOLUME ERROR =,F8.3,9H  PERCENT)
116 FORMAT (/,10X,64HNUMBER OF NODES EXCEEDS THAT ALLOWED FOR BY DIMEN
   1SION STATEMENTS)
117 FORMAT (/,5X,19HSEDIMENT CONTINUITY,/,5X,19(1H-),/,5X,19HCUMULATIV
   1E YIELD = ,F6.3,3H KG,//,5X,23HSEDIMENT VOLUME ERROR =,F8.3,9H  PE
   2RCENT)
118 FORMAT (/,10X,76HUPSTREAM BOUNDARY HYDROGRAPH NOT DEFINED FOR FULL
   1 DURATION OF ROUTING PERIOD)
120 FORMAT (/,10X,100HNUMBER OF DISCRETE POINTS DESCRIBING THE HYDROGR
   1APH EXCEEDS THAT ALLOWED FOR BY DIMENSION STATEMENTS)
124 FORMAT (/,10X,38HLATERAL INFLOW HYDROGRAPH AT SUB REACH,I4,56H NOT
   1 DEFINED FOR THE FULL DURATION OF THE ROUTING PERIOD)
126 FORMAT (/,10X,76HUPSTREAM SEDIMENT HYDROGRAPH NOT DEFINED FOR FULL
   1 DURATION OF ROUTING PERIOD)
128 FORMAT (/,9X,109HNUMBER OF DISCRETE POINTS DESCRIBING THE SEDIMENT
   1 HYDROGRAPH EXCEEDS THAT ALLOWED FOR BY DIMENSION STATEMENTS)
130 FORMAT (/,5X,15HSCOUR HOLE DATA,/,5X,15(1H-),/,5X,12HLENGTH (M) =,
   1F6.3,14H ,DEPTH (MM) =,F6.2,7H ,L/H =,F6.3)
    END
```

```
      SUBROUTINE ADJUST
C
C ***************************************************************************
C
C     SUBROUTINE ADJUSTS THE ELEVATIONS COORDINATES OF EACH CROSS
C     SECTION DATA POINT AND CALCULATES THE DISCHARGE AND STAGE ON
C     THE T+1 TIME LINE
C
C ***************************************************************************
C
C
      COMMON /A/ T,N,T1
      COMMON /B/ G,DT,QBASE,THETA,Q(50),OPTION
      COMMON /E/ MANN1(50),MANN(50),NP(50),XNODE(50),YB(50,12),ZB(50,12)
      COMMON /G/ A(50),ALPHA(50),B(50),DX,K(50),DEPTH(50),P(50),R(50),
     1           THALWG(50),Z(50)
      COMMON /H/ DQ(50),DZ(50)
      COMMON /O/ BETA,D35,D50,D65,GS(50),POROS,SG,USCRIT,VISCOS,W
      COMMON /R/ DABED(50),DG(50),GSF,NL
      COMMON /T/ DY(50,12),SUBK(50,12)
C
      REAL       KSUM,MANN,MANN1
      INTEGER    OPTION
C
      T = T1
C
      DO 6 J=1,N
      NUP = NP(J)-1
C
      WS = Z(J) + DZ(J)
      CALL PROPS (2,J,WS,AT,BAT,KSUM,PT,RT,RBT,ALPT,THALD)
C
C     THE CONVEYANCE SCHEME PROPOSED BY LI AND BROWN (1979) IS USED TO
C     DETERMINE THE BED ELEVATION CHANGE AT A POINT. FOR COMPLEX
C     CHANNEL GEOMETRY INSERT
C
C     DO 4 I = 2,NUP
C     IF( ZB(J,I).LT.ZB(J,I-1).AND.WS.LT.ZB(J,I) ) GO TO 4
C     IF( ZB(J,I).GT.ZB(J,I-1).AND.WS.LT.ZB(J,I) ) GO TO 4
C     DZB = (SUBK(J,I-1)+SUBK(J,I))*DABED(J)/(KSUM*(DY(J,I-1)+DY(J,I)))
C     ZB(J,I) = ZB(J,I) + DZB
C   4 CONTINUE
C
C     INSTEAD OF THE FOLLOWING SCHEME WHICH ONLY APPLIES TO A
C     RECTANGULAR CHANNEL
C
      DO 4 I = 2,3
C
      DZB = DABED(J)/BAT
      ZB(J,I) = ZB(J,I) + DZB
C
    4 CONTINUE
C
      Q(J) = Q(J) + DQ(J)
      Z(J) = Z(J) + DZ(J)
C
      MANN(J) = MANN1(J)
C
    6 CONTINUE
C
      RETURN
      END




      SUBROUTINE FCONT (N,DTT,VOLERR)
C
C ***************************************************************************
C
C     SUBROUTINE CHECKS FLOW CONTINUITY
C
C ***************************************************************************
C
C
      COMMON /B/ G,DT,QBASE,THETA,Q(50),OPTION
      COMMON /E/ MANN1(50),MANN(50),NP(50),XNODE(50),YB(50,12),ZB(50,12)
      COMMON /G/ A(50),ALPHA(50),B(50),DX,K(50),DEPTH(50),P(50),R(50),
     1           THALWG(50),Z(50)
      COMMON /H/ DQ(50),DZ(50)
C
      DIMENSION  DA(50)
C
      REAL       MANN,MANN1
```

```
C
      VOLIN = DTT*(Q(1) - (1.-THETA)*DQ(1))
      VOLOUT = DTT*(Q(N) - (1.-THETA)*DQ(N))
      BDYVOL = VOLIN - VOLOUT
      IF( BDYVOL.EQ.0. ) GO TO 6
C
C     CALCULATE STORAGE VOLUME
C
      DO 4 J = 1,N
      ST = Z(J) - DZ(J)
      CALL PROPS (1,J,ST,AT,BT,KT,PT,RT,RBT,ALPT,THALD)
      ST = Z(J)
      CALL PROPS (1,J,ST,AT1,BT,KT,PT,RT,RBT,ALPT,THALD)
      DA(J) = AT1 - AT
    4 CONTINUE
C
      CALL SIMPSN (1,N,DA,XNODE,STORVL)
C
      VGAIN = STORVL - BDYVOL
      VOLERR = (VGAIN/VOLIN) * 100.
      GO TO 8
    6 VOLERR = 0.
C
    8 RETURN
      END




      SUBROUTINE GEO (J,IFLAG,JFLAG)
C
C ***************************************************************************
C
C     SUBROUTINE EVALUATES CHANNEL PROPERTIES AT A NODE FOR ANY GIVEN
C     STAGE
C
C ***************************************************************************
C
C
      COMMON /A/ T,N,T1
      COMMON /D/ AA(50),BB(50),BDERIV(50),DF,KDERIV(50),ALPDER(50)
      COMMON /E/ MANN1(50),MANN(50),NP(50),XNODE(50),YB(50,12),ZB(50,12)
      COMMON /G/ A(50),ALPHA(50),B(50),DX,K(50),DEPTH(50),P(50),R(50),
     1           THALWG(50),Z(50)
C
      REAL       K,KT,KDERIV,MANN,MANN1
C
C     CALCULATE HYDRAULIC PROPERTIES OF THE CROSS SECTION
C
      CALL PROPS (1,J,Z(J),A(J),B(J),K(J),P(J),R(J),RB,ALPHA(J),
     1            THALWG(J))
C
      DEPTH(J) = Z(J) - THALWG(J)
C
C     IFLAG = 0  CALCULATE HYDRAULIC PROPERTIES ONLY
C             1  CALCULATE HYDRAULIC PROPERTIES AND DERIVATES
C
      IF( IFLAG.EQ.0 ) RETURN
C
      WS = Z(J) + 0.005
      CALL PROPS (1,J,WS,AT,BT,KT,PT,RT,RBT,ALPT,THALD)
      BDERIV(J) = (BT - B(J)) / 0.005
      KDERIV(J) = (KT - K(J)) / 0.005
      ALPDER(J) = (ALPT - ALPHA(J)) / 0.005
C
C     JFLAG = 0 SET AA(J) = AA(J-1), BB(J) = BB(J-1)
C             1 CALCULATE AA(J), BB(J)
C
      IF( JFLAG.EQ.0 ) GO TO 8
      GO TO 10
    8 AA(J) = AA(J-1)
      BB(J) = BB(J-1)
      GO TO 16
C
   10 CALL QUAD (J,Z,WS,DX,XNODE)
      KOUNT = 0
   12 CALL PROPS (1,J  ,WS,AT1,BT,KT,PT,RT,RBT,ALPT,THALD)
      CALL PROPS (1,J+1,WS,AT2,BT,KT,PT,RT,RBT,ALPT,THALD)
      IF( KOUNT.EQ.1 ) GO TO 14
      AA(J) = (AT2 - AT1) / DX
      KOUNT = KOUNT + 1
      WS = WS + 0.005
      GO TO 12
```

```
   14 BB(J) = (((AT2-AT1)/DX) - AA(J)) / 0.005
   16 IF( J.NE.N ) RETURN
      DF = KDERIV(J)*SQRT((THALWG(J-1)-THALWG(J))/DX)
      GO TO 20
   20 RETURN
C
      END




      FUNCTION GSB (GB,TG,T,NPG)
C
C *********************************************************************
C
C     THIS FUNCTION ROUTINE EVALUATES THE SEDIMENT INFLOW AT THE
C     UPSTREAM BOUNDARY AT TIME T
C
C *********************************************************************
C
C
      DIMENSION  GB(20),TG(20)
C
      J = NPG - 1
      DO 2 I = 1,J
      IF( T.GE.TG(I).AND.T.LT.TG(I+1) ) GO TO 4
    2 CONTINUE
    4 GSB = GB(I) + (GB(I+1)-GB(I))/(TG(I+1)-TG(I))*(T-TG(I))
C
      RETURN
      END




      SUBROUTINE HOLE (NB,L,H,LF,HF)
C
C *********************************************************************
C
C     SUBROUTINE CALCULATES SCOUR HOLE PROPERTIES AT TIME T USING
C     CALIBRATED EQUATIONS
C
C *********************************************************************
C
C
      COMMON /A/ T,N,T1
      COMMON /B/ G,DT,QBASE,THETA,Q(50),OPTION
      COMMON /G/ A(50),ALPHA(50),B(50),DX,K(50),DEPTH(50),P(50),R(50),
     1           THALWG(50),Z(50)
      COMMON /H/ DQ(50),DZ(50)
      COMMON /O/ BETA,D35,D50,D65,GS(50),POROS,SG,USCRIT,VISCOS,W
      COMMON /P/ GB(20),TG(20),NPG
      COMMON /Q/ COEF(50),COEF1(50),DCOEF(50),DUSED(50),GSE(50),GSE1(50)
     1           ,USED(50),USED1(50),DGSE(50)
      COMMON /R/ DABED(50),DG(50),GSF,NL
C
      REAL       KT,L,LF,LONH
      DATA       PI/3.14159/
C
      QQ = Q(NL-1)+DQ(NL-1)
      WS = Z(NL-1)+DZ(NL-1)
C
      CALL PROPS (2,NL-1,WS,AT,BT,KT,PT,RT,RB,ALPT,THAL)
C
C     DETERMINE FLOW PROPERTIES AT UPSTREAM SECTION
C
C
      Y = WS-THAL
      U = QQ/AT
      SF = (QQ/KT)**2
      USTARB = SQRT(G*RB*SF)
      UCRIT = U*USCRIT/USTARB
      IF( UCRIT.GT.U ) GO TO 26
      ASTAR = VISCOS**2/((SG-1.)*G*D50**3)
      DELTA = (U-UCRIT)/(W*ASTAR**0.3334)
C
C     SCOUR HOLE STEEPNESS RELATION CALIBRATED AGAINST DATA OF
C     DIETZ (1969) AND BELL (1980)
C
      IF( DELTA.GT.150.) GO TO 6
      LONH = 65.48/DELTA**0.5094
      GO TO 8
    6 LONH = 5.1
```

```
C
    8 CALL SED (2,NB,Q(NB))
C
C
C     TEST FOR THRESHOLD BED CONDITIONS
C
      GSLIM = 0.000000001
      IF( GSE(NB).LE.GSLIM.OR.GSE1(NB).LE.GSLIM.AND.T.GT.0. ) GO TO 26
C
C
C     SOLVE FOR LOCATION OF MAX SCOUR DEPTH ON FOWARD TIME LINE
C
      C2 = COEF1(NB)
      G2 = THETA*GSE1(NB)*COEF1(NB)+(1.-THETA)*GSE(NB)*COEF(NB)
C
      EE = 0.791*LONH
      FF = 0.582*H*LONH + 1./C2
      GG = 0.209*(H*L-LONH*H*H)-(G2/C2-GSB(GB,TG,T1,NPG))*DT/(BT*
     1     (1.-POROS))
C
C     DTERMINE CHANGE IN SCOUR DEPTH OVER TIME INCREMENT USING A
C     NEWTON-RAPHSON ALGORITHM. ERROR CRITERION IS PER < 2 %.
C
      DH = -DT*COEF(NB)*(GS(NB)-GSE(NB))/(BT*(1.-POROS))
C
   10 DO 16 I = 1,20
      F = EE*DH*DH + FF*DH + GG
      FDASH = 2.*EE*DH + FF
      ERR = F/FDASH
C
      IF( DH.EQ.0. ) GO TO 12
      PER = ERR/DH*100.
      GO TO 14
   12 PER = 999.
   14 DH = DH-ERR
      IF( ABS(PER).LE.2. ) GO TO 18
   16 CONTINUE
      GO TO 28
C
C
C     SECTION PROPERTIES ON FOWARD TIME LINE
C
   18 HF = H+DH
      IF( HF.LE.0.00005 ) GO TO 20
C
C     CALCULATE SEDIMENT TRANSPORT RATE ON FOWARD TIME LINE
C
      LF = LONH*HF
      GSF = BT*(0.791*(LF*HF-L*H) - H*(LF-L))*(1.-POROS)/DT +
     1      GSB(GB,TG,T1,NPG)
      IF( GSF.LT.0. ) GO TO 26
      GO TO 22
C
C     IF ZERO SCOUR OR AGGRADATION ENCOUNTERED LOCATE THE MOBILE
C     SECTION 0.5 MM DOWNSTREAM OF UPSTREAM INTERFACE
C
   20 HF = 0.00005
      LF = 0.0005
      GSF = GSB(GB,TG,T1,NPG)
C
   22 RETURN
C
C
C     THRESHOLD CONDITIONS AT TOE OF VORTEX
C
   26 HF = H
      LF = L
      GSF = 0.
      LONH = LF/HF
      RETURN
C
   28 WRITE(6,30) PER
   30 FORMAT( //,5X,40HDH PERCENTAGE ERROR AT LAST ITERATION =,F6.2,
     19H  PERCENT)
      RETURN
C
      END
```

```
      SUBROUTINE IMPLCT
C
C ***************************************************************************
C
C     SUBROUTINE EVALUATES THE CHANGE IN DISCHARGE AND SURFACE ELEVATION
C     NODES FOR TIME T1 USING THE IMPLICIT FINITE DIFFERENCE SCHEME AND
C     SWEEP ALGORITHM TO SOLVE THE FLOW CONTINUITY AND MOMENTUM EQUATION
C
C ***************************************************************************
C
      COMMON /A/ T,N,T1
      COMMON /B/ G,DT,QBASE,THETA,Q(50),OPTION
      COMMON /C/ QQ(20),TQ(20),NPQ
      COMMON /D/ AA(50),BB(50),BDERIV(50),DF,KDERIV(50),ALPDER(50)
      COMMON /E/ MANN1(50),MANN(50),NP(50),XNODE(50),YB(50,12),ZB(50,12)
      COMMON /F/ DLAT(50),QI(10,50),TI(10,50),QLAT(50),NPQI(50)
      COMMON /G/ A(50),ALPHA(50),B(50),DX,K(50),DEPTH(50),P(50),R(50),
     1           THALWG(50),Z(50)
      COMMON /H/ DQ(50),DZ(50)
C
      DIMENSION  L(50),M(50),E(50),F(50),W(50)
C
      REAL       K,KDERIV,L,M,MANN,MANN1
      INTEGER    OPTION
C
C     UPSTREAM BOUNDARY CONDITION
C
      J = 1
      T1 = T + DT
      CALL QLTF
      E(1) = 0.0
      F(1) = QB(QQ,TQ,T1,NPQ) - QB(QQ,TQ,T,NPQ)
    2 DX = (XNODE(J+1)-XNODE(J))
      CALL GEO (J,1,1)
      CALL GEO (J+1,1,0)
C
C     IMPLICIT FINITE DIFFERENCE SCHEME
C
C
C     CONTINUITY EQUATION
C     -------------------
C
C     COEFFICIENT FOR DZ(J+1)
C
      H1 = 1.0-4.*THETA*DT/DX*(Q(J+1)-Q(J))/(B(J+1)+B(J))**2*BDERIV(J+1)
     1     +4.*THETA*QLAT(J)*BDERIV(J+1)/(B(J+1)+B(J))**2*DT
C
C     COEFFICIENT FOR DQ(J+1)
C
      B1 = 4.*THETA*DT/(DX*(B(J+1)+B(J)))
C
C     COEFFICIENT FOR DZ(J)
C
      C1 =-1.+4.*THETA*DT/DX*(Q(J+1)-Q(J))/(B(J+1)+B(J))**2*BDERIV(J)-4.
     1     *THETA*QLAT(J)*BDERIV(J)/(B(J+1)+B(J))**2*DT
C
C     COEFFICIENT FOR DQ(J)
C
      D1 = 4.*THETA*DT/(DX*(B(J+1)+B(J)))
C
C     CONSTANT
C
      G1 = -4.*DT*(Q(J+1)-Q(J))/(DX*(B(J+1)+B(J)))+4./(B(J+1)+B(J))*
     1     (QLAT(J)+DLAT(J)*THETA)*DT
C
C
C     MOMENTUM EQUATION
C     -----------------
C
C
C     COEFFICIENT FOR DZ(J+1)
C
      H2 = -0.5*(Q(J+1)*B(J+1)/A(J+1)+Q(J)*B(J)/A(J))+THETA*DT/DX*((Q(J+
     1     1)-Q(J))*(Q(J+1)/A(J+1)*ALPDER(J+1)-Q(J+1)*B(J+1)*ALPHA(J+1)/
     2     (A(J+1)**2))+G*B(J+1)*(Z(J+1)-Z(J))-Q(J+1)**2*B(J+1)/(2.*A(J+
     3     1)**2)*(ALPHA(J+1)-ALPHA(J))+G*(A(J+1)+A(J))+0.5*(Q(J+1)**2/A
     4     (J+1)+Q(J)**2/A(J))*ALPDER(J+1))+G*THETA*DT*Q(J+1)*ABS(Q(J+1)
     5     )/(K(J+1)**2)*(B(J+1)-2.*A(J+1)/K(J+1)*KDERIV(J+1))-THETA*QLA
     6     T(J)*DT*(Q(J+1)*B(J+1)/(A(J+1)**2))-THETA*DT/DX*((Q(J+1)**2*A
     7     A(J+1)*ALPDER(J+1)/(A(J+1)**2)+Q(J+1)**2*ALPHA(J+1)*BB(J+1) /
     8     A(J+1)**2-2.*ALPHA(J+1)*AA(J+1)*Q(J+1)**2*B(J+1)/A(J+1)**3)*D
     9     X+ALPHA(J+1)*Q(J+1)**2*B(J+1)/(A(J+1)**2)+ALPHA(J)*B(J)*Q(J)*
     $     *2/(A(J)**2)+(Z(J+1)-Z(J))*(ALPHA(J+1)*Q(J+1)**2*BDERIV(J+1)/
     $     (A(J+1)**2)+B(J+1)*Q(J+1)**2*ALPDER(J+1)/(A(J+1)**2)-2.*ALPHA
     $     (J+1)*B(J+1)*Q(J+1)**2*B(J+1)/(A(J+1)**3)))
```

```
C
C     CONSTANT
C
      G2 = -DT/DX*((Q(J+1)-Q(J))*(ALPHA(J+1)*Q(J+1)/A(J+1)+ALPHA(J)*Q(J)
     1     /A(J))+G*(Z(J+1)-Z(J))*(A(J+1)+A(J))+(ALPHA(J+1)-ALPHA(J))*(Q
     2     (J+1)**2/(2.*A(J+1))+Q(J)**2/(2.*A(J))))-G*DT*(Q(J+1)*ABS(Q(J
     3     +1))*A(J+1)/(K(J+1)**2)+Q(J)*ABS(Q(J))*A(J)/(K(J)**2))-THETA*
     4     DLAT(J)*DT*(Q(J+1)/A(J+1)+Q(J)/A(J))-QLAT(J)*DT*(Q(J+1)/A(J+1
     5     )+Q(J)/A(J))+DT/DX*((ALPHA(J+1)*Q(J+1)**2*AA(J+1)/(A(J+1)**2)
     6     +ALPHA(J)*Q(J)**2*AA(J)/(A(J)**2))*DX+(Z(J+1)-Z(J))*(ALPHA(J+
     7     1)*Q(J+1)**2*B(J+1)/(A(J+1)**2)+ALPHA(J)*B(J)*Q(J)**2/(A(J)**
     8     2)))
C
C     COEFFICIENT FOR DQ(J+1)
C
      B2 = 1.+THETA*DT/DX*(ALPHA(J+1)*Q(J+1)/A(J+1)+ALPHA(J)*Q(J)/A(J)+(
     1     Q(J+1)-Q(J))*ALPHA(J+1)/A(J+1)+(ALPHA(J+1)-ALPHA(J))*Q(J+1)/A
     2     (J+1))+2.*G*THETA*DT*A(J+1)*ABS(Q(J+1))/K(J+1)**2+QLAT(J)*THE
     3     TA*DT/A(J+1)-2.*THETA*DT/DX*((Q(J+1)*ALPHA(J+1)*AA(J+1)/(A(
     4     J+1)**2))*DX+(Z(J+1)-Z(J))*(Q(J+1)*B(J+1)*ALPHA(J+1)/A(J+1)**
     5     2))
C
C     COEFFICIENT FOR DZ(J)
C
      C2 = 0.5*(Q(J+1)*B(J+1)/A(J+1)+Q(J)*B(J)/A(J))-THETA*DT/DX*((Q(J+1
     1     )-Q(J))*(Q(J)/A(J)*ALPDER(J)-Q(J)*B(J)*ALPHA(J)/(A(J)**2))+G*
     2     B(J)*(Z(J+1)-Z(J))-Q(J)**2*B(J)/(2.*A(J)**2)*(ALPHA(J+1)-ALPH
     3     A(J))-G*(A(J+1)+A(J))-0.5*(Q(J+1)**2/A(J+1)+Q(J)**2/A(J))*ALP
     4     DER(J))-G*THETA*DT*Q(J)*ABS(Q(J))/(K(J)**2)*(B(J)-2.*A(J)/K(J
     5     )*KDERIV(J))+THETA*QLAT(J)*B(J)*Q(J)/(A(J)**2)*DT-THETA*DT/DX
     6     *((-ALPHA(J)*Q(J)**2*BB(J)/(A(J)**2)-AA(J)*Q(J)**2*ALPDER(J)/
     7     (A(J)**2)+2.*ALPHA(J)*AA(J)*Q(J)**2*B(J)/A(J)**3)*DX+ALPHA(J+
     8     1)*Q(J+1)**2*B(J+1)/(A(J+1)**2)+ALPHA(J)*B(J)*Q(J)**2/(A(J)**
     9     2)-(Z(J+1)-Z(J))*(ALPHA(J)*Q(J)**2*BDERIV(J)/(A(J)**2)+B(J)*Q
     $     (J)**2*ALPDER(J)/(A(J)**2)-2.*ALPHA(J)*(B(J)*Q(J))**2/A(J)**3
     $     ))
C
C     COEFFICIENT FOR DQ(J)
C
      D2 = -1.-THETA*DT/DX*(-ALPHA(J+1)*Q(J+1)/A(J+1)-ALPHA(J)*Q(J)/A(J)
     1     +(Q(J+1)-Q(J))*ALPHA(J)/A(J)+(ALPHA(J+1)-ALPHA(J))*Q(J)/A(J))
     2     -2.*G*THETA*DT*A(J)*ABS(Q(J))/(K(J)**2)-THETA*DT*QLAT(J)/A(J)
     3     +2.*THETA*DT/DX*((Q(J)*ALPHA(J)*AA(J)/(A(J)**2))*DX+(Z(J+1)-Z
     4     (J))*Q(J)*ALPHA(J)*B(J)/A(J)**2)
C
C
C     DOUBLE SWEEP ALGORITHM
C     ----------------------
C
      L(J) = H1/(C1+D1*E(J))
      M(J) = B1/(C1+D1*E(J))
      W(J) = -(G1+D1*F(J))/(C1+D1*E(J))
      E(J+1) = (H1*(C2+D2*E(J))-H2*(C1+D1*E(J)))/(B2*(C1+D1*E(J))-B1*(C2
     1         +D2*E(J)))
      F(J+1) = ((G2+D2*F(J))*(C1+D1*E(J))-(G1+D1*F(J))*(C2+D2*E(J)))/(B2
     1         *(C1+D1*E(J))-B1*(C2+D2*E(J)))
      IF( (J+1).EQ.N ) GO TO 4
      J = J+1
      GO TO 2
    4 J = N
C
C     DISCHARGE AND STAGE AT NEW TIME T1 FOR EACH NODE
C
C
C     STEADY UNIFORM RATING CURVE USED AT THE DOWNSTREAM BOUNDARY
C
C
      QN = K(N)*SQRT((THALWG(N-1)-THALWG(N))/DX)
      DZ(N) = (QN-F(N)-Q(N))/(E(N)-DF)
      DQ(N) = E(N)*DZ(N) + F(N)
      IF( OPTION.EQ.1 ) GO TO 6
      Z(N) = Z(N) + DZ(N)
      Q(N) = Q(N) + DQ(N)
    6 J = J-1
    8 DZ(J) = L(J)*DZ(J+1) + M(J)*DQ(J+1) + W(J)
      DQ(J) = E(J)*DZ(J) + F(J)
      IF( OPTION.EQ.1 ) GO TO 10
      Q(J) = Q(J) + DQ(J)
      Z(J) = Z(J) + DZ(J)
   10 IF( J.EQ.1 ) RETURN
      GO TO 6
C
      END
```

```
      SUBROUTINE PROPS (FLAG,J,WS,A,B,K,P,R,RB,ALP,THAL)
C
C ***************************************************************************
C
C     SUBROUTINE CALCULATES HYDRAULIC PROPERTIES OF A SECTION FOR A
C     GIVEN STAGE
C ***************************************************************************
C
C
      COMMON /E/ MANN1(50),MANN(50),NP(50),XNODE(50),YB(50,12),ZB(50,12)
      COMMON /T/ DY(50,12),SUBK(50,12)
C
      REAL       K,KI,MANN,MANN1,N
      INTEGER    FLAG
C
      A = 0.0
      B = 0.0
      K = 0.0
      P = 0.0
      R = 0.0
      ALP = 0.0
      THAL = 0.0
      DO 2 M = 1,12
      DY(J,M) = 0.
    2 SUBK(J,M) = 0.
      SUMK = 0.0
      N = MANN(J)
      IF( FLAG.EQ.2 ) N = MANN1(J)
C
      NPP = NP(J)
      DO 16 I = 2,NPP
C
      IF( ZB(J,I).GT.ZB(J,I-1) ) GO TO 4
      THAL = ZB(J,I)
    4 DELY = (YB(J,I) - YB(J,I-1)) + 1.0E-6
      IF( ZB(J,I).GE.WS ) GO TO 8
      IF( ZB(J,I-1).GE.WS ) GO TO 6
C
      DELZ = ABS( ZB(J,I)-ZB(J,I-1) )
      DA = WS - 0.5*( ZB(J,I-1) + ZB(J,I) )
      AR = DELY * DA
      WP = SQRT( DELY**2 + DELZ**2 )
      GO TO 12
C
    6 DELZ = WS - ZB(J,I)
      DELY = DELY*DELZ/(ZB(J,I-1)-ZB(J,I))
      GO TO 10
C
    8 IF( ZB(J,I-1).GE.WS ) GO TO 16
      DELZ = WS - ZB(J,I-1)
      DELY = DELY*DELZ/(ZB(J,I)-ZB(J,I-1))
   10 AR = 0.5*DELY * DELZ
      WP = SQRT( DELY**2 + DELZ**2 )
   12 HR = AR / WP
      KI = AR * HR**(2./3.) / N
C
      SUBK(J,I-1) = KI
      DY(J,I-1) = DELY
C
      B = B + DELY
      A = A + AR
      P = P + WP
      K = K + KI
      SUMK = SUMK + KI**3/AR**2
   16 CONTINUE
C
      IF( WS.LE.THAL ) GO TO 18
C
      Y  = WS - THAL
      ALP= SUMK * A**2/K**3
C
C     FOR COMPLEX CHANNEL GEOMETRY INSERT
C
C     R  = A/P
C
C     INSTEAD OF THE FOLLOWING STATEMENTS WHICH APPLY ONLY TO A
C     RECTANGULAR CHANNEL
C
      R  = (K*N/A)**1.5
      RB = Y/(1.+0.591*Y)
      K  = A*RB**(2./3.) / N
C
      RETURN
   18 WRITE(6,20) J,WS,THAL
   20 FORMAT(//,10X,50HA NEGATIVE FLOW DEPTH HAS BEEN ENCOUNTERED AT NOD
     1E,I4,16H  WHERE: STAGE =,F8.3,15H  AND THALWEG =,F8.3,/)
      STOP
      END
```

```
      FUNCTION QB (QQ,TQ,T,NPQ)
C
C ***************************************************************************
C
C     THIS FUNCTION ROUTINE EVALUATES THE INFLOW AT THE UPSTREAM
C     BOUNDARY AT TIME T
C
C ***************************************************************************
C
C
      DIMENSION  QQ(20),TQ(20)
      J = NPQ - 1
      DO 2 I = 1,J
      IF( T.GE.TQ(I).AND.T.LT.TQ(I+1) ) GO TO 4
    2 CONTINUE
    4 QB = QQ(I) + (QQ(I+1)-QQ(I))/(TQ(I+1)-TQ(I))*(T-TQ(I))
      RETURN
      END




      SUBROUTINE QLTF
C
C ***************************************************************************
C
C     SUBROUTINE EVALUATES THE LATERAL INFLOWS AT TIMES T AND T1 FOR
C     EACH SUB REACH
C
C ***************************************************************************
C
C
      COMMON /A/ T,N,T1
      COMMON /F/ DLAT(50),QI(10,50),TI(10,50),QLAT(50),NPQI(50)
C
      DIMENSION  QLAT1(50)
C
      M = N-1
      TIME = T
    2 DO 6 I = 1,M
      MM = NPQI(I) - 1
      DO 4 L = 1,MM
      IF( TI(L,I).LE.TIME.AND.TI(L+1,I).GT.TIME ) GO TO 5
    4 CONTINUE
C
    5 QL = QI(L,I) + (QI(L+1,I)-QI(L,I))*(TIME-TI(L,I))/(TI(L+1,I)-
     1     TI(L,I))
      IF( TIME.EQ.T ) GO TO 7
      QLAT1(I) = QL
      GO TO 6
    7 QLAT(I) = QL
    6 CONTINUE
C
      IF( TIME.EQ.T1 ) GO TO 10
      TIME = T1
      GO TO 2
   10 DO 12 IL = 1,M
      DLAT(IL) = QLAT1(IL) - QLAT(IL)
   12 CONTINUE
C
      RETURN
      END




      SUBROUTINE QUAD(J,Z,ST,DX,XNODE)
C
C ***************************************************************************
C
C     SUBROUTINE EVALUATES THE DEPTH AT TWO ADJACENT NODES CORRESPONDING
C     TO THE SURFACE ELEVATION MIDWAY BETWEEN THESE NODES USING
C     QUADRATIC INTERPOLATION FOR NODES WITH UNEQUAL SPACING
C
C ***************************************************************************
C
C
      DIMENSION  Z(50),XNODE(50)
C
      INTEGER    R
C
```

```
      IF( J.EQ.1) GO TO 2
      M = J
      L = J-1
      R = J+1
      X = DX/2.
      GO TO 4
    2 M = 2
      L = 1
      R = 3
      X = (XNODE(1)-XNODE(2))/2.
    4 H = (XNODE(M)-XNODE(L))
      RATIO = (XNODE(R)-XNODE(M))/(XNODE(M)-XNODE(L))
      A = (Z(R)+Z(L)*RATIO-Z(M)*(1.+RATIO))/(RATIO*(1.+RATIO)*H*H)
      B = (Z(M)-Z(L))/H+(Z(R)+RATIO*Z(L)-Z(M)*(1.+RATIO))/(H*RATIO*(1.+
     1    RATIO))
      ST = A*X**2 + B*X + Z(M)
C
      RETURN
      END




      SUBROUTINE SCONT (N,DTT,THETA,SVLOUT,VOLERS)
C
C ***************************************************************************
C
C     SUBROUTINE CHECKS SEDIMENT CONTINUITY
C
C ***************************************************************************
C
C
      COMMON /E/ MANN1(50),MANN(50),NP(50),XNODE(50),YB(50,12),ZB(50,12)
      COMMON /O/ BETA,D35,D50,D65,GS(50),POROS,SG,USCRIT,VISCOS,W
      COMMON /R/ DABED(50),DG(50),GSF,NL
C
      REAL       MANN,MANN1
C
      SVLIN = DTT*(GS(NL)-(1.-THETA)*DG(NL))
      SVLOUT = DTT*(GS(N) - (1.-THETA)*DG(N))
      SDVOL = SVLIN - SVLOUT
      IF( SDVOL.EQ.0..OR.SVLOUT.EQ.0. ) GO TO 4
C
C     CALCULATE SEDIMENT VOLUME ERODED/DEPOSITED
C
      BEDVL = 0.
C
      CALL SVOL (NL,N,DABED,XNODE,BEDVL)
C
      SEDVL = BEDVL*(1.-POROS)
C
      SVGAIN = SEDVL - SDVOL
      VOLERS = (SVGAIN/SVLOUT) * 100.
      GO TO 6
    4 VOLERR = 0.
C
    6 RETURN
      END




      SUBROUTINE SED (TFLAG,J,Q)
C
C ***************************************************************************
C
C     SUBROUTINE CALCULATES SEDIMENT PROPERTIES ON T TIME LINE IF TFLAG
C     = 1 AND ON T+1 TIME LINE IF TFLAG = 2
C
C ***************************************************************************
C
C
      COMMON /G/ A(50),ALPHA(50),B(50),DX,K(50),DEPTH(50),P(50),R(50),
     1           THALWG(50),Z(50)
      COMMON /H/ DQ(50),DZ(50)
      COMMON /O/ BETA,D35,D50,D65,GS(50),POROS,SG,USCRIT,VISCOS,W
      COMMON /Q/ COEF(50),COEF1(50),DCOEF(50),DUSED(50),GSE(50),GSE1(50)
     1           ,USED(50),USED1(50),DGSE(50)
C
      REAL       K,KT,KT1,LAMBDA
      INTEGER    TFLAG
      DATA       G/9.81/,AL/4000./
```

```
C
      DENOM    = (SG-1.)*G*D50
      THETC    = USCRIT**2./DENOM
C
C     CALCULATE SEDIMENT PROPERTIES ON THE T TIME LINE
C
      CALL PROPS (1,J,Z(J),AT,BT,KT,PT,RT,RB,ALPT,THAL)
C
      U        = Q / AT
      SF       = (Q/KT)**2
      RT       = Z(J) - THAL
      USTAR    = SQRT(G*RT*SF)
      USTARB   = SQRT(G*RB*SF)
      IF( USTARB.LE.USCRIT ) GO TO 8
      USED(J) = 8.5*USTARB*SQRT(1.-USCRIT/USTARB)
      GSE(J)   =  SEDCAP(U,USTARB,USCRIT,B(J)) / (G*SG*1000.)
      IF( GS(J).LE.0.      ) GO TO 12
C
C     CALCULATE  SPATIAL LAG COEFFICIENT
C
      THETB    = USTARB**2./DENOM
      COEF(J) = 1./(AL*D50*(THETB-THETC))
      GO TO 16
C
    8 GSE(J)   = 0.
   12 USED(J) = 0.
      COEF(J) = 0.
C
   16 IF( TFLAG.EQ.1 ) RETURN
C
C     CALCULATE SEDIMENT PROPERTIES ON THE T+1 TIME LINE
C
      WS       = Z(J) + DZ(J)
      CALL PROPS (2,J,WS,AT1,BT1,KT1,PT1,RT1,RB1,ALPT1,THAL)
C
      U1       = (Q+DQ(J))/AT1
      SF1      = ((Q+DQ(J))/KT1)**2
      RT1      = WS - THAL
      USTAR    = SQRT(G*RT1*SF1)
      USTARB   = SQRT(G*RB1*SF)
      IF( USTARB.LE.USCRIT ) GO TO 20
      USED1(J)= 8.5*USTARB*SQRT(1.-USCRIT/USTARB)
      GSE1(J) = SEDCAP(U1,USTARB,USCRIT,B(J)) / (G*SG*1000.)
C
      THETB    = USTARB**2./DENOM
      COEF1(J)= 1./(AL*D50*(THETB-THETC))
      GO TO 24
C
   20 GSE1(J)   = 0.
      USED1(J) = 0.
      COEF1(J) = 0.
C
   24 DUSED(J)= USED1(J) - USED(J)
      DCOEF(J)= COEF1(J) - COEF(J)
      DGSE(J) = GSE1(J) - GSE(J)
C
      RETURN
      END
```

```
      FUNCTION SEDCAP (U,USTARB,USCRIT,B)
C
C ***************************************************************************
C
C     FUNCTION CALCULATES BED-LOAD SEDIMENT TRANSPORT CAPACITY FOR ANY
C     GIVEN FLOW CONDITIONS. AN 'EFFECTIVE STREAM POWER' TRANSPORT
C     EQUATION IS ASSUMED AND SEDIMENT TRANSPORT CAPACITY IS IN (N/S/M)
C
C ***************************************************************************
C
C
      COMMON /S/  COEFA,COEFB
C
      UCRIT = USCRIT*U/USTARB
      IF( UCRIT.GE.U ) GO TO 5
      SEDCAP = COEFA*(U-UCRIT)**COEFB*B
      RETURN
    5 SEDCAP = 0.
C
      RETURN
      END
```

```
      SUBROUTINE SIMPSN (JL,N,O,X,VOL)
C
C ***************************************************************************
C
C     SUBROUTINE EVALUATES A VOLUME FROM SUPPLIED AREAS USING SIMPSON'S
C     RULE
C
C ***************************************************************************
C
C
      DIMENSION  O(N),X(N)
      REAL       L
C
C     DETERMINE IF THE NUMBER OF SUB REACHES IS ODD OR EVEN
C
      RM = (N-JL)/2
      NN = RM
      RN = NN
      RES = RM - RN
      IF( RES.EQ.0. ) GO TO 2
      JUP = N-2
      GO TO 4
    2 JUP = N-1
    4 VOL = 0.
      IF(N.EQ.2 ) GO TO 8
      JLOW = JL+1
      DO 6 J = JLOW,JUP,2
      L = X(J) - X(J-1)
      R = X(J+1) - X(J)
      DENOM = R*L**2 + L*R**2
      A = ( R*O(J-1) - (R+L)*O(J) + L*O(J+1) ) / DENOM
      B = (-R**2*O(J-1) + (R**2-L**2)*O(J) + L**2*O(J+1) )/DENOM
      C = O(J)
C
      VOL = VOL + A/3.*(R**3+L**3) + B/2.*(R**2-L**2) + C*(R+L)
    6 CONTINUE
C
      IF( RES.EQ.0. ) RETURN
    8 VOL = VOL + 0.5*(X(N)-X(N-1))*(O(N)+O(N-1))
C
      RETURN
      END




      SUBROUTINE SOLVE (C,NB,N)
C
C ***************************************************************************
C
C     SUBROUTINE SOLVES SIMULTANEOUS LINEAR EQUATIONS USING GAUSSIAN
C     ELIMINATION WITH PIVOTAL CONDENSATION
C
C ***************************************************************************
C
C
      DIMENSION  C(100,101)
C
      NR = 2*N
      NLAST = 2*N-1
      NC = 2*N+1
C
      DO 12 I = NB,NLAST
      I1 = I+1
      IBIG = I
      BIG = ABS( C(I,I) )
      DO 2 K = I1,NR
      IF( ABS(C(K,I)).LT.BIG ) GO TO 2
      IBIG = K
      BIG = ABS( C(K,I) )
    2 CONTINUE
      IF( I.EQ.IBIG ) GO TO 6
      DO 4 J = NB,NC
      T = C(I,J)
      C(I,J) = C(IBIG,J)
      C(IBIG,J) = T
    4 CONTINUE
C
C     FORWARD ELIMINATION PASS
C     ------------------------
C
    6 DO 10 J = I1,NR
      IF( ABS(C(J,I)).LT.1.E-10 ) GO TO 10
      R = C(I,I) / C(J,I)
```

```
      DO 8 K = I1,NC
    8 C(J,K) = C(J,K)*R - C(I,K)
   10 CONTINUE
   12 CONTINUE
C
C     BACK SUBSITITUTION PASS
C     -----------------------
C
      C(2*N,2*N+1) = C(2*N,2*N+1) / C(2*N,2*N)
C
      NLOW = 2*N-NB
      DO 16 I = 1,NLOW
      II = 2*N-I
      IJ = II+1
      S = 0.
      DO 14 J = IJ,NR
   14 S = S + C(II,J)*C(J,2*N+1)
   16 C(II,2*N+1) = (C(II,2*N+1)-S) / C(II,II)
C
      RETURN
      END




      SUBROUTINE SROUT
C
C ***************************************************************************
C
C     SUBROUTINE EVALUATES THE CHANGE IN SEDIMENT TRANSPORT RATE AND
C     AREA OF SCOUR/DEPOSITION AT THE NODES FOR TIME T1 USING GAUSSIAN
C     ELIMINATION WITH PARTIAL PIVOTING TO SOLVE THE SEDIMENT CONTINUITY
C     AND SPATIAL LAG EQUATIONS
C
C ***************************************************************************
C
C
      COMMON /A/ T,N,T1
      COMMON /C/ QQ(20),TQ(20),NPQ
      COMMON /B/ G,DT,QBASE,THETA,Q(50),OPTION
      COMMON /E/ MANN1(50),MANN(50),NP(50),XNODE(50),YB(50,12),ZB(50,12)
      COMMON /G/ A(50),ALPHA(50),B(50),DX,K(50),DEPTH(50),P(50),R(50),
     1           THALWG(50),Z(50)
      COMMON /H/ DQ(50),DZ(50)
      COMMON /O/ BETA,D35,D50,D65,GS(50),POROS,SG,USCRIT,VISCOS,W
      COMMON /P/ GB(20),TG(20),NPG
      COMMON /Q/ COEF(50),COEF1(50),DCOEF(50),DUSED(50),GSE(50),GSE1(50)
     1           ,USED(50),USED1(50),DGSE(50)
      COMMON /R/ DABED(50),DG(50),GSF,NL
C
      DIMENSION  CSOLVE(100,101)
C
      INTEGER    OPTION,FLAG
      REAL       K,LN,LF,MANN,MANN1,N1
C
      DO 2 I = 1,100
      DO 2 J = 1,101
    2 CSOLVE(I,J) = 0.
C
C
C     UPSTREAM BOUNDARY CONDITION
C     ---------------------------
C
      DG(NL) = GSF-GS(NL)
C
C
      J = NL
      JF = 0
      NS = NL
      NB = 2*NL-1
      JUP = N-1
      CALL SED (2,J,Q(J))
      IF( GS(J).EQ.0..AND.DG(J).EQ.0. ) DUSED(J) = 0.
C
C
    4 DX = XNODE(J+1) - XNODE(J)
      CALL SED (2,J+1,Q(J+1))
C
      GSLIM = 0.000000001
      IF( JF.EQ.1 ) GO TO 5
      IF( GSE(J+1).GT.GSLIM.OR.T.EQ.0. ) GO TO 5
      NS = J+1
      NB = 2*J+1
```

```
      GS(NS) = 0.
      DG(NS) = 0.
      DABED(NS) = 0.
      IF( NS.EQ.N ) GO TO 11
      J = J+1
      GO TO 4
    5 CONTINUE
      JF = 1
C
C
C     ESTABLISH ELEMENTS OF MATRIX TO BE SOLVED BY GAUSSIAN ELIMINATION
C
C
C     SEDIMENT CONTINUITY EQUATION
C     ----------------------------
C
C
C     COEFFICIENT FOR DG(J+1)
C
          IF( USED(J).EQ.0..AND.DUSED(J).EQ.0..AND.USED(J+1).EQ.0..AND.
     1        DUSED(J+1).EQ.0. ) GO TO 50
          IF( USED1(J+1).EQ.0. ) GO TO 52
              GO TO 54
C
   50 H1 = 2.*THETA*DT/DX
         GO TO 56
   52 H1 = 2./(THETA*(DUSED(J+1)+DUSED(J))+(USED(J+1)+USED(J))) + 2.*
     1  THETA*DT/DX
         GO TO 56
   54 H1 = 2./(THETA*(DUSED(J+1)+DUSED(J))+(USED(J+1)+USED(J))) - THETA/
     1   2.*(DUSED(J+1)+DUSED(J))/USED1(J+1)**2 + 2.*THETA*DT/DX
C
C     COEFFICIENT FOR DABED(J+1)
C
   56 B1 = 1.-POROS
C
C     COEFFICIENT FOR DG(J)
C
          IF( USED(J).EQ.0..AND.DUSED(J).EQ.0..AND.USED(J+1).EQ.0..AND.
     1        DUSED(J+1).EQ.0. ) GO TO 58
          IF( USED1(J).EQ.0. ) GO TO 60
              GO TO 62
   58 C1 = -2.*THETA*DT/DX
         GO TO 64
   60 C1 = -(2./(THETA*(DUSED(J+1)+DUSED(J))+(USED(J+1)+USED(J))) - 2.*
     1  THETA*DT/DX)
         GO TO 64
C
   62 C1 = -(2./(THETA*(DUSED(J+1)+DUSED(J))+(USED(J+1)+USED(J))) -
     1   THETA/2.*(DUSED(J+1)+DUSED(J))/USED1(J)**2 - 2.*THETA*DT/DX)
C
C     COEFFICIENT FOR DABED(J)
C
   64 D1 = -(1.-POROS)
C
C     CONSTANT
C
          GT1 = 0.
          GT2 = 0.
          GT3 = 0.
          GT4 = 0.
C
          IF( USED1(J+1).GT.0. ) GT1 = GS(J+1)/USED1(J+1)**2.
          IF( USED1(J)   .GT.0. ) GT2 = GS(J)/USED1(J)**2.
          IF( USED(J+1)  .GT.0. ) GT3 = GS(J+1)/USED(J+1)**2.
          IF( USED(J)    .GT.0. ) GT4 = GS(J)/USED(J)**2.
                                  GT5 = 2.*DT/DX*(GS(J+1)-GS(J))
C
C
      G1 = (THETA/2.*(GT1+GT2)+(1.-THETA)/2.*(GT3+GT4))*(DUSED(J+1)+
     1  DUSED(J)) - GT5
C
C     SPATIAL LAG EQUATION
C     --------------------
C
C
C     COEFFICIENT FOR DG(J+1)
C
      H2 = -DT*COEF1(J+1)
C
C     COEFFICIENT FOR DABED(J+1)
C
      B2 = 1.-POROS
C
C     COEFFICIENT FOR DG(J)
C
      C2 = DT*COEF1(J)
```

```
C
C     COEFFICIENT FOR DABED(J)
C
      D2 = -(1.-POROS)
C
C     CONSTANT
C
      G2 = DT*(COEF1(J+1)*(GS(J+1)-THETA*GSE1(J+1)) + COEF1(J)*(GS(J)-
     1     THETA*GSE1(J)) - (1.-THETA)*(GSE(J+1)*COEF(J+1)+GSE(J)*
     2     COEF(J)))
C
C     SET UP MATRIX ELEMENTS
C
      CSOLVE(2*J-1,2*J-1) = -C1
      CSOLVE(2*J-1,2*J  ) = -D1
      CSOLVE(2*J-1,2*J+1) =  H1
      CSOLVE(2*J-1,2*J+2) =  B1
      CSOLVE(2*J-1,2*N+1) =  G1
C
      CSOLVE(2*J,2*J-1)   = -C2
      CSOLVE(2*J,2*J  )   = -D2
      CSOLVE(2*J,2*J+1)   =  H2
      CSOLVE(2*J,2*J+2)   =  B2
      CSOLVE(2*J,2*N+1)   =  G2
C
      IF( J.EQ.JUP ) GO TO 6
      J = J + 1
      GO TO 4
C
C     UPSTREAM BOUNDARY CONDITION
C
    6 CSOLVE(2*N-1,NB) = 1.
      CSOLVE(2*N-1,2*N+1) = DG(NS)
C
C     DOWNSTREAM BOUNDARY CONDITION
C
      CSOLVE(2*N,2*N-1) = -DT*COEF1(N)
      CSOLVE(2*N,2*N) = 1.0
      CSOLVE(2*N,2*N+1) = DT*GS(N)*COEF1(N) - THETA*DT*GSE1(N)*COEF1(N)
     1                  - (1.-THETA)*DT*GSE(N)*COEF(N)
C
C
   10 CALL SOLVE (CSOLVE,NB,N)
C
C     CALCULATE SEDIMENT DISCHARGES AND AREAS OF SCOUR/DEPOSITION ON THE
C     FORWARD TIME LINE
C
      DO 40 J = NS,N
      DG(J)    = CSOLVE(2*J-1,2*N+1)
      DABED(J) = CSOLVE(2*J  ,2*N+1)
   40 CONTINUE
   11 GS(NL-1) = GSB(GB,TG,T1,NPG)
      DO 12 J = NL,N
      GS(J) = GS(J) + DG(J)
   12 CONTINUE
C
      RETURN
      END



      SUBROUTINE SVOL (IL,IU,DA,X,VOL)
C
C ***************************************************************************
C
C     SUBROUTINE CALCULATES VOLUME USING THE TRAPEZOIDAL RULE
C
C ***************************************************************************
C
C
      DIMENSION  DA(50),X(50)
C
      VOL = 0.
      IUP = IU-1
C
      DO 20 I = IL,IUP
      VOL = VOL + 0.5*(DA(I)+DA(I+1))*(X(I+1)-X(I))
   20 CONTINUE
C
      RETURN
      END
```

F.4.2 Temporal Lag Model Modifications

Temporal lag effects were simulated by modifying the preceeding numerical model, which only simulates spatial lag effects, in the following manner:

The MAIN program modifications are:

Insertion, in the Common block, of

```
      COMMON /W/ NFLAG,QBL,QMAX
```

Insertion, after data Output statements, of

```
      QBL  = Q(1)/0.305
      QMAX = QQ(2)/0.305
```

Replacement of the bed roughness scheme by

```
C     DETERMINE ROUGHNESS ON FOWARD TIME LINE
C
      DO 520 J = 2,N
C
      NFLAG = 1
      CALL SED (2,J,Q(J))
C
      IF( MANN1(J).LE.0.01610 ) MANN1(J) = 0.01610
  520 CONTINUE
```

Insert the following two new subroutines (QU and TLAG) and replace subroutin SED with the following modified version of this subroutine.

```
      FUNCTION QU (QL,SF,AA,T)
C
C  ***********************************************************************
C
C     THIS FUNCTION ROUTINE CALCULATES EQUIVALENT STEADY FLOW RATE. THE
C     TIME SCALE RELATION WAS OBTAINED BY SUBSTUTING THE VARIOUS FLOW
C     AND SEDIMENT PROPERTIES OF BELL (1980) INTO THE GENERAL TIME
C     SCALE RELATION OF PHILLIPS (1984).
C
C  ***********************************************************************
C
C     QU        - SUPERPOSITION SOLUTION EQUIVALENT STEADY FLOW RATE
C
C     T90       - TIME SCALE OF TEMPORAL RESPONSE OF EQUIVALENT
C                 STEADY FLOW RATE
C
C  ***********************************************************************
C
C
      T90 = 1.873*QL**0.7208/SF**1.2748
      TT  = 0.111*T90
      ARG = TT/(TT+T)
      QU  = AA*T+AA*TT*ALOG(ARG)
C
      RETURN
      END
```

```
      SUBROUTINE TLAG (J,IUP,SF,T,UN,UU,USB)
C
C  ***************************************************************************
C
C     SUBROUTINE CALCULATES EQUIVALENT STEADY PROPERTIES USING TEMPORAL
C     LAG SCHEME AND RELATIONS OBTAINED BY SUBSTITUTING THE VARIOUS
C     FLOW AND SEDIMENT PROPERTIES OF BELL (1980) INTO THE GENERAL
C     FLOW PROPERTY RELATIONS OF PHILLIPS (1984).
C
C  ***************************************************************************
C
C     AA        - SLOPE OF SUPERPOSITION SOLUTION DISCHARGE LIMB
C
C     QBL       - BASE DISCHARGE (M**3/S/M)
C     QE        - INSTANTANEOUS EQUIVALENT STEADY FLOW RATE
C     QL        - DISCHARGE ON DISCHARGE LIMB AT TIME T
C     QS        - EXCESS EQUIVALENT STEADY FLOW RATE
C
C     T         - TIME
C     T0        - TIME ORIGIN OF DISCHARGE LIMB
C
C     UN        - EQUIVALENT STEADY BED ROUGHNESS VALUE
C     UU        - EQUIVALENT STEADY FLOW VELOCITY
C     USB       - EQUIVALENT STEADY BED SHEAR VELOCITY
C
C  ***************************************************************************
C
C
      COMMON /W/ NFLAG,QBL,QMAX
      COMMON /X/ AA(50,200),T0(50,200),BB(50,200)
C
      QS = 0.
      DO 8 I = 1,IUP
      TD = T-T0(J,I)
      IF(AA(J,I).EQ.0. ) GO TO 8
      QL = ABS(AA(J,I)*TD)+QBL
      IF( QL.GE.QMAX ) QL = QMAX
      QS = QS + QU(QL,SF,AA(J,I),TD)
    8 CONTINUE
      QE = QS+QBL
C
      UN = 0.0359    *SF**0.0910*QE**0.07264
      UU = 33168000.*UN**4.6164/SF**0.16667
      USB= 1368930. *UN**4.2123
C
      RETURN
      END




      SUBROUTINE SED (TFLAG,J,Q)
C
C  ***************************************************************************
C
C     SUBROUTINE CALCULATES SEDIMENT PROPERTIES ON T TIME LINE IF TFLAG
C     = 1 AND ON T+1 TIME LINE IF TFLAG = 2
C
C  ***************************************************************************
C
C
      COMMON /A/ T,N,T1
      COMMON /E/ MANN1(50),MANN(50),NP(50),XNODE(50),YB(50,12),ZB(50,12)
      COMMON /G/ A(50),ALPHA(50),B(50),DX,K(50),DEPTH(50),P(50),R(50),
     1           THALWG(50),Z(50)
      COMMON /H/ DQ(50),DZ(50)
      COMMON /O/ BETA,D35,D50,D65,GS(50),POROS,SG,USCRIT,VISCOS,W
      COMMON /Q/ COEF(50),COEF1(50),DCOEF(50),DUSED(50),GSE(50),GSE1(50)
     1           ,USED(50),USED1(50),DGSE(50)
      COMMON /W/ NFLAG,QBL,QMAX
      COMMON /X/ AA(50,200),T0(50,200),BB(50,200)
C
      REAL K,KT,KT1,MANN,MANN1
      INTEGER TFLAG
      DATA G/9.81/,AL/4000./
C
      DENOM    = (SG-1.)*G*D50
      THETC    = USCRIT**2./DENOM
C
C     CALCULATE SEDIMENT PROPERTIES ON THE T TIME LINE
C
      CALL PROPS (1,J,Z(J),AT,BT,KT,PT,RT,RB,ALPT,THAL)
C
```

```
      U       = Q / AT
      SF      = (Q/KT)**2
      RT      = Z(J) - THAL
      USTAR   = SQRT(G*RT*SF)
      USTARB  = SQRT(G*RB*SF)
      IF( USTARB.LE.USCRIT ) GO TO 28
      USED(J) = 8.5*USTARB*SQRT(1.-USCRIT/USTARB)
C
   28 IF( T.EQ.0. ) GO TO 40
      DO 32 I = 1,200
      IF( T.EQ.T0(J,I) ) GO TO 36
   32 CONTINUE
C
   36 CALL TLAG (J,I-1,SF,T,UN,UU,USB)
C
      IF( USB.LE.USCRIT ) GO TO 8
      GSE(J) = SEDCAP (UU,USB,USCRIT,B(J))/(G*SG*1000.)
      GO TO 44
   40 IF( USTARB.LE.USCRIT ) GO TO 8
      GSE(J)  =  SEDCAP(U,USTARB,USCRIT,B(J)) / (G*SG*1000.)
   44 IF( GS(J).LE.0.      ) GO TO 12
C
C     CALCULATE  SPATIAL LAG COEFFICIENT
C
      THETB   = USTARB**2./DENOM
      COEF(J) = 1./(AL*D50*(THETB-THETC))
      GO TO 16
C
    8 GSE(J)  = 0.
   12 USED(J) = 0.
      COEF(J) = 0.
C
   16 IF( TFLAG.EQ.1 ) RETURN
C
C     CALCULATE SEDIMENT PROPERTIES ON THE T+1 TIME LINE
C
      WS      = Z(J) + DZ(J)
      CALL PROPS (2,J,WS,AT1,BT1,KT1,PT1,RT1,RB1,ALPT1,THAL)
C
      U1      = (Q+DQ(J))/AT1
      SF1     = ((Q+DQ(J))/KT1)**2
      RT1     = WS - THAL
      USTAR   = SQRT(G*RT1*SF1)
      USTARB  = SQRT(G*RB1*SF)
      IF( USTARB.LE.USCRIT ) GO TO 46
      USED1(J)= 8.5*USTARB*SQRT(1.-USCRIT/USTARB)
C
C     DETERMINE SLOPES AND TIME ORIGINS OF DISCHARGE LIMBS IN THE
C     SUPERPOSITION SOLUTION
C
   46 IF( T.GT.0. ) GO TO 48
      I = 1
      AA(J,1) = DQ(J)/(T1-T)/BT1
      BB(J,1) = AA(J,1)
      T0(J,1) = T
      GO TO 52
C
   48 BB(J,I) = DQ(J)/(T1-T)/BT1
      AA(J,I) = BB(J,I)-BB(J,I-1)
   52 T0(J,I+1) = T1
C
      CALL TLAG (J,I,SF1,T1,UN1,UU1,USB1)
C
      IF( USB1.LE.USCRIT ) GO TO 20
      GSE1(J) = SEDCAP (UU1,USB1,USCRIT,B(J))/(G*SG*1000.)
C
      THETB   = USTARB**2./DENOM
      COEF1(J)= 1./(AL*D50*(THETB-THETC))
      GO TO 24
C
   20 GSE1(J)  = 0.
      USED1(J) = 0.
      COEF1(J) = 0.
C
   24 DUSED(J)= USED1(J) - USED(J)
      DCOEF(J)= COEF1(J) - COEF(J)
      DGSE(J) = GSE1(J) - GSE(J)
C
      IF( NFLAG.EQ.1 ) MANN1(J) = UN1
      IF( USB1.LE.USCRIT ) MANN1(J) = 0.01610
      NFLAG = 0
      RETURN
      END
```

SPATIAL AND TEMPORAL LAG EFFECTS IN BEDLOAD SEDIMENT TRANSPORT

B.C. Phillips

ABSTRACT: A spatial lag equation and a temporal lag scheme for bedload transport are developed and tested against measured data. A numerical model which incorporates the spatial lag equation and temporal lag effects, via the sediment transport capacity term, is formulated. Model runs are compared with previously measured data and good agreement obtained. It is concluded that the numerical model is well able to simulate spatial and temporal bedload lag effects.

U. of Cant., Civil Eng. Dept., Ph.D. Thesis.